Technical Report Documentation Page

1. Report No.	2. Government Accession No.	3. Recipient's Catalog No.
FHWA/TX-05/1872-2		

4. Title and Subtitle	5. Report Date
DEVELOPMENT OF A NEW METHOD FOR ASSESSING ASPHALT BINDER DURABILITY WITH FIELD VALIDATION	August 2005
	6. Performing Organization Code
7. Author(s) Charles J. Glover, Richard R. Davison, Chris H. Domke, Yonghong Ruan, Pramitha Juristyarini, Daniel B. Knorr, Sung H. Jung	8. Performing Organization Report No. Report 0-1872-2
9. Performing Organization Name and Address Texas Transportation Institute The Texas A&M University System College Station, Texas 77843-3135	10. Work Unit No. (TRAIS)
	11. Contract or Grant No. Project No. 0-1872
12. Sponsoring Agency Name and Address Texas Department of Transportation Research and Technology Implementation Office P.O. Box 5080 Austin, Texas 78763-5080	13. Type of Report and Period Covered Research: September 1998 - August 2002
	14. Sponsoring Agency Code

15. Supplementary Notes

Research performed in cooperation with the Texas Department of Transportation and the U.S. Department of Transportation, Federal Highway Administration.
Research Project Title: Evaluate Non-Specification Properties for Performance Graded Asphalts Which May Affect Performance

16. Abstract

This project was a comprehensive study directed at developing an improved method of screening asphalt binders for long-term pavement performance. A new dynamic shear rheometer (DSR) function and a new aging procedure should warn of premature asphalt hardening and resulting fatigue cracking.

For unmodified asphalts the new DSR function $G'/(\eta'/G')$ correlated well with ductility (at 15 °C, 1 cm/min) below 10 cm. The correlation was originally developed for DSR measurements at 15 °C and 0.005 rad/s. These conditions were time-temperature superposition shifted to 44.7 °C and 10 rad/s to produce a method that is easily accessible to standard laboratory rheological equipment and methods.

The recommended aging procedure uses the pressure aging vessel (PAV) apparatus but takes advantage of the higher average aging rate when the asphalt is aged in thinner films. This change, combined with somewhat longer aging, results in a more rigorous test of durability than the standard PAV method. At the same time, the resulting rankings of aged materials are more representative of rankings that are obtained from aging at atmospheric air pressure and 60 °C.

For modified asphalts, the results were complex. Generally for a given value of the DSR function, the ductility was better than indicated by the unmodified asphalt DSR-ductility correlation. Larger amounts of modifier produced increasing values of ductility for a given function value. This result was very asphalt dependent, however, so no general correlation could be found. As modified binders oxidize, the asphalt hardens and the improvement to ductility imparted by modifiers decreases. After enough aging, the improvement is gone and modified binders perform no better than their aged unmodified counterpart. A critical issue is whether the life extension produced by modifiers is life-cycle cost effective.

Long-Term Pavement Performance (LTPP) and SH 21 binders indicate: sealcoats may provide an opportunity for significant and very cost-effective in-place binder rejuvenation; $G'/(\eta'/G')$ is an excellent function for tracking pavement aging; pavements can oxidize rather uniformly with depth; brittle binders can be tolerated in stiff pavements; aggregates appear to have little effect on asphalt oxidation reactions; rolling thin-film oven test (RTFOT) plus PAV aging is not severe aging, in the context of pavement life.

17. Key Words	18. Distribution Statement
Asphalt Oxidation, Ductility, Asphalt Durability, Asphalt Aging, Superpave, Maxwell Model, Failure Stress, Failure Strain, Aging Test	No restrictions. This document is available to the public through NTIS: National Technical Information Service 5285 Port Royal Road Springfield, Virginia 22161

19. Security Classif.(of this report)	20. Security Classif.(of this page)	21. No. of Pages	22. Price
Unclassified	Unclassified	334	

Form DOT F 1700.7 (8-72) Reproduction of completed page authorized.

DEVELOPMENT OF A NEW METHOD FOR ASSESSING ASPHALT BINDER DURABILITY WITH FIELD VALIDATION

by

Charles J. Glover
Richard R. Davison
Research Engineers
Chemical Engineering/Texas Transportation Institute

and

Chris H. Domke
Yonghong Ruan
Pramitha Juristyarini
Daniel B. Knorr
Sung H. Jung
Graduate Students
Chemical Engineering/Texas Transportation Institute

Report 1872-2
Project Number 0-1872
Research Project Title: Evaluate Non-Specification Properties for Performance Graded Asphalts Which May Affect Performance

Sponsored by the
Texas Department of Transportation
In Cooperation with the
U.S. Department of Transportation
Federal Highway Administration

August 2005

TEXAS TRANSPORTATION INSTITUTE
and Chemical Engineering Department
The Texas A&M University System
College Station, Texas 77843-3135

DISCLAIMER

This research was performed in cooperation with the Texas Department of Transportation (TxDOT) and the U.S. Department of Transportation, Federal Highway Administration (FHWA). The contents of this report reflect the views of the authors, who are responsible for the facts and accuracy of the data presented herein. The contents do not necessarily reflect the official view or policies of the FHWA or TxDOT. This report does not constitute a standard, specification, or regulation, nor is it intended for construction, bidding, or permit purposes. Trade names are used solely for information and not for product endorsement. The engineer in charge of this project was Charles James Glover, Ph.D., P.E. (Texas, 48732).

ACKNOWLEDGMENTS

The authors wish to express their appreciation for contributions made by several individuals during the project. Gerald Peterson, Texas Department of Transportation project director, was very helpful with technical suggestions and in serving as the project contact. The excellent staff support of the Chemical Engineering Department and the Texas Transportation Institute of The Texas A&M University System is greatly appreciated. Also, we recognize the assistance of Todd Hausman of the Center for Asphalt and Materials Chemistry for assistance with laboratory analyses and operations. Finally, the contributions of Dorothy Jordan to project administration and preparation of this report are especially valued and appreciated.

The financial support provided by the Texas Department of Transportation in cooperation with the Federal Highway Administration, the Texas Transportation Institute, the Texas Engineering Experiment Station, and the Chemical Engineering Department at Texas A&M University is also greatly appreciated.

TABLE OF CONTENTS

TABLE OF CONTENTS (CONT.)

TABLE OF CONTENTS (CONT.)

TABLE OF CONTENTS (CONT.)

LIST OF FIGURES

LIST OF FIGURES (CONT.)

LIST OF FIGURES (CONT.)

LIST OF FIGURES (CONT.)

LIST OF FIGURES (CONT.)

LIST OF FIGURES (CONT.)

LIST OF FIGURES (CONT.)

LIST OF FIGURES (CONT.)

LIST OF TABLES

LIST OF TABLES (CONT.)

LIST OF TABLES (CONT.)

CHAPTER 1. INTRODUCTION AND BACKGROUND

PROBLEM STATEMENT

Performance grade specifications (PG) are intended to predict pavement performance. By basing the specification on a model of pavement structure and pavement life, the PG system should ideally be able to ignore the content of the asphalt binder in determining the behavior of the material. In actuality, it is known that asphalts of the same grade may behave differently, displaying markedly different aging characteristics, water or stripping susceptibilities, fatigue resistance, and low-temperature strength and flexibility. Refineries will be investigating methods to meet specifications at a low cost, and in some cases, may provide products which meet specifications but do not perform as expected or desired.

The objectives of this research were as follows:

1. Determine asphalt properties which will affect the performance of hot mix asphalt concrete (HMAC). Performance should be related to general pavement behavior, such as rutting, stripping, fatigue cracking, and thermal cracking.
2. Develop methods to measure the identified properties.
3. Determine acceptable criteria for the identified properties.
4. Evaluate existing asphalts which are manufactured to meet the performance grade specifications, including modified systems such as latex, block copolymer, and tire rubber, with respect to performance-related properties and acceptable criteria previously identified.

BASIS AND THEORY OF SUPERPAVE™ SPECIFICATIONS

The Strategic Highway Research Program (SHRP) was conducted from 1988 to 1993. A significant part of this effort was a study of asphalt binder properties leading to performance-based specifications for their selection and use. Specifically, these specifications address the major failure properties of pavements, namely, rutting, fatigue cracking, and thermal cracking. The work of the SHRP program built upon early asphalt work, added new data and theory, and provided updated specifications.

The Superpave™ binder testing protocol calls for a combination of conditioning and property measurement steps (Figure 1-1). First, the binder is tested in an unaged condition at the desired maximum pavement temperature to assess the likelihood that it will produce a tender mix. This test is assessed with a dynamic shear rheometer (DSR) $G^*/\sin\delta$ measurement, and a minimum value of 1.0 kPa is required. Second, the binder is subjected to the rolling thin-film oven test (RTFOT) to mimic the binder aging that would occur in the hot-mix plant and then tested again for the likelihood of permanent deformation (rutting) (DSR, $G^*/\sin\delta$, measured at the maximum pavement temperature, a minimum value of 2.2 kPa is required). Third, the binder is subjected to the pressure aging vessel (PAV) at a high temperature and high pressure to mimic

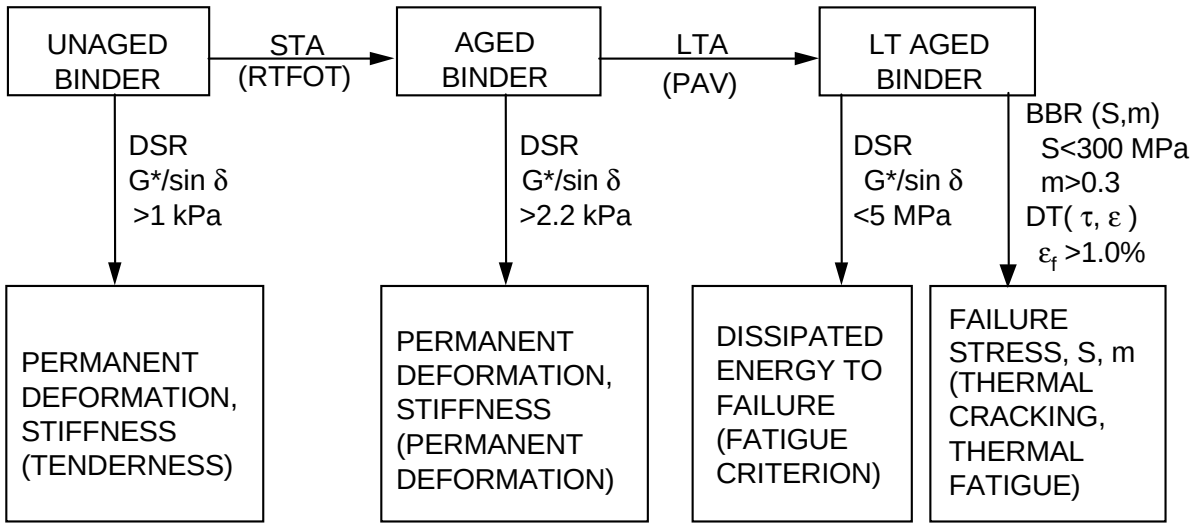

Note: DSR measurements at 10 rad/s

Figure 1-1. Superpave Asphalt Binder Test.

the aging that would occur over extended periods of time in pavement use. Then it is tested a) at moderate temperatures for a tendency to fail due to fatigue cracking (DSR, $G^*\sin\delta$, a maximum value of 5 MPa is allowed) and b) at low temperature (10 °C above the minimum pavement temperature) to obtain a stiffness (S, maximum 300 MPa allowed) and the slope (m) of the log creep stiffness versus log loading time curve to determine the likelihood that the material will fail due to low temperature cracking and thermal fatigue (bending beam rheometer, BBR, S, and m measured at 60 s loading time). Furthermore, the direct tension failure test at low temperature on this long-term aged material may be performed to provide additional information about the likelihood of low-temperature cracking failure (tested at 10 °C above the minimum pavement temperature, 1 percent strain at failure, minimum).

Thermal Cracking Specifications

Early Work

Recent work in the SHRP program leading to Superpave specifications is based upon work which occurred during the mid 1960s by Heukelom and others which led to the concept of a limiting stiffness and limiting stiffness temperature. When an asphalt reaches a certain limiting stiffness, presumably either by temperature or by oxidative aging, then it is susceptible to cracking. The early work of Heukelom (1966) produced considerable data on binder properties and especially binder stiffness, stress, and strain. From these data, he determined that over a wide range of stiffness, Log elongation at break for road bituminous binders versus Log stiffness followed two linear correlations which intersected at a stiffness of about 3 kPa (Figure 1-2). This

common relationship was found for a number of different bitumens and for a number of different rheological measurement techniques. With stiffnesses above 3 kPa, the correlation was especially good, and he extrapolated it to the theoretical glassy modulus of elasticity for bitumens of about 3 Gpa (Figure 1-3). This range of stiffnesses from 3 kPa to 3 GPa covered the failure strain range from about 10% to a little over 0.1%. From these data Heukelom also calculated failure stress data and obtained a common curve for tensile strength versus log stiffness for bituminous binders. The tensile strength at the glassy elastic limit was found to be about 3.5 MPa. This tensile strength curve passed through a maximum tensile strength of about 5.5 MPa at a stiffness value of about 40 MPa. It should be noted that while he recognized that loading time was a factor in the measurements, his measurements were made for common loading rates, and he reported simply "stiffness," bypassing the issue of dependence of stiffness on temperature and time. Nevertheless, the data are very valuable for establishing the importance of stiffness to thermal cracking.

Parallel with the work of Heukelom, Hills and Brien (1966) demonstrated a procedure for determining a cracking temperature for bituminous binders. This technique was based upon the data of Heukelom and recognized that cooling binders, while being restrained from contracting, generated tensile stresses. When these tensile stresses exceed the tensile strength of the binders, whose values as a function of stiffness were determined by Heukelom, the binders will crack. This work then, together with the work of Heukelom, establishes two concepts: the limiting stiffness and the limiting stiffness temperature. For typical coefficients of thermal expansion for asphalt binders, and for pavements, a typical thermal-induced strain is of the order of 1 percent. Therefore, when the stiffness is high enough that a 1 percent strain causes the tensile strength of the binder to be exceeded, we would expect the binder to crack. From Heukelom's data, 1 percent failure strain occurs at a (limiting) stiffness of approximately 400 MPa. Thus, in the literature, one sees limiting stiffness values that approach this value, e.g., 240 MPa at 0.5 hour loading time (McLeod, 1972), 138 MPa at 2.8 hours (Fromm and Phang, 1970), and 200 MPa at 2 hours (Readshaw, 1972). Hills and Brien (1966), as reported by Anderson et al. (1990) use a thermal expansion coefficient of $2 \times 10^{-4}/^{o}C$ to calculate thermal strains.

McLeod (1972) reports much data on thermal cracking in Ontario test roads. Using his data, Readshaw (1972) reports a critical stiffness for bitumen of 240 MPa at 0.5 hr loading time. These field data would seem to match quite well the laboratory data of Heukelom on binder stiffnesses and tensile strengths.

Work of the SHRP Program

Within the SHRP program, a number of thermal cracking theories and procedures were considered (Anderson et al., 1990), including the limiting stiffness concepts discussed above, an empirical/mechanistic model for computing thermal cracking as a function of time (Shahin-McMulin model TC-1), the program COLD, the Ruth model, statistical models, and fracture mechanics models, including the Lytton model. These latter models all attempt to do more than establish a limiting stiffness temperature; they also attempt to calculate the onset-of-cracking

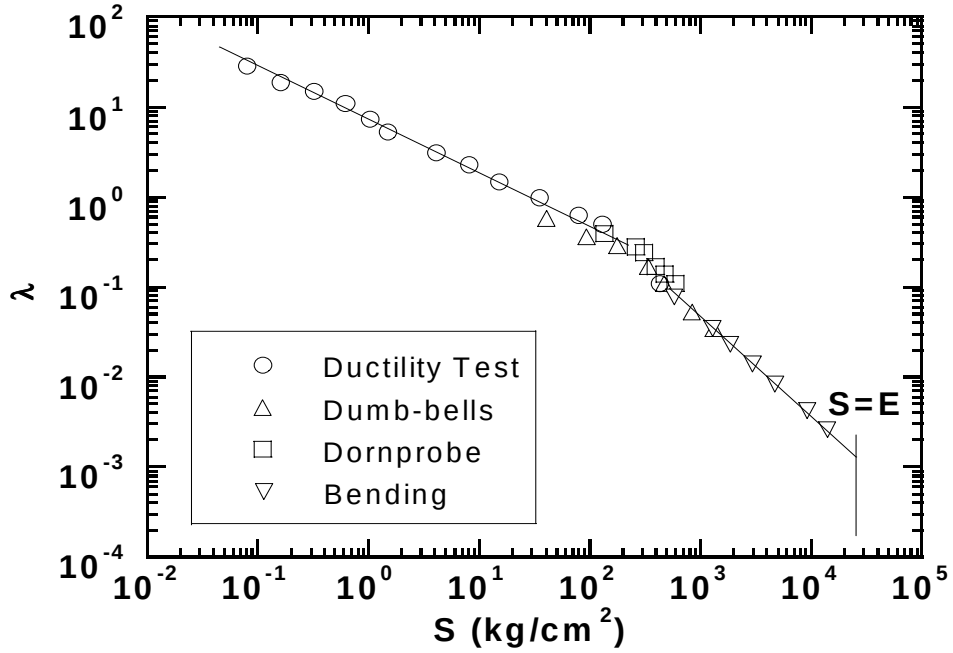

Figure 1-2. Elongation at Break (λ) as a Function of the Stiffness Modulus (S). (1 kg / cm² = 98 kPa) (Heukelom, 1966)

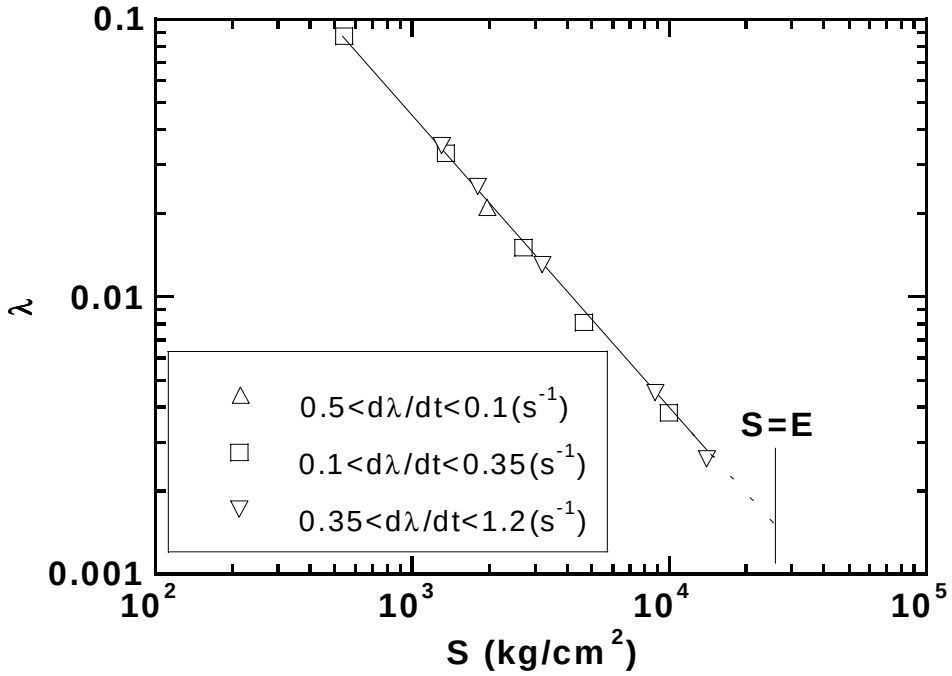

Figure 1-3. Elongation at Break (λ) as a Function of the Stiffness Modulus (S) at High Stiffnesses. (Heukelom, 1966)

time and the extent of cracking over time. All are based variously upon either empirical data, theory, or combinations of the two. These more sophisticated and detailed models, although evaluated as part of the SHRP effort, were considered to be inappropriate for specification purposes (Anderson et al., 1991). In the area of thermal cracking, the limiting stiffness of 300 MPa at a loading time of 2 hours was finally selected for the asphalt binder specification for Superpave (Anderson and Kennedy, 1993). However, this value was time-temperature shifted so that the measurement was actually made at a 10 °C higher temperature and at 60 s instead of 2 hours (i.e., a measurement made at a 10 °C above the specified pavement temperature after 60 s loading is equivalent to one made at the actual pavement temperature and after 2 hours loading) (Anderson and Kennedy, 1993). Additionally, it was specified that the magnitude of the slope of the Log(S) versus Log(t) curve must be greater than 0.3 measured at 10 °C above the minimum pavement temperature. This forces the material to still exhibit relaxation and therefore to exhibit a failure strain greater than its failure strain at its elastic limit. Based on Heukelom's work, an asphaltic material which is at its elastic limit can sustain a strain of only 0.13 percent. The values of 300 MPa and m=0.3 were based upon field data and observations of cracking (Stoffels et al., 1994).

Rutting Specifications

The tenderness and permanent deformation tests which are based on the $G^*/\sin\delta$ parameter measured at the maximum pavement temperature have been related to laboratory rutting tests conducted on compacted mixes (Anderson and Kennedy, 1993). These results have been obtained for both original asphalts and modified asphalt binders. A higher G^* (stiffness) at the maximum pavement temperature and a greater elasticity (smaller $\sin\delta$) will each contribute to a reduced tendency for the binder to deform under load, and therefore, should characterize a binder that is less susceptible to rutting.

Fatigue Cracking Specification

The fatigue cracking specification is the least supported in the literature and, evidently, the least successful. Fatigue cracking is evaluated in the Superpave system from measurements of $G^*\sin\delta$ ($=G''$), which is a measure of energy dissipation, along with the low-temperature value of the slope of the log creep stiffness versus log time curve, m (Anderson and Kennedy, 1993).

ASPHALT DURABILITY AND SUPERPAVE™

Introduction

Perhaps the greatest shortcoming of Superpave specifications for unmodified binders is in regard to the hardening of asphalt. It has been recognized for years that while asphalt roadways can fail for a variety of reasons, if they are properly constructed and designed for the loads they must carry, failure will finally occur when the binder is so oxidized that it becomes very brittle.

Thus one of the most desired properties of asphalt is that it resist the effect of weathering or aging.

For example, in a report to the Virginia Highway and Transportation Committee, Halstead (1984) said: "Thus, the durability of the asphalt cement is a major consideration. A durable asphalt is sometimes defined as one where properties are resistant to change for the worse with time. However, a better definition is that used by Petersen (1984). He defines a durable asphalt as one that 1) possesses the physical properties necessary to produce the desired initial product performance, and 2) is resistant to change in physical properties during long-term, in-use environmental aging."

Superpave™ and Fatigue Cracking

While it is assumed Superpave specifications do a creditable job of guarantying good initial properties, they do not guarantee good aging characteristics. Since this statement is strong it deserves elaboration.

The PAV was introduced to ensure that the fatigue cracking parameter $G^*\sin\delta$ and the low temperature transverse cracking parameters S and m from the bending beam would reflect aging effects. The problem is that none of these parameters is particularly sensitive to aging. This is less important for the low temperature parameters since asphalt physical properties become relatively constant at very low temperature, but it is very important for the fatigue cracking parameters. The literature is replete with studies showing that when penetration, ductility, or other rheological properties reach certain critical levels, roads fail through cracking. Many of these properties are discussed later.

Figure 1-4 is a plot of $G^*\sin\delta$ at 19 and 28 ^oC after 20, 40, and 60 hours in the PAV. Little change in $G^*\sin\delta$ with increased aging is observed. Note that very few asphalts fail this specification (i.e., exceed 5 Mpa) which implies, falsely, that fatigue cracking is not a problem. The specifications could be tightened until some asphalts fail, but that hardly deals with the problem that an aging insensitive property is being used to control for a very aging sensitive malady. In fact Figure 1-4 indicates $G^*\sin\delta$ can even go in the wrong direction with continued aging.

Asphalt Oxidation and Hardening

Before continuing this analysis it is necessary that we digress to discuss the nature of asphalt oxidation and hardening. Over the last decade, we (CMAC) have done extensive studies on asphalt oxidation.

Asphalt hardening is broken into independent parameters as indicated by equation 1-1 relative to viscosity changes with oxidation.

$$\frac{d \ln \eta_o^*}{dt} = \frac{d \ln \eta_o^*}{dCA} \frac{dCA}{dt} \qquad (1\text{-}1)$$

where η_o^* is the low shear rate limiting dynamic complex viscosity, t is time, and carbonyl area (CA) is the area under the carbonyl curve as measured by infrared analysis. We have shown the CA is a good surrogate for oxygen and much easier to measure (Liu et al., 1996). We discovered some years ago (Martin et al., 1990) that the first term in equation 1-1 was independent of aging temperature below about 100-110 °C and was a constant for each asphalt. We called this term the hardening susceptibility (HS). It is not a measure of how fast an asphalt oxidizes, but it is a measure of its tendency to harden when it oxidizes. Obviously a low value is desirable.

Figure 1-5 shows a typical plot of how carbonyl changes with time when diffusion is eliminated. There is an initial jump that is characteristic of the asphalt and then a constant slope. The change in $\ln \eta_o^*$ behaves the same way, so that when $\ln \eta_o^*$ is plotted versus CA as in Figure 1-6, a straight line is obtained with data from all temperatures collapsing to a single line.

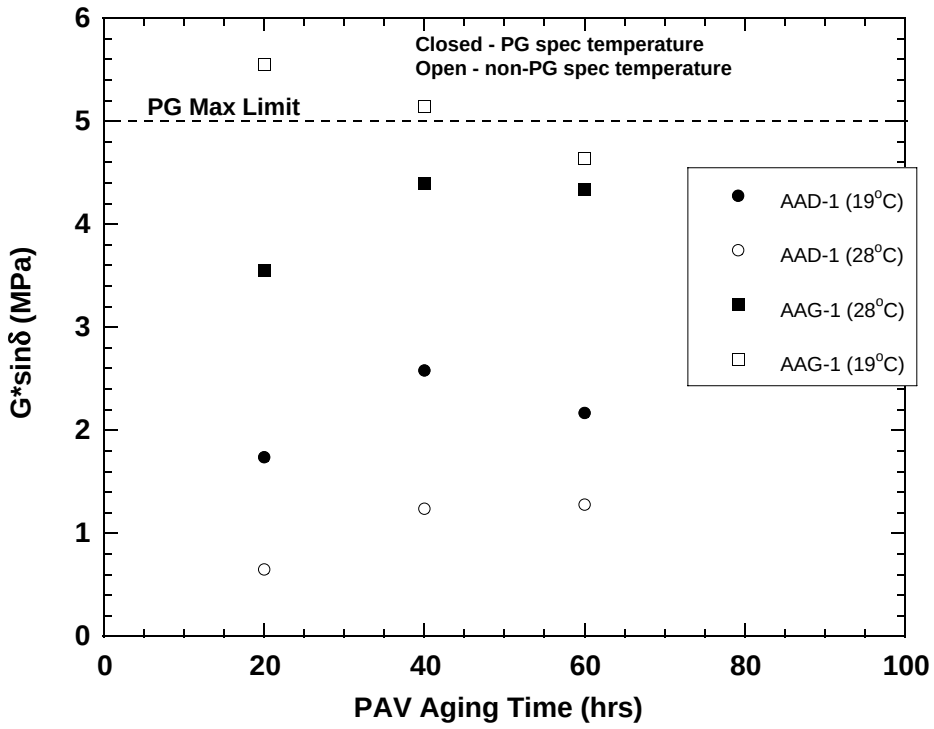

Figure 1-4. G*sin δ versus Aging Time.

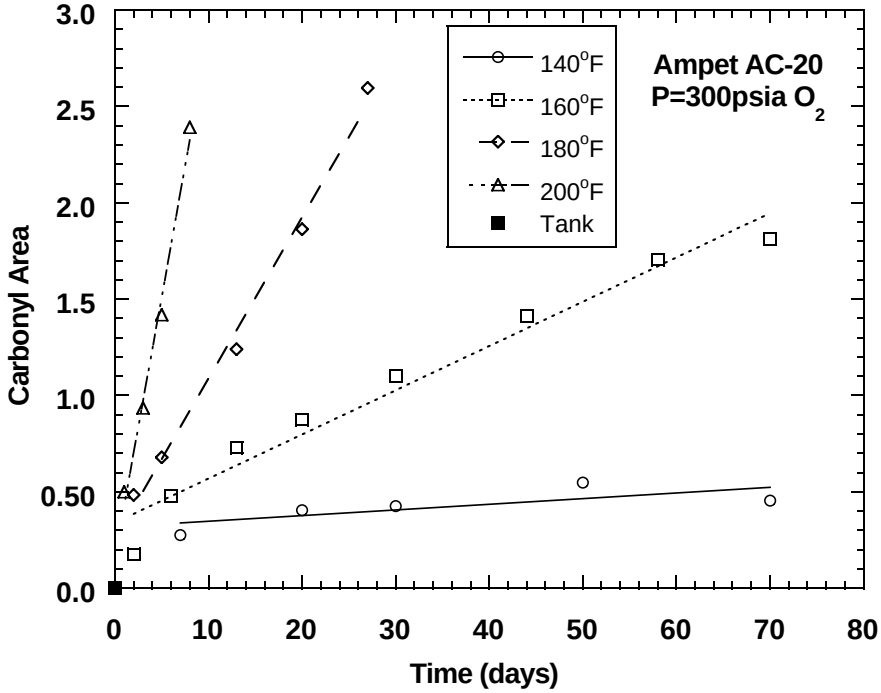

Figure 1-5. Carbonyl Area versus Aging Time.

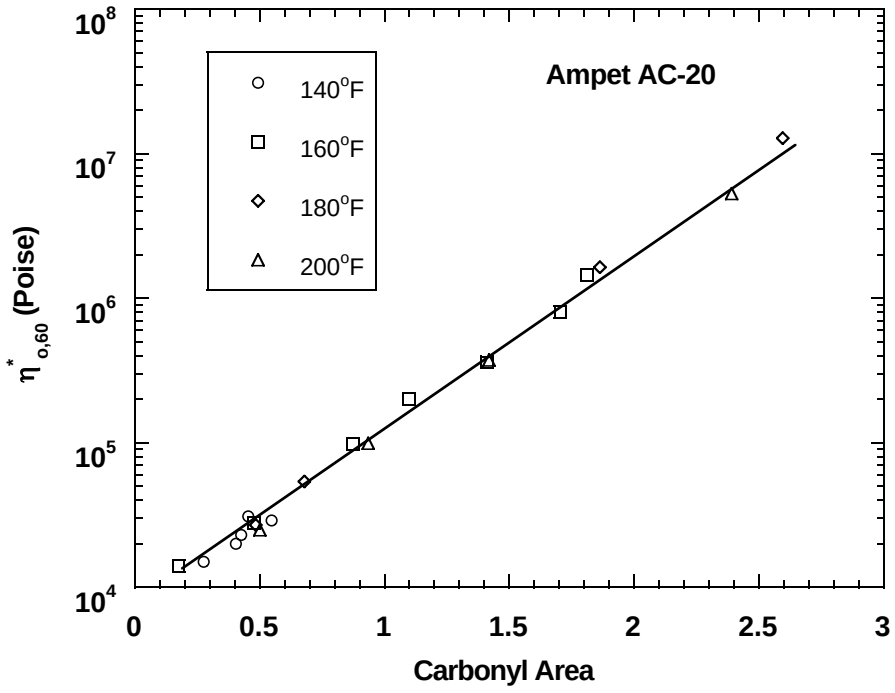

Figure 1-6. Hardening Susceptibility.

We have also done extensive studies on how to manipulate asphalt composition to affect the HS. Though as equation 1-1 shows, it is only part of the picture. It is usually the most variable term, and we also know generally how those changes affect the oxidation rate (Liu et al., 1997a; Liu et al., 1997b; Jemison et al., 1995; Stegeman et al., 1991).

The realization that asphalt hardening rate is of paramount importance is indicated by the large number of attempts to simulate road aging with short term tests. The thin film oven test (TFOT) and the rolling thin film oven test are reasonably accurate at simulating the hot-mix process, at least for conventional, unmodified materials (Jemison et al., 1991). The two tests produce almost identical results and simulate changes in viscosity as accurately as could be expected. The literature of the development and use of these tests were extensively reviewed in Davison et al. (1989). There are some differences in chemical properties between the oven tests and hot mix operation as indicated by gel permeation chromatography (GPC) and carbonyl formation, but overall, these oven tests are as good at simulating the hot mix operations as could be expected and need not be changed.

On the other hand, attempts to relate the results of these tests to road aging have generally been unsatisfactory. Many attempts have been made to alter these tests to better simulate road aging. Welborn (1984) lists 18 of these. Frequently it is stated that one of these tests is equal to so many years on the road. For instance, Huang et al. (1996) stated that the RTFOT at 185 °C can simulate one year of aging and that 168 hours in the California tilt oven is equivalent to eight years on the road. They also claim that high temperature aging is satisfactory because when, for a single asphalt, penetration is plotted versus log viscosity of oven aged, PAV aged and road aged materials, they more or less fall on the same curve. This is naive not only because asphalts differ but because the effect of voids often overwhelms other factors affecting road life (Davison et al., 1989).

The Superpave specified PAV is based on earlier work on pressure oxidation (Lee, 1968; Lee and Huang, 1973) even though Jamieson and Hattingh (1970) reports pressure oxidation at 65 °C and 300 psi oxygen did not agree with road performance. Since asphalt oxidation rates increase with pressure, it shortens the time for the test. The problem is that asphalt oxidation is not simple. The second term in equation 1 is represented by (Liu et al., 1996)

$$\frac{dCA}{dt} = AP^{\alpha}EXP\left(-\frac{E}{RT}\right) \qquad (1\text{-}2)$$

where P is pressure, T absolute temperature, and A, α and E are constants that are characteristic of each asphalt. Later we discovered that both E and HS were functions of pressure, (Figures 1-7 and 1-8) as well as the initial jump shown in Figure 1-5. This means that it is quite probable that relative hardening rates measured in the PAV will differ from those experienced on roadways. Figure 1-9 shows relative oxidation rates experienced in the PAV versus those obtained by aging asphalt in thin films in a 60 °C environmental room.

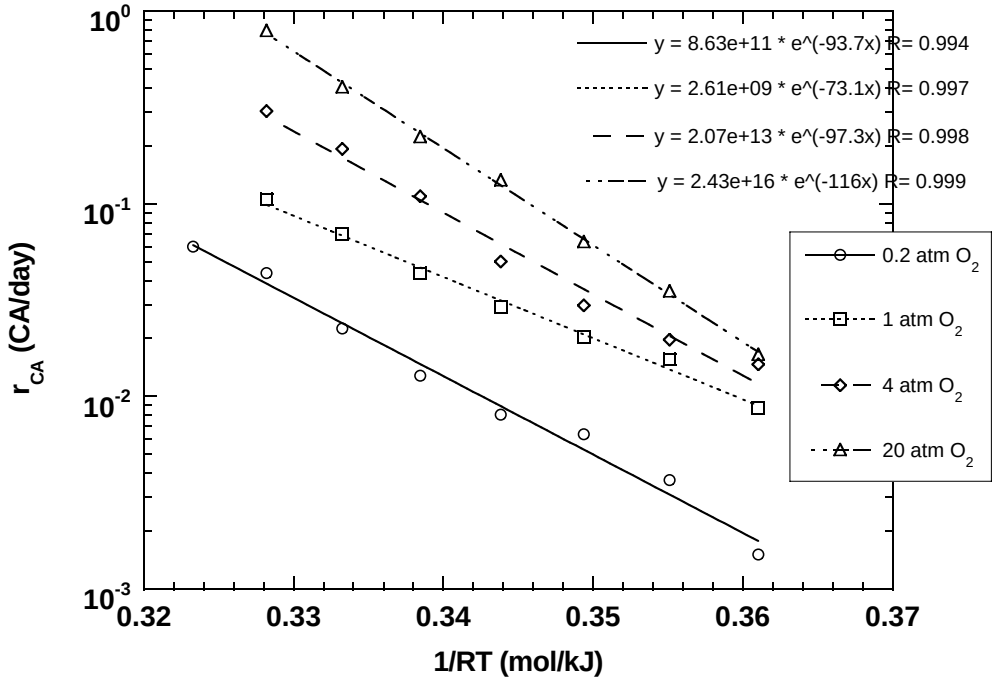

Figure 1-7. Activation Energy as a Function of Aging Pressure.

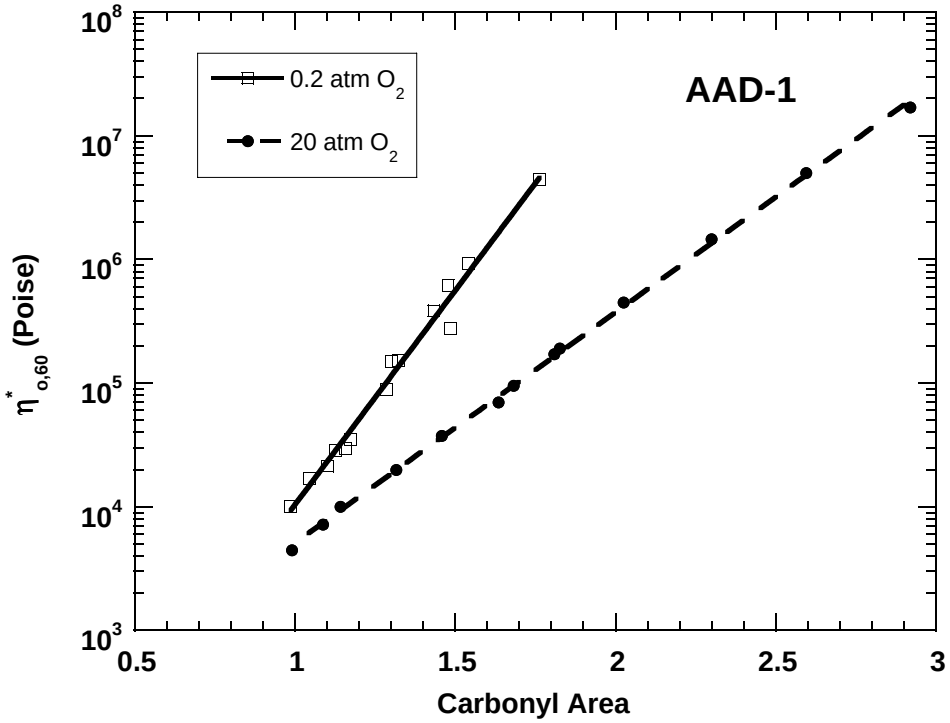

Figure 1-8. Hardening Susceptibility as a Function of Aging Pressure.

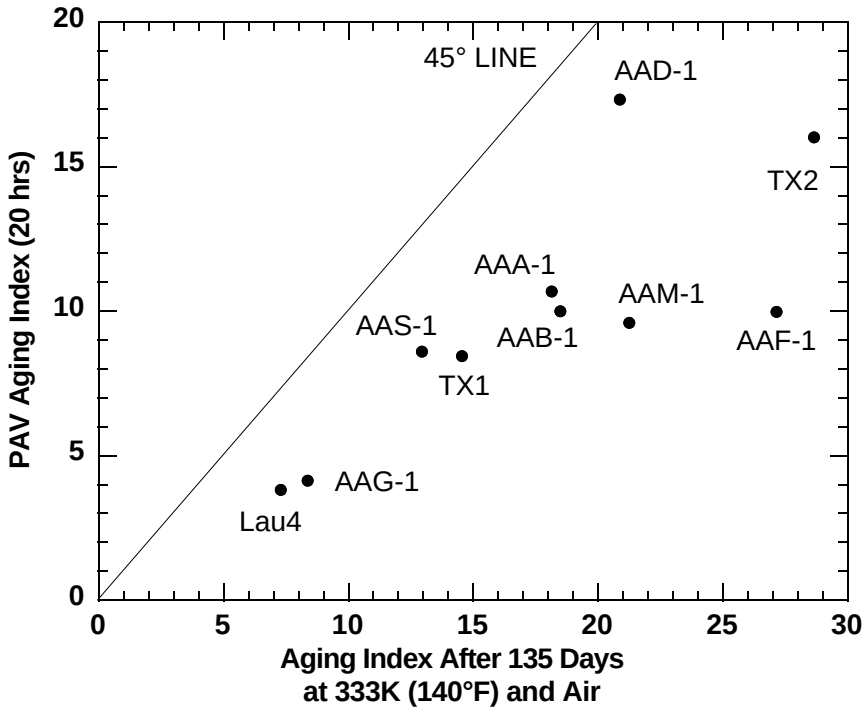

Figure 1-9. PAV Aging Index versus Environmental Room Aging Index.

While the degree of aging in the environmental room does not correspond to the 20 hours in the PAV, very large variations are still apparent. For instance, there are six asphalts that aged almost the same in the PAV, while aging in the 60 °C room varies over twofold. Similarly, AAD-1 and AAM-1 aged the same in the 60 °C room but differ nearly twofold in the PAV.

Any short-term aging test will have problems because E in equation 1-2 is asphalt dependent, but the accuracy should be improved by running at atmospheric pressure and eliminating the effect of α and the pressure dependence of E, HS, and the initial jump.

Chemistry of Asphalt Hardening

Again we will digress in order to show how asphalt composition may be manipulated to affect properties. Many attempts have been made to relate asphalt properties to chemical measurements. These attempts are reviewed in Davison et al. (1991). Generally they have not been very successful, and we have no intention of recommending a chemical specification. However, in a general sense we know how to move properties in the desired direction.

The hardening of asphalt on oxidation is almost entirely caused by the increase in asphaltene content (Lin et al., 1995a; Lin et al., 1995b). This is primarily the result of the

oxidation of polar aromatics. The presence of original asphaltenes accelerates the process. However, the asphaltenes formed by oxidation, while hardening the material, do not change the rate of hardening.

Saturates do not oxidize and they lower the viscosity and improve the low temperature grade, but in the presence of high original asphaltenes they increase the HS. Thus at high asphaltenes content, they may actually increase the viscosity (Figure 1-10).

Figure 1-11 shows the effect of recycling agent saturate content on the HS of recycling material. The top line is the result of blending agents of varying saturate content with a 85,000 poise hardened SHRP AAF-1 asphalt (Chaffin et al., 1997). The bottom line is the result of blending saturate-free agents of varying viscosity with a 55,000 poise hardened SHRP AAA-1 asphalt (Madrid, 1997). The abscissa shows the blend saturate content. The principal effect of the agents is to dilute asphaltene content and for the bottom line, saturate content also.

The Effect of Composition on Grade and Hardening

Figure 1-12 shows the result of another recycling experiment. Four hardened asphalts were mixed with four recycling agents to produce 16 blends of about 5000 poise. Three of the agents were asphaltene free and relatively low in saturates. The fourth was an AC-10 asphalt. As can be seen, there is little difference overall in the Superpave grade span: (64-22 is a ΔT of 86) but the HS is much higher when using the AC-10. The oxidation rate also probably will be higher for AC-10 blends.

One of the most interesting studies is shown in Figure 1-13 (Domke et al., 1997). In this study a vacuum tower bottom grading 64-22 was separated on a “Giant Corbett” column (Peterson et al., 1994) into asphaltenes, aromatics, and saturates. These components were reblended to form a variety of materials which were graded and aged in our reactors (Lau et al., 1992; Liu et al., 1997a) to get the HS values.

The line drawn across the top shows how one can improve the top grade as much as four levels while maintaining the bottom grade simply by adding asphaltenes to a high saturate material. Figure 1-14 shows what this does to the HS. The point in the upper right is the original vacuum tower bottom with its high HS. The point in the lower left corner shows the good HS and poor grade of the aromatic alone. Interestingly, at low asphaltenes, a little saturate actually lowers HS while improving the grade span.

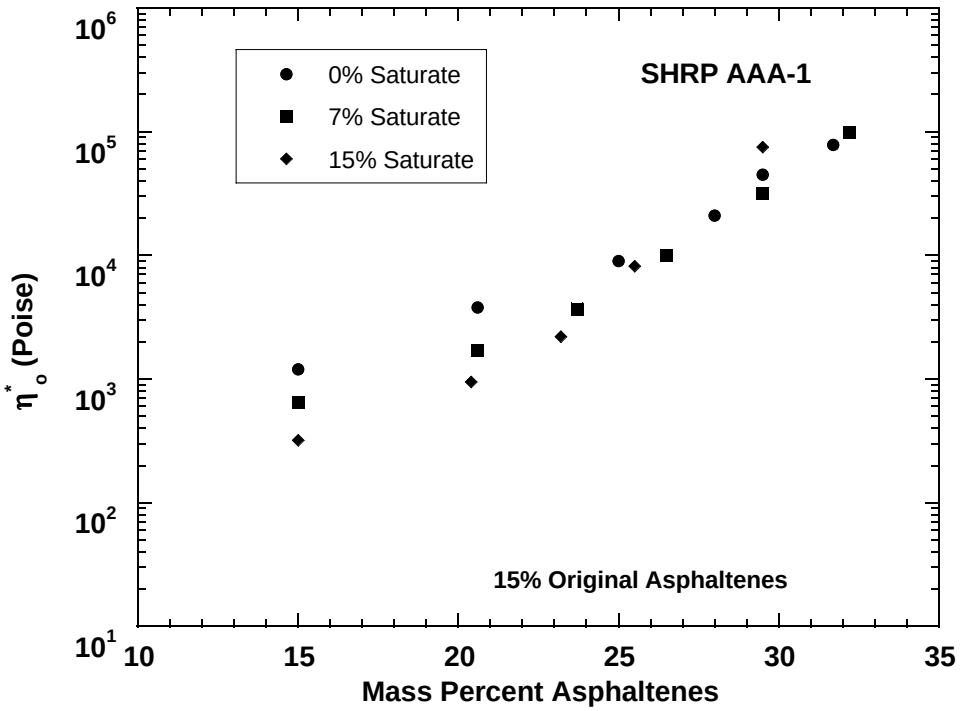

Figure 1-10. Viscosity versus Asphaltene Content at Varying Saturate Levels.

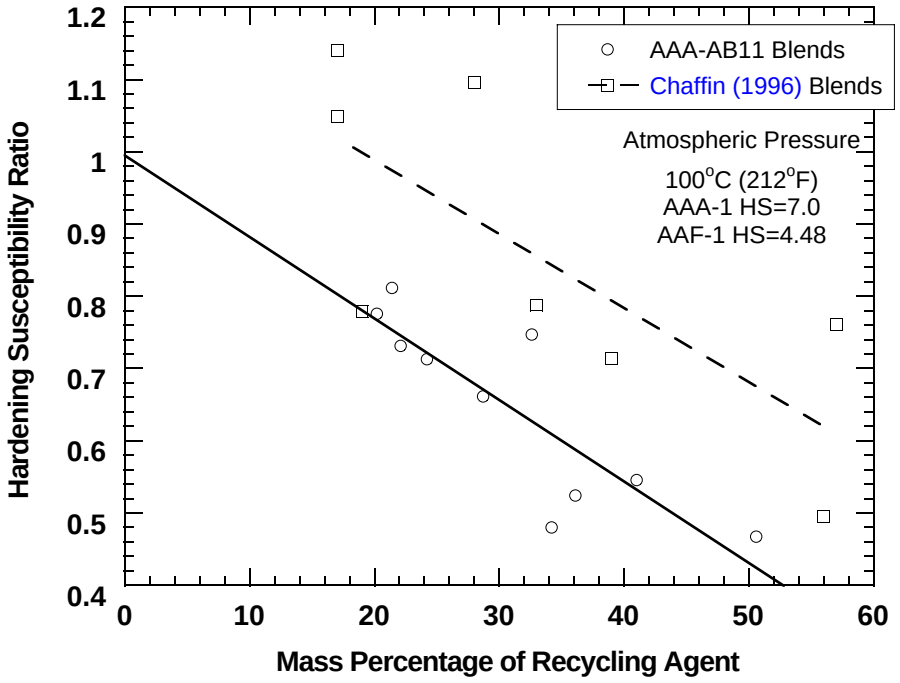

Figure 1-11. Hardening Susceptibility Ratio versus Percent of Recycling Agent.

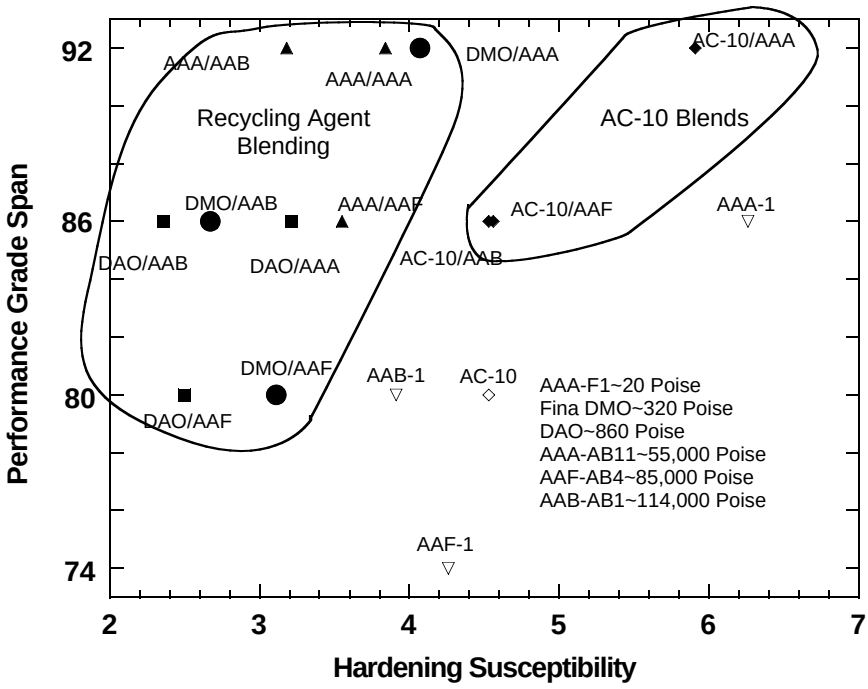

Figure 1-12. Recyling Performance Grades versus Hardening Susceptibility.

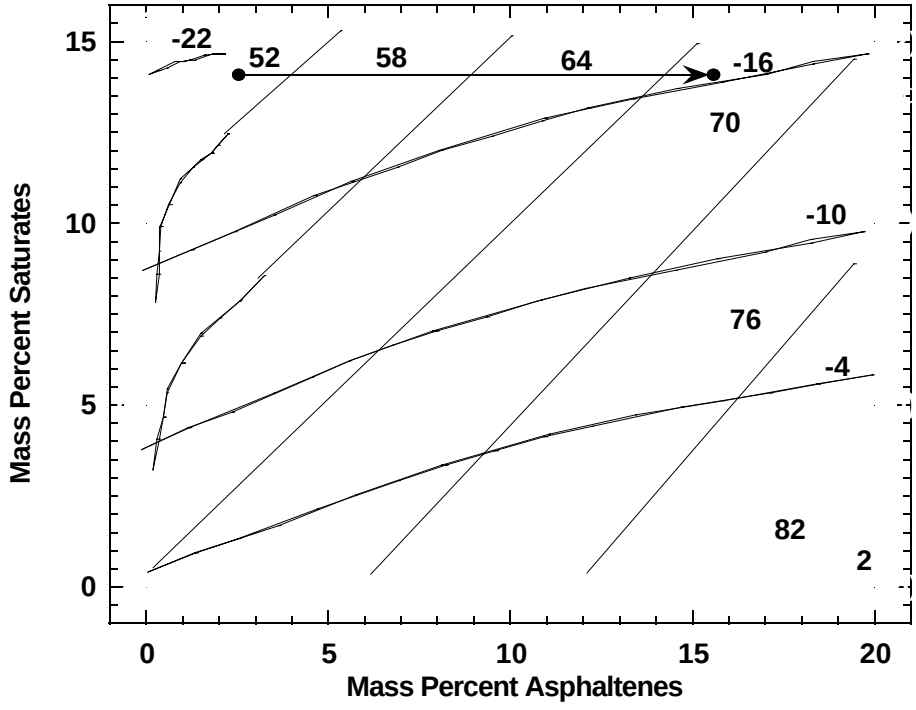

Figure 1-13. Performance Grading for VTB Aromatics Compounds.

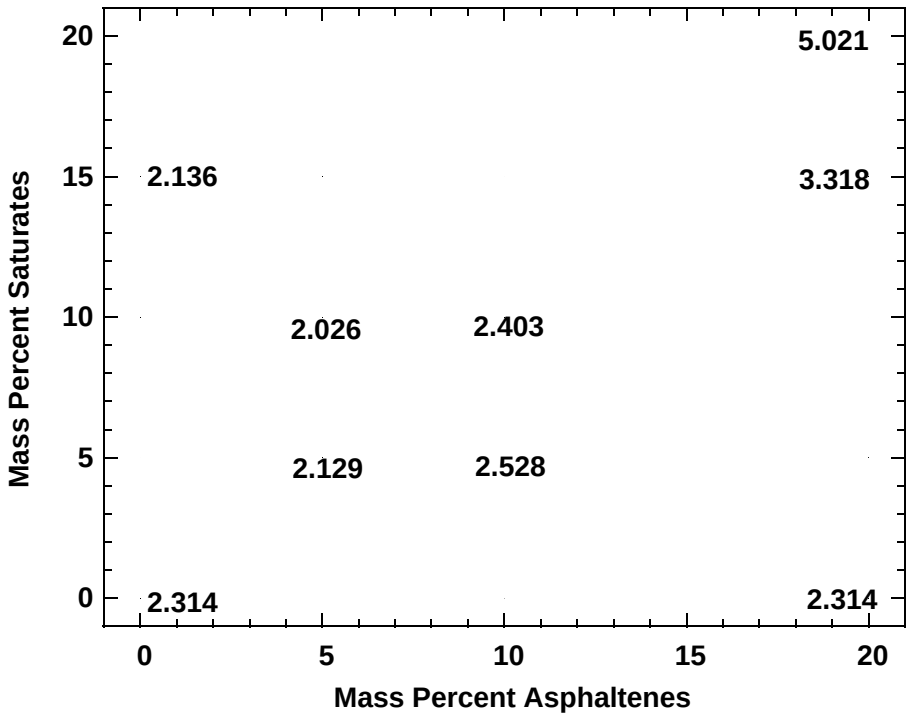

Figure 1-14. Hardening Susceptibility for VTB Aromatic Compounds.

HISTORICAL ATTEMPTS TO RELATE PROPERTIES TO PERFORMANCE

As mentioned earlier, attempts to correlate asphalt chemical properties with performance have not been very successful, but of course it is chemical composition that actually determines physical properties. However, the relationship is so complex that while we know the general effect for compositional manipulations, the magnitude of these effects are asphalt specific. For this reason one would expect changes in physical properties with aging to be better predictors of asphalt durability.

Even so, one of the most interesting and controversial proposals for specifications to reduce road aging was the suggestion by Jennings that the percent large molecular size region (LMS) as determined by GPC be used as a specification. It is controversial because LMS is primarily an indication of asphaltene formation which is the main cause of asphalt hardening but not a measure of the changes in physical properties that actually cause road failure. On the other hand, it is very easy to measure and made possible the collection of a very large body of data.

His first study was of Montana roads (Jennings et al., 1980) which was later expanded to include many parts of the country (Jennings and Pribanic, 1985). The significant findings of these studies were that in each region there was a level of LMS above which all roads were in bad condition. There were bad roadways with lower LMS, but these had likely failed for non-

binder related causes. In general, the critical LMS was higher in warmer climates, and in hotter regions some very low LMS roadways had rutted.

This work showed that, first, parameters are needed that are sensitive to aging and that have critical values that indicate failure. Then, secondly, an aging procedure is needed will indicate the rate at which individual asphalts approach these values. The work of this project was directed at meeting these needs.

The attempts to find such parameters was not new. The literature concerning these attempts is both interesting and informative. For instance, in 1937, Hubbard and Gollomb (1937) reporting on an Ohio field study stated "---that out of 9 pavements rated good or excellent all but one showed the recovered asphalt to have a penetration of 30 or higher. Out of 12 pavements rated as bad, all but two showed the recovered asphalt to have a penetration of 20 or less." In a comparison of lab and field aging of asphalts in an Iowa study, Lee (1973) suggested a critical pen of 20 and a critical viscosity of 20-30 megapoise at 25 ^{o}C.

In a study of roads in Utah, the condition of 20 controlled sections were correlated with a wide variety of effects (Anderson et al.,1976). The best correlation was the accumulated total (7 years) of 18-kip loads. Transverse cracking went up with saturate content, which is interesting considering that increasing saturates improves the low temperature Superpave grade. This is consistent, however, with the effect of saturates on hardening (Figure 1-10). Some correlation was also obtained between force ductility and transverse cracking.

Doyle (1958) reporting on the performance of Ohio test sections says, "Ductility at 25 ^{o}C shows an inconsistency as far as these two carefully observed test roads are concerned; however, ductility at 12.8 ^{o}C, 1 cm or lower does apparently correlate with results on these roads." He gave data on other roads, and one showed no cracking after 5 years for which the recovered asphalt had a ductility of 29 at 12.8 ^{o}C and 1 cm/min. Two others with considerable cracking showed ductilities of 3 and 4.

Skog (1967) aged these same asphalts and showed that the shear susceptibility versus aging time was much lower for the good road than for the two cracked roadways with low ductilities. Welborn et al. (1966) showed that there was a fairly good correlation between 60 ^{o}F ductility and shear susceptibility before and after TFOT. Kandahl and Wenger (1973) also showed a good correlation between shear susceptibility at 25 ^{o}C and 15.6 ^{o}C ductility for TFOT residues.

Kandahl and others (1975, 1977, 1984) have published a series of papers on performance of Pennsylvania test sections. Four sections were laid in 1960-61 and after 10 years all showed some cracking, while one with high voids had cracked after 5 years. All cracked between a penetration of 20-25 at viscosities ranging from about 40,000 to 70,000 poise and at ductilities between 5 and 6 cm measured at 60 ^{o}F and 5 cm/min. Of these variables only ductility gave the proper ranking in road condition after 10 years.

Six more pavements were laid in 1964, each with a different asphalt. These sections were cored periodically until 1974 or 113 months after construction. This time road condition was correlated with viscosity at 25 °C, viscosity at 60 °C, shear susceptibility at 25 °C, and ductility at 15.6 °C and 1 cm/min. Also included was the slope of low shear viscosity versus shear susceptibility. Both ductility and the viscosity-shear susceptibility slope perfectly ordered the performance rating of the six pavements.

A third set of sections were laid in 1976 and were evaluated after 6 years. Again relative rankings agreed with the ordering of ductilities measured at 60 °C and 5 cm/min. Halstead (1963) studied road conditions relative to penetration and ductility and concluded, "the amount of hardening of the asphalt during construction and in service are the primary factors affecting durability of the pavement. However, the data discussed in this report demonstrate that the accompanying decrease in ductility of the asphalt is an important secondary factor that must not be overlooked. Pavements containing asphalt with penetrations in the range normally considered satisfactory (30 to 50) but with low ductility are likely to show poorer service than those pavements containing asphalts of the same penetration but with higher ductility." In fact some of his data indicated that at very low ductility (below 6 at 25 °C) a roadway with lower penetration such as below 20 was less likely to fail than a roadway with asphalt having a penetration above 30.

Clark (1958) reported results comparing laboratory oven aging at 65.6 °C with hot-mix and road aging for 46 roadways with respect to ductility and penetration. In general, oven aging ranked the roadways correctly, but low ductility particularly was a good predictor of roadway condition and life.

A variation in the use of shear susceptibility is given by Reese and Goodrich (1993). They plotted the shear susceptibility of DSR phase angle, defined by

$$\frac{\delta_{10\,\mathrm{rad/s}} - \delta_{1\,\mathrm{rad/s}}}{\log(10\,\mathrm{rad/s}) - \log(1\,\mathrm{rad/s})} \tag{1-3}$$

versus the viscosity shear susceptibility defined by

$$\frac{\log\ \eta_{10\,\mathrm{rad/s}} - \log\ \eta_{1\,\mathrm{rad/s}}}{\log\ (10\,\mathrm{rad/s}) - \log\ (1\,\mathrm{rad/s})} \tag{1-4}$$

Note that the denominator in both relations is numerically equal to one so that actually it is a plot of the difference in phase angle versus the difference in log viscosity. A slightly off vertical plot for asphalts extracted from California desert roadways perfectly separated 10 uncracked sections

from 9 cracked sections. These results are easily obtained from the DSR and are not subject to the difficulty with ductility for which critical values may be small. Road aging simulation is still required.

SPECIFICATION FOR MODIFIED ASPHALTS

Modifiers present different problems and require different test procedures. We have considerable experience with asphalt rubber, and we can enumerate several problems with current testing procedures. The first is that the TFOT and RTFOT no longer simulate the hot-mix operation. For instance, with asphalt rubber, material from the RTFOT is of consistently higher viscosity than that from the TFOT because of the shorter time in RTFOT. The much shorter time in the hot-mix should yield material of even higher viscosity.

The relative reaction rates for rubber and asphalt are affected by temperature and diffusion of oxygen into rubber particles which makes reaction time an important factor. Since time is so short in the hot-mix operation, the difference between it and the oven tests may be large and probably more hardening will occur than in the oven tests because of the greater dependence of rubber reaction on diffusion. Unfortunately this is not easily confirmed because extraction of asphalt-rubber from a mix can have a major effect on the recovered binder properties. As the rubber oxidizes it is broken into smaller materials decreasing the viscosity. This is why many asphalt rubber materials pass $G^*/\sin\delta$ before RTFOT or TFOT but then fail after. Another problem is using an elevated temperature to simulate road aging. The problems are even greater than those already enumerated for unmodified binders. Figure 1-15 compares HS measured at different temperatures. For unmodified binder this is independent of temperature below about 100-110 ^oC. This temperature dependency of HS for rubber modified asphalts indicates that major changes in the reaction mechanism are encountered with changing temperatures. This varying HS with temperature makes it extremely difficult to simulate road aging at elevated temperatures.

UNDERLYING PRINCIPLES AND SCOPE OF PROBLEM

The purpose of this study was to recommend specifications for asphalt binders that will ensure that in meeting Superpave specifications, other important properties will not be sacrificed. At the same time these specifications will replace the inadequate $G^*\sin\delta$ criterion for fatigue cracking. This study also addresses the issue of how testing procedures and specifications need to be modified for asphalts containing additives such as polymers or ground tire rubber. This research then naturally falls into two areas: 1) development of specifications and methods for existing asphalts and for asphalts whose composition has been manipulated by blending and/or air blowing, and 2) development of testing methods and specifications for asphalts modified by additives.

In either event, the specification $G^*\sin\delta$ is inadequate to protect against age hardening and fatigue cracking. Since the parameters used to predict fatigue cracking must be sensitive to

oxidative hardening, the adequacy of the laboratory hardening procedures must be established. Since Superpave specifications that refineries must meet can only refer to the binder and it is difficult to study aged materials in mixes, this project does not directly address mix specifications or tests. However, because some compositional changes could negatively impact adhesion, cohesion and thus water susceptibility, these composition factors have been checked.

OUTLINE OF THE REPORT

The work of this project consisted of fundamental experimental studies in a number of areas. These studies were directed at developing an appropriate aging procedure, identifying an appropriate physical property parameter (preferably to be measured using the DSR) which would be indicative of binder durability in pavements, assessing the effect of the aging procedure on this durability parameter and on low-temperature properties, and assessments of water susceptibility. These issues would be addressed for both unmodified and modified binders.

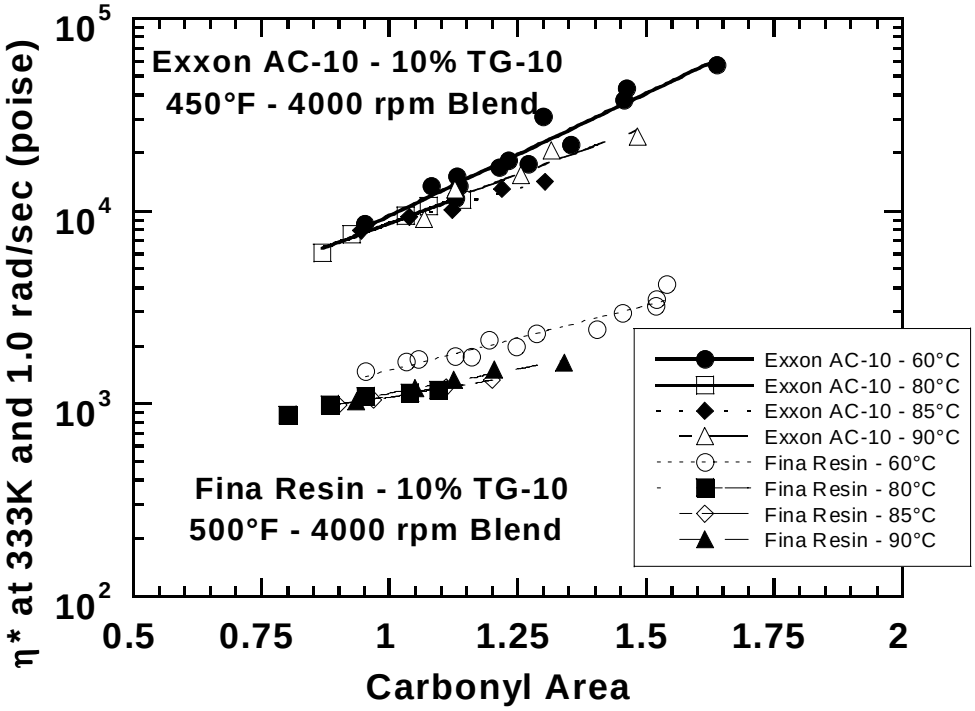

Figure 1-15. Hardening Susceptibility of Asphalt-Rubber Aged in Atmospheric Air.

Chapter 2 presents a fundamental investigation of the effect of oxidation pressure on the reaction kinetics. This information is important for devising an appropriate aging procedure for condition asphalt materials in an aging test. Chapter 3 is a study of the effect of aging on low-temperature Superpave properties and performance grades. Chapter 4 is a study of the effect of aging on asphalt durability, as measured by ductility and a newly developed surrogate DSR function. Chapter 5 presents data on the effect of modifiers on physical, chemical, and aging properties of asphalts. Chapter 6 compares various accelerated aging methods in their ability to rank asphalts in agreement with 60 °C environmental room aging. Chapter 7 is a detailed study of the hardening rates and hardening susceptibilities from the perspective of the DSR function. Chapter 8 provides results on adhesion and water susceptibility, as measured by the Texas DOT test, Tex 531-C. Chapter 9 presents significant field results using binders recovered in multiple years from SH 21 and from 16 long-term pavement performance (LTPP) sites in Texas. Chapter 10, based on the work of all the previous chapters, presents a recommended test protocol for unmodified asphalts and recommendations for modified materials. Finally, Chapter 11 provides an executive summary, including conclusions and recommendations.

CHAPTER 2. EFFECT OF OXYGEN PRESSURE ON ASPHALT OXIDATION KINETICS

(Pages 2-1 through 2-18 reprinted, with permission, from C. H. Domke, R. R. Davison, and C. J. Glover, "Effect of Oxygen Pressure on Asphalt Oxidation Kinetics," *Ind. Eng. Chem. Res.*, Volume 39, 2000, pp. 592-598.)

ABSTRACT

The oxidation of asphalt is a major cause of pavement failure. At a given temperature and pressure, the asphalt oxidizes in two stages: (1) a rapid-rate period followed by (2) a long period with constant oxidation rate. The degree of oxidation that occurs in the constant oxidation region is asphalt dependent and varies with oxygen pressure and with temperature. Using pavement-temperature oxidation kinetics obtained for eight asphalts in this study, it has been determined that the activation energies for the constant-rate region are dependent on the oxygen pressure and can be related to the asphaltene composition of the asphalt. An oxidation kinetic model is developed to predict the rate of oxidation in the constant rate region knowing an initial asphaltene composition variable for the asphalt.

INTRODUCTION

Millions of dollars are spent every year to build and maintain roads. A large percentage of these roads are built with asphalt. Over the lifetime of the road, an asphalt binder oxidizes and subsequently hardens eventually causing failure of the road.

Several authors have shown that carbonyl formation is a major product of oxidation (Lee and Huang, 1973; Martin et al., 1990; Lau et al., 1992; Peterson et al., 1993). The formation of carbonyl-containing compounds varies between asphalts, but for each asphalt the carbonyl content, CA, can be used as a surrogate for total oxidative changes (Liu et al., 1998b). This is because the carbonyl growth varies linearly with total oxygen increase even though the slopes vary somewhat for different asphalts.

Many accelerated aging tests have been devised to simulate the aging that occurs on the roads. Most of these tests use elevated temperatures and oxygen pressures to accelerate the aging process. However, studies have indicated that elevated temperatures and pressures may not adequately simulate the road aging conditions (Domke et al., 1999).

It would be ideal to save time and effort to produce a model that would allow for a prediction of the oxidation rate of an asphalt at a given temperature and pressure. There have been few attempts to describe the oxidation kinetics of an asphalt (Peterson et al., 1993; Liu et al., 1996). Liu et al. (1996) had described the carbonyl formation rate as a function of the temperature and pressure in an Arrhenius form:

$$r_{CA} = AP^{\alpha} \exp\left(\frac{-E}{RT}\right) \qquad (2\text{-}1)$$

For the 10 asphalts Liu et al. (1996) studied A, E, and α were calculated by determining the rates at atmospheric air (0.2 atm O_2) and 20 atm O_2 and various temperatures and fitting equation 2-1 to the data. In this study, rates have been determined for eight asphalts using the same range of temperatures, but additional oxygen pressures have been included, and additional rates were measured at the previously used conditions.

EXPERIMENTAL METHODS

Eight asphalts were used in this study: seven SHRP asphalts (AAA-1, AAB-1, AAD-1, AAF-1, AAG-1, AAM-1, and AAS-1) and one Texas asphalt, Lau4 (Lau et al., 1992). Each of these asphalts was weighed into several 4 cm x 7 cm aluminum trays using approximately 2.4 grams of material. This yielded a uniform thickness of less than 1 mm. Thin films were used to minimize the effects of diffusion (Domke et al., 1997).

The asphalts were placed in our pressure oxygen vessels (POV) (Lau et al., 1992). The POV is immersed in a triethylene glycol bath used for temperature control. Each POV holds approximately 60-70 sample trays. For each asphalt a tray was removed periodically depending on the temperature and pressure of the POV. The temperatures varied from 60 °C to 98.9 °C (140 °F>210 °F), and the oxygen pressures varied from atmospheric air (0.2 atm O_2) to 20 atm O_2.

Each sample was analyzed using a Mattson Galaxy 5000 FT-IR and the attenuated total reflectance (ATR) method described by Jemison et al. (1992). The carbonyl area was determined by finding the area under the absorbance peaks from 1650-1820 cm^{-1}. The CA was used to monitor the progress of the asphalt oxidation.

Heptane asphaltene (C7) content from Lau4 was determined by dissolving 7 grams of asphalt in 200 mL of n-heptane. After heating and stirring the sample for one hour, the solution was allowed to settle overnight. A Whatman #2 quantitative filter was used for the vacuum filtration procedure to determine the mass of the asphaltenes. The asphaltene content of the SHRP asphalts was taken from the SHRP Material Reference Library (1993).

Pentane asphaltene content for each of the eight asphalts was determined by dissolving 0.2 grams of asphalt in 20 mL of n-pentane. The samples were sonicated for 20 minutes and allowed to settle overnight. A Whatman #2 quantitative filter was used for the vacuum filtration procedure to determine the mass of the asphaltenes.

RESULTS

Reaction Rate

Lau et al. (1992) determined that the rate of carbonyl formation became constant after an initial, higher rate period. Figure 2-1 shows how pressure affects the constant oxidation rate of AAG-1 at 200 °F. The regression line determines the initial jump of the asphalt (CA_o) and the aging rate (r_{CA}) given by:

$$CA = CA_o - r_{CA} t \tag{2-2}$$

where t is the aging time.

Figure 2-1 shows that r_{CA} increases with increasing pressure while keeping the temperature constant. The rates also increase with increasing temperature when keeping the pressure constant (Figure 2-2), a fact that is true of all eight asphalts studied (Table 2-1).

From Figures 2-1 and 2-2 it is also observed that the initial jump may be pressure dependent but, with considerable scatter, probably is temperature independent. This fact was also observed by Liu et al. (1996). Table 2-2 shows CA_o for all eight asphalts, and shows that within the scatter, that CA_o may be pressure dependent depending on the asphalt. This phenomenon will be discussed later.

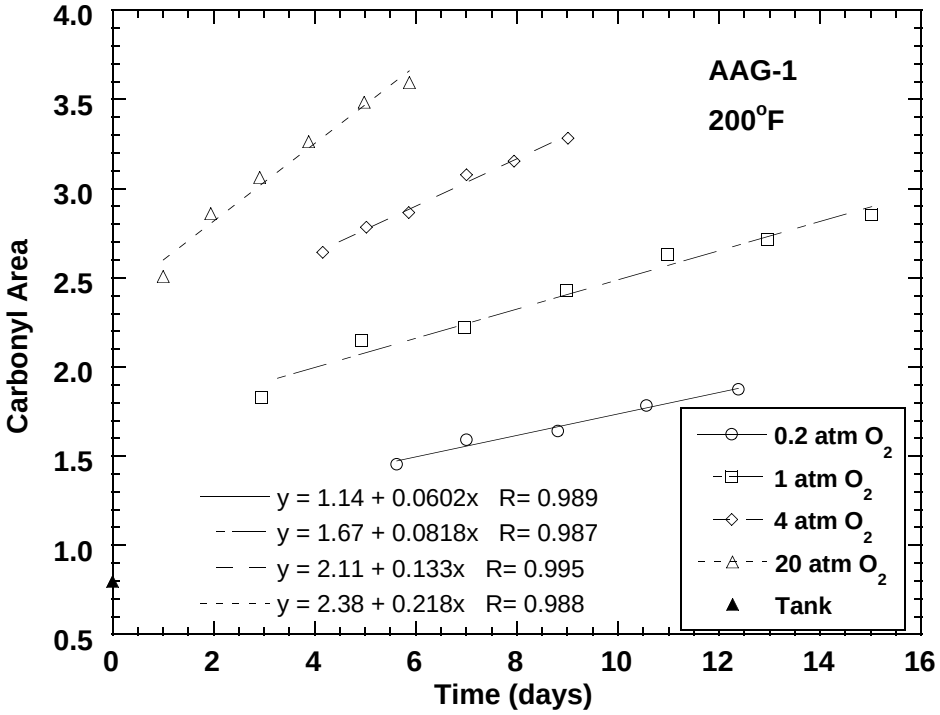

Figure 2-1. How Oxygen Pressure Affects Oxidation Rate of AAG-1.

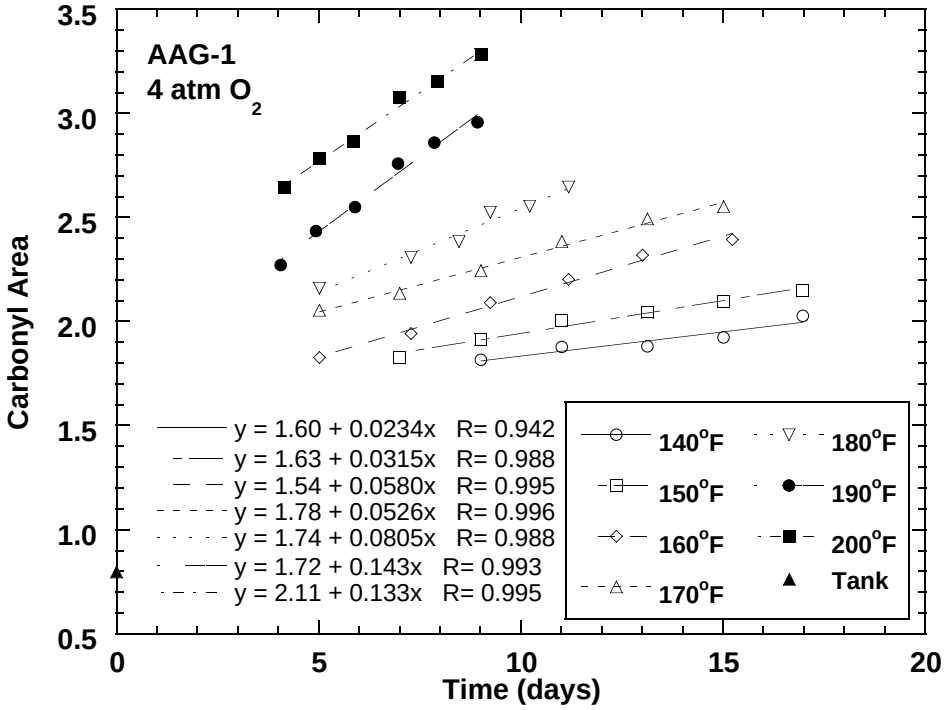

Figure 2-2. How Temperature Affects Oxidation Rate of AAG-1.

Table 2-1. Carbonyl Formation Rates x 10^3.

0.2 atm O_2

°F	AAA-1			AAB-1			AAD-1			AAF-1		
140	2.0	±	0.4	2.4	±	0.1	1.5	±	0.8	2.6	±	0.6
150	3.8	±		4.3	±		3.7	±	0.5	5.5	±	
160	6.9	±		8.1	±		6.4	±	0.8	7.2	±	
170	10.7	±	1.6	12.2	±	0.7	8.0	±	1.8	10.1	±	1.3
180	11.9	±	1.9	15.7	±	2.0	12.8	±	2.3	12.3	±	1.3
180	11.4	±	5.1	14.9	±	2.4	11.4	±	6.9	12.6	±	6.4
190	19.8	±	11.4				22.6	±	5.3	31.8	±	8.4
190	21.8			27.4			21.0			31.1		
200	44.9	±	13.5	55.5	±	15.6	42.3	±	16.2	41.7	±	36.0
210	58.7	±	7.8	80.4	±	5.6	60.0	±	8.1	65.0	±	6.5

°F	AAG-1			AAM-1			AAS-1			Lau4		
140	4.1	±	0.7	2.2	±	0.4	1.9	±	0.3	2.0	±	0.3
150	6.4	±		4.5	±		4.5	±		4.8	±	
160	10.2	±		6.4	±		6.5	±		6.7	±	
170	11.9	±	3.1	8.5	±	1.7	9.4	±	1.0	10.9	±	1.6
180	16.3	±	3.6	9.7	±	2.0	14.0	±	3.3	14.4	±	4.5
180	24.3	±	4.7	13.1	±	6.4	11.4	±	5.5	15.2	±	5.5
190	41.4	±	7.9	22.3	±	4.7						
190	42.4			33.2			23.5			26.1		
200	60.2	±	16.7	39.1	±	18.5	42.1	±	9.4	56.7	±	6.9
210	87.5	±	15.3	56.3	±	8.2	64.6	±	6.9	83.0	±	5.4

Table 2-1. Carbonyl Formation Rates x 10^3 (continued).

1 atm O_2

°F	AAA-1	AAB-1	AAD-1	AAF-1
140	6.7 ± 2.1	8.1 ± 2.2	9.4 ± 3.6	9.3 ± 3.2
150	15.3 ± 3.9	16.3 ± 3.4	15.1 ± 4.1	20.5 ± 1.8
160	18.5 ± 4.3	21.3 ± 2.8	20.3 ± 3.4	23.8 ± 3.6
170	24.6 ± 2.2	24.9 ± 4.4	25.0 ± 5.8	31.6 ± 5.0
180	34.1 ± 3.3	37.2 ± 2.8	33.7 ± 8.1	37.4 ± 7.0
190	58.6 ± 13.7	78.6 ± 5.3	70.3 ± 4.9	66.2 ± 13.1
200	89.5 ± 13.9	110.2 ± 9.5	107.6 ± 14.4	145.5 ± 25.8

°F	AAG-1	AAM-1	AAS-1	Lau4
140	24.5 ± 6.9	13.5 ± 3.6	6.6 ± 2.0	11.0 ± 1.5
150	25.9 ± 6.1	23.0 ± 4.3	14.5 ± 8.8	18.7 ± 4.1
160	30.8 ± 5.0	24.4 ± 4.2	14.7 ± 4.3	23.3 ± 3.3
170	38.6 ± 5.5	24.6 ± 3.6	22.7 ± 2.8	28.1 ± 2.1
180	42.4 ± 3.8	33.9 ± 5.3	28.8 ± 8.8	39.8 ± 9.1
190	67.3 ± 7.3	41.9 ± 9.4	67.5 ± 2.5	71.8 ± 5.8
200	81.8 ± 15.3	64.0 ± 11.1	92.3 ± 10.4	121.5 ± 19.1

4 atm O_2

°F	AAA-1	AAB-1	AAD-1	AAF-1
140	11.7 ±	13.4 ±	11.1 ±	16.1 ±
150	16.2 ± 3.0	16.6 ± 6.4	20.0 ± 4.4	26.8 ± 3.7
160	31.2 ± 5.8	25.3 ± 4.9	24.6 ± 4.3	30.7 ± 5.0
170	48.2 ± 6.1	44.4 ± 10.1	45.8 ± 4.5	39.4 ± 8.8
180	97.0 ± 19.1	110.3 ± 13.4	136.8 ± 19.9	118.3 ± 20.3
190	144.8 ± 31.5	190.9 ± 44.4	192.8 ± 18.9	156.3 ± 6.0
200	182.1 ± 38.0	295.0 ± 48.3	289.6 ± 42.2	241.7 ± 30.9

°F	AAG-1	AAM-1	AAS-1	Lau4
140	23.4 ±	18.2 ±	13.8 ±	13.7 ±
150	31.5 ± 6.8	23.0 ± 5.9	17.6 ± 2.5	18.6 ± 4.8
160	58.0 ± 8.0	25.5 ± 20.4	22.2 ± 4.6	28.6 ± 7.7
170	52.6 ± 7.0	33.9 ± 4.1	35.5 ± 2.9	43.4 ±
180	80.5 ± 17.3	59.9 ± 5.8	96.7 ±	103.3 ± 14.0
190	143.4 ± 23.4	78.7 ± 20.3	141.0 ± 19.8	153.8 ±
200	132.5 ± 18.3	109.1 ± 20.2	210.9 ± 29.4	284.5 ± 24.7

20 atm O_2

°F	AAA-1	AAB-1	AAD-1	AAF-1
140	16.2 ± 0.9	10.6 ± 0.8	16.5 ± 0.7	12.2 ± 1.8
150	29.7 ± 7.8	24.8 ± 9.0	32.9 ± 8.9	35.0 ± 11.0
160	60.4 ± 9.5	36.6 ± 5.8	63.0 ± 8.4	43.4 ± 5.4
170	121.7 ± 11.9	78.3 ± 18.1	133.2 ± 19.1	63.9 ± 6.1
180	179.5 ± 25.7	132.5 ± 11.6	223.5 ± 37.5	86.3 ± 8.0
190	349.8 ± 27.2	222.1 ± 7.6	403.9 ± 86.6	164.4 ± 16.5
200	425.7 ± 70.5	593.5 ± 75.7	726.4 ± 140.5	415.5 ± 81.5

Table 2-1. Carbonyl Formation Rates x 10^3 (continued).

°F	AAG-1			AAM-1			AAS-1			Lau4		
140	18.1	±	2.8	10.7	±	2.7	10.3	±	1.9	13.1	±	1.1
150	39.2	±	17.1	30.3	±	22.8	25.8	±	11.4	30.5	±	14.5
160	50.9	±	10.9	36.0	±	4.8	34.6	±	3.7	38.5	±	4.4
170	74.7	±	12.6	52.3	±	8.0	73.0	±	23.3	82.5	±	9.0
180	102.0	±	23.3	65.4	±	13.8	105.3	±	12.3	125.0	±	21.0
190	163.3	±	10.9	112.0	±	13.1	197.7	±	16.2	149.3	±	14.8
200	217.9	±	47.3	239.5	±	46.9	496.1	±	99.5	491.6	±	59.3

Table 2-2. CA_0 for All Asphalts.

Pressure (atm O_2)	AAA-1	AAB-1	AAD-1	AAF-1	AAG-1	AAM-1	AAS-1	Lau4
0.2	0.215	0.177	0.201	0.280	0.475	0.297	0.153	0.247
	±0.085	±0.043	±0.092	±0.069	±0.157	±0.072	±0.040	±0.029
1	0.185	0.206	0.157	0.221	0.605	0.299	0.140	0.149
	±0.086	±0.097	±0.071	±0.092	±0.172	±0.133	±0.060	±0.062
4	0.305	0.291	0.216	0.372	0.934	0.487	0.193	0.289
	±0.149	±0.064	±0.140	±0.120	±0.190	±0.145	±0.063	±0.054
20	0.254	0.374	0.194	0.580	1.490	0.669	0.128	0.093
	±0.272	±0.075	±0.141	±0.119	±0.159	±0.072	±0.054	±0.083

The oxidation rate of an asphalt can be estimated by determining a kinetic rate equation. Assuming classical kinetics, the carbonyl rate (r_{CA}) is given by equation 2-1 where A is the frequency (preexponential) factor, P is the oxygen pressure, α is the reaction order with respect to oxygen pressure, E is the activation energy, R is the universal gas constant, and T is the temperature. To find E, A, and α graphically one must plot ln r_{CA} vs 1/RT and find the slope (E) and intercept (AP^{α}) of the line. Figure 2-3 shows an example of this plot. Both E and AP^{α} vary with respect to oxygen pressure. As oxygen pressure is increased from 0.2 to 20 atm O_2, AP^{α} and E go through a minimum near 1 atm O_2. This occurs for all eight asphalts studied.

Equation 2-1 can be linearized by taking the natural logarithm of both sides

$$\ln(r_{CA}) = \ln A + \alpha \ln P - E/RT \qquad (2\text{-}3)$$

Equation 2-3 could be used to determine A, E, and α if they were independent of pressure. However, Domke et al. (1999) explain how pressure can affect the properties of an asphalt upon oxidation with a layered particle model. Figure 2-4 is taken from their work. They explain that as oxygen pressure is changed, the different diffusional fluxes of oxygen cause oxidation to occur at different layers (Figure 2-4a) of the "particle." At low pressures the oxygen would react primarily with the maltene phase of the asphalt (Figure 2-4b). As oxygen pressure is increased, the

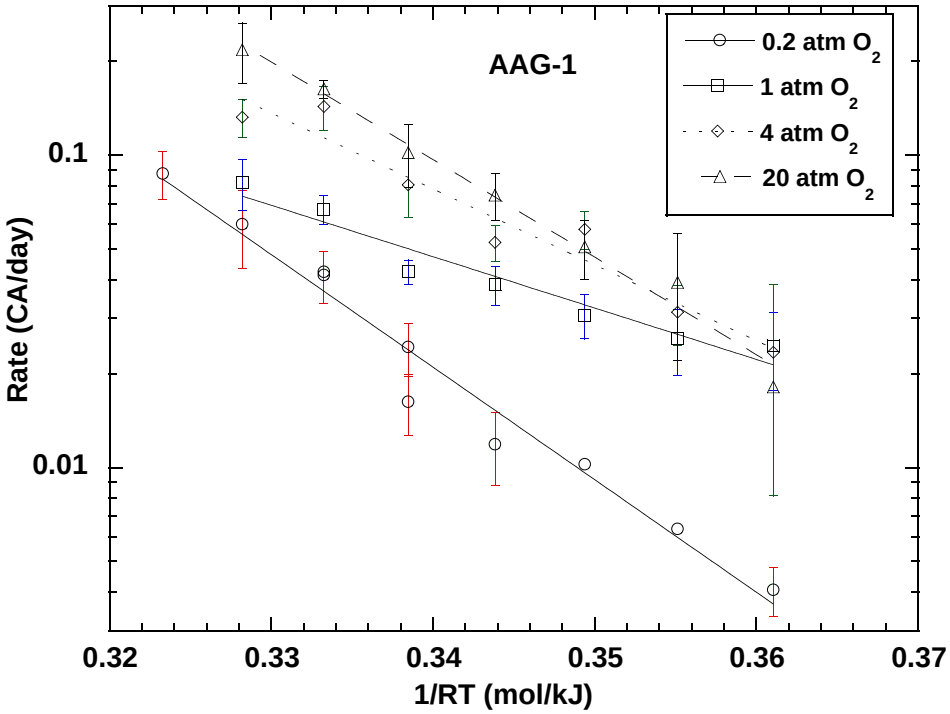

Figure 2-3. How Temperature and Pressure Affect the Oxidation Rate of AAG-1.

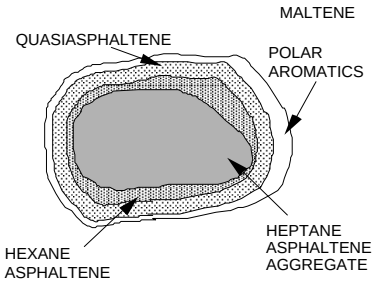

Figure 2-4a

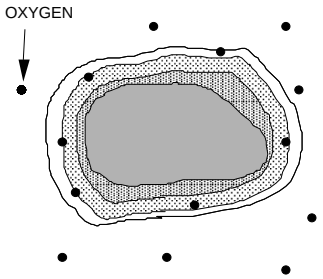

Figure 2-4b

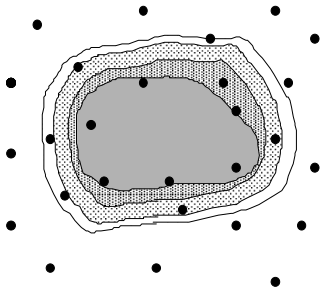

Figure 2-4c

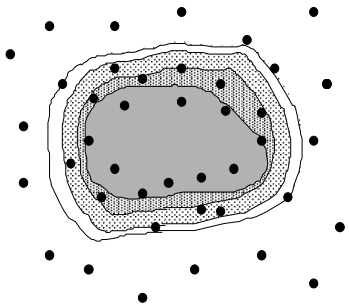

Figure 2-4d

Figure 2-4. Hypothesized Particle Model of Asphalt (Reproduced with Permission from Domke et al., 1999).

increased oxygen flux would allow for oxidation to occur with the "quasiasphaltenes" (Figure 2-4c), the hexane asphaltenes, and finally the heptane asphaltenes (Figure 2-4d). This molecular diffusion concept complicates the use of equation 2-3.

Liu et al. (1998c) showed that naphthene aromatics and polar aromatics displayed different rate constants A, E, and α. Because different molecules are reacting at different oxygen pressures, one cannot assume that the observed A, E, and α are independent of pressure. This pressure dependency causes difficulty in estimating the rate constants individually. E can be determined for each oxidation pressure; however, A and α are linked together in equation 2-1. Rather than estimating A and α separately, they were combined into one variable thus modifying equation 2-1 to:

$$r_{CA} = A' \exp\left(\frac{-E}{RT}\right) \tag{2-4}$$

where

$$A' = AP^{\alpha} \tag{2-5}$$

By combining the pressure dependent constants of A and α into one pressure dependent variable, A´, the oxidation kinetic model is simplified without damaging its integrity. Tables 2-3 and 2-4 show the values of E and ln A , respectively, for the eight asphalts at the four different oxygen pressures. It can be seen that both E and A´ go through a minimum value at 1 atm O_2. This minimum is likely tied to the layered particle model by Domke et al. (1999) and the difference in the kinetic parameters observed by Liu et al.(1998c). This is also supported by Liu et al. (1997) who determined kinetic parameters for seven fractions separated from asphalt AAF-1 by supercritical extraction. The parameters of Equation 2-3 were fitted to the data and a minimum occurred in the pressure dependency parameter, α, at fraction 4. We can speculate that the average composition reacting at 1 atm has a lower activation energy than the average material reacting at both lower and higher pressures.

Table 2-3. Activation Energy for All Asphalts at Various Pressures.

Pressure (atm O_2)	AAA-1	AAB-1	AAD-1	AAF-1	AAG-1	AAM-1	AAS-1	Lau4
0.2	85.6	90.2	92.3	82.9	83.1	84.8	88.2	86.4
	±12.7	±10.6	±11.8	±16.5	±13.4	±16.1	±13.2	±11.5
1	72.4	75.0	70.9	71.9	37.9	40.4	76.0	67.8
	±13.8	±16.7	±15.7	±21.9	±11.0	±13.5	±19.5	±15.7
4	89.9	102	105	84.7	56.0	56.4	89.8	95.0
	±13.0	±22.1	±22.5	±23.4	±15.5	±14.0	±22.1	±20.5
20	104	116	115 ±5.2	93.7	72.0	81.9	110	96.6
	±12.0	±16.3		±27.7	±15.8	±31.1	±22.2	±26.7

Table 2-4. ln (Pre-exponential Factor) for All Asphalts at Various Pressures.

Pressure (atm O_2)	AAA-1	AAB-1	AAD-1	AAF-1	AAG-1	AAM-1	AAS-1	Lau4
0.2	24.7	26.6	27.0	24.0	24.4	24.5	25.7	25.3
	±4.3	±3.6	±4.0	±5.6	±4.6	±5.5	±4.5	±3.9
1	21.3	22.3	20.9	21.4	9.8 ±3.8	10.3	22.5	19.9
	±4.8	±5.7	±5.4	±7.5		±4.7	±6.7	±5.4
4	27.9	32.1	33.1	26.3	16.5	16.2	27.9	29.8
	±4.5	±7.6	±7.8	±8.1	±5.3	±4.8	±7.6	±7.1
20	33.3	37.2	37.5	29.6	22.7	25.2	35.0	30.5
	±4.1	±5.6	±1.8	±9.5	±5.5	±10.7	±7.7	±9.2

Isokinetic Rate

An isokinetic temperature has been determined for other petroleum reactions (Liu et al., 1996; Boudart, 1991). At this temperature, all compounds in a homologous series have the same reaction rate. In order to determine the isokinetic temperature A´ vs E, data, are plotted and fit by an exponential model. The slope of the line is 1/RT, and thus the isokinetic temperature is determined. The isokinetic rate at this temperature would be the intercept of the curve-fit.

Figure 2-5 shows the A´ vs E for all oxidation pressures studied. It is interesting to see that for oxidation pressures above atmospheric pressure the data overlay extremely well. From the curve-fits in Figure 2-5 we can determine that the isokinetic temperature for atmospheric air (0.2 atm O_2) is 105 °C (221 °F) with a rate of 0.0975 CA/day. For pressures of 1 atm O_2 and higher the isokinetic temperature is calculated to be 65.7 °C (150 °F) with a rate of 0.0189 CA/day. Figures 2-6 through 2-8 show how well these calculations approximate the data. We can see that the calculated isokinetic rates appear to fall in the middle of the experimental rate data near the isokinetic temperature. We can also see that near the calculated isokinetic temperature, the oxidation rates of the asphalts are fairly close together indicating that there is a convergence in the oxidation rates, but error is also associated with the measurements.

Figures 2-6 through 2-8 also show that as oxidation rates are measured at temperatures increasingly distant from the isokinetic temperature, a larger disparity in the rates occurs. This is

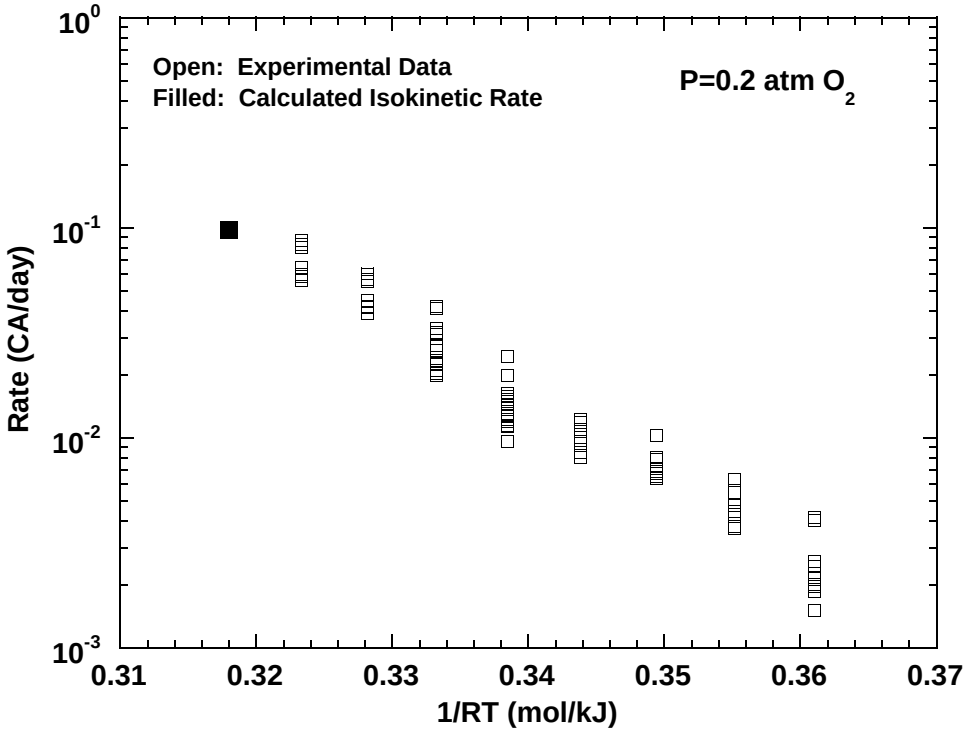

Figure 2-5. Relationship Between A' and E for Isokinetic Temperature.

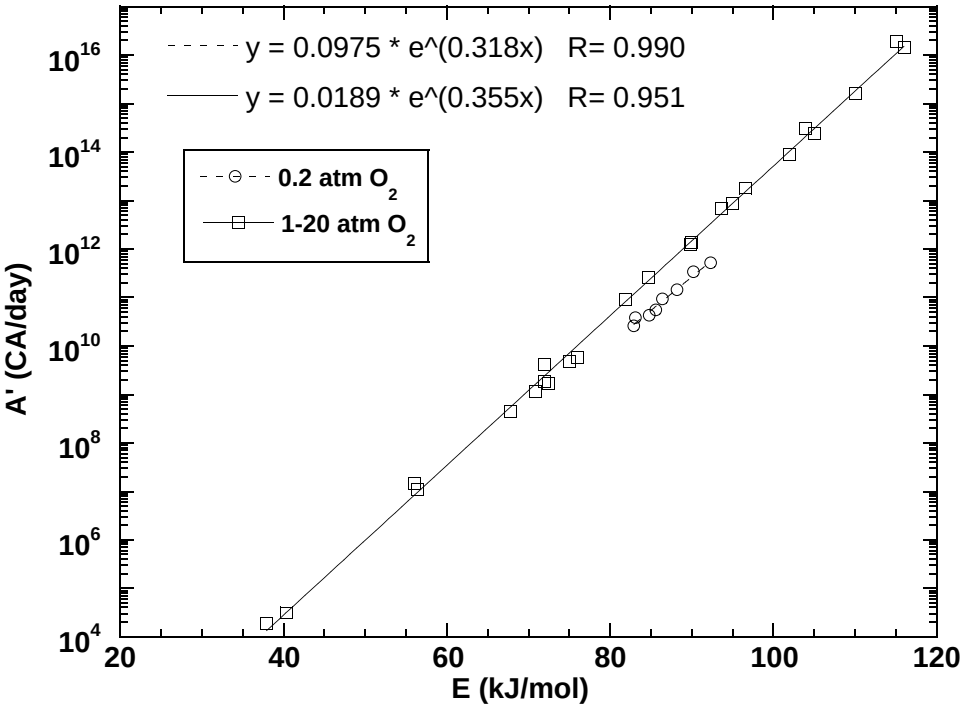

Figure 2-6. Calculated 0.2 atm O_2 Isokinetic Temperature with Experimental Results.

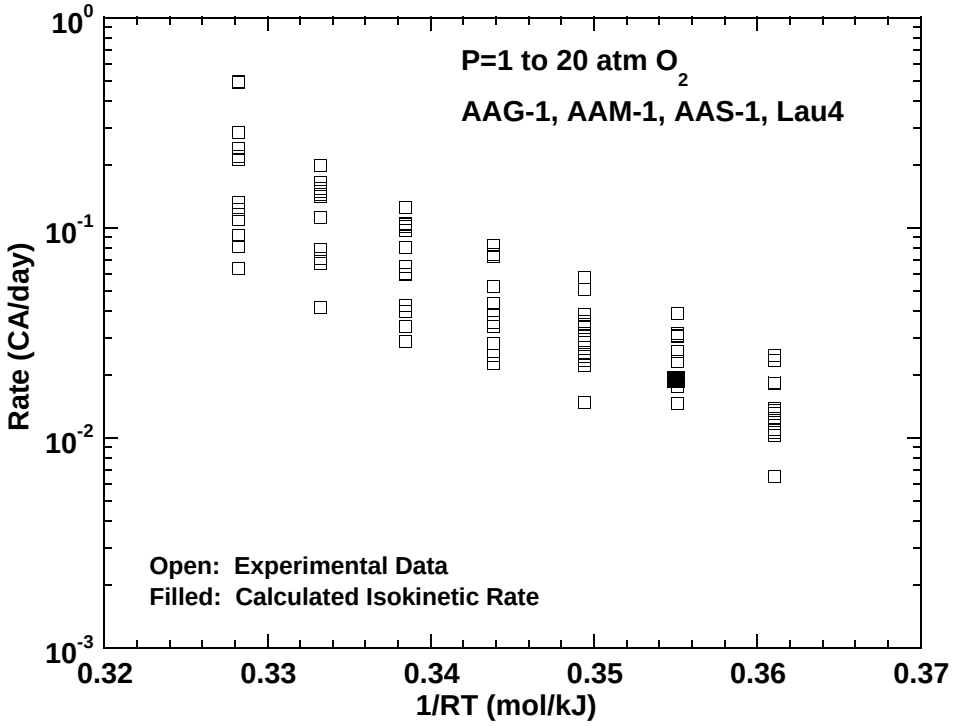

Figure 2-7. Calculated Isokinetic Temperature with Experimental Results for P=1 to 20 atm O_2 (AAA-1, AAB-1, AAD-1, AAF-1).

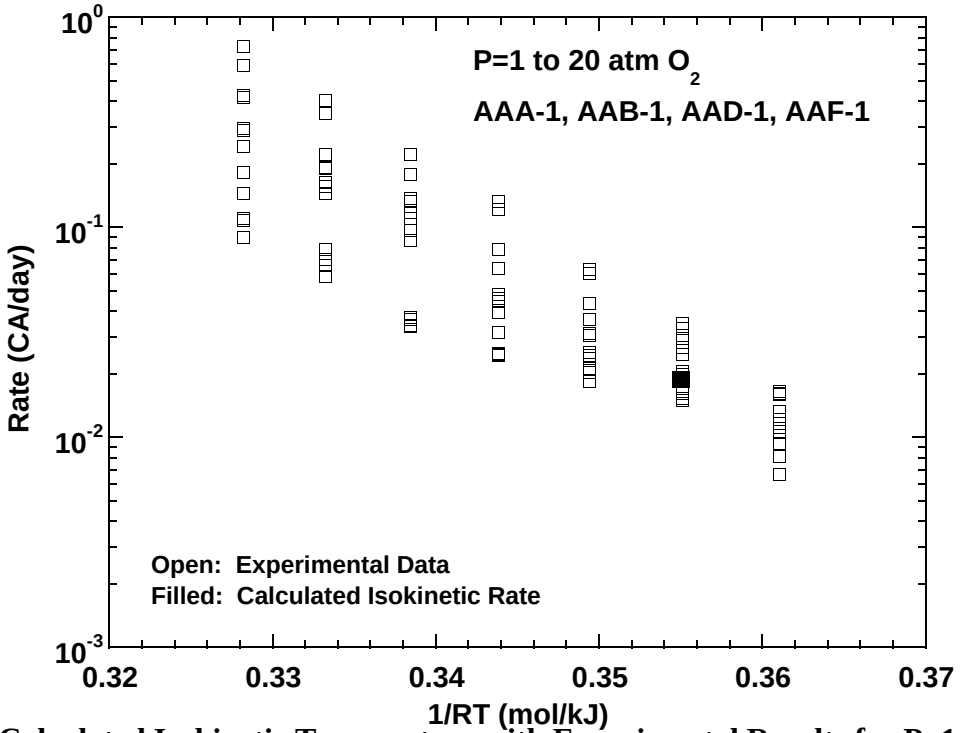

Figure 2-8. Calculated Isokinetic Temperature with Experimental Results for P=1 to 20 atm O_2 (AAG-1, AAM-1, AAS-1, Lau4).

due to the different activation energies that have been observed. Figure 2-6, which shows oxidation rates at atmospheric air, does not show this effect as well as Figures 2-7 and 2-8. This is because the activation energies at atmospheric air only range from 83-92 kJ/mol as opposed to 56-116 kJ/mol for 1 to 20 atm O_2.

The reason for the overlap of A´ vs E in Figure 2-5 (1-20 atm O_2) could be explained by the molecular diffusion hypothesis (Domke et al., 1999). As oxygen pressure is increased the asphaltenes are able to react. Once the asphaltenes can react, the overall oxidation mechanisms would be similar, thus allowing for a constant isokinetic temperature even as oxygen pressure varies.

Reaction Rate Model

Using the above results, a model can be used to estimate the kinetic parameters of the rate model in Equation 2-4. In turn A´ and E can be expressed in terms of an asphalt compositional parameter, oxygen pressure, and the results in Figure 2-5. The ratio of heptane asphaltenes (C7) to pentane asphaltenes (C5) is used as the asphalt compositional parameter (Table 2-5).

Table 2-5. Asphaltene Content of Tank Asphalts.

Asphalt	Heptane %AS	Pentane %AS	C7/C5
AAA-1	16.2	31.1	0.521
AAB-1	17.3	32.9	0.526
AAD-1	20.5	37.9	0.541
AAF-1	13.3	29.3	0.454
AAG-1	5.0	21.6	0.23
AAM-1	4.0	12.4	0.323
AAS-1	18.4	32.8	0.561
Lau4	13.6	29.7	0.458

From the data in Figure 2-9, E can be expressed in terms of the heptane:pentane asphaltene ratio and oxygen pressure. For the single pressure P=0.2 atm O_2:

$$E = 77.8 + 19.7\frac{C7}{C5} \quad \text{(for 0.2 atm } O_2\text{)} \tag{2-6}$$

For the other pressures, the data can be expressed as a single function of oxygen pressure and C7/C5 because of the single relationship between A´ and E at these higher pressures. For these pressures, the slopes from Figure 2-9 were averaged, and the intercepts were modeled as a function of oxygen pressure to find:

$$E = \left[11.3\ln(P) + 5.19\right] + 134.6\frac{C7}{C5} \quad \text{(for 1, 4, 20 atm } O_2\text{)} \tag{2-7}$$

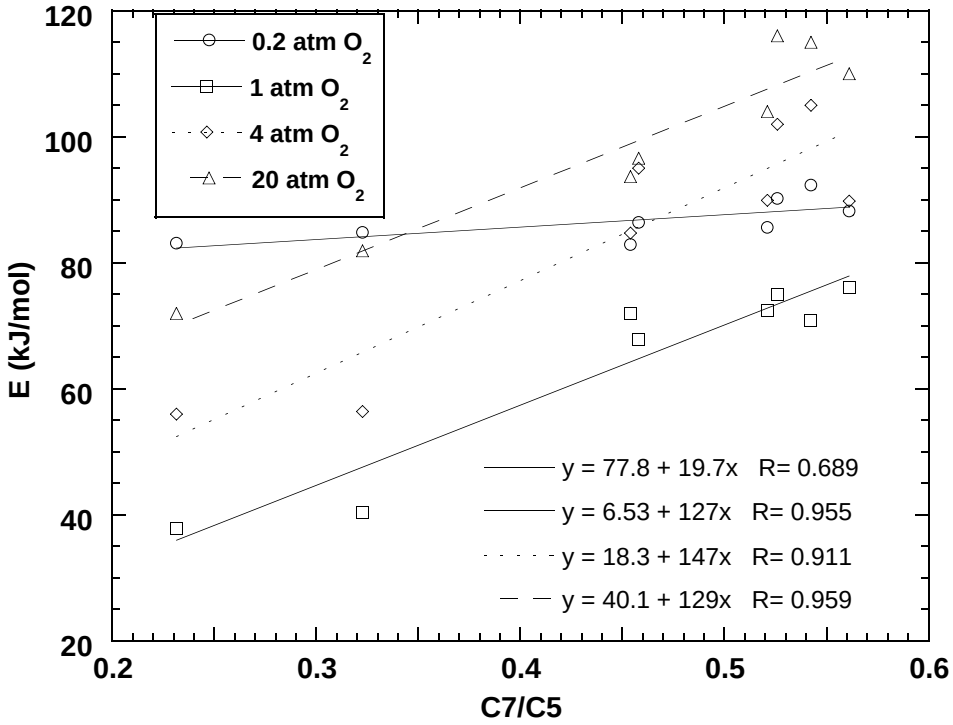

Figure 2-9. Relationship between E and Asphaltene Ratio.

Once E is known, A´ can be determined knowing the oxidation pressure by use of Figure 2-5:

$$\text{for P=0.2 atm } O_2 \quad A' = 0.0975 \exp(0.318E) \tag{2-8}$$

$$\text{for P} \geq 1 \text{ atm } O_2 \quad A' = 0.0189 \exp(0.356E) \tag{2-9}$$

It can be seen by comparing Tables 2-3, 2-4, 2-6, and 2-7 that ln A and E from the model are both within the error of the experimental data. However, when these values are substituted into equation 2-4 with the experimental error that is present, the model-calculated carbonyl formation rate for an asphalt may be in error by as much as 157 percent (Table 2-8). This is because with even a small error in the rate constants in equation 4, the exponential nature of the model can cause a very large error in the model calculation of the individual oxidation rates.

Table 2-6. Model Calculations for E.

Pressure (atm O_2)	AAA-1	AAB-1	AAD-1	AAF-1	AAG-1	AAM-1	AAS-1	Lau4
0.2	88.0	88.1	88.5	86.7	82.3	84.1	88.8	86.8
1	75.3	76.0	78.2	66.3	36.4	48.6	80.7	66.8
4	91.0	81.6	93.8	81.9	52.0	64.3	96.3	82.5
20	109	110	112	100	70.1	82.4	115	101

Table 2-7. Model Calculations for ln(A′).

Pressure (atm O_2)	AAA-1	AAB-1	AAD-1	AAF-1	AAG-1	AAM-1	AAS-1	Lau4
0.2	25.7	25.7	25.8	25.3	23.9	24.5	25.9	25.3
1	22.8	23.1	23.9	19.6	9.0	13.4	24.8	19.8
4	28.4	28.6	29.4	25.2	14.6	18.9	30.3	25.4
20	34.8	35.1	35.9	31.6	21.0	25.4	36.7	31.8

It is important to note that this model predicts that the rates of two different asphalts containing the same C7/C5 asphaltene ratio would be the same. This is not necessarily the case. The individual molecules that make up the C5 and C7 asphaltenes between two different asphalts will not likely be the same let alone in the same amounts, with inevitable effect on the oxidation rates. It would be ideal to create an oxidation model that would be based on the amount of types of molecules; however, this would be extremely difficult. It is interesting that the results are unaffected by the ratio of carbonyl to oxygen content. It is lower than average for AAG-1 and above average for AAD-1, but these asphalts correlate as well as the others.

Initial Jump

Initial jump data, CA_o-CA_t, are recorded in Table 2-9, where CA_t is the carbonyl value of the tank asphalt. There is much scatter but within the scatter the results appear to be independent of temperature as reported by Liu et al. (1996) for more extensive data. Liu et al. did report pressure dependence for some asphalts and fitted the data with

$$CA_o - CA_t = \beta P^{\gamma} \tag{2-10}$$

Table 2-8. Model-Calculated Rates x 10^3.

0.2 atm O_2

°F	AAA-1	AAB-1	AAD-1	AAF-1	AAG-1	AAM-1	AAS-1	Lau4
140	2.2	2.2	2.2	2.3	2.8	2.6	2.1	2.3
150	3.7	3.7	3.7	3.9	4.6	4.3	3.6	3.9
160	6.2	6.2	6.1	6.4	7.4	7.0	6.0	6.4
170	10.1	10.0	10.0	10.4	11.7	11.1	9.9	10.4
180	16.2	16.1	16.0	16.6	18.2	17.5	15.9	16.6
180	16.2	16.1	16.0	16.6	18.2	17.5	15.9	16.6
190	25.6		25.4	26.1	27.9	27.2		
190	25.6	25.6	25.4	26.1	27.9	27.2	25.3	26.1
200	40.0	25.6	39.8	40.5	42.3	41.6	39.6	40.5
210	61.5	39.9	61.4	62.0	63.4	62.8	61.3	61.9

1 atm O_2

°F	AAA-1	AAB-1	AAD-1	AAF-1	AAG-1	AAM-1	AAS-1	Lau4
140	12.3	12.3	12.1	13.0	15.4	14.3	11.9	12.9
150	19.2	19.2	19.2	19.2	19.1	19.1	19.3	19.2
160	29.6	29.7	30.1	28.1	23.5	25.3	30.6	28.2
170	45.0	45.3	46.5	40.6	28.7	33.1	47.9	40.8
180	67.5	68.3	70.9	58.0	34.9	43.0	73.9	58.5
190	100.0	101.4	106.5	81.9	42.2	55.4	112.6	82.9
200	146.3	148.9	158.2	114.5	50.8	70.8	169.4	116.2

4 atm O_2

°F	AAA-1	AAB-1	AAD-1	AAF-1	AAG-1	AAM-1	AAS-1	Lau4
140	11.3	11.2	11.1	11.8	14.1	13.1	10.9	11.8
150	19.3	19.3	19.3	19.3	19.1	19.2	19.3	19.3
160	32.5	32.6	33.1	30.8	25.8	27.7	33.6	30.9
170	53.9	54.3	55.7	48.6	34.4	39.6	57.3	48.9
180	87.9	88.9	92.3	75.5	45.5	56.0	96.3	76.2
190	141.2	143.3	150.5	115.7	59.7	78.2	159.1	117.1
200	223.7	227.7	241.9	175.1	77.6	108.3	259.0	177.6

20 atm O_2

°F	AAA-1	AAB-1	AAD-1	AAF-1	AAG-1	AAM-1	AAS-1	Lau4
140	10.2	10.1	10.0	10.7	12.7	11.8	9.8	10.7
150	19.4	19.4	19.4	19.3	19.2	19.3	19.4	19.3
160	36.2	36.4	36.9	34.3	28.7	30.9	37.4	34.4
170	66.4	66.9	68.6	59.9	42.4	48.8	70.7	60.2
180	119.4	120.8	125.4	102.5	61.8	76.1	130.8	103.5
190	210.9	214.0	224.8	172.8	89.1	116.9	237.6	174.8
200	366.1	372.8	396.0	286.6	127.0	177.3	424.0	290.8

Table 2-9. Initial Jump Data for All Asphalts at Various Pressures.

Pressure (atm O_2)	AAA-1	AAB-1	AAD-1	AAF-1	AAG-1	AAM-1	AAS-1	Lau4
0.2	0.215	0.177	0.201	0.280	0.475	0.297	0.153	0.247
	±0.085	±0.043	±0.092	±0.069	±0.157	±0.072	±0.040	±0.029
1	0.185	0.206	0.157	0.221	0.605	0.299	0.140	0.149
	±0.086	±0.097	±0.071	±0.092	±0.172	±0.133	±0.060	±0.062
4	0.305	0.291	0.216	0.372	0.934	0.487	0.193	0.289
	±0.149	±0.064	±0.140	±0.120	±0.190	±0.145	±0.063	±0.054
20	0.254	0.374	0.194	0.580	1.490	0.669	0.128	0.093
	±0.272	±0.075	±0.141	±0.119	±0.159	±0.072	±0.054	±0.083

Pressure dependence and composition dependence are indicated by a plot of the results in Figure 2-10. It appears however, that the pressure dependence, if any, is obscured by the scatter for the asphalts having high C7/C5 value. Perhaps the most interesting result is the high pressure dependence and high values of CA_o-CA_t at low values of C7/C5.

Values of β and γ are shown in Table 2-10 together with C7/C5 ratios. The values of β correlate rather well with C7/C5, being almost linear except that Lau4 and AAM-1 are a little low. The values for γ scatter badly. Only four asphalts AAG-1, AAM-1, AAF-1, and Lau4 show

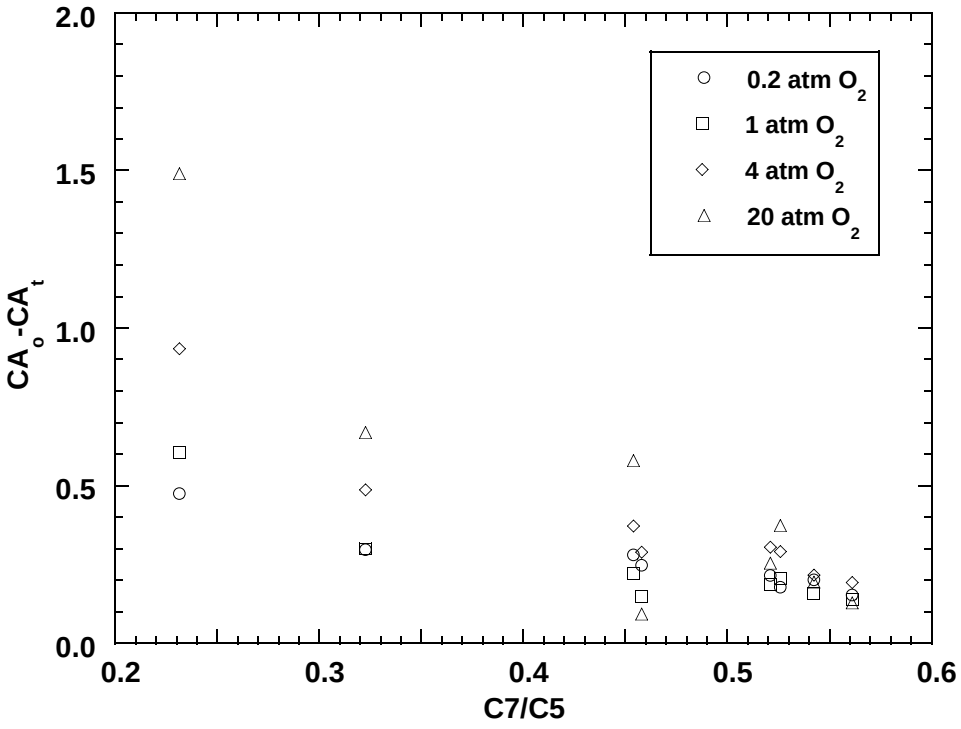

Figure 2-10. CA_0-CA_t versus Asphaltene Ratio.

Table 2-10. β, γ, and C_7/C_5 for All Asphalts.

Asphalt	β	γ	C_7/C_5
AAA-1	0.226	0.0632	0.521
AAB-1	0.223	0.17	0.526
AAD-1	0.189	0.0121	0.541
AAF-1	0.301	0.176	0.454
AAG-1	0.667	0.254	0.231
AAM-1	0.361	0.191	0.323
AAS-1	0.153	-0.0163	0.561
Lau4	0.197	-0.155	0.458

enough pressure effect on the initial jump (Figure 2-10) to be significant and the 20 atm datum for Lau4 (Table 2-9) looks bad as does the γ value. The other values of γ, except perhaps AAB-1, move in the same direction, increasing with decreasing C7/C5.

CONCLUSIONS

The oxidation kinetics of asphalts is hypothesized to be affected by oxygen diffusion through maltenes to polar aromatic and asphaltene aggregates. This causes an effect of oxygen pressure on oxidation which varies with asphaltene composition.

Several asphalts were oxidized at various temperatures and pressures to determine how the aging conditions affected their oxidation kinetics. An Arrhenius equation was assumed to fit the constant-rate region using a classical kinetics model for reactions:

$$r_{CA} = A' \exp\left(\frac{-E}{RT}\right) \tag{2-4}$$

Thus, the oxidation rate for each asphalt was assumed to be explicit in aging temperature and effects of oxygen pressure could be included implicitly through the parameters A′ and E.

In fact, it was determined that the oxidation pressure did play a role in the kinetic model constants. In particular, the activation energy and the preexponential factor are both surprisingly a function of oxygen pressure. They appear to have a minimum value at approximately 1 atm O_2, and these values are asphalt dependent. This pressure dependency is hypothesized to be caused by molecular diffusion.

An isokinetic temperature was determined for all the asphalts studied. This isokinetic temperature also appears to be a function of oxidation pressure. For low pressures, the asphalts tested have the same model-calculated rate at one isokinetic temperature, while at higher pressures, they have a different model-calculated rate and a second isokinetic temperature.

A model was developed to relate the kinetic parameters for different asphalts to their composition. This model was based on the asphaltene content of an individual asphalt, and the

oxidation temperature and pressure. The activation energy (E) of the oxidation is determined knowing the C7:C5 asphaltene ratio and oxygen pressure (P). The preexponential factor (A′) is then determined knowing E and P.

The model-estimated parameters calculate A′ and E within experimental error for the asphalts studied. However, this error may still lead to large errors in carbonyl formation rates due to the exponential nature of the kinetic model. Model-calculated rates were sometimes in error by as much as 150%.

The extent of initial jump of CA oxidation is asphalt dependent. For all asphalts the initial jump is independent of oxidation temperature. However, for some asphalts the initial jump is pressure dependent, and for others it is within experimental error. This also appears to be due to the composition of the asphalt. It appears as though low C7:C5 asphaltene ratio asphalts had a stronger pressure dependency and a higher value of the initial jump than the higher asphaltene ratio content asphalts.

CHAPTER 3. THE EFFECT OF ASPHALT AGING TECHNIQUES ON LOW-TEMPERATURE PROPERTIES

ABSTRACT

This project includes three test phases wherein the effects of various aging techniques on asphalt low-temperature properties were investigated. In addition, two other studies were conducted: air-blowing was investigated as a possible long-term aging test, and modifier performance was compared with respect to aging.

In Phase I of this project it was shown that 38 days of aging at 60 ^{o}C and 1 atmosphere of air is approximately equivalent to 20 hours in the PAV at 100 ^{o}C after both have been RTFOT-aged. Low-temperature properties of the samples did not vary significantly between the PAV and environmental room aged material.

In Phase II of this work, a correlation was developed using the high-temperature parameter $G^{*}/\sin(\delta)$ at 58 ^{o}C and 10 rad/s to correct the low-temperature performance grade when one desires to skip the long-term aging procedure. The correlation proved to give a maximum error of ±1.6 ^{o}C for the low-temperature performance grade.

In Phase III of this project it was shown that as asphalts are aged for extended periods their relative ranks with respect to Superpave low-temperature specifications change. This indicates that the Superpave long-term aging specifications result in an arbitrary ranking of asphalts with respect to low-temperature properties.

Air-blowing was investigated as a possible alternative for long-term aging in this project. Upon examining the data obtained by long-term air-blowing, it was concluded that air-blowing is not a suitable long-term test because it did not consistently produce samples comparable to those aged in the environmental room.

To summarize the work in comparing various modifiers, the higher weight percent modified samples showed considerably better low-temperature properties. The 18% RSGF-20 modified samples showed the best improvement in low-temperature properties followed by 4%SBS and 4%SBR. Polymer modifiers, therefore, should be used in concentrations of at least 4 percent by weight, where SBS rather than SBR is recommended. If ground tire rubber is to be used, a high-cure process with 18 percent by weight rubber provides excellent benefits for both high- and low-temperature properties but faces a significant cost hurdle.

INTRODUCTION

Asphalt Aging

A significant characteristic of asphalts is the fact that they undergo oxidative aging in the presence of oxygen. Oxidative aging has a profound effect on physical properties of asphalts and therefore a great deal of research has gone into understanding the nature and effects of oxidative aging.

Oxidative aging results in changing the composition of the asphalt itself. As an asphalt undergoes oxidation, the polar aromatics transform to asphaltenes, and naphthene aromatics become polar aromatics (Liu et al., 1998). Saturates, however, do not readily oxidize in significant portions (Petersen, 1998). After naphthene aromatics become polar aromatics they may then continue to oxidize and become asphaltenes, but for limited aging times this transformation is negligible. Liu (1996) showed that the rates of reaction for the polar aromatic fraction and the naphthene aromatic fraction vary from asphalt to asphalt. Therefore, the overall amount of the aromatic fractions may increase or decrease, while the asphaltene fraction always increases, and the saturate fraction does not generally change.

The oxidative aging process begins with an initial jump region, wherein the asphalt viscosity greatly increases with oxidation time (Lau et al., 1992; Petersen et al., 1993). The initial jump region is followed by a region of slower viscosity increase at a constant rate. Petersen (1998) has presented an explanation for the two regions based on a dual sequential oxidation mechanism. Petersen suggests that the initial jump region is due to the oxidation of polycyclic hydroaromatics to hydroperoxides. The hydroperoxides then may decompose into ketones or radicals or may react with sulfur groups to form sulfoxides. Following the initial jump, the constant rate region begins wherein benzylic carbons present in the asphalt complex react with oxygen to form ketones (carbonyls).

In a general sense these mechanisms describe asphalt aging, but the mechanisms themselves and the products of the oxidation are both highly dependent upon the asphalt composition and the aging conditions. Aging conditions and composition influence oxidation primarily due to the configuration of the asphalt matrix itself. It has been shown, for example, that pressure has a profound effect on the relative size of the initial jump region while temperature has no effect at all (Lau et al., 1992). This makes sense when one considers that at atmospheric pressure there is considerable diffusion resistance to oxygen transport into the asphalt. Higher pressures allow oxygen to be transported into the asphalt more readily and therefore lead to greater overall oxidation (Domke, 1999).

Considerable work has also been done to model the rate of asphalt oxidation in terms of temperature and pressure. Lau et al. (1992) showed that the rate of asphalt oxidation can be expressed as an Arrhenius model. Lunsford (1994) expounded upon this model, adding an

oxygen pressure effect. For the constant rate region, the rate of carbonyl area formation (a measure of oxidation rate) is given as:

$$r = AP^{\alpha} \exp\left(\frac{-E(P)}{RT}\right) \quad (3\text{-}1)$$

where P is the partial pressure of oxygen. Equation 3-1 illustrates that aging which occurs at atmospheric air pressure and a pavement temperature of 60 °C will have a significantly different rate than pressurized aging occurring at 20 atmospheres air and 100 °C.

Domke (1999) illustrated that aging conditions can also affect asphalt physical properties as he compared the 60 °C viscosities obtained by high pressure (20 atm air) aging with those obtained from asphalts in an environmental room maintained at 60 °C and 1 atm air. Domke showed that the degree of asphalt oxidation, as seen by the change in carbonyl area, differed between the two groups, proving that asphalt aging conditions have an effect on physical properties.

Upon aging, the physical properties of an asphalt may change dramatically. The viscosity of the material increases, as does its stiffness. These physical changes are due primarily to the increased amount of asphaltenes in the asphalt, although some volatilization of lighter saturates may contribute as well. As asphaltene concentration increases, the maltene concentration simultaneously decreases, resulting in larger colloidal particles with fewer solvating molecules. The resulting material tends to behave more like an elastic material at high temperatures, and more like a glassy solid at moderate to low temperatures. In service, aging leads to thermal and fatigue cracking susceptibility and is responsible, in part, for road failure.

Because the physical properties of asphalt binders are changed by oxidation, it is important to know the extent of the oxidation effect both by the hot-mix process and while in service on the road. Therefore, in order to evaluate asphalt binders, Strategic Highway Research Program researchers needed methods of asphalt aging that simulated both the hot-mix process and field aging (Anderson et al., 1991). In order to simulate the hot-mix process, researchers chose the existing rolling thin film oven test (ASTM D-2872). The RTFOT ages asphalt at elevated temperatures (325 °F) by blowing hot air over a thin film of asphalt. For field aging simulation, researchers chose to age asphalt binders in a Pressurized Aging Vessel for 20 hours at temperatures from 90 to 110 °C and a pressure of 20 atmospheres of air (Harrigan et al., 1994). SHRP goals, findings, and methods will be discussed in further detail in the following section.

Overview of SHRP (Superpave) Tests and Specifications

In 1987, the Strategic Highway Research Program was launched in order to improve asphalt pavement performance. As part of the program, researchers developed new methods for

testing asphalt binders and new specifications in accordance with the new testing methods (Anderson et al. 1994). Performing the SHRP (subsequently called Superpave) tests on an asphalt binder results in a performance grade for the binder. The PG reflects the maximum and minimum design temperatures under which the asphalt will have satisfactory performance.

Asphalt binder physical properties are critical to road performance. If an asphalt binder is too soft, rutting may occur soon after completion of the road due to traffic loads. On the other hand, if the binder is too hard or brittle, thermal cracking will occur during periods of cold weather. In addition, oxidative aging causes the binder to harden, thereby compounding its thermal cracking susceptibility over the life of the pavement (Domke, 1999). In light of these issues, SHRP formulated binder tests and specifications that determine the high-temperature and low-temperature physical properties of aged binders. In order to determine high-temperature properties, a material is aged for a short time, in the previously mentioned RTFOT test, which simulates the hot-mix process. Low-temperature properties, on the other hand, are measured using material aged in the PAV to simulate long-term aging.

Several tests are involved in obtaining the performance grade of an asphalt binder. The top grade is determined by a dynamic shear rheometer, which is used to characterize the high-temperature rheological properties of the binder. Low-temperature properties (and therefore bottom grade) are measured using a bending beam rheometer and a direct tension tester.

Overall, the Superpave standards for asphalt binder testing have provided a beneficial framework wherein binders can be evaluated and compared (Hoare and Hesp, 2000). However, Superpave standards are still relatively new and may yet be improved in some areas. Of particular concern is the long-term aging test, which takes place at pressures and temperatures well above road aging conditions. These elevated temperatures and pressures affect the mechanism of oxidation for the binder, leading to physiochemical property relations that may be different from those obtained at road aging conditions. A different mechanism for oxidation may also produce different relative aging rates between materials.

Since Superpave standards require long-term aging for low-temperature property measurement, it stands to reason that low-temperature properties are of primary interest after long-term aging. The long-term aging tests, unfortunately, are quite time consuming. The Superpave specified aging time, for example, is 20 hours within the PAV. In light of this time-consuming procedure, it would be beneficial to determine if the low-temperature properties of short-term aged material correlated with those obtained from long-term aged material. With an accurate correlation relating the physical properties of long-term aged material with those of short-term aged material, one could bypass the time-consuming long-term test. Low-temperature data collected by Domke (1999) indicate that the development of a correlation of this type may be possible.

Many previous researchers have observed that air blowing asphalt binders at elevated temperatures results in oxidation and change in physical properties (Quddus et al., 1995;

Gallagher et al., 1996). Concurrent with this project, the Center for Asphalt and Materials Chemistry has developed an alternative short-term aging procedure by air blowing to replace the existing RTFOT procedure (TxDOT project 0-1742). Also, an air-blowing procedure was sought to replace the long-term aging tests. A portion of the research reported in this chapter was devoted to establishing the validity of these new procedures.

Research Objectives

The research presented in this chapter had five primary objectives. The first objective was to compare the long-term high pressure, high-temperature aging to aging at simulated road conditions in the environmental room (Phase I). The second (Phase II) objective was to determine if long-term aging could be skipped when obtaining the performance grade of an asphalt. Third, it was hoped to gain insight into how extended aging affects the relative rankings of asphalt binders as given by the Superpave specifications (Phase III). Fourth, air-blown aging of asphalt was examined as a possible replacement for the PAV long-term aging test. Finally, the effect of modifiers on low-temperature performance was evaluated.

To accomplish the first objective, a comprehensive comparison of the RTFOT/ environmental room aged material to RTFOT/PAV aged material was performed. This comparison was intended to reveal the relative amount of road aging the PAV simulates and the accuracy with which the PAV models road conditions. In addition, the comparison revealed differences between the oxidation mechanisms for the two aging methods.

The Phase II objective of this research involved determining how the low-temperature physical properties of short-term aged material compare with those of long-term aged material. Specifically, a correlation was sought between the performance grade of long-term aged material with the apparent performance grade of short-term aged material. Hopefully, such a correlation would enable laboratories to obtain reliable performance grades for a material without running long-term aging tests.

Third, this research was intended to determine if the differing mechanisms for asphalt oxidation have significant impact on low-temperature properties. If so, the relative rankings of asphalts based on their performance grade would be entirely dependent upon the type, and perhaps length, of the aging test performed on the asphalts. For example, the degree of oxidation observed at atmospheric air concentration and 60 ^{o}C are significantly different from that observed in the PAV (Domke, 1999). These differences may result in significant differences in low-temperature properties. If this is the case, Superpave standards may need to be modified to reflect the difference.

In order to find a long-term aging test that was more representative of road conditions and yet still of reasonable length, a long-term air-blowing test was investigated. This test was intended to reflect, as much as possible, the conditions and oxidation mechanisms observed in road aging, while still accelerating the rates enough for timely testing.

The study of modifier performance used the same base asphalt with SBR, SBS, and high-cure ground tire rubber to assess their effect on low-temperature and high pavement temperature performance grade.

MATERIALS AND METHODS

Materials

Selection of Asphalts

Asphalt binders used in this project were selected from the inventory of the Center for Asphalt and Materials Chemistry (CAMC) at Texas A&M University. In order to ensure that the results of the study were not confined to a specific type of asphalt, many different asphalt binders were chosen for the study. In selecting asphalts, a wide variety of initial viscosities were sought as well as a variety of asphalt manufacturers. Table 3-1 presents the various unmodified asphalt binders used in the study as well as their initial unaged, or tank 60 ºC viscosities. The values presented in Table 3-1 tend to be higher than the literature values for the selected SHRP asphalts. The asphalts used in this study have been stored in a facility which was not temperature controlled, and some have been there for a number of years. It is conceivable, therefore, that some oxidation has taken place during storage, which would account for the higher viscosities.

Table 3-1. Unmodified Asphalt Binders and Their Unaged Viscosities Measured at 60 ºC and 0.1 rad/s.

Asphalt Binder	Unaged 60 ºC Viscosity @ 0.1 rad/s (P)
SHRP AAA-1	1081
SHRP AAD-1	1366
SHRP AAF-1	2261
SHRP AAS-1	3162
SHRP ABM-1	3313
Conoco AC-20	3870
Exxon AC-10	1203
Exxon AC-20	2267
GSAC AC-15P Base	858
Shell AC-20	2232

Preparation of Modified Samples

The 10 binders listed in Table 3-1 are unmodified materials, that is, no polymer modifiers have been added to them to enhance their rheological properties. Since the scope of this work includes modified material as well, we prepared six additional modified binders for the study. The six modified binders are listed in Table 3-2. All of the modified binders share the same base, the GSAC AC-15P base, and were modified with either styrene-butadiene rubber (SBR), styrene-butadiene-styrene block co-polymer rubber (SBS), or Rouse ground tire rubber of –20 mesh (RSGF-20).

The first pair of samples listed in Table 3-2 were modified using an SBR Latex emulsion (Sample number 140-0) received from Gulf States Asphalt Company (GSAC). The emulsion contains 72 percent solids, with the balance being water. Two percent solids by mass were added to the first sample, and four percent solids by mass to the second sample. In order to maintain the emulsion while mixing into the base asphalt, the emulsion was added drop-wise while stirring the base asphalt. To accomplish this, the base asphalt was poured into a one gallon can and heated to 325 ^{o}F. A Central Machinery drill press (model T-726) was used to mix the hot asphalt at a speed of 1550 rpm. The emulsion was then added drop-wise over a period of about 10 minutes. After the addition of the emulsion, the asphalt was stirred at 1550 rpm for 1.5 hours to ensure

Table 3-2. Modified Asphalt Binders and Their Unaged Viscosities Measured at 60 ^{o}C and 1.0 rad/s.

Asphalt Binder	Unaged 60 ^{o}C Viscosity @ 1.0 rad/s (P)
GSAC AC-15P Base W/2% SBR	1886
GSAC AC-15P Base W/4% SBR	2721
GSAC AC-15P Base W/2% SBS	1613
GSAC AC-15P Base W/4% SBS	3521
GSAC AC-15P Base W/10% RSGF-20	1750
GSAC AC-15P Base W/18% RSGF-20	2300

good mixing and to ensure the vaporization of the water in the emulsion. During the entire mixing process a nitrogen blanket was maintained on the system to prevent the asphalt from oxidizing.

The second pair of modified samples was made with 2 and 4 weight percent SBS, which was received from GSAC (D-1101 polymer, sample number 139-0). In contrast to the SBR modified material, wherein the emulsion simply needed to be mixed in, the SBS polymer had to be dissolved in the asphalt. In order to accomplish this a different procedure was used. To dissolve the polymer into the base asphalt the mixture was heated in a one gallon can to 350 ^{o}F, and mixed using a Silverson mixer (model L4RT) at 4000 rpm. The 2%SBS sample was blended for 2 hours at these conditions, and the 4%SBS sample was blended for four hours. A nitrogen blanket was maintained on the system throughout the mixing process to prevent oxidation of the binder.

The final pair of the modified samples, GSAC AC-15P Base w/10% RSGF-20 (Rouse Rubber, -20 mesh) and GSAC AC-15P Base w/18% RSGF-20, was modified using RSGF-20. These samples were cured using a high-cure process recommended by Chipps (2001) which gives adequate disintegration of the crumb rubber and thorough dispersion of the modifier throughout the base. For the first sample, 10 percent by mass RSGF-20 was added to the GSAC AC-15P base. Similarly, the second sample contains18% RSGF-20 by mass. After the rubber was added, each sample was cured in a one gallon can using a Silverson Mixer (model L4RT) for 6.5 hours at 500 ^{o}F and 8000 rpm. In order to prevent oxidation during the curing process a sparger was used to blow nitrogen through the sample. In addition, a blanket of nitrogen was maintained above the sample.

Aging Procedures

Short-Term Aging

During the road manufacturing process, asphalt is heated and mixed with aggregate, a procedure known as the hot-mix process. Asphalt hardening occurs during the hot-mix process by loss of volatile components within the asphalt and by oxidative aging due to contact with atmospheric oxygen. For laboratory purposes, it is necessary to simulate the hot-mix aging process before any other long-term aging procedure is performed on the asphalt.

There are a number of ways to simulate the hot-mix process. The most common is the rolling thin film oven test, ASTM D2872, which was developed by Hveem et al. (1963). Another hot-mix simulation, the thin film oven test, ASTM D1754, is available, but as Jemison et al. (1991) pointed out, these tests give essentially identical results. Finally, the CAMC at Texas A&M University, has developed a new air-blowing procedure to simulate the hot-mix process. In this study, the RTFOT was used for the bulk of short-term aging tests, but the new air-blowing procedure was used as well. Both the RTFOT and the new CAMC test are described in this section.

The RTFOT test simulates the hot-mix process by bringing a heated asphalt film in contact with hot air. Oxygen in the air reacts with the asphalt film, thus simulating oxidative aging, and the heating of the asphalt results in volatilization of the lighter components. The RTFOT procedure begins by pouring 35 grams of asphalt into each of eight RTFOT bottles. Within the oven, the bottles are inserted into a rack where they sit horizontally, with the mouth of the bottle facing outward. The rack itself rotates at 15 revolutions per minute, thereby passing each bottle in front of a nozzle that directs hot air into the bottle at a rate of 4 L/min. The oven temperature is maintained at 163 ^{o}C (325 ^{o}F) and the test runs for 85 minutes. For more information concerning the RTFOT test see ASTM D2872.

Figure 3-1 illustrates the apparatus used in the new air-blowing procedure developed at the CAMC. The apparatus consists of a main vessel, a temperature control system, air flow control system, and a mixer. For the prototype apparatus, the main vessel itself is made of a copper alloy with an approximately 3 1/2 inch outer diameter. The vessel has a stainless steel lid, which contains ports for the spindle, the thermocouple, and the air sparger. The vessel also was insulated with 2 inch thick fiberglass insulation. The temperature control system consists of a heating mantle (Glas-Col Model TM610), a temperature controller (Omega Model CN9000A), a variac (Staco Model 3PN1010B), and a thermocouple (Omega Part Number 010801). Temperature is continuously measured by the thermocouple, which sends a signal to the controller. The controller then varies the power sent to the heating mantle. The operator controls the maximum output to the heating mantle by adjusting the setting on the variac. Compressed air enters the system and flows through a flow controller (Cole-Parmer), which maintains a constant air flow rate. The air then proceeds into the vessel through the sparger and exits directly under the spindle. The mixing system consists of an Arrow 1750 Mixer and a spindle with four sets of six cylindrical prongs.

The procedure is straightforward. Two hundred and fifty grams of asphalt are poured into the main vessel. The vessel is then inserted into the heating mantle, and the apparatus is assembled. The temperature controller is set to 325 ^{o}F, and the Variac to about 70 percent. Once the temperature reaches about 270 ^{o}F, the Variac is adjusted to 50 percent. Once the temperature within the vessel reaches 320 ^{o}F, the air flow is turned on and controlled at a constant rate of 4L/min. The mixer is set at a constant speed of 700 rpm. When run for 75 or 80 minutes, this apparatus and procedure was found to be comparable to the RTFOT in terms of viscosity increase and carbonyl area production. The interested reader is directed to Vassiliev (2001) for details concerning the new air-blowing apparatus.

Long-Term Aging

Once asphaltic concrete is installed in road applications, the asphalt continues to age. Atmospheric oxygen reacts with the asphalt binder in periods of hot weather, thereby changing the chemical composition and material properties of the binder. As aging progresses, the binder's viscosity increases, and the binder itself becomes more brittle. This may lead to

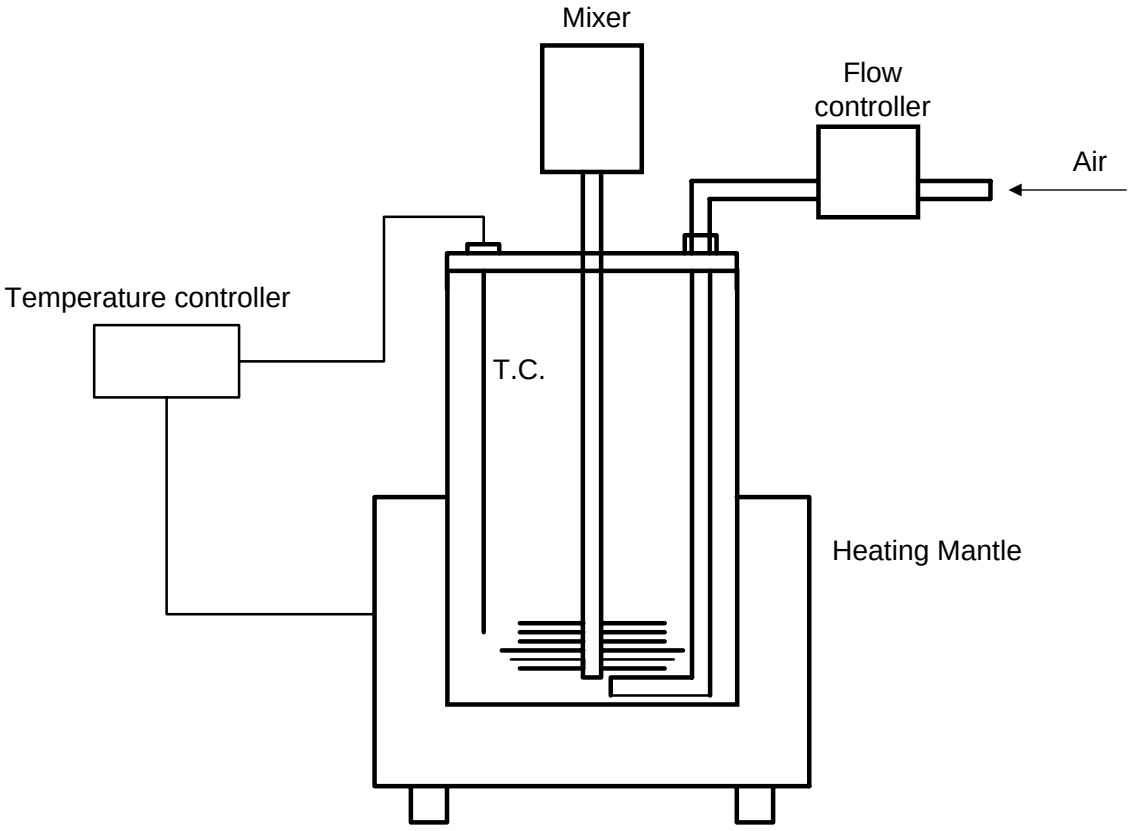

Figure 3-1. Air Blowing Short-Term Aging Apparatus.

increased thermal and fatigue cracking susceptibility of the asphaltic concrete. In order to design roads which are durable, that is, resistant to thermal and fatigue cracking, it is necessary to simulate the long-term in-service aging of asphalt binders.

As with the short-term aging simulation, several long-term aging options are available. The most common long-term aging test is performed at high temperatures and pressures using a pressure aging vessel. Asphalt binders may also be long-term aged at simulated road conditions with atmospheric pressure and temperatures similar to those encountered in summer months. Simulations of road conditions are performed in an environmental room, where temperature and humidity are held constant. Finally, asphalt binders may be air-blown at elevated temperatures in an apparatus similar to the one presented in Figure 3-1. All three of these long-term options were used during the course of this project, and as such, they are described in this section.

The PAV testing equipment consists of a pressure vessel with pressure and temperature controls, a sample rack, and a sample pan. Fifty grams of asphalt that has been RTFOT aged are poured into a sample pan giving an asphalt layer which is 3 mm thick. The sample pans are then placed onto the sample rack, which is then placed inside the vessel. Once the vessel is sealed, the temperature and pressure control systems bring the sample to the temperature and pressure

chosen by the operator. Typically, the test itself is performed at a pressure of 20 atmospheres of air and temperatures of either 90, 100 or 110 °C. For this study, all PAV tests were conducted at 100 °C. For further information regarding the PAV test, the reader is directed to AASHTO PP1.

Long-term asphalt aging can also be carried out in an environmental room, where conditions can be kept close to those seen in road service. For this study, asphalt materials were aged in an environmental room maintained at 60 °C, atmospheric pressure, and 50 percent relative humidity. These conditions were chosen because they are comparable to Texas road conditions during the summer months. Before environmental room aging, all samples are RTFOT short-term aged. Following the RTFOT, 20 grams of asphalt are poured into 5.5″ by 5.5″ aluminum trays. The resulting film of asphalt in each tray should be approximately 1.0 mm thick. The thin film of asphalt allows the oxidation to take place with little or no diffusion resistance, thereby producing a uniform sample that accurately represents aging at the environmental room conditions.

The final type of long-term aging is air-blowing. Figure 3-2 illustrates the apparatus used in the long-term air-blowing procedure. As with the short-term air-blowing apparatus, the system is comprised of a main vessel, a temperature control system, a mixer, and an air control system. The main vessel used for this apparatus is a quart can. The temperature controller receives a signal from the thermocouple and controls the power sent to the heating tape. A variac is included to allow the operator to control the maximum power sent to the heating tape. Air flow rate is controlled by a rotameter set to a specific flow rate by the operator. The air flows through the rotameter and into the sparger, which distributes the air into the asphalt sample. A Central Machinery drill press (Model T-726) with an attached impeller was used to mix the sample during the procedure.

The long-term air-blowing procedure begins by placing 250 grams of asphalt into a quart can. The apparatus is then assembled and the temperature controller is set to 325 °F. While the system achieves temperature, a nitrogen line is connected to the sparger in place of the air line. This prevents any oxidation of the asphalt prior to testing. After the system achieves temperature, the air line is connected, and the rotameter is set to a flowrate of 24,680 mL/min. The drill press is then turned on at a speed of 1550 rpm. Typically, the long-term aging test is run for 20 hours at these conditions.

High-Temperature Material Properties

High-temperature properties of binders are very important in the proper design of asphaltic concrete, for they contribute to the pavement's susceptibility to rutting. A binder having minimum hardness is desired for preventing rutting.

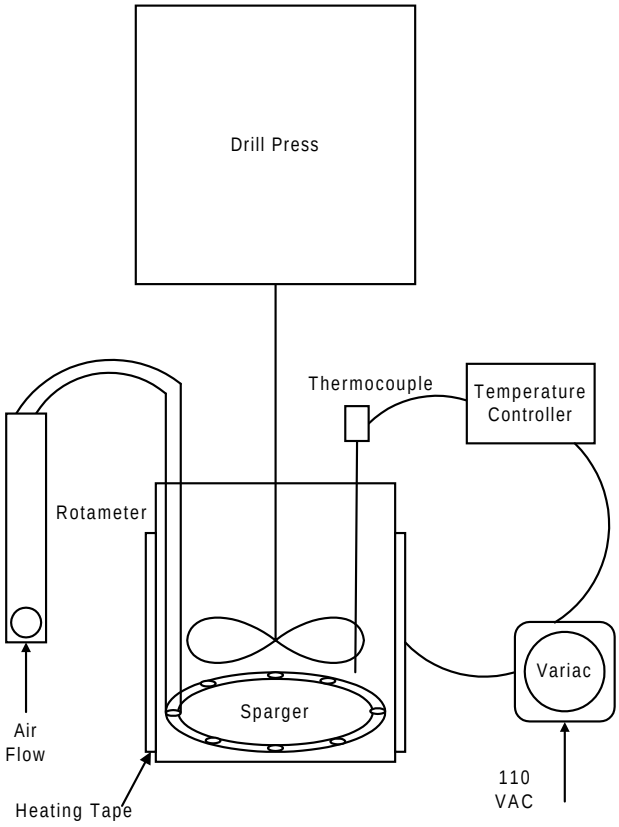

Figure 3-2. Air Blowing Long-Term Aging Apparatus.

Dynamic Shear Rheometer

In order to measure the high-temperature properties of the asphalt material, a Carri-Med CSL-500 dynamic shear rheometer was used. For all samples the 60 ºC complex viscosity was obtained by running a frequency sweep at constant torque for each material. A 2.5 cm composite plate was used with a 500 micron gap for the majority of the samples, and a 1500 micron gap for rubber-modified (RSGF-20) samples. For unmodified samples the limiting complex viscosity was taken at a strain rate of 0.1 rad/s, whereas for modified samples the value at 1.0 radians per second was recorded. Since the rubber modified materials were outside of the Newtonian flow regime at 60 ºC, the viscosity at 1.0 radians per second was chosen arbitrarily as a convenient value for comparative purposes.

All samples were also top graded according to Superpave specifications. For these measurements the frequency was fixed at 10 rad/s, and a torque sweep was performed on the material. Once the material reached the Newtonian limit, the complex shear modulus, G^*, and the phase angle, δ, were recorded. $G^*/\sin(\delta)$, an important parameter in Superpave specifications, was then calculated. Measurements of this type were conducted at two of the

following temperatures for each material: 52, 58, 64, 70 and 76 ºC. As with the 60 ºC viscosity, all runs were performed at a 500 micron gap for all samples except those modified with crumb rubber, which were performed at 1500 microns.

Low-Temperature Material Properties

Low-temperature material properties are also important for proper asphaltic concrete design. While a relatively hard asphalt is necessary to prevent rutting at high temperatures, an asphalt which is too hard will exhibit thermal cracking at low temperatures.

Bending Beam Rheometer and Direct Tension Tester

The bending beam rheometer (BBR) was used to measure the low-temperature stiffness and the m-value of an asphalt binder. The direct tension tester (DTT) was used to measure low-temperature failure strain and stress of asphalt subjected to a uniaxial load. The standard SHRP procedures were used for these tests.

From the DSR, BBR, and DTT measurements, Superpave grading of the materials was determined. Interpolation of data was used to obtain continuous gradesand values are reported as continuous grades

Analytical Techniques for Asphalt Oxidation

Two analytical techniques were used during this study to determine the degree of asphalt aging. Infrared spectroscopy was used to determine the carbonyl area of samples after various aging techniques (Jemison et al., 1992). Gel permeation chromatography was used to determine the shift in molecular weight as a result of oxidative aging.

Methodology

For this project, the low-temperature properties of asphalt material were studied in three different test phases. First, high-pressure PAV aging was compared to road-condition aging as simulated in the 60 ºC environmental room. Second, the current standard aging procedure for obtaining the bottom grade (RTFOT/PAV 20 hours) was compared to material that was short-term aged only. Finally, some materials were PAV aged for an extended period of time, and these were compared to the conventional long-term aging times.

Figure 3-3 illustrates the methodology for the first phase of the project. All 16 asphalt binders were RTFOT aged. Following this aging the top performance grades were obtained for each asphalt using the DSR techniques previously described in this chapter. After RTFOT aging, sample Set A was PAV aged for 20 hours at 100 ºC. The bottom grade and 60 ºC viscosity of Set A was then determined. Sample Set A represents the standard Superpave method of binder aging to determine low-temperature physical properties. A second sample set, Set B, was aged in the

environmental room at 60 ºC after RTFOT aging. Periodically, the 60 ºC viscosities of the samples in Set B were obtained using the DSR and were compared to those of Set A. Once the 60 ºC viscosities of Set B were approximately equivalent to those of sample Set A, Set B was removed from the environmental room. Low-temperature properties and performance grades were then determined for both Sets A and B.

In the second phase of the project (Figure 3-4), the conventional testing method (Set A) was compared to material that had been short-term aged only. Set C consists of the short-term aged only samples that were aged by either the RTFOT method or the air-blowing method developed by Vassiliev (2001). Low-temperature properties, 60 ºC viscosities, and bottom grades for Set C were obtained and compared to those of Set A.

Figure 3-5 illustrates phase III of the project. In this phase Set D was made with five asphalts: AAF-1, AAS-1, Exxon AC-10, Exxon AC-20, and Shell AC-20. These asphalts were RTFOT aged and then aged in the PAV for 48 hours at 100 ºC. After aging, their 60 ºC viscosities were determined as well as their low-temperature physical properties and bottom performance grade. These values were compared to those of Set A.

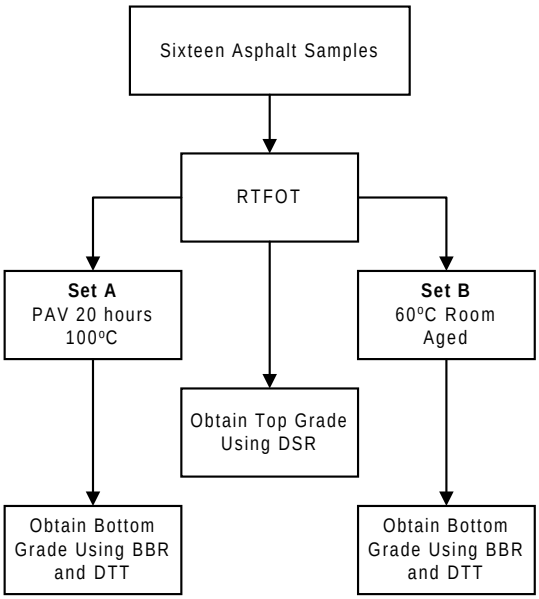

Figure 3-3. Methodology for Comparison of PAV and Environmental Room Aging.

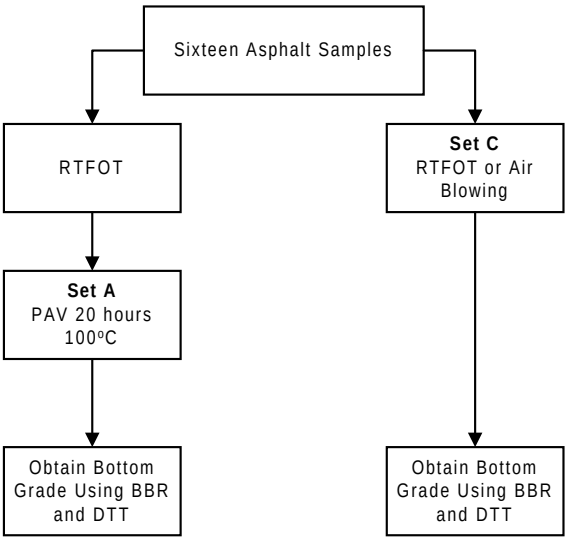

Figure 3-4. Methodology for Comparison of PAV Aged and Short-Term Aged Material.

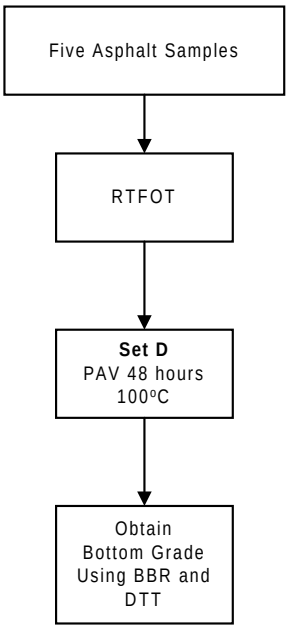

Figure 3-5. Methodology for Obtaining Extended PAV Aging Data.

RESULTS AND DISCUSSION

Phase I Results

As explained in the methodology section, sample Set B, aged in the 60 ºC environmental room was removed from the room when the viscosities of the samples, as a whole, approximately equaled that of the sample Set A values. This criterion was satisfied at an aging time of 38 days in the environmental room. Figure 3-6 shows a comparison between the 60 ºC limiting complex viscosity of unmodified members of sample Sets A and B (Figure 3-3) .

As shown in Figure 3-6, most materials fall on or near the line of equal viscosity. This indicates that an aging time of 38 days in the environmental room results in materials which have approximately equivalent viscosities to those aged in the PAV for 20 hours at 100 ºC. Also in support of this conclusion is the fact that the carbonyl areas for the same samples also show good agreement, as presented in Figure 3-7.

Figure 3-7 does seem to indicate, however, that the carbonyl area for the PAV tends to be higher than that of the environmental room. The only exceptions to this are asphalts AAD-1 and ABM-1, which showed greater carbonyl area increase in the environmental room. According to the work done by Liu (1996) and Domke et al. (1999), the hardening susceptibility of an asphalt is pressure dependent. This would explain why even though the carbonyl area of AAD-1 is quite different for Sets A and B, the viscosities are about equal. Indeed, Domke et al. (1999) showed that the hardening susceptibility for asphalts actually reaches a minimum in the vicinity of 4 atmospheres of oxygen, where the PAV operates. This is supported by Figures 3-6 and 3-7, as they indicate that although the viscosities of both sets are about equal, the carbonyl areas for the PAV tend to be slightly higher. That is, the hardening susceptibility of Set A is lower than that of Set B as a whole, presumably because it is being aged at a higher pressure.

In addition to the unmodified asphalts, modified asphalts of Sets A and B were investigated. Figure 3-8 shows the 60 ºC viscosities of modified asphalts of Sets A and B. As shown, the viscosities of the modified materials indicate good agreement between the PAV and environmental room aging. Modified samples, like the unmodifieds, were removed from the environmental room after 38 days of aging.

At this point it is important to note that the results obtained here, namely the equivalence of 38 days in the environmental room to 20 hours at 100 ºC in the PAV are in disagreement with the results obtained by Domke (1999). Domke showed that environmental room aging of 135 days gave viscosities close to those obtained from 40 hours in the PAV at 100 ºC, seeming to indicate that 20 hours in the PAV would approximate 67.5 days aging in the environmental room. This discrepancy can be easily explained since Domke did not RTFOT the samples before either aging procedure, as has been done in this project. As has been pointed out, the extent of the initial jump region of an asphalt is dependent on pressure, but not on temperature (Liu et al., 1996; Petersen, 1998; Domke et al., 2000). Therefore, since Domke did not RTFOT the

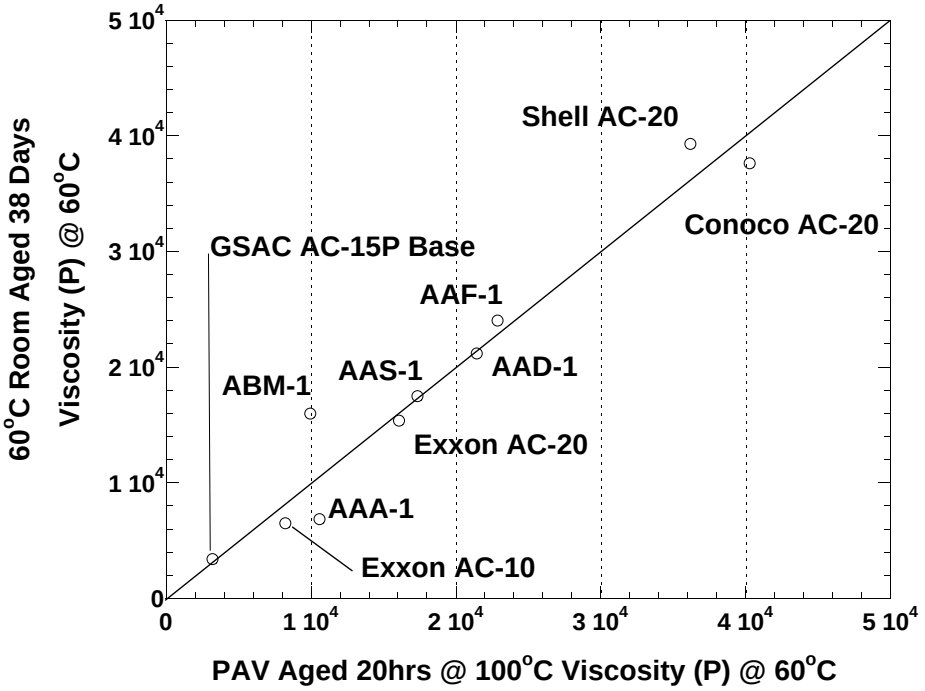

Figure 3-6. Comparison of PAV Aged and 60 ºC Room Aged 60 ºC Viscosity: Unmodified Materials.

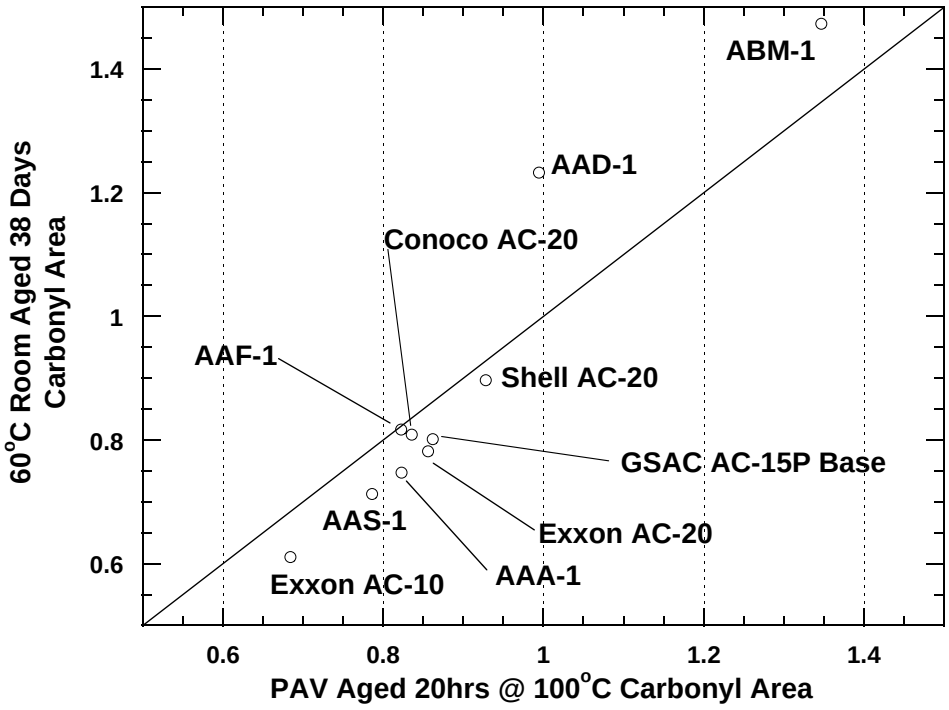

Figure 3-7. Comparison of PAV Aged and 60 ºC Room Aged Carbonyl Area: Unmodified Materials.

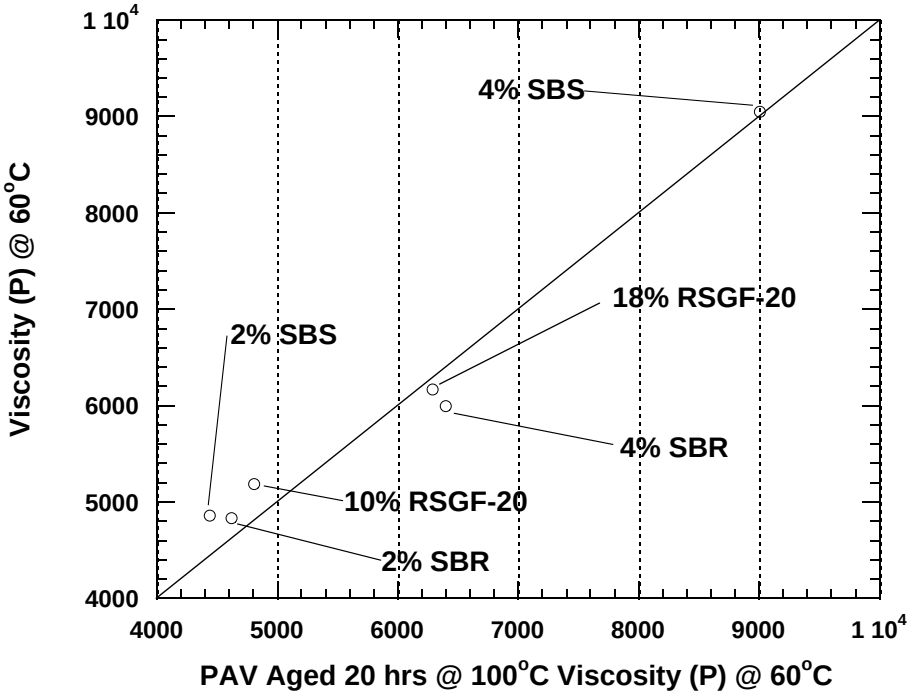

Figure 3-8. Comparison of PAV Aged and 60 ºC Room Aged 60 ºC Viscosity: Modified Material.

materials first, the initial jump regions for the environmental room samples and the PAV samples would naturally be quite different. Additionally, since increasing pressure increases the initial jump, the PAV would have a large head start on the environmental room, so that longer environmental room aging times would be necessary to match the extent of aging seen in the PAV. In this study, the initial jump regions for both sample sets A and B occurred, for the most part, in the RTFOT, so both samples had roughly the same starting point. The added pressure can, however, add to the initial jump. Presumably, each sample was in its constant rate region when long-term environmental room or PAV aging began.

If one assumes that the environmental room accurately simulates road aging during a summer in Texas, the road aging equivalent for the environmental room can be estimated. In this case and as a very rough approximation, the assumption is made that most aging occurs for four months, June through September for 8 hours per day. (A calibration based on field data will improve this calculation.) Then, for 38 days in the environmental room:

$$38\ \text{days(ER)}\ \frac{24\ \text{hours}}{1\ \text{day(ER)}}\ \frac{1\ \text{day(road)}}{8\ \text{hours}}\ \frac{1\ \text{month}}{30\ \text{days}}\ \frac{1\ \text{year(road)}}{4\ \text{months}} \cong 0.95\ \text{years} \qquad (3\text{-}2)$$

This value also applies to PAV aging for 20 hours at 100 ºC, since they have been shown to be approximately equivalent. This result is quite surprising, since the intention of the PAV in the SHRP specifications is to determine whether or not roads will fail in the long term. Clearly, the long-term aging test should simulate several years in service, so the aging time in the PAV may need to be modified.

It is important to note here that although this research is presenting 20 hours in the PAV at 100 ºC as equivalent to 38 days in the 60 ºC environmental room, this does not necessarily mean that multiples of these (e.g. 40 PAV hours and 76 days) are also equivalent. As numerous researchers have shown (Liu, 1996; Domke, 1999; Lunsford, 1994), the constant rate region of asphalt oxidation is dependent upon pressure and temperature conditions. The conditions studied in this work indicate merely an intersection of these two aging conditions with respect to carbonyl area and viscosity. Indeed, upon further aging the materials may not show such equivalence at any other point, not even, as might be expected, at 40 hours in the PAV and 76 days in the environmental room or 10 hours in the PAV and 19 days in the environmental room.

Although sample Sets A and B (Figure 3-3) look similar so far, it was still necessary to determine if their low-temperature properties and SHRP grades were considerably affected by the different aging treatments. In order to accomplish this, the stiffness and m-value for all samples were obtained using the BBR Superpave procedure. These values resulted in a continuous performance grade, wherein the passing temperature of each sample was determined by interpolation or extrapolation of the data. This procedure was repeated with DTT data by averaging the values over the four specimens tested.

Table 3-3 gives the resulting continuous bottom grades for all the asphalts included in this study. Figure 3-9 provides a comparison between sample Sets A and B for the SHRP asphalts tested. The plot shows that the BBR continuous grades for both the PAV aged material and the environmental room aged material are comparable. In fact, all the SHRP asphalts tested vary by less than 1 degree between the two sample sets. DTT data have considerably more variance, varying by as many as 5 degrees for the AAD-1 sample.

Figure 3-10 presents the same bottom continuous grade comparison for the remaining unmodified asphalts. These asphalts also indicate good agreement between the BBR continuous grades of Sets A and B, with the largest variance being for Conoco AC-20 at 1.15 ºC. In addition, the DTT data are also in good agreement, with the largest variance being that of Exxon AC-10, which showed a 4.2 ºC difference between the PAV and environmentally aged material. Considering the fact that the DTT data are notorious for scatter, the results here are well within the experimental error of the DTT equipment.

Table 3-3. Continuous Grade Values for Sample Sets A and B.

Material	PAV BBR Grade (°C)	60 °C Room BBR Grade (°C)	PAV DTT Grade (°C)	60 °C Room DTT Grade (°C)
AAA-1	-33.12	-32.51	-37.48	-35.43
AAD-1	-31.85	-31.14	-30.73	-25.25
AAF-1	-20.05	-19.42	-11.28	-12.90
AAS-1	-29.14	-29.45	-25.20	-21.71
ABM-1	-14.05	-13.67	-15.47	-17.30
Conoco AC-20	-24.60	-25.85	-27.24	-24.39
Exxon AC-10	-30.28	-30.48	-28.12	-32.32
Exxon AC-20	-24.74	-25.10	-24.07	-24.20
GSAC AC-15P Base	-27.61	-27.88	-27.00	-27.79
Shell AC-20	-28.98	-28.15	-25.43	-25.43
GSAC AC-15P w/2% SBR	-28.57	-28.29	-23.56	-25.98
GSAC AC-15P w/4% SBR	-28.95	-28.79	-30.17	-33.49
GSAC AC-15P w/2% SBS	-28.98	-28.15	-32.52	-29.23
GSAC AC-15P w/4% SBS	-28.91	-27.44	-29.66	-34.53
GSAC AC-15P w/10% RSGF-20	-29.30	-28.84	-30.87	-29.63
GSAC AC-15P w/18% RSGF-20	-30.71	-29.61	-36.95	-37.13

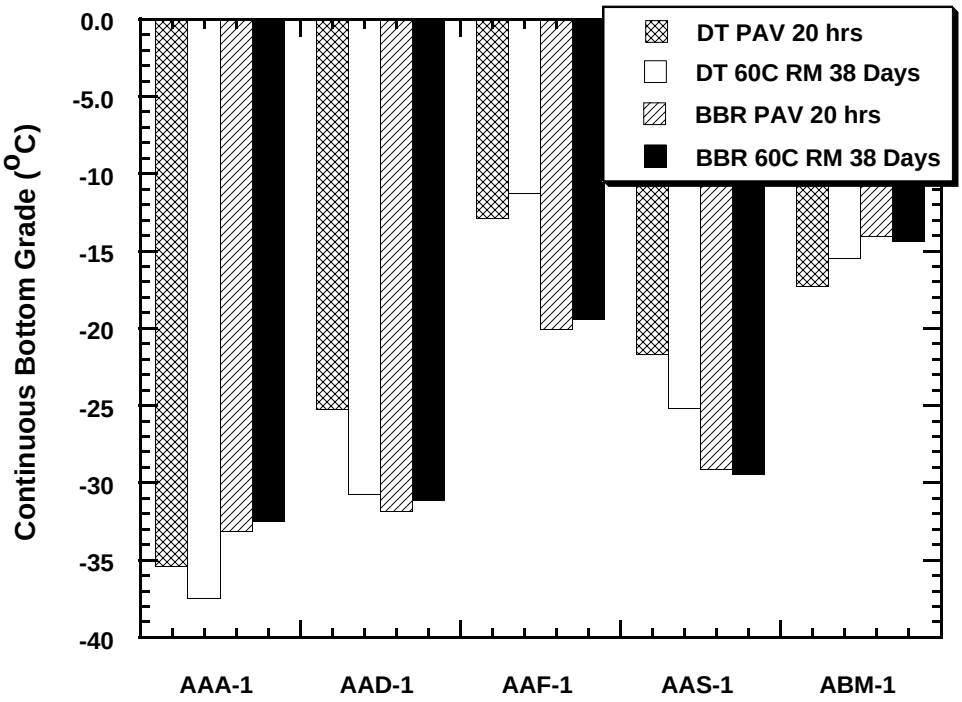

Figure 3-9. Bottom Continuous Grade Comparison for SHRP Asphalts.

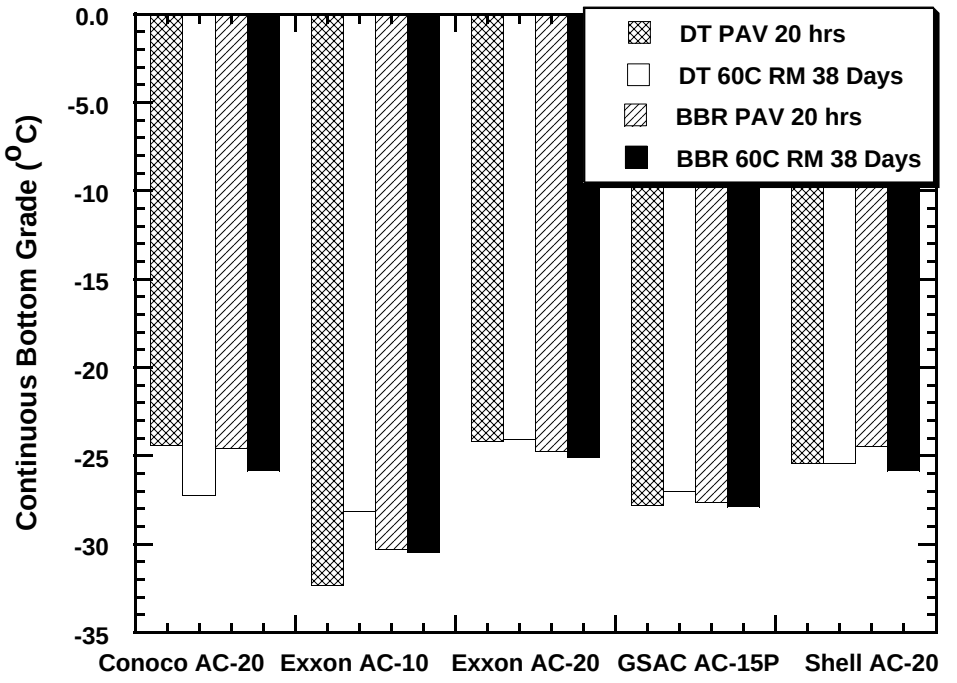

Figure 3-10. Bottom Continuous Grade Comparison for non-SHRP Asphalts.

Low-temperature physical property results for modified materials are presented in Figure 3-11. The modified materials' common base, GSAC AC-15P Base, is also included for comparative purposes. As shown, the BBR data for both Sets A and B are comparable, with the greatest variance being 1.47 °C for 4% SBS. There is considerably more scatter in the DTT data for the modified samples than for the unmodified samples. The reason is unknown.

Also of interest as far as low-temperature properties are concerned, is how the different aging mechanisms may have affected the way the asphalt is graded, particularly on the BBR. Specifically, does one method of aging make the PG limited by the m-value criterion whereas the other is limited by the stiffness criterion? Figure 3-12 presents data for m-value and S for sample Sets A and B. As seen in Figure 3-12 the data occur in pairs, which are the same material with the two different aging procedures. With the exception of data occurring very near the line, no sample seems to have changed from being S dominated or m dominated. As a group, the data show that S typically determines performance grade, rather than m.

As part of the Phase I project, the top performance grade was also obtained for all of the materials studied. Table 3-4 presents these data as well as the low-temperature performance grade obtained by the Superpave specifications for the PAV aged material. These data are intended as a characterization of the materials involved in this research and were not further investigated.

Phase II Results

In Phase II of this project the low-temperature properties for short-term aged samples (Set C) were compared with those of samples aged long term in hope of determining whether or not the long-term aging of a sample could be skipped without loss of accuracy when determining performance grade. As explained in the previous chapter, the same samples were used as in Phase I, and the samples were either RTFOT aged or air-blown according to the procedure developed by Vassiliev (2001). Table 3-5 lists the 60 °C viscosity for all of the unmodified materials and compares them to values obtained by RTFOT in Phase I. Table 3-6 presents the same data for modified materials.

For the most part the air-blowing values are comparable to the RTFOT values, the exceptions being the crumb rubber modified asphalts and AAF-1. In the case of the crumb rubber modified asphalts, the viscosity discrepancy is likely due to the fact that, unlike the RTFOT, the air-blowing apparatus allows the operator to recover most of the rubber in the sample. After RTFO aging of a sample a considerable portion of the rubber settles out during aging and remains stuck in the film of asphalt within the bottle after the test. The increased rubber concentration of the air-blown sample relative to the RTFOT would increase the viscosity while not necessarily increasing the aging of the sample. AAF-1 also seems to be quite different from the previous RTFOT value. This may be an error running the air-blowing apparatus or may simply be an outlying point. In any case, the sample was not rerun because no material was left from the original AAF-1 material used in this study.

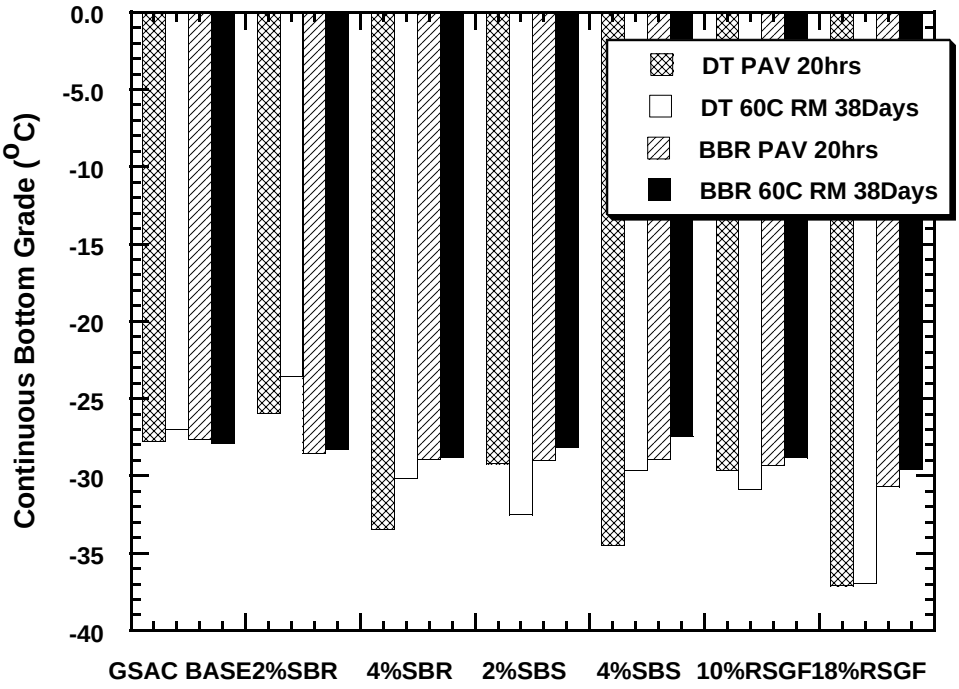

Figure 3-11. Bottom Continuous Grade Comparison for Modified Asphalts.

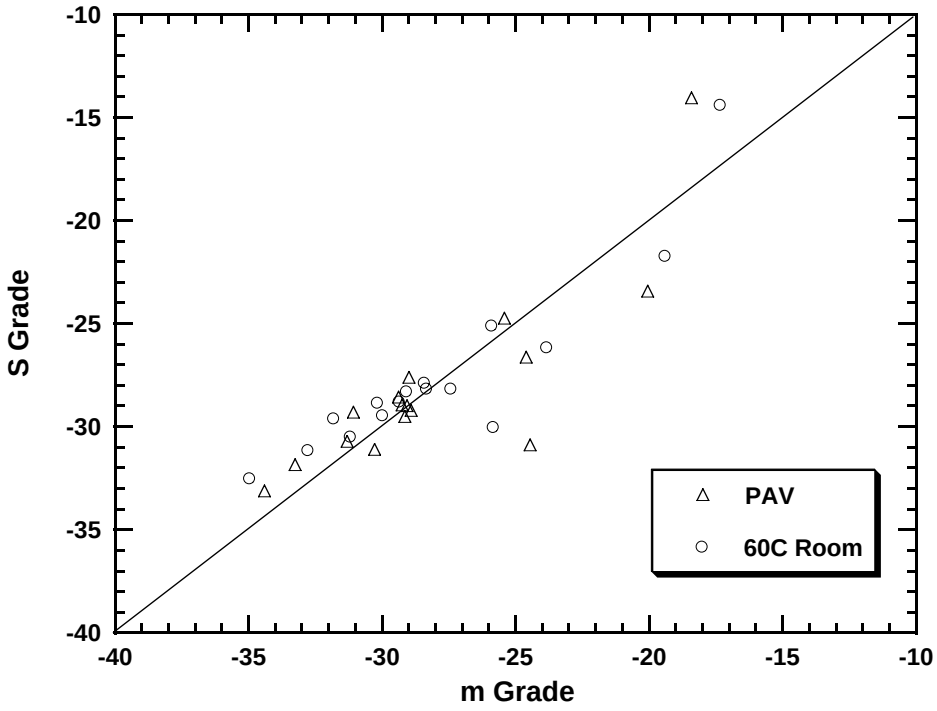

Figure 3-12. Comparison of m and S Continuous Grade for Sample Sets A and B.

Table 3-4. Overall Performance Grades.

Material	Overall PG
AAA-1	58-28
AAD-1	58-28
AAF-1	58-16
AAS-1	64-28
ABM-1	64-10
Conoco AC-20	64-22
Exxon AC-10	58-28
Exxon AC-20	64-22
GSAC AC-15P Base	52-22
Shell AC-20	64-22
GSAC AC-15P w/2% SBR	58-28
GSAC AC-15P w/4% SBR	58-28
GSAC AC-15P w/2% SBS	58-28
GSAC AC-15P w/4% SBS	58-34
GSAC AC-15P w/10% RSGF-20	58-28
GSAC AC-15P w/18% RSGF-20	58-34

Table 3-5. Comparison of 60 ºC Viscosity for Unmodified Materials Used in Phase II with RTFOT Values.

Materials	Method of Short-Term Aging	60 ºC Viscosity of Short-Term Aged Material	RTFOT 60 ºC Viscosity
AAA-1	RTFOT	2092	2177
AAD-1	Air Blown	4555	4341
AAF-1	Air Blown	5713	4723
AAS-1	Air Blown	5217	5012
ABM-1	Air Blown	5251	4937
Conoco AC-20	Air Blown	7016	6756
Exxon AC-10	RTFOT	2246	2007
Exxon AC-20	RTFOT	4630	4714
GSAC AC-15P Base	RTFOT	1266	1420
Shell AC-20	Air Blown	6505	7138

Table 3-6. Comparison of 60 ºC Viscosity for Modified Materials Used in Phase II with RTFOT Values.

Materials	Method of Short-Term Aging	60 ºC Viscosity of Short-Term Aged Material	RTFOT 60 ºC Viscosity
GSAC AC-15P w/2% SBR	RTFOT	2455	2905
GSAC AC-15P w/4% SBR	RTFOT	3651	3689
GSAC AC-15P w/2% SBS	RTFOT	2305	2191
GSAC AC-15P w/4% SBS	RTFOT	4339	4367
GSAC AC-15P w/10% RSGF-20	Air Blowing	2152	3526
GSAC AC-15P w/18% RSGF-20	Air Blowing	2572	3630

One of the first tests performed on the short-term aged samples was the bending beam rheometer determination of the continuous bottom performance grade. Figure 3-13 illustrates this comparison for the SHRP asphalts. It is interesting to note here that although the AAF-1 sample showed a higher viscosity than the RTFOT sample, the continuous bottom grade is still significantly better than the long-term aged samples. For the remainder of the samples, it is apparent that although the short-term aged material has a better grade, the grade is typically only 3 or 4 degrees better.

Figure 3-14 presents BBR data for the non-SHRP unmodified asphalts studied. Again in this plot all of the short-term aged materials provide bottom grades that are better than their long-term aged counterparts. For the three middle asphalts, Exxon AC-10, Exxon AC-20, and GSAC AC-15P Base, the continuous grades of Set C are very close to those of the long-term aged materials. Shell AC-20 and Conoco AC-20, the two asphalts which showed the highest viscosities after aging (Figure 3-6), show a considerably different grade, with Conoco AC-20 being 6.65 degrees different.

BBR data for modified materials are given in Figure 3-15, with the common base, GSAC AC-15P included as well for comparison. As shown, the modified materials behave just as the base material does, showing a better bottom grade for short-term aging, although not dramatically better. This may suggest that in the case of modified asphalts, that long-term aging could be justifiably skipped when obtaining performance grades. While the data clearly indicate that this is true for this case, an alternate conclusion may be appropriate. Rather than suggesting that all modified asphalts can be graded without long-term aging, the data suggest that the modified asphalt mimics the aging characteristics of the base. If, for example, Conoco AC-20 from Figure 3-14 was modified with these same additives, it is likely that the bottom grade difference between the short-term and long-term aged material would be just as significant as for the unmodified Conoco AC-20. Repeating the experiments with other bases and the same modifiers would allow for a more accurate assessment.

In Phase II the continuous bottom grade as obtained by the DTT was also studied for short-term aged materials. Figure 3-16 presents the results of this investigation for unmodified SHRP materials. As with the BBR measurements, all of the short-term aged material demonstrated better performance grades. The DTT data show significant differences for AAD-1, AAF-1, and AAS-1 in terms of variance from the long-term aged values. AAA-1 and ABM-1 short-term bottom grades are similar to their long-term aged counterparts.

Data for non-SHRP materials are presented in Figure 3-17. As with the SHRP materials, all show a better low-temperature PG for the short-term aged material, but some vary more drastically than others. Exxon AC-10, for example, shows a high degree of variance from the long-term aged material while Exxon AC-20 seems to show almost no difference at all.

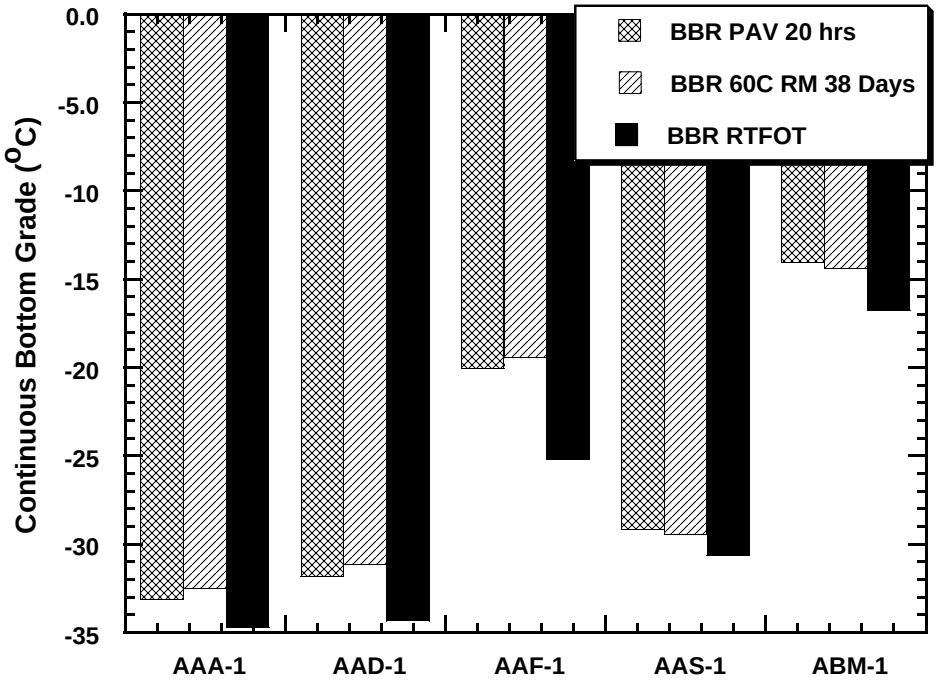

Figure 3-13. Comparison of Continuous Bottom Grade as Measured Using the BBR for Short-Term and Long-Term Aged SHRP Materials.

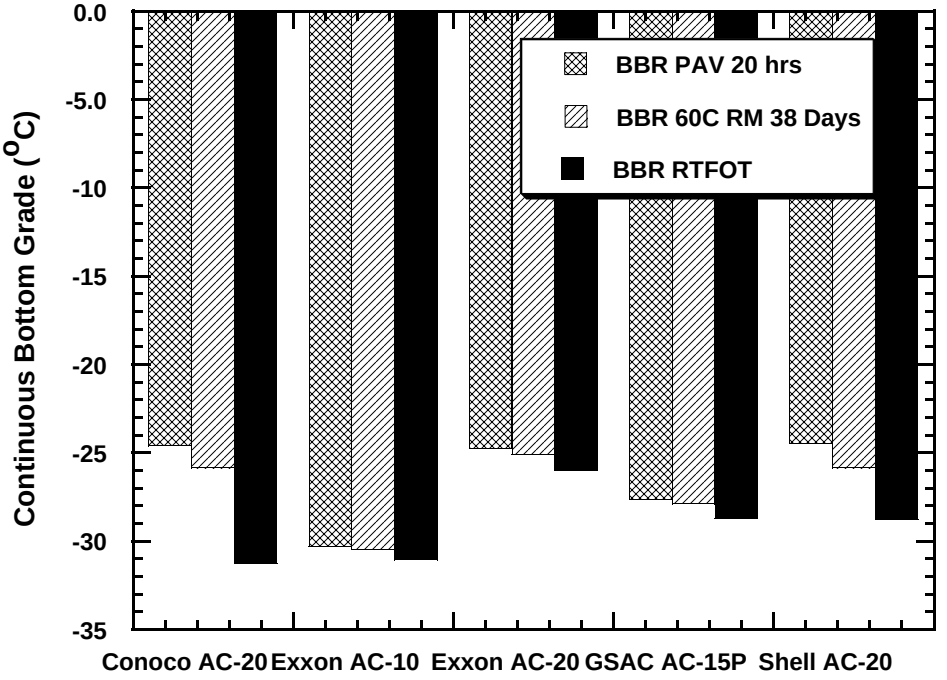

Figure 3-14. Comparison of Continuous Bottom Grade as Measured Using the BBR for Short-Term and Long-Term Aged Non-SHRP Materials.

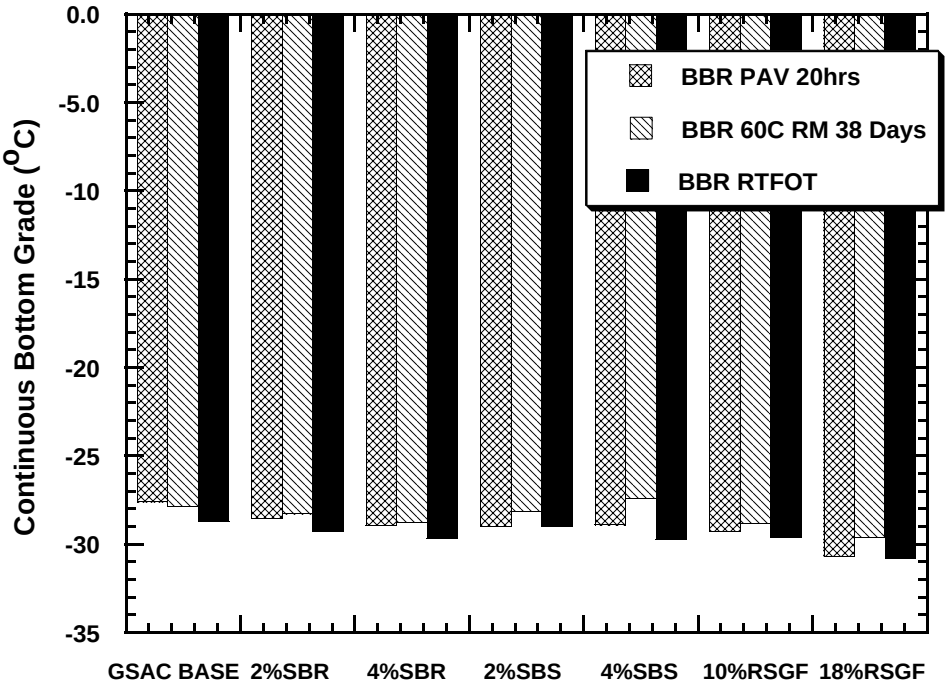

Figure 3-15. Comparison of Continuous Bottom Grade as Measured Using the BBR for Short-Term and Long-Term Aged Modified Materials.

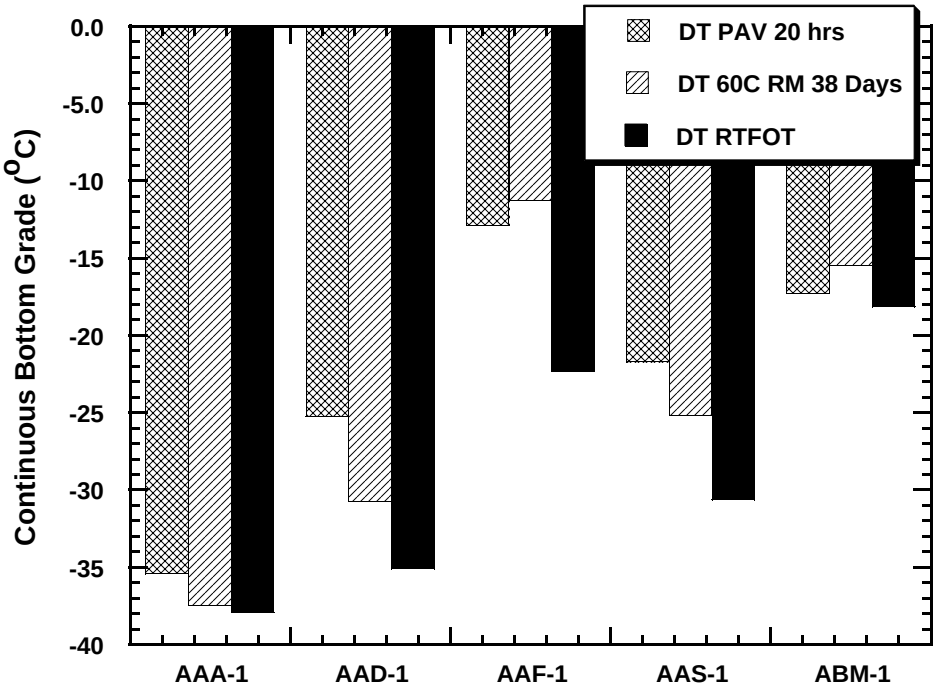

Figure 3-16. Comparison of Continuous Bottom Grade Measured Using the DTT for Short-Term and Long-Term Aged SHRP Materials.

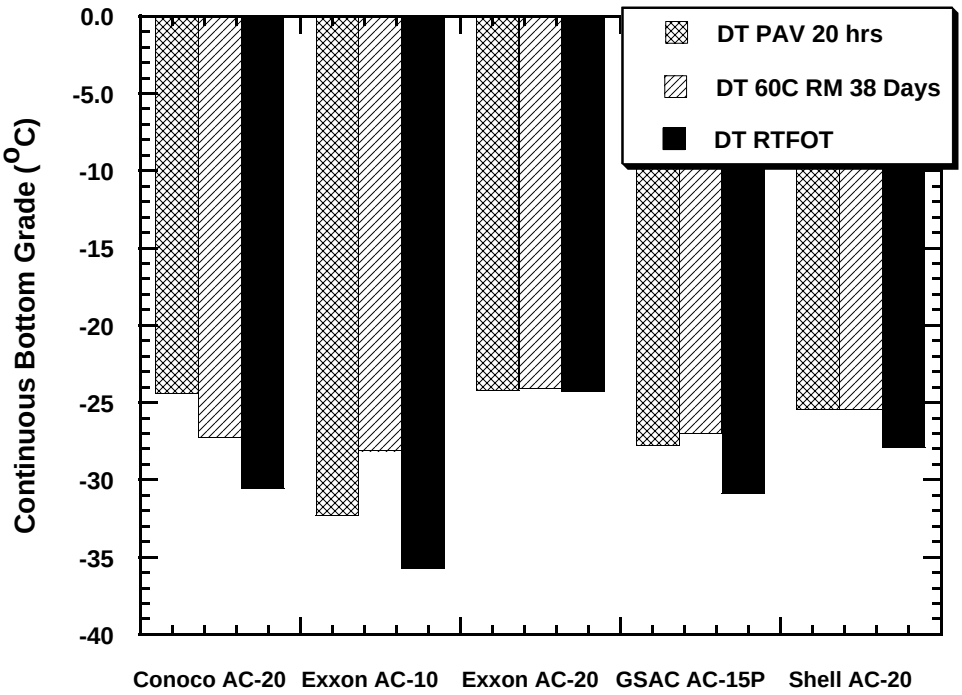

Figure 3-17. Comparison of Continuous Bottom Grade Measured Using the DTT for Short-Term and Long-Term Aged non-SHRP Materials.

DTT data for modified materials are presented in Figure 3-18. Again, this plot indicates that the modified materials behave in a similar fashion to the base material. For most of these materials, a significant difference is seen between the long-term and short-term aged materials.

A summary of the results of Phase II is presented in Figures 3-19, 3-20, and 3-21. These plots are included to enable comparison between the DTT and BBR continuous bottom grades. For the unmodified materials, the scatter in the DTT data makes it difficult to come to solid conclusions regarding the performance of the DTT data versus the BBR. For modified materials it seems that the DTT data typically give a better performance grade and therefore should be run for all modified materials.

It is also instructive to determine whether or not a correction for low-temperature performance grade can be determined by another parameter that would enable one to skip the long-term aging test. In order to do this it would be beneficial to find a parameter that may be measured while obtaining the top grade of the material. Figure 3-22 shows the difference between the PG of the PAV long-term aged set (PG_{LT}) and the PG of the short-term aged set (PG_{ST}) as measured on the BBR, as a function of the unaged viscosity of the material (Table 3-1). As can be seen from the plot, all of the softer asphalts show little difference between long-term and short-term performance grades. Harder asphalts tend to show more difference, but in some cases, such as AAS-1 and Exxon AC-20, the harder asphalts are still within 2 degrees of the

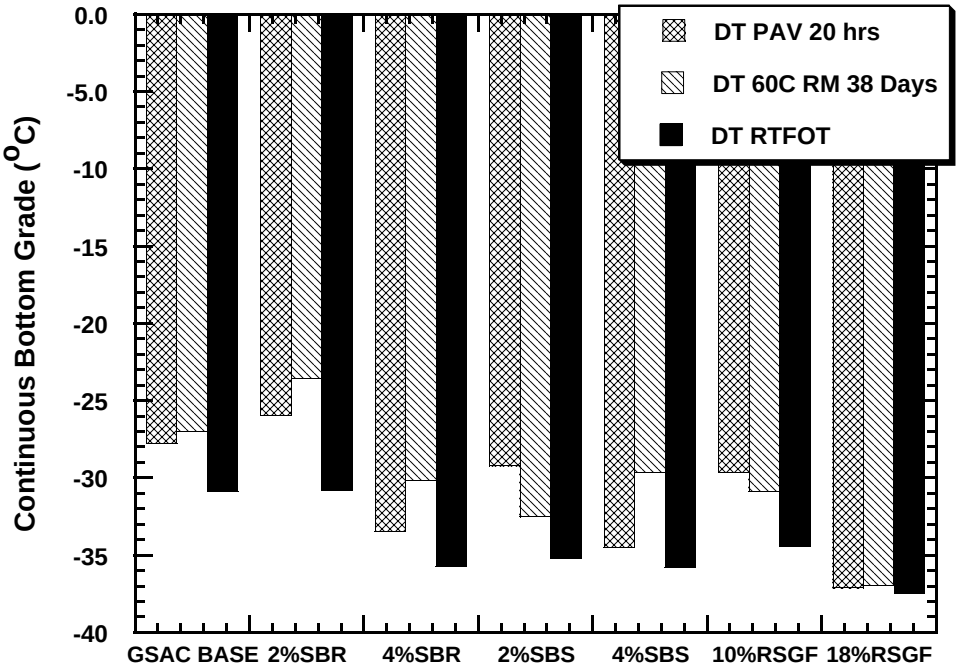

Figure 3-18. Comparison of Continuous Bottom Grade as Measured Using the DTT for Short-Term and Long-Term Aged Modified Materials.

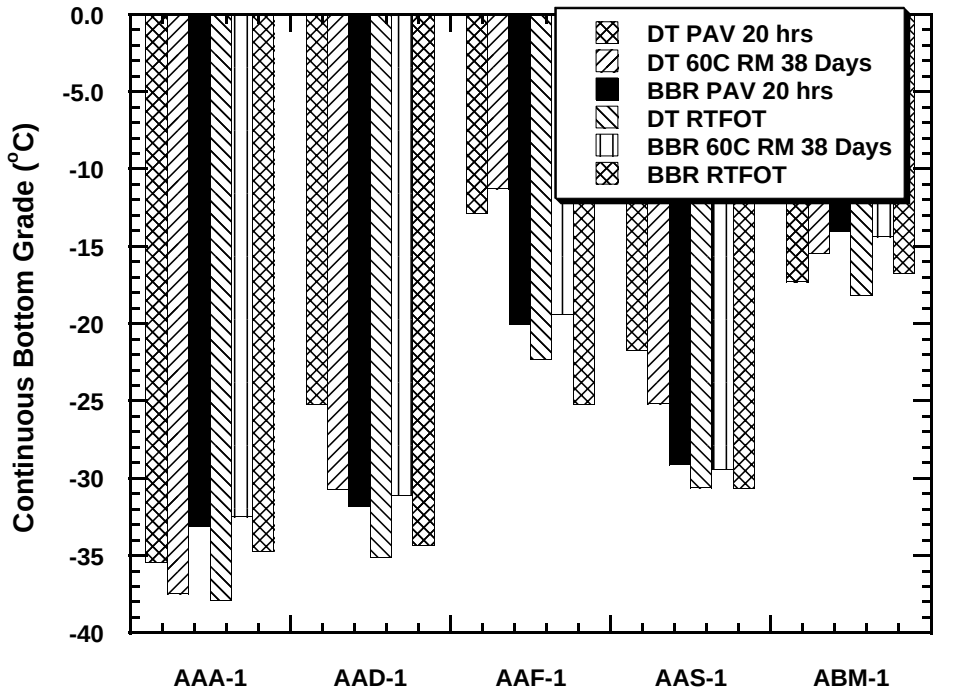

Figure 3-19. Comparison of Continuous Bottom Grade for Short-Term and Long-Term Aged SHRP Materials.

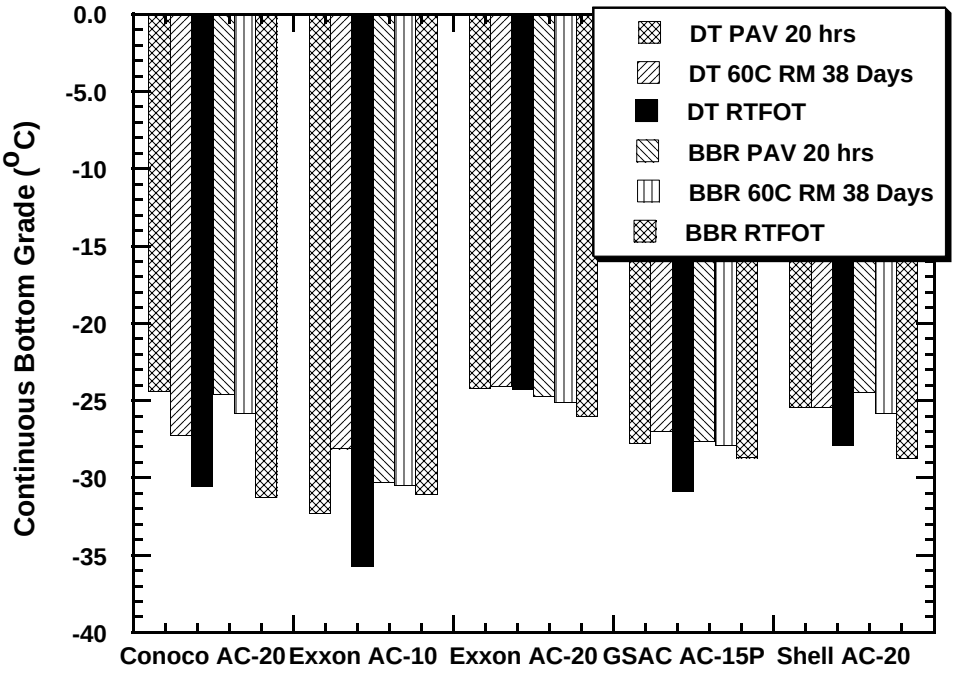

Figure 3-20. Comparison of Continuous Bottom Grade for Short-Term and Long-Term Aged non-SHRP Materials.

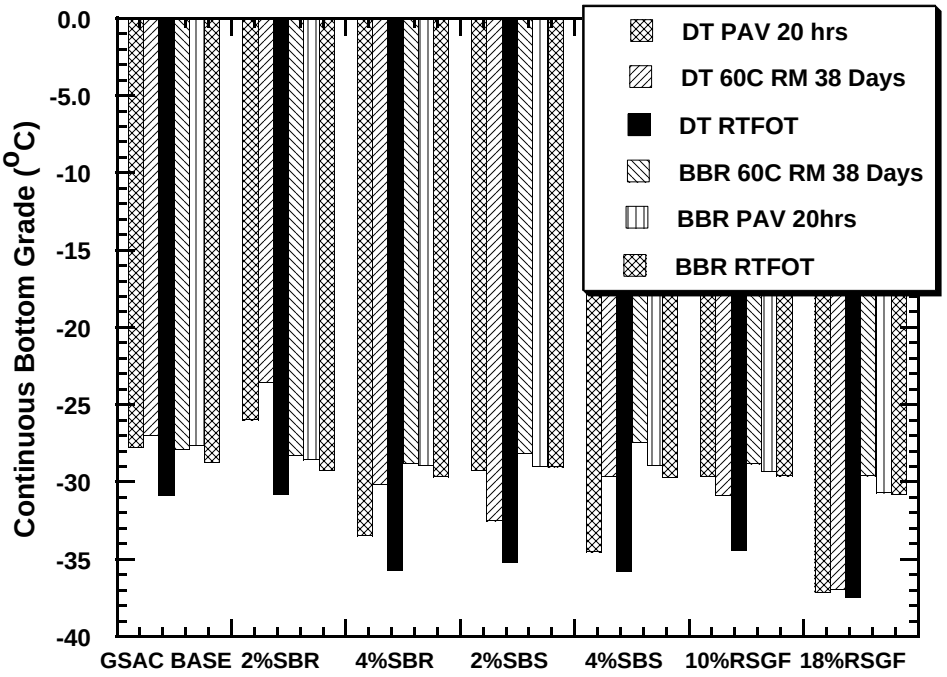

Figure 3-21. Comparison of Continuous Bottom Grade for Short-Term and Long-Term Aged Modified Materials.

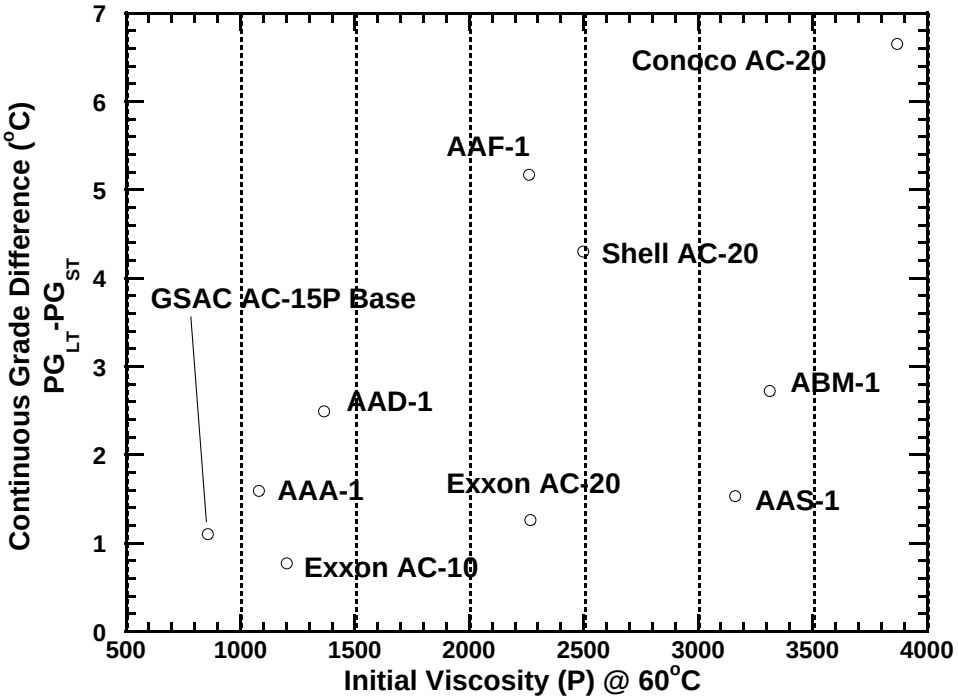

Figure 3-22. Bottom Continuous Performance Grade Difference between PAV Long-Term Aged Material and Short-Term Aged Material as a Function of Initial Viscosity.

long-term aged bottom grade. It is also interesting to note that all the asphalts studied provided grade differences of less than 7 degrees.

Figure 3-23 shows the correlation between the continuous bottom grade difference and $G^*/\sin(\delta)$ at 58 °C for the RTFOT aged material, a parameter measured to obtain the top performance grade of a material. As shown in Figure 3-23, an exponential relationship fits the data rather well. It seems that a $G^*/\sin(\delta)$ value of less than 6000 Pa would allow one to skip the long-term aging test and obtain the bottom grade on the RTFOT aged material only without gross error. This procedure is only recommended if time cannot be spared for the long-term test. The operator may also wish to performance grade the short-term aged material and simply add the given correction function value to the obtained grade. From the plot, the correction factor is obtained using the following equation:

$$C = 0.6225 \exp\left(0.0002095 G^*/\sin(\delta)\right) \quad (3\text{-}3)$$

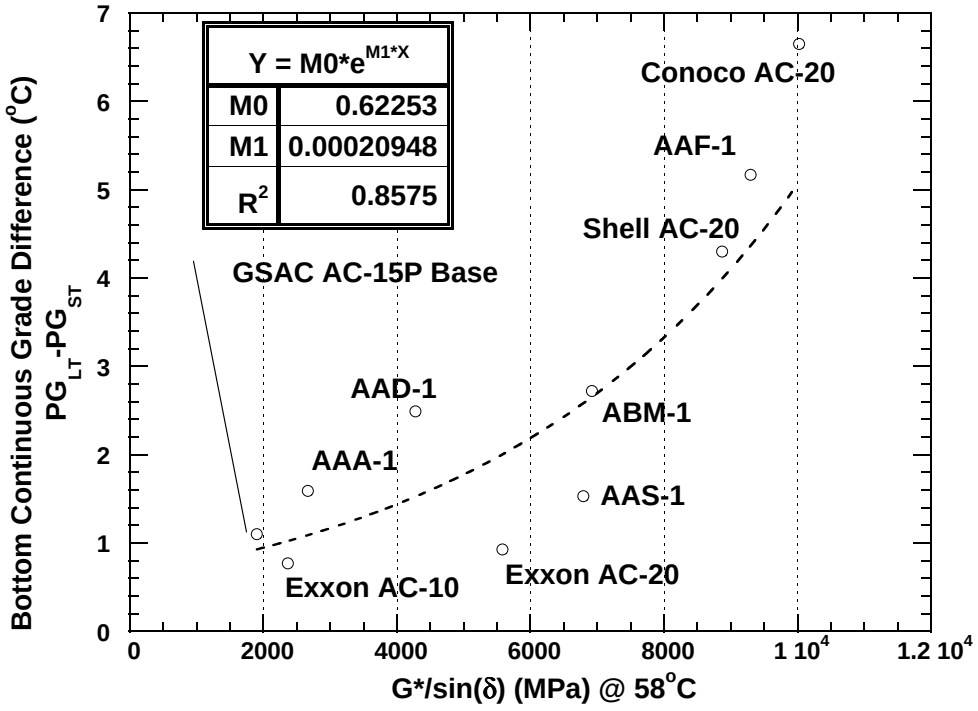

Figure 3-23. Bottom Continuous Performance Grade Difference between PAV Long-term Aged Material and Short-Term Aged Material as a Function of $G^*/\sin(\delta)$ at 58 °C and 10 rad/s.

Where $G^*/\sin(\delta)$ is measured at 58 °C and 10 rad/s on the RTFOT aged material. The low-temperature PG for the long-term aged material can be estimated from the short-term aged PG using the correction factor:

$$PG_{LT} = PG_{ST} + C \qquad (3\text{-}4)$$

Table 3-7 lists the measured low-temperature performance grades for the long-term aged materials as well as those estimated from the short-term aged materials using the correction factor. The absolute error is always within ±1.6 °C. More importantly, in all cases the estimated PG value is identical to the measured PG value, indicating that despite errors the estimation method can produce accurate low-temperature PG values. The convenience of this estimation method should not overshadow the fact that it is a rough correlation and is not intended to replace the proper SHRP specification method, which calls for long-term aging of material before low-temperature performance grading.

Table 3-7. Comparison between Estimated and Experimental PAV Bottom Performance Grades.

Material	$\frac{G}{\sin(\delta)}$	RTFO Grade (°C)	PAV Grade (°C)	PAV Grade Estimate (°C)	Error (°C)	% Error	PAV PG (°C)	Est'd PAV PG (°C)
AAA-1	2665.3	-34.71	-33.12	-33.62	0.502	-1.52%	-28	-28
AAD-1	4276.8	-34.34	-31.85	-32.82	0.965	-3.03%	-28	-28
AAF-1	9298.2	-25.22	-20.05	-20.85	0.804	-4.01%	-16	-16
AAS-1	6793.2	-30.67	-29.14	-28.09	-1.053	3.61%	-28	-28
ABM-1	6920.3	-16.77	-14.05	-14.12	0.067	-0.48%	-10	-10
Conoco AC-20	10024	-31.25	-24.6	-26.17	1.567	-6.37%	-22	-22
Exxon AC-10	2365.9	-31.05	-30.28	-30.03	-0.252	0.83%	-28	-28
Exxon AC-20	5581.9	-25.664	-24.74	-23.66	-1.080	4.37%	-22	-22
GSAC AC-15P	1901.6	-28.71	-27.61	-27.78	0.173	-0.63%	-22	-22
Shell AC-20	8870.4	-28.75	-24.45	-24.76	0.308	-1.26%	-22	-22

Phase III Results

As mentioned in the methodology section, five asphalts were aged for extended periods to determine the effect of extended aging on relative ranking of asphalts. The five asphalts studied were Exxon AC-10, Exxon AC-20, Shell AC-20, AAF-1, and AAS-1. This section presents data relating to performance grade changes with aging time, as well as changes in m-value and stiffness with aging. The section concludes with a discussion of how the m and S criteria determine performance grade for a variety of aging times.

Figure 3-24 depicts the bottom grade of each sample as a function of aging time. Zero aging time in the figure represents the continuous bottom grade of the RTFOT aged sample. As can be seen in the figure the relative rankings of asphalts do change with aging time. The Exxon AC-20 sample and the Shell AC-20 sample provide the best illustration of this phenomenon.

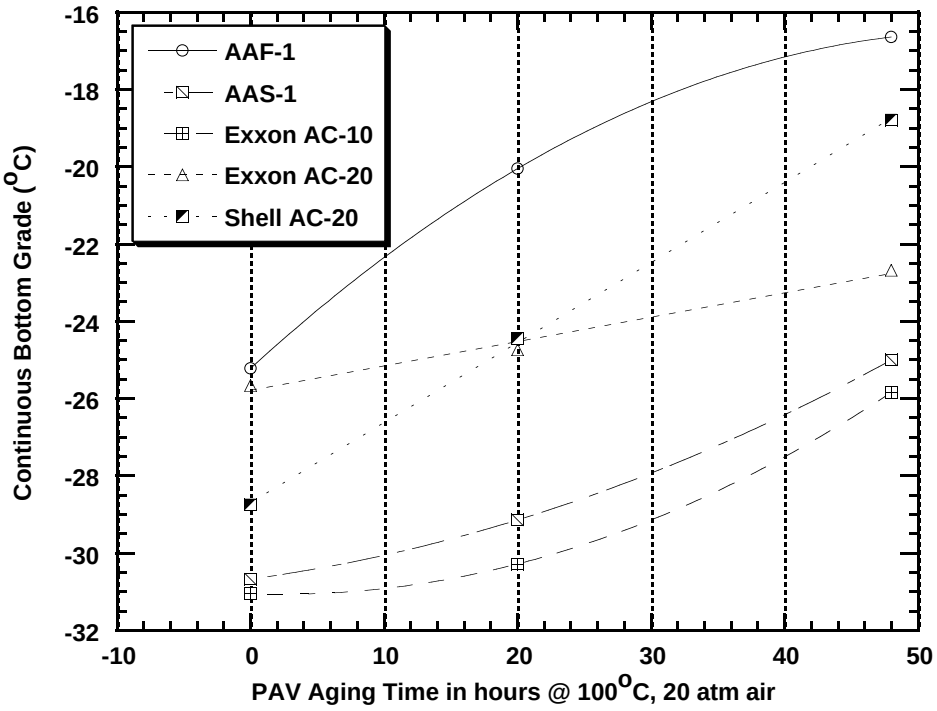

Figure 3-24. Continuous Bottom Grade as a Function of PAV Aging Time.

Before PAV aging Shell AC-20 shows a continuous bottom grade that is about 2 degrees lower than that of Exxon AC-20. After 20 hours of PAV aging, the grades are very similar, both being around −24.5 ºC. After 48 hours of PAV aging, Exxon AC-20 displays a better bottom grade by about 4 ºC.

From Figure 3-24, one may conclude that the relative ranking of asphalts will change depending upon the specified aging time. This indicates that the Superpave long-term aging specifications result in an arbitrary ranking of asphalts with respect to low-temperature properties. Figure 3-24 clearly shows that the low-temperature physical properties of Exxon AC-20 are much less affected by aging than those of Shell AC-20. Exxon AC-20 therefore is more resistant to the effects of aging on low-temperature properties, but, from the current Superpave specification, they would be given identical low-temperature grades.

Agreeing with the work of Domke (1999), Figures 3-25 through 3-28 depict how stiffness and m-value change as a function of aging time. The line in each figure indicates the Superpave specification; the sample must have an m-value greater than 0.300 and a stiffness of less than 300 MPa. Figure 3-25 shows that, for AAF-1, the m-value decreases steadily with aging time. Stiffness, as shown in Figure 3-26, increases with increased aging time. Figures 3-27 and 3-28 depict the variation of m-value and stiffness for Exxon AC-20.

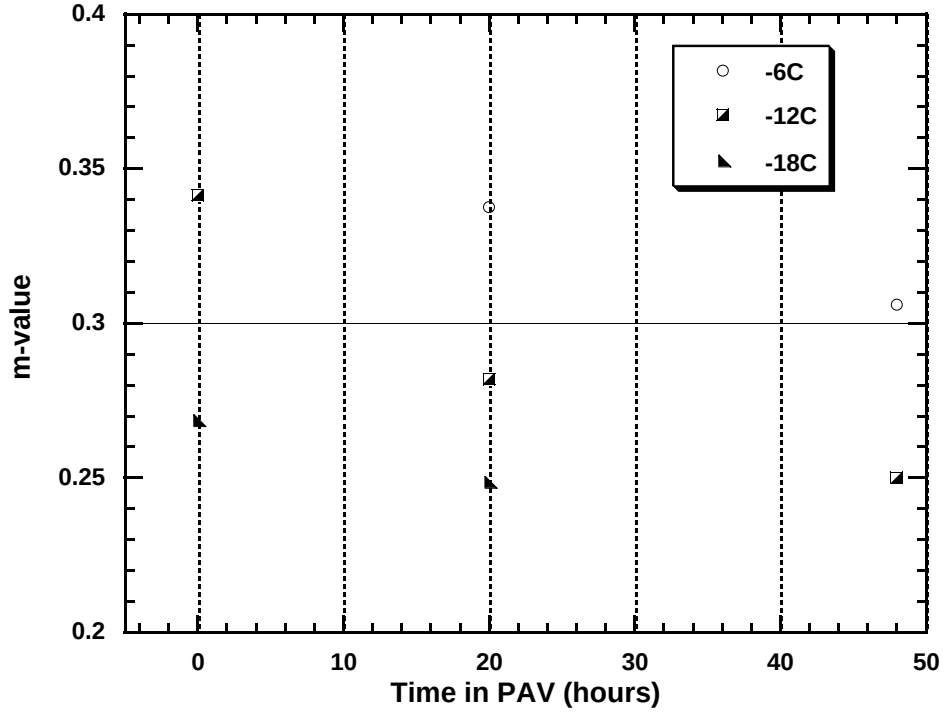

Figure 3-25. m-Value as a Function of Aging Time for AAF-1.

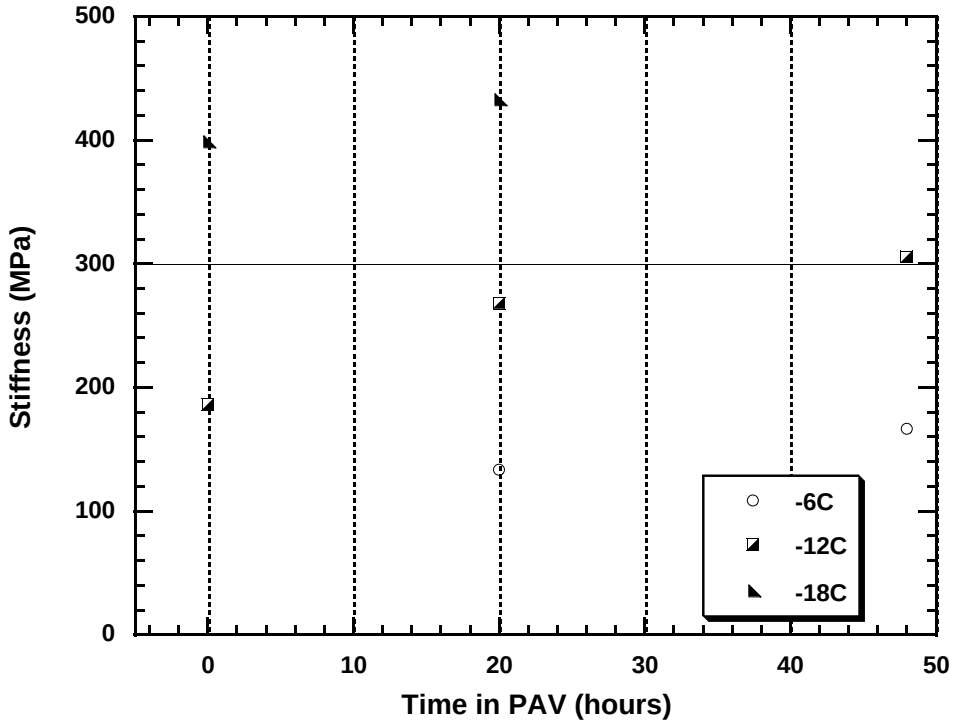

Figure 3-26. Stiffness as a Function of Aging Time for AAF-1.

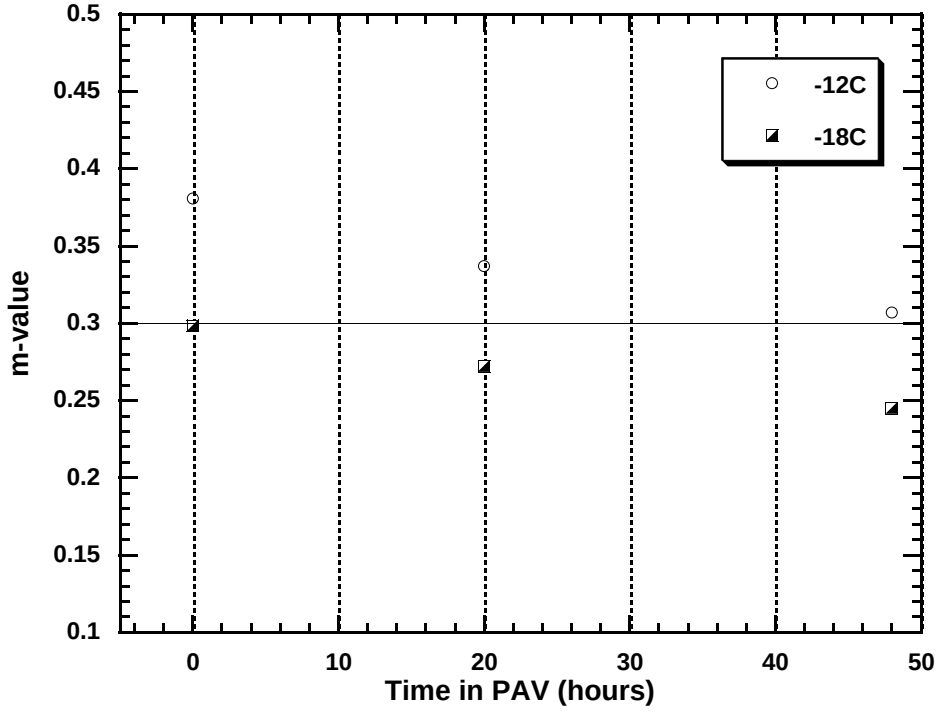

Figure 3-27. m-Value as a Function of Aging Time for Exxon AC-20.

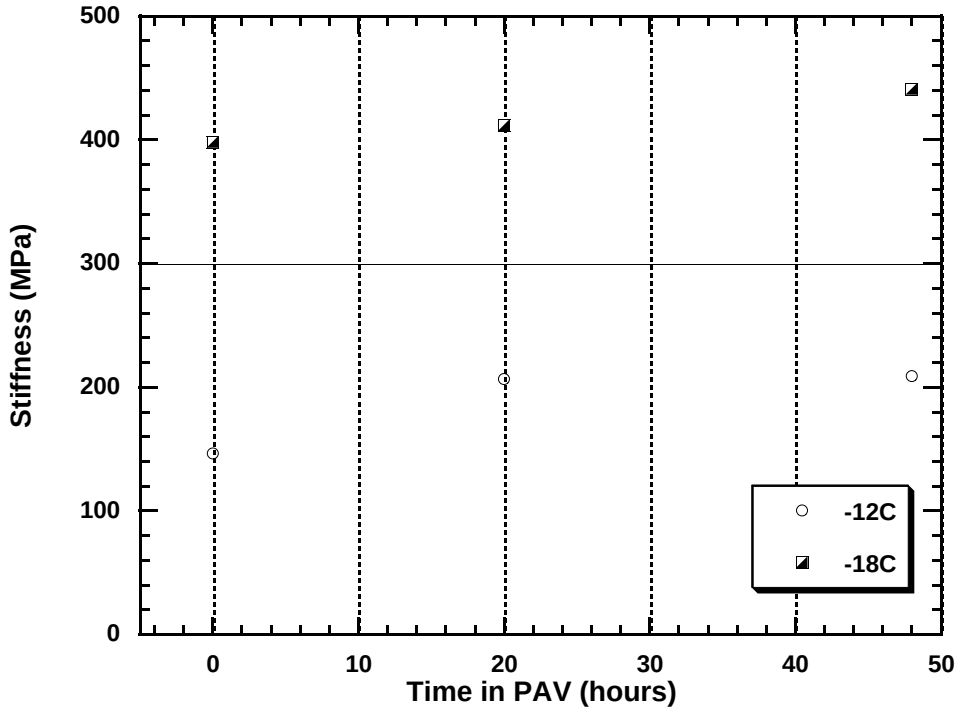

Figure 3-28. Stiffness as a Function of Aging Time for Exxon AC-20.

Another interesting result of this work is that, since the Superpave specification has two requirements which must be satisfied, the bottom PG of an asphalt is determined predominantly by stiffness at shorter aging times and m-value at longer aging times. Figure 3-29 shows that a performance grade obtained for short-term aged material is dictated by the stiffness criterion. In contrast, material aged for 48 hours in the PAV was limited by the m-value criterion. Materials aged for 20 hours in the PAV, like materials aged 38 days in the 60 °C room may be limited by either criterion, depending upon the material. Since the clutter in Figure 3-29 makes it hard to determine the change in grading for a specific asphalt, Figure 3-30 has been included. This plot depicts the change in m grade and S grade for two asphalts, AAS-1 and Exxon AC-20. As shown in Figure 3-30, the grades move linearly with aging from being limited by stiffness at short aging times, to being limited by m-value at longer aging times.

Air Blowing as a Long-Term Aging Test

Another objective of this research was to determine if a suitable long-term aging test could be developed by air-blowing asphalt. It was hypothesized that the kinetics involved in air-blowing would match those of road conditions more closely because air-blowing is carried out at atmospheric pressure. The air-blowing procedure used was described in the aging procedures section. Infrared spectroscopy and GPC were used to analyze the resulting samples to determine if they were comparable in carbonyl area and molecular weight to those obtained from 60 °C room aging and PAV aging. Ideally, an air-blowing procedure would produce viscosities, carbonyl areas and GPC results similar to those of the 60 °C room. In this project an attempt was made to find a time at which air-blowing produced carbonyl areas and viscosities similar to those obtained from RTFOT and 38 days aging in the 60 °C room. The air-blown samples were short-term aged before being air-blown for extended periods of time.

Of the asphalts used in the first three phases of this project, Exxon AC-10, Exxon AC-20 and Shell AC-20 were all air-blown for 20 hours following the short-term air-blowing procedure. Figure 3-31 depicts the carbonyl region of the Fourier transform infrared (FTIR) spectrum of Shell AC-20 for the various aging methods used. Viscosities are included in the legend for comparison. As shown, the viscosity produced by air-blowing the sample was similar to that obtained in the environmental room. The carbonyl areas, however, were quite different. This difference may indicate that a different oxidation mechanism is at work for the air-blowing procedure.

Figure 3-32 provides the FTIR spectra for Exxon AC-10 in the carbonyl region. As shown for this asphalt the carbonyl area of the air-blown sample agrees quite well with that of the 60° C room, but the viscosity obtained is still considerably different, and no better than that obtained from the PAV. Figure 3-33 shows the FTIR spectra for Exxon AC-20. As with Shell AC-20, the viscosity obtained is similar to that of the environmental room, but the carbonyl area is significantly lower.

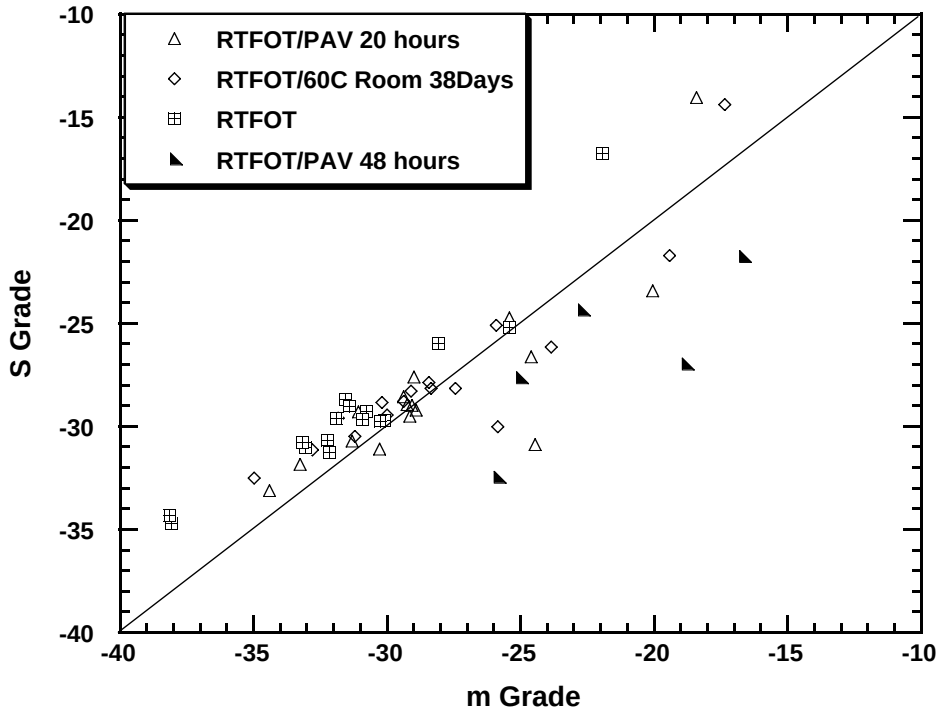

Figure 3-29. Comparison of m-Value Grade and S Grade for Materials at Various Aging Times.

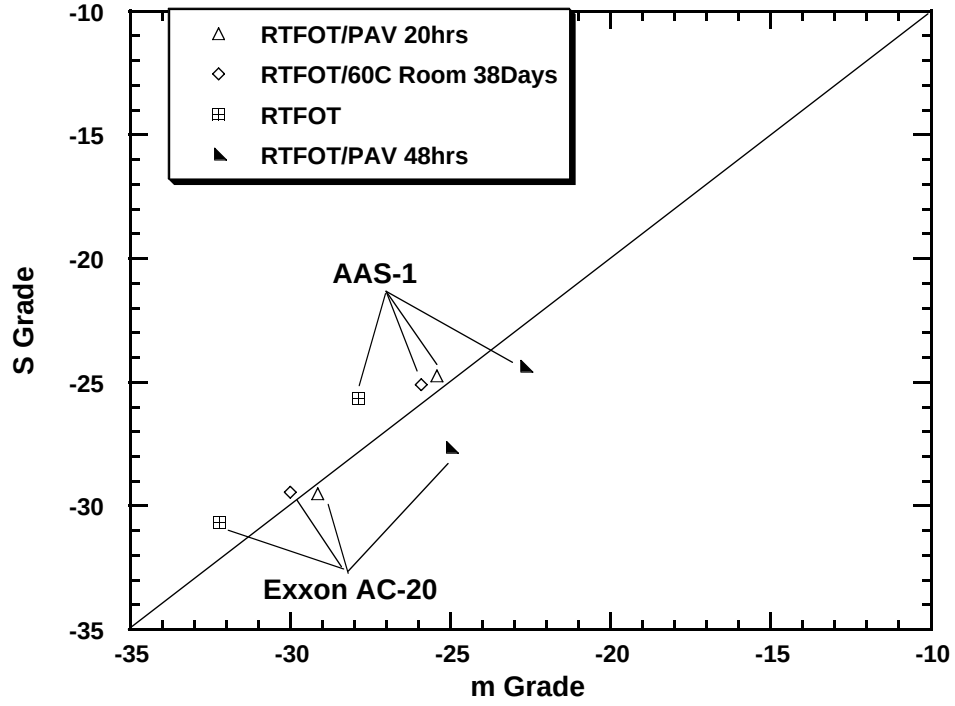

Figure 3-30. Comparison of m-Value Grade and S Grade for AAS-1 and Exxon AC-20 at Various Aging Times.

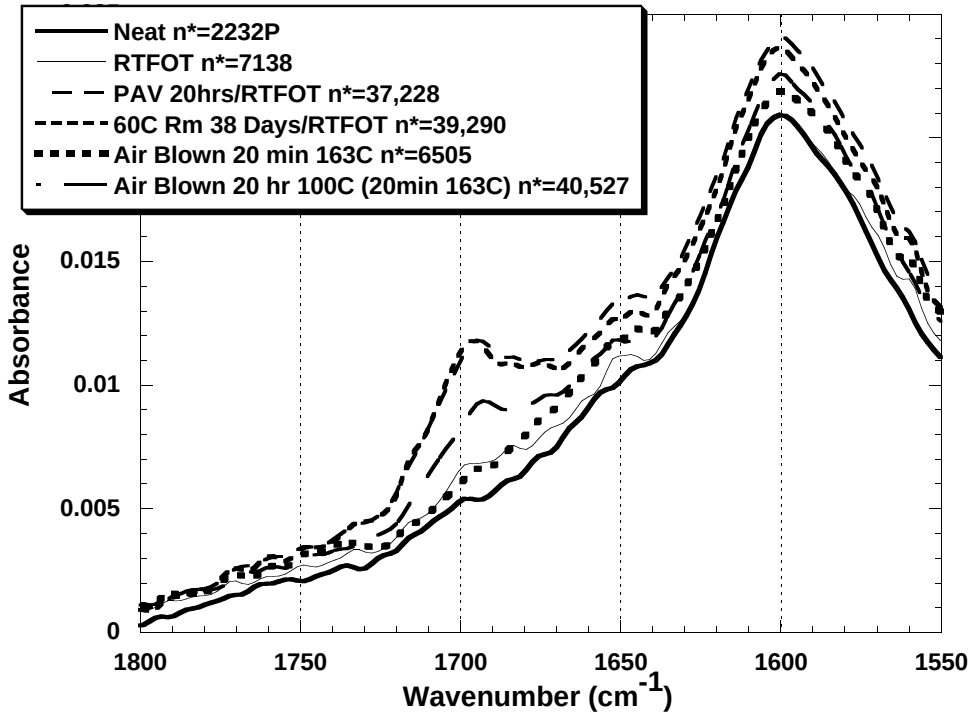

Figure 3-31. FTIR Spectra for Shell AC-20 for Various Aging Procedures.

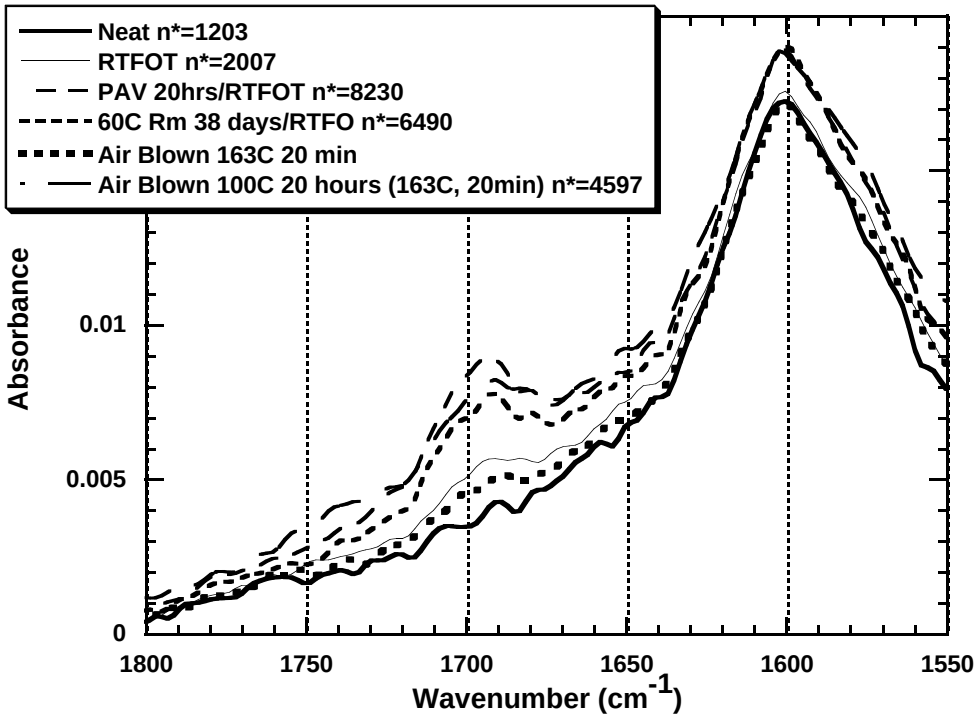

Figure 3-32. FTIR Spectra for Exxon AC-10 for Various Aging Procedures.

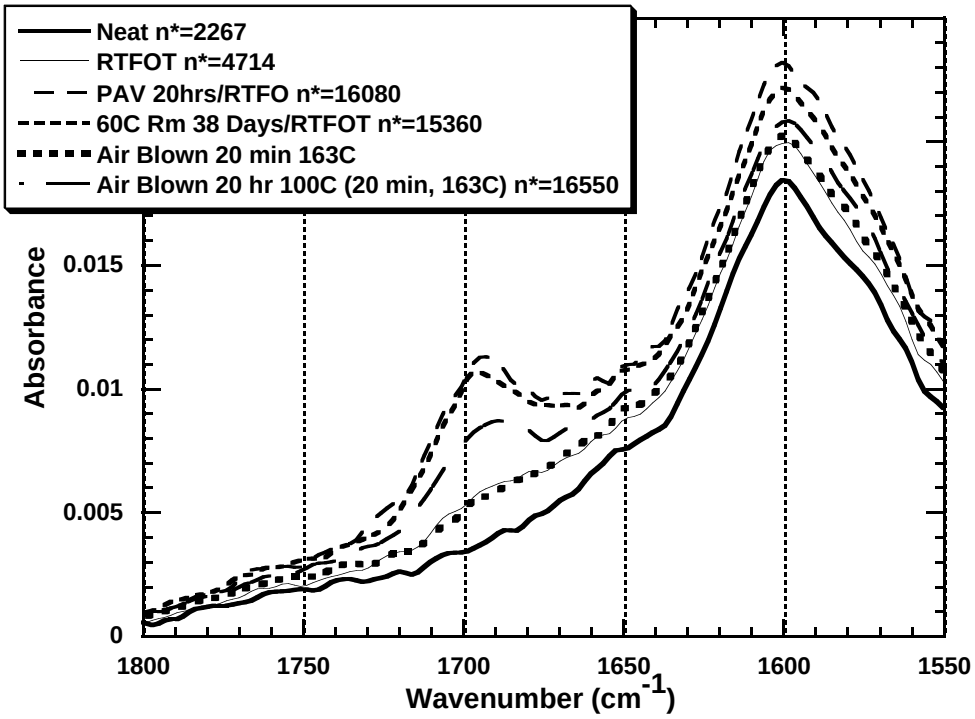

Figure 3-33. FTIR Spectra for Exxon AC-20 for Various Aging Procedures.

Several other asphalts were air-blown at various times and compared with RTFOT and 20 hour PAV aged material. As discussed in the results of Phase I, the PAV results should be similar to those obtained in the environmental room. Figure 3-34 shows that air blowing at 20 hours gives good agreement with PAV aged material both in viscosity and carbonyl area for AAS-1. Figure 3-35 indicates good agreement as well, but for an air-blowing time of 30 hours rather than 20 hours.

Since the air-blowing was taking place at elevated temperatures and high air flow rates, it was thought possible that volatilization and not oxidation was accounting for some of the viscosity increase in the samples. This would also explain why, in the cases of Exxon AC-20 and Shell AC-20, a similar viscosity was reached upon air-blowing, but a much lower carbonyl area was observed. In order to determine if this was the case, the Shell AC-20 samples were analyzed by GPC. The GPC results are presented in Figure 3-36. As shown, the air-blown sample shows asphaltene growth similar to that of the environmental room and the PAV. Also, the sample does not show significant differences in the lower molecular weight (higher time) region. Therefore, volatilization is not likely to be significantly affecting the viscosity increase.

Upon examining the data obtained by long-term air blowing of the samples, it was concluded that air-blowing is not a suitable long-term test. Air blowing did not provide carbonyl area data which were consistently in line with data obtained from the environmental room.

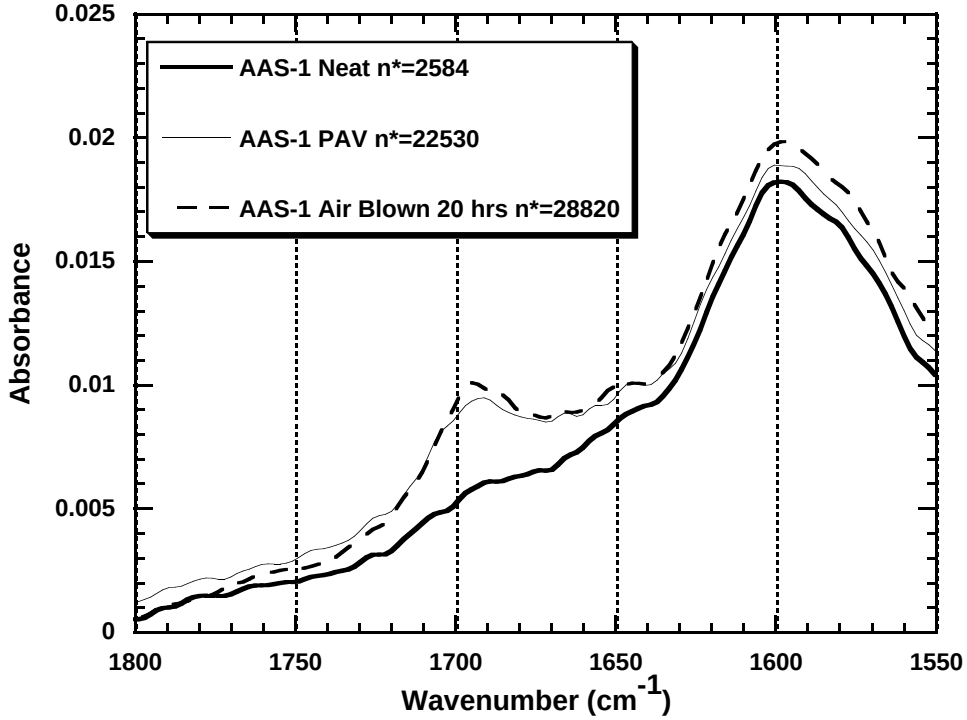

Figure 3-34. FTIR Spectra for AAS-1 for Various Aging Procedures.

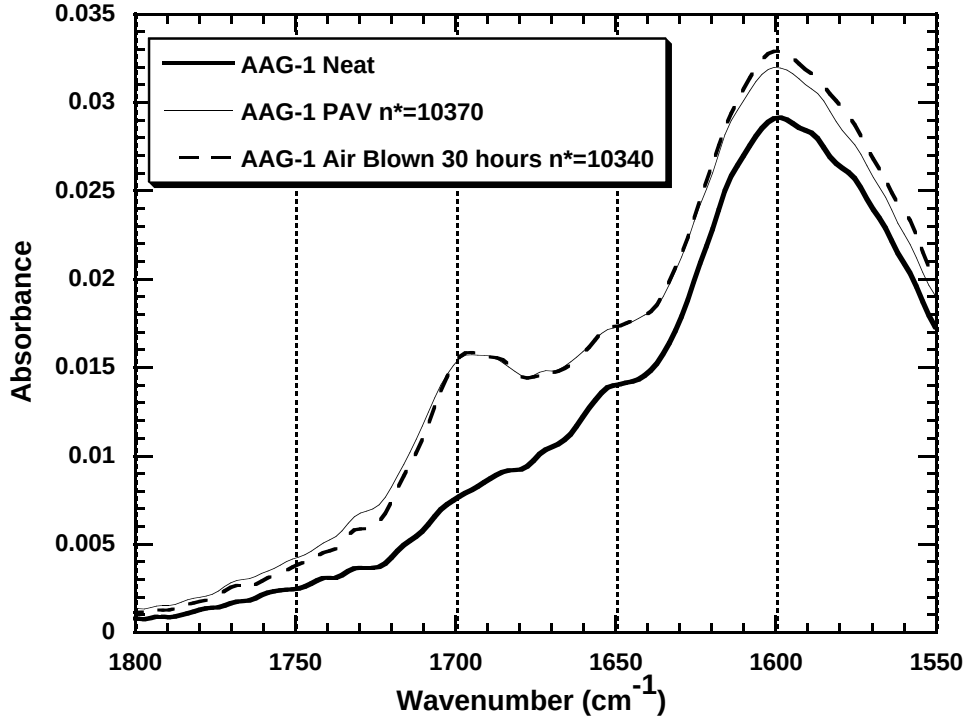

Figure 3-35. FTIR Spectra for AAG-1 for Various Aging Procedures.

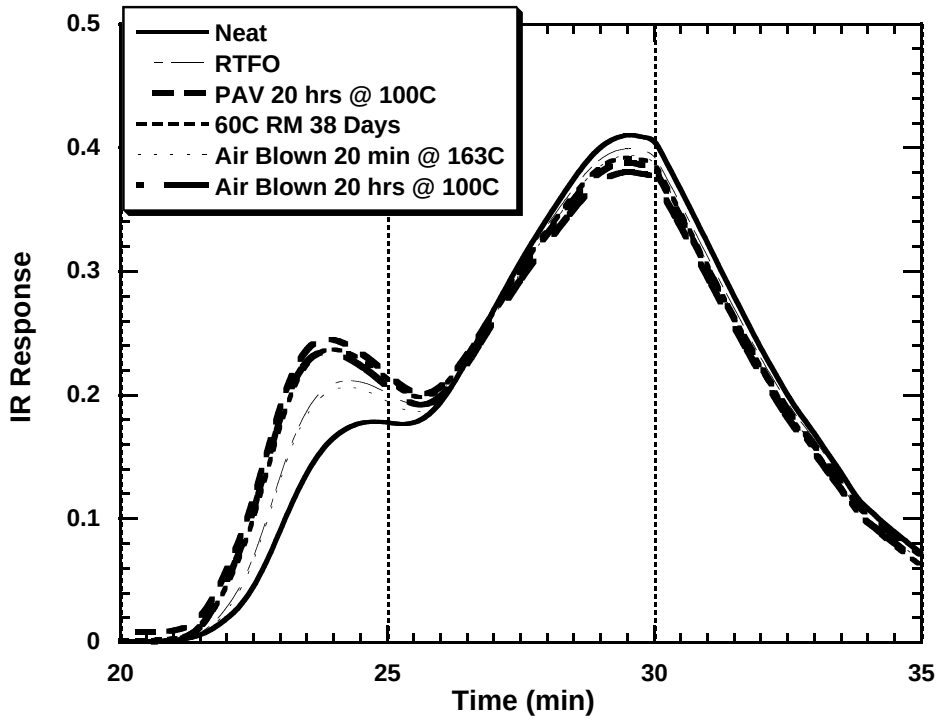

Figure 3-36. GPC Results for Shell AC-20 for Various Aging Procedures.

Several samples showed a similar viscosity while the carbonyl areas were drastically different. In addition, no time could be established where air blowing seemed to be identical to either the PAV or the environmental room aging procedures. The air-blowing test was also very difficult to run. Because high-temperature asphalt was being agitated at high rpm the apparatus could not be left on overnight unattended. This made the test tedious to monitor. In light of these problems with air blowing as a long-term aging test, the conclusion is that it would not be a suitable test.

Modifier Performance

In addition to the other results obtained in this project, some attention should be directed toward the modifiers used. All modified asphalts were made using the same base to enable a comparison between them. In this section the effect of modifiers will be discussed as it relates to the low-temperature properties and high-temperature performance grade of the material.

Beginning with the low-temperature properties, the bottom performance grades have been repeated in Figure 3-37 for convenience. A significant observation in the data of Figure 3-37 is that, although each modifier pulled the base past the –28 °C mark, and therefore bettered its performance grade, the true impact of the modifiers on the BBR measurements does not seem to be that significant. The greatest impact on the BBR bottom continuous performance grade was

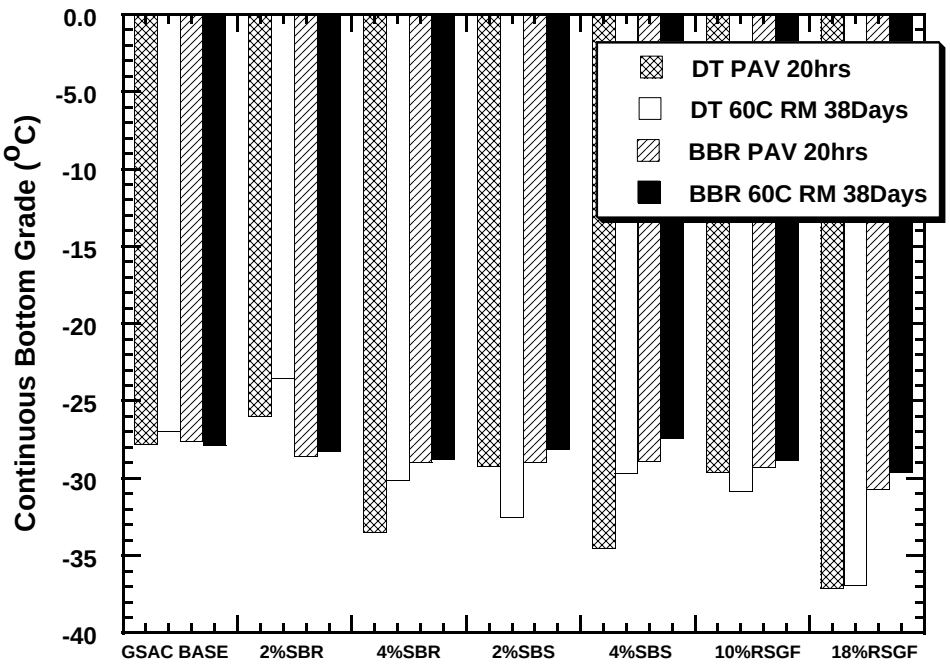

Figure 3-37. Continuous Grade Comparison for Modified Asphalts.

the 18% RSGF-20 modifier, which improved the grade 3.1 °C from the base material. The improvement seen in the remaining modifiers was modest, with most showing just over 1 degree of improvement. It seems, therefore, that modifiers have relatively little impact on the bottom grade as determined by BBR measurements.

The DTT data scatter prevents one from drawing concrete conclusions regarding modifier performance, but it seems clear that while the modifier's improvement may not be seen on the BBR, a direct tension test may allow for a better PG. The samples modified with 4% SBS and 18% RSGF-20 in Figure 3-37 illustrate this for the PAV aged materials.

Figure 3-38 presents data comparing the failure stress measured at –24 °C for each of the modified samples with that of the GSAC AC-15P base. All samples were RTFOT aged, then PAV aged for 20 hours at 100 °C. As shown in the figure, all of the modifiers increase the failure stress of the material by significant amounts. Even the smallest increases, as seen by the 2% SBR and 2% SBS modified systems show an increase from 3 to 4 MPa. The 10% RSGF-20 modified sample, while better than the 2% SBS and 2% SBR samples, clearly is inferior to the 4% SBR and 4% SBS samples, which improve failure stress by about 2 MPa. By far the best modifier in terms of raising the failure stress is the sample modified by 18% RSGF-20. This sample nearly doubles the failure stress of the base asphalt.

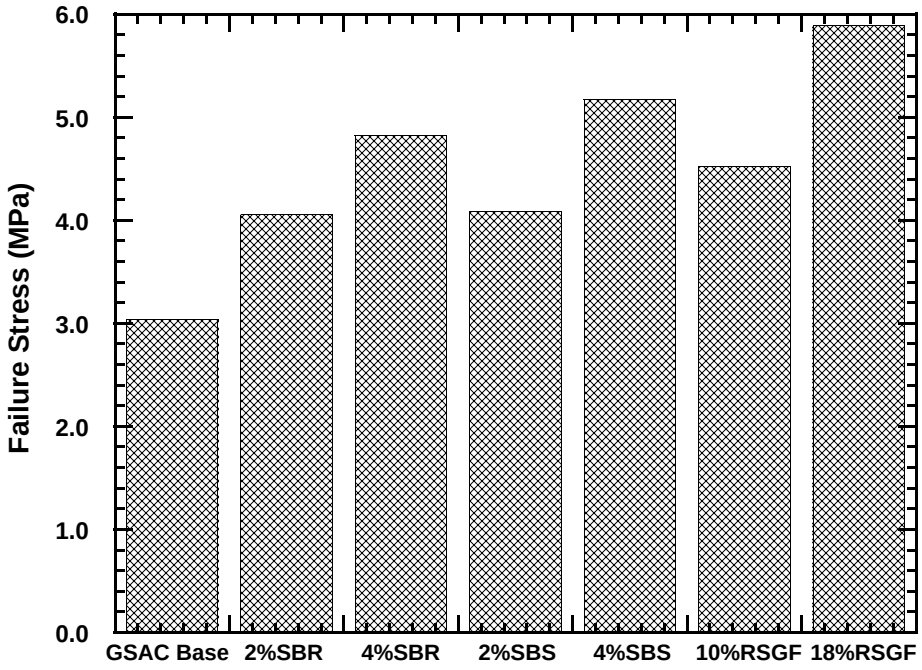

Figure 3-38. DTT Failure Stress at –24 ºC for Modified Materials.

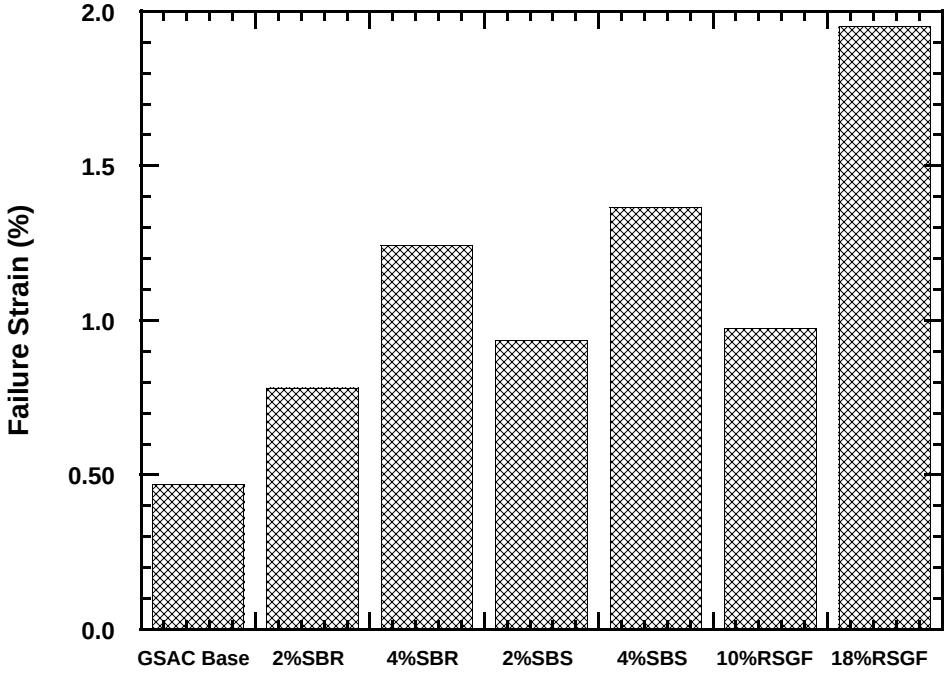

Figure 3-39. DTT Failure Strain Measured at –24 ºC for Modified Materials.

Figure 3-39 shows a comparison between the failure strain at break for modified asphalt samples. As with the failure stress, the 2%SBR, 2%SBS, and 10%RSGF-20 samples improve failure strain, but are clearly not as effective as the more heavily modified samples. In this case the improvement seen by the 18%RSGF-20 is an amazing four times the elongation at break of the base asphalt. The data presented in Figures 3-38 and 3-39 are tabulated in Table 3-8.

Table 3-8. DTT Results for Modified Samples at –24 ºC.

Material	Failure Stress at -24 ºC (MPa)	Failure Strain (%)
GSAC AC-15P	3.0340	0.46800
GS AC AC-15 w/2%SBR	4.0520	0.78100
GS AC AC-15 w/4%SBR	4.8260	1.2410
GS AC AC-15 w/2%SBS	4.0890	0.93400
GS AC AC-15 w/4%SBS	5.1730	1.3640
GS AC AC-15 w/10%RSGF-20	4.5180	0.97500
GS AC AC-15 w/18%RSGF-20	5.8910	1.9510

In addition to evaluating the direct tension data for modifiers it is interesting to note the changes in BBR data that the modifiers bring as well. Table 3-9 gives the BBR results for the modified materials and the base at −24 ºC. As can be seen in the table, all modifiers improve the stiffness of the base material, but to varying degrees. All modifiers also improve the m-value, but the changes are not as significant as the changes in the stiffness. It was hypothesized that the improvements in these DTT data could be correlated with the data obtained from the BBR. While no such correlation exists for m, stiffness correlates well with both failure stress and strain as seen in Figures 3-40 and 3-41. These data indicate that the decrease in stiffness is accompanied by increases in both the failure stress and the failure strain.

Modifiers may improve these low-temperature properties by lowering the glass transition temperature of the base material. Kumar and Gupta (1998) define the glass transition temperature as “the temperature at which a hard glassy polymer becomes a rubber material.” Asphalt, like polymers, exhibits glass transitions, and some glass transition temperatures have been measured for SHRP materials by Bahia and Anderson (1993). On a molecular level, these modifiers may prevent or help to control some of the associations between highly polar molecules which form as temperature drops, thereby lowering the glass transition temperature and improving low-temperature physical properties.

Table 3-9. BBR Results for Modified Samples at -24 ºC.

Material	Failure Stress at -24 ºC (MPa)	Failure Strain (%)
GSAC AC-15P	3.0340	0.46800
GS AC-15 w/2%SBR	4.0520	0.78100
GS AC-15 w/4%SBR	4.8260	1.2410
GS AC-15 w/2%SBS	4.0890	0.93400
GS AC-15 w/4%SBS	5.1730	1.3640
GS AC-15 w/10%RSGF-20	4.5180	0.97500
GS AC-15 w/18%RSGF-20	5.8910	1.9510

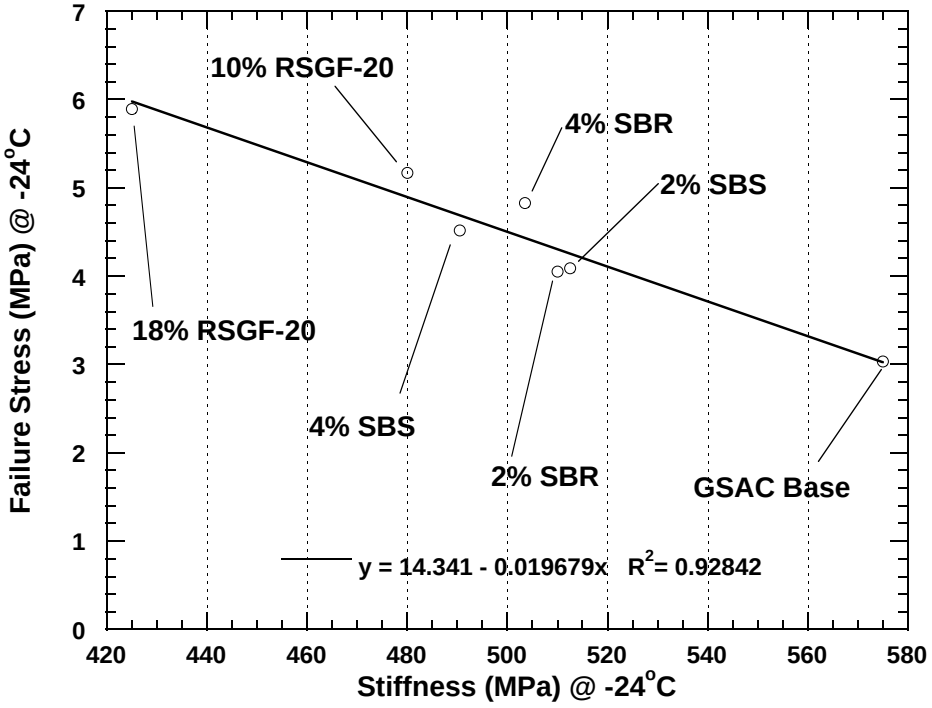

Figure 3-40. Failure Stress as a Function of Stiffness at -24 ºC for Modified Materials.

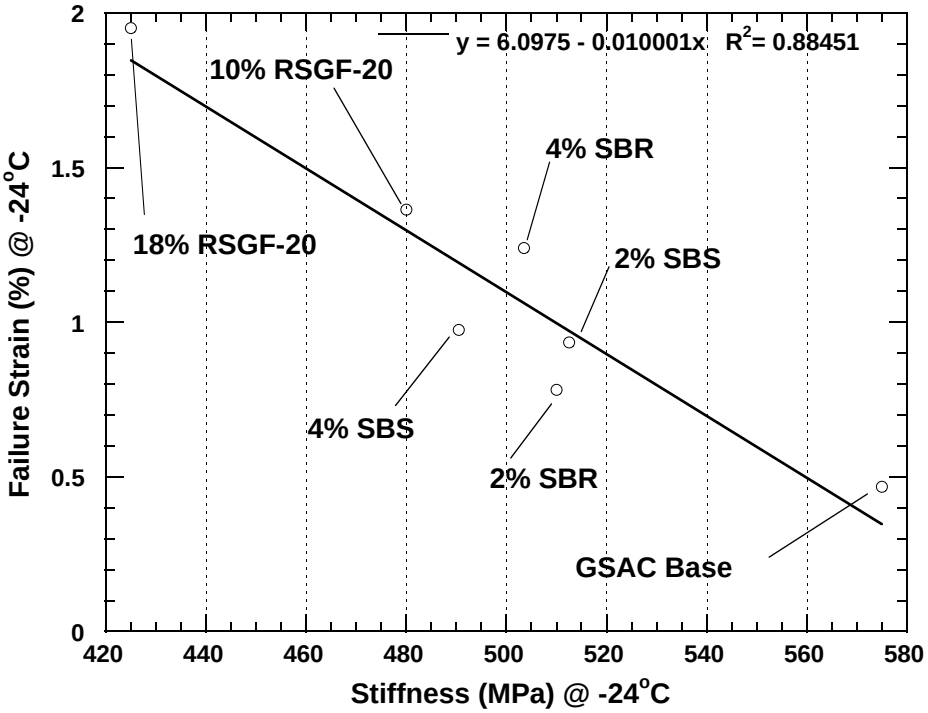

Figure 3-41. Failure Strain as a Function of Stiffness at -24 ºC for Modified Materials.

In addition to having a significant impact on low-temperature properties, modifiers also help to improve high-temperature properties and performance grades. High-temperature performance grades are determined by DSR measurement of $G^*/\sin(\delta)$ at various temperatures for unaged and RTFOT-aged materials.

Figure 3-42 illustrates $G^*/\sin(\delta)$ at 10 rad/s as measured for the unaged base and modified materials. The horizontal line on the plot indicates the SHRP specification that an unaged material must have a $G^*/\sin(\delta)$ value of 1000 Pa to pass. From the plot, 4% SBR and 4% SBS modifiers increase the value of the base $G^*/\sin(\delta)$ more than any other modifiers. They are followed closely by the 18% RSGF-20 modified material. It is interesting to note in this plot that the effect of 2% SBS at 58 ºC is similar to that of the 18% RSGF-20, but as the temperature increases to 70 ºC, 2% SBS becomes only slightly better than the base material. The remaining modifiers 2% SBR and 10% RSGF-20 showed only modest improvement to the base asphalt. The data of Figure 3-42 are also presented in Table 3-10.

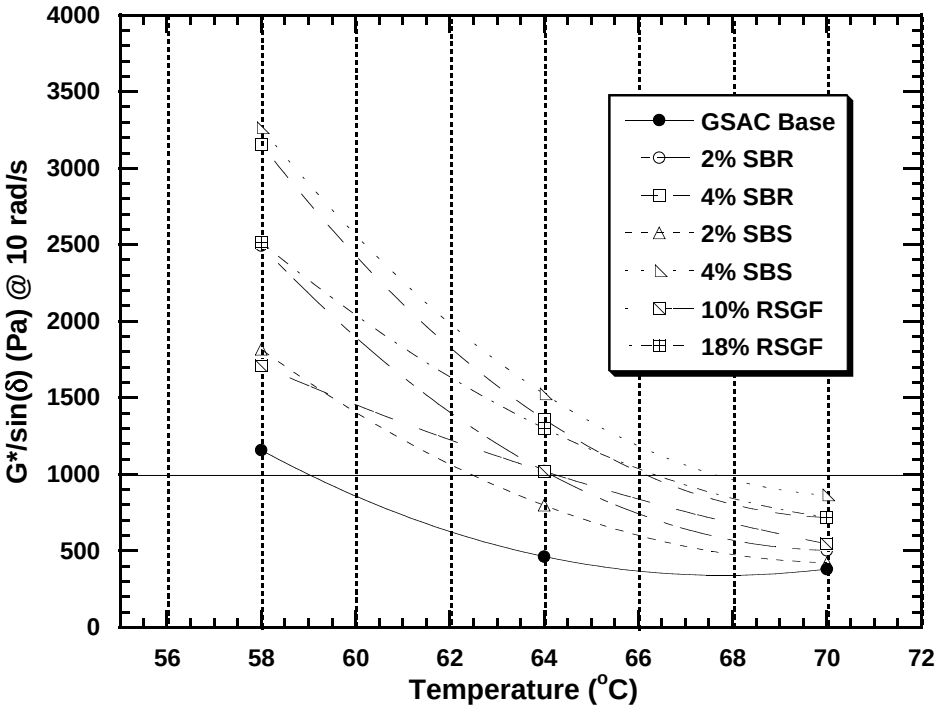

Figure 3-42. G */sin(δ) @ 10 rad/s for Unaged Modified Materials.

Table 3-10. G*/sin(δ) for Unaged Modified Materials.

Material	G*/sin(δ) (Pa) at 10 rad/s		
	58 ºC	64 ºC	70 ºC
GSAC AC-15P Base	1158.1	463.3	---
GS AC-15 w/2%SBR	2494.1	1021.3	503.7
GS AC-15 w/4%SBR	3156.4	1360.0	717.9
GS AC-15 w/2%SBS	1817.0	798.0	422.7
GS AC-15 w/4%SBS	3264.4	1525.7	864.9
GS AC-15 w10%RSGF-20	1709.1	1020.3	546.3
GS AC-15 w18%RSGF-20	2517.2	1301.7	719.4

Figure 3-43 illustrates $G^*/\sin(\delta)$ as measured for the RTFOT-aged base and modified materials. As with Figure 3-42, the horizontal line on the plot indicates the SHRP specification that a short-term aged material must have a $G^*/\sin(\delta)$ value of 2200 Pa to pass. Like the unaged material, the 4% SBR and 4% SBS modifiers increase the value of the base $G^*/\sin(\delta)$ more than any other modifiers. The 4% samples are followed by 2% SBR and 2% SBS. As before with the unaged material, the data indicate that for the 2% SBS sample, the modifier helps at lower temperatures but shows little improvement for the higher temperatures. In this case the 18% modifier does not show improvement that is as significant as that seen in the unaged material. This is likely due to the fact that after RTFOT aging, much of the ground rubber remains in the RTFOT bottle and is not collected in the sample. This loss of modifier would explain the reduced benefit. Unfortunately, the loss of modifier in a simulation does not mean that the modifier will not have benefit in service. The remaining modifier, 10% RSGF-20, showed only modest improvement to the base asphalt. The data of Figure 3-43 are also presented in Table 3-11.

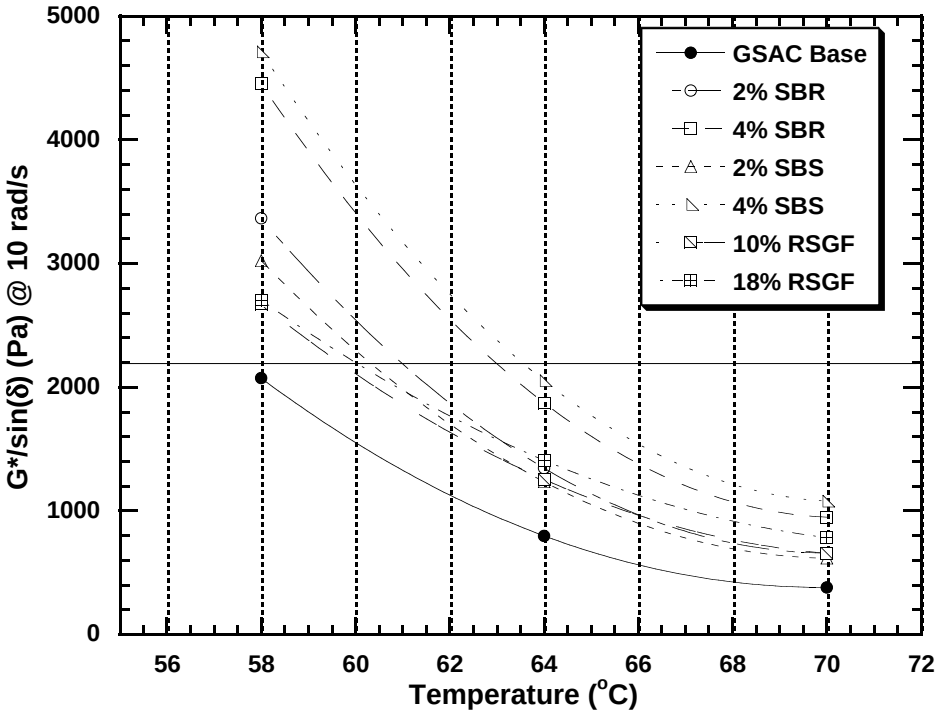

Figure 3-43. $G^*/\sin(\delta)$ for RTFOT-Aged Modified Materials.

Table 3-11. $G^*/\sin(\delta)$ for Modified Materials after RTFOT Aging.

Material	$G^*/\sin(\delta)$ (Pa) at 10 rad/s		
	58 °C	64 °C	70 °C
GSAC AC-15P	2072.7	798.0	381.4
GS AC-15P w/2%SBR	3364.9	1345.4	658.5
GS AC-15P w/4%SBR	4454.4	1873.4	949.1
GS AC-15P w/2%SBS	3024.5	1235.5	618.2
GS AC-15P w/4%SBS	4712.8	2052.5	1078.7
GS AC-15 w/10%RSGF-20	2672.2	1255.2	657.2
GS AC-15 w/18%RSGF-20	2704.7	1409.9	783.3

To summarize, the higher weight percent modified samples showed considerably better low-temperature properties. The 18% RSGF-20 modified sample showed the best improvement to low-temperature properties followed by 4% SBS and 4% SBR. For high-temperature properties 4% SBS proved to be the best modifier, followed by 4% SBR. For the base asphalt used in this project (PG 52-22), all modifiers provided a 12 °C improvement in PG to 58-28. Two modifiers, 4% SBS and 18% RSGF-20, provided an 18 °C improvement in PG to 58-34.

CONCLUSIONS AND RECOMMENDATIONS

In Phase I of this project it was shown that 38 days of aging at 60 °C and 1 atmosphere of air is approximately equivalent to 20 hours in the PAV at 100 °C, after both have been RTFOT aged. This indicates that the PAV simulates roughly one year of aging on Texas roads. Clearly this aging test should be extended or modified if the SHRP performance specifications are to accurately predict intermediate and long-term binder failure.

Low-temperature properties of the samples were found not to vary significantly between the PAV and environmental room aged material. The DTT and the BBR both gave the same performance grade for each material at each aging condition. In addition, for the BBR, the bottom grade was determined by the same parameter (S or m) for each aging procedure. Therefore, the current Superpave specification gives consistent values for PAV aged materials as well as for environmental room aged materials.

For Phase II a correlation was developed from the high-temperature parameter $G^*/\sin(\delta)$ at 58 °C and 10 rad/s to correct the low-temperature performance grade when one desires to skip the long-term aging procedure. The correction factor for the continuous bottom performance grade is given by:

$$C = 0.6225 \exp\left(0.0002095 G^{*}/\sin(\delta)\right) \quad (3\text{-}3)$$

Where the bottom continuous performance grade for long-term aged material can be estimated from that of the short-term material and the correction factor by:

$$PG_{LT} = PG_{ST} + C \quad (3\text{-}4)$$

The correlation proved to give a maximum error of ±1.6 °C for the low temperature performance grade.

In Phase III of this project it was shown that as asphalts are aged for extended periods their relative ranks with respect to Superpave low-temperature specifications change. This indicates that the Superpave long-term aging specifications result in an arbitrary ranking of asphalts with respect to low-temperature properties. In addition it was shown that as asphalts are aged for extended periods, the low-temperature grades move linearly with aging from being limited by stiffness at short aging times, to being limited by m-value at longer aging times.

Upon examining the data obtained by long-term air blowing of the samples, it was concluded that air blowing is not a suitable long-term test. Air blowing did not provide carbonyl area data which were consistently in line with data obtained from the environmental room. In addition, no time could be established where air blowing seemed to be identical to either the PAV or the environmental room aging procedures. The air-blowing test also was difficult and tedious to run. In light of these problems with air blowing as a long-term aging test, it was concluded that it would not be a suitable test.

A portion of the work in this project dealt with comparing various modifiers. To summarize, the higher weight percent modified samples showed considerably better low-temperature properties. The 18% RSGF-20 modified sample showed the best improvement to low-temperature properties followed by 4% SBS and 4% SBR. For high temperature properties 4% SBS proved to be the best modifier, followed by 4% SBR. It is recommended that polymer modifiers be used in concentrations of at least 4% by weight, where SBS rather than SBR is recommended. If ground tire rubber is to be used, a high-cure process with 18% by weight rubber provides excellent benefit for both high- and low-temperature properties.

CHAPTER 4. AN INVESTIGATION OF ASPHALT DURABILITY: RELATIONSHIPS BETWEEN DUCTILITY AND RHEOLOGICAL PROPERTIES FOR UNMODIFIED ASPHALTS

ABSTRACT

Literature reports indicate that the ductility of binders recovered from asphalt pavements correlate with cracking failure. However, ductility measurement is a time and material consuming process and is subject to reproducibility difficulties, as are all failure tests. The purpose of this study was to correlate ductility with DSR properties analogous to the SHRP procedure of using BBR S and m to screen for the thermal cracking. DSR measurements are much faster and consume much less material than ductility measurement.

Fourteen unmodified asphalts were oxidized to different levels of aging at temperatures ranging from 60 to 200 ºC. Experimental data show that the extensional flow of conventional asphalt binders can be qualitatively described with a simple elongation model using a viscoelastic Maxwell element. Based on this model, a map of the dynamic shear modulus G' versus η'/G' was used to track changes in ductility with aging. Also, ductility correlated remarkably well with $G'/(\eta'/G')$ for different binders aged at different conditions.

INTRODUCTION

Field data suggest that asphalt binder ductility correlates quite well with pavement cracking, provided it is measured at the appropriate temperature. Doyle (1958) found from the performance of Ohio test sections that while the ductility measured at 25 ºC was not a good indicator of pavement cracking, ductilities measured at 12.8 ºC, 1 cm/min or less correlated quite well. He also gave data on other roads, and one showed no cracking after 5 years for which the recovered asphalt had a ductility of 29 cm when measured at 12.8 ºC and 1 cm/min. Two others with considerable cracking showed ductilities of only 3 and 4 cm.

Four test sections were laid during 1960-61, and after 10 years all of them showed some cracking (Kandhal and Koehler, 1984; Kandhal and Wenger, 1975). Among penetration at 25 ºC, viscosity at 60 ºC, and ductility at 15.6 ºC, only ductility gave the proper ranking in road condition (cracking) after 10 years. The pavement condition was good if the ductility at 15.6 ºC was above 10 cm, and when the ductility value decreased to about 3 to 5 cm, cracking began to develop. It was also found that ductility at 15.6 ºC was more reproducible and better defined than that at higher temperature, such as 25 ºC. In 1964, six more pavements were laid, each with a different asphalt. Road cracking condition was correlated with viscosity at 25 and 60 ºC, shear susceptibility at 25 ºC, and ductility at 15.6 ºC, 1 cm/min. Among these parameters, both ductility and viscosity-shear susceptibility slope ordered the performance rating (cracking) of the six pavements correctly. A third set of test sections was laid in 1976, and again relative rankings of pavement performance agreed with the ordering of ductility measured at 15.6 ºC, 1 cm/min. Kandhal (1977) summarized results from these three test sections and concluded that when the

binder ductility decreased to 3-5 cm (measured near 15 °C), there would be serious cracking and the pavement needed resurfacing.

Clark (1958) reported results comparing laboratory oven aging with hot-mix and road aging for 46 roadways with respect to ductility and penetration and found that low-temperature ductility was a good predictor of roadway condition (cracking) and life.

Halstead (1963) showed that the pavements containing asphalts with penetration in the range normally considered satisfactory (30 to 50) but with low ductility were likely to show poorer service than pavements containing asphalts of the same penetration but with high ductility. Vallerga and Halstead (1971) studied 53 highway pavements located throughout the United States and concluded that severe raveling occurred in cold climates when the ductility at 15.6 °C, 1 cm/min decreased to 3 cm or lower.

From the above discussion we can conclude that ductility measured at reduced temperature and elongation rate (e.g., 15 °C and 1 cm/min) is a good indicator of cracking condition of asphalt binders. However, ductility measurement is a time-consuming process and requires several grams of material, according to ASTM D 113-86 (1994), 75 grams. Thus, it was the objective of this work to devise alternate measurements using viscoelastic properties to assess durability in conventional asphalt binders, similar to the concept of using bending beam rheometer S and m to indicate low-temperature thermal cracking.

METHODOLOGY

Seventeen unmodified asphalt binders were compared and evaluated through a number of physical properties. The binder materials were aged at two temperatures, 93.3 and 204 °C (200 and 400 °F), by air blowing and at a third temperature, 60 °C (140 °F), in a controlled environment room to obtain properties ranging from those of a slightly aged material to one which would be near the end of its service life. Table 4-2 summarizes the materials and their aging methods.

The air blowing was conducted by placing approximately 500 grams of asphalt binder in a 0.9-L (1 qt) can and controlling to the desired temperature. Air was blown through a sparger in the bottom of the can, and the binder was stirred continuously by a mixer at a low speed.

Physical properties measured on the aged binders were viscoelastic properties, ductility, and force ductility. The viscoelastic properties were measured with a Carri-Med CSL500 dynamic shear rheometer (DSR). Ductilities were obtained at 15 °C and an extensional speed of 1 cm/min in accordance with ASTM D113-86 (1994). The ductility sample has a 3 cm initial gauge length and a tapered throat. Ductility is recorded as the extension in centimeters of the asphalt specimen before break. Force ductility (F-D) measurements were made at 4 °C and 1 cm/min elongation speed. In this case the specimen was similar to the ductility specimen except that the initial gauge length, while still 3 cm in length, had a uniform rectangular cross-section of 1 cm by

0.5 cm. A strain gauge provided for force measurements up to 100 N. The force measurement allowed stress as a function of extension ratio to be calculated, assuming a constant cross-section and an incompressible binder. F-D measurements were made to better understand the phenomenological relationship between a material's rheological properties and ductility and thus the impact of aging on durability.

Table 4-1. List of Asphalts Studied.

Aging Method	Asphalt Binders
204 °C (400 °F) Air-blowing	DS AC-5, Exxon AC-5, Fina AC-5 Exxon AC-10, Fina AC-10, GSAC AC-10 Exxon AC-20, Fina AC-20, Shell AC-20
93.3 °C (200 °F) Air-blowing	SHRP AAA-1, AAB-1, AAD-1
60 °C (140 °F) Environmental Room	Exxon AC-30, Fina AC-5, Fina AC-10 Fina AC-20, GSAC AC-10, Neste AC-20 Wright AC-10, Wright AC-20, UR AC-10

In addition to these physical properties measurements, FTIR spectra were obtained on a number of the asphalt materials as a measure of the amount of oxidation. The area under the carbonyl absorbance band from 1650 to 1820 cm^{-1} represents the extent of oxidation in asphalt materials and is reported as carbonyl area (CA).

RESULTS AND DISCUSSION

Effect of Aging on Rheological Properties and Master Curves

Figure 4-1 shows dynamic viscosity (η') and storage modulus (G') master curves at two aging conditions at a reference temperature of 4 °C. At high frequency or low temperature the viscosity curves merge together, approaching a single asymptote. At low frequency or high temperature there is a significant increase with aging in the low shear rate, limiting viscosity.

Figure 4-2 shows typical storage modulus G' and loss modulus G'' versus aging time behavior for asphalt, and Figure 4-3 shows increases in G' and G'' with FTIR carbonyl area. From Figure 4-2, note that G'' increases less with aging time than G'. Hence, it may be said that G'' is less sensitive to aging than is G', and this is seen within the context of oxidation, as represented by the FTIR carbonyl band, by comparing the relationships in Figure 4-3. This smaller sensitivity of G'' to aging than G' means that their ratio ($\tan \delta$) and hence the phase angle, δ, decreases with aging. Phase angle master curves are shown in Figure 4-4. Thus with increased aging, asphalts tend to become more solidlike and less liquidlike at moderate temperatures. This decrease in phase angle over aging time is shown in Figure 4-5. The relationship between δ and carbonyl area (Figure 4-6) is also linear.

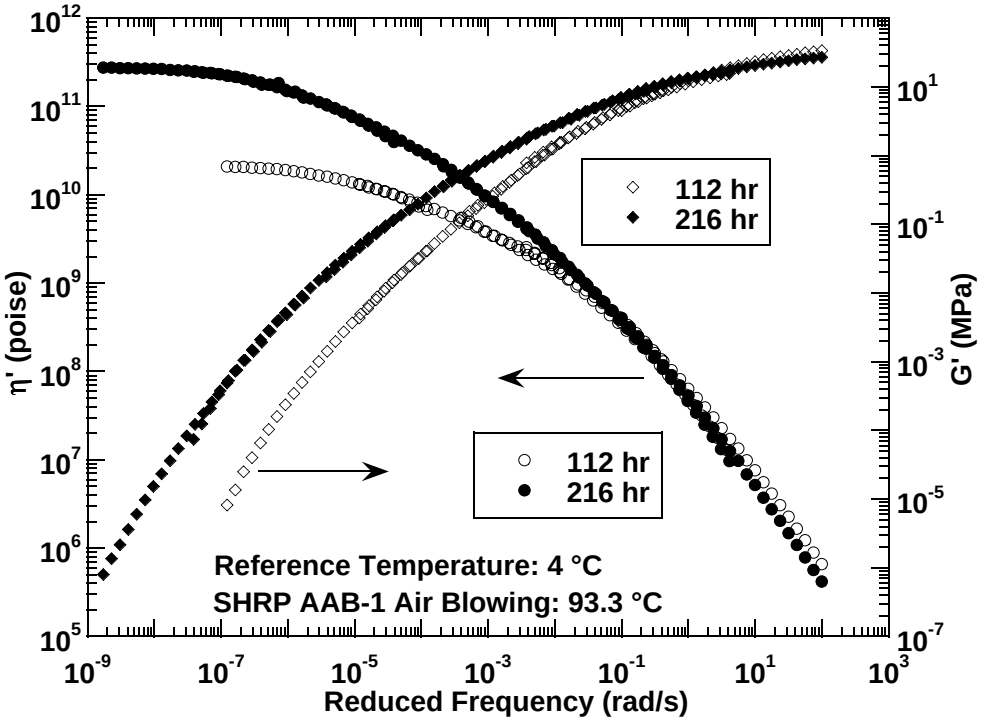

Figure 4-1. Master Curves for SHRP AAB-1 at Two Aging Times.

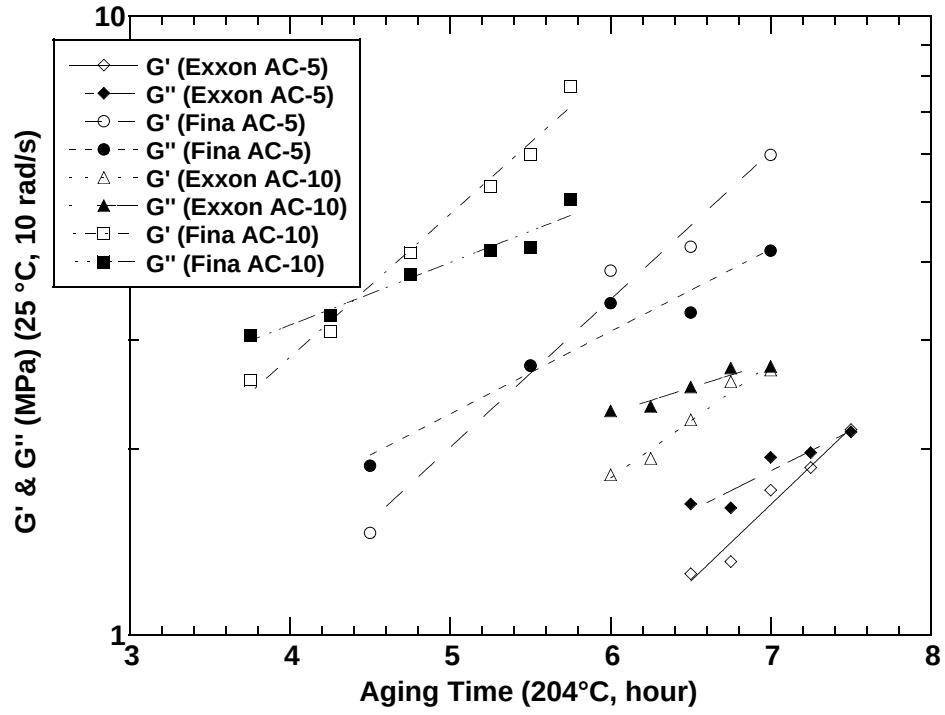

Figure 4-2. Effect of Aging on Storage and Loss Moduli.

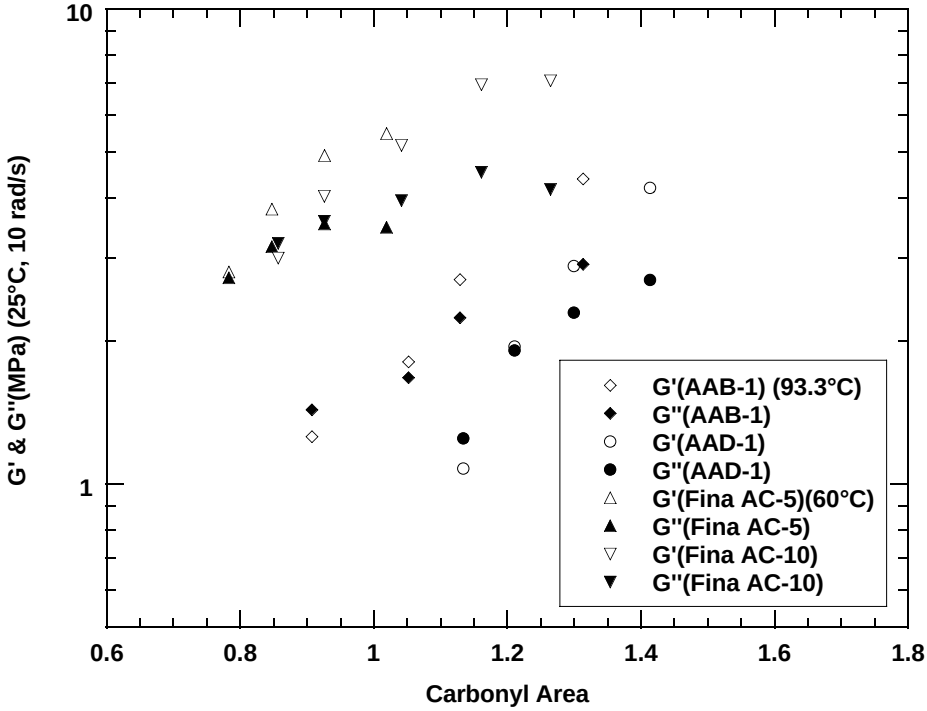

Figure 4-3. Storage and Loss Moduli Related to Oxidation Carbonyl Area.

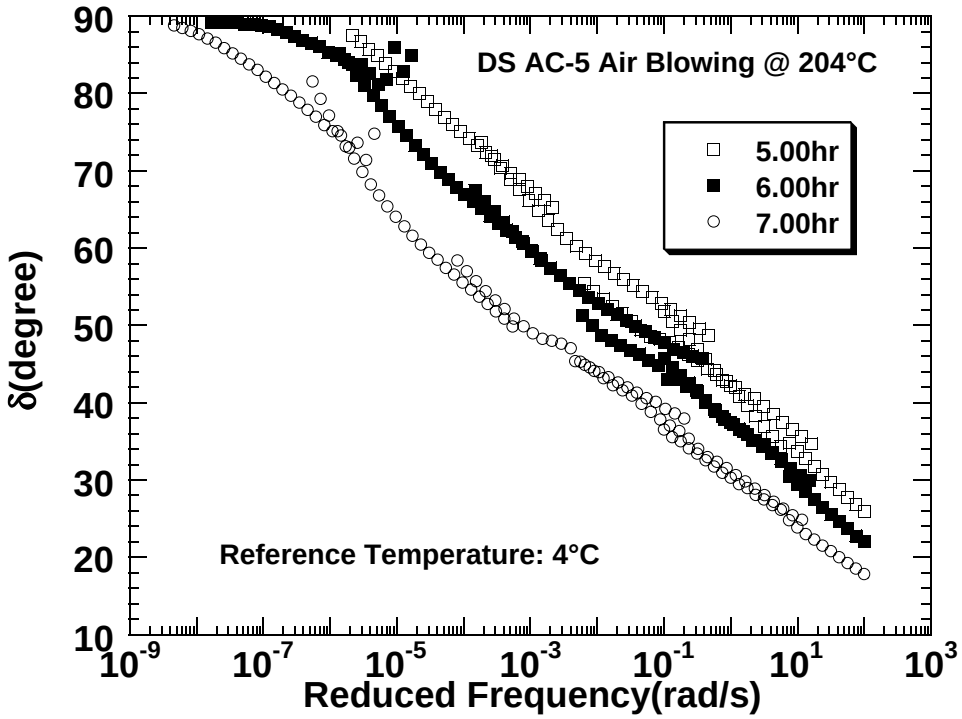

Figure 4-4. Effect of Aging on the Phase Angle Master Curve.

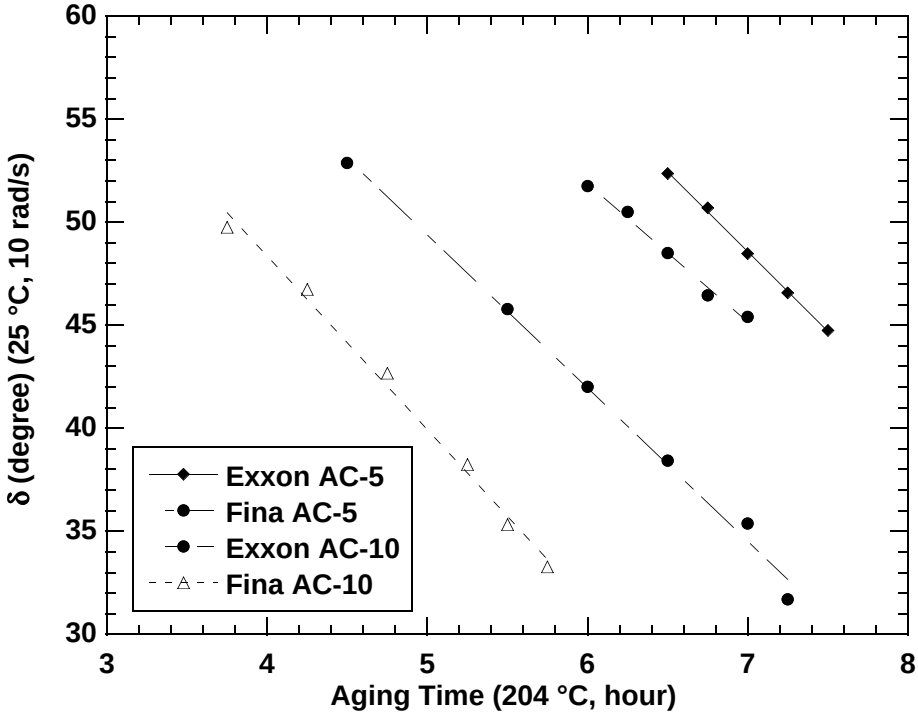

Figure 4-5. Decrease in Phase Angle (25 ºC, 10 rad/s) with Aging Time.

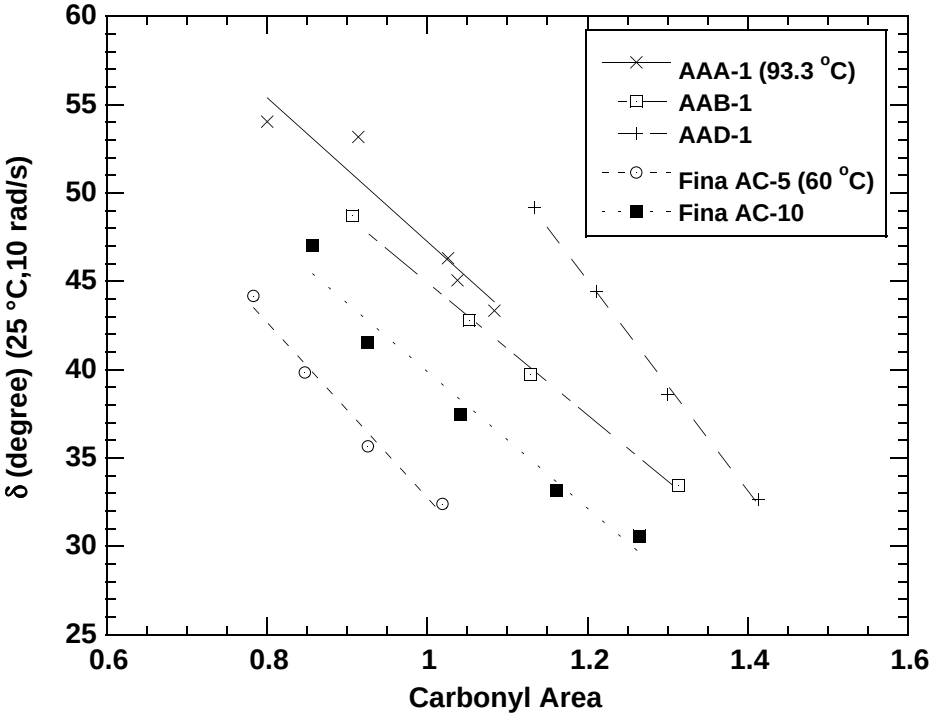

Figure 4-6. Decrease in Phase Angle with Oxidation Carbonyl Area.

The imperfections in the phase angle master curves (Figure 4-4) should be noted. Whereas G′ and η′ master curves show very consistent behavior in accordance with time-temperature superposition (TTSP) when created from measurements at different temperatures, there are obvious problems with the phase angle master curve. This has been pointed out as evidence of structuring in asphalt resulting from associations of asphaltenes and resins, associations that change with temperature, thereby bringing into question the validity of TTSP (Lesueur et al., 1996). Nevertheless, TTSP is commonly used with asphalts and we do so in this chapter.

To summarize the effect of aging on the rheological properties, aging increases the dynamic viscosity (η′) and storage modulus (G′) at intermediate frequencies (temperatures). Furthermore, G′ increases more rapidly than G″ so that the phase angle decreases with aging, thereby producing a more solidlike material over time at intermediate temperatures. These changes have a profound effect on ductility, as discussed below.

Maxwell Model

With aging, ductility decreases dramatically (Figure 4-7). This can also be seen in Figure 4-8, which shows two experimental force ductility curves for an unmodified asphalt aged to two conditions. The measurements are made at 4 °C. The abscissa is the extension ratio so that an alpha of 3 with a gauge length of 3 cm would be a ductility of 6 cm. The ductility of the 216-hour aged sample is only about 0.45 cm.

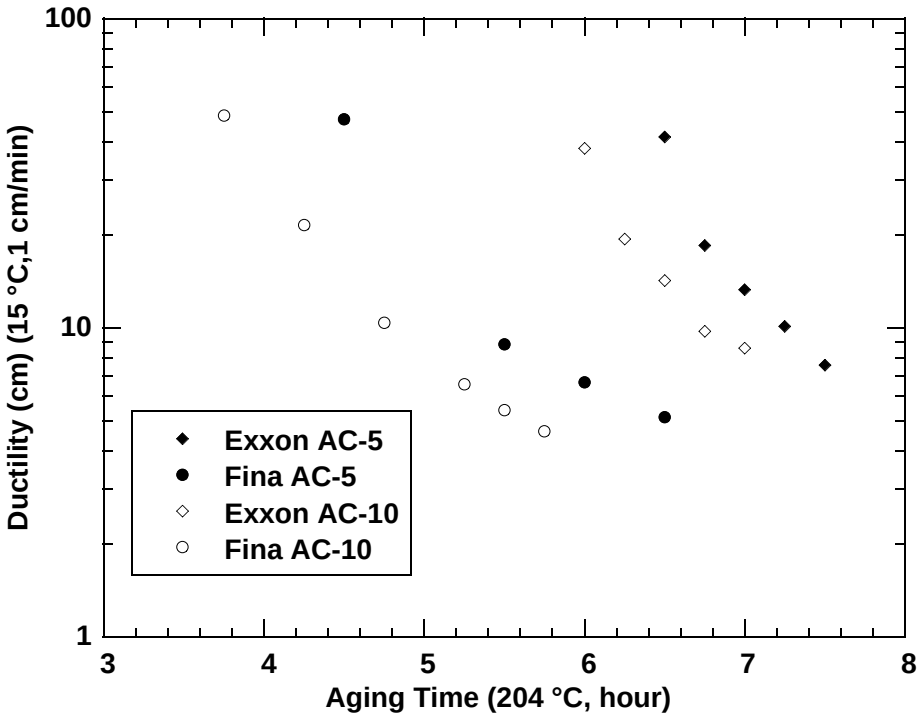

Figure 4-7. Decrease in Ductility with Aging Time.

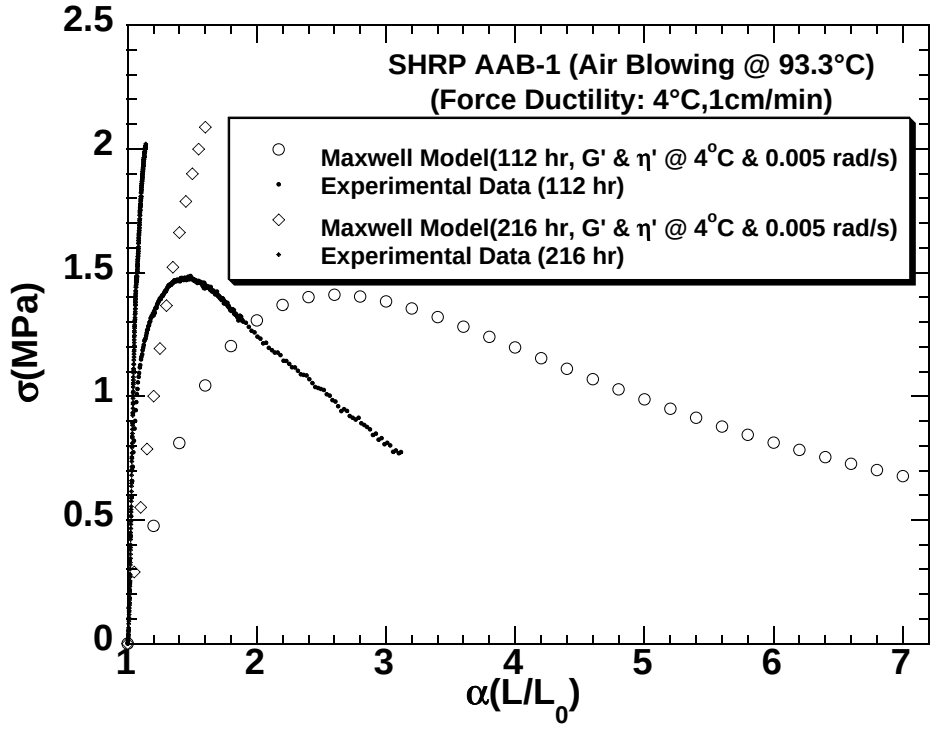

Figure 4-8. Force-Ductility Data and Maxwell Model Simulation for Two Aging Times.

As a sample is extended, the initial (short time) response is from the elastic properties of the material, and hence the initial slope is dominated largely by its elastic modulus. At longer times, i.e., larger extension ratios for the 112-hour sample, the stress actually declines with extension ratio. In this region the viscosity allows the material to flow. Furthermore, for heavilyaged asphalt samples, both the elastic modulus and viscosity are greater so that the stress reaches a higher level before the deformation can transition to flow. This is a simplistic description, but appears to embody the essential elements of these stress elongation curves.

To continue with this simplistic analysis, we have used a spring and dashpot in series (Maxwell model). Here, our emphasis is not on precise modeling of the extensional flow of asphalt binders. Previous work has shown that a multiple relaxation time model is more appropriate for such a purpose (Christensen and Anderson, 1992). Rather, our purpose is to gain sufficient insight into the nature of elongation and failure of asphalt materials, especially as they harden at low temperature or with oxidation, to provide guidance into possible correlations between ductility and linear viscoelastic rheological properties. Such a concept is similar to the use of low-temperature bending beam stiffness (S) and creep rate (d log S/dt, defined as m) together as a surrogate for the low-temperature direct-tension failure strain, as defined by the Superpave asphalt binder specifications (Asphalt Institute, 1994). Both rely upon the existence of a common failure stress in asphalt materials at the test conditions and common qualitative behavior of the stress-strain relation. In both situations, stresses build with deformation due to the elastic modulus but are relieved as the material undergoes flow. The balance between these

two phenomena determines the level of stress that is achieved as a result of deformation; the amount of stress the material can sustain without failure interacting with this balance establishes the failure strain. Such a correlation will allow failure to be estimated from DSR master curves for aged materials.

The Maxwell model represents the asphalt by a linear elastic element (linear spring) in series with a newtonian viscous element (Figure 4-9). Here we are concerned with deformation

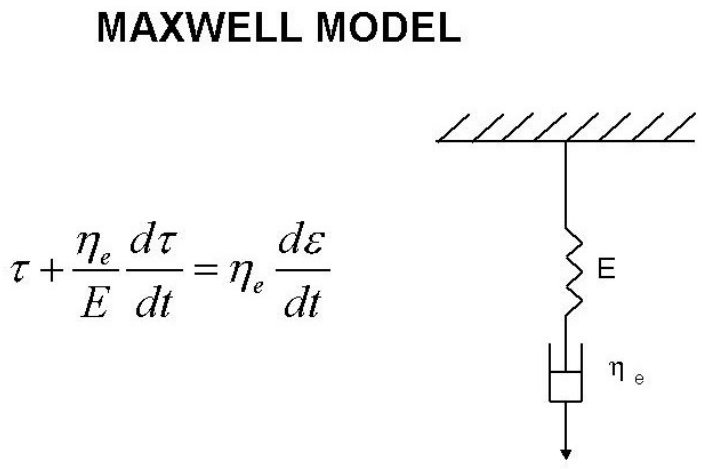

Figure 4-9. The Maxwell Model: An Elastic and Viscous Element in Series.

at constant elongation rate under uniaxial load. Because these elements are in series the stress in each is the same, but the strain rate in each depends on its own constitutive relation. Specifically, the elastic element's total stress (T) under elongation is proportional to the strain through the elastic modulus (E). Hence, the rate of strain across the spring is directly proportional to the rate of change of stress:

$$\frac{d\varepsilon_E}{dt} = \frac{1}{E}\frac{dT}{dt}. \qquad (4\text{-}1)$$

For the viscous element of an incompressible material, the rate of strain is proportional to the total stress through the elongational viscosity (η_e) (McCrum et al., 1997):

$$\frac{d\varepsilon_\eta}{dt} = \frac{1}{\eta_e} T. \qquad (4\text{-}2)$$

Combining the strain rates of these two elements gives the total strain rate as

$$\frac{d\varepsilon}{dt} = \frac{1}{\eta_e} T + \frac{1}{E}\frac{dT}{dt}, \tag{4-3}$$

which is rearranged to give

$$T + \frac{\eta_e}{E}\frac{dT}{dt} = \eta_e \frac{d\varepsilon}{dt}. \tag{4-4}$$

It is useful to transform the independent variable time to the elongation ratio. For constant elongation ratio, ($dL/dt = U_o$), $L = L_o + U_o t$. The elongation ratio $\alpha = L/L_o = 1 + U_o/L_o\, t$ so that $d\alpha/dt = U_o/L_o$, and thus

$$\frac{d\varepsilon}{d\alpha} = (d\varepsilon/dt)/(d\alpha/dt) = (U_o/L)/(U_o/L_o) = 1/\alpha, \tag{4-5}$$

leading to the differential equation for total stress as a function of elongation ratio:

$$\left(\frac{L_o}{U_o}\right)\left(\frac{E}{\eta_e}\right)\frac{T}{E} + \frac{1}{E}\frac{dT}{d\alpha} = \frac{1}{\alpha}. \tag{4-6}$$

Converting to shear modulus ($E = 2G(1 + \nu)$) and noting that $\eta_e = 3\eta$ (by Trouton's rule) then gives

$$\frac{L_o}{U_o}\,\frac{G(2(1+\nu))}{\eta}\,\frac{T}{G(2(1+\nu))} + \frac{3}{G(2(1+\nu))}\,\frac{dT}{d\alpha} = \frac{3}{\alpha}. \tag{4-7}$$

Letting $\nu = 0.5$ for an incompressible material and simplifying leads to

$$\frac{L_o}{U_o}\left(\frac{G}{\eta}\right)\frac{T}{G}+\left(\frac{1}{G}\right)\frac{dT}{d\alpha}=\frac{3}{\alpha} \tag{4-8}$$

This can be converted to a dimensionless form by defining a dimensionless stress $T' = T/T_f$ where T_f is the asphalt's failure stress (generally 3 to 5 MPa for unmodified asphalts) and dimensionless groups that involve G and (η/G):

$$\left(\frac{L_o / U_o}{\eta / G}\right)T' + \frac{dT'}{d\alpha} = \frac{3}{\alpha}\left(\frac{G}{T_f}\right). \tag{4-9}$$

This result is expressed in terms of shear modulus G and viscosity η. For the purposes of further discussion, we assume that these can be replaced by their respective dynamic shear properties, i.e., $G = G'$, $\eta = \eta'$.

With this model we can make some approximate comparisons between force-ductility data and DSR data. The data were measured at 4 °C and at an elongation rate of 1 cm/min, which is equivalent to the strain rate of approximately 0.005 s^{-1}. Using this strain rate as an angular frequency and 4 °C master curves, we obtained values for η' and G' to use in this Maxwell model.

Data and model calculations for the SHRP AAB-1 air blowing at 93.3 °C (200 °F) at both 112 and 216 hours are shown in Figure 4-8. Experimental data are from the force-ductility apparatus, and the calculations are based solely on the DSR experimental data and the Maxwell model with no empirical adjustments. While there are significant quantitative differences between the data and the calculations, the general trends are in agreement, and considering the total predictive nature of the calculations based upon the viscoelastic property data and the simplistic Maxwell model, the comparisons are really quite reasonable. Model limitations will be discussed more extensively below. The material air blown for 112 hours shows an increase in stress to a maximum followed by a relaxation, which, according to the Maxwell model, is the result of viscous flow of the material, whereas for the material air blown for 216 hours the increase in stress occurs much more rapidly (i.e., at smaller elongation ratios) so that the material breaks before it can reach a maximum in stress and a transition to viscous flow.

As noted above, the elongation model based on a Maxwell viscoelastic element is very approximate in a number of ways. First, the material's viscosity and shear modulus are assumed constant over the elongation. In fact, because the experiment is performed at a constant elongation rate, as the material lengthens the strain rate decreases. This error, while less at the small failure elongation ratios of heavily aged materials, still is a consideration. Second, like other viscoelastic materials, asphalts have many more than one relaxation time and modulus. This is likely a significant error in quantitatively modeling the extensional flow. Third, unmodified materials

tend to neck down in elongation, violating the uniform cross-section assumption of our calculations. For heavily aged materials, for which failure occurs before transition to viscous flow, this error is reasonably small.

So, in view of these model uncertainties, we would not expect to have close quantitative agreement between calculations based on the rheological properties and the experimental force-ductility data. Nevertheless, the Maxwell model qualitatively describes the extensional flow of asphalt binders, thereby providing guidance on defining physical parameters that are important for understanding and correlating the binder's extensional flow, as discussed in the next section.

Relationship between Ductility and G′, η′/G′

From this elongation model using a Maxwell element (Equation 4-9), it is seen that two rheological parameters are suggested to represent the extensional behavior of asphalt binders: the ratio of the dynamic viscosity to the storage modulus (η′/G′) and the value of the storage modulus G′. Figures 4-10a and 4-10b are maps of G′ versus η′/G′ for materials measured at 15 °C in the DSR. Figure 4-10a shows the data with each material identified at different levels of aging, and Figure 4-10b has the data grouped by regions of ductility, also measured at 15 °C.

The general trend is clear. As an asphalt ages, it moves from the lower right to the upper left and the ductility declines dramatically along this path. For some materials this path is significantly steeper than for others. The boundaries between regions of ductility are not perfect, as one might imagine from the normal experimental scatter that is observed in any kind of failure test. These maps show clearly that ductility is not related to just one parameter, i.e., to just the ratio η′/G′ or to just the modulus G′ (stiffness) of the material. Rather, the ductility is dependent upon both.

As an alternate way of viewing these same data, ductility is plotted versus the ratio of G′ to (η′/G′) (Figure 4-11). This plot shows a good correlation between these parameters, especially for ductilities less than 10 cm. Note that it is in this region below 10 cm that Reese (1997) and Reese and Goodrich (1993) observed binder ductility as playing a significant role in binder road performance. At this level of ductility, evidently the stiffness and viscosity of the binder are great enough that the binder will fail because of excessive stresses that develop because of insufficient material flow.

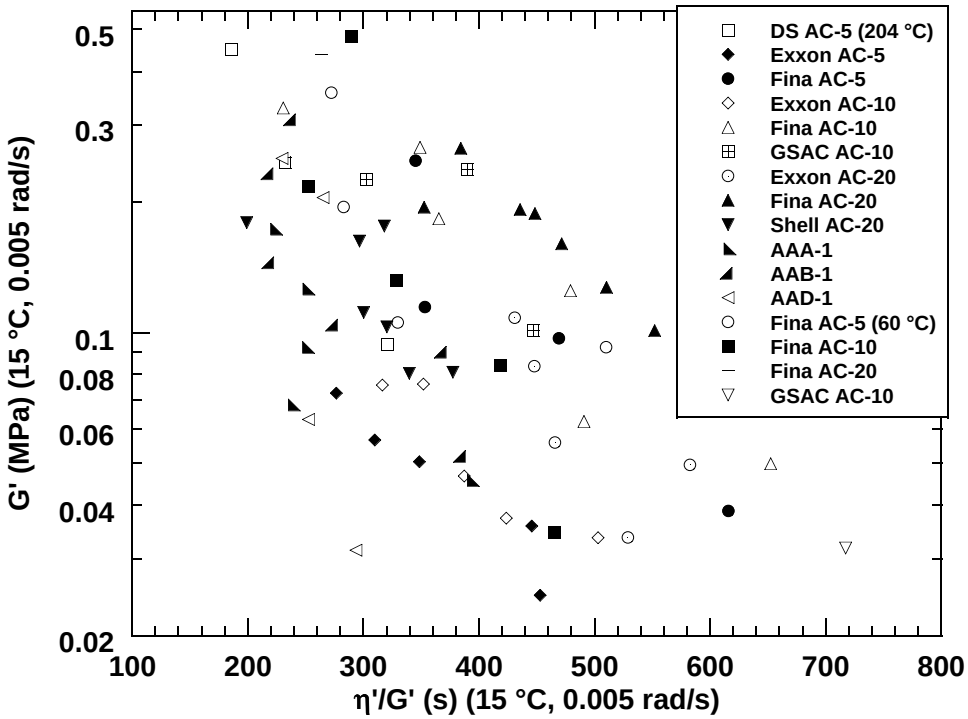

Figure 4-10a. G′ versus η′/G′ Map as Asphalts Oxidize, by Asphalt.

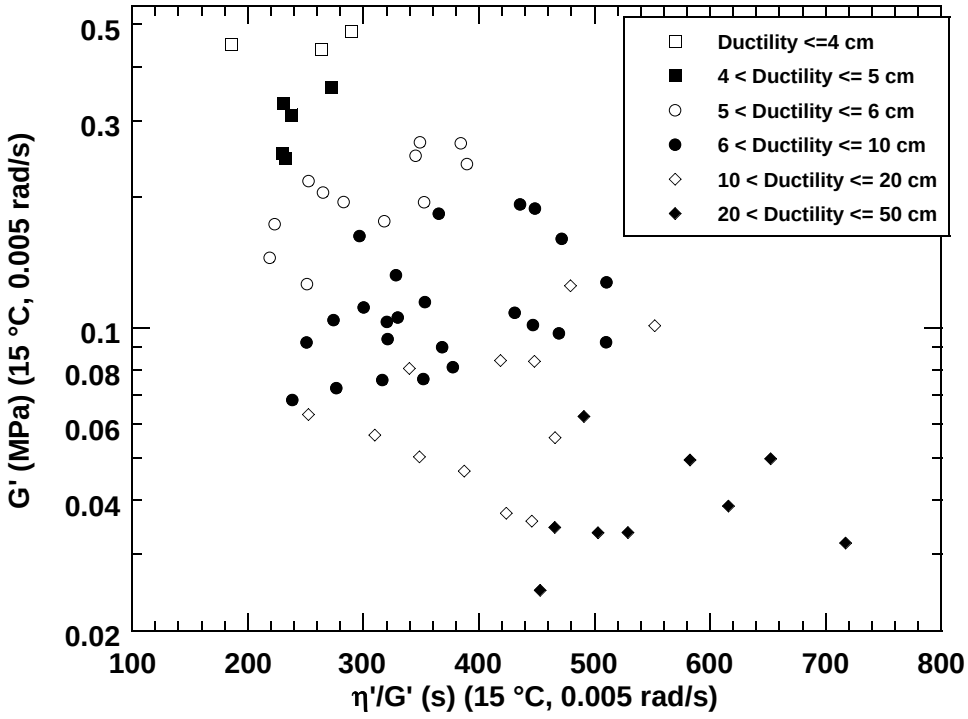

Figure 4-10b. G′ versus η′/G′ Map as Asphalts Oxidize, by Ductility Regions.

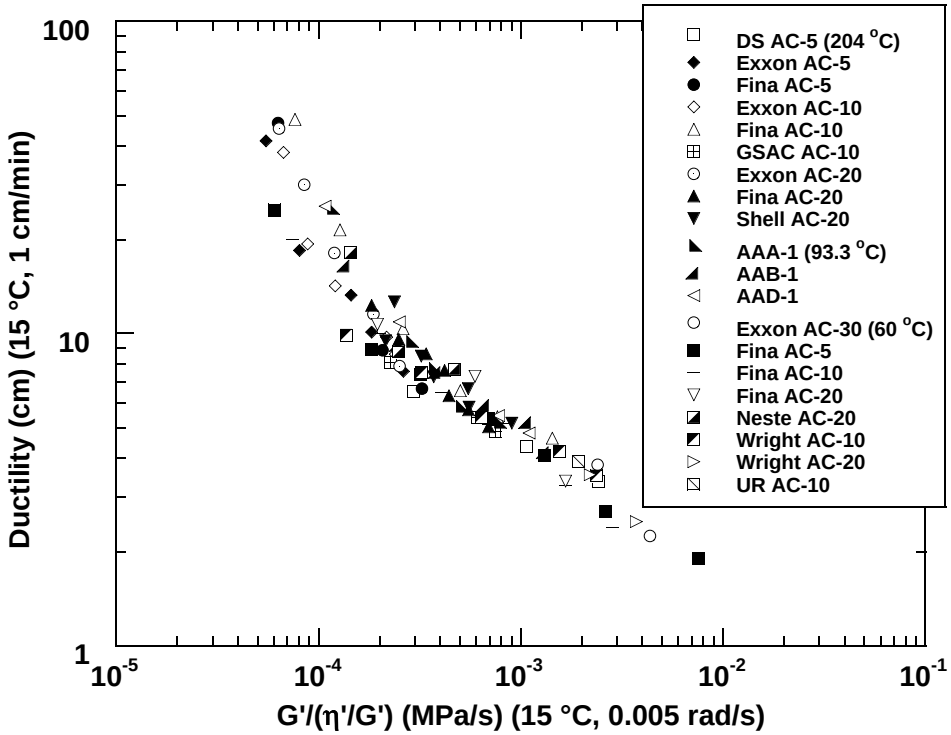

Figure 4-11. Ductility versus DSR Parameter G′/(η′/G′), All Ductilities.

Figure 4-12 shows the linear region below 10 cm, and from this a map with curves of constant ductility is produced and is shown in Figure 4-13. Each point on the line in Figure 4-12 produces a line of constant ductility, which is also a line of constant G′ to η′/G′ ratio in Figure 4-13. This produces the ductility regions shown in the figure and the data are shown in the figure as well. That the data do not fall in the regions perfectly is the result of the scatter of the data around the line in Figure 4-12. Again, we make the observation that a whole range of values of G′ and η′/G′ can produce the same asphalt ductility.

The point of Figure 4-12 is that for conventional asphalts the function G′/(η′/G′) can serve as a surrogate for ductility, is easier to measure, and requires less material.

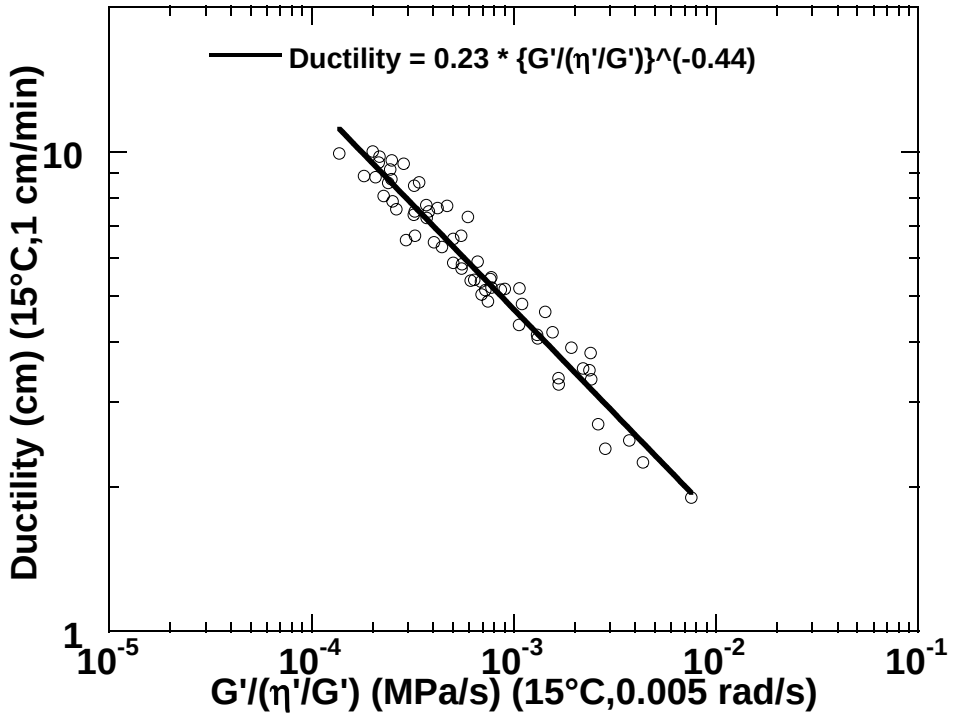

Figure 4-12. Ductility versus DSR Parameter G′/(η′/G′), Low Ductilities.

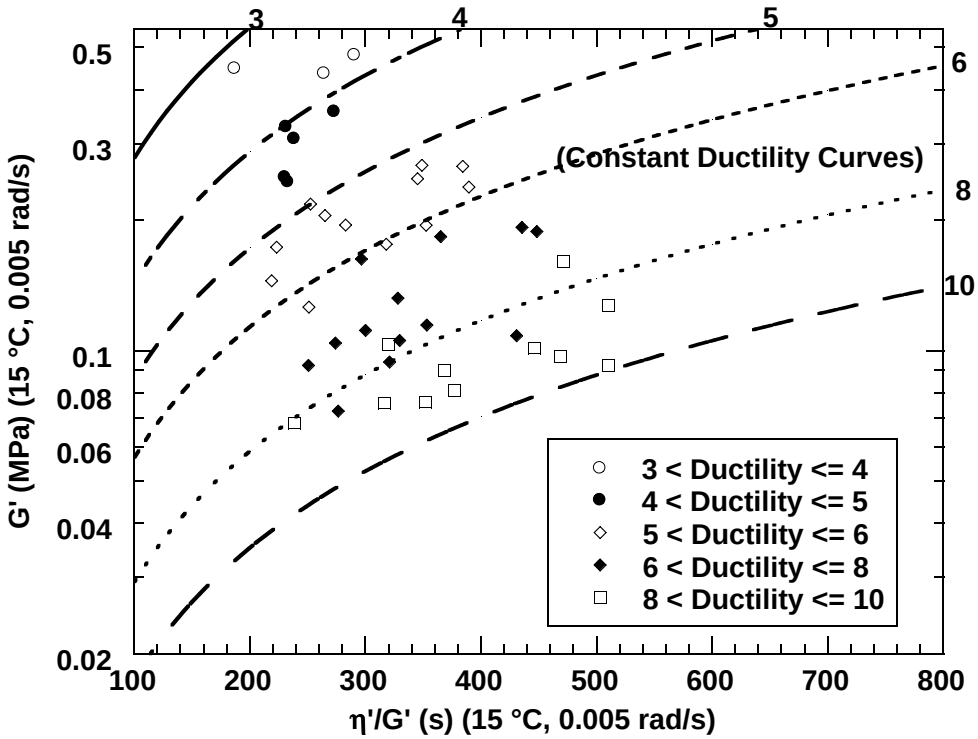

Figure 4-13. G′ versus η′/G′ Map at Low Ductilities with Lines of Constant Ductility.

Ductility-DSR Correlation at 10 rad/s

If ductility at 15 °C, 1 cm/min can be used as an indication of durability, as the literature indicates, then through the correlation of the above section, so can $G'/(\eta'/G')$ at 15 °C, 0.005 rad/s. However, this low a frequency is not accessible to most instruments except through data taken at several temperatures and over a range of several orders of magnitude in frequency, followed by use of the time-temperature superposition principle. Consequently, it is desirable to shift this correlation by using TTSP to measurements at the SHRP standard of 10 rad/s.

In accordance with TTSP, a viscoelastic property measured at two different temperatures will be the same value if the frequency of measurement is also shifted appropriately. The shift factor a_T is used to to characterize this required shift in frequency (or equivalently, time): $a_T = \omega_o/\omega_T$, where ω_o is a particular frequency of interest on the master curve for a particular reference temperature and ω_T is the frequency that gives the same value of the property at a different temperature, T. If the shift factor is known for a material, then measurements at one frequency-temperature condition can be shifted to another frequency and temperature.

The dependence of the shift factor on temperature commonly is described by using an empirical expression known as the WLF (Williams-Landel-Ferry) (Williams et al., 1955) equation:

$$\log a(T)_R = - C1(T - T_R) / (C_2 + T - T_R), \quad (4\text{-}10)$$

where

T = the selected temperature, °C or K,
T_R = the reference temperature, °C or K,
$a(T)_R$ = the shift factor at temperature T relative to the reference temperature T_R, and
C_1, C_2 = empirically determined coefficients.

Anderson et al. (1994) found that for pavement asphalts, the appropriate WLF form was

$$\log a(T)_d = - C_1(T - T_d) / (C_2 + T - T_d), \quad (4\text{-}11)$$

where $a(T)_d$ is the shift factor at temperature T relative to the "defining" temperature T_d. Also, they found that with fixed values of C_1 and C_2 (equal to 19 and 92, respectively) the defining temperature T_d was a characteristic parameter for each asphalt and varied from −14.5 °C to 6 °C. Their values for T_d are shown in Table 4-2.

Table 4-2. Defining Temperature T_d for PAV-Conditioned SHRP Asphalts (Anderson et al., 1994).

Sample	T_d (°C)
AAA-1	-14.5
AAB-1	-6.0
AAC-1	3.5
AAD-1	-8.7
AAF-1	5.2
AAG-1	2.7
AAK-1	-9.2
AAM-1	6.0

For our work, we used the values of C_1 and C_2 from Anderson et al. (1994) and an average of their values for T_d. Thus, all parameters in the WLF equation were fixed. From a practical point of view, this will be necessary for a test procedure on unknown asphalts. To determine the temperature T that is appropriate for DSR measurements at 10 rad/s in the sense that it would be equivalent to measurements AT 15 °C and 0.005 rad/s, we proceeded in two steps. First, the shift factor is calculated for a temperature shift from 15 °C to −2.63 °C (T_d) and from this the appropriate test frequency at the defining temperature.

$$\log a(T)_d = -19(15-(-2.63))/(92+15-(-2.63)), \quad (4\text{-}12)$$

which gives $a(T)_d = 8.8(10^{-4})$. Thus, the appropriate test frequency at −2.63 °C would be $\omega(T_d) = a(T)_d\omega(15) = 4.4(10^{-6})$ rad/s; testing at -2.63 °C and $4.4(10^{-6})$ rad/s is equivalent to testing at 15 °C and 0.005 rad/s.

Second, the shift factor from $\omega(T)_d$ to 10 rad/s, $4.4(10^{-7})$, is used to calculate the appropriate test temperature at 10 rad/s. Equation 4-11 with the appropriate substitutions gives

$$\log (4.4(10^{-7})) = -19(T-(-2.63))/(92+T-(-2.63)), \quad (4\text{-}13)$$

from which T = 43 °C.

From data at temperatures close to 43 °C we determined that 44.7 °C was a better choice than 43 °C . Figures 4-14 through 4-18 compare the DSR function $G'/(\eta'/G')$ measured at 15 °C and 0.005 rad/s to measurements at 10 rad/s and 44.7 °C for several asphalts. All show reasonable, although not perfect, agreement between these two conditions. It should be noted that discrepancies are not unexpected due to the simplifying assumptions that were made, i.e., that TTSP is valid, and that the constants C_1 and C_2 and the defining temperature T_d were assumed to

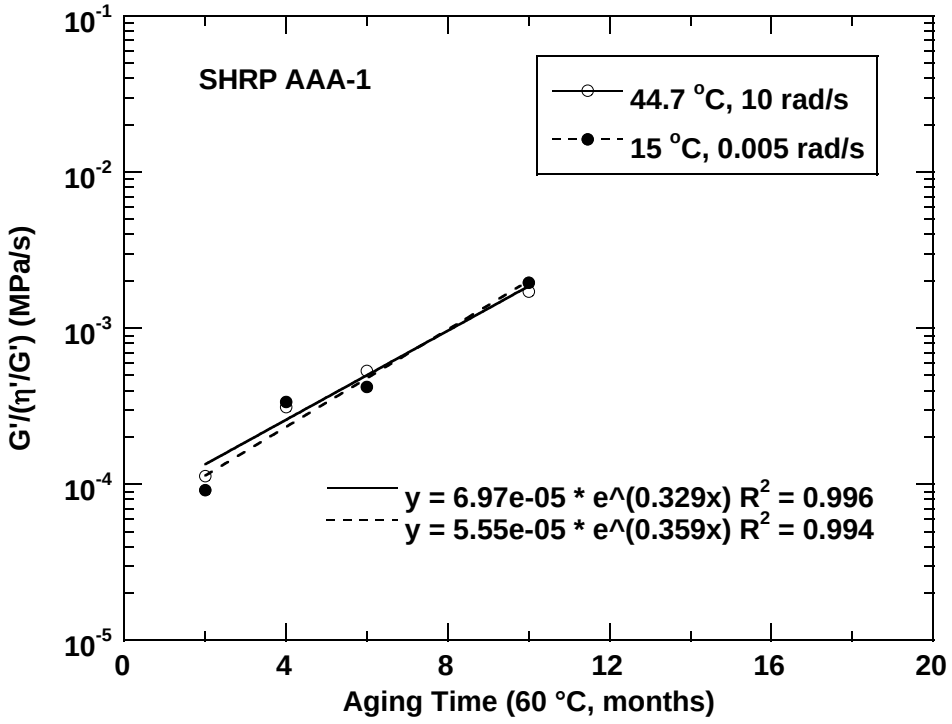

Figure 4-14. Increase in G′/(η′/G′) with Aging at Two Test Conditions: SHRP AAA-1.

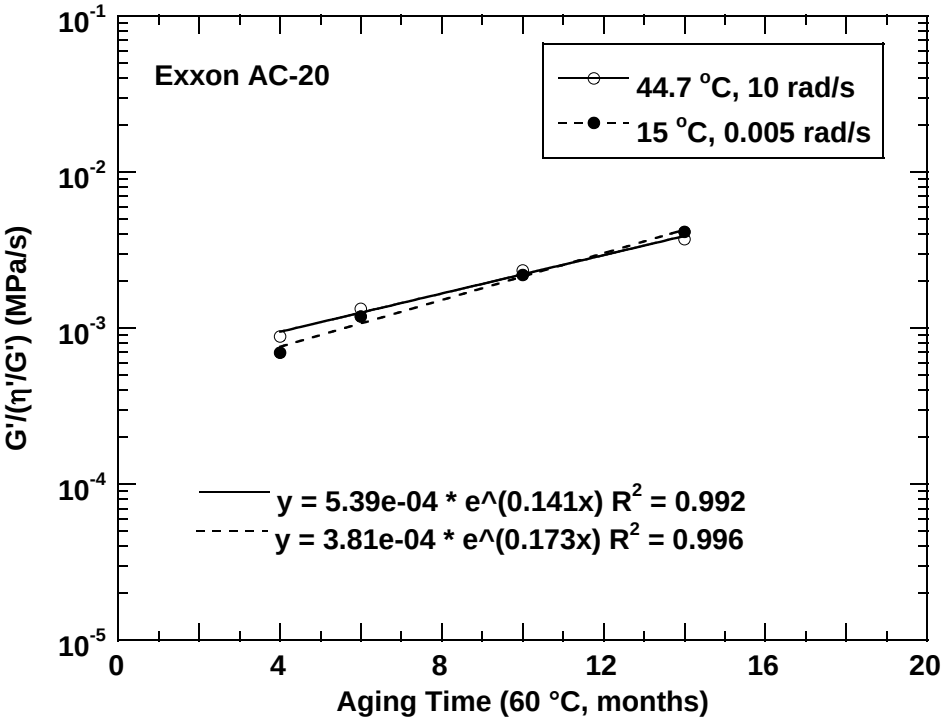

Figure 4-15. Increase in G′/(η′/G′) with Aging at Two Test Conditions: Exxon AC-20.

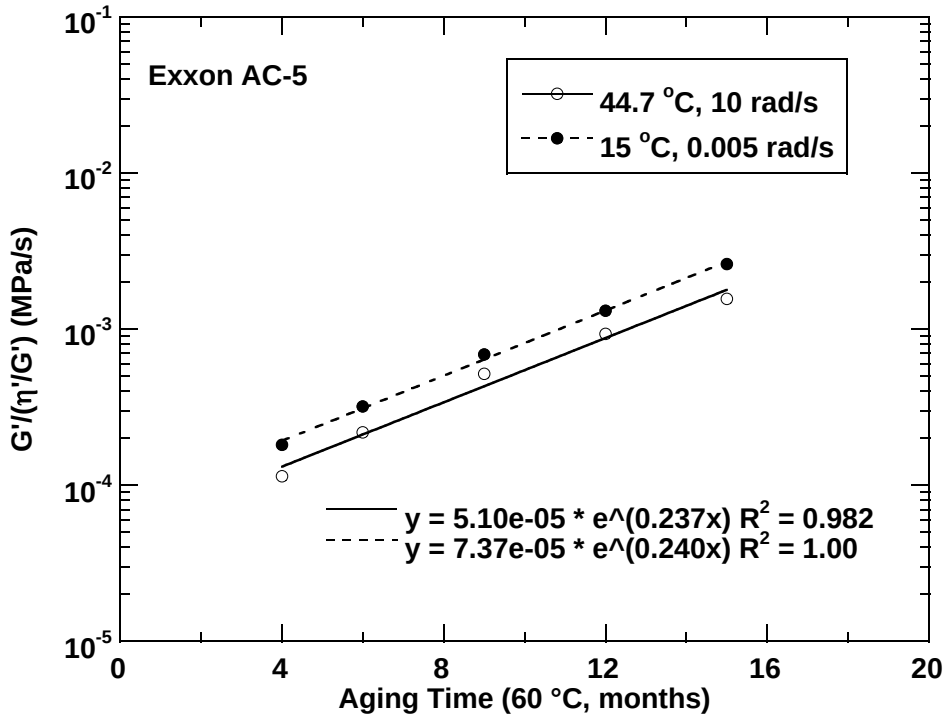

Figure 4-16. Increase in G′/(η′/G′) with Aging at Two Test Conditions: Fina AC-5.

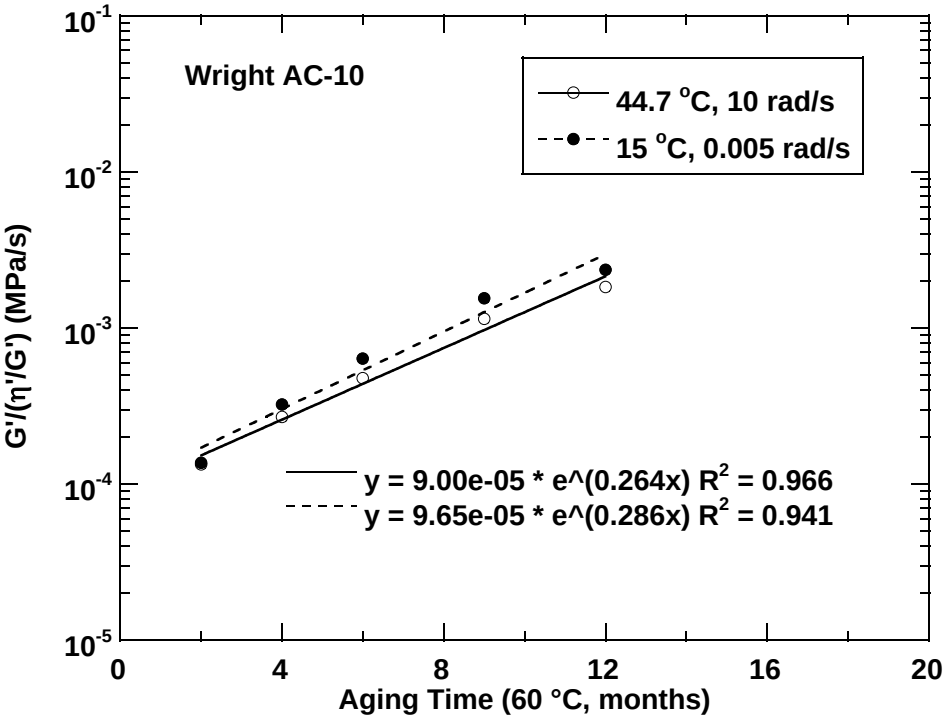

Figure 4-17. Increase in G′/(η′/G′) with Aging at Two Test Conditions: Wright AC-10.

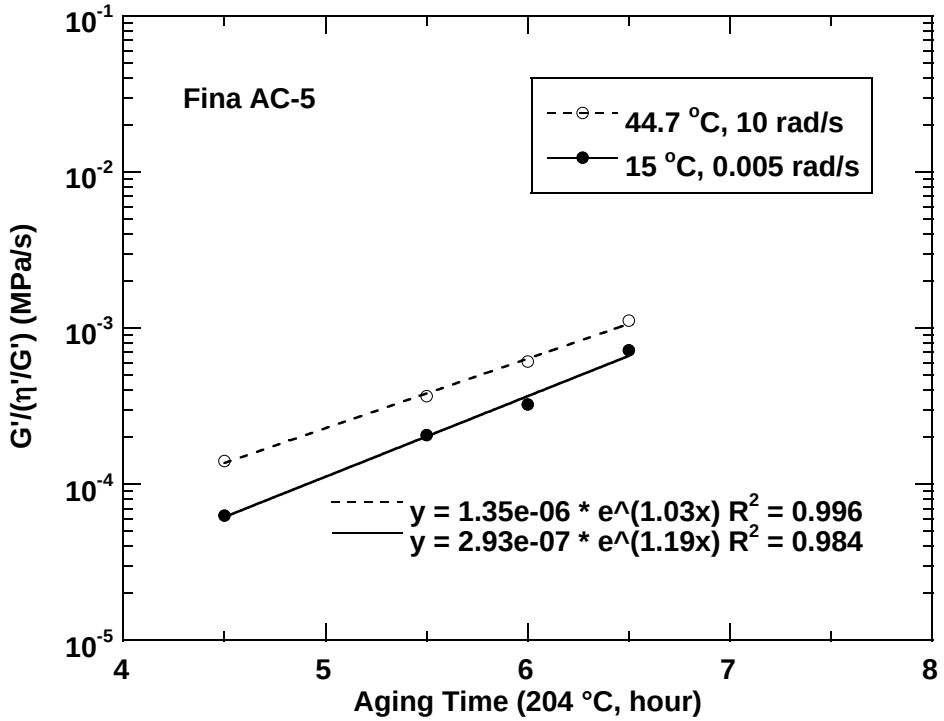

Figure 4-18. Increase in G′/(η′/G′) with Aging at Two Test Conditions: Fina AC-5.

be the same for all the asphalts. As mentioned previously, TTSP is most certainly invalid to some degree, as evidenced by the problems with the phase angle master curve, Figure 4-4. Furthermore, the fact that Anderson et al. (1994) saw a range of values for T_d suggests that our use of a single value is less than ideal. Finally, the best WLF parameters may, in fact, be different from theirs for the reason that our materials are more heavily aged than the PAV conditions that they tested. So, all things considered, the agreement between the two test conditions actually is quite good.

Figure 4-19 shows the ductility-DSR correlation for DSR properties measured at the shifted conditions of 44.7 °C and 10 rad/s. In the low-ductility region, again there is a good linear relationship between these two parameters, although there is somewhat more scatter than that of Figure 4-12. Note that the line shown is the same as that in Figure 4-12 and that the scatter of the 44.7 °C, 10 rad/s measurements bracket the line quite well.

This correlation, together with an aging procedure (Chapter 6) form a basis for a new test procedure for predicting asphalt binder durability in pavements. Chapter 8 presents this new procedure.

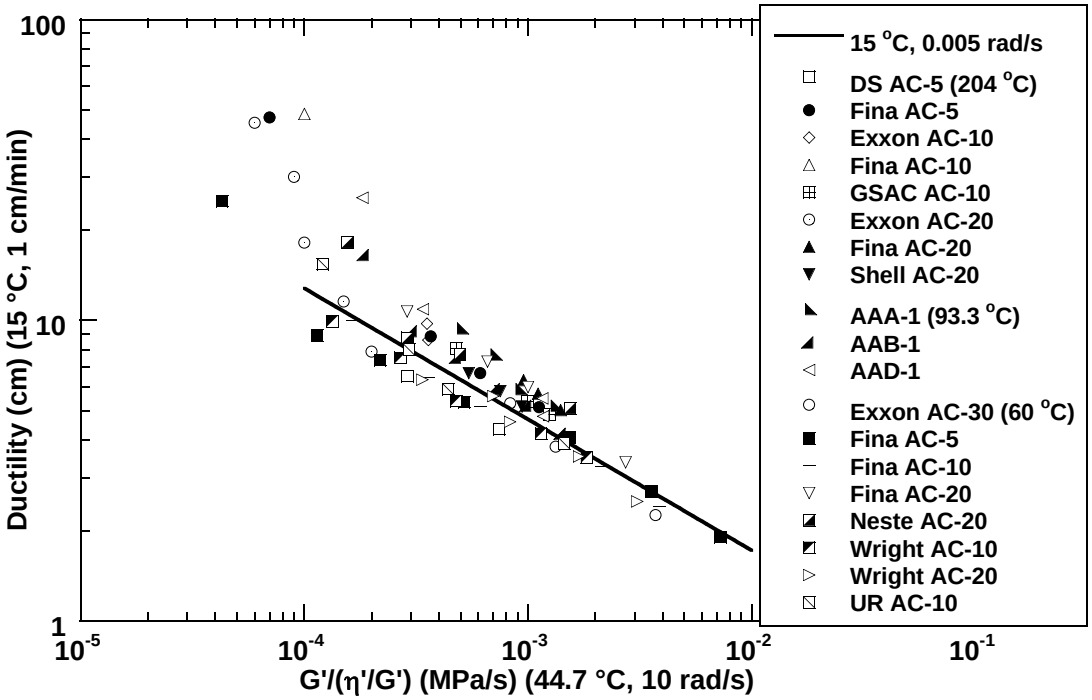

Figure 4-19. Ductility (15 °C, 0.005 rad/s) versus DSR Parameter G′/(η′/G′) (44.7 °C, 10 rad/s), All Ductilities.

CONCLUSION

Field tests indicate that ductility measured at low temperature is a good indicator of age-related cracking of asphalt binders. When a pavement's binder ductility decreases to a certain critical value, cracking is inevitable.

Binder ductility decreases dramatically with oxidative aging due to increases in both the viscosity and elastic modulus that result in a more solidlike material. Changes in ductility can be conceptually understood in the context of these changes in rheological properties through an elongation flow model that utilizes a simple Maxwell element.

Ductility correlates very well with G′/(η′/G′) for conventional asphalt binders aged at different conditions, especially when ductility is below 10 cm. In this region, the logarithm of ductility varies approximately linearly with the logarithm of G′/(η′/G′), and ductility measurements potentially can be replaced by G′/(η′/G′), measured at 10 rad/s, 44.7 °C using the DSR. This provides the basis for a new asphalt durability test, presented in Chapter 8.

CHAPTER 5. POLYMER MODIFIED ASPHALTS: OXIDATIVE AGING, RHEOLOGY, AND DUCTILITY

ABSTRACT

The effect of different polymeric modifiers on properties of asphalt binders was investigated. All samples are commercially used materials and came from the suppliers directly. Modifiers include diblock poly (styrene-b-butadiene) rubber (SBR), triblock poly (styrene-b-butadiene-b-styrene) (SBS), and tire rubber. Binder properties investigated include aging properties (hardening and oxidation). In addition, the effect of aging on modifiers was studied by means of size exclusion chromatography (SEC).

For the modifiers studied in this work, modified binders have a lower hardening rate than their corresponding base asphalts. Modified binders also have lower oxidation rates than their base materials, but the difference is not as big as for the hardening rates, and there are even some exceptions. Finally, modified binders have lower hardening susceptibility compared with their base materials.

With aging, the asphaltene content in binders increases, and modifiers such as SBR and SBS molecules will degrade.

INTRODUCTION

Asphalt is a viscoelastic material that behaves like an elastic solid at low temperature or high frequency, and like a viscous liquid at high temperature or low frequency. The purpose of asphalt modification is to minimize the effects of this behavior and thus minimize stress cracking at low temperatures and plastic deformation at high temperatures (Bouldin et al., 1991; Lewandowski, 1994).

Bouldin et al. (1992) found that polymer modification with SBS resulted in binders having superior rutting resistance compared to the straight asphalt due to a polymeric network structure, which led to enhanced performance especially at elevated temperatures.

The effect of adding modifiers to asphalt was to increase molecular associations and provide elastic stability at higher temperatures, resulting in a decrease in loss tangent (Tayebali et al., 1992).

Linde and Johansson (1992) used size exclusion chromatography (SEC) to study the aging of SBS-modified binders and found that pronounced molecular size change occurred both in the bitumen and the polymer phase, resulting in changes in mechanical properties.

As for extensional properties, Srivastava et al. (1992) found that the ductility of the binder was increased by an order of magnitude by SBS. The aging of modified binders was also

less pronounced than base asphalts. The authors' explanation was that the active components of asphalt, such as naphthene and polar aromatics, carried out micro-structural interactions with the modifier (being the styrene-component of SBS) that prevented active components from oxidizing. The rubbery properties of the butadiene became evident in a ductility test. Modified binders needed more energy to deform than the base asphalt. Also, the elastic recovery of SBS-modified binder was much higher than unmodified asphalt. This resulted in an increased flexibility at low temperatures.

Muncy et al. (1987) found that SBR modification generally could improve the aging and consequent hardening characteristics of the asphalt, as indicated by the viscosity ratio, but there were some exceptions.

Shuler et al. (1987) noted that SBS was composed of glassy polystyrene end blocks and rubbery polybutadiene midblocks and that the polystyrene and polybutadiene blocks existed as two separate phases at typical pavement service temperatures. The resulting structure is a 3-D network of hard, spherical polystyrene domains in a rubbery matrix. This rubbery network imparted elastic properties to the modified binders.

Because of the importance of successes with polymer modification of asphalt binders, the purpose of the work of this chapter was to further investigate the effect of polymers on binder properties and especially the effect of oxidative aging on polymer modified properties. The work is presented in three sections. The first study addresses the effect of modifiers on aging properties, specifically on oxidation and viscosity hardening. The second part is a more detailed study of the rheology of modified binders, in the context of master curves, and the impact of aging on these properties. The third section is a study of the effect of modification on the ductility of aged binders, as it relates to the correlations of Chapter 4 and to the results of the previous sections of this chapter.

OXIDATION AND VISCOSITY HARDENING OF POLYMER MODIFIED ASPHALTS

Methodology

Dynamic viscosity was measured with a Carimed CSL500 dynamic shear rheometer.

In addition to these physical property measurements, FTIR infrared spectra were obtained on a number of asphalt materials as a measure of the amount of oxidation following the method of Jemison et al. (1992). The area under the carbonyl absorbance band (1650 to 1800 cm^{-1}) represents the extent of oxidation in asphalt materials (Liu et al., 1998) and is reported as carbonyl area (CA). A Waters HPLC-SEC system was used to measure the molecular size distribution of the asphaltic materials.

Materials used were nine conventional asphalt cements from six suppliers. These base asphalts were modified with poly (styrene-butadiene) rubber and/or poly (syrene-butadiene-

styrene) and in addition, one of the asphalts was modified with highly-cured ground tire rubber plus SBS. Another material, available from a high-cure rubber test section placed by our group in June 2000, also was included in the study.

All asphaltic materials were aged at 60 ºC in a controlled environment room to simulate the long-term road aging. Aging times ranged from 2 to 18 months. Previous aging kinetics studies showed that accelerated aging at elevated temperature and pressure produces different rankings of asphalts than aging at road conditions (Domke et al., 1999; Liu et al., 1996). This is especially true of modified materials and necessitates measurements at conditions closer to actual pavement service in order to be more meaningfully related to expected pavement performance.

Results and Discussion

Asphalt Composition and Aging

Conventional asphalt binders can be separated by means of the Corbett precipitation and alumina column chromatographic procedure (ASTM D4124) into four fractions: saturates, naphthene aromatics, polar aromatics, and asphaltenes. According to Corbett (1979), asphalt can be viewed as an associated system of asphaltenes dissolved in the maltene (non-asphaltene) phase. Asphaltenes contribute to a good viscosity temperature susceptibility, and they are important viscosity builders. Polar aromatics greatly contribute to ductility and the dispersion of asphaltenes. Both saturates and naphthene aromatics work against good ductility.

Pfeiffer and Saal (1940) proposed a peptization model to represent the associated nature of asphalt binder. In this model, asphaltenes (the most polar and heaviest of the asphalt constituents) form the center of some associated entities surrounded and stabilized by resins and other constituents of the maltenes. Whenever a shortage of resin occurs, attractive forces are enhanced and increase the molecular associations and ultimately extend the gel-type structure.

As an asphalt oxidizes, the heaviest naphthene aromatics convert to polar aromatics, and the heaviest polar aromatics to asphaltenes (Petersen, 1984; Liu et al., 1998a). As a result, a shortage of resin occurs, and the asphaltene associations increase in size and number according to the above model. These increased associations result in the asphalt becoming stiffer and more difficult to flow and to relieve stress (Lin et al., 1998; Lin et al., 1996).

Effect of Modifiers on Oxidation of Asphalt Binders

With aging, asphalt binders harden because of these increased associations, thereby losing their ability to flow and deform under external loads (Chapter 4). After enough aging, this hardening results in serious pavement cracking. Consequently, it is important to investigate the effect of modifiers on the oxidation and hardening of asphalts. The introductory discussion indicated that polymeric modifiers could slightly improve the asphalt binder's aging resistance (Dhalaan et al., 1992; Ista and Choquet, 1992; Srivastava et al., 1992; Muncy et al., 1987).

Here, the parameter hardening rate (HR) is used to describe this effect. It is found that the logarithm of low shear rate dynamic viscosity (η_0^*) is linear with aging time after the "initial jump" aging period (Lau et al., 1992), and the slope of this linear relationship is called the hardening rate:

$$\text{Hardening rate} = \partial (\ln \eta_0^*) / \partial t \tag{5-1}$$

where t is aging time and η_0^* typically is at 60 °C and at a sufficiently low frequency (0.1 rad/s or lower) that the material is very nearly Newtonian.

From its definition, the hardening rate is a measure of how sensitive an asphalt binder's viscosity is to aging time. Obviously, binders having low hardening rates are desired.

Recognizing that η_0^* is a function of the extent of oxidation, which in turn increases with time according to appropriate oxidation kinetics, i.e., $\eta_0^* = \eta_0^*(CA(t))$, the hardening rate can be expressed as the product of two derivatives:

$$\partial (\ln \eta_0^*) / \partial t = [\partial (\ln \eta_0^*)/ \partial CA] [\partial CA / \partial t] \tag{5-2}$$

where CA is carbonyl area measured by FTIR. Carbonyl area is used as an indicator of oxidation extent because it represents the oxidation product, including ketones, carboxylic acids and anhydrides, and other compounds with the C = O bond in a way that relates directly to viscosity hardening and total oxidation (Lau et al., 1992; Liu et al., 1998b).

The first term on the right side of Equation 5-2 is called the hardening susceptibility (HS), which is a characteristic property for asphalts. It indicates the sensitivity of the viscosity change due to carbonyl content increase. A desirable asphalt binder would have a comparatively low value of hardening susceptibility, which means that the binder's viscosity would increase slowly with oxidation.

The second term is the oxidation rate, and Lau et al. (1992) reported that after the initial jump period, asphalt oxidation as represented by carbonyl area can be described by:

$$CA = CA_0 + r_{CA}\, t \tag{5-3}$$

where CA_0 is the intercept, and r_{CA} is the constant reaction rate (oxidation rate) after the early time initial jump period.

Table 5-1 and Figures 5-1a, 5-1b, and 5-1c show the effect of modifiers on hardening rate, oxidation rate, and hardening susceptibility of asphalt binders. The hardening rate is the bottom-line viscosity performance indicator while the oxidation rate and the HS reflect underlying causes of hardening. In each case in Figure 5-1a, the polymer-modified binders have

a lower hardening rate than their corresponding base asphalts. In addition, the difference in hardening rate varies with the base asphalt, modifier type, and modifier concentration.

Generally, modified binders have a lower oxidation rate than their base materials (Figure 5-1b). However, the difference in oxidation rate between them is much smaller than the difference in hardening rate. There are even some exceptions: Fina AC-10 1 percent SBR, GSAC AC-10 3 percent SBS, and Wright AC-20 5 percent tire rubber plus from 2 to 5 percent SBS have a higher oxidation rate than their corresponding base asphalts.

Similar to hardening rate, modified binders have lower hardening susceptibility than unmodified ones, i.e. the viscosity of modified binders is less sensitive to oxidation than that of base asphalts (Figure 5-1c). This is true for each material tested in this project, although the effect is relatively minor in some cases. At this point, we can only hypothesize possible reasons for this phenomenon as:

1) polymer modifiers interfere with asphalt associations to the extent that in the presence of polymer, asphalt oxidation does not produce as much or as strong associations as in its absence and

2) with aging, polymer modifiers may decompose, resulting in a decrease in viscosity enhancement on the modifiers part and perhaps even serving to increase the resin portion of the asphalt so as to improve solubilization of the asphaltenes.

Due to the strong viscosity increases which occur with asphaltene production, the net effect of this such polymer degradation and asphalt oxidation would still be to increase the binder's viscosity, just not as much as the base asphalt.

The combined effect of oxidation rate and HS reductions is to produce the improved hardening rates in Table 5-1 and Figure 5-1a, but some significant differences appear in asphalt response to modifiers. As was noted above, the HS is reduced (compared to the base asphalt) for all of the asphalt/modifier combinations studied and the oxidation rate is reduced more often than not, but the effect is not universal. For most cases, the reductions are mild and do not generally favor either oxidation rate or HS significantly. However, for three asphalts, the comparisons are more striking. For both the Wright AC-10 and the UR AC-10, the oxidation rate has the greatest improvement (approximately 30 percent) while for the TFA AC-20, the oxidation rate improvement is marginal and the HS improvement is nearly 50 percent. Also, note that the Wright AC-20 modified by both tire rubber and SBS has by far the best improvement in HS (although the oxidation rate is actually increased). These results suggest that there can be some significant compositional effects on asphalt/polymer interactions that impact oxidation and subsequent hardening and that bear further study.

Table 5-1. Effect of Modifiers on Oxidation Properties of Asphalt Binders.

Sample	Hardening Rate (ln [poise]/day)	Oxidation Rate (day^{-1})	Hardening Susceptibility
Fina AC-5	0.00563	0.00122	4.61
Fina AC-5 2% SBR	0.00438	0.00116	3.77
Fina AC-10	0.00552	0.00139	3.96
Fina AC-10 2% SBR	0.00491	0.00132	3.71
Fina AC-20	0.01061	0.00245	4.32
Fina AC-20 1% SBR	0.00780	0.00213	3.66
Wright AC-10	0.00821	0.00153	5.38
Wright AC-10 2% SBR	0.00459	0.00093	4.94
Wright AC-10 3% SBR	0.00372	0.00093	4.01
Wright AC-10 3% SBS	0.00510	0.00102	5.02
Wright AC-20	0.00776	0.00127	6.09
Wright Ac-20 3% SBR	0.00452	0.00108	4.20
Wright AC-20 3% SBS	0.00499	0.00103	4.84
Wright AC-20 5% Tire Rubber + 2~ 5% SBS	0.00380	0.00150	2.53
TFA AC-20	0.00935	0.00118	7.90
TFA AC-20 3% SBR	0.00458	0.00101	4.52
Exxon AC-30	0.00702	0.00123	5.71
Exxon Base 1% SBR	0.00440	0.00088	4.98
UR AC-10	0.00768	0.00197	3.89
UR AC-10 3% SBR	0.00347	0.00122	2.85
GSAC AC-10	0.00438	0.00149	2.94
GSAC AC-10 3% SBS	0.00342	0.00155	2.21

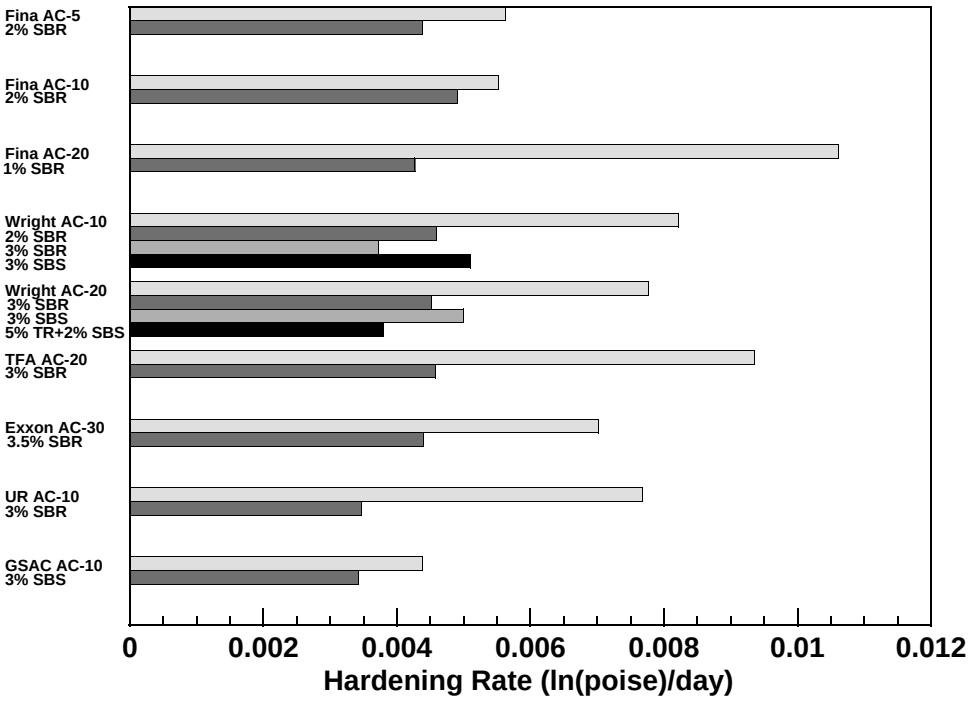

Figure 5-1a. The Effect of Modifiers on Binder Hardening Rates.

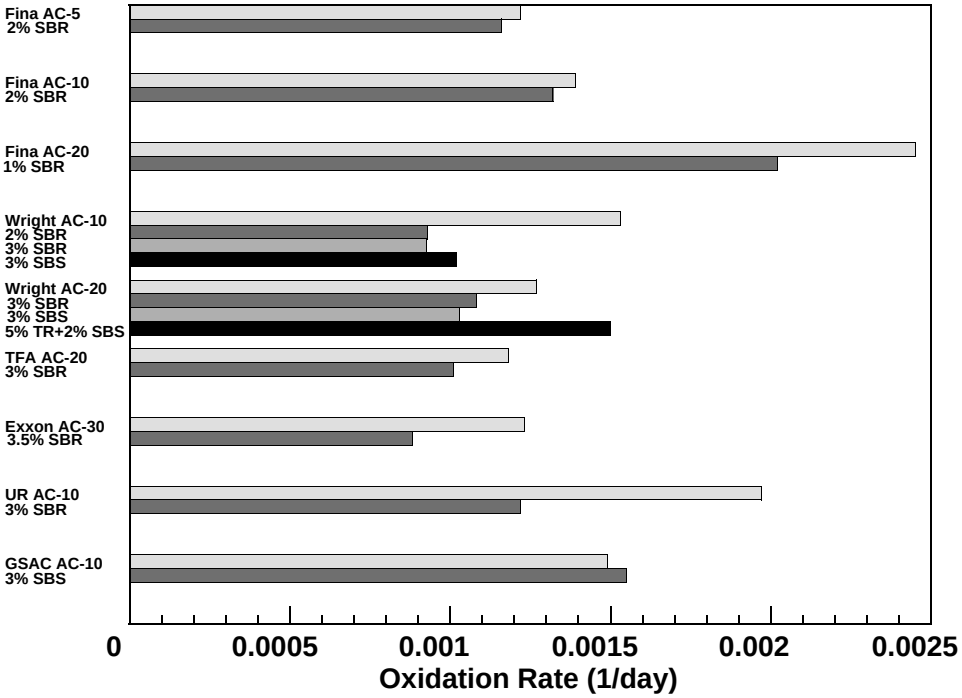

Figure 5-1b. The Effect of Modifiers on Binder Oxidation Rates.

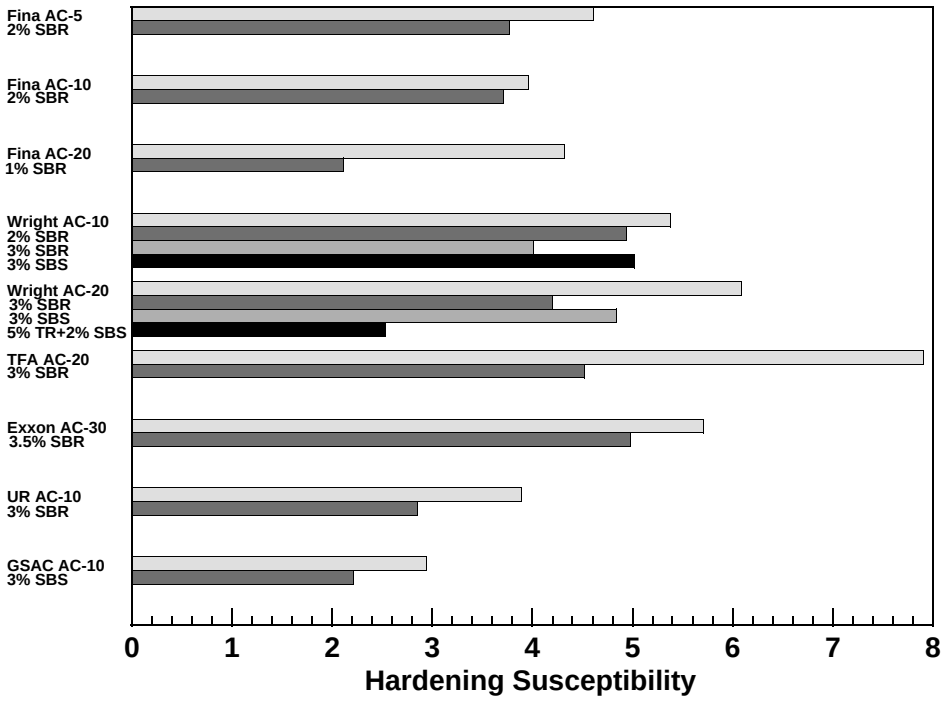

Figure 5-1c. The Effect of Modifiers on Binder Hardening Susceptibilities.

Effect of Aging on Modifiers

Linde and Johansson (1992) aged SBS-modified asphalt at 200 °C for different times and found that after a few hours, there was a significant change in the polymer phase. After 24 hours, almost all of the original SBS had degraded to lower molecular size. The asphalt phase showed the opposite behavior; larger molecular size fractions were formed.

Figure 5-2a, 5-2b, and 5-2c are SEC chromatograms for the Wright AC-10 group aged at 60 °C for zero, six, and 12 months, respectively. In these figures, the chromatogram is the bottom plot and the top plot is the difference between the modified and unmodified chromatograms for the same amount of aging. For unaged binders (Figure 5-2a), the three peaks (from left to right) correspond to modifiers (polymers), primarily asphaltenes, and primarily maltenes. Polymer molecules elute from the column before asphaltenes, which means that both SBR and SBS molecules are larger than the associations of asphaltene. The peak of SBS is narrower and higher than that of SBR, meaning that the molecular weight distribution of SBS is narrower than SBR. In addition, the SBS peak elutes somewhat earlier than the SBR peak, indicating that the molecular weight of SBS is a little higher than that of SBR.

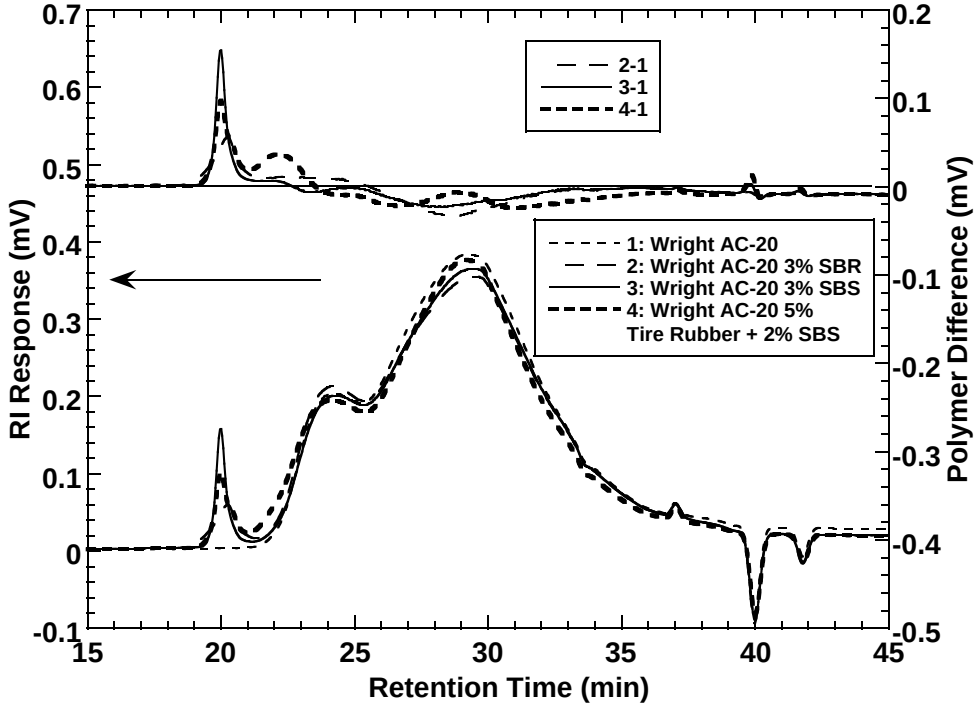

Figure 5-2a. SEC Chromatograms for Wright AC-10/SBR or SBS: Unaged.

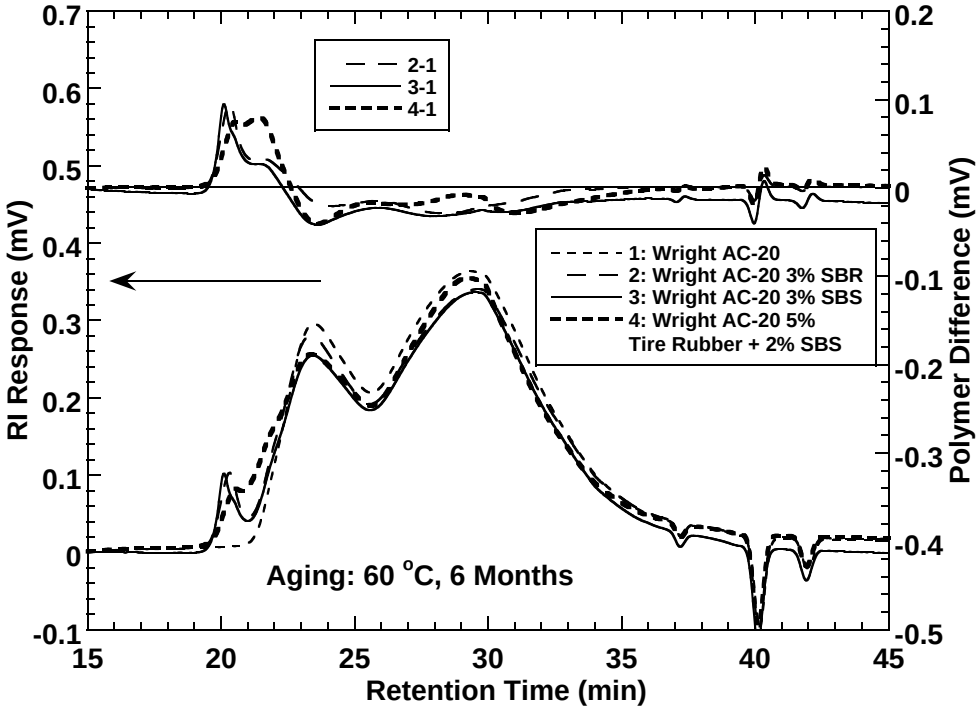

Figure 5-2b. SEC Chromatograms for Wright AC-10/SBR or SBS: Aged 6 Months.

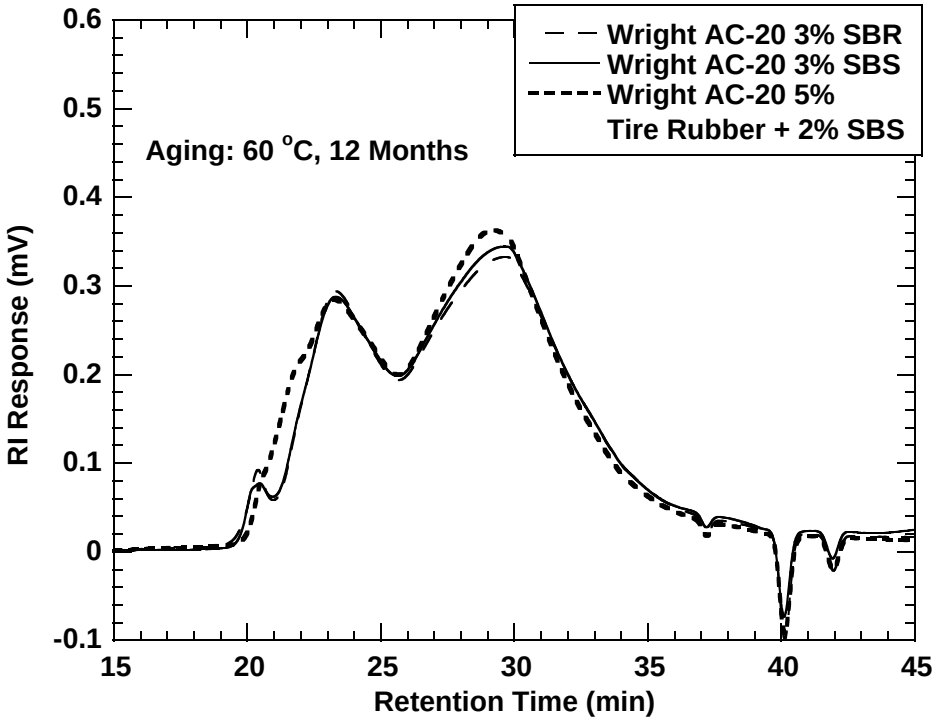

Figure 5-2c. SEC Chromatograms for Wright AC-10/SBR or SBS: Aged 12 Months.

After six months aging at 60 °C, three prominent differences between Figure 5-2b and Figure 5-2a are evident. First, the asphaltene peak increased dramatically in size and shifted earlier in time. This phenomenon is the result of production of more asphaltene from naphthene and polar aromatics and from an increase in the size of the asphaltene structures due to increasing molecular interactions (Mullins and Sheu, 1998). Second, the polymer peak has shifted to a later time, indicating that the large polymer molecules decompose to smaller ones. Third, there is almost no difference between SBS (3 percent) peak and SBR peak (3 percent). By a full 12 months aging (Figure 5-2c), the polymer peak almost merges into the asphaltene peak, meaning that the polymers further decomposed. In addition, there is almost no difference between the asphaltene peaks in Figures 5-2b and 5-2c. While this might be attributed to minimal asphaltene growth in subsequent aging, the HS value of about five would argue against this. It may be more likely that large "asphaltene" growth in the first 6 months actually is due to a combination of degraded polymer and asphaltene and that further aging actually reduces the polymer contribution as asphaltenes continue to grow.

Figures 5-3a and 5-3b are SEC chromatograms for the PG70 group aged for zero and six months at 60 °C, respectively. From the bottom chromatogram, we can see that with the increase in tire rubber concentration, the asphaltene peak decreases. Our explanation is that tire rubber particles can adsorb asphaltene, and some rubber particles are larger than the filter pore (0.45 μm), so they could not go though the filter, and GPC could not measure these large particles. The upper spectrum indicates that tire rubber particles are larger than asphaltene.

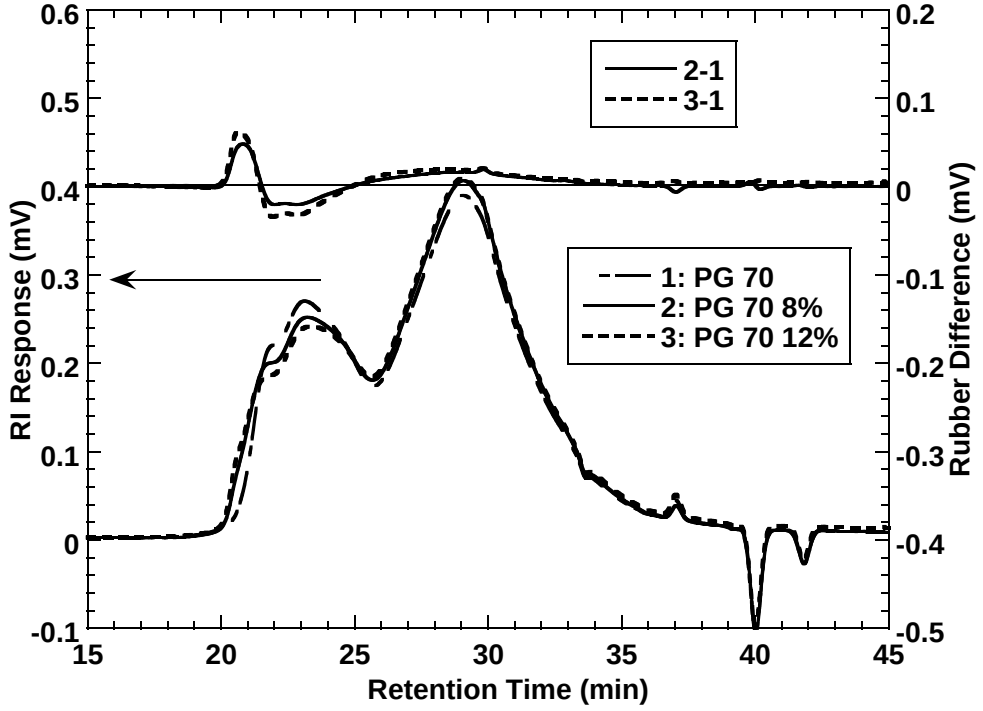

Figure 5-3a. SEC Chromatograms of a PG-70/HC-CRM: Unaged.

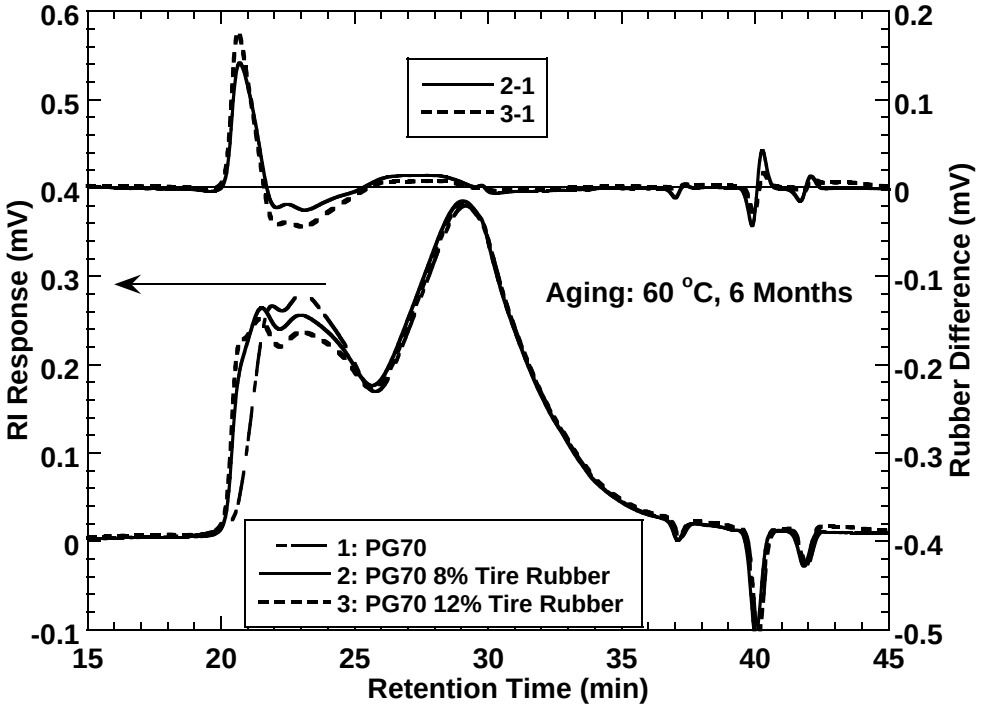

Figue 5-3b. SEC Chromatograms of a PG-70/HC-CRM: Aged 6 Months.

After six months aging (Figure 5-3b), the asphaltene peak increases and moves to the left slightly, meaning these asphalts have not produced much asphaltene upon aging. The upper spectrum indicates that the height of the tire rubber peak increases with aging. Our explanation is that during the aging procedure, oxygen could break down rubber particles so that more tire rubber particles pass through the filter. As a result, the rubber concentration in the SEC sample increases.

Conclusion

Polymer-modified binders tend to have a lower hardening rate than their corresponding base asphalts. The extent of decrease in hardening rate is different for different base asphalts and occurs due to the combined effects of aging on oxidation rate and hardening susceptibility. Modified binders also have a lower oxidation rate than their base materials, but the difference is not as large as that of hardening rate, and there are even some exceptions. Finally, modified binders have lower hardening susceptibility compared with their base materials, and in some cases the results can be dramatic. Chapter 6 presents additional results on oxidation and hardening of asphalts and modified asphalts.

With oxidative aging, the asphaltene content in binders increases, and modifiers, such as SBR, SBS, and tire rubber, degrade to smaller molecules. The next sections discuss the impact of this degradation and other effects of aging polymer-modified asphalts on binder properties.

EFFECT OF POLYMER MODIFIERS AND OXIDATION ON RHEOLOGICAL PROPERTIES

Abstract

The effect of different polymer modifiers and long-term aging on rheological properties of asphalt binders is presented. Modifiers include diblock poly (styrene-butadiene) rubber, triblock poly (styrene-butadiene-styrene), and tire rubber.

The addition of polymer to unmodified asphalt can lead to a higher complex modulus at high pavement temperature and a lower stiffness at low pavement temperature, meaning polymer modification can bring better rutting (high-temperature permanent deformation) and thermal cracking (low-temperature failure) resistance to pavement. Also polymer-modified binders have broader relaxation spectra than their base asphalts. The existence of a plateau region in loss tangent master curves of modified asphalts indicates the formation of a polymeric network. In addition, polymer additives impart more non-Newtonian properties to base asphalts. Aging increases the complex modulus (especially at high temperatures), decreases the phase angle, lowers the ductility, and damages the polymer network in binders. Aging can also decrease phase angle and destroy the polymeric network inside binders. Finally, aging can broaden the relaxation spectrum of asphalt binders.

Only one linear region where stress increases with elongation exists for unmodified asphalt binders. However, for modified binders, there is an additional region characteristic of the polymer network. SBR-modified asphalt binders can extend longer but build smaller stress than SBS-modified samples due to stronger interaction between SBS and asphalt components and the higher modulus of the polymer network.

With aging, the asphaltene content in binders increases, and modifiers such as SBR and SBS molecules degrade. The result is a reduction in the polymer benefit.

Introduction

Polymer modification of asphalt led to superior rutting resistance compared to the straight asphalt, and it was explained that SBS incorporated in binders could help to form a polymeric network structure that led to enhanced performance, especially at elevated temperatures (Bouldin and Collins, 1992; Lu and Isacsson, 1999). In addition, the formation of a polymeric network depends on both asphalt source and polymer type (Newman, 1998). Gahvari (1997) investigated the effect of SBR, SBS, and poly (styrene-ethylene-butylene-styrene) (SEBS) on the rheology of pavement asphalt and found that the addition of polymers into straight asphalt could decrease their temperature sensitivity and loss tangent and also broaden their relaxation spectra. Another study found that the addition of from 3 to 6 percent polymer into asphalt cement could result in higher viscosity and lower penetration, improved elasticity, and adhesion and tensile characteristics (Dhalaan et al., 1992). Apart from the beneficial environmental impact of the disposal of degrading wastes by recycling rather than by dumping, the introduction of waste tire rubber into asphalt results in a series of improvements, including resistance to fatigue cracking, greater flexibility at low temperatures, improved elasticity, greater adhesion, and higher aging resistance (Ista and Choquet, 1992).

The aging of polymer-modified asphalts is another important issue. Polymer-modified binders were aged for a short time with different methods, and it was found that aging resulted in the degradation of polymer additives (Lu and Isacsson, 1999) and improved elasticity of binders (Newman, 1998).

There are some studies about the effect of aging on the rheology of polymer-modified binders, but they address short-term (hot-mix) aging rather than long-term aging that is more relevant to pavement durability. Also there is no detailed research on the effect of polymer modification on extensional flow and failure of asphalt binders, an important issue to thermal and fatigue cracking in pavements. These two issues are assessed in this section.

Experimental Methodology

Materials

The unmodified asphalt is an AC-20, and polymer additives include diblock poly

(styrene-b-butadiene) rubber, triblock poly (styrene-b-butadiene-b-styrene), and ground tire rubber well-cured in the asphalt.

Aging Method

All asphaltic materials were aged at 60 °C in a controlled environmental room for six months to simulate long-term road aging of approximately 4.5 years (Jemison et al., 1992). Aging at 60 °C was selected to approximate the temperature at which the bulk of pavement oxidation occurs. Higher temperatures, while speeding the process, do not accurately duplicate the balance of reactions that occur, and this is likely to be especially significant for polymer-modified materials.

Test Methods

Dynamic shear properties were measured with a Carri-Med CSL500 dynamic shear rheometer. Measurements were conducted at five temperatures: 0, 10, 25, 40, and 60 °C and frequencies from 0.1 to 100 rad/s, and the time-temperature superposition principle was used to construct master curves for complex modulus G^* and loss tangent tan δ (phase angle δ).

Ductility was obtained at 15 °C and an extensional speed of 1 cm per minute in accordance with ASTM D113-86 (1994). The ductility sample has a 3-cm initial gauge length and a tapered throat. Ductility is recorded as the amount of extension in centimeters of the asphalt specimen before break. Force ductility measurements were obtained at 4 °C and 1 cm per minute elongation speed. In this case, the specimen was similar to the ductility specimen except that the initial gauge length, while still 3 cm in length, had a uniform crosssection 1 cm by 0.5 cm. A strain gauge measured force up to 100 Newton and this measurement was used to estimate stress as a function of extension ratio.

A Waters GPC system was used to measure the molecular size distribution of the asphaltic materials.

Results and Discussion

1. Effect of Modifiers on Dynamic Shear Modulus

An AC-20 asphalt binder was selected for study, and it was modified by the supplier with 3 percent SBR, 3 percent SBS, and 5 percent tire rubber plus 2 percent SBS. Figure 5-4a shows the dynamic shear modulus (G^*) master curves for the base and modified asphalt binders at a reference temperature of 0 °C. Compared with their base, modified binders showed a marked increase in the complex modulus at low angular frequency (high temperature). This means that the addition of polymers into asphalt makes it stiffer at high temperature, and as a result, polymer-modified binders have better rutting resistance than their base. At high angular frequency (low temperature), the trend is the opposite: the addition of polymer brings a lower

stiffness to asphalt binders to make it easier to deform, and this will bring better thermal cracking resistance to the pavement. However, the effect of polymer on asphalt binder at high temperature is much more obvious than that at low temperature. At high temperature, the addition of 5 percent tire rubber plus 2 percent SBS increased the complex modulus approximately 10 times, but at low temperature, it decreased the complex modulus by only about 15 percent.

Polymers vary in their ability to change the complex modulus. Comparing 3 percent SBR and 3 percent SBS for this base material, the SBR was somewhat more effective at increasing the base asphalt's stiffness at high temperature.

Figure 5-4a also indicates the effect of polymer modification on the slope of complex modulus master curve (Gahvari, 1997). Over almost the entire frequency range, the addition of polymers into the base asphalt brings a considerable decrease in the slope of complex modulus master curve. This decrease in the slope means the polymer-modified asphalt binders have improved temperature susceptibility over the unmodified binder with respect to G*.

Figure 5-4b shows the effect of six months of aging at 60 °C relative to the unaged materials in Figure 5-4a and indicates that oxidative aging increases G*, especially at high temperatures (low frequency). At low temperature (high frequency), the change in G* is relatively small with aging. As a result, the slope of G* versus ω curve decreases with aging, meaning that aging makes the asphalt binder less temperature sensitive in G*. Note that these effects are true of both the modified and unmodified materials.

2. Effect on Phase Angle

Loss tangent is another very important rheological parameter for asphalt binders. The desired effect of polymer modification is to provide a polymer network that imparts elastic stability at higher temperatures, and this is indicated by a decrease in loss tangent (Tayebali et al., 1992). Figure 5-5a shows loss tangent master curves for the unaged AC-20 series. It is clear that except for the high angular frequency (low temperature) region, the addition of polymers to asphalt decreases the loss tangent (or phase angle) value significantly, meaning that these polymers bring elasticity to the base asphalt. SBR is more effective than SBS in this regard, and AC-20 modified with 5 percent tire rubber plus 2 percent SBS has the lowest phase angle due to the inclusion of the more elastic tire rubber.

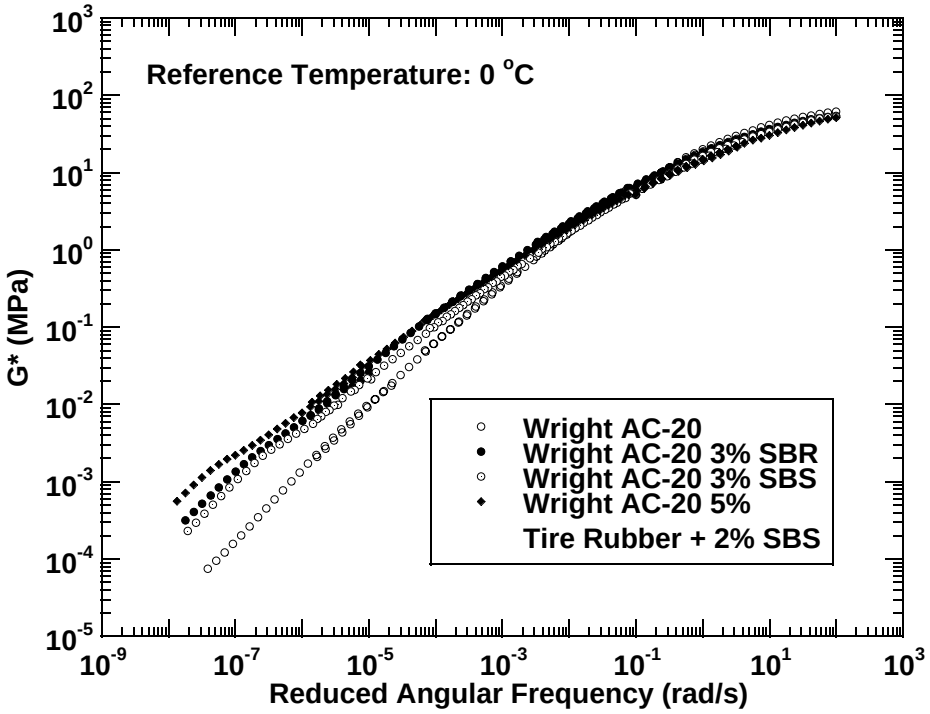

Figure 5-4a. G* Master Curves at 0 °C: Unaged.

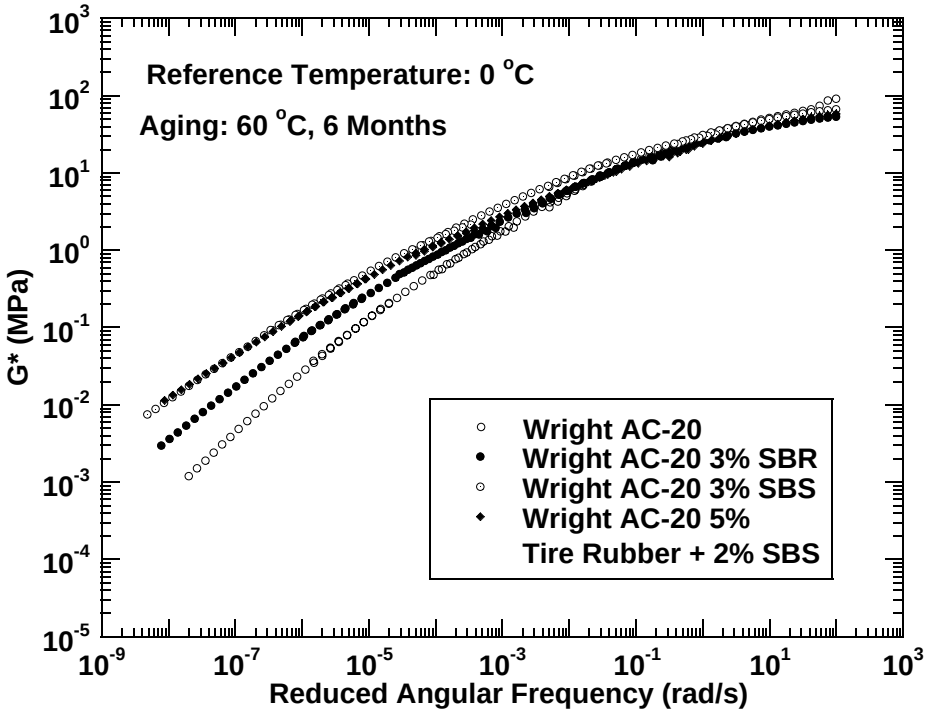

Figure 5-4b. G* Master Curves at 0 °C: Six Months Aging at 60 °C.

Figure 5-5a also indicates that the addition of polymer brings a plateau region to the loss tangent master curves over the intermediate angular frequency range (approximately from 10^{-6} to 10^{-3} rad/s at the 0 °C reference temperature). A true plateau region is absent for the SBR- and SBS-modified AC-20, but for the asphalt modified with 5 percent tire rubber plus 2 percent SBS, there is a well-defined plateau region, suggesting the formation of a strong polymer network (Goodrich, 1988; Collins et al. 1991).

Aging results in a significant shift of the entire loss tangent (also phase angle) curve in the direction of more elastic (G′ increases even more than G″) behavior (Figure 5-5b). Also, the plateau region becomes less pronounced, suggesting that the polymer network has been damaged by oxidation.

3. Effect on Relaxation Spectrum

According to Anderson et al. (1992), polymer modifiers can extend the relaxation processes to longer times. Figure 5-6a shows the relaxation spectra for this AC-20 series. Derivation of the spectra was based on the procedure of Ferry (1980). Experimental data indicate that the inclusion of polymer into base asphalt results in a broader relaxation spectrum. In addition, the broadening effect of polymer modification on relaxation spectrum of asphalt binders is a function of polymer type, and AC-20 with 5 percent tire rubber plus 2 percent SBS has the broadest spectrum in this series. The reason for longer relaxation time for modified binders is that the polymer modification results in an increase in both in-phase and out-of-phase components of G*, but the relative amounts of increase are different; polymer modification enhances elasticity more than viscosity.

Figure 5-6b shows relaxation spectra after six months of aging. The spectra at longer times are shifted upward, indicating that aging makes asphalts more solidlike (Ferry, 1980).

4. Effect on Shift Factor

Anderson et al. (1994) found that for asphalt cements, the temperature dependence of the viscoelastic behavior, as indicated by the shift factors determined from construction of master curves, can be represented by the Williams, Landel, and Ferry (WLF) equation above the defining temperature, T_d:

$$\log a(T)_d = -C_1(T-T_d)/(C_2+T-T_d) \qquad (5\text{-}4)$$

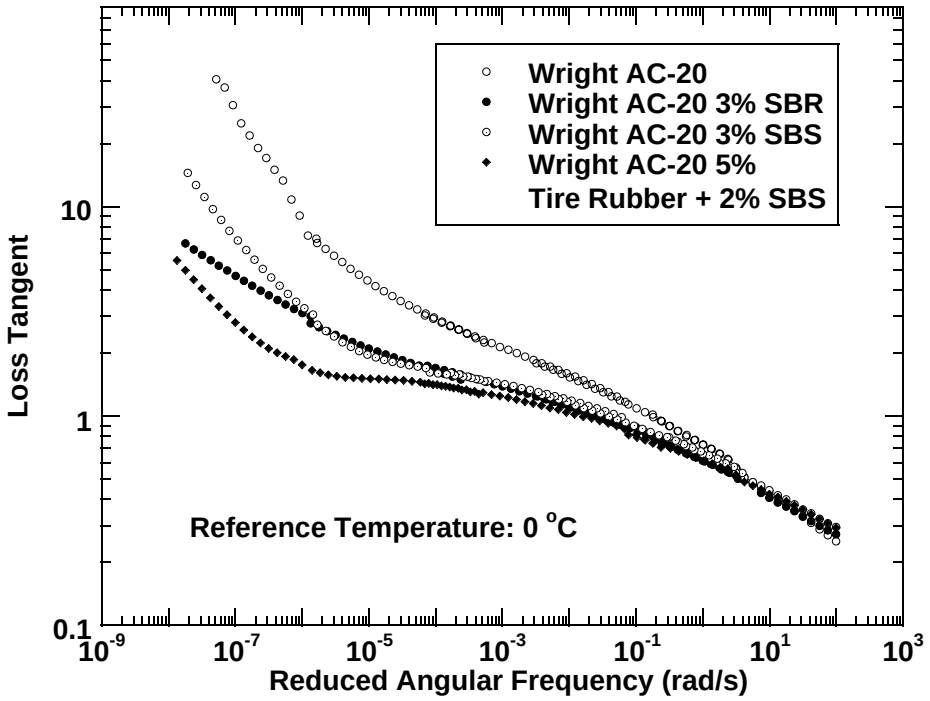

Figure 5-5a. Loss Tangent Master Curves at 0 °C: Unaged.

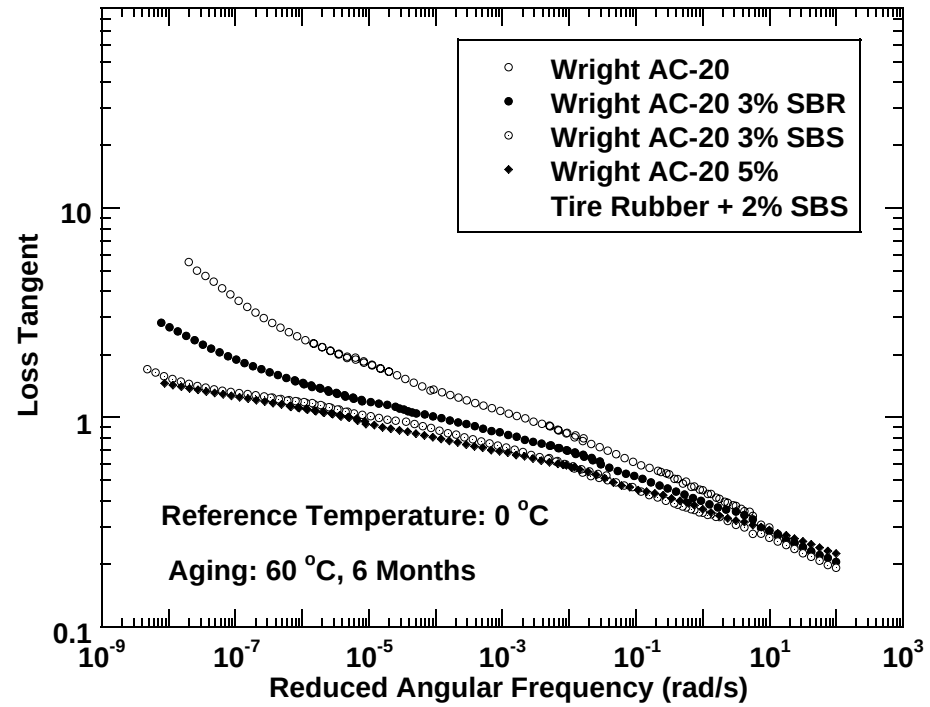

Figure 5-5b. Loss Tangent Master Curves at 0 °C: Six Months Aging at 60 °C.

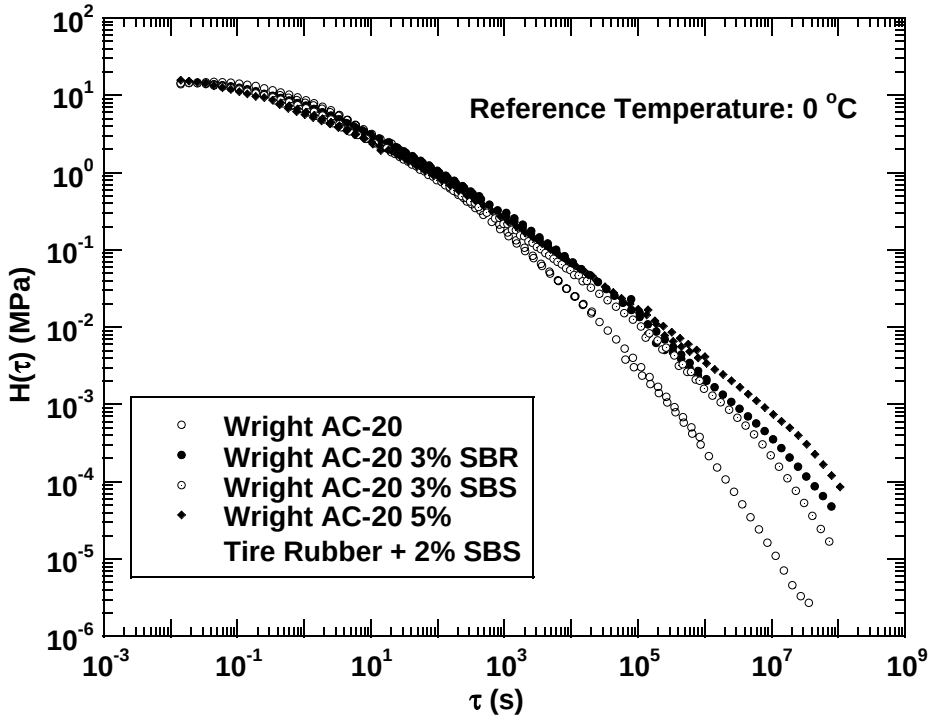

Figure 5-6a. Relaxation Spectra at 0 °C: Unaged.

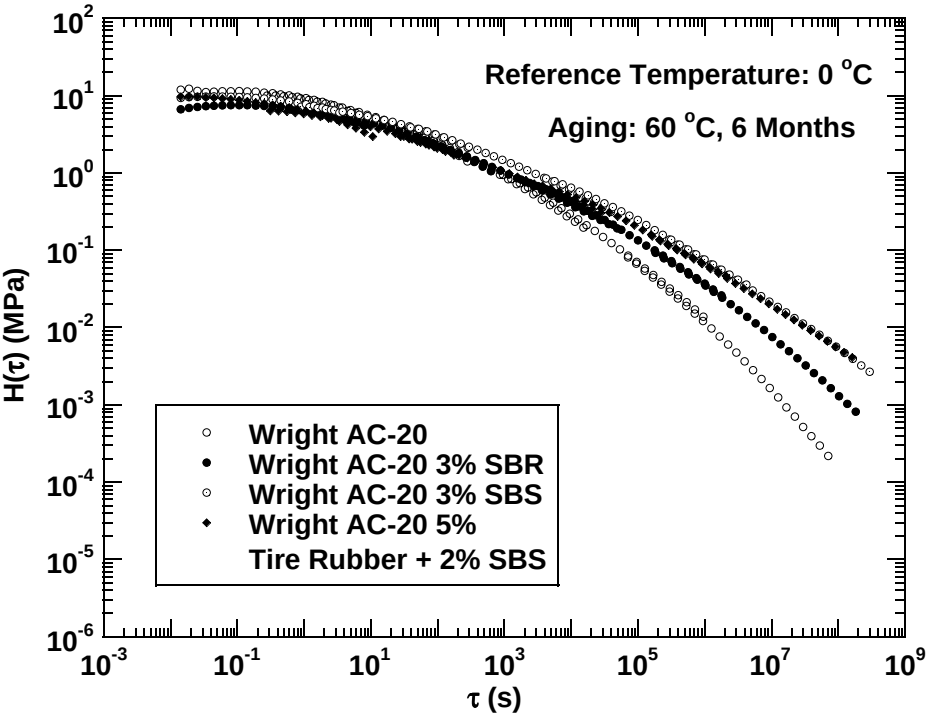

Figure 5-6b. Relaxation Spectra at 0 °C: Six Months Aging at 60 °C.

where $a(T)_d$ is the shift factor relative to the defining temperature; C_1 and C_2 are experimental constants; T is temperature (°C or K); and T_d is the defining temperature, a characteristic parameter for each asphalt cement.

Anderson et al. (1994) analysis on Strategic Highway Research Program (SHRP) asphalts found that the values of C_1 and C_2 could be approximated by the fixed values 19 and 92, respectively. As an approximation, these constants were also assumed for the AC-20 series, although it would be reasonable to assume that other values might be more appropriate, especially for the polymer-modified materials. From experimentally determined values of the shift factor, the WLF equation was used to estimate the best value of T_d for each material, using the fixed values of C_1 and C_2. Figure 5-7a is the comparison between the WLF equation and the experimental shift factor values. The legend for each material shows the values of T_d. There is some difference between the model and the experimental data, and this may be the result of using universal values for the two constants C_1 and C_2.

Aging does not have much effect on shift factor a(T) (Table 5-2, Figure 5-7b, c). The defining temperature T_d for the aged SHRP asphalts is the average value for the PAV-aged binders, as reported by Anderson et al. (1994).

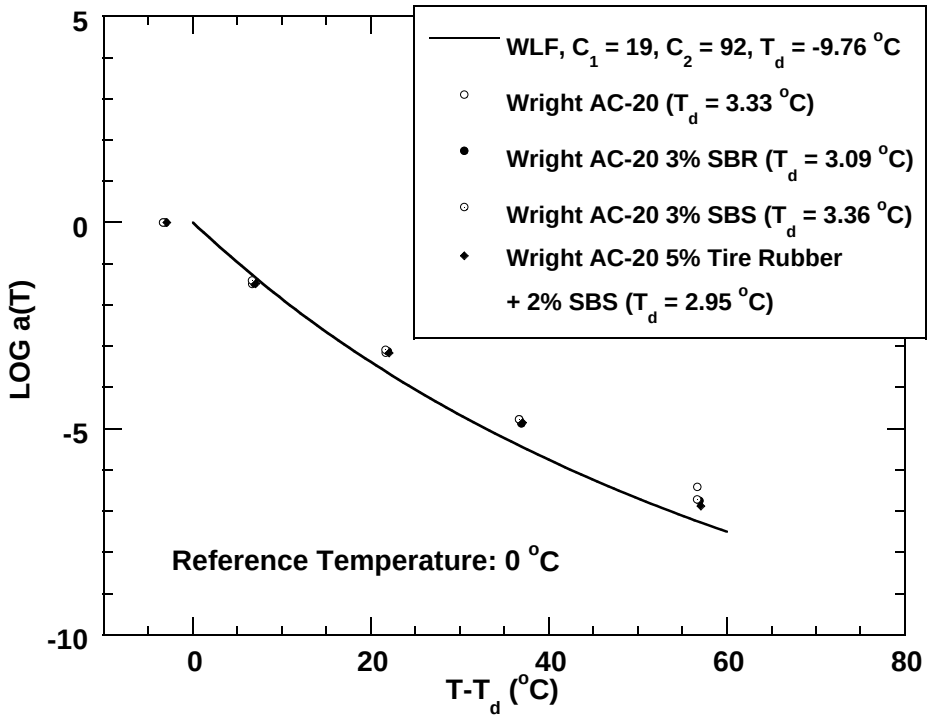

Figure 5-7a. Shift Factors Variation with Temperature for 0 °C Master Curves: Unaged.

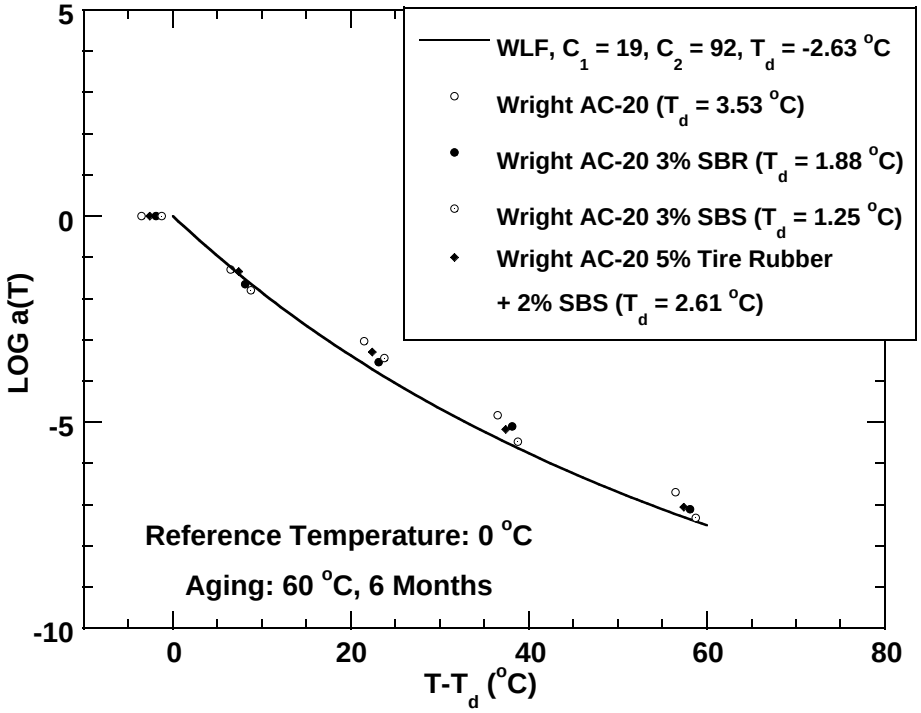

Figure 5-7b. Shift Factors Variation with Temperature for 0 °C Master Curves: Aged Six Months at 60 °C.

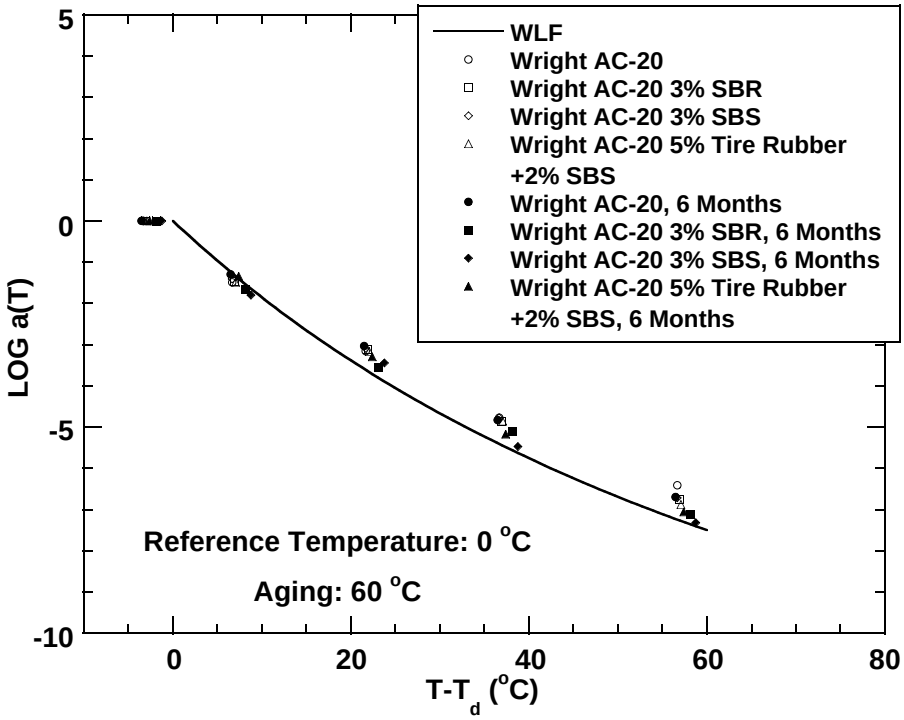

Figure 5-7c. Shift Factors Variation with Temperature for 0 °C Master Curves: All.

Table 5-2. Effect of Modifiers and Aging on Asphalt Shift Factors.

Material	Temperature (°C)				
	0	10	25	40	60
Wright AC-20	1.00	3.24×10^{-2}	6.92×10^{-4}	1.68×10^{-5}	3.87×10^{-7}
Wright AC-20 6 months	1.00	5.07×10^{-2}	9.24×10^{-4}	1.48×10^{-5}	2.00×10^{-7}
Wright AC-20 3% SBR	1.00	3.38×10^{-2}	7.54×10^{-4}	1.34×10^{-5}	1.29×10^{-7}
Wright AC-20 3% SBR 6 months	1.00	2.25×10^{-2}	2.89×10^{-4}	7.92×10^{-6}	7.73×10^{-8}
Wright AC-20 3% SBS	1.00	3.93×10^{-2}	8.20×10^{-4}	1.69×10^{-5}	1.93×10^{-7}
Wright AC-20 3% SBS 6 months	1.00	1.58×10^{-2}	3.60×10^{-4}	3.36×10^{-6}	4.79×10^{-8}
Wright AC-20 5% tire rubber plus 2% SBS	1.00	3.28×10^{-2}	6.83×10^{-4}	1.40×10^{-5}	1.33×10^{-7}
Wright AC-20 5% tire rubber plus 2% SBS 6 months	1.00	4.56×10^{-2}	5.07×10^{-4}	6.75×10^{-6}	8.70×10^{-8}

5. Effect on the Frequency Dependence of η_o^*

Figure 5-8 indicates the frequency dependence of the complex viscosity of this AC-20 series of asphalts. For both the unaged and aged samples, polymer modification results in an extension in non-Newtonian behavior to lower frequencies. In addition, aging alone can increase the non-Newtonian behavior. Also, modifiers have different abilities to increase the non-Newtonian property of asphalt binders. For the unaged group, the neat asphalt displays a reasonably Newtonian behavior, and the dynamic viscosity does not change much with the angular frequency. Both 3 percent SBR and 3 percent SBS impart almost the same extent of non-Newtonian property into the neat binders. But for the asphalt modified with 5 percent tire rubber plus 2 percent SBS, due to the presence of more elastic tire rubber particles, it displays a much more non-Newtonian property. Oxidative aging will produce asphaltene from polar aromatics inside asphalt binder, and asphaltene is a kind of solid particle. As a result, aged asphalt will display more non-Newtonian property than an unaged one. Figure 5-8 shows that after six months of aging at 60 °C, even the neat AC-20 begins to show apparent non-Newtonian behavior. For aged modified binders, there will be two opposite effects as to their non-Newtonian property. The first one is that the aging will produce more elastic asphaltene particles, and this will increase the content of non-Newtonian property. The second one is that the oxidative degradation of polymeric additives will decrease the content of non-Newtonian behavior. The experimental data show that the first effect is predominant.

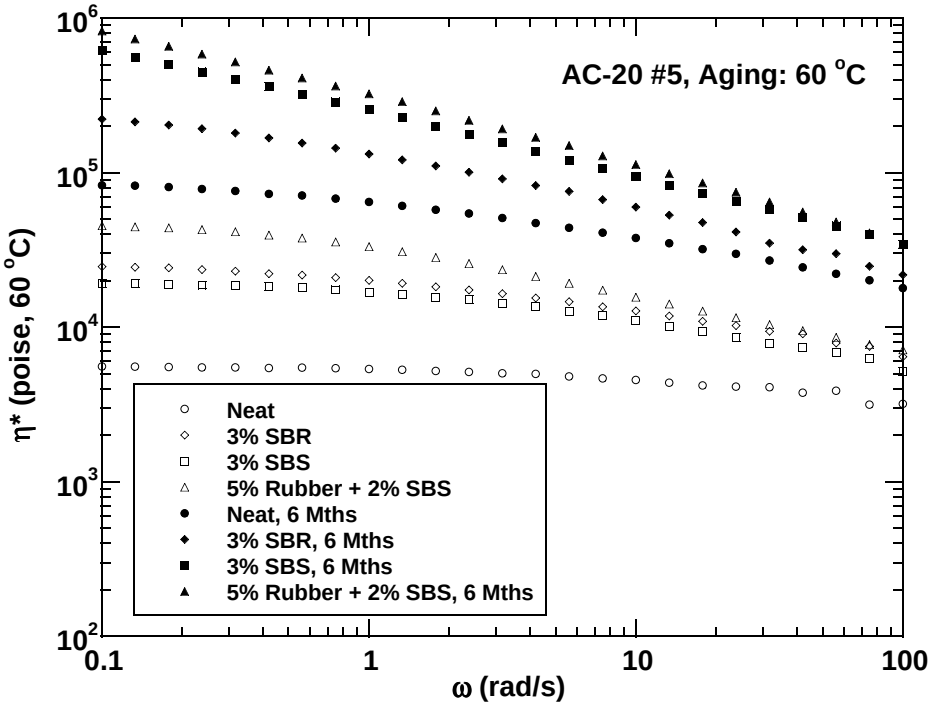

Figure 5-8. Shift in Complex Viscosity Behavior with Aging at Low Frequency.

Effect of Aging on Modifiers

Linde and Johansson (1992) aged SBS-modified asphalt at 200 °C for various times and found that after a few hours, there was a significant change in the polymer phase. After 24 hours, almost all of the original SBS had been degraded to a lower molecular size. The asphalt phase showed opposite behavior as larger molecular size fractions were formed.

Figures 5-2a and 5-2b, presented earlier, are SEC chromatograms for this AC-20 group aged for zero and six months at 60 °C, respectively. Each of these figures include two sets of chromatograms: the upper chromatograms are differences between modified and unmodified asphalt chromatograms, and the bottom chromatograms are the corresponding complete SEC chromatograms. In these complete chromatograms, the three peaks (from left to right) correspond to modifiers (polymers), asphaltenes, and maltenes. The larger molecular size polymer elutes from the column before the asphaltenes. Note also that for the material containing ground tire rubber the polymer peak consists of two peaks. The first peak is believed to be primarily SBS, based upon the material with 3 percent SBS modifier only, while the second peak is well-cured ground tire rubber, i.e., rubber that is small enough to pass through the 0.45 μm pre-column filter.

After six-months of aging at 60 °C, there are several apparent differences between Figures
5-2a and 5-2b. First, the asphaltene peak increases dramatically with aging. This phenomenon results from the production of more asphaltene from naphthene and polar aromatics and from the increase in asphaltene associations (Liu et al. 1998a, Mullins and Sheu, 1998). Secondly, the SBS peak shifts somewhat to later times and decreases dramatically in size, indicating that the polymer molecules decompose to smaller ones. The SBR peak also shifts to the right, but the shift is not as apparent as that of SBS. Third, the upper difference chromatograms indicate that the height of the second polymer peak, the tire rubber peak, increases with aging. We believe that this is the result of oxidation serving to digest more of the rubber to the point that it passes through the prefilter and on to the column (Chipps, 2001).

Effect of Modifiers on Extensional Properties of Asphalt Binders

We found that the addition of modifiers to asphalt binders could significantly increase their ductility. In addition, the effect of the polymer became more pronounced with increasing polymer content (Srivastava et al., 1992). Our experimental data confirm these trends. However, we also found that modifiers can improve binder ductility. The effect is dramatic for lightly-aged materials but diminishes with increased aging to the point that eventually the polymer benefit is gone (Table 5-3). This decrease could be the result of polymer degradation with aging, as seen in Figure 5-2. However, it also could be the result of the underlying asphalt binder stiffening with aging, resulting in failure that the polymer cannot overcome. This hypothesis suggests that when the base asphalt is stiff enough, it will fail regardless of the presence of the polymer.

With the significant caveat that our data are limited, SBS-modified binders have lower ductility than SBR-modified ones (Table 5-3), especially at the beginning of oxidation. SBR is the abbreviation for diblock poly (styrene-butadiene) rubber. SBS represents triblock poly (styrene-butadiene-styrene). These molecular structures are shown below:

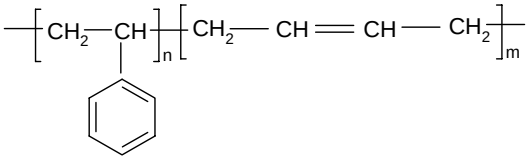

Diblock poly (styrene-b-butadiene) rubber (SBR)

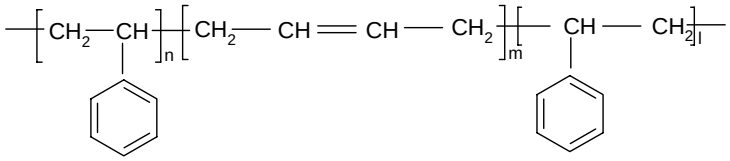

Triblock poly (styrene-b-butadiene-b-styrene) (SBS)

The different elongation properties of SBR-modified and SBS-modified binders could be explained by the different chemical structures of SBR and SBS and the difference in their interactions with asphalt components. The difference in these two polymers is that SBS has two polystyrene blocks, compared to one polystyrene block in SBR. This extra polar and rigid polystyrene block makes the polymer system more resistant to deformation (Linde and Johansson, 1992). In addition, more polar groups in the polymer mean larger interactions between the polymer molecules and asphaltenes and polar aromatics. As a result, the interaction between SBS and asphalt likely is greater than that between SBR and asphalt. So, it is more difficult for SBS-modified asphalt to flow, and thus, stresses that arise from deformation are less easily relieved.

Table 5-3. Effect of Modifiers on Ductility (15 °C, 1 cm/min) of Asphalt Binders.

	Aging Time (Months at 60 °C, 1 atm Air)				
Material	2	4	6	9	12
Wright AC-20	6.35	5.6	4.6	3.53	2.5
Wright AC-20 3% SBR	39.42	24.35	17.53	6.85	2.3
Wright AC-20 3% SBS	22.13	19.12	13.32	10.7	2.93
Wright AC-20 5% tire rubber plus 2% SBS	16.73	9.17	5.32	3.37	2

Force ductility measurements can provide more details about the effect of modifiers on elongation of asphalt binders. Figure 5-9a shows the effect of SBS and tire rubber plus SBS on the elongation properties of asphalt Wright AC-20. SBR is not included on the graph because the AC-20 modified with 3 percent SBR began to neck down at an extension ratio around four, and stress could not be calculated after this point.

The stress-elongation curve for SBS-modified asphalt and polymer-modified materials, in general, may be described in four stages. Initially, the unmodified and modified binders behave very similarly, and stress is linear with elongation ratio. According to Shuler et al. (1987), in this region, stress arises mainly from deformation of the asphalt itself; the modifier's contribution is very small. Consequently, the initial slope of the stress-extension ratio curve in the linear region will be referred to as "asphalt modulus." Secondly, upon additional extension, stress first reaches a maximum value (yield stress) and then begins to decline because of the flow of asphalt specimen. The yield stress of polymer-modified asphalts is a little bit higher than that of the straight asphalt. Thirdly, with further elongation, polymer molecules also extend, and at the same time, these molecules reorientate themselves along the direction of elongation (Kaufman, 1978). This results in an increase in stress arising from the polymer deformation that compensates for the decrease in stress due to the flow of asphalt. These two opposite effects produce an approximately flat region designated as "C" in Figure 5-9a. Lastly, as deformation

proceeds, the reorientation of polymer molecules continues and increases the crystallinity of the polymer domain, resulting in further increases in stress, as shown in region "E" in Figure 5-9a. In this region, stress is linear with elongation again, and the slope is smaller than "asphalt modulus." This slope is called the "asphalt-polymer modulus" (Lu and Isacsson, 1999). The slope difference comes from the difference in molecular interactions. The "asphalt modulus" is the result of interactions between asphalt components, and these interactions include primary bonding, but also strong polar bonding and the effect of suspended solids (asphaltenes). However, the "asphalt-polymer modulus" is from the interaction between asphalt components and polymer molecules, which are mainly weaker secondary bonds. Note also that the "asphalt-tire rubber-SBS modulus" is larger than "asphalt-SBS modulus." Region D (not shown) is a transition between regions C and E.

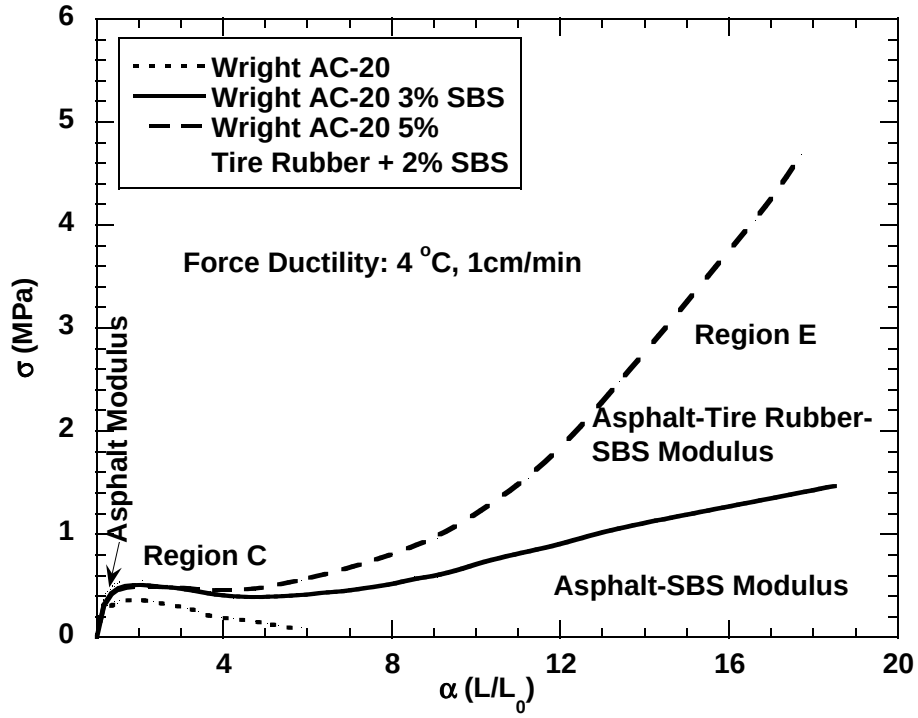

Figure 5-9a. Stress-Elongation Curves at 4 °C: Unaged.

In spite of the significant effect that polymers can have on extensional properties, these effects deteriorate with oxidative aging. Figure 5-9b indicates that after six months of aging at 60 °C, there is almost no difference remaining between the unmodified and modified binder ductilities and failure stresses, measured at 4 °C. Likely, this is the result of the stiffening that occurs in the asphalt due to oxidation so that the failure stress is reached without a beneficial effect of the polymer. Alternatively, the polymer degradation that has been noted with binder oxidation may also be a contributing factor to this loss of ductility.

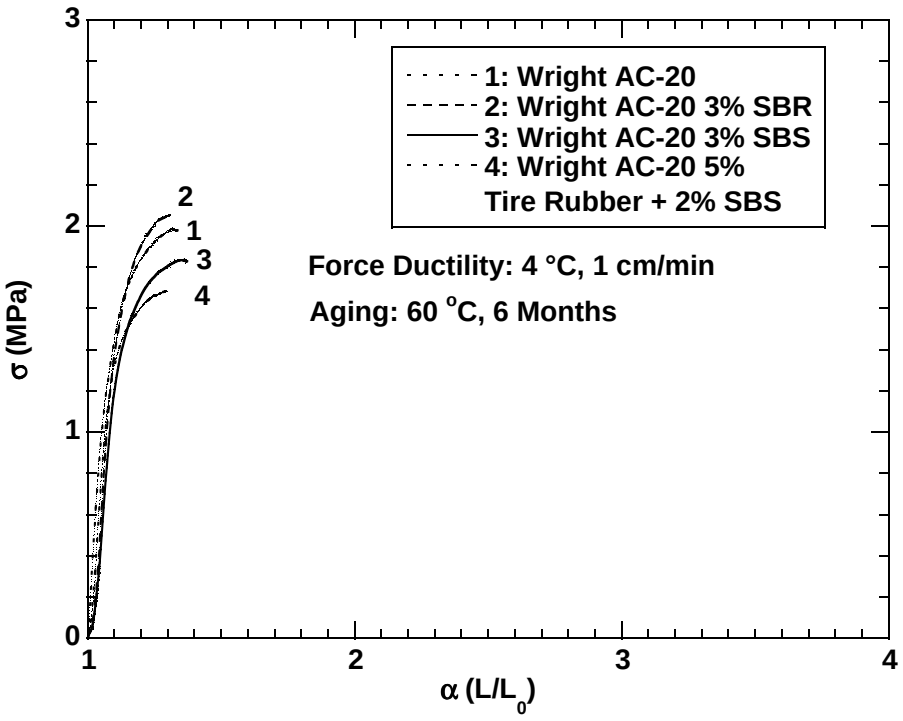

Figure 5-9b. Stress-Elongation Curves at 4 °C: Six Months Aging at 60 °C.

Conclusion

Polymer modification can improve asphalt binder physical properties at both high and low temperatures. However, the benefits tend to be greater to rutting resistance than to improved thermal cracking. Polymer-modified binders have a broader relaxation spectrum than their base asphalt. The existence of a plateau region in loss tangent master curves of modified asphalts suggests the formation of a polymer network. In addition, polymeric additives make the asphalt's complex viscosity a stronger function of frequency (shear rate) at high pavement temperatures.

Aging can improve the temperature susceptibility of asphalt binders. Aging can also make asphalt more elastic, damage the polymer network in binders, and result in an extended relaxation spectrum for asphalt binders. These effects result from increases in asphaltene content and degradation of modifiers such as SBR and SBS.

For unaged polymer-modified binder, ductility is improved greatly over the unmodified base binder. This is due to the polymer having a lower elastic modulus than the asphalt or the polymer-modified material having a higher failure stress, or both. However, with aging, the benefit from modifiers decreases.

RELATIONSHIPS BETWEEN DUCTILITY AND DSR PROPERTIES FOR MODIFIED ASPHALTS

In Chapter 4 we reported that for unmodified asphalts ductility correlates well with the DSR parameter $G'/(\eta'/G')$. In addition, for different unmodified binders, this appears to be a universal correlation in the low-ductility region of aged binders. In the previous sections of this chapter, we investigated oxidation of polymer-modified asphalts and the impact on fundamental rheological properties. In this section we return to the ductility correlation and evaluate it for modified asphalts.

Methodology

Seventeen modified asphalt binders were compared and evaluated through a number of physical properties. The binders were aged at 204 °C (400 °F) by air blowing and at a second temperature, 60 °C (140 °F), in a controlled environment room to obtain properties ranging from those of a slightly aged material to one which would be near the end of its service life. The materials and their aging methods are summarized in Table 5-4.

The experimental methods were the same as for the unmodified asphalts of Chapter 4.

Results and Discussion

Relationship between Ductility and G', η'/G'

In Chapter 4, consistent with the Maxwell model of linear viscoelasticity, asphalt ductilities measured at 15 °C and 1 cm/min were found to correlate with the DSR parameter $G'/(\eta'/G')$ for aged unmodified binders. Accordingly, this correlation was evaluated for the polymer-modified asphalts.

Figure 5-10 shows a map of G' versus η'/G' for polymer-modified materials measured at 15 °C, 0.005 rad/s. The general trend is similar to unmodified binders. As modified asphalt ages, it also moves from the lower right to the upper left, and the ductility declines dramatically along this path. This map clearly shows that for modified asphalts, ductility is related to both η'/G' and G' (stiffness) of the material.

As an alternate way of viewing these same data, ductility is plotted versus the ratio of G' to (η'/G') (Figure 5-11). In comparison to the correlation for unmodified asphalts (Figure 4-12 and the line in Figure 5-11), there is significantly more scatter as well as deviation from the unmodified correlation. There is no linear relationship even in the low ductility region. Obviously, polymer-modified asphalts behave much differently from unmodified asphalts, consistent with the stress elongation curves shown in Figure 5-9a.

Figure 5-12 is another version of Figure 5-11, showing asphalts divided into three rather distinct groups (also shown by the boundary lines in Figure 5-11). The Fina group includes all modified Fina asphalts plus GSAC AC-10 three percent SBS. The Wright group includes all modified Wright asphalts. The UltraPave group includes modified Texas Fuel and Asphalt, Exxon, and UR asphalts. For all of the modified materials, for a given value of $G'/(\eta'/G')$, ductility is signific ntly better than for the unmodified binders. With aging, all three groups move from the upper left to the lower right, with the differences between them, and also between the unmodified binders, decreasing with aging.

So, for the modified asphalts, there is no universal correlation between ductility and $G'/(\eta'/G')$. However, for different asphalts within the same group, ductility correlates reasonably well with $G'/(\eta'/G')$ (Figure 5-12).

Table 5-4. List of Modified Asphalts Studied.

Aging Method	Asphalt Binders
204 °C Airblowing:	Fina AC-5 with 2% SBR
	Fina AC-10 with 2% SBR
	GSAC AC-10 with 3% SBS
	Wright AC-10 with 2%, 3 % SBR
	Wright AC-10 with 3% SBS
	Wright AC-20 with 3% SBR
	Wright AC-20 with 3% SBS
	Wright AC-20 with 5% tire rubber + 2% SBS
60 °C Environmental Room:	Exxon AC-30 with 3.5% SBR
	Fina AC-5 with 1%, 2% SBR
	Fina AC-10 with 1%, 2% SBR
	Fina AC-20 with 1%, 3.5% SBR
	GSAC AC-10 with 3% SBS
	Neste AC-20 with 3% SBR
	TFA AC-20 with 3% SBR
	Wright AC-10 with 2%, 3% SBR
	Wright AC-10 with 3% SBS
	Wright AC-20 with 3% SBR
	Wright AC-20 with 3% SBS
	Wright AC-20 with 5% tire rubber + 2% SBS
	UR AC-10 with 3% SBR

Effect of Polymeric Modifiers on Ductility of Asphalt Binders

Srivastava (1992) found that the addition of polymeric additives made asphalts more ductile. Furthermore, when the ductility of the asphalt in a pavement decreased to the range of 3 to 5 cm, there was serious cracking that developed (Kandhal, 1977). Using a ductility of 5 cm as a critical value, the additional aging time beyond that of its unmodified base asphalt for a modified asphalt to reach this critical ductility value we use the term “modifier benefit.”

Figure 5-13 indicates the modifier benefit for Fina AC-10 asphalt group. When its ductility is low enough due to aging, the logarithm of ductility is linear with aging time. For unmodified Fina AC-10, the aging time to reach the critical ductility value is 8.5 months in the environmental room, and for Fina AC-10 with 1 percent SBR and 2 percent SBR, the times are

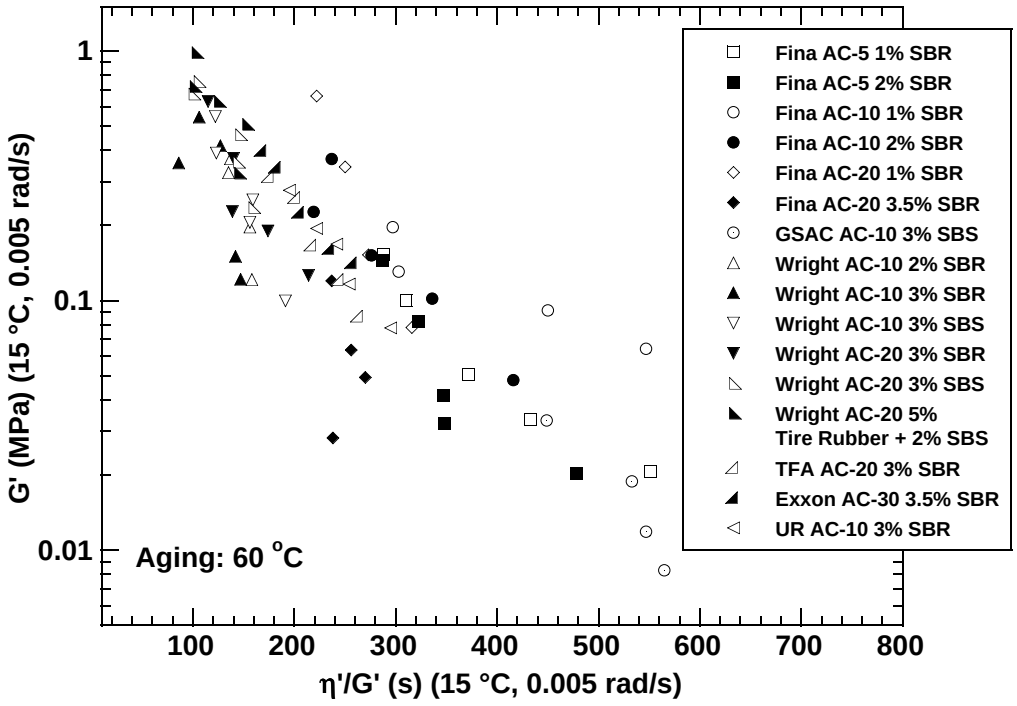

Figure 5-10. Ductility Map for Modified Asphalts.

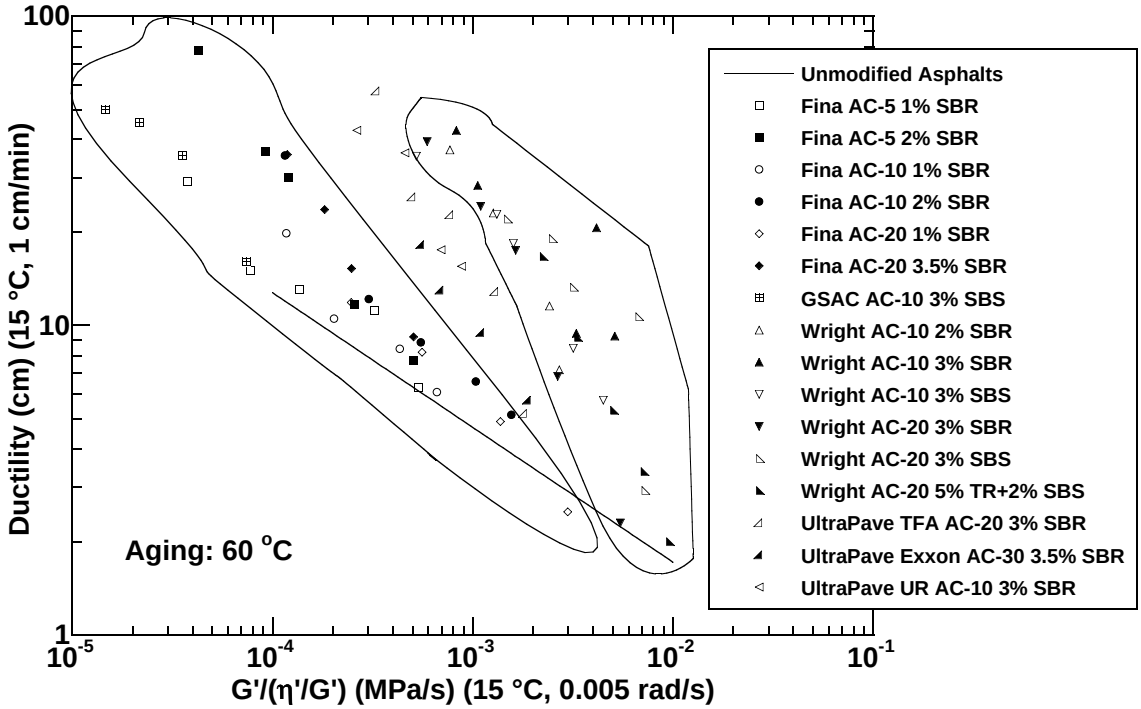

Figure 5-11. Ductility versus G′/(η′/G′) for Modified Asphalts.

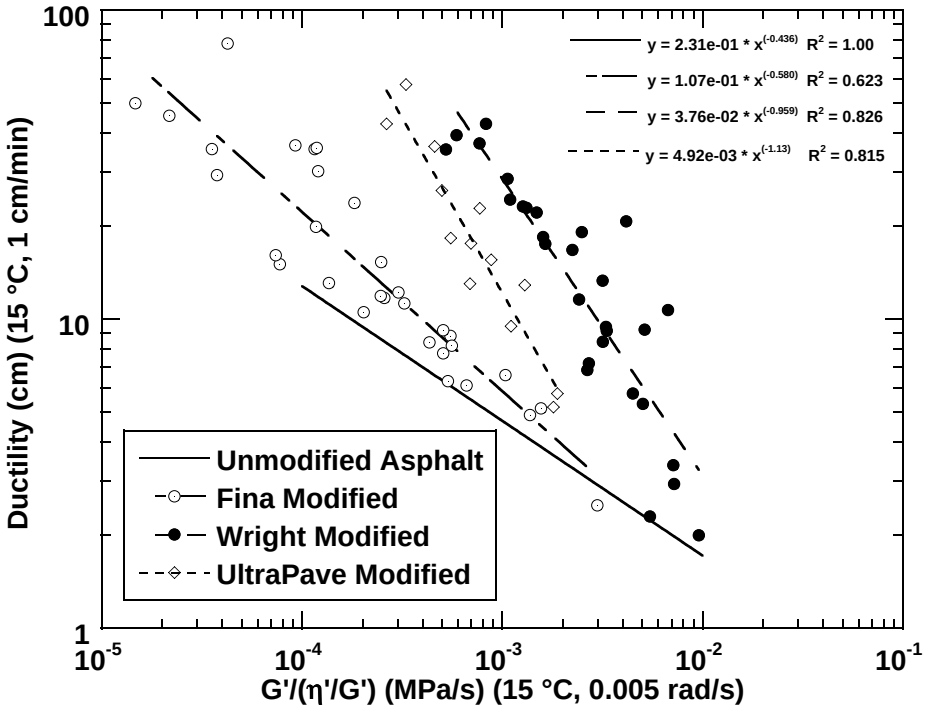

Figure 5-12. Ductility versus G′/(η′/G′) for Modified Asphalt Groupings.

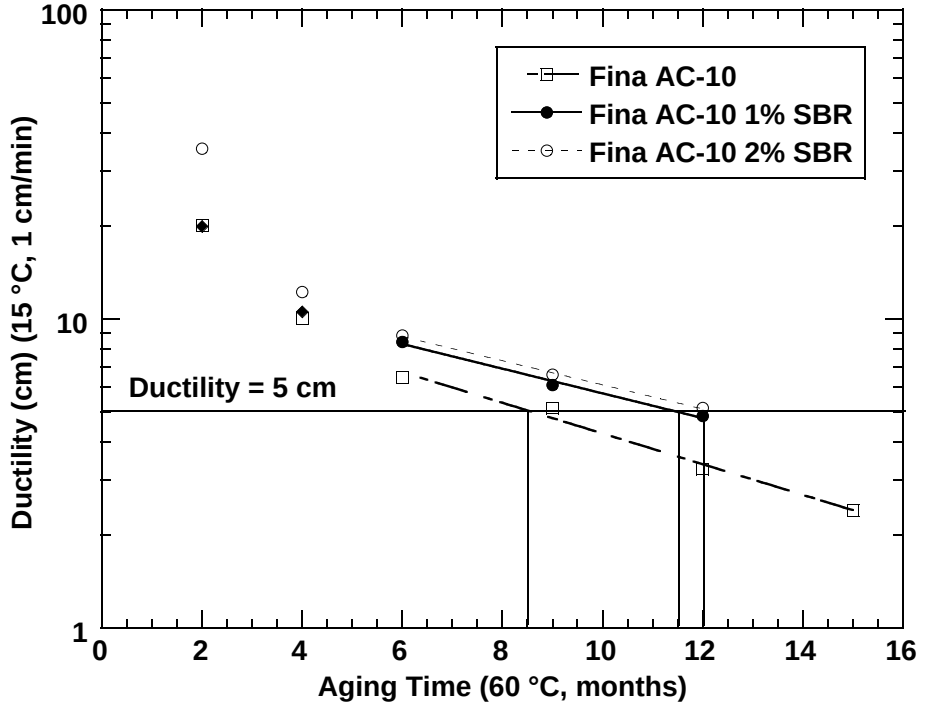

Figure 5-13. Effect of Modifiers on Ductility: Fina AC-10.

11.5 and 12 months, respectively. So for these data the benefits of 1 percent and 2 percent SBR for Fina AC-10 would be calculated as three and 3.5 months, respectively. For the Fina AC-20 group (Figure 5-14), the benefit of 1 percent SBR is calculated to be negative, -0.8 months, although this difference is almost certainly statistically insignificant, and 3.5 percent SBR produces a benefit of 5.8 months.

Table 5-5 is a summary of these calculated benefits for several unmodified and modified asphalts. Table 5-5 generally indicates that the addition of several percent of polymer modifiers can result in a benefit of from two to six months at 60 °C aging. Note, however, that this benefit is asphalt and modifier dependent. The benefit values are also shown as a percent extension of aging time, relative to the base material.

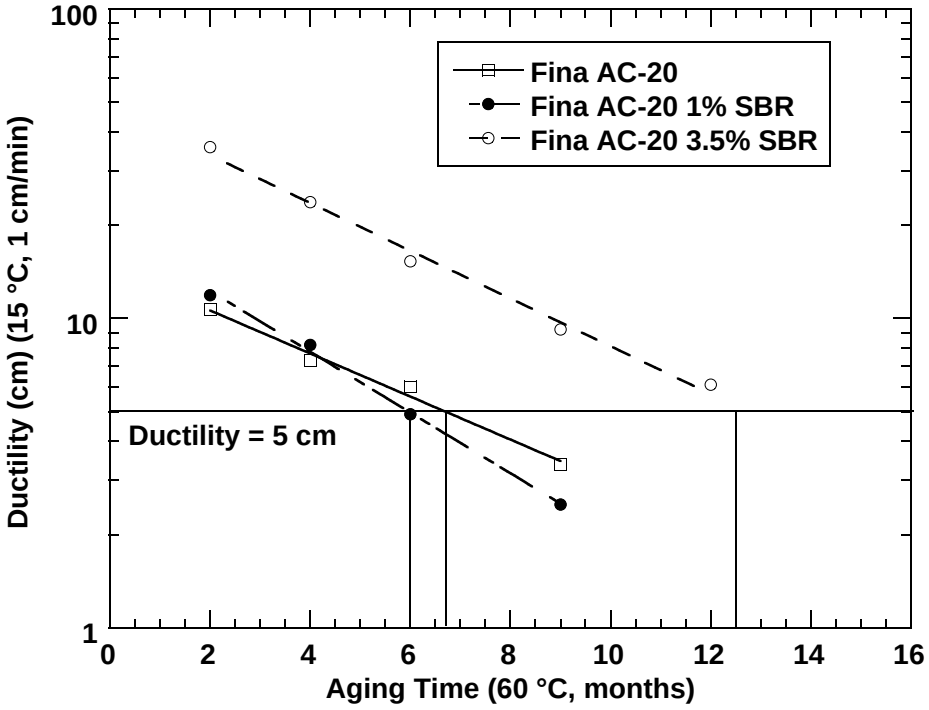

Figure 5-14. Effect of Modifiers on Ductility: Fina AC-20.

Table 5-5. Summary of Modifier Benefit on Ductility.

Sample	Aging Time to Reach 5 cm Ductility (Months at 60 °C)	Modifier Benefit	
		(Months)	(Percent)
Fina AC-10	8.5	–	–
Fina AC-10 1% SBR	11.5	3.0	35
Fina AC-10 2% SBR	12.0	3.5	41
Fina AC-20	6.8	–	
Fina AC-20 1% SBR	6.0	-0.8	-12
Fina AC-20 3.5% SBR	12.5	5.7	84
Wright AC-10	7.75	–	–
Wright AC-10 2% SBR	14.0	6.2	80
Wright AC-10 3% SBR	13.3	5.5	71
Wright AC-10 3% SBS	13.0	5.3	68
Wright AC-20	5.0	–	–
Wright AC-20 3% SBR	9.8	4.7	94
Wright AC-20 3% SBS	9.8	4.7	94
Wright AC-20 5% tire rubber plus 2% SBS	7.0	2.0	40
Exxon AC-30	6.5	–	–
Exxon AC-30 3.5% SBR	10.0	3.5	54
TFA AC-20	9.0	–	–
TFA AC-20 3% SBR	12.8	3.7	41

Summary

For modified asphalts, there is no universal correlation between ductility and $G'/(\eta'/G')$, even in the low ductility region. However, there are reasonably good correlations between these two parameters for different asphalt groups.

Generally, the addition of several percent of polymer modifiers can result in a benefit of from two to six months continuous aging at 60 °C. In addition, this benefit is asphalt and modifier dependent.

COMPARISON OF DUCTILITY TO DIRECT TENSION FAILURE STRAIN

In the previous chapter, a correlation between ductility and the DSR function (G'/[η'/G']) at 15 °C and 0.005 rad/s was presented for unmodified asphalts. The actual measurement of the DSR properties can be made at 44.7 °C, 10 rad/s for convenience and then easily time-temperature superposition shifted to 15 °C , 0.005 rad/s with a frequency ratio of 2000. This correlation is quite good and provides a method for estimating binder ductility from DSR measurements.

As noted in the previous section, however, this correlation does not work well for polymer-modified materials. Thus, a substitute method using the Superpave direct tension procedure was briefly investigated. Direct tension failure strain and ductility were measured for a number of unmodified and polymer-modified materials aged for a range of times in the 60 °C environmental room to achieve a span of ductility values. The ductility was measured at 15 °C, 1 cm/min and the direct tension failure strain at -12 °C and -18 °C, although the set of asphalts at the two temperatures was not exactly the same. Ductility values ranged from 0.4 cm to 80 cm and direct tension ranged from 0.2 percent to over 2 percent. Figures 5-15 (-12 °C) and 5-16 (-18 °C) report the comparisons.

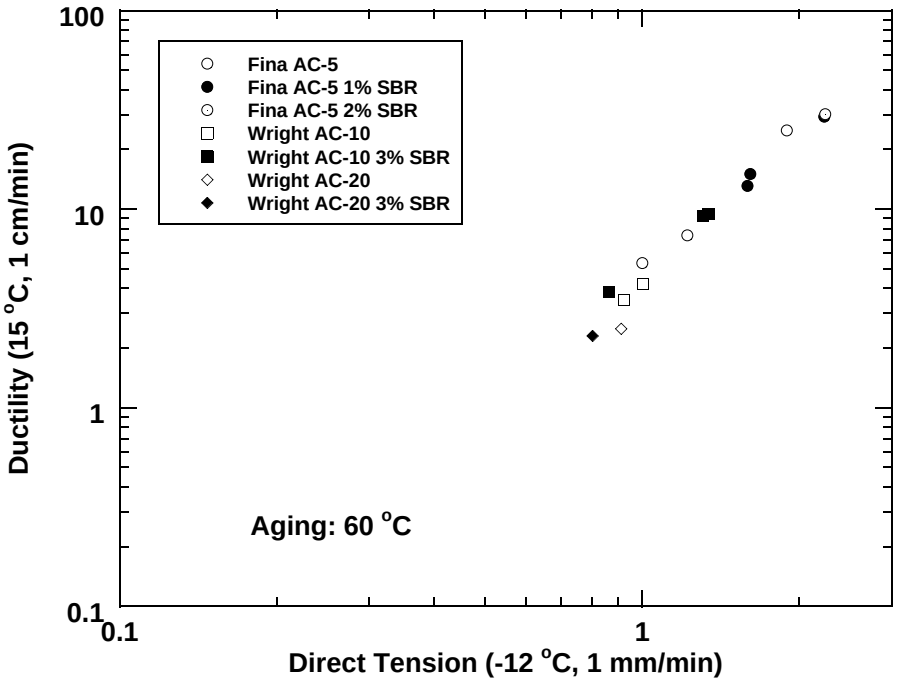

Figure 5-15. Ductility-Direct Tension Comparison at -12 °C.

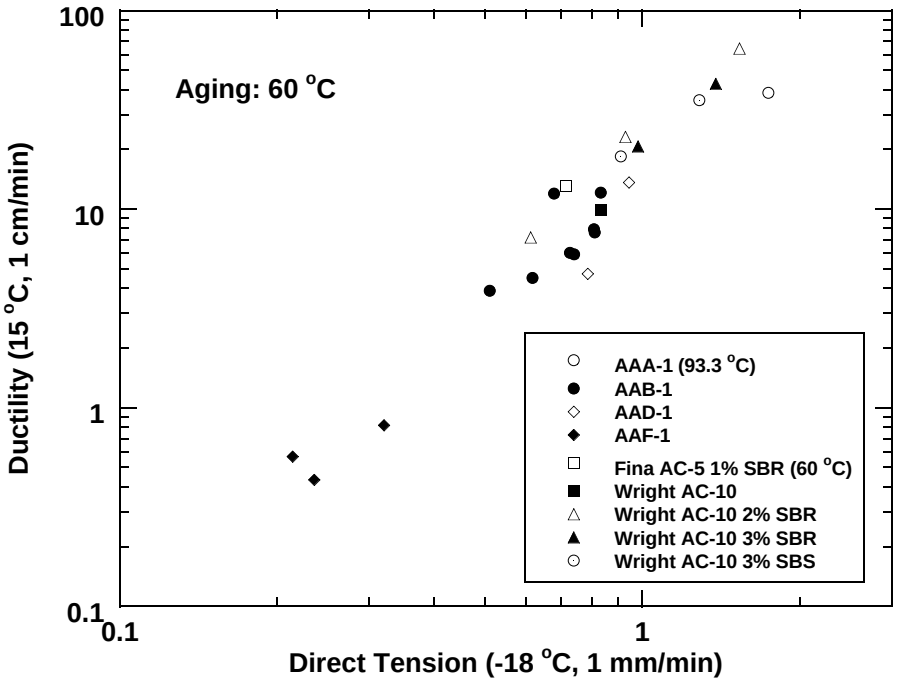

Figure 5-16. Ductility-Direct Tension Comparison at -18 °C.

In spite of the scatter (which because of the log-log relation is considerable), the linearity of the relations is quite good. The slope of both plots is close to 2.5 so they are the same correlation except for a shift to greater failure strain at the higher temperature, as would be expected. The shift is approximately a factor of two.

The intriguing aspect of these data is that the correlation is the same for both the unmodified and modified materials, even to the high ductility values, suggesting that direct tension failure strain data could be used in a binder durability test procedure in lieu of ductility and in lieu of the DSR function, especially for modified materials. Although direct tension is not as convenient to measure as DSR properties, it is considerably more convenient than ductility and is available to many laboratories as part of the Superpave test protocol. Further evaluation of this ductility-direct tension correlation using a greater number of both unmodified and modified materials is recommended and would further quantify the utility of using direct tension measurements in this way.

CHAPTER 6. DEVELOPMENT OF AN ASPHALT AGING PROCEDURE

INTRODUCTION

The primary objective of this project has been the development of a procedure to identify asphalts that are particularly subject to failure resulting from oxidative hardening. To accomplish this two things are required: 1) an aging procedure to harden asphalts so that those most susceptible to oxidative hardening will fail the test, and 2) a test that correlates with pavement failure caused by binder hardening.

The aging procedure should age asphalts to the same relative extent as will occur in service, i.e., the best and worst asphalts in service should be best and worst in the test. This is particularly true with the worst, as it is the one that will be most likely to fail the test. It is, of course, highly desirable that the aging procedure require a relatively short time. Unfortunately, this introduces considerable difficulty into the choice of test conditions.

Strictly speaking, the problem is in theory intractable. Exhaustive data from prior studies and this one show that asphalts respond differently to temperature, pressure, and time so that a relatively rapidly hardening asphalt at road conditions may not be so at test conditions, and the reverse is also true. Using viscosity as a general surrogate for hardening, Equation 6-1 shows the mechanisms by which hardening occurs in the absence of diffusion resistance:

$$\ln \eta_t = \ln \eta_o + \Delta(\ln \eta_{ot}) + \Delta(\ln \eta_j) + r_\eta \cdot \text{time}, \qquad (6\text{-}1)$$

where η_o is the original viscosity, η_t is the viscosity at any time, $\Delta(\ln \eta_{ot})$ is the hardening in the hot-mix plant simulated by an oven test, $\Delta(\ln \eta_j)$ is the hardening that occurs in an early rapid "initial jump" stage, and r_η is the subsequent constant rate of hardening. This sequence is shown in Figure 6-1 in which η_{ot} is the viscosity after the oven test and η_j is the viscosity after the initial jump defined by the intercept of the constant-rate line. Region A will be defined as the time for the initial jump, and region B is a constant-rate region. If there is diffusional resistance, this rate will decline as the asphalt hardens. The first term is not a problem, as oven tests do a good job of simulating the hot-mix hardening (Jemison et al., 1991). The initial jump, however, is quite complex, being both asphalt dependent and pressure dependent. Interestingly, it is not temperature dependent. The oven test may reduce the initial jump but usually not nearly enough to eliminate it.

Asphalt oxidative hardening is almost entirely caused by asphaltene formation (Lin et al., 1995, 1996 and 1998), and the rate can be expressed as follows:

$$r_\eta = \frac{\partial \ln \eta}{\partial t} = \frac{\partial \ln \eta}{\partial AS} \cdot \frac{\partial AS}{\partial CA} \cdot \frac{\partial CA}{\partial t}, \qquad (6\text{-}2)$$

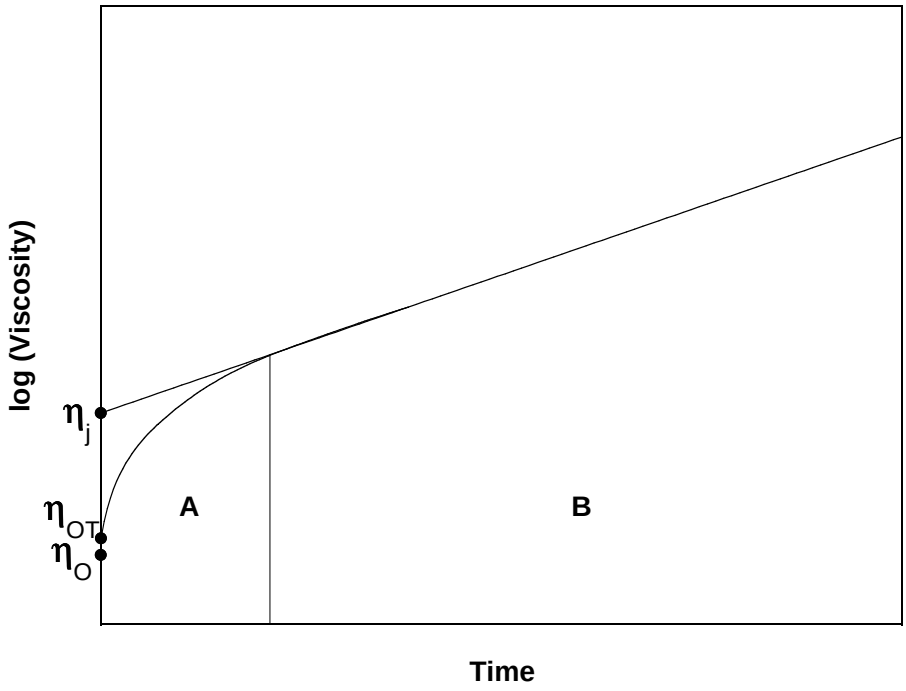

Figure 6-1. The Variation of Asphalt Viscosity with Aging.

where $\partial \ln \eta / \partial AS$ is the impact of asphaltene (AS) increase on increasing viscosity and is affected by asphaltene size, which in turn is affected by maltene solvent power. $\partial AS / \partial CA$ is the rate at which carbonyl formation produces asphaltenes, and $\partial CA / \partial t$ is the rate of carbonyl formation. Carbonyl increase correlates linearly with oxidation (Liu et al., 1998b).

This can be simplified as:

$$r_\eta = HS \cdot r_{CA} \tag{6-3}$$

where HS is the combination of the first two terms in Equation 6-2. This combination is remarkably constant as oxidation proceeds and is independent of oxidation temperature below about 100-110 °C. It has a characteristic value for each asphalt except that it is pressure dependent. This term is called the hardening susceptibility (Lau et al. 1992; Domke, 1999).

The rate of carbonyl formation is (Lin et al., 1996; Lin et al., 1998; Liu et al., 1997a)

$$r_{CA} = \frac{\partial CA}{\partial t} = AP^{\alpha} e^{-(E/RT)} \tag{6-4}$$

where A is the frequency (pre-exponential) factor, P is the pressure, α is the reaction order with respect to oxygen pressure, E is the activation energy, R is the gas constant, and T is the absolute temperature. Values of A, E, and α are very asphalt dependent, though A and E are generally correlated (Liu, 1996). Recent studies described in this report and in Domke et al. (2000) show that the activation energy, E, is also pressure dependent for many asphalts, and this dependence is a function of asphaltenes. The following equation summarizes these results:

$$\ln \eta_t = \ln \eta_{ot} + \Delta(\ln \eta_j)(P) + r_{CA}(T,P) \cdot HS(P) \cdot time \qquad (6\text{-}5)$$

As only one term is multiplied by time, this means that the relative rankings of asphalts from any accelerated aging procedure will change with the length of the test as well as with the temperature and pressure. Because of these complexities, the only recourse is to conduct accelerated aging at a variety of conditions and compare the results with long-term aging at or near road conditions. In this study, this long-term simulation was done in an environmental room held at 60 ºC (140 ºF). The asphalts were aged in thin films to minimize diffusion effects. All other tests were then compared as to relative rankings with results from the environmental room.

THE AGING CONDITIONS

The accelerated aging tests were performed in the pressure aging vessel (PAV) and in the pressure oxygen vessel (POV) as well as in the environmental room (ER). Table 6-1 gives the aging conditions. The samples were oxidized at high temperature and pressure to increase the aging rate.

Table 6-1. Aging Conditions.

	Vessel	Pressure	Temperature (ºC)	Sample Thickness (mm)
ER Test	Environmental Room	1 atm Air	60	1
Test 1	PAV	20 atm Air	100	3
Test 2	PAV	20 atm Air	90	1
Test 3	POV	5 atm O_2	100	1
Test 4	POV	1 atm O_2	110	1
Test 5	POV	1 atm Air	110	1
Test 6	POV	1atm O_2	100	1
Test 7	POV	1 atm O_2	93	1
Test 8	POV	1 atm Air	88	1
Test 9	POV	1 atm O_2	82	1
Test 10	POV	5 atm O_2	110	1

The asphalt film thickness for all aging conditions except for Test 1 (PAV test) was 0.86 mm, approximately one third as thick as the standard PAV test, to limit the effects of diffusion resistance on aging rates (Domke, 1999). Tests 1 and 2 were conducted in the PAV apparatus. For Test 1, 50 g were placed in a standard PAV pan to give the 3-mm thick film; in Test 2, 2.4 g samples were aged in 4-cm by 7-cm trays to give a approximate 0.86-mm thick film. Tests 3 through 10 were conducted in the POV. Tests 1 through 7 took place for four days, and the materials were sampled for analysis every day. Tests 8 and 9 were conducted for 16 days with sampling occurring on days 3, 5, 9, 10, and 16. The condition of Test 10 was very severe so that the asphalts were too brittle to measure after only one day of aging, so the results are not included in this report.

COMPARISON OF AGING TESTS USING η^*_o

Nine asphalts – AAA-1, AAB-1, AAD-1, AAF-1, ABM-1, AAM-1, AAS-1, Lau 4, and TS2K – after being subjected to a form of SAFT aging were aged at the 11 aging conditions listed in Table 6-1, previously. (Lau4 is asphalt Exxon AC-20 used in the SH 21 pavement discussed in Chapter 9.) Even though it is fundamentally inaccurate to simulate road hardening of an asphalt binder by conducting an aging procedure at elevated pressure and temperature at a given fixed time, still it is necessary to investigate how much error actually results from an accelerated aging test for a fixed time and to search for a condition that might agree reasonably well with ER aging while being conducted in a much shorter length of time.

Figure 6-2 shows the hardening rate of the nine asphalts measured by complex dynamic viscosity, η^*_o, measured at 60 ºC, 0.1 rad/s after aging in the environmental room. The plot also shows the complexities of ranking asphalts with respect to their hardening.

The horizontal line at 300,000 poise represents an assumed approximate failure limit of an asphalt binder. When the viscosity of an asphalt binder exceeds 300,000 poise, the asphalt is considered too hard and is likely to fail. The criterion is determined based on an indirect correlation with a ductility value of 3-5 cm.

Note that asphalts come from different sources, and each asphalt has different portions of saturates, naphthene aromatics, polar aromatics, and asphaltenes, which in turn will result in different activation energies and, thus, in different oxidation rate and hardening rate dependencies on temperature.

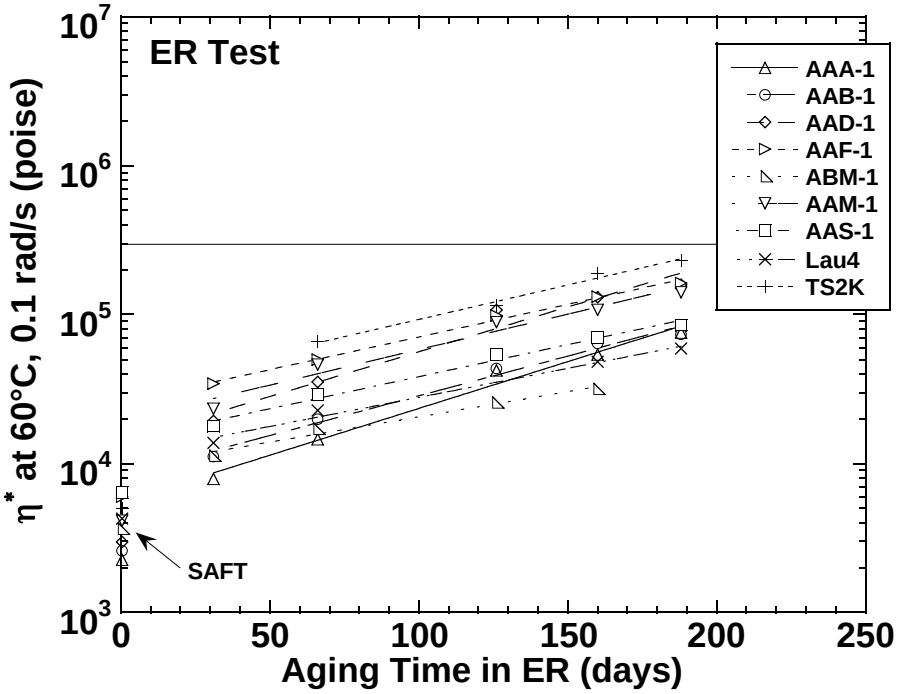

Figure 6-2. Environmental Room η^*_o Hardening Rates.

The hardening rates, i.e. the slope of viscosity versus aging time, of different asphalts also vary. The first set of samples aged in the environmental room was obtained after 30 days of aging. Unfortunately, the TS2K measurement was defective, probably as a result of overheating prior to DSR measurement. The viscosity of AAA-1 is the lowest as shown in Figure 6-2, and extrapolation of the TS2K data corresponding to 30 days of aging will show that TS2K has the highest viscosity. However, with time, the ranking shuffles and at 188 days ABM-1 is ranked best (lowest viscosity), while TS2K is still the worst. Although the initial jump for ABM-1 is not the lowest, its very low hardening rate, i.e. the slope of the line, compensates, and after enough time, it is the least hardened. Table 6-2 tabulates the values of hardening rate and initial jump. More complete hardening rate data are shown in Table A-6-1 in Appendix A. Asphalt AAA-1, on the other hand, has a very high hardening rate, which in turn offsets its very low initial jump; hence, its rank slipped from best at 30 days to third best at 188 days. The hardening rate of TS2K is nearly the same as that of AAF-1 and AAM-1, but the high initial jump of TS2K contributes heavily to its poor ranking. As shown in Figure 6-2, asphalts AAD-1 and AAF-1 are very close to each other after 188 days. Although asphalt AAD-1 starts relatively low, its hardening rate is in fact the second highest such that with time AAD-1 catches up with AAF-1 and eventually will be higher in viscosity compared to AAF-1 after an extended aging period.

Figures 6-3 to 6-11 present the viscosity hardening rates for the other nine aging tests. Each plot shows the hypothetical failure line at 300,000 poise (based on the DSR function, discussed in the next section). The aging times are much shorter than the environmental room aging as discussed previously under the section on aging conditions.

Table 6-2. Environmental Room Aging, Viscosity Hardening Rates.

Asphalt	Viscosity Hardening Rate x 10^3 ln(poise)/day	Initial Jump ln(poise)
AAA-1	14.5	1.65
AAB-1	12.3	1.84
AAD-1	13.8	2.28
AAF-1	10.1	2.51
ABM-1	7.8	1.36
AAM-1	11.0	2.28
AAS-1	9.9	1.79
Lau4	8.8	1.44
TS2K	10.7	2.17

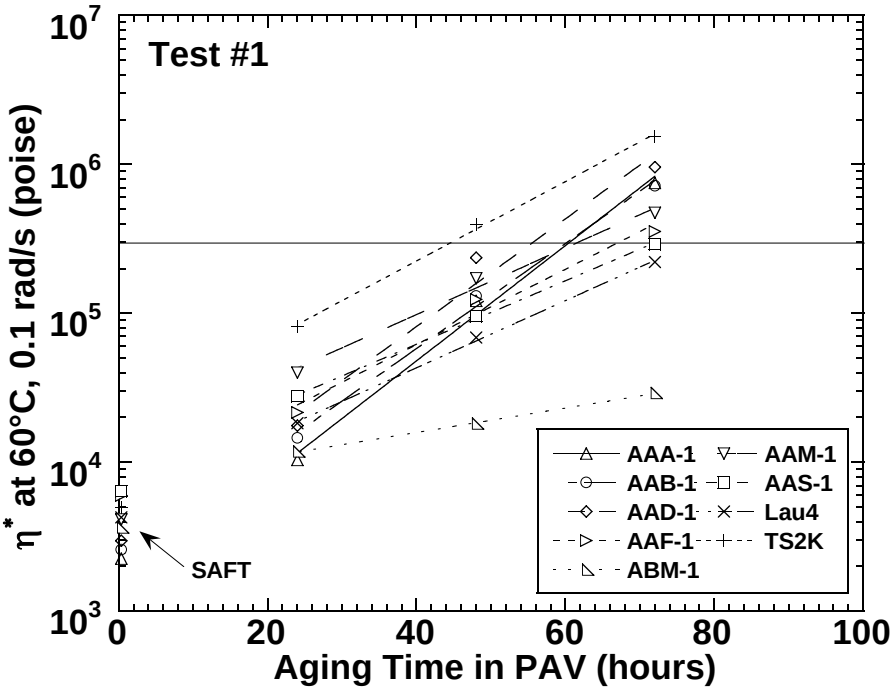

Figure 6-3. Viscosity versus Aging Time in Test #1 (20 atm Air, 100 °C).

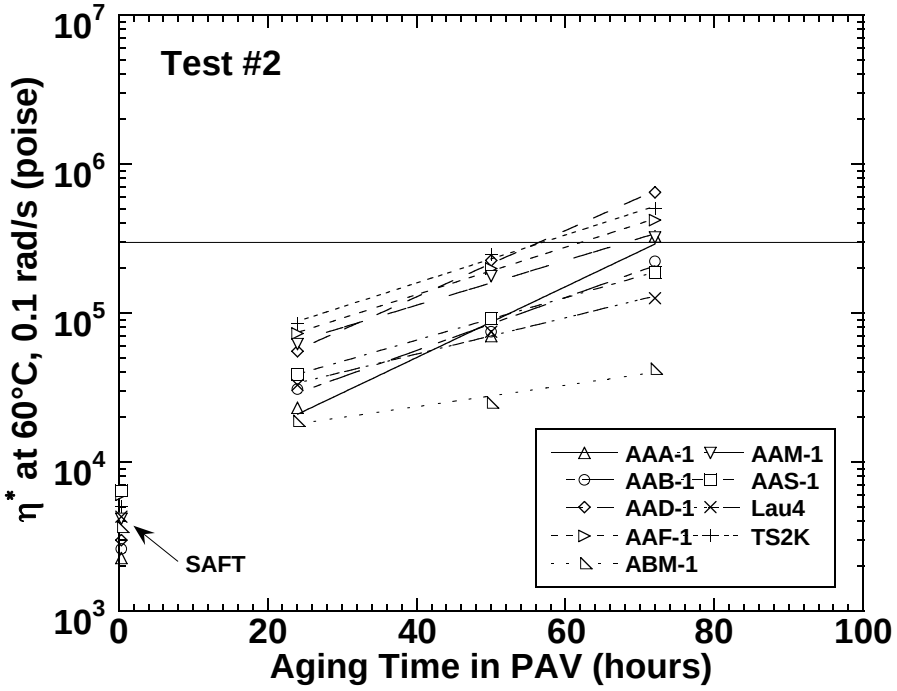

Figure 6-4. Viscosity versus Aging Time in Test #2 (20 atm Air, 90 °C).

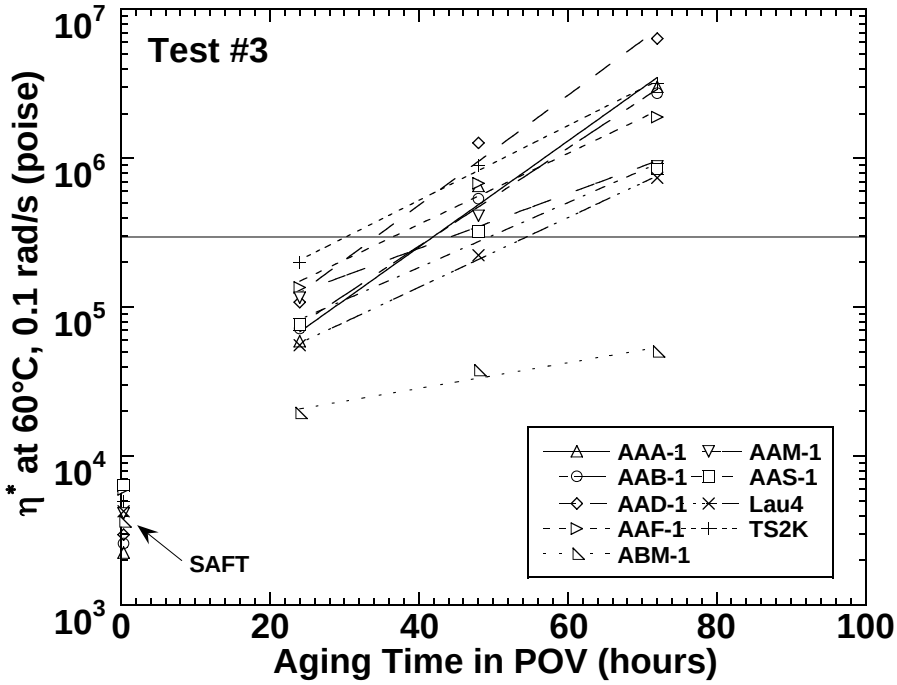

Figure 6-5. Viscosity versus Aging Time in Test #3 (5 atm O_2, 100 °C).

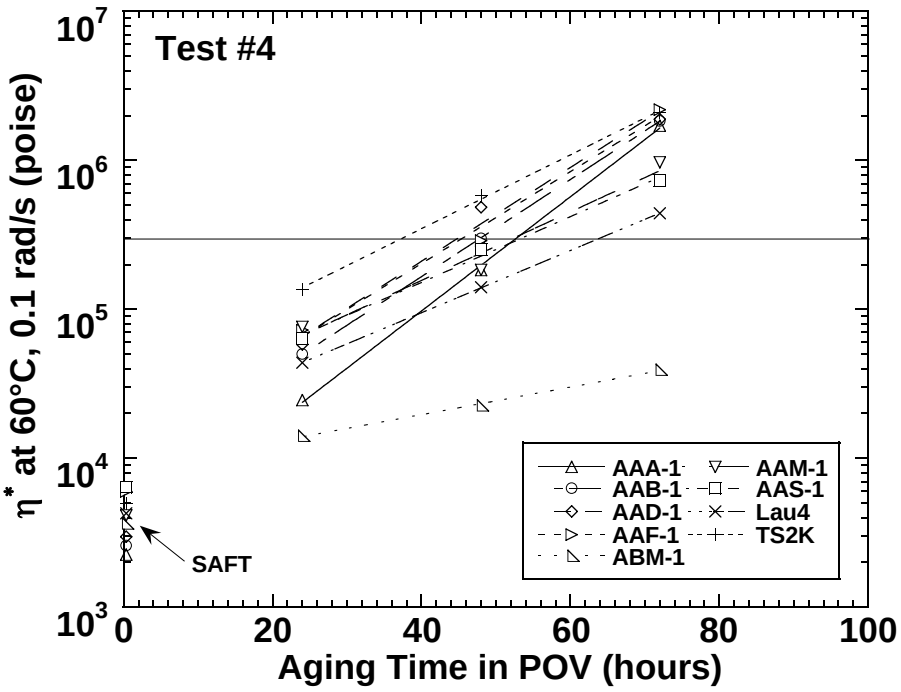

Figure 6-6. Viscosity versus Aging Time in Test #4 (1 atm O_2, 110 °C).

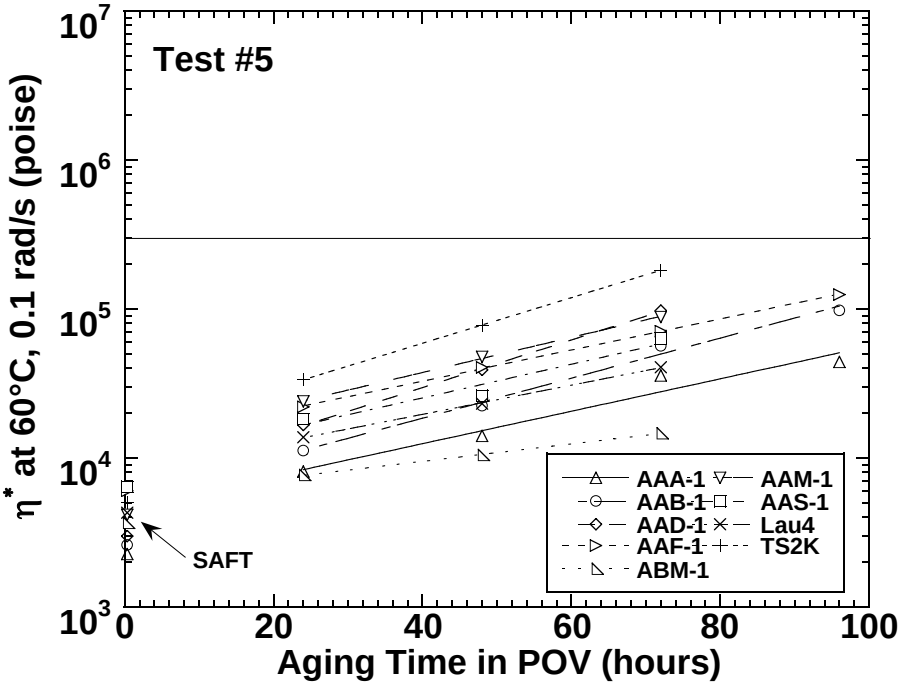

Figure 6-7. Viscosity versus Aging Time in Test #5 (1 atm Air, 110 °C).

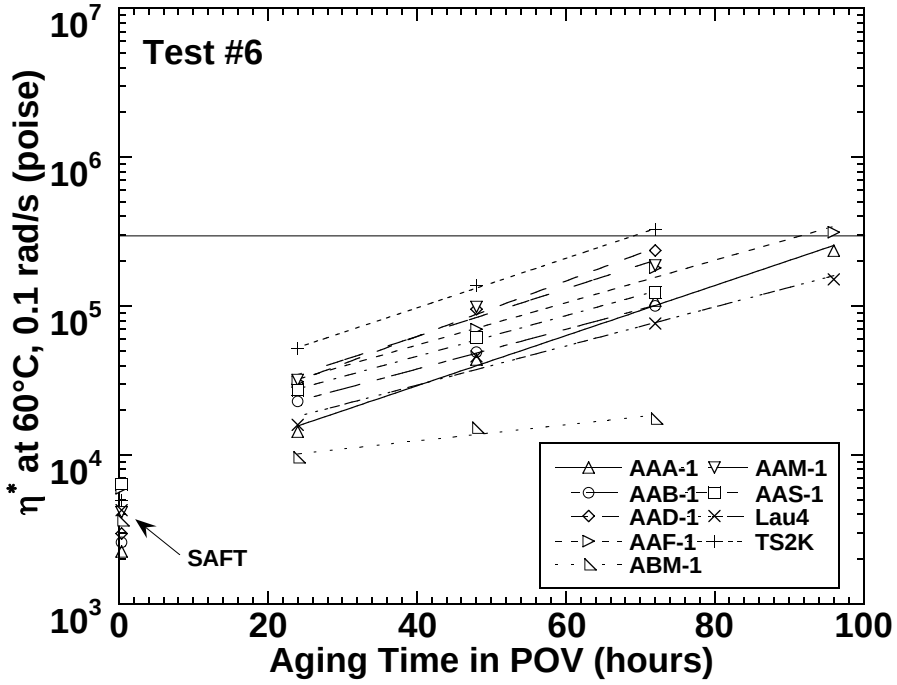

Figure 6-8. Viscosity versus Aging Time in Test #6 (1 atm O_2, 100 °C).

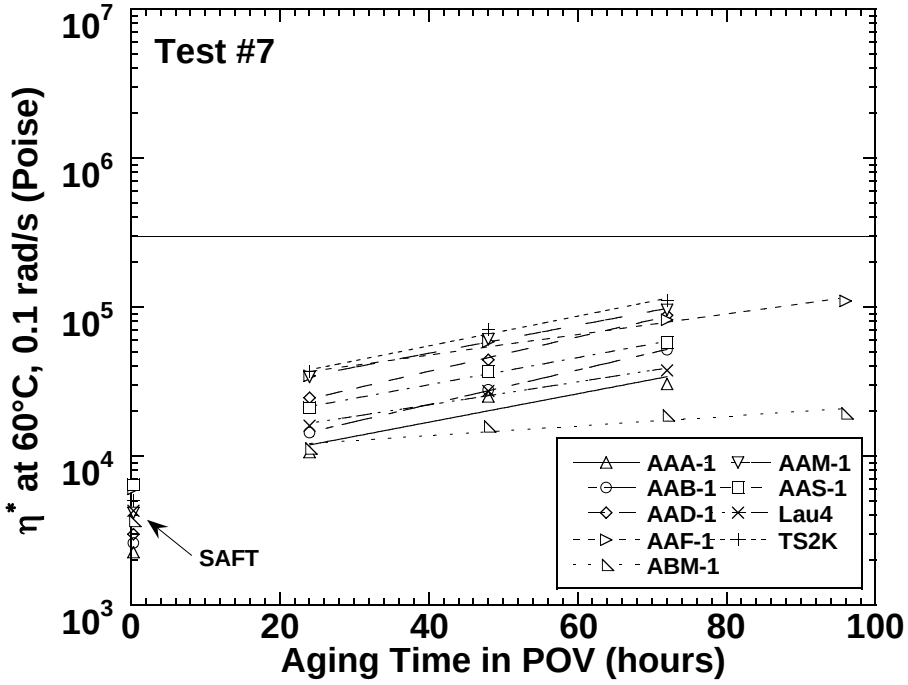

Figure 6-9. Viscosity versus Aging Time in Test #7 (1 atm O_2, 93 °C).

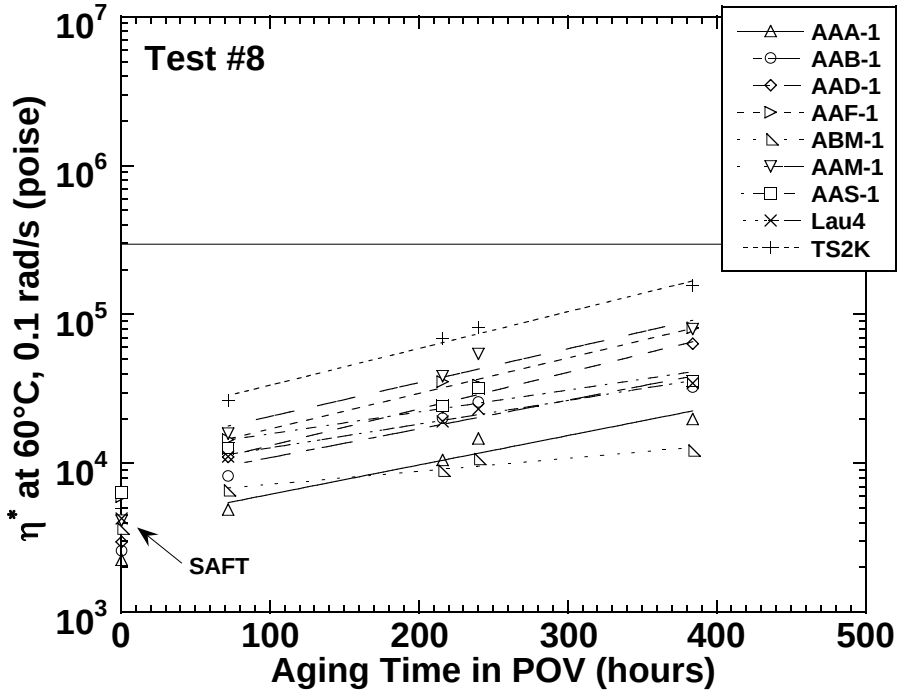

Figure 6-10. Viscosity versus Aging Time in Test #8 (1 atm Air, 88 °C).

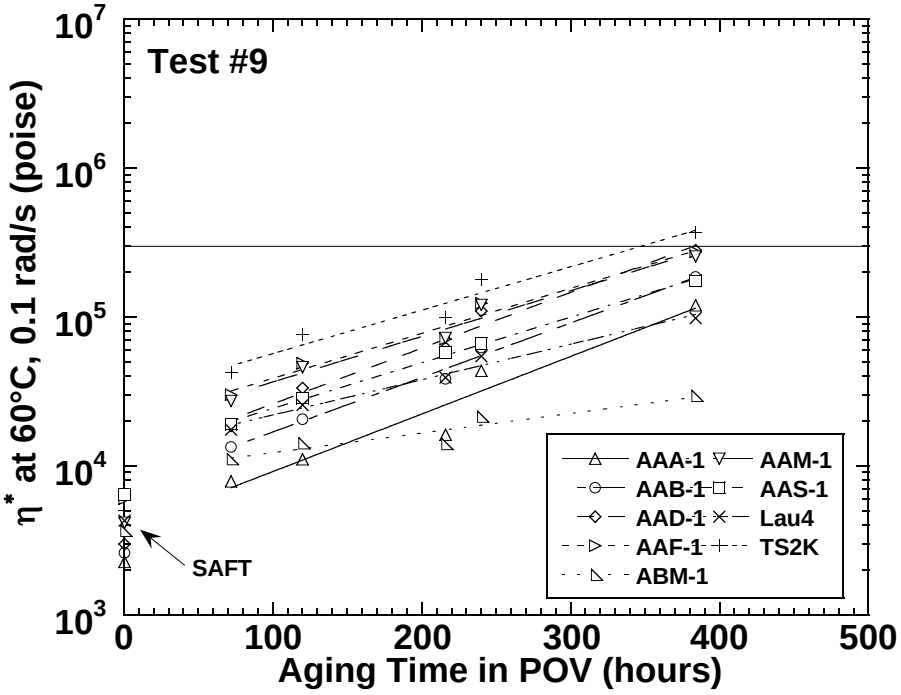

Figure 6-11. Viscosity versus Aging Time in Test #9 (1 atm O_2, 82 °C).

For all aging conditions, just like in the environmental room aging, asphalt ABM-1 slowly ages in all nine conditions. Asphalt AAA-1, on the other hand, shows a very rapid hardening rate in Tests 1-4. In most cases, asphalts TS2K, AAD-1, and AAA-1 turn out to be high in viscosity, although in some cases, AAB-1 and AAM-1 also have very high viscosities.

The time when the hardest asphalt has reached a viscosity of 300,000 poise can be determined from these hardening rate plots. For all aging conditions, it is clearly shown that TS2K crosses the failure line first, except for Test 2, for which AAD-1 takes less than one hour less time than TS2K to fail. The number of days for TS2K to reach 300,000 poise in the environmental room is estimated to be 210 days (Figure 6-2).

The calculated aging time, the corresponding viscosity for each sample, and the absolute error values, which are a measure of how much the accelerated aging tests deviate from the environmental aging, for all aging conditions are tabulated in Table 6-3. The percent error in log viscosity is reported because hardening varies logarithmically with time. It should be noted that asphalt ABM-1 is so far below the critical value that its value is irrelevant; therefore, it is not a part of the average value. In the short-term tests (Tests 1 through 7), the time for TS2K to reach 300,000 poise varies between 34 hours and 114 hours. In the long-term aging, the times are 486 hours and 348 hours for Tests 8 and 9, respectively.

The absolute relative errors were defined as the absolute value of the difference between the log viscosity of a sample aged in a PAV or POV and the log viscosity of the same asphalt aged in the environmental room divided by the log viscosity of the environmental room aged asphalt. Tests 2 and 3 yield the smallest errors of 0.8 percent and 0.7 percent, respectively. It is appealing to choose Test 3 over 2 as the former has a slightly smaller error; however, it is also important to consider the time required for the worst asphalt to fail. Test 2 requires 57 hours, and Test 3 requires 34 hours, but its accuracy may not be as reliable. Test 1 has a high absolute error. This might be due to a diffusion problem associated with thick films (Domke, 1999). In Test 7, where the aging condition is relatively moderate (93 ºC, 1 atm O_2), no asphalt reaches the failure limit after four days of aging. The time required to failure is approximately 114 hours by extrapolation and again TS2K fails first.

Tests 8 and 9 were designed to determine if longer aging time would produce better results. The results show that a longer aging time does not guarantee the error will decrease. The absolute log error of Test 9 is 1.3 percent, whereas that of Test 8 is 4.4 percent, the biggest error among all nine tests. Thus, if one is to choose a long-term aging condition based on viscosity, it is preferable to choose Test 9 over Test 8. Moreover, the former requires less aging time than the latter.

Table 6-3. Value of the Viscosity when the TS2K Value is 300,000 Poise.

	ER Test 210 days (poise)	Test #1 56 hours (poise)	Test #2 57 hours (poise)	Test #3 34 hours (poise)	Test #4 37 hours (poise)	Test #5 86 hours (poise)	Test #6 69 hours (poise)	Test #7 114 hours (poise)	Test #8 486 hours (poise)	Test #9 348 hours (poise)
AAA-1	115,340	72,874	128,393	115,312	77,401	39,663	91,221	85,517	35,819	83,317
AAB-1	110,145	84,925	112,944	123,974	136,311	77,252	93,420	158,626	60,677	136,681
AAD-1	258,291	120,490	308,913	213,959	174,094	162,683	220,518	263,410	116,953	221,306
AAF-1	214,985	81,153	248,644	212,326	168,877	99,505	143,582	153,800	141,468	217,377
AAM-1	195, 040	125,052	203,644	165,244	136,116	131,319	185,022	242,743	155,986	210,368
AAS-1	114,065	78,151	115,308	114,148	132,917	84,040	116,047	142,279	58,330	140,007
Lau4	68,643	55,015	85,579	81,078	83,793	55,578	71,765	82,016	52,323	85,249
TS2K	300,000	300,000	300,000	300,000	300,000	300,000	300,000	300,000	300,000	300,000
ABM-1	48,598	17,354	31,157	23,617	18,600	17,627	17,990	23,809	15,730	25,98
Absolute Log Error (%)										
AAA-1		3.9	0.9	0.0	3.4	9.2	2.0	2.6	10.0	2.8
AAB-1		2.2	0.2	1.0	1.8	3.1	1.4	3.1	5.1	1.9
AAD-1		6.1	1.4	1.5	3.2	3.7	1.3	0.2	6.4	1.2
AAF-1		7.9	1.2	0.1	2.0	6.3	3.3	2.7	3.4	0.1
AAM-1		3.6	0.4	1.4	3.0	3.2	0.4	1.8	1.8	0.6
AAS-1		3.2	0.1	0.0	1.3	2.6	0.1	1.9	5.8	1.8
Lau4		2.0	2.0	1.5	1.8	1.9	0.4	1.6	2.4	1.9
TS2K		0.0	0.0	0.0	0.0	0.0	0.0	0.0	0.0	0.0
ABM-1		9.5	4.1	6.7	8.9	9.4	9.2	6.6	10.5	5.8
Average (ABM-1 excluded)		3.6	0.8	0.7	2.1	3.7	1.1	1.7	4.4	1.3
(ABM-1 included)		4.3	1.1	1.4	2.8	4.4	2.0	2.3	5.0	1.8

COMPARISON OF AGING TESTS USING THE DSR FUNCTION

In the previous section, viscosity has been used as a measure of asphalt aging in determining a reliable aging test. However, Ruan et al. (2003) developed a rheological function, G'/(η'/G'), and found that it correlated well with ductility (and, thus, to long-term pavement failure) and thus may be a better value to use in an aging test procedure than η^*_o. The parameters are measured using a dynamic shear rheometer (DSR), a much less cumbersome and more reliable means than a ductility procedure. They found that a DSR function value of 0.003 MPa/s, measured at 15 °C and 0.005 rad/s, corresponds to a critical ductility value of about 3 cm measured at 15 °C and 1 cm/min. They based their correlation on DSR measurements at 15 ºC and 0.005 rad/s. For this current work, a higher temperature (44.7 ºC) was determined through time-temperature superposition (TTSP) to accommodate measurements at the Superpave frequency of 10 rad/s. Thus, the DSR function values were measured at 44.7 ºC and 10 rad/s and then shifted to 15 ºC and 0.005 rad/s; it is these shifted values that are reported in this work.

Figure 6-12 is a plot of the DSR function measured at 44.7 ºC and 10 rad/s versus 60 °C viscosity measured at 0.1 rad/s of all asphalts aged in all conditions in this project. Clearly, there is not a one-to-one correspondence between viscosity and the DSR function value of 0.003 MPa/s (taken to be the failure limit). In fact, at the critical DSR function value of 0.003 MPa/s, the viscosity ranges from about 80,000 to 600,000 poise. From a regression procedure, η^*_o is approximately 300,000 poise when the DSR function reaches the value of 0.003 MPa/s.

The growth of asphalt hardening based on DSR shares a similar trend with that based on viscosity. Both parameters grow exponentially with aging time. Figure 6-13 shows the DSR function hardening rate for asphalts aged in the environmental room.

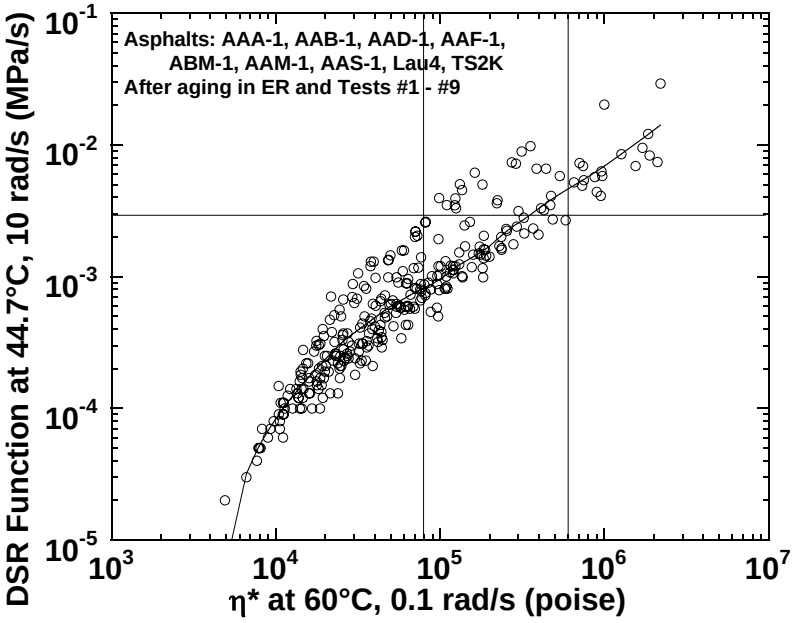

Figure 6-12. Comparison of DSR Function with Viscosity.

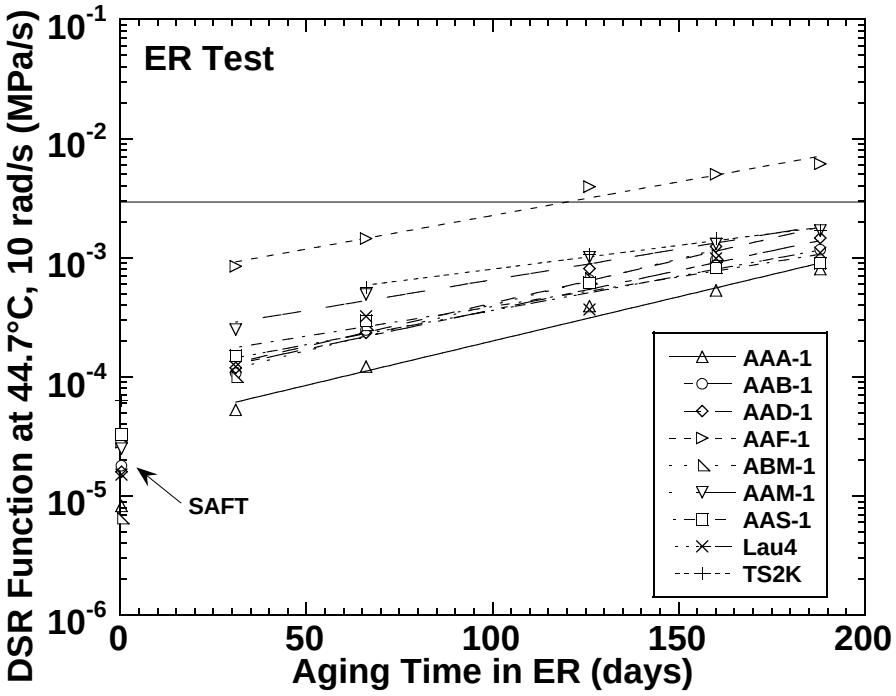

Figure 6-13. Environmental Room DSR Function Hardening Rates.

The line crossing 0.003 MPa/s is taken to be the failure limit in accordance with the findings discussed above. As expected, the relative ranking of viscosity will not be the same as those based on the DSR function. Asphalt TS2K appears to be the hardest asphalt based on viscosity, but asphalt AAF-1 fails the DSR function criterion (0.003 MPa/s) first in the same environmental aging condition. Asphalt AAF-1 is ranked first, and TS2K is second. Again, asphalt AAA-1 has a low initial jump but a high hardening rate; yet in this case, the initial jump is very low compared to the others so that the hardening rate does not greatly affect the ranking. Longer aging times, however, will result in a different ranking. Eventually, asphalt TS2K will reach failure first although its high initial jump puts this after a very long time. Consideration of choosing the right property on which to base the test proves to be a critical issue in designing an asphalt aging test. However, it is encouraging that this particular test based on the DSR function fails the same asphalt for all aging conditions in this project.

Table 6-4 gives the DSR function hardening rates for all asphalts aged in the environmental room. They vary between 0.009 and 0.018 ln(MPa/s)/day. It is very surprising that the DSR hardening rate of ABM-1 is the highest compared to the other asphalts; however, its initial jump is relatively low. On the other hand, AAF-1 has a reasonably low hardening rate but an extremely high initial jump. As noted before, hardening rate and initial jump can offset each other, and thus both values should be taken into consideration for binder aging evaluation. Referring back to Figure 6-13, it is clear that the high initial jump of AAF-1 causes this asphalt to fail the criterion of 0.003 MPa/s in advance of the other asphalts. It takes only 122 days for asphalt AAF-1 to cross the 0.003 MPa/s limit.

Table 6-4. Environmental Room Aging, DSR Function Hardening Rates.

Asphalt	DSR Function Hardening Rate ln(MPa/s)/day	Initial Jump ln(MPa/s)
AAA-1	0.017	3.52
AAB-1	0.015	3.68
AAD-1	0.017	3.43
AAF-1	0.013	5.84
ABM-1	0.018	4.07
AAM-1	0.012	4.11
AAS-1	0.011	3.29
Lau4	0.013	3.57
TS2K	0.009	2.72

Figures 6-14 to 6-22 show the hardening rate plots for the other nine tests. The data for these plots, including Figure 6-13, were collected from the same samples covered in the previous section discussing the viscosity. Similar behavior was observed for all aging conditions studied. Asphalt AAF-1 is shown to reach the critical value of 0.003 MPa/s before the other asphalts. Asphalt ABM-1 is ranked lowest in some cases, and AAA-1 in other cases. Recall that based on viscosity the constant hardening rate lines of TS2K, in most cases, are the highest of the group; however, with the DSR function as a means of evaluating asphalt hardening, AAF-1 is the highest, except for Test 3, where the hardening rate line of asphalt AAA-1 crosses the line of AAF-1 after 60 hours of aging.

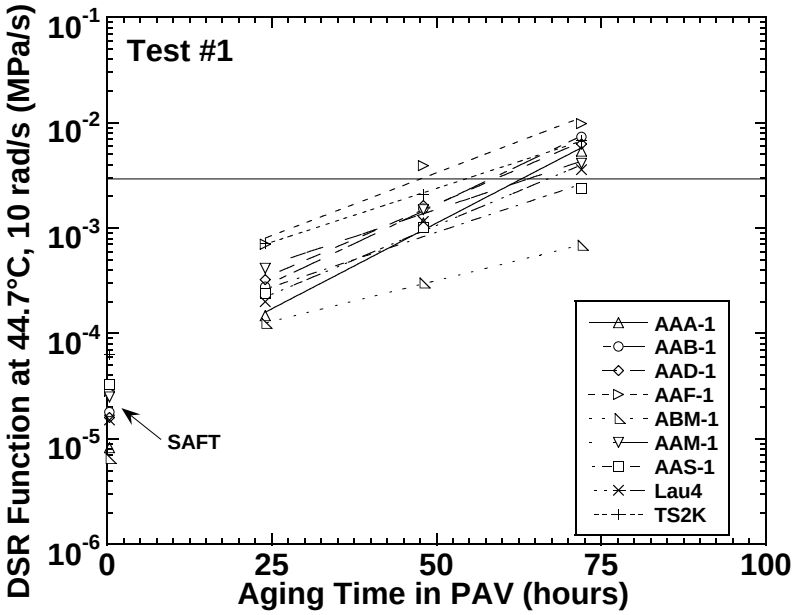

Figure 6-14. DSR Function versus Aging Time in Test #1 (20 atm Air, 100 °C).

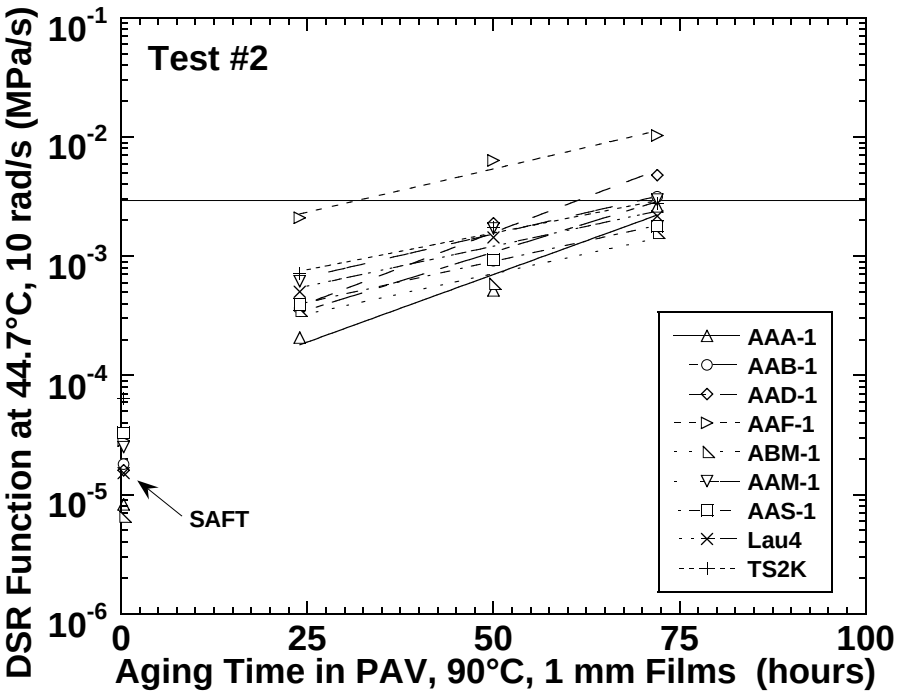

Figure 6-15. DSR Function versus Aging Time in Test #2 (20 atm Air, 90 °C).

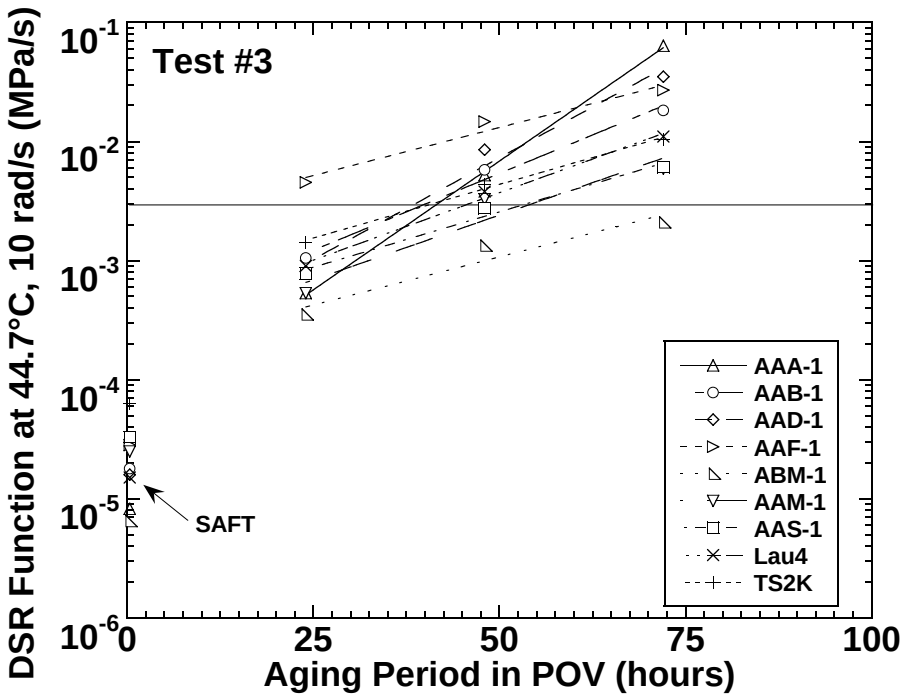

Figure 6-16. DSR Function versus Aging Time in Test #3 (5 atm O_2, 100 °C).

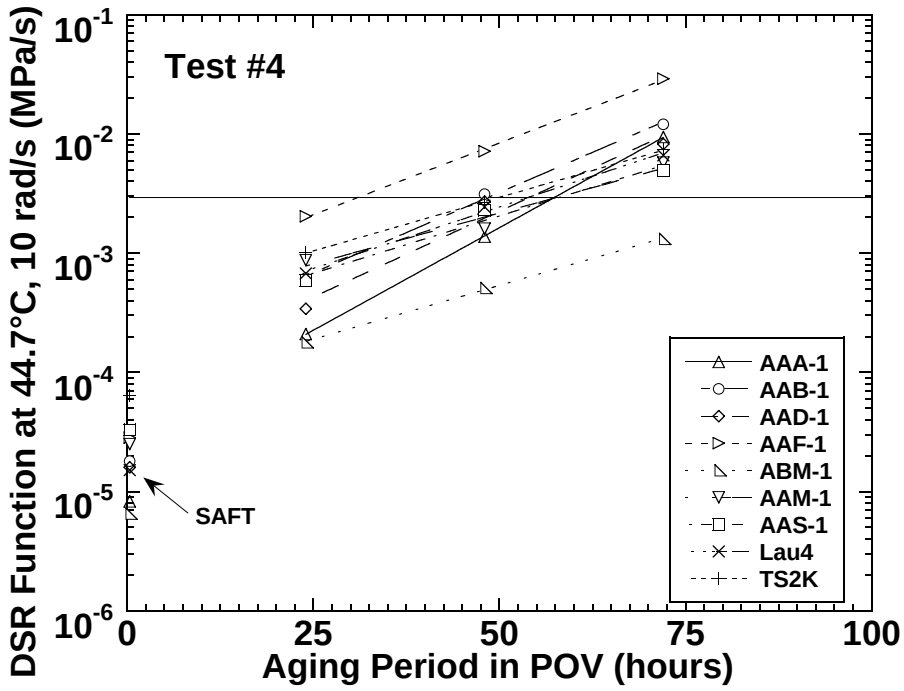

Figure 6-17. DSR Function versus Aging Time in Test #4 (1 atm O_2, 110 °C).

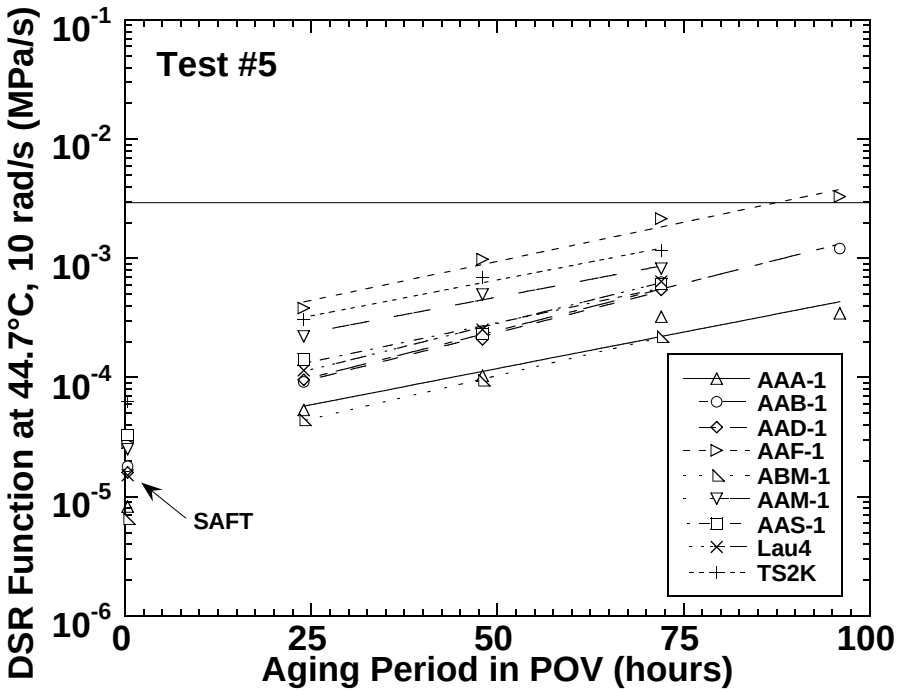

Figure 6-18. DSR Function versus Aging Time in Test #5 (1 atm Air, 110 °C).

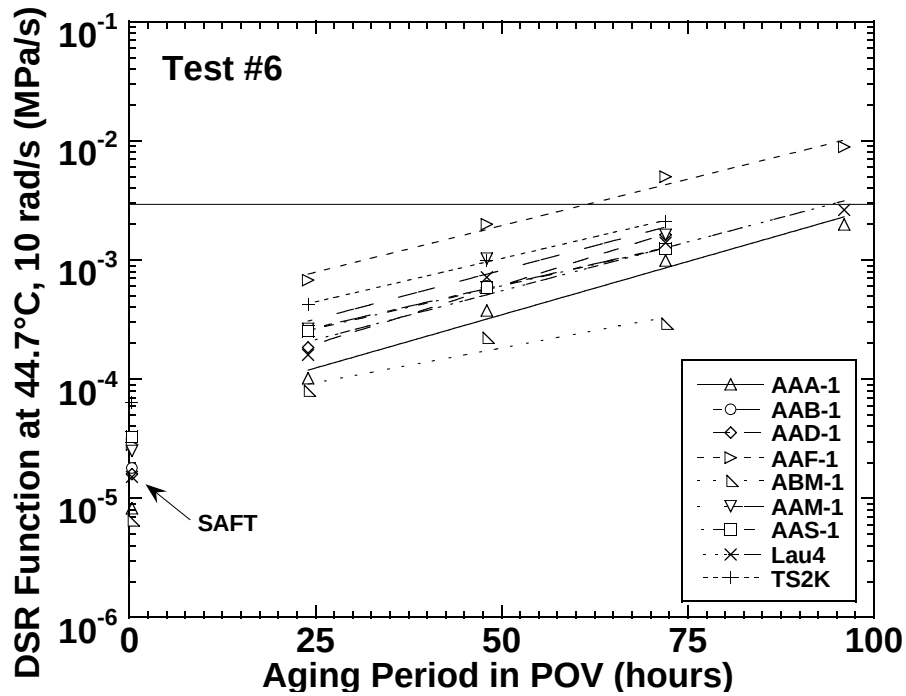

Figure 6-19. DSR Function versus Aging Time in Test #6 (1 atm O_2, 100 °C).

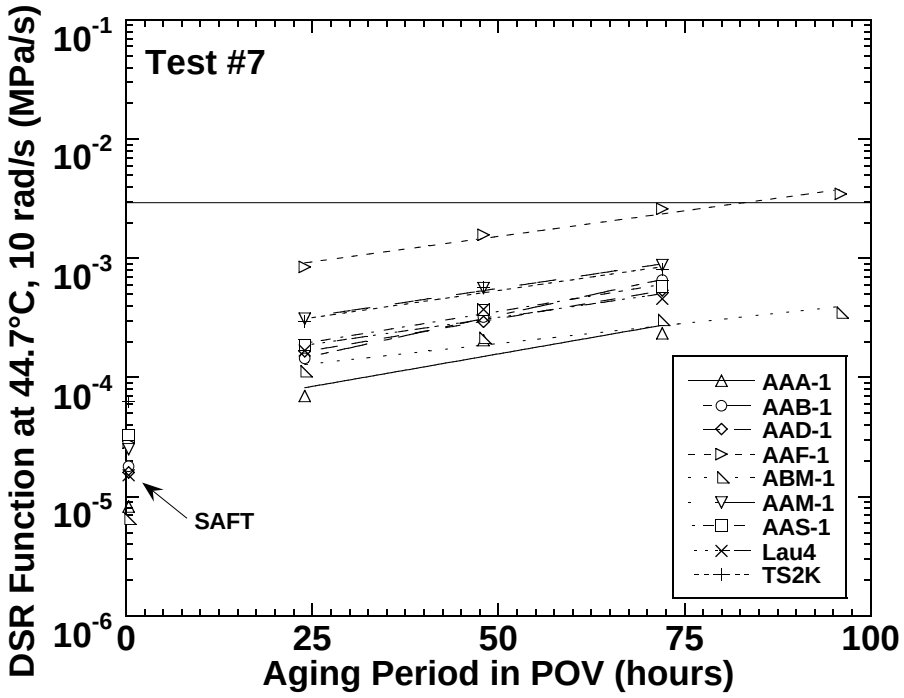

Figure 6-20. DSR Function versus Aging Time in Test #7 (1 atm O_2, 93 °C).

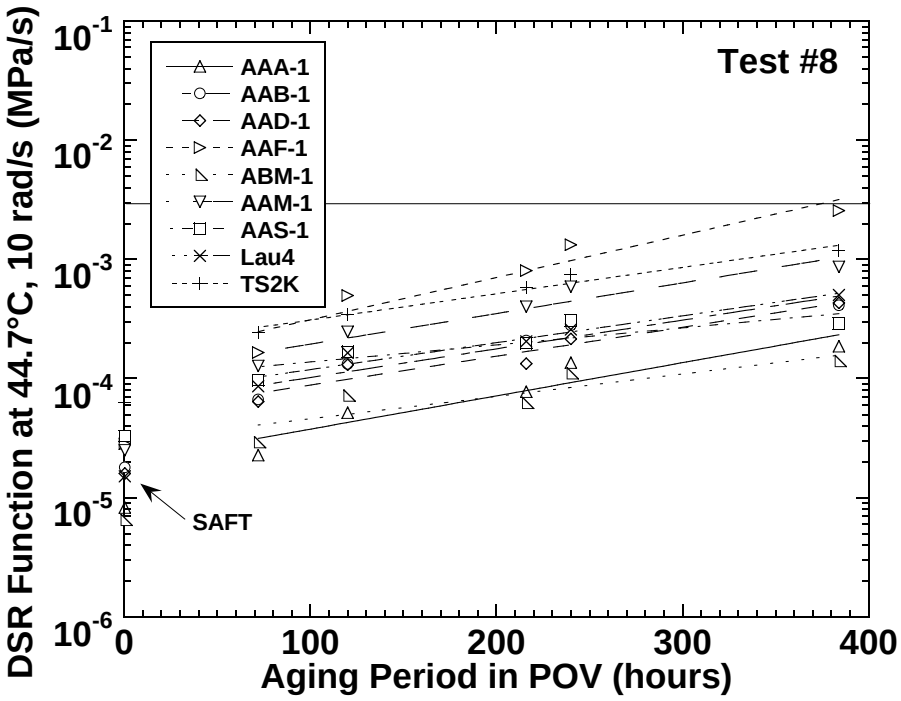

Figure 6-21. DSR Function versus Aging Time in Test #8 (1 atm Air, 88 °C).

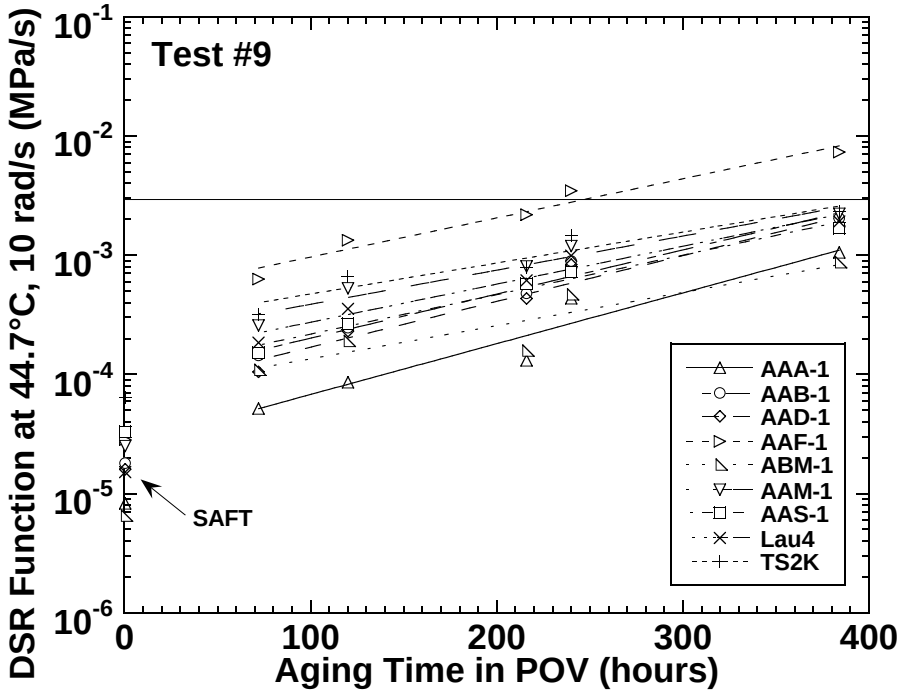

Figure 6-22. DSR Function versus Aging Time in Test #9 (1 atm O_2, 82 °C).

In Test 1, the initial jumps of AAF-1 and TS2K are very high compared to the other asphalts, while the highest hardening rate belongs to asphalt AAA-1 (Figure 6-14). The initial jump values and hardening rates of all tests are given in Table A-6-2 of Appendix A. In Figure 6-15, asphalt AAF-1 is shown to oxidize very fast in the thin-film PAV at 20 atm air and 90 ºC, requiring only 32 hours to reach the critical function value. Asphalt AAD-1 has a high hardening rate. After only two days of aging it fails. Asphalt AAA-1 also has a high hardening rate, but its initial jump is not very high. Also in Test 3, AAF-1 has a higher initial jump (5.84 ln[MPa/s]) than the other eight asphalts, followed by TS2K. In less than 1 day of aging, asphalt AAF-1 has reached the critical value. The hardening rates of these two asphalts are not as high as AAA-1. The high hardening rate rapidly changes the DSR function of asphalt AAA-1; thus, after the second day of aging, the line of AAA-1 surpasses the line of AAF-1. Again in Test 4, AAF-1 fails the criterion earlier than the other asphalts and AAA-1 also has a very high hardening rate.

The long-term aging tests are shown in Figures 6-21 and 6-22. It takes approximately 377 hours for the first asphalt, again AAF-1, to fail in the POV at 88 ºC, 1 atm air and 250 hours in the POV at 82 ºC, 1 atm O_2.

In comparing the accelerated vessel aging conditions against environmental room aging, an early-failing asphalt was used as the reference for ranking the DSR function. As mentioned earlier, the DSR function of AAF-1 was overall the highest after aging in the environmental room as well as in the thin-film PAV at 20 atm air and 90 ºC. It appears that AAF-1 was consistently the worst asphalt in terms of the DSR ranking for all aging conditions. Accordingly, the DSR functions of other asphalts after 122 days of environmental room aging (the time for AAF-1 to reach 0.003 MPa/s) were calculated and ranked, one being the best asphalt while nine is the worst, in this case AAF-1. Similarly, the PAV and POV data were used to determine times at which the hardest asphalt reached 0.003 MPa/s.

To compare the different aging conditions against the environmental room aging, the absolute log errors were calculated for each sample, and the averages were taken for each PAV or POV aging condition. The DSR function at the time when the first asphalt fails the limit of 0.003 MPa/s, the absolute log errors, and the averages of the errors are tabulated in Table 6-5. As shown, asphalt AAA-1 is consistently the best asphalt with respect to the DSR function, while, again, AAF-1 is the worst and TS2K is the second worst, except for Test 7. Asphalt ABM-1 is excluded from the average since its deviation was always large; it hardened so slowly in the PAV and POV aging that its value was of no significance.

The average absolute errors for aging conditions studied range from 0.9 percent to 7.45 percent. Test 2 for 32 hours shows the least average deviation from the environmental room compared to the other aging conditions, while the other PAV condition (Test 1) gave the worst agreement. Again, this difference could be due to the diffusion problem associated with the sample thickness. For the long-term runs, the two conditions (POV 88 ºC, 1 atm air and POV 82 ºC, 1 atm O_2) have almost the same average error (2.6 and 2.8 percent), but the latter takes less time, 250 hours as opposed to 377 hours.

Table 6-5. Value of the DSR Function when the AAF-1 Value is 0.003 MPa/s.

	DSR Function at 44.7 ºC, 10 rad/s x10^4 (MPa/s)									
	ER Test 122 days	Test #1 48 hours	Test #2 32 hours	Test #3 10 hours	Test #4 31 hours	Test #5 88 hours	Test #6 62 hours	Test #7 77 hours	Test #8 377 hours	Test #9 250 hours
AAA-1	2.90	9.59	2.80	1.31	3.73	3.48	5.70	3.13	2.23	2.95
AAB-1	5.08	14.5	4.93	5.08	10.2	9.97	9.16	7.86	4.74	7.22
AAD-1	5.97	14.9	6.03	3.24	6.54	9.53	10.6	6.08	4.14	6.37
AAF-1	30.0	30.0	30.0	30.0	30.0	30.0	30.0	30.0	30.0	30.0
AAM-1	8.45	13.7	8.57	3.31	10.5	13.4	13.0	10.1	10.0	10.4
AAS-1	4.99	8.31	5.19	4.69	8.99	9.19	9.08	6.84	3.43	6.83
Lau4	4.81	9.39	7.05	4.69	10.1	11.2	8.70	5.62	5.02	8.23
TS2K	9.79	21.7	9.52	8.38	13.6	19.1	15.5	9.50	12.7	11.6
ABM-1	5.91	2.96	4.13	2.45	2.47	3.74	2.53	2.95	1.61	4.11
Absolute Log Error (%)										
AAA-1		14.7	0.4	9.7	3.1	2.3	8.3	1.0	3.2	0.2
AAB-1		13.9	0.4	0.0	9.2	8.9	7.8	5.7	0.9	4.6
AAD-1		12.3	0.1	8.3	1.2	6.3	7.7	0.2	4.9	0.9
AAF-1		0.0	0.0	0.0	0.0	0.0	0.0	0.0	0.0	0.0
AAM-1		6.8	0.2	13.3	3.0	6.6	6.1	2.5	2.4	2.9
AAS-1		6.7	0.5	0.8	7.7	8.0	7.9	4.1	4.9	4.1
Lau4		8.8	5.0	0.3	9.7	11.0	7.8	2.0	0.6	7.0
TS2K		11.5	0.4	2.3	4.8	9.6	6.6	0.4	3.8	2.4
ABM-1		9.3	4.8	11.8	11.7	6.1	11.4	9.3	17.5	4.9
Average (ABM-1 excluded)		9.3	0.9	4.3	4.8	6.6	6.5	2.0	2.6	2.8
(ABM-1 included)		9.3	1.3	5.2	5.6	6.5	7.1	2.8	4.2	3.0

Figure 6-23 shows the aging time to reach the same DSR function value in the environmental room and the aging time in the PAV thin film at 90 ºC and 20 atm air for all nine asphalts. The time when the first asphalt fails the criterion, AAF-1, after aging in the environmental room is 122 days, and this corresponds to 32 hours of aging in the PAV thin film. The other asphalts, except ABM-1 and Lau4, converge around the 122 days and 32 hours time frame, suggesting that aging in the PAV thin film 90 ºC, 20 atm air for 32 hours best simulates the aging in the environmental room. The convergence of most of the lines in Figure 6-23 is because there is a rough inverse correlation between initial jump and subsequent hardening rate.

Another attempt was made to rank the asphalts based on the same DSR function except using TS2K as the reference and the time at which it reached 0.003 MPa/s. The values are given in Table 6-6. It took considerably longer for TS2K to reach the critical value than it did for AAF-1. In the environmental room, the time for TS2K to reach 0.003 MPa/s was 244 days. Due to the effects of the initial jump and hardening rate, the ranking based on AAF-1 is not the same as the ranking based on TS2K. The best condition is still PAV thin-film at 90 ºC and 20 atm air, but the time is nearly 73 hours and the average percent error is larger. It is not surprising that even using TS2K as the reference and hence a longer aging time, asphalt AAF-1 is still consistently the worst asphalt. On the other hand, asphalt AAA-1 is not always the best asphalt, i.e. the lowest DSR value, although for some conditions it is. Asphalt AAA-1 is comparable to AAS-1, and in one case (Test 1), the DSR function value of AAA-1 is close to those of AAM-1 and Lau4 as well.

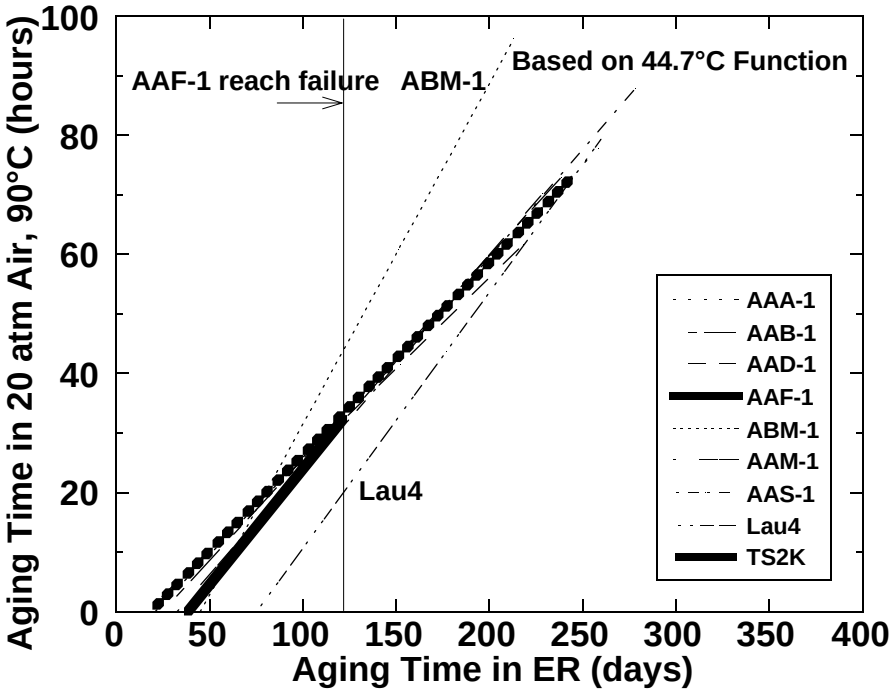

Figure 6-23. Lines of Equal DSR Function for Two Aging Conditions.

Table 6-6. Value of the DSR Function when the TS2K Value is 0.003 MPa/s.

	DSR Function at 44.7 ºC, 10 rad/s x10^4 (MPa/s)									
	ER Test 244 days	Test 1# 55 hours	Test #2 73 hours	Test #3 41 hours	Test #4 50 hours	Test #5 104 hours	Test #6 82 hours	Test #7 132 hours	Test #8 546 hours	Test #9 408 hours
AAA-1	23.5	16.1	23.2	28.0	16.9	5.50	12.9	12.5	6.60	14.0
AAB-1	32.6	23.3	29.9	31.6	33.2	18.0	17.5	44.4	12.1	28.0
AAD-1	46.0	22.9	55.3	36.0	23.1	17.2	26.0	23.3	10.6	26.0
AAF-1	147	43.8	11.6	93.8	86.2	49.0	61.0	108	119	99.7
AAM-1	36.0	19.0	32.8	15.4	22.1	20.9	27.4	32.7	27.2	29.6
AAS-1	20.2	11.6	18.7	17.5	20.9	15.0	17.5	25.1	5.99	23.0
Lau4	24.3	14.2	24.6	23.2	25.0	19.9	18.4	17.5	12.1	26.4
TS2K	30.0	30.0	30.0	30.0	30.0	30.0	30.0	30.0	30.0	30.0
ABM-1	51.7	3.78	14.5	7.68	5.46	6.44	4.30	6.94	3.37	11.6
Absolute Log Error (%)										
AAA-1		6.2	0.2	2.9	5.4	24.0	9.9	10.4	20.9	8.5
AAB-1		5.9	1.5	0.5	0.3	10.4	10.9	5.4	17.3	2.7
AAD-1		13.0	3.4	4.5	12.8	18.3	10.6	12.6	27.2	10.6
AAF-1		28.7	5.6	10.6	12.6	26.0	20.8	7.3	4.9	9.2
AAM-1		11.3	1.7	15.1	8.7	9.7	4.9	1.7	5.0	3.5
AAS-1		9.0	1.3	2.4	0.5	4.8	2.4	3.5	19.7	2.0
Lau4		8.9	0.2	0.7	0.4	3.3	4.7	5.4	11.6	1.4
TS2K		0.0	0.0	0.0	0.0	0.0	0.0	0.0	0.0	0.0
ABM-1		49.7	24.1	36.2	42.7	39.6	47.2	38.1	51.9	28.4
Average (ABM-1 excluded)		10.4	1.7	4.6	5.1	12.1	8.0	5.8	13.3	4.7
(ABM-1 included)		14.7	4.2	8.1	9.3	15.1	12.4	9.4	17.6	7.4

FURTHER AGING TEST COMPARISONS

A second set of asphalts was aged in the 60 ºC environmental room, consisting of 10 unmodified asphalts. The values of the DSR function are given in Table 6-7 after 233 days in the environmental room, which was the time required for the first asphalt to reach the critical value chosen for the DSR function of 0.003 MPa/s. This value corresponds to a ductility at 15 ºC of 3 cm/min. Complete environmental room data for these asphalts are given in Table A-6-3 in Appendix A. In Figure 6-24 the DSR data are shown versus time, and in Figure 6-25 60 ºC (140 ºF) viscosity data are plotted versus time. Asphalt TX03-F is the first to reach the critical DSR parameter of 0.003 MPa/s and also the chosen viscosity parameter of 300,000 poise, although for this asphalt it took considerably longer to reach the viscosity limit (291 days for viscosity and 233 days for DSR function).

Tables 6-5 and 6-6 of the previous section show that the thin-film PAV at 90 ºC and 20 atm air had the smallest deviation from the environmental room. Consequently these asphalts were run in thin films in the PAV but at 100 ºC to reduce the time required. Another condition in the POV at 100 ºC and 1 atm oxygen was also chosen.

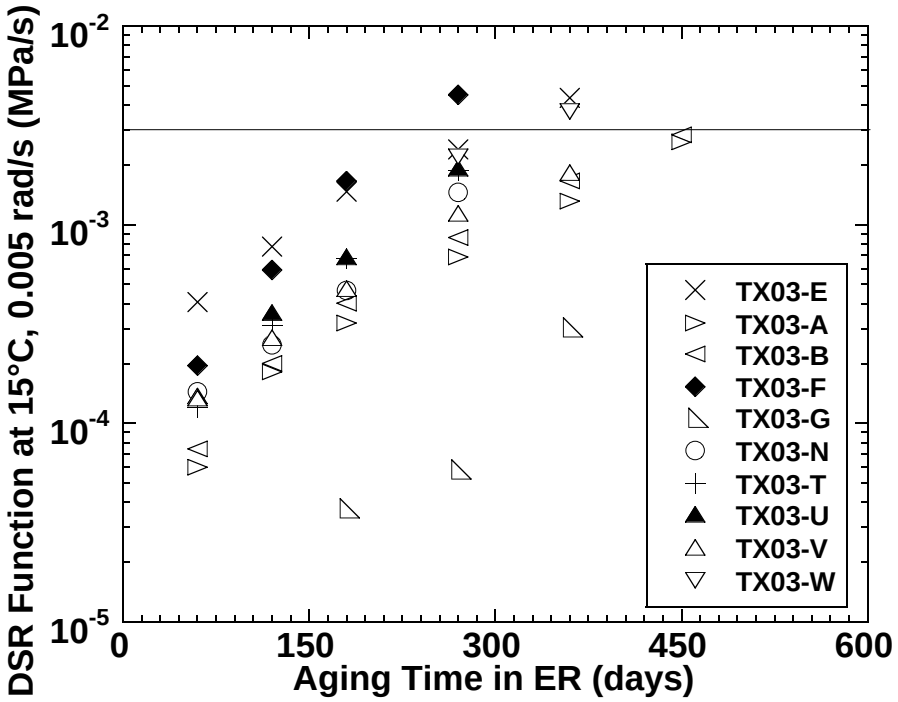

Figure 6-24. DSR Hardening Rates after Aging in Environmental Room.

Table 6-7. Rank and Absolute Error of Asphalts Based on DSR Function at Various Aging Conditions.

	Environmental Room at 233 hours		POV 100 ºC, 1 atm O_2 at 52 hours			PAV 100 ºC, 20 atm Air at 30 hours		
	DSR Function at 15 ºC, 0.005 rad/s (MPa/s)	Rank	DSR Function at 44.7 ºC, 10 rad/s (MPa/s)	Rank	Absolute Log Error wrt ER (%)	DSR Function at 44.7 ºC, 10 rad/s (MPa/s)	Rank	Absolute Log Error wrt ER (%)
TX03-E	$1.80x10^{-3}$	6	$1.71x10^{-3}$	5	0.9	$1.25x10^{-3}$	4	5.7
TX03-F	$3.00x10^{-3}$	7	$3.19x10^{-3}$	7	1.0	$2.45x10^{-3}$	6	3.5
TX03-N	$9.14x10^{-4}$	2	$1.19x10^{-3}$	2	3.7	$1.04x10^{-3}$	1	1.9
TX03-T	$1.24x10^{-3}$	3	$1.05x10^{-3}$	1	2.6	$1.46x10^{-3}$	5	2.3
TX03-U	$1.29x10^{-3}$	4	$1.26x10^{-3}$	3	0.4	$1.06x10^{-3}$	2	3.1
TX03-V	$7.03x10^{-4}$	1	$1.70x10^{-3}$	4	12.2	$1.22x10^{-3}$	3	7.6
TX03-W	$1.78x10^{-3}$	5	$2.65x10^{-3}$	6	6.3	$2.52x10^{-3}$	7	5.5
Average Error for Hardest 7 Asphalts					3.9			4.2
TX03-A	$4.02x10^{-4}$		$1.96x10^{-4}$		9.2	$1.55x10^{-4}$		12.2
TX03-B	$5.08x10^{-4}$		$3.90x10^{-4}$		3.5	$2.28x10^{-4}$		10.5
TX03-G	$5.71x10^{-5}$		$5.83x10^{-5}$		0.2	$7.22x10^{-5}$		2.4

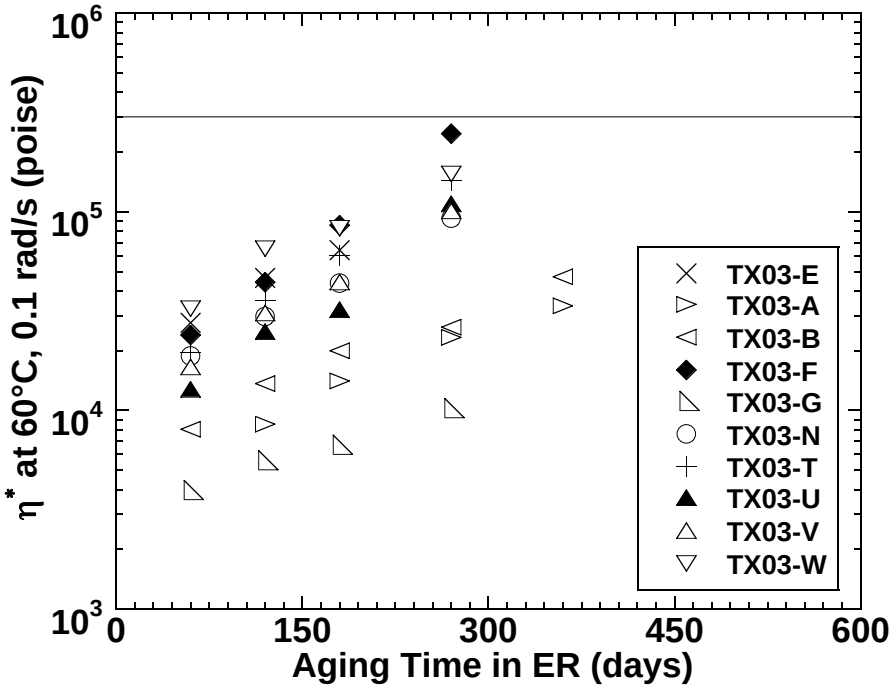

Figure 6-25. Viscosity Hardening Rates after Aging in Environmental Room.

Figure 6-26 shows the POV data (100 ºC and 1 atm O_2) for the DSR function. It is interesting that the most rapidly hardening asphalt reached the critical DSR function value of 0.003 MPa/s in about 52 hours, 10 hours shorter than the time required for asphalt AAF-1 to fail in Test 6, as shown in Figure 6-19. Figure 6-27 shows that the first asphalt reached the critical viscosity of 300,000 poise in approximately the same time, but it was not the same asphalt.

Figure 6-28 shows the DSR function versus time for the PAV run (100 ºC, 20 atm air, 1 mm film). Here, the first asphalts reach the critical DSR function value of 0.003 MPa/s in about 30 hours. It took 32 hours for asphalt AAF-1 of the first set to reach the critical value.

Both accelerated aging runs seem to discriminate against the TX03-W and TX03-V, though the latter is still well below the critical value. DSR functions for both of these runs at the critical times are given in Table 6-7, and complete data are given in Table A-6-4 of Appendix A. Figure 6-29 shows viscosity versus DSR function for the second set of asphalts aged in the environmental room and the two accelerated aging conditions. It is very similar to the results for the first set shown in Figure 6-12.

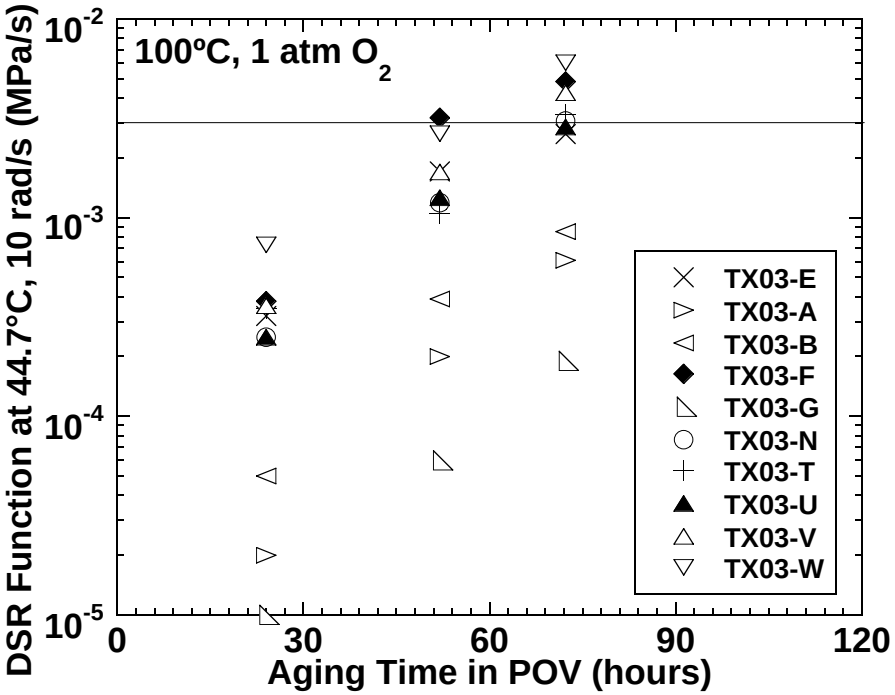

Figure 6-26. DSR Hardening Rates after Aging at 100 ºC, 1 atm O_2.

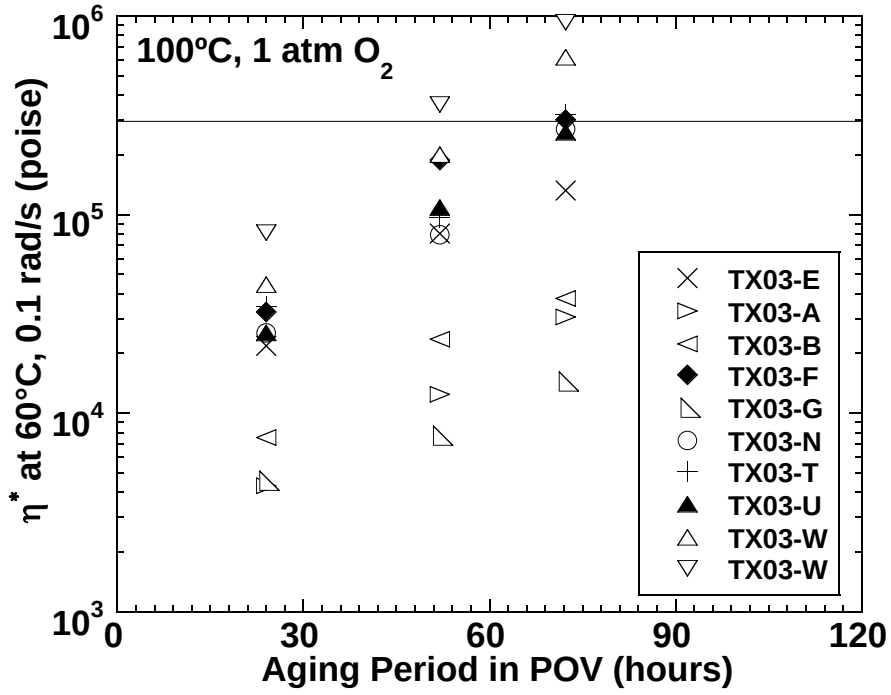

Figure 6-27. Viscosity Hardening Rates after Aging at 100 ºC, 1 atm O_2.

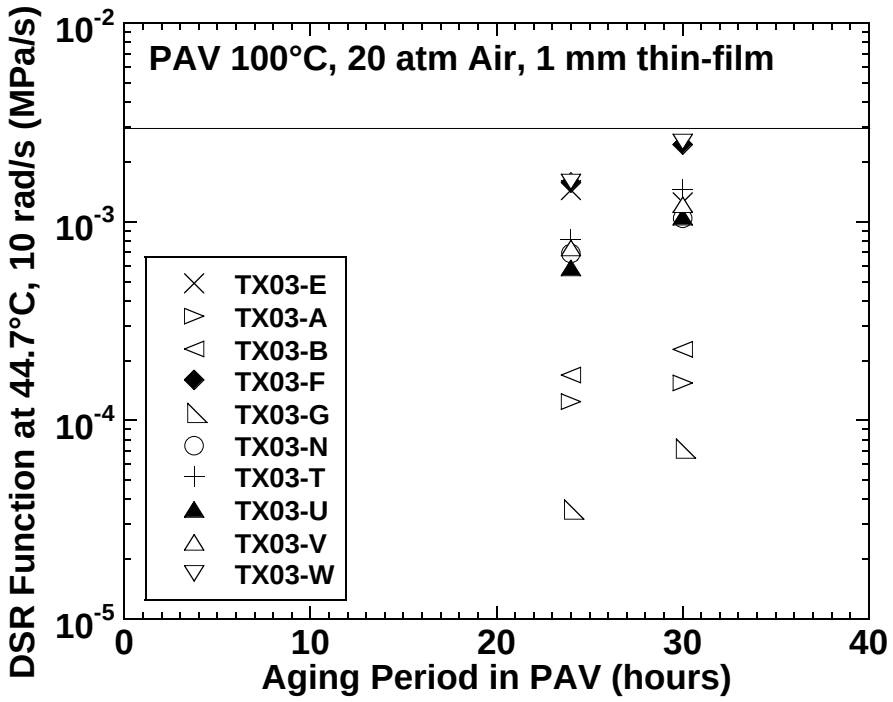

Figure 6-28. DSR Hardening Rates after Aging in Thin-Film PAV.

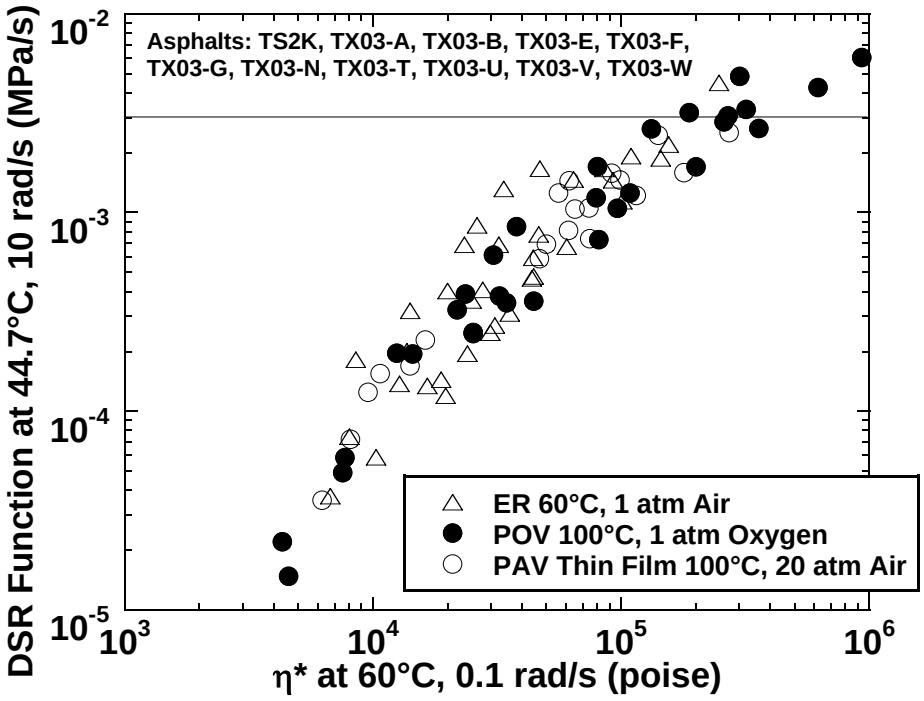

Figure 6-29. Relation between DSR Function and η^*_o for Several Aging Methods.

Percent error in the DSR function is calculated for each run, but TX03-G, TX03-A, and TX03-B are excluded because they are so far below critical that their values are irrelevant. The average errors are close, but the large errors in TX03-V and TX03-W distort the results. Again, because aging is logarithmic, the error in the log of the function is more meaningful, so these values are given. In this case, the POV at 100 ºC and 1 atm O_2 error is smaller than thin-film PAV at 100 ºC, 20 atm air error. The relative agreement of the two conditions with the environmental room is shown visually in Figure 6-30 and 6-31, where the PAV values at 30 hours and the POV values at 52 hours are compared to the environmental room at 233 days. Agreement is very good for TX03-F, especially for the POV, and this is fortuitous in that the environmental room and the POV show TX03-F as first to reach the critical value and this asphalt is very close to first in the PAV. Unfortunately, for both accelerated aging runs TX03-W is very close to the critical value, while in the environmental room it is still well below this value. Overall, one can see that the POV data (100 ºC, 1 atm O_2) are closer except for TX03-V and TX03-W asphalts, but the difference is not great.

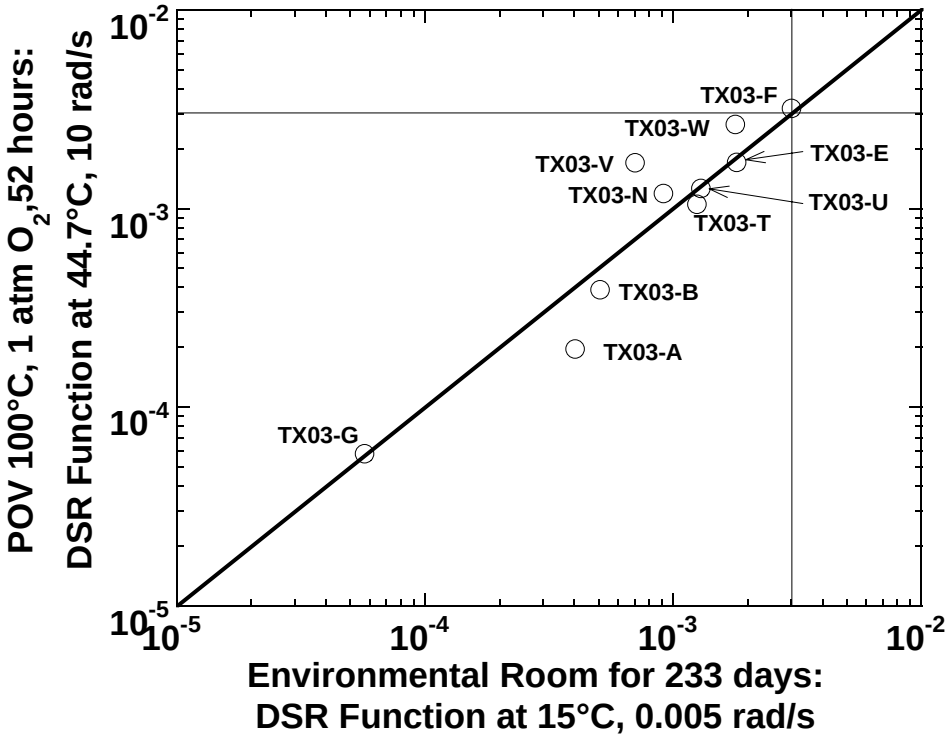

Figure 6-30. Comparison of ER Aging with POV Aging: DSR Function.

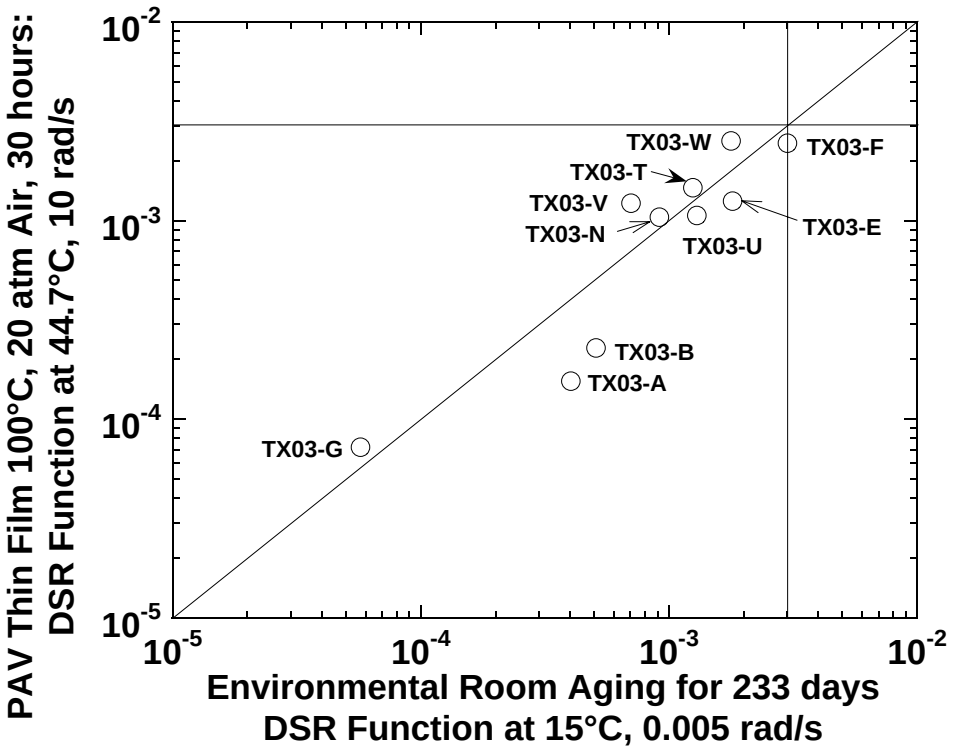

Figure 6-31. Comparison of ER Aging with PAV Aging: DSR Function.

TESTS INCLUDING MODIFIERS AND THEIR BASE ASPHALTS

A series of runs were made with unmodified and modified asphalts as listed in Table 6-8; the asphalts in the left column are the base materials. Asphalts TX03-EM and TX03-FM contain 3.5 percent SBR latex, while TX03-UM contains 3 percent SBR latex, as does the TX03-WM material. Asphalt TS2K was used as the base material for a 12 percent high-cure ground tire rubber blend.

In the previous section, good results were obtained at 100 ºC and 1 atm O_2, so this was repeated except air was used at 5 atm to obtain the same oxygen partial pressure. The results are listed in Table 6-9 at 77 hours of aging along with rankings and errors when compared to the 60 ºC environmental room at 233 days. Only eight of the asphalts were run in the environmental room. The values of the DSR function versus time are shown in Figure 6-32 for the unmodified asphalts. Asphalts AAD-1 and AAF-1 were also included to gain continuity with the first set of runs with mostly SHRP asphalts.

Table 6-8. List of Modified Materials with their Base Materials.

Unmodified Materials	Modified Materials
TS2K	TS2K 12% Rubber
TX03-E	TX03-EM 3.5% SBR Latex
TX03-F	TX03-FM 3.5% SBR Latex
TX03-U	TX03-UM 3% SBR Latex
TX03-W	TX03-WM 3% SBR Latex

Surprisingly, 77 hours were required for the first asphalt (TX03-W) to reach the critical DSR function value of 0.003 MPa/s. In the previous runs at 100 ºC and 1 atm O_2, Figures 6-19 and 6-26, at most 62 hours were required. Figure 6-33 is a comparison of the DSR function at 77 hours for the current run with the 52-hour results using 1 atm O_2. The agreement is not bad, although TX03-F has improved from the worst to third from worst. It seems far from obvious that the presence of inert nitrogen would slow the reaction to this extent. The increase in average error for the unmodified asphalts is not surprising, as only four of them were run here, and this includes the TX03-W asphalt that always exhibited large errors.

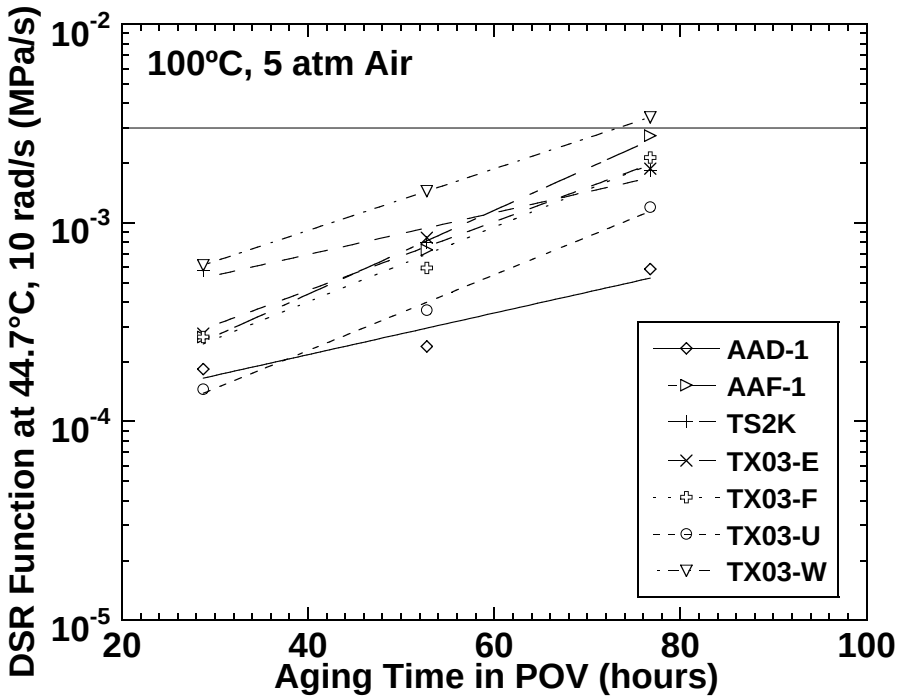

Figure 6-32. Change in DSR Function with Aging Time in POV.

Table 6-9. Rank and Absolute Error of Base and Modified Asphalts Based on the DSR Function.

	Environmental Room at 233 hours		POV 100 ºC, 20 atm Air at 26 hours			POV 100 ºC, 5 atm Air At 77 hours		
	DSR Function at 15 ºC, 0.005 rad/s (MPa/s)	Rank	DSR Function at 44.7 ºC, 10 rad/s (MPa/s)	Rank	Absolute Log Error wrt ER (%)	DSR Function at 44.7 ºC, 10 rad/s (MPa/s)	Rank	Absolute Log Error wrt ER (%)
AAD-1	$3.84x10^{-3}$		$4.52x10^{-4}$			$5.87x10^{-4}$		
AAF-1	$12.8x10^{-3}$		$3.11x10^{-3}$			$2.76x10^{-3}$		
TS2K	$2.72x10^{-3}$		$1.11x10^{-3}$			$1.84x10^{-3}$		
TX03-E	$1.80x10^{-3}$	6	$1.39x10^{-3}$	4	4.2	$1.88x10^{-3}$	5	0.7
TX03-F	$3.00x10^{-3}$	8	$2.78x10^{-3}$	7	1.3	$2.14x10^{-3}$	6	5.8
TX03-U	$1.29x10^{-3}$	3	$7.31x10^{-4}$	2	8.6	$1.20x10^{-3}$	3	1.1
TX03-W	$1.78x10^{-3}$	5	$2.96x10^{-3}$	8	8.0	$3.41x10^{-3}$	7	10.3
Average Error					5.5			4.5
TS2K 12% Rubber	-		$5.26x10^{-4}$			$6.47x10^{-4}$		
TX03-EM 3.5% SBR Latex	$1.36x10^{-3}$	4	$1.82x10^{-3}$	6	4.4	$1.77x10^{-3}$	4	4.0
TX03-FM 3.5% SBR Latex	$3.83x10^{-4}$	1	$3.07x10^{-4}$	1	2.8	$3.15x10^{-4}$	1	2.5
TX03-UM 3% SBR Latex	$7.67x10^{-4}$	2	$1.34x10^{-3}$	3	7.7	$5.96x10^{-4}$	2	3.5
TX03-WM 3% SBR Latex	$2.22x10^{-3}$	7	$1.52x10^{-3}$	5	6.2	$6.57x10^{-3}$	8	17.8
Overall Average Error					5.4			5.7

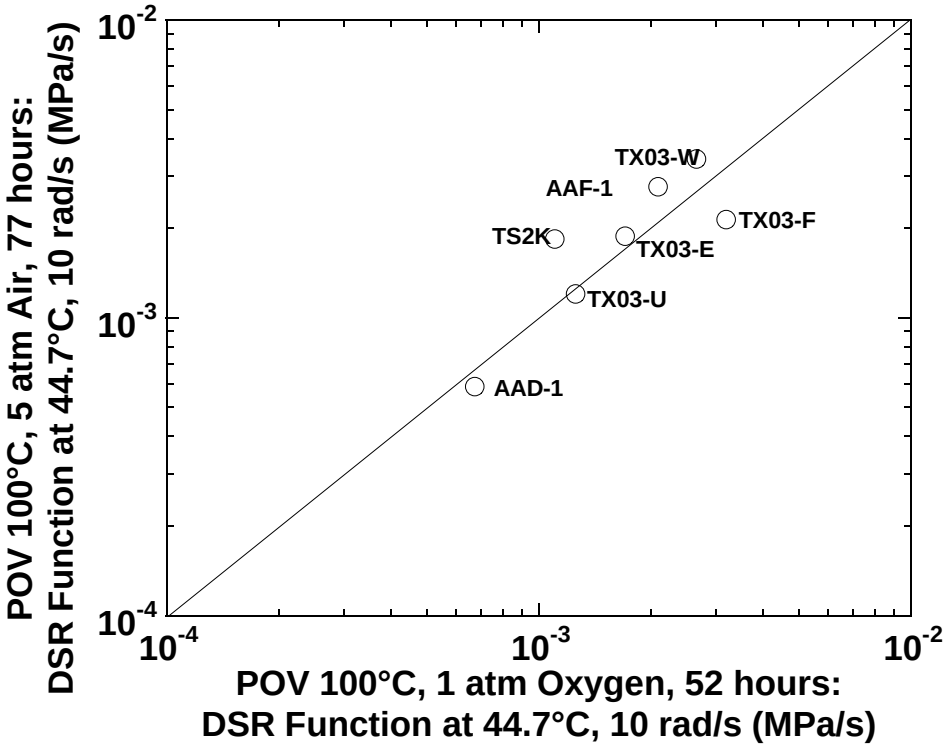

Figure 6-33. Comparison of POV Aging: 5 atm Air, 77 Hours versus 1 atm O_2, 52 Hours.

Figure 6-34 compares POV aging at 100 ºC and 5 atm O_2 to environmental room aging for the modified asphalts (closed symbols) and their base asphalts (open symbols) for the asphalts for which data at both conditions are available. The modified asphalts appear to behave fairly well as far as aging is concerned. Figure 6-35 shows the DSR function versus aging time for all five modified asphalts and their base asphalts. The aging of the TX03-F asphalt is much improved by modification, and it is significantly improved for the TS2K asphalt. The TX03-U and TX03-E asphalts do not change much, and the TX03-W asphalt appears to have suffered significantly by modification. This is deceptive. Chapter 5 reported that the TX03-U and TX03-W asphalts have very high ductility values at given values of the DSR function and much better than those of the base asphalt for a given DSR function value; therefore, if the decline in function with aging is improved by the modifier, then the ductility is definitely improved. The reverse is not necessarily so, especially for the TX03-W asphalts. Complete data for the aging times in Figures 6-32 and 6-35 are given in Appendix A, Table A-6-5.

The results in Table 6-9 for the PAV at 100 ºC and 20 atm air were promising, so they were repeated for the same materials, modified and unmodified, as were tested at 100 ºC, 5 atm air, but for 26 and 30 hours. However, there was trouble with the pressure on the apparatus; the 30-hour run was lost, and results for the 26-hour run are suspect as they do not fit with the previous data at 24 and 30 hours. The 26-hour data are shown in Table 6-9, and the error compared to the environmental room is poorer than the 100 ºC, 5 atm O_2 run, 5.5 as opposed to 4.5 percent. All three PAV runs at 100 ºC and 20 atm air are shown in Figure 6-36.

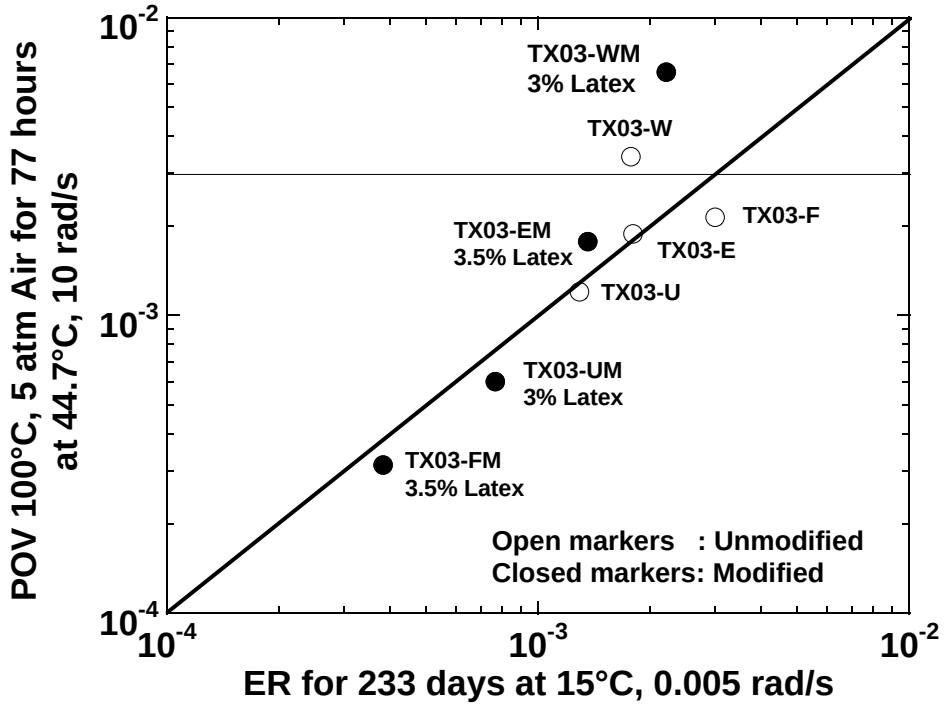

Figure 6-34. Comparison of POV (100 ºC, 5 atm Air, 77 Hours) and ER (233 Days) Aging.

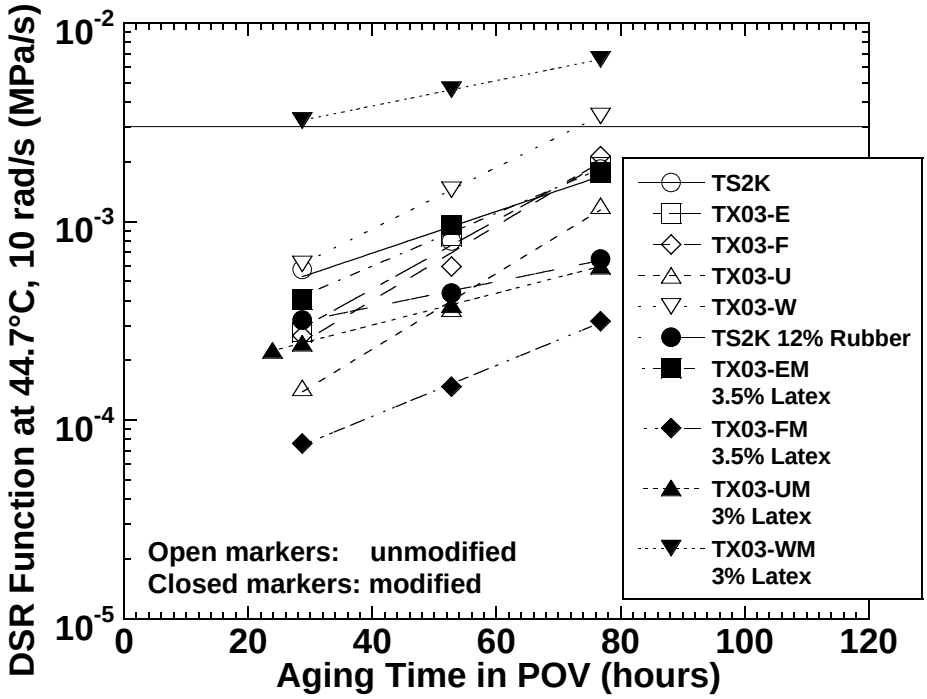

Figure 6-35. Effect of Modifiers on DSR Function Aging at 100 ºC, 5 atm Air.

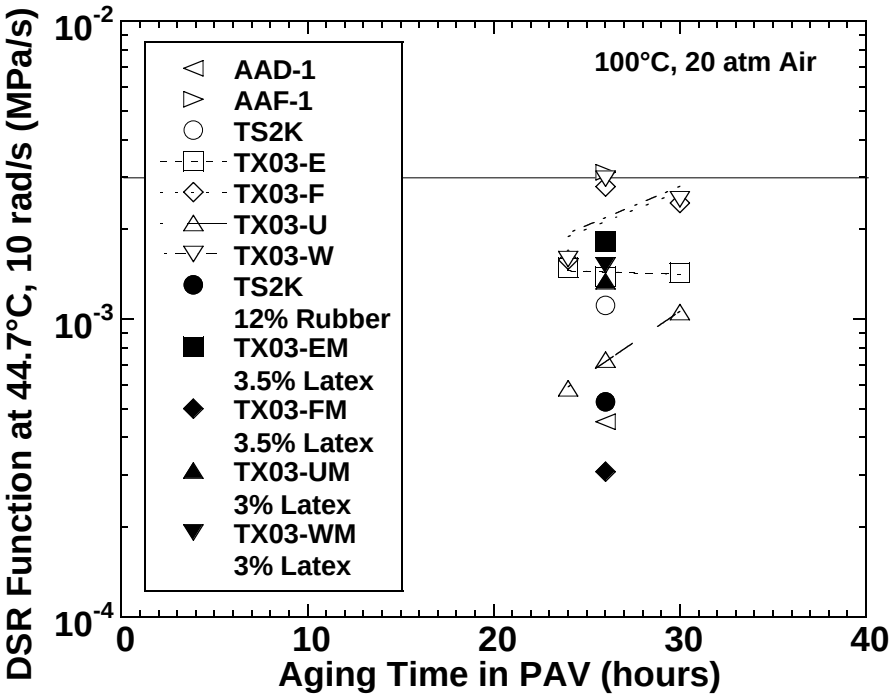

Figure 6-36. Thin-Film PAV Hardening Rates.

AGING BY AIR BLOWING

An attempt was made to replace the PAV with an air-blowing procedure so that RTFOT and PAV aging could be accomplished in the same apparatus. Various combinations of air flow, mixer speed, and mixer design were investigated, and the results are rather impressive except for two serious problems. First, operating a mixer unit overnight poses both safety and design issues, and second, the carbonyl area at a given viscosity was different from that obtained in the environmental room (Knorr, 2002). As both are oxidizing at 1 atm air, a study by Lau et al. (1992) has shown that the carbonyl to viscosity ratio should be the same.

Table 6-10 and Figure 6-37 are part of a study to attempt to use air-blowing at 163 ºC (325 ºF) to simulate the RTFOT. The figure shows that 20 minutes is sufficient. In Table 6-10, results are given for a number of asphalts. They were first air blown for 20 minutes at 163 ºC (325 ºF) at 6 L/min to simulate the RTFOT and then at 100 ºC (212 ºF) and 24 L/min to simulate the PAV. It can be seen that PAV viscosities were reached at times ranging from less than 20 hours for asphalt AAS-1 to about 30 hours for asphalt AAG-1. These times should not all agree with the PAV time of 20 hours because the difference in pressure changes the relative hardening rates of the asphalts. The remarkable thing is that similar aging rates have been achieved at 1 atm air as obtained in the PAV at 20 atm air. This shows that the PAV is extremely limited by diffusion.

Table 6-10. Viscosities of Airblown Asphalts.

Airblow Time	Limiting 60 ºC Viscosity (poise)								
	TX03-4	Lau4	SHRP AAA-1	SHRP AAB-1	SHRP AAD-1	SHRP AAF-1	SHRP AAG-1	SHRP AAM-1	SHRP AAS-1
0	1287	2305	1130	1569	1479	2166	2250	2429	2584
20 minutes SAFT	2158	4090	2337	4076	4374	5128	3827	6196	6372
5 hours	2776								
10 hours			4274	8005	10,828	14,810	6,574		15,361
20 hours	4132	23,900	6895	14,947	23,827	26,128	8,240		28,820
30 hours			10,105	24,771	95,587	45,900	10,340		50,488
40 hours			15,450	51,652	594,000	136,000	10,910		99,745
50 hours			26,310	112,351	-	252,000	15,403		264,000
Conventional RTFOT + PAV	5211		11,940	18,070	29,310	25,760	10,370		22,530

All asphalts were airblown at the following conditions: 163 ºC, 1600 rpm, 6 L/min of air (short-term) and 100 ºC, 1600 rpm, 24 L/min of air (long-term); except for AAG-1: 163 ºC, 1550 rpm, 6 L/min of air (short-term) and 100 ºC, 1550 rpm, 24 L/min of air (long-term)

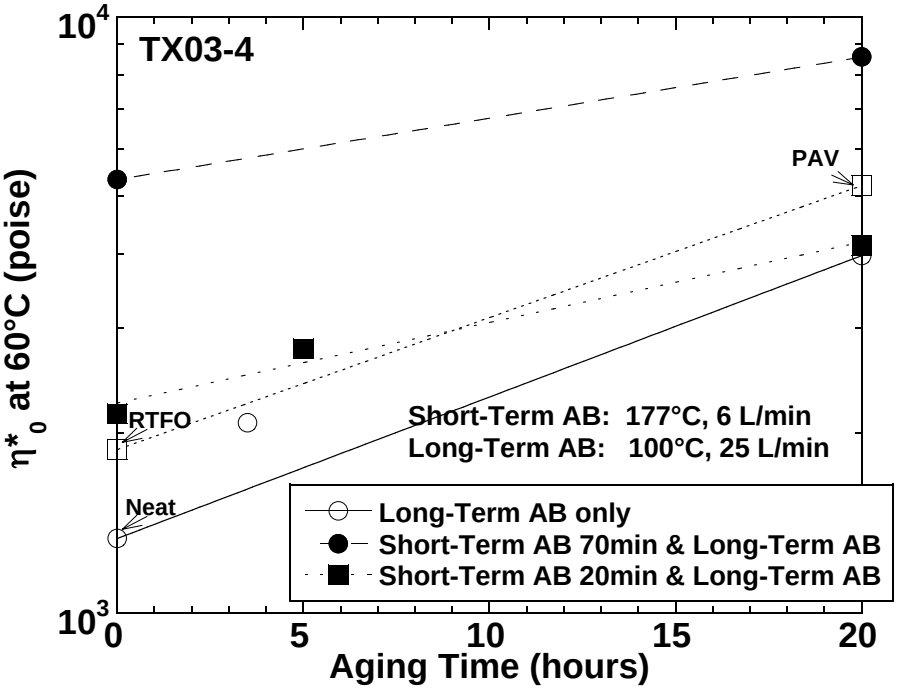

Figure 6-37. Simulation of RTFOT Aging in Air-Blowing Apparatus.

SUMMARY

Many aging conditions have been investigated and compared to environmental room aging at 60 ºC and 1 atm air. As suspected, no condition is able to accurately accelerate the aging rates so that the relative rates of hardening are the same as the simulated road condition in the environmental room. It is encouraging, however, that the same asphalts failed the DSR function criterion at a large number of conditions, and this was true at conditions that do not require an extended aging time. Therefore, a procedure that reasonably identifies asphalts that experience excessive oxidative hardening that is likely to lead to premature roadway failure can be specified with a great level of confidence.

Of nine asphalts (the first set), asphalt AAF-1 consistently was the worst. TX03-F and TX03-W of the second set of asphalts were limiting in all cases, but asphalt TX03-W aged in the POV, and the PAV is high in the DSR function value compared to the environmental room and is not a good guide. Among the aging conditions studied, thin-film PAV at 20 atm air and 90 ºC best agreed with the environmental room aging in that the average error in the log of the DSR function was the smallest.

CHAPTER 7. DSR FUNCTION HARDENING KINETICS OF ASPHALTS

The previous chapter discussed the oxidation of asphalts at different conditions. Two rheological properties were used, i.e., the low shear rate limiting viscosity (η^*_o) and a newly developed DSR function, G'/(η'/G'). While η^*_o is a good surrogate of hardening, it does not represent road aging properties that relate to cracking failure very well. The DSR function that has been shown to correlate well with ductility, a new measurement of road aging (Ruan et al., 2003), offers an alternative method of evaluating premature aging and subsequent pavement cracking.

This chapter discusses the kinetics of asphalt aging based on the DSR function. A number of previous studies have dealt with the kinetics of aging using viscosity and carbonyl area measurements (Domke et al., 2000, Domke et al., 1997, Lin, 1995, Lau et al., 1992). However, there are no studies of how the temperature and/or pressure affect the kinetics of the DSR function, and how the kinetic parameters, based on the DSR function, correlate with pressure or temperature.

INTRODUCTION

A study suggests that oxygen pressure affects the hardening of aged asphalt through a competition between the oxidation kinetics reaction and diffusion of oxygen through layers of particles in a maltene media (Domke, 1999). The author removed a portion of the heavy polar aromatics and light asphaltenes from a whole asphalt. The layers consisted of polar aromatics on the outside that coated layers of asphaltenes, namely quasiasphaltenes, hexane asphaltenes, and heptane asphaltenes. Quasiasphaltenes are molecules left in pentane asphaltenes after the removal of heptane asphaltenes. Hypothetically, at low oxygen pressure, the major oxidation takes place in the maltene fraction. As the oxygen pressure increases, the oxygen is able to penetrate to reach the polar aromatics.

As mentioned in the previous chapter, asphalt oxidation occurs in two steps, the initial rapid-rate region and the much slower constant-rate region. During the rapid oxidation, the properties of the aging asphalt, such as viscosity and carbonyl content, increase tremendously. Then the asphalt undergoes a much slower aging process in the constant-rate region. In the previous chapter, asphalt AAF-1 consistently reaches the critical value of 0.003 MPa/s for the DSR function much quicker than the other asphalts. This is the result of the rapidly increasing function at the early stage of aging, the initial jump. It appears that the aging conditions, such as pressure and temperature, influence the aging process, during the initial rapid rate as well as during the constant rate. In their separate studies, Liu et al. (1996) and Domke (1999) observed that the magnitude of the initial jump may be pressure dependent but is temperature independent.

Figure 7-1 shows the oxidation rate of asphalt AAF-1 after being aged at four different conditions, which can be grouped into two temperatures, 100 ºC (the dashed lines in the figure) with oxygen pressures at 1 and 5 atm and 110 ºC (the solid lines) with oxygen pressures at 0.2

and 1 atm. At the same temperature, the rate goes up as the pressure increases. It also goes up as the temperature increases. However, an increase in pressure from 1 atm O_2 (open symbols) to 5 atm O_2 (solid symbols), while keeping the temperature the same at 100 ºC is more significant than raising the temperature from 100 °C to 110 °C and while keeping the pressure constant at 1 atm O_2.

As expected, the asphalt stiffens and oxidizes during aging, as shown by the carbonyl area (Figure 7-1) and also the log of viscosity and the log of the DSR function as seen in Figures 7-2 and 7-3, again for asphalt AAF-1. Similar plots for the other eight asphalts are shown in Figures B-7-1 to B-7-24 of Appendix B. The increase in the log of viscosity and the log of the DSR function shows a similar trend in that the regression lines at 100 ºC, 5 atm O_2 and 110 ºC, 1 atm O_2 cross after 3 days of aging, shown in Figures 7-2 and 7-3. This cross-over does not take place in carbonyl area (Figure 7-1) indicating a major effect on the hardening susceptibility (the slope of the log physical property versus carbonyl content relation) by the change in aging conditions.

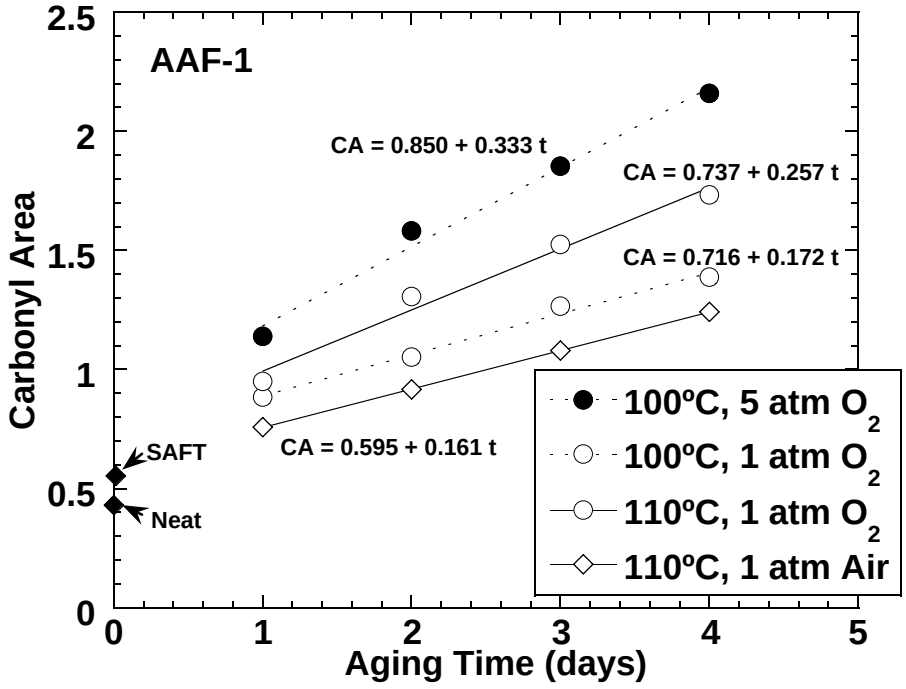

Figure 7-1. Carbonyl Area versus Aging Time for SHRP AAF-1.

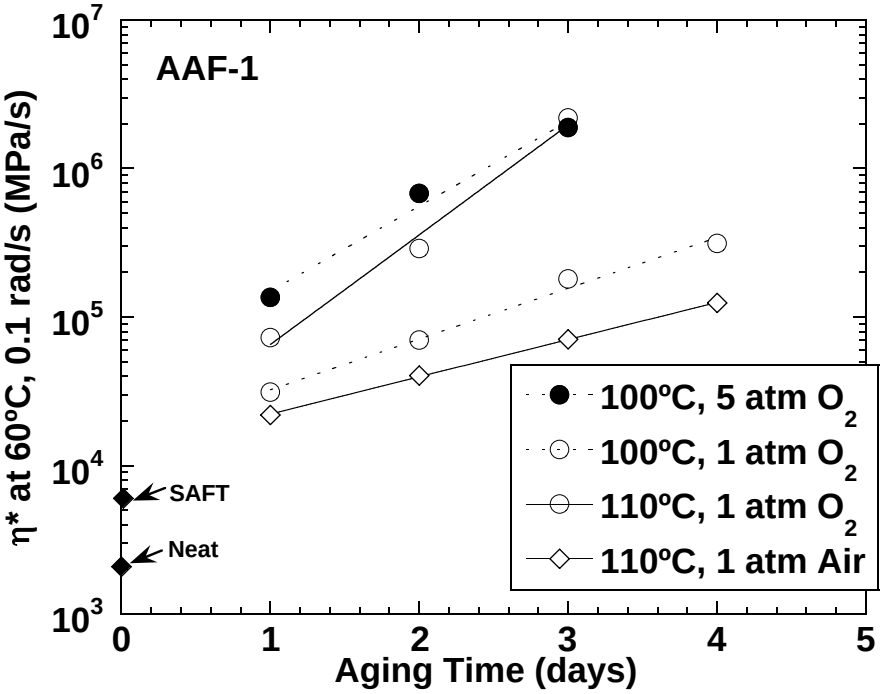

Figure 7-2. η^*_o Hardening Rates of SHRP AAF-1.

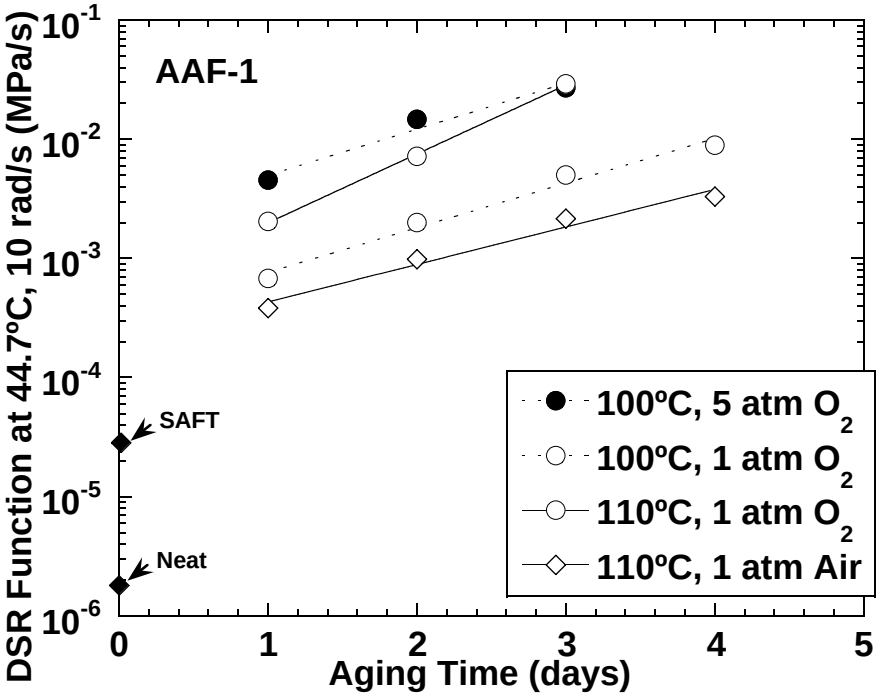

Figure 7-3. DSR Function Hardening Rates of SHRP AAF-1.

DSR FUNCTION KINETICS

Initial Jump

Liu et al (1996) and Domke (1999) found that based on the carbonyl growth data the initial jump does not depend on temperature yet does depend on pressure. The same phenomenon is seen using DSR function as presented in Figures 7-4 and 7-5. The plots show the rate of DSR function for asphalt AAF-1 aged at different conditions, varying temperature in Figure 7-4 and varying pressure in Figure 7-5. The difference between Fn_0 (the intercept of the constant rate line) and the DSR function value of the unaged asphalt is defined as the initial jump. In Figure 7-4, the pressure is kept constant, while varying the temperature. The result shows the scatter in the initial jump appears random, suggesting that temperature has no effect on the initial jump. On the other hand, when pressure is varied, Figure 7-5, the initial jump is shown to be dependent on pressure. As the pressure increases, the initial jump goes up. Unfortunately, there is a lack of data for which pressure is varied while keeping temperature constant. The data presented in Figure 7-5 are obtained at different temperatures. However, as previously mentioned and supported by previous studies, the initial jump is independent of temperature, making it plausible to draw this conclusion. In fact, given that the initial jump is independent of temperature, the regression lines in Figure 7-4 where the asphalt was aged at 110 ºC and at 93 ºC, both at 1 atm of O_2, show how close the initial jumps are (0.000527 and 0.000572 MPa/s) in spite of the different rates. The other asphalts studied show similar results, shown in Figures B-7-25 through B-7-39 of Appendix B.

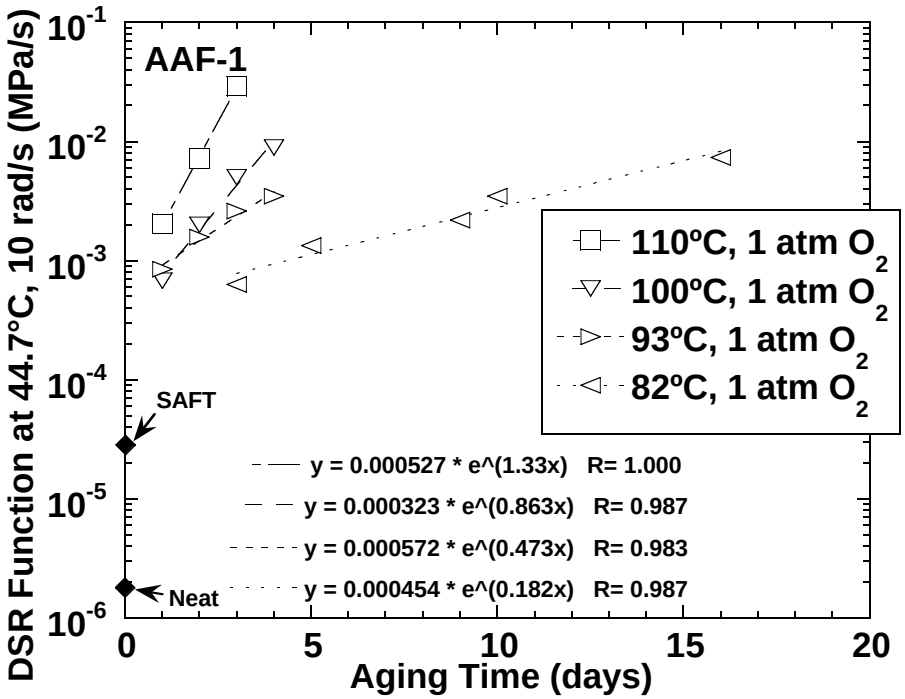

Figure 7-4. DSR Function Hardening for SHRP AAF-1 at Four Aging Temperatures.

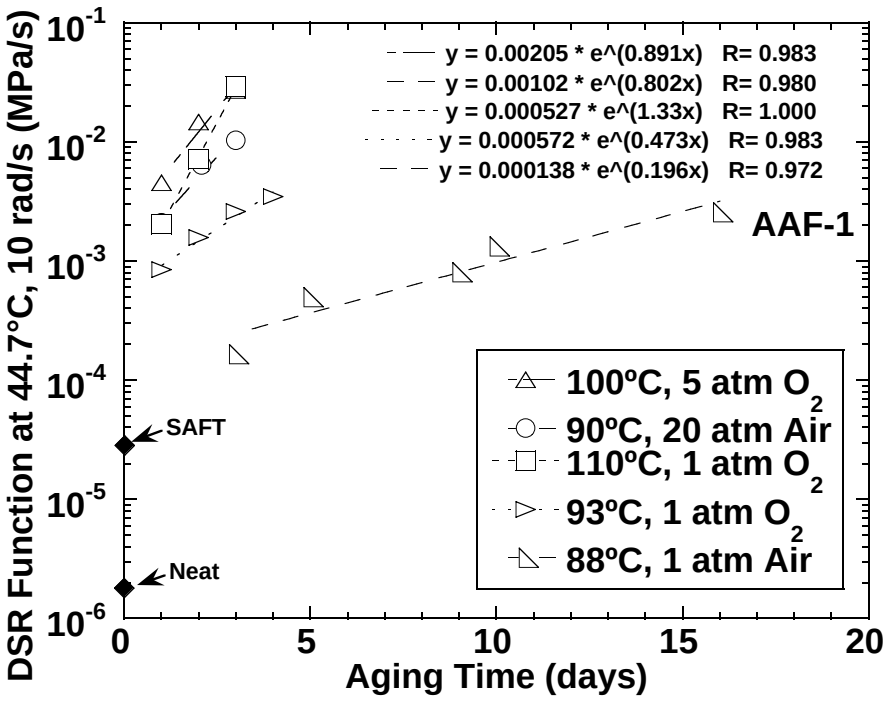

Figure 7-5. DSR Function Hardening for SHRP AAF-1 at Five Aging Pressures.

Table 7-1 lists the initial jumps of all asphalts, defined as the difference between the logarithmic of the intercept of the regression line and the logarithmic of the DSR function of a neat asphalt binder, at various pressures. The data for oxygen pressures of 4 and 5 atm were obtained at a single temperature, 90 ºC and 100 ºC, respectively. In all conditions, the initial jumps of asphalt AAF-1 appear to be significantly higher than the rest of the asphalts. At high pressure, the initial jump of AAF-1 is almost four times higher than the next highest initial jump, that is of TS2K. This high initial jump could very well be a factor as to why asphalt AAF-1 hardens faster than the rest of the asphalts, as observed in Chapter 6.

Table 7-1. Initial Jump Values for All Asphalts.

O_2 Press (atm)	$\ln(Fn_0) - \ln(Fn_{tank})$ (ln(MPa/s))								
	AAA-1	AAB-1	AAD-1	AAF-1	ABM-1	AAM-1	AAS-1	Lau 4	TS2K
0.2	3.25 ±0.30	3.35 ±0.34	3.05 ±0.35	4.97 ±0.78	3.39 ±0.63	3.74 ±0.33	2.99 ±0.34	3.24 ±0.35	2.32 ±0.36
1	3.49 ±0.28	3.91 ±0.33	3.39 ±0.16	5.54 ±0.25	4.08 ±0.27	4.09 ±0.37	3.34 ±0.36	3.87 ±0.42	2.45 ±0.32
4	3.87	4.06	3.69	6.33	4.86	4.49	3.70	4.57	2.89
5	3.78	4.92	4.04	7.03	4.97	4.10	4.18	4.62	3.25

How pressure affects the initial jump for each asphalt binder can be seen in Figure 7-6, where the initial jump, defined as $\ln(Fn_0) - \ln(Fn_{tank})$, is plotted against the aging pressure. In general, the initial jump increases with oxygen pressure in the following fashion:

$$\ln(Fn_0) - \ln(Fn_{tank}) = \beta P^{\gamma} \qquad (7\text{-}1)$$

where β and γ are the model parameters obtained from the regression fit.

This is similar to the correlation developed by Liu et al. (1996), which used carbonyl area as the aging measurement.

Table 7-2 tabulates the values of β and γ. It shows that among the nine asphalts studied, asphalt AAF-1 has the highest values of β while asphalt TS2K has the smallest value. As for γ value, asphalt ABM-1 has the highest value and asphalt AAM-1 is the lowest. How these parameters affect asphalt aging is discussed in the following section.

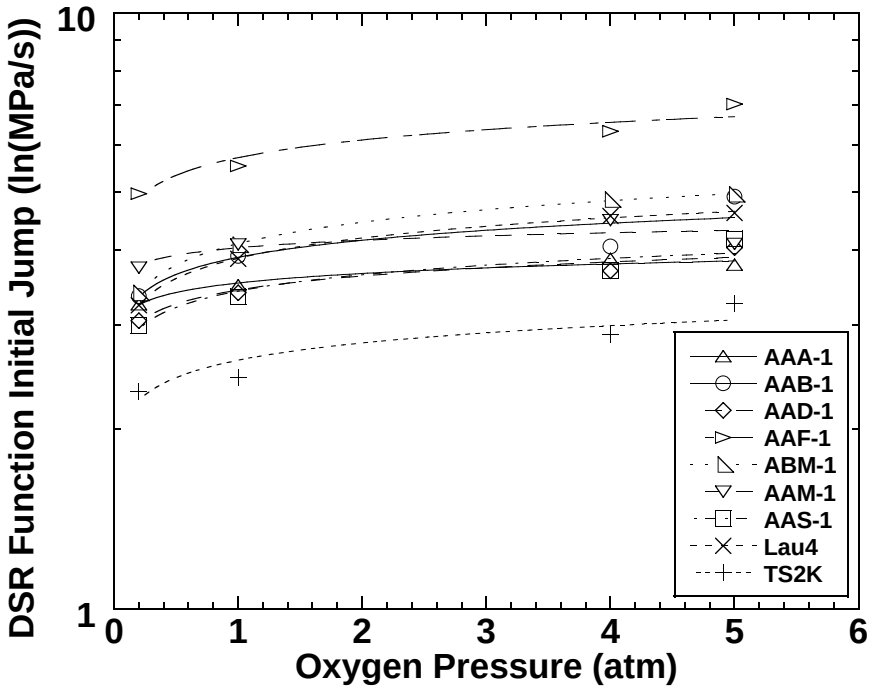

Figure 7-6. DSR Function Initial Jump versus Oxygen Pressure for Nine Asphalts.

Table 7-2. Pressure Dependent Function Initial Jump Parameters, β and γ.

Asphalt	β	γ
AAA-1	3.52	0.053
AAB-1	3.89	0.095
AAD-1	3.43	0.078
AAF-1	5.72	0.098
ABM-1	4.10	0.120
AAM-1	4.04	0.042
AAS-1	3.42	0.091
Lau4	3.88	0.113
TS2K	2.61	0.097

Constant-Rate Reaction Rate

Studies have shown that during aging the carbonyl grows linearly with time after the initial jump region is past, as described in Equation 2-2. And using η^*_o as the surrogate of asphalt hardening, the log of η^*_o also increases linearly with time (Equation 6-1).

By the same token, the rate of DSR function growth can be expressed as:

$$\ln(Fn) = \ln(Fn_0) + r_{Fn} \cdot t \qquad (7\text{-}2)$$

where Fn is the DSR function at any given time, Fn_0 is the intercept of the regression line, r_{Fn} is the hardening rate based on the DSR function, and t is the aging time. All plots of hardening rates based on η^*_o, as well as DSR function of the nine asphalts aged in 10 different conditions, are presented in Chapter 6. Table 7-3 lists the function rates The highest value is 2.39 ln(MPa/s)/day (asphalt AAA-1 aged in 100 ºC, 5 atm O_2) while the lowest value is 0.0092 ln(MPa/s)/day (asphalt TS2K aged in environmental room).

The hardening rate of the DSR function can be calculated from the kinetic rate equation, provided the model parameters are known. Liu et al. (1996) reported that the rate of carbonyl growth during asphalt aging varies linearly with the reciprocal of the aging temperature in an Arrhenius-type of equation and was pressure dependent such that:

$$r_{CA} = \frac{\partial(CA)}{\partial t} = A_{CA} P^a e^{-\left(\frac{E_{CA}}{RT}\right)} \qquad (7\text{-}3)$$

Table 7-3. DSR Function Hardening Rates for All PAV and POV Aged Asphalts.

	r_{Fn} (ln(MPa/s)/day)									
	ER Test	Test #1[a]	Test #2	Test #3	Test #4	Test #5	Test #6	Test #7	Test #8	Test #9
T (ºC):	60	100	90	100	110	110	100	93	88	82
P, (atm O_2):				5	1		1	1		1
(atm Air):	1	20	20			1			1	
AAA-1	0.0171	1.80	1.25	2.39	1.90	0.67	0.99	0.61	0.15	0.24
AAB-1	0.0152	1.64	1.07	1.43	1.49	0.87	0.79	0.76	0.13	0.21
AAD-1	0.0167	1.48	1.31	1.88	1.59	0.87	1.10	0.59	0.13	0.21
AAF-1	0.0130	1.32	0.80	0.89	1.33	0.73	0.86	0.47	0.20	0.18
ABM-1	0.0178	0.86	0.75	0.89	1.00	0.80	0.65	0.37	0.10	0.15
AAM-1	0.0119	1.15	0.80	1.20	0.94	0.65	0.91	0.52	0.14	0.16
AAS-1	0.0115	1.15	0.76	1.03	1.06	0.73	0.80	0.57	0.08	0.18
Lau4	0.0133	1.44	0.74	1.25	1.14	0.86	0.91	0.50	0.13	0.18
TS2K	0.0092	1.13	0.68	1.00	1.00	0.67	0.81	0.50	0.12	0.14

Note: [a] Test 1 was conducted with 3mm-thick sample films. All other tests were approximately 0.86-mm thick films.

where r_{CA} is the carbonyl formation rate, A is the pre-exponential factor, P is the oxygen pressure, α is the reaction order with respect to oxygen pressure, E is the activation energy, R is the universal gas constant (0.008314 kJ/mol.K), and T is the aging absolute temperature (K). The expression is valid if α is independent of temperature and E is independent of pressure (Liu et al., 1996).

Similarly, the hardening rate using the DSR function as the aging measurement can be described as:

$$r_{Fn} = \frac{\partial(\ln Fn)}{\partial t} = A_{Fn} P^{a} e^{-\left(\frac{E_{Fn}}{RT}\right)} \qquad (7\text{-}4)$$

where all parameters are evaluated based on the DSR function. The kinetics parameters E, α, and the log of the pre-exponential factor, A, are obtained using multivariable regression and are presented in Table 7-4.

The pressure effect on the initial jump, γ in the constant rate region, is plotted against the reaction order, α, with respect to oxygen pressure in Figure 7-7. It shows that the reaction order, α, is inversely correlated with γ and the values for all but two asphalts (AAF-1 and AAM-1) fall along a straight line. The correlations suggests that there is an offsetting effect between the initial jump and the DSR function rate in the constant rate region. A high initial jump is compensated by a lower DSR function rate.

Table 7-4. Kinetic Parameters for All Asphalts – DSR Function (Equation 7-4).

Asphalt	E kJ/mol	ln A	α
AAA-1	77.8±1.6	25.1±0.5	0.62±0.02
AAB-1	81.6±7.2	26.2±2.3	0.50±0.08
AAD-1	80.3±5.4	25.8±1.8	0.57±0.06
AAF-1	83.7±7.4	26.6±2.4	0.37±0.09
ABM-1	75.9±7.2	23.9±2.3	0.40±0.08
AAM-1	80.8±7.1	25.7±2.3	0.48±0.08
AAS-1	83.9±8.9	26.6±2.9	0.50±0.10
Lau4	84.6±5.6	27.0±1.8	0.44±0.06
TS2K	87.3±7.1	27.7±2.3	0.45±0.08

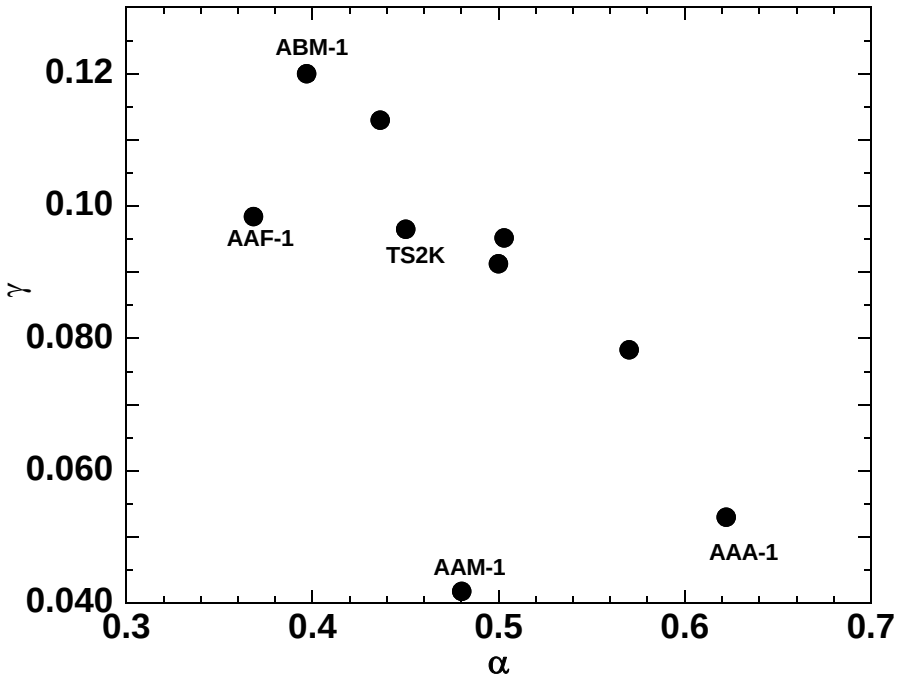

Figure 7-7. Initial Jump γ and Pressure Reaction Order α Relationship.

Figure 7-8 shows the plot of initial jump model parameter β against α. Generally, the constant β varies inversely with α. Asphalt TS2K is somewhat anomalous since it is air-blown and suspected to have been overheated and cracked during the air-blowing process. As a result, the DSR function value of unaged TS2K is very high.

Both correlations, γ and β versus α, confirm that the reaction rate alone does not represent the complete oxidation mechanism of an asphalt. The early stage of oxidation, where aging takes place rapidly, must be taken into account. Therefore, ranking of asphalts cannot be determined from the rates only. The correlations also validate the reason as to why AAF-1 reached the DSR function failure limit first in all aging conditions in this project (Chapter 6) although its rate is not the highest. The α value of AAF-1 of 0.37 is the lowest α compared to the others, but its β value is the highest. Asphalts with low α values are more sensitive to aging pressure, shown by large β values.

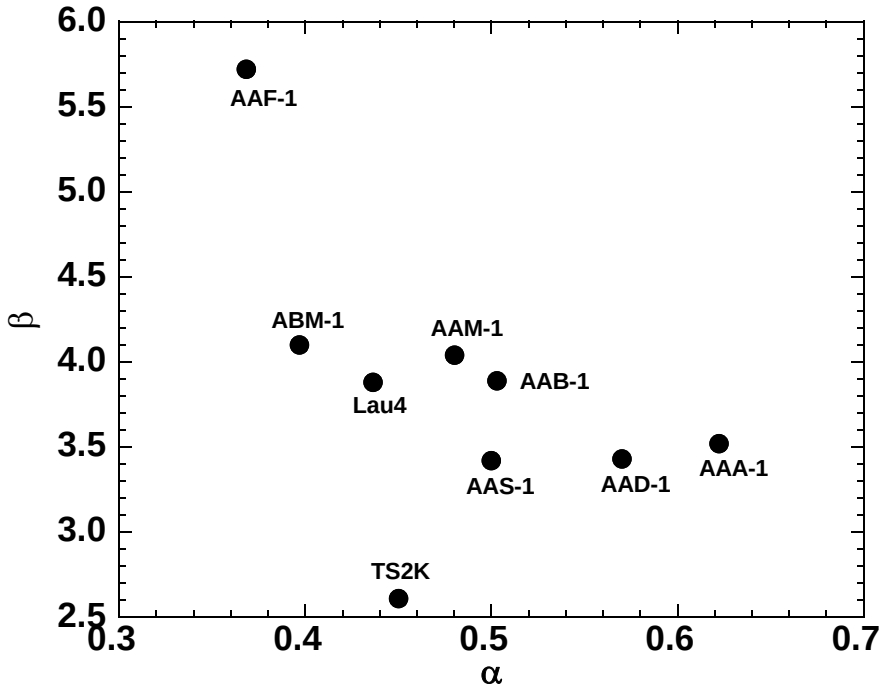

Figure 7-8. Initial Jump Constant β and Reaction Order α Relationship.

Figure 7-9 shows the plot of activation energy, E, versus pressure reaction order, α. In this figure, E decreases as α increases, suggesting that it is possible to simulate aging using different conditions due to the inverse effects between pressures and temperatures.

Domke (1999), in conjunction with his hypothesized layer particle model, suggested that the pressure dependency caused complications in estimating the rate constants, such as A and α, individually. Hence he attempted to combine the first terms on the right-hand side of Equation 7-3 without damaging its integrity. Thus, the equation becomes:

$$r_{CA} = \frac{\partial(CA)}{\partial t} = A'_{CA}\, e^{-\left(\frac{E_{CA}}{RT}\right)} \qquad (7\text{-}5)$$

where A' is a combination of AP^{α}. All parameters are based on carbonyl area.

By the same token, Equation 7-4 becomes :

$$r_{Fn} = \frac{\partial(\ln Fn)}{\partial t} = A'_{Fn}\, e^{-\left(\frac{E_{Fn}}{RT}\right)} \qquad (7\text{-}6)$$

Here, all parameters are based on the DSR function.

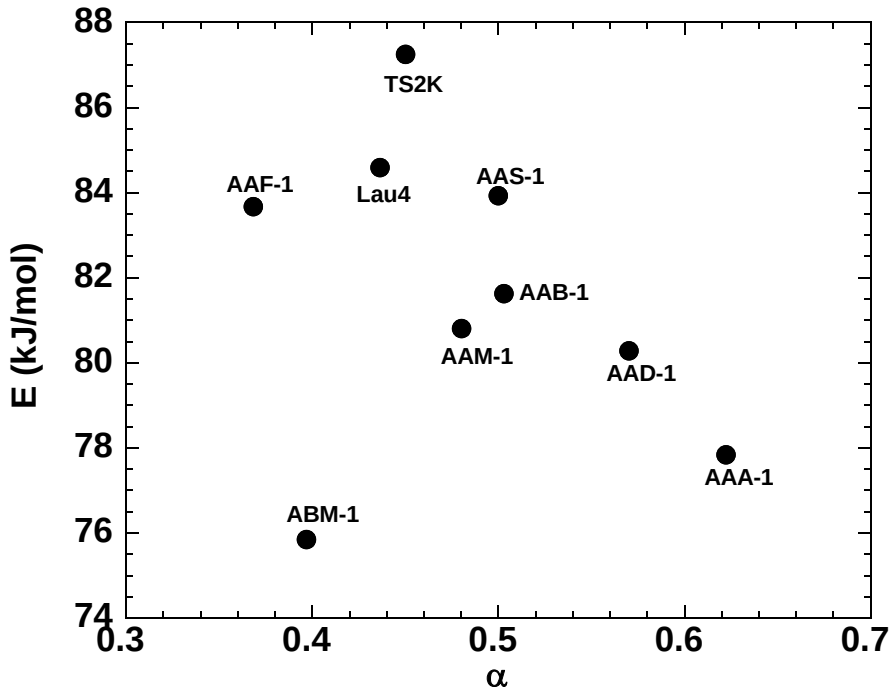

Figure 7-9. Activation Energy E and Reaction Order α Relationship.

Figures 7-10 and 7-11 show the Arrhenius plots, the function rates versus the inverse of temperature, for all asphalts aged at 0.2 and 1 atm O_2, respectively. The plots show that activation energy, E, which is the slope of the regression line, is a function of pressure. The activation energy decreases with increasing pressure. However, this could be misleading because the range of pressures in this study is small. A plot of function rates as a function of oxygen pressures for all nine asphalts at 90 ºC is shown in Figure 7-12. It shows that the log of DSR function rate increases linearly with pressure.

Table 7-5 tabulates the values for E and log A'. It shows that, except for asphalt AAA-1, E and the pre-exponential factor, A', decrease with pressure in this study. Figure 7-13 shows how the activation energy of an asphalt binder changes with aging pressure. Domke (1999) studied the oxidation kinetics of several asphalts at various temperatures and pressures ranging between 0.2 and 20 atm O_2, and reported that the kinetic parameters E and A' reached a minimum at 1 atm O_2. It is worth mentioning that the E and ln A' values of AAF-1 are not significantly higher or not at all higher than the other asphalts. Again, this confirms that it is the high initial jump values of AAF-1 that cause the properties of the asphalt to reach the failure value quicker than the rest.

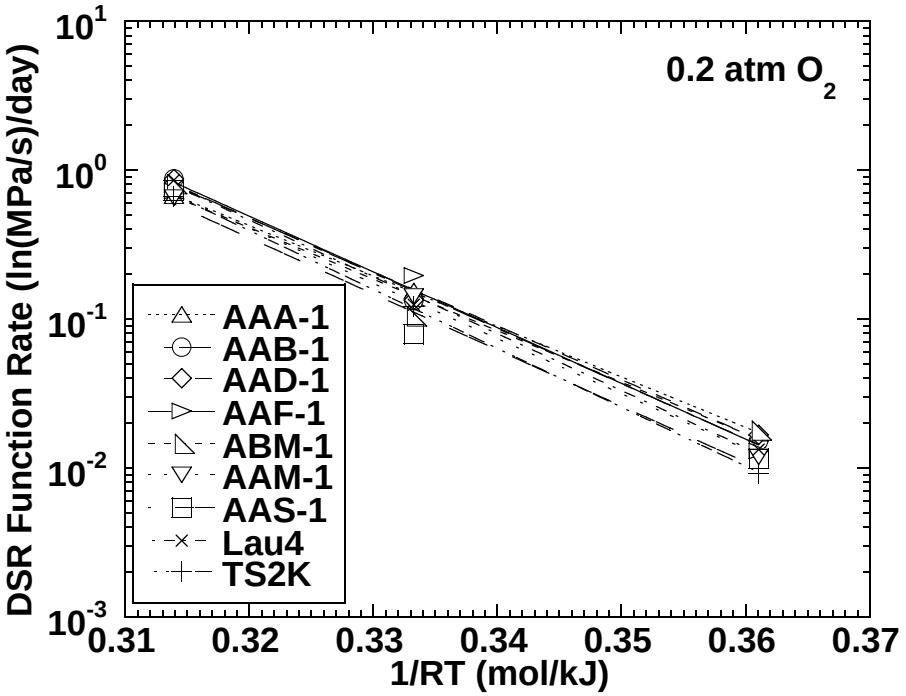

Figure 7-10. Arrhenius Plots for All Asphalts Aged at 0.2 atm O_2.

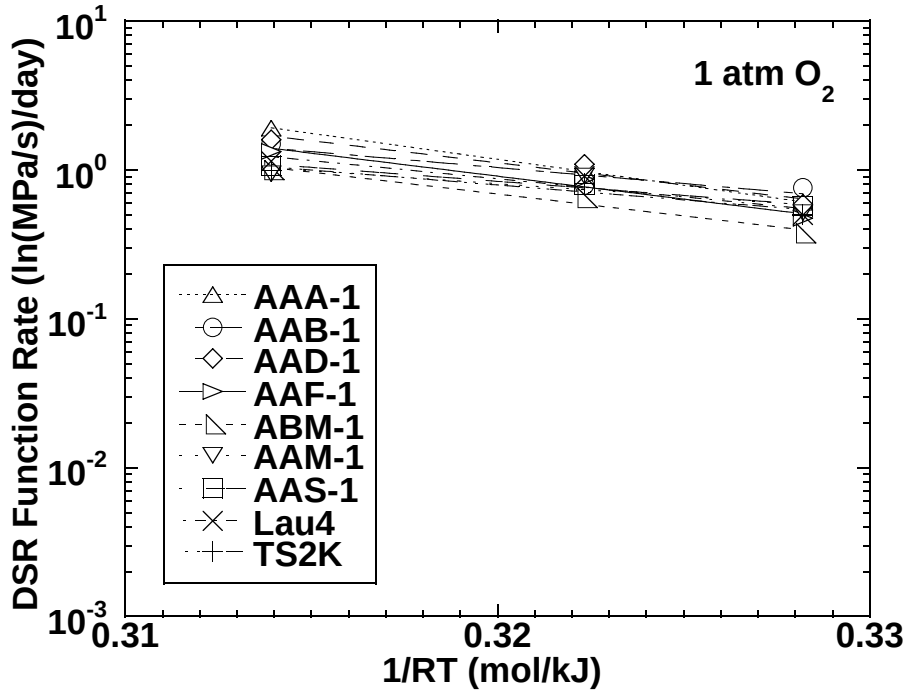

Figure 7-11. Arrhenius Plots for All Asphalts Aged at 1 atm O_2.

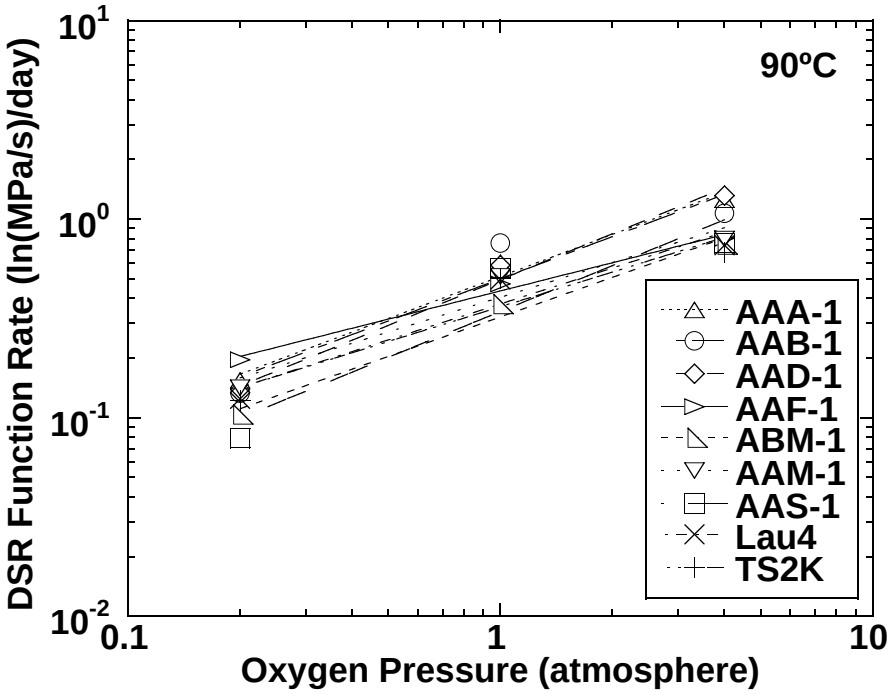

Figure 7-12. DSR Function Growth Rate versus Aging Pressure at 90 ºC for All Asphalts.

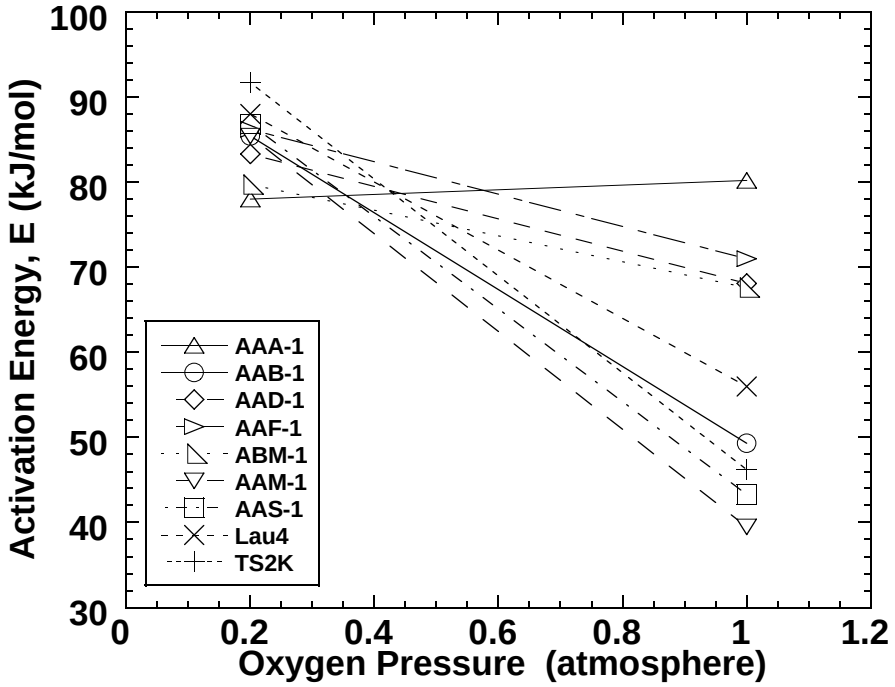

Figure 7-13. Pressure Dependency of Activation Energy.

Table 7-5. Kinetic Parameters for All Asphalts – DSR Function (Equation 7-6).

Asphalt	E kJ/mol		ln A'	
	0.2 atm O_2	1 atm O_2	0.2 atm O_2	1 atm O_2
AAA-1	78.0±0.8	80.2±1.7	24.1±0.3	25.8±0.5
AAB-1	85.4±5.3	49.3±19.1	26.6±1.8	15.8± 6.1
AAD-1	83.3±6.0	68.1±16.6	25.9±2.0	21.9±5.3
AAF-1	86.2±8.3	71.0±14.1	26.9±2.8	22.6±4.6
ABM-1	79.7±11.7	67.6±11.4	24.6±3.9	21.2±3.7
AAM-1	85.4±2.8	39.5±25.4	26.4±1.0	12.4±8.2
AAS-1	86.8±12.5	43.3±6.4	26.7±4.2	13.7±2.1
Lau4	88.0±5.3	56.0±20.7	27.4±1.8	17.8±6.7
TS2K	91.2±1.5	46.2±15.3	28.2±0.5	14.5±4.9

The standard error for the activation energy obtained from this method of combining the pre-exponential factor is higher than the standard error for E obtained from Equation 7-4, primarily because the latter has more data points than the former, which only has three or four values analyzed at each pressure.

Isokinetic Temperature

Isokinetic temperature is a temperature where all asphalts have the same rate (Boudart, 1991). It is obtained by setting ln r_{Fn} = 0, in other words by plotting ln A + α ln P or ln A' against E data as shown in Figures 7-14 and 7-15, respectively. The slope of the line is the inverse of temperature, and the intercept of the regression line is the logarithmic value of the isokinetic rate.

From the regression fit, the isokinetic temperature determined from the DSR function analysis is estimated to be 102.6 ºC for oxidation at 0.2 atm O_2 and 115.5 ºC for 1 atm O_2 based on the first method of kinetic parameters estimation, Equation 7-4. Another set of isokinetic temperatures based on kinetic parameters in Equation 7-6 is 105.9 ºC at 0.2 atm O_2 and 96.3 ºC at 1 atm O_2. Domke (1999), using the carbonyl growth as the aging measurement, calculated the isokinetic temperature to be 105 ºC for atmospheric air and 65.7 ºC for oxygen pressures of 1, 4, and 20 atm. It is very interesting indeed that estimations based on the carbonyl growth and on the DSR function produce similar isokinetic temperature values at 0.2 atm O_2. They only differ by less than 1 ºC, which is quite trivial for this approximation. The values for higher pressure do not seem to agree since the determination based on the DSR function was evaluated at one pressure only, i.e., 1 atm O_2 as opposed to 1, 4, and 20 atm O_2 as in the work of Domke (1999). The isokinetic rates at 0.2 atm O_2 and 1 atm O_2 are 0.413 ln(MPa/s)/day and 2.14 ln(MPa/s)/day (based on Equation 7-4) and 0.541 ln(MPa/s)/day and 0.654 ln(MPa/s)/day (based on Equation 7-6), respectively.

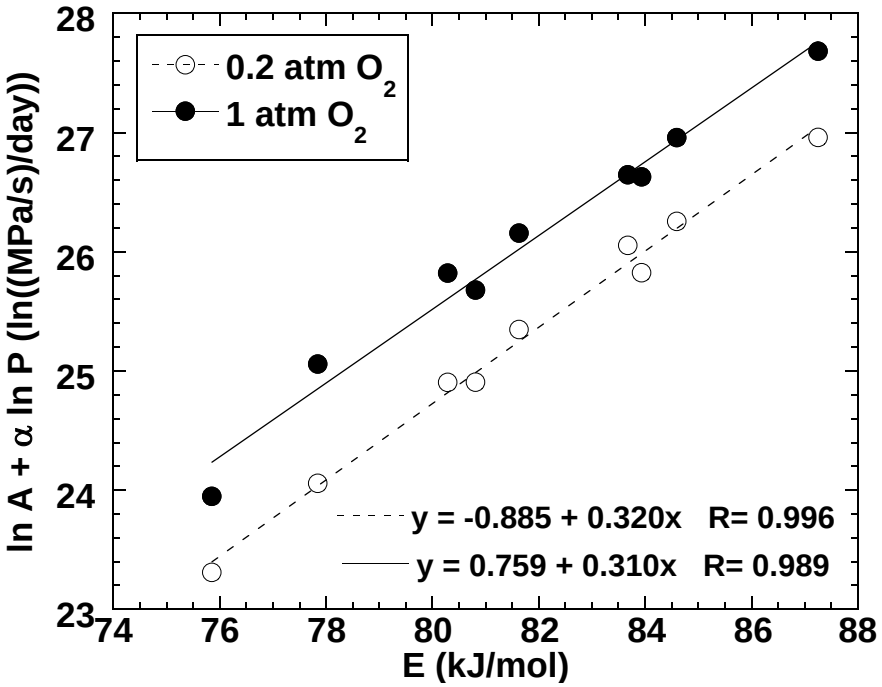

Figure 7-14. Isokinetic Diagrams for All Aged Asphalts at 0.2 and 1 atm O_2 (Equation 7-4).

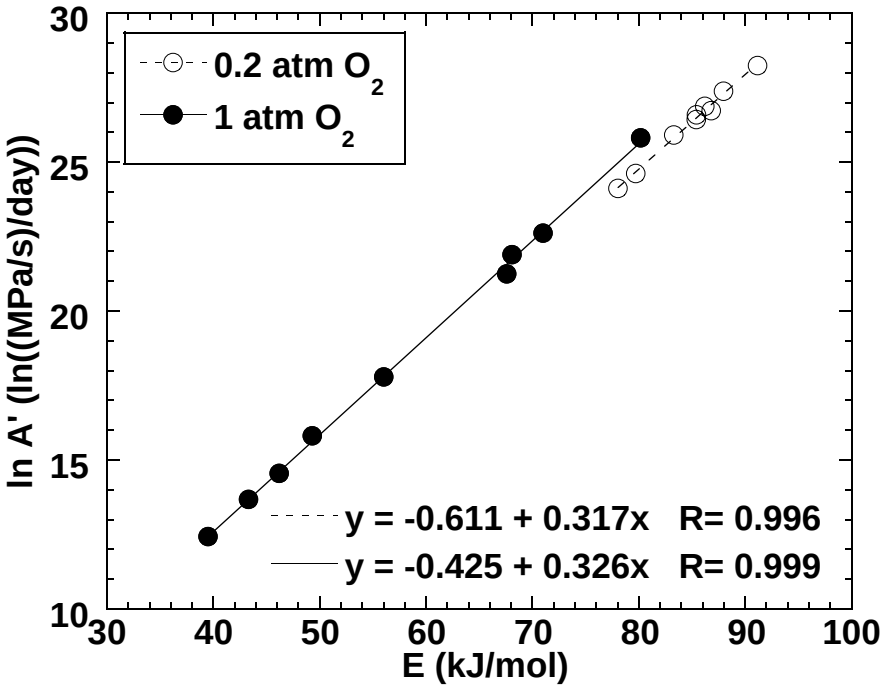

Figure 7-15. Isokinetic Diagrams for All Aged Asphalts at 0.2 and 1 atm O_2 (Equation 7-6).

It is also interesting to note that the calculated values of isokinetic rate and its corresponding temperature appear to fall within the experimental data as shown in Figures 7-16 and 7-17. The calculated rate at 1 atm O_2 using Equation 7-4, however, is not within the range. This suggests that Equation 7-4 does not precisely model the kinetics of the asphalt aging mechanism. The aging pressure does affect the rate constant. Here, Equation 7-6 is a better representation. It was determined earlier that standard errors are bigger for Equation 7-6 parameters than Equation 7-4. But again, this is a result of a small number of values.

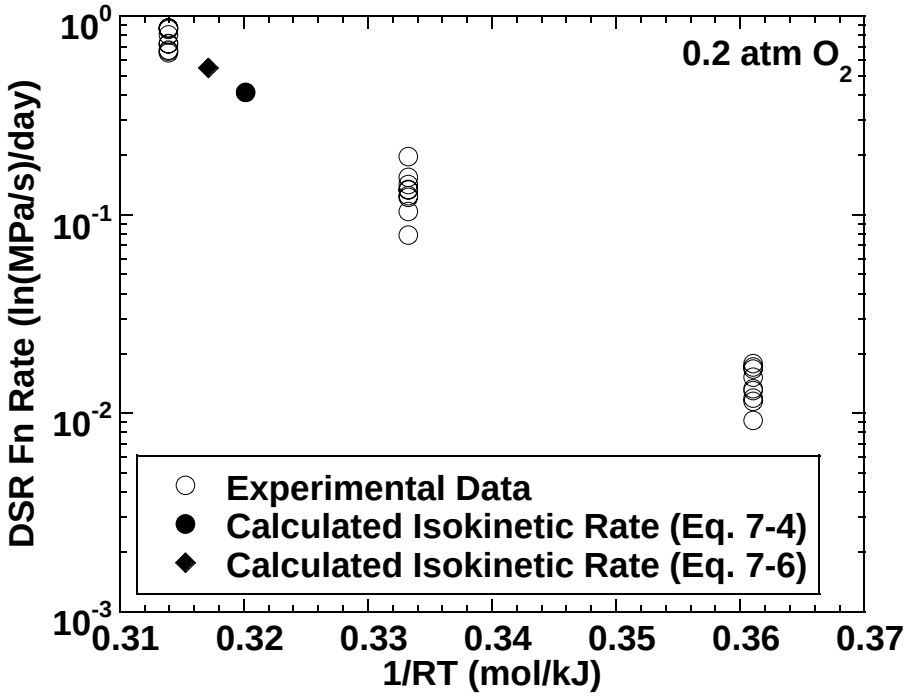

Figure 7-16. Calculated Isokinetic Temperature (Solid Symbols) at 0.2 atm O_2.

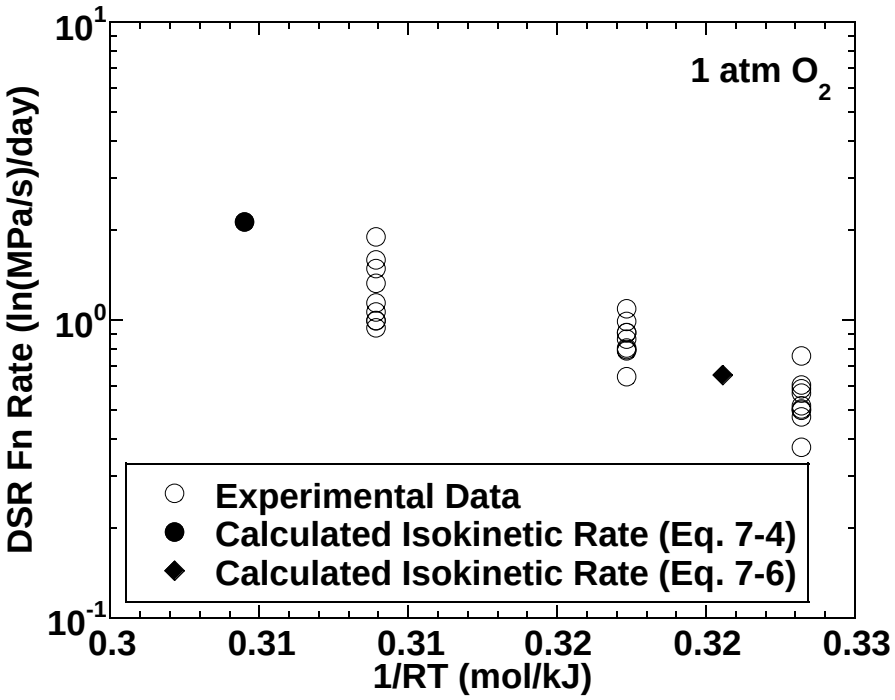

Figure 7-17. Calculated Isokinetic Temperature (Solid Symbols) at 1 atm O_2.

Physico-Chemical Correlations

During aging, asphalt comes into contact with oxygen, resulting in an increase in asphaltene content, carbonyl content, and rheological properties. Previous studies have shown that log η^*_o of an asphalt varies linearly with its carbonyl content during the course of oxidative aging (Lee and Huang, 1973; Martin et al., 1990; Lau et al., 1992; Liu, 1996; Domke, 1999):

$$\ln \eta^*_0 = \ln m + HS \bullet CA \tag{7-7}$$

where m is a model parameter and HS is the hardening susceptibility or the slope of the regression line for ln η^*_o versus CA. Hardening susceptibility is a function of pressure but not temperature and is characteristic for each asphalt (Liu et al., 1998). With respect to the asphalt hardening rate, the hardening susceptibility can be expressed as:

$$\frac{\partial \ln \eta}{\partial t} = \left(\frac{\partial \ln \eta}{\partial CA} \right) \left(\frac{\partial CA}{\partial t} \right) \tag{7-8}$$

Here, the asphalt is more susceptible to hardening as the HS value gets larger.

This project has demonstrated that the log of the DSR function grows linearly with time. Hence, the correlation between the log of the DSR function and carbonyl content during oxidative aging of an asphalt binder should be linear. And Equation 7-7 becomes:

$$\ln (Fn) = \ln m + HS \bullet CA \qquad (7\text{-}9)$$

The plots of hardening susceptibility can be seen in Figures 7-18 and 7-19 for asphalts AAF-1 and TS2K, and the remaining can be found in Appendix B (Figures B-7-40 to B-7-46). The values of the hardening susceptibility for each asphalt and its corresponding m-value are tabulated in Table 7-6. For most of the asphalts, the value of HS decreases as the pressure increases from 0.2 to 1 atm O_2. Domke (1999) also observed a similar trend in which the pressure was varied from 0.2 to 20 atm O_2 and there was a minimum in the hardening susceptibility at 4 atm O_2, attributed to molecular diffusion of oxygen in the sample.

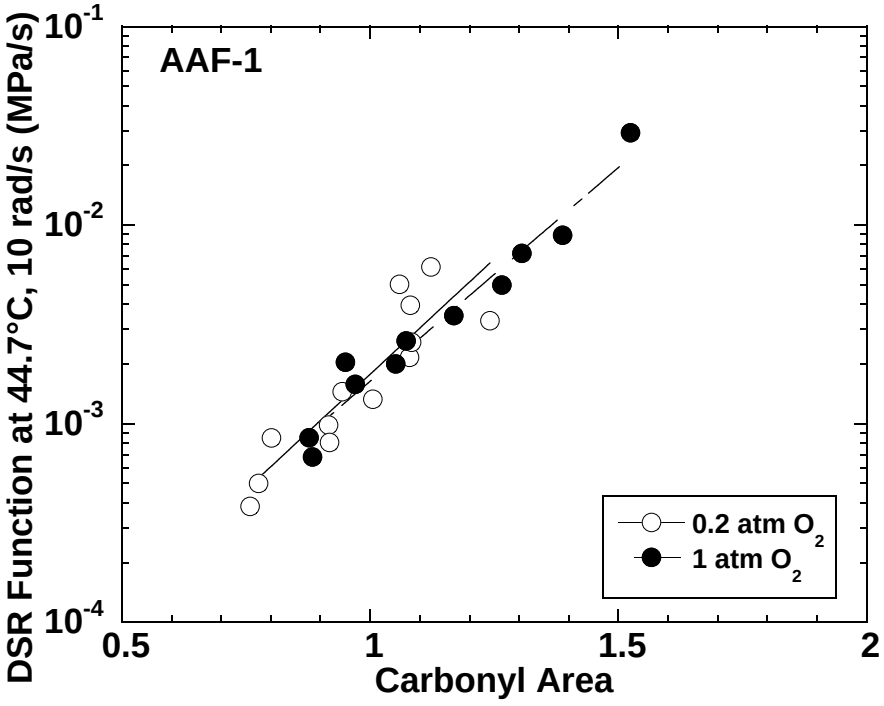

Figure 7-18. Hardening Susceptibility Plot for SHRP AAF-1.

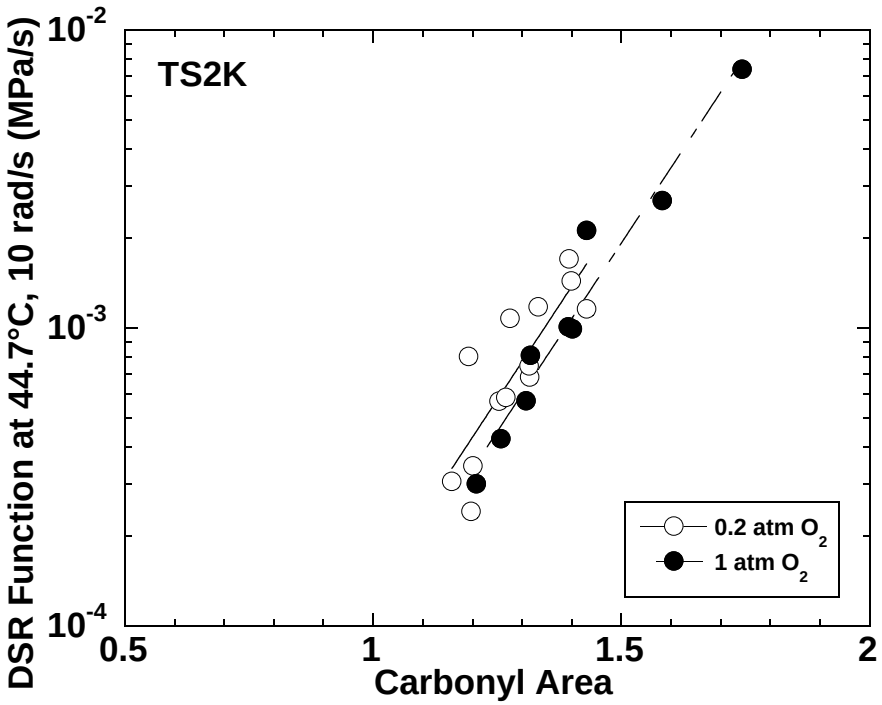

Figure 7-19. Hardening Susceptibility Plot for TS2K.

Table 7-6. Hardening Susceptibility Parameters for All Nine Asphalts.

Asphalt	0.2 atm O_2		1 atm O_2		5 atm O_2	
	HS	m x 10^9 (MPa/s)	HS	m x 10^9 (MPa/s)	HS	m x 10^9 (MPa/s)
AAA-1	8.61	88.35	6.79	479.8	7.49	164.2
AAB-1	6.26	1,103	4.99	3,784	3.31	34,355
AAD-1	9.49	7.60	6.24	226.2	3.84	14,321
AAF-1	6.08	3,874	4.95	11,566	2.51	264,879
ABM-1	4.35	356.9	2.54	3,850	2.98	868.2
AAM-1	4.39	9,602	4.57	7,120	5.58	984.4
AAS-1	4.70	6,375	5.09	4,832	3.78	23,242
Lau4	6.68	862.4	5.23	3,013	4.65	7,160
TS2K	5.83	394.5	5.85	287.0	6.24	272.9

The pressure dependency of hardening susceptibility is plotted in Figure 7-20 and can be modeled as:

$$HS = \theta P^{\delta} \quad (7\text{-}12)$$

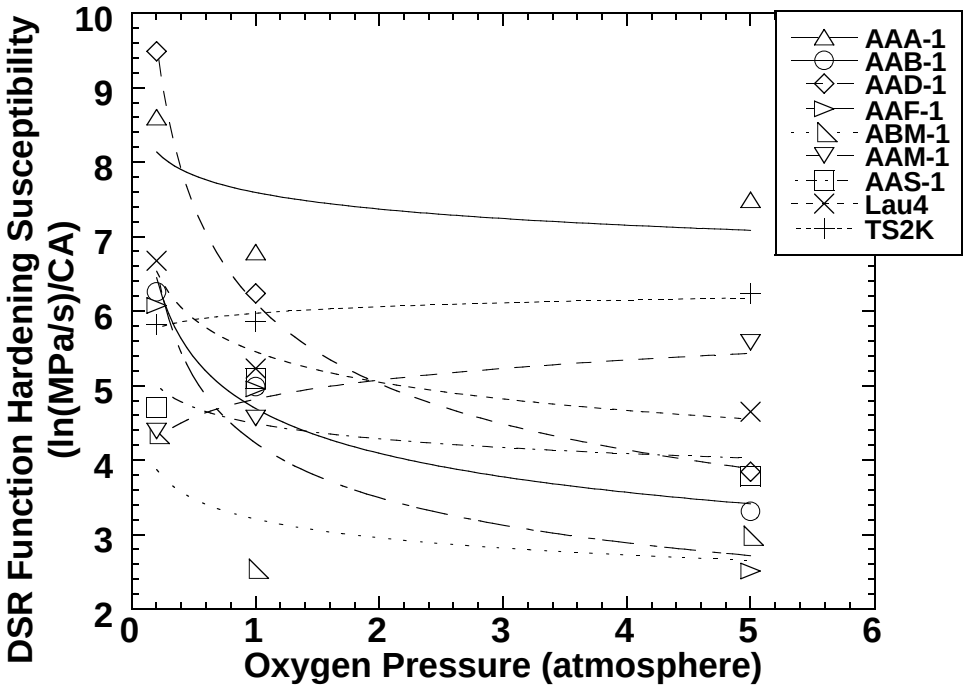

Figure 7-20. Pressure Dependency of Hardening Susceptibility.

Table 7-7 lists the resulting parameters θ and δ. For all asphalts except asphalts AAM-1 and TS2K, the hardening susceptibility decreases with pressure. The anomaly of these two asphalts could be due to the source of the materials. Asphalt TS2K is suspected to have been cracked during the air-blowing process as mentioned in the previous section.

Figure 7-21 compares the pressure dependency of hardening susceptibility, δ, versus that of DSR function hardening rate, α. Unfortunately, no correlation can be established possibly due to the complication in deriving a rate constant, such as α, as a result of pressure dependency. The plot, however, shows how sensitive AAF-1 and AAD-1 are to pressure.

Table 7-7. Pressure Dependency of Hardening Susceptibility.

Asphalt	θ	δ
AAA-1	7.59	-0.0430
AAB-1	4.69	-0.198
AAD-1	6.11	-0.281
AAF-1	4.23	-0.275
ABM-1	3.21	-0.117
AAM-1	4.82	0.0746
AAS-1	4.49	-0.0679
Lau4	5.45	-0.112
TS2K	5.97	0.0211

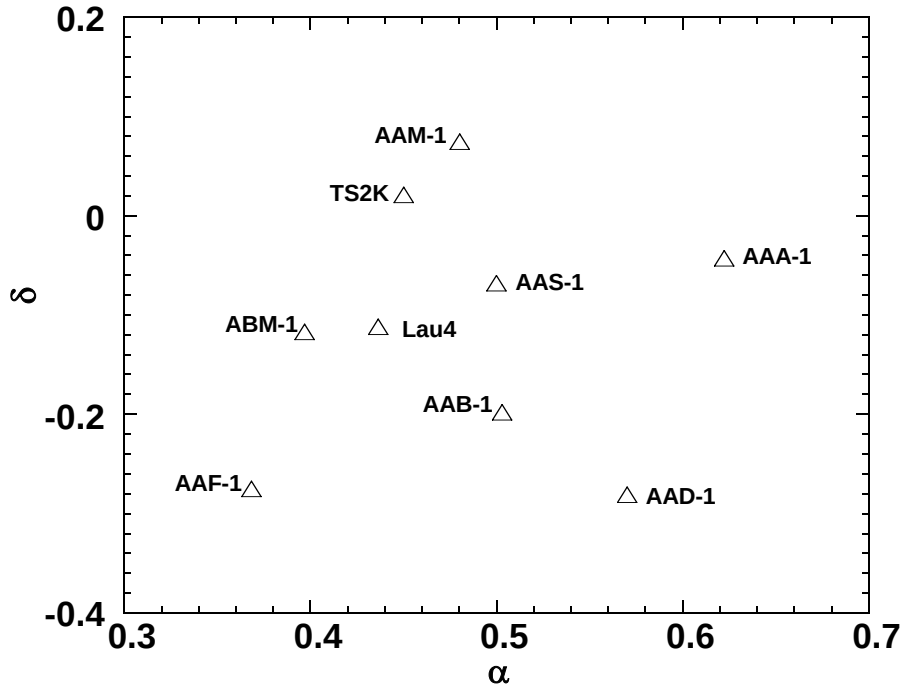

Figure 7-21. Reaction Order versus Pressure Dependency of Hardening Susceptibility.

The hardening susceptibility parameter, δ, is plotted against the initial jump pressure factor, γ, in Figure 7-22. Again, there is no direct correlation between γ and δ. It only suggests that, in general, asphalts with higher γ values are more sensitive to pressure in terms of HS. The correlation between the asphalt hardening and the initial jump is more noticeable in the θ versus β relationship as shown in Figure 7-23. Asphalts with high initial jump are likely to harden at a slower rate than those with low initial jump. Thus, there tends to be an offsetting effect between the initial jump and the DSR function hardening rate.

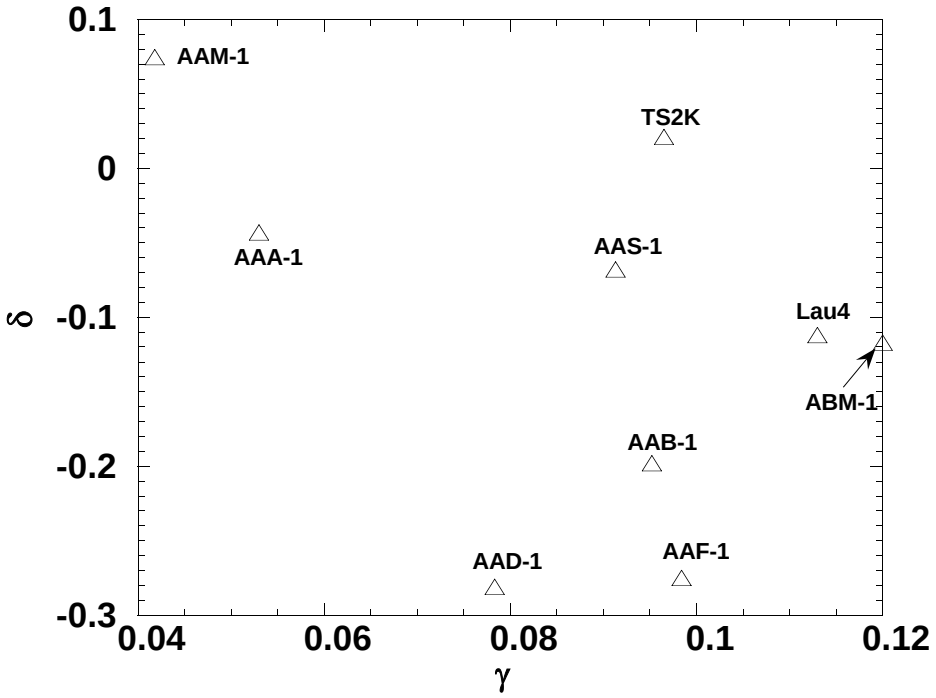

Figure 7-22. Initial Jump Pressure Dependency versus HS Pressure Dependency.

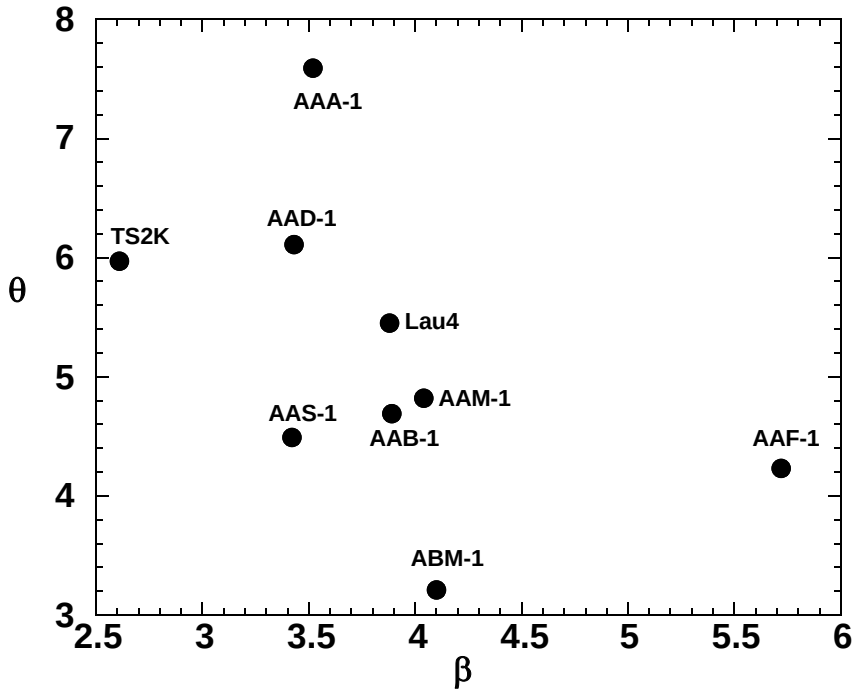

Figure 7-23. DSR Function Hardening Susceptibility and Initial Jump Relationship.

Asphalt Aging Model

All asphalt aging parameters, such as initial jump, activation energy E, and pre-exponential factor A', have been determined for each asphalt binder at different pressures. These parameters can be used to estimate the road condition aging resistance of an asphalt binder. For a chosen temperature, the rate of the DSR function hardening of an asphalt binder can be calculated by Equation 7-6 using the constants in Table 7-5.

By Equation 7-2 and initial jump constants in Table 7-1, the critical time at which the asphalt will be likely to deteriorate can be calculated. The failure limit is 0.003 MPa/s as suggested earlier in Chapter 6.

Table 7-8 lists the estimated number of days when an asphalt binder is expected to fail the criterion after being aged at atmospheric air. Increasing the aging temperature from 60 ºC to 90 ºC while keeping the pressure constant at 1 atm air reduces the aging time required more than ten fold. And again, asphalt AAF-1 requires the shortest time among nine asphalts, 98 days at 60 ºC and 8 days at 90 ºC (based on Equation 7-4) and 157 days at 60 ºC and 12 days at 90 ºC (based on Equation 7-6).

Table 7-8. Calculated Critical Time for All Asphalts Aged at 1 atm Air.

Asphalt	Critical Time Based on Equation 7-6 (Days)		Critical Time Based on Equation 7-8 (Days)	
	60 ºC	90 ºC	60 ºC	90 ºC
AAA-1	252	26	270	26
AAB-1	204	18	273	21
AAD-1	215	20	255	21
AAF-1	98	8	157	12
ABM-1	213	22	278	26
AAM-1	196	18	248	19
AAS-1	265	22	346	26
Lau4	220	18	299	22
TS2K	219	16	278	18

Reaction Rate Constants Derived From G' and (η'/G') Values

The DSR function is comprised of two rheological components, G' and η'/G', which represent the extensional behavior of asphalt binders. An attempt was made to determine the rate constants expressed in these parameters using both Equations 7-4 and 7-6. The values are tabulated in Tables 7-9 through 7-12. Interestingly, the α value of asphalt AAF-1 is the lowest when expressed in terms of G' (Table 7-9). As indicated earlier, asphalts with low α value tend to have a high initial jump. However, when expressed in terms of η'/G', the α value of AAF-1 is not exactly the lowest (Table 7-11). This is because the dynamic viscosity, η', behaves

differently than the storage modulus, G', which is proportional to the elasticity of a material. During aging the increase of the viscous part is less sensitive than the elastic part. This suggests that the two parameters may not be analyzed individually, instead they should be combined as G'/(η'/G').

Listed in Tables 7-10 and 7-12 are the kinetic parameters calculated using Equation 7-6 based on G' and (η'/G') values, respectively. Based on G', the activation energy E and the pre-exponential factor A' decrease when the aging pressure increases from 0.2 to 1 atm O_2. And again, when expressed in terms of (η'/G'), the E and A' values decrease with pressure in this study for some asphalts and increase for others, such as asphalts AAA-1 and AAF-1, emphasizing the importance of combining the two rheological components, G' and (η'/G').

Table 7-9. Kinetic Parameters for All Asphalts – G' (Equation 7-4).

Asphalt	E kJ/mol	ln A	α
AAA-1	77.2±1.5	24.5±0.5	0.60±0.02
AAB-1	79.8±9.0	25.2±3.0	0.46±0.10
AAD-1	79.6±7.4	25.2±2.4	0.51±0.09
AAF-1	82.4±10.9	25.6±3.6	0.25±0.13
ABM-1	75.5±7.7	23.4±2.5	0.39±0.09
AAM-1	80.8±8.2	25.2±2.7	0.44±0.10
AAS-1	82.4±10.2	25.7±3.4	0.47±0.12
Lau4	84.5±7.5	26.5±2.4	0.39±0.09
TS2K	89.5±9.1	28.0±3.0	0.42±0.11

Table 7-10. Kinetic Parameters for All Asphalts – G' (Equation 7-6).

Asphalt	E kJ/mol		ln A'	
	0.2 atm O_2	1 atm O_2	0.2 atm O_2	1 atm O_2
AAA-1	78.0±1.4	72.7±2.0	23.8±0.49	23.1±0.65
AAB-1	85.2±5.0	34.9±14.5	26.2±1.7	10.8±4.6
AAD-1	83.2±5.8	62.4±22.4	25.6±1.9	19.7±7.2
AAF-1	87.2±9.9	48.4±19.9	26.7±3.3	14.7±6.4
ABM-1	80.0±13.3	65.1±8.6	24.3±4.5	20.0±2.8
AAM-1	86.6±3.2	35.5±22.0	26.5±1.1	10.7±7.1
AAS-1	85.3±15.2	37.0±8.7	25.9±5.1	11.3±2.8
Lau4	89.1±5.9	13.4±0.7	27.4±2.0	3.81±0.22
TS2K	94.3±2.9	35.8±19.0	28.9±1.0	10.8±6.1

Table 7-11. Kinetic Parameters for All Asphalts – η'/G' (Equation 7-4).

Asphalt	E kJ/mol	ln A	α
AAA-1	79.4±3.3	24.3±1.1	0.68±0.04
AAB-1	85.2±4.6	26.2±1.5	0.59±0.05
AAD-1	82.2±3.1	25.2±1.0	0.70±0.04
AAF-1	84.7±5.0	26.2±1.7	0.49±0.06
ABM-1	76.4±6.4	23.1±2.1	0.42±0.07
AAM-1	80.6±5.9	24.6±1.9	0.54±0.07
AAS-1	88.2±6.4	26.9±2.1	0.57±0.07
Lau4	84.2±5.8	25.9±1.9	0.53±0.07
TS2K	123.6±12.2	38.3±4.0	0.60±0.14

Table 7-12. Kinetic Parameters for All Asphalts – η'/G' (Equation 7-6).

Asphalt	E kJ/mol		ln A'	
	0.2 atm O_2	1 atm O_2	0.2 atm O_2	1 atm O_2
AAA-1	78.1±1.2	97.5±1.8	22.8±0.4	30.2±0.6
AAB-1	85.6±6.1	77.0±27.0	25.4±2.0	23.6±8.7
AAD-1	83.6±7.0	81.2±1.6	24.5±2.3	24.9±0.5
AAF-1	84.6±5.5	96.2±9.2	25.4±1.9	29.9±3.0
ABM-1	79.1±8.5	72.1±16.5	23.3±2.9	21.7±5.3
AAM-1	82.8±2.0	47.1±31.9	24.4±0.7	13.8±10.3
AAS-1	91.0±5.9	57.1±1.5	26.9±2.0	16.9±0.5
Lau4	85.4±3.8	47.5±0.8	25.3±1.3	14.2±0.3
TS2K	131.8±19.6	68.4±7.7	40.1±6.6	20.5±2.5

SUMMARY

A number of asphalt binders have been aged at various temperatures and pressures to determine the effects of aging conditions on oxidation kinetics. With the DSR function as a measure of oxidation, the constant reaction rates vary linearly with the reciprocal of absolute temperature in the usual Arrhenius form:

$$r_{Fn} = A'_{FN}\, e^{-\left(\frac{E_{Fn}}{RT}\right)} \qquad (7\text{-}6)$$

This is the same form used to describe oxidation kinetics using carbonyl area and viscosity as aging measurements. The kinetic parameters are asphalt dependent.

From another form of reaction rate which takes into account the aging pressure (Equation 7-4), the value of α indicates a relationship with initial jump. For asphalts with low α, the initial jump tends to be very sensitive to aging pressure.

The initial jump, $\ln(Fn_0) - \ln(Fn_{tank})$, is pressure dependent but temperature independent. Hardening susceptibility is also pressure dependent.

There is an inverse relationship between E and α, suggesting that if aging temperature and pressure are increased, the asphalts most affected by temperature increase will be least affected by pressure increase. Moreover, there is also a crude negative correlation between γ and α, indicating that asphalts with a large initial jump tend to have lower hardening rates. Hence, it is possible to simulate road aging by accelerated aging due to the offsetting effect between pressure and temperature as well as the inverse correlation between initial jump and hardening rate.

Asphalt's road aging resistance can be predicted using the kinetic parameters E and A' as well as initial jump. Among the nine asphalts studied, asphalt AAF-1 fails the 0.003 MPa/s criterion much earlier than the other asphalts. Increasing aging temperature by 30 ºC, while maintaining the same pressure, reduces the number of days required to obtain significant changes in asphalt by ten fold.

CHAPTER 8. WATER SUSCEPTIBILITY

We conducted a brief study of water susceptibility to make sure that modifiers did not adversely affect the water resistance of asphalt mixes and to see if there was any relation between water susceptibility of unmodified asphalts and PG grade and hardening tendencies.

The asphalts included the control and two levels of CRM asphalts (project 1460 test section 2000) SHRP asphalts AAA-1 and ABM-1, Wright asphalt AC-10 and Wright AC-10 modified with 3 percent SBR latex, and Wright AC-30P, which is Wright AC-10 modified with 3 percent SBS. The mix design is shown in Table 8-1. Binder content was 5.1 percent and no lime was used. Lottman's were run in accordance with Tex 531-C, "Prediction of Moisture Induced Damage to Bituminous Paving Materials Using Molded Specimens."

The results are shown in Figure 8-1 and 8-2. The modifiers seem to help the dry strength except for SBS, but wet strength less so. Rubber at 12 percent and 3 percent SBR seemed to give some improvement in the TSR ratio, while 8 percent rubber and SBS were slightly deleterious. In general, it appears that modifiers will have only a minor effect on water susceptibility.

The most striking effect is the superiority of asphalt ABM-1. Continuous PG grades as well as DSR functions as obtained in Chapter 8 for asphalts aged at 100 ^{o}C (212 ^{o}F), 1 atm O_2 and 52 hours are listed in Table 8-2 for the unmodified asphalts. At least for this small sample, no connection between grade, DSR function, or water susceptibility is discernible, except that ABM-1 has a good DSR function, the best wet and dry strength, and the worst grade span. These relations do not continue for the other asphalts, however.

Table 8-1. Aggregate Gradation and Materials for the Laboratory Specimens.

	Colo Materials D Rock Hunter		Colo Materials F Rock Hunter		Gifford-Hill Wash Scr. New Braunfels		Young Matls Sand Riverbend		Source 6 Aggr. Num 6 Lab Num 6		Total % 100.0			
Sieve Size	Bin#1 39.4	Total %	Bin#2 21.2	Total %	Bin#3 29.3	Total %	Bin#4 10.1	Total %	Bin#5 0.0	Total %	Cum. Pass	TxDOT Specs.	Ind. Ret.	Cum. Ret.
1"	100.0	39.4	100.0	21.2	100.0	29.3	100.0	10.1	100.0	0.0	100.0	100 - 100	0.0	0.0
7/8"	100.0	39.4	100.0	21.2	100.0	29.3	100.0	10.1	100.0	0.0	100.0	100 - 100	0.0	0.0
5/8"	99.5	39.2	100.0	21.2	100.0	29.3	100.0	10.1	100.0	0.0	99.8	98 - 100	0.2	0.2
3/8"	76.4	30.1	100.0	21.2	100.0	29.3	100.0	10.1	100.0	0.0	90.7	85 - 100	9.1	9.3
#4	6.0	2.3	70.7	14.9	99.5	29.2	100.0	10.1	100.0	0.0	56.5	50 - 70	34.2	43.5
#10	2.4	0.9	7.6	1.6	72.0	21.1	100.0	10.1	100.0	0.0	33.7	32 - 42	22.8	66.3
#40	1.9	0.7	2.6	0.5	22.6	6.7	99.3	10.0	100.0	0.0	17.9	11 - 26	15.8	82.1
#80	1.7	0.7	2.2	0.5	8.6	2.5	12.8	1.3	100.0	0.0	5	4 - 14	12.9	95
#200	0.8	0.3	0.7	0.1	4.1	1.2	0.5	0.1	100.0	0.0	1.7	1 - 6	3.3	98.3

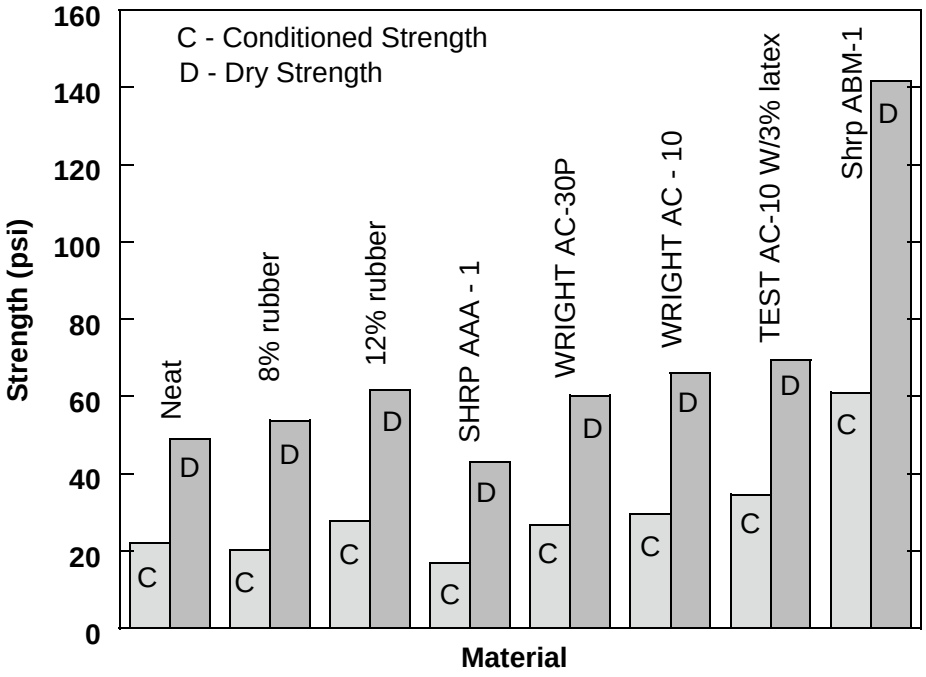

Figure 8-1. Dry and Conditioned Strengths for the Laboratory Specimens.

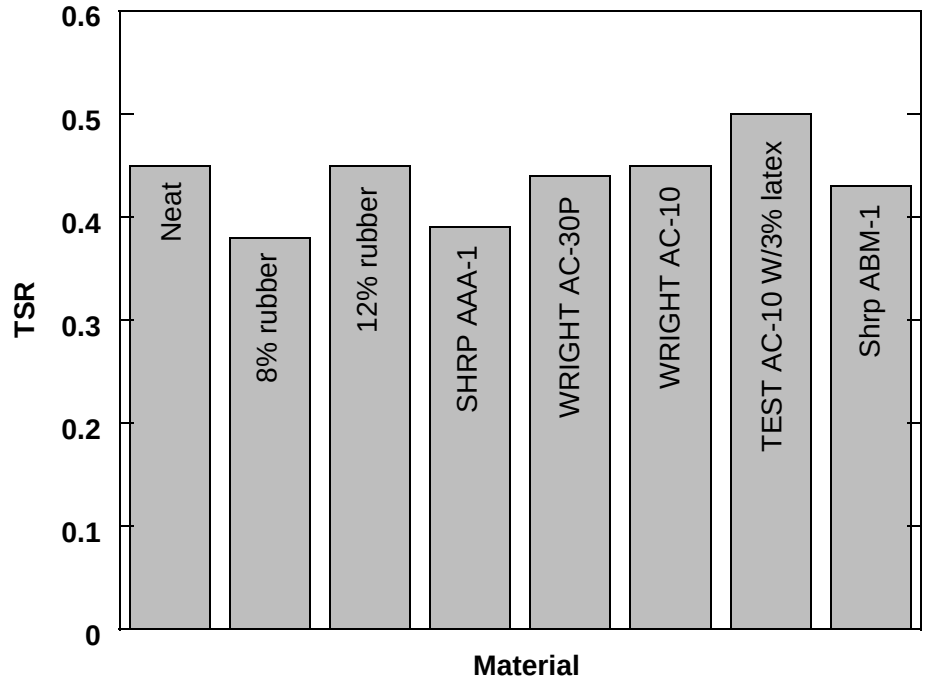

Figure 8-2. Tensile Strength Ratios for the Laboratory Specimens.

Table 8-2. Comparison of PG Grade Span and DSR Function.

Asphalt	DSR Function	Continuous Grade	Grade Span
AAA-1	3.77×10^{-4}	60-33	93
ABM-1	1.93×10^{-4}	66-14	80
TS 2000	1.10×10^{-3}	68-29	97
Wright AC-10	1.70×10^{-3}	61-29	90

CHAPTER 9. FIELD AGING OF ASPHALT BINDERS

INTRODUCTION

Previous chapters have described several important aspects of laboratory binder aging, including oxidation kinetics (Chapter 2), the effect of oxidation on low-temperature properties (Chapter 3), resulting changes in ductility and DSR properties (Chapter 4), polymer-modified binders (Chapter 5), and studies of aging procedures (Chapter 6).

These results are necessary to understand the effects of oxidation, the rates at which they occur, and for developing a practical laboratory aging procedure but are not sufficient for predicting pavement aging. Actual field aging data are needed to relate field aging rates to laboratory rates, to determine if aging mechanisms are the same in both situations, and finally, to establish the level of field aging that can be tolerated before failure occurs.

The work that is reported in this chapter addresses these issues of field aging in a novel manner. As much as possible, the pavements have been evaluated over a period of time, allowing aging rates and binder hardening susceptibilities to be measured and compared to laboratory-determined values. Also, these longitudinal determinations have provided results that allow tracking the march of a binder across the ductility-DSR map (Chapter 4) as the result of oxidation and provide insight into the state of the binder at the time of pavement cracking failure. Additionally, data were obtained on aging rates as a function of pavement depth. Serendipitously, intriguing results on the effect of sealcoats on binder properties were observed and suggest further studies of maintenance methods that could lead to significant extensions of pavement life.

METHODOLOGY

This section describes the material, equipment, and procedures followed in this research. The materials primarily were binders recovered from field cores although these data also are compared with the original binder in the case of SH 21. Size exclusion chromatography, also called gel permeation chromatography (GPC) was used to ensure complete solvent removal in the binder recovery process. Then, a dynamic shear rheometer was used to measure the rheological properties of the binder. Finally, infrared spectroscopy was used to measure the carbonyl content in the binder. Details of these methods follow.

Field Pavements

Data were obtained from a combination of Texas Highway 21 between Bryan and Caldwell , Strategic Highway Research Program (SHRP) long-term pavement performance (LTPP) general pavement study (GPS) sites, and other pavements submitted by districts for investigation. In all, 19 pavements were studied and one (Texas Highway 21) was evaluated at six different stations and combined with extensive data from previous years' studies.

Texas Highway 21

Texas Highway 21 (SH 21) is the most investigated pavement of this project. The construction of this road, a two-lane divided highway, began on July 22, 1986, and was completed on July 21, 1988. The tank asphalt used in this road was an Exxon AC-20. The hotmix was produced at Young Brothers hotmix plant in Bryan, Texas, a counter-flow drum plant manufactured by Standard Havens with a capacity of 350 tons per hour. The aggregate used in this pavement was Texas crushed limestone and field sand. The highway was seal coated and over laid in July 2000, 12 months before 2002 cores were taken.

The westbound lanes of this road were cored several times during the 13-month construction period between the Brazos River and Caldwell, Texas. In previous projects, stations were sampled in 1989 (nine locations), 1992 (seven locations), and 1996 (six locations) (Davison et al., 1989; Davison et al., 1994, Bullin et al., 1997). In this current project, six stations were sampled in 2002 and are located within about 4.5 miles of each other between the east end of the railroad overpass and County Road 212. Cores from 1989 and 1992 were analyzed in an earlier study (Lunsford, 1994). In this current research, measurements were obtained for the 1996 and 2002 cores.

In March 1996, four cores were taken from stations 1483, 1465, 1295 and 1277 and five cores from stations 1500 and 1392 because of the thinness of their top lifts. Those cores were four inches in diameter. In July 2002, six cores were taken at each of these six stations, with three cores from the wheel path and the other three from the center of the lane. Their descriptions follow.

Station 1500. This station is located 0.1 mile west of the "zero" reference point (which is the east end of the concrete embankment for the railroad track overpass west of the Brazos River). The cores were taken from the right westbound lane. They are located 225 feet from the west end of the concrete embankment for the railroad overpass. The wheel-path cores were taken from the right-hand lane, from the right wheel path in 1996 and the left wheel path in 2002. This station is the reference point located at 0 mile and to which the other stations are referenced.

Station 1483. This station is located at the crossover, 0.5 mile west of the zero reference point. The cores were located about 26.6 feet east of County Road 221. The wheel-path cores were taken from the right lane, from the right wheel path in 1996 and from the left path in 2002.

Station 1465. This station is located 1.0 mile west of the reference point. The cores were taken 55.3 feet east of the crossover at County Road 229. The wheel-path cores were taken in the left-hand lane in 1996 and in the right-hand lane in 2002. Both were taken from the left wheel path.

Station 1392. Station 1392 is located 2.2 miles west of the reference point. The cores are located 58.2 feet west of the "Historical Marker 1 Mile" sign. The wheel-path cores were taken in the right-hand lane from the right wheel path in 1996 and from the left path in 2002.

Station 1295. This station is located 4.0 miles west of the reference point. The cores were taken 1021 feet west of FM 1392. The wheel-path cores were taken in the right-hand lane from the right wheel path in 1996 and from the left path in 2002.

Station 1277. Station 1277 is located 4.4 miles west of the reference point. The cores were taken 195.8 feet east of County Road 212. The wheel-path cores were taken in the left-hand lane from the center of the lane in 1996 and from different paths and lanes in 2002.

The center-lane cores were only taken in 2002 and from the right-hand lane.

Cores taken in 1989 and 1992 were immediately extracted and recovered; the cores taken in 1996 and 2002 were recovered in 2002.

Texas LTPP GPS Sites

Sixteen long-term pavement performance general pavement studies sites in Texas were evaluated. Their site numbers and locations are listed in Table 9-1 and Figure 9-1. Cores (12-inch diameter) were obtained by the LTPP program during the 1989-1990 time period and stored at the materials reference library (MRL). These cores were obtained from the MRL for study under this program. Additionally, new cores (6 or 4 inch) were obtained from the same locations during the summer of 2002 from pavements that were still in the study. Note that two cores were not available from 1989-1990; six pavements were removed from the program because of maintenance or rehabilitation so that 2002 cores were not taken; two cores, though taken in 1989, were no longer available; and one pavement did not exist in 1989.

The MRL cores taken in 1989-1990 were stored a warehouse without temperature control and temperatures ranged from 7 to 32 ^{o}C (45 to 90 ^{o}F). Thus, it is likely that there was further aging in the warehouse, but the rate of aging undoubtedly was significantly slowed.

Other Pavements

Some additional pavements were submitted by TxDOT districts for inclusion in the program. Interstate 10, both the northbound and southbound frontage roads over the Southern Pacific and Missouri Pacific railroad (Hollywood Overpass), was evaluated. Both pavements were 2 inches of asphalt cement pavement over a box beam and 15 years old. However, the northbound lane was observed to be "very oxidized" while the southbound lane was stated to be "like new." The district engineer was interested in why these two pavements appeared to be so different.

Table 9-1. Locations and Coring Dates for the Sixteen Texas LTPP Sites.

LTPP Site	Lat	Long	Route	County	Year Constructed	'89-'90 Cores Date Taken	2002 Cores Date Taken
48-1046	35.2 N	101.34 W	I 40	Carson	1955	8/3/89	Aug 02
48-1049	31.65 N	94.67 W	US 59	Nacogdoches	1984	3/28/90	NA
48-1050	30.35 N	95.92 W	SH 105	Grimes	1984	6/7/89	NA
48-1056	36.19 N	100.71 W	US 83	Ochiltree	1969	8/2/89	Sep 02
48-1060	28.5 N	97.05 W	US 77	Refugio	1986	3/5/90	NA
48-1068	33.50 N	95.58 W	SH 19	Lamar	1985	NA	7/24/02
48-1109	30.75N	95.52 W	SH 19	Walker	1984	3/21/90	NA
48-1168	32.67 N	95.46 W	FM 564	Wood	1985	NA	7/8/02
48-2108	29.34 N	94.92 W	Spur 37	Galveston	1985	6/6/89	6/26/02
48-2133	31.07 N	97.31 W	SH 36	Bell	1984	5/12/89	7/9/02
48-3679	31.37 N	94.50 W	SH 103	Angelina	1988	3/27/90	NA
48-3689	30.7 N	94.85 W	US 190	Polk	1987	3/20/90	NA
48-3769	31.79 N	106.25 W	US 62	El Paso	1976	7/11/89	7/9/02
48-3835	30.73 N	96.43 W	SH 6	Brazos	1991	-	Sep 02
48-6086	28.17N	97.86 W	I 37	Live Oak	1971	8/3/90	July 02
48-9005	29.51 N	98.72 W	FM 1560	Bexar	1986	2/6/90	7/10/02

NA = Not Available

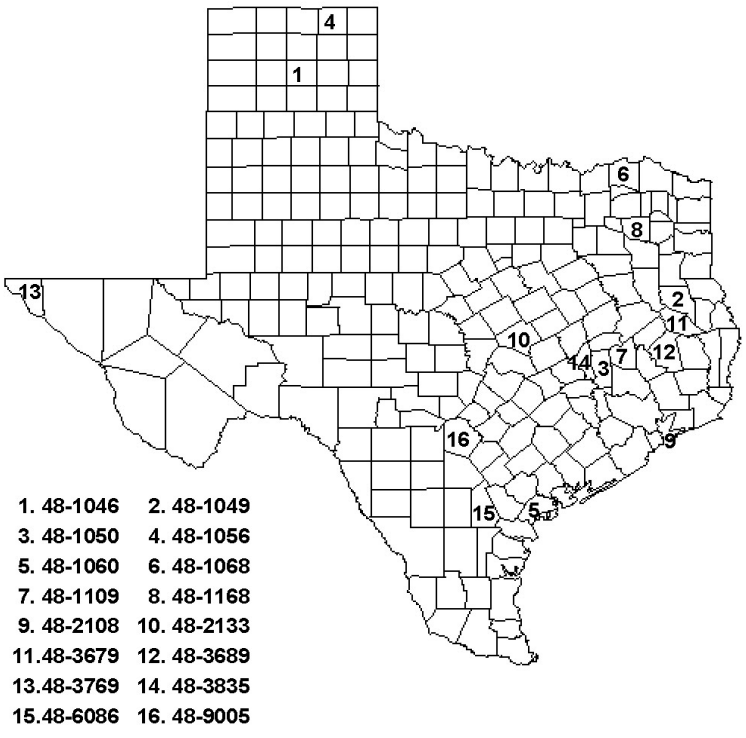

Figure 9-1. Locations of the 16 LTPP Sites in Texas.

Extraction and Recovery

The pavement cores (after separating the lifts either by sawing or by freezing and then cleaving apart) were broken into small pieces with a hammer before solvent-extracting the binder from the aggregate. The binder content of the pavement was approximately 5 percent by mass, so about 130 g of core material were extracted to obtain about 6 g of binder. The extraction used three successive washes: one wash of 100 mL toluene followed by two washes of a mixture of 15 mL ethanol plus 100 mL toluene. After the binder was extracted from the aggregate, the solvent was filtered five times using basket coffee filters to remove all aggregate particles from the binder solution.

The binder was recovered from the solvent with a Büchi, RE 111 rotovap. The rotavap "flask" was specially designed as a straight glass tube that would mate with a 55-mm diameter ointment tin. Binder was recovered from solution in 100 mL batches and retained in the ointment tin. During recovery, nitrogen gas was introduced to the vessel to drive off any remaining solvent and to prevent contact with oxygen.

Before the removal of the solvent from the last batch of the solution, the bath temperature was kept at 100 °C (212 °F) to avoid hardening or softening of the asphalt in dilute solution (Burr et al. 1991; Burr et al., 1994). When no more solvent could be detected visually, the temperature was increased to 173.9 °C (345 °F) for an additional 30 minutes to ensure sufficient solvent removal. The extraction and recovery procedure took from three to four hours for each sample of pavement.

Each lift from each core had its binder extracted and recovered in at least two replicate batches to assess variability and to ensure accuracy. The properties of the recovered binders were compared to each other or to other lifts, paths, or years. When inconsistencies occurred in these recovered binder properties, additional replicates were extracted, up to four replicates total for a given station and lift.

Size Exclusion Chromatography (SEC)

After the binder was extracted and recovered, it was analyzed by SEC to ensure complete solvent removal using previously reported methodology (Leicht et al., 2001). Test samples were prepared by dissolving 0.2 ± 0.005 g of binder in 10 mL of carrier. The sample of interest was then sonicated to ensure complete dissolution. The sonicated sample was then filtered through a 0.45 µm PTFE syringe filter. Samples of 100 µL were injected into 1000, 500, and 50 Å columns in series with tetrahydrofuran (THF) carrier solvent flowing at 1.0 mL/min.

The chromatograms of binder obtained from replicate extractions should overlay each other. Incomplete solvent removal will result in a peak located at 38 minutes on the chromatogram.

Dynamic Shear Rheometer (DSR)

After complete solvent removal, the rheological properties of the binder were determined. The DSR used in this research was a Carri-Med CSL 500 Controlled Stress Rheometer.

The rheological properties of interest were the complex viscosity (η_o^*) measured at 60 °C and 0.1 rad/s (approximately equal to the low-shear rate limiting viscosity) and the storage modulus (G') and the dynamic viscosity (η'), both at 44.7 °C and 10 rad/s in time sweep mode. A 2.5-cm composite parallel plate geometry was used with a 500 μm gap between the plates.

DSR measurement was also important for deciding whether the binder was changed in some way by the extraction and recovery process (Burr et al., 1990; Burr et al., 1991; Burr et al., 1994; Cipione et al., 1991). If two extraction and recovery processes yielded binders with matching SEC chromatograms but significantly different complex viscosities, then at least one of the binders was suspected of having undergone solvent hardening or softening.

Fourier Transform Infrared (FTIR) Spectrometer

Carbonyl area was measured using a Galaxy 5000 FTIR spectrometer with an attenuated total reflectance, ATR zinc selenide prism (Jemison et al., 1992). This absorption band (from 1650 to 1820 cm^{-1}) relates directly to oxygen content (Liu et al., 1998) and, thus, provides a good measure of binder oxidation.

RESULTS AND DISCUSSION

Texas Highway 21

Experimental Data

Binder was extracted and recovered from the individual lifts of the pavement cores, analyzed by several methods, and the results compared to laboratory aging of the same binder that was obtained during construction. Analyses included FTIR, SEC (GPC), and DSR. From the data obtained from binders recovered from cores of different age, we determined binder hardening rates (in terms of both low-shear-rate complex dynamic viscosity, also called the zero shear viscosity, ZSV, and the DSR function that was reported in Chapter 4), carbonyl growth rates, and binder hardening susceptibilities. Each of these values was compared to laboratory values to evaluate similarities of field and laboratory aging, and relative rates of aging. One issue of considerable importance has been the question of what one month (for example) of aging in a 60 °C environmental room is equivalent to on the road. This comparison will vary from climate to climate and pavement to pavement, but beginning the task of obtaining such data was very important. A second issue was how aging rates in the top 2-inch lift compared to aging rates in

the other lifts. Data on the top and bottom lifts (0 to 2 inches and 4 to 6 inches below the surface) were obtained to address this issue.

Table 9-2 summarizes the number and size of cores taken at the various stations and in different years from SH 21 in this and earlier TxDOT projects. In this current project, measurements were made on 1996 and 2002 cores. Data reported in this chapter from 1989 and 1992 cores are taken from an earlier study (Lunsford, 1994).

Table 9-2. Texas Highway 21 Cores Taken in 1989, 1992, 1996, and 2002.

Station	1989		1992		1996		2002	
	Diam. (in)	No. of Cores	Diam. (in)	No. of Cores	Diam. (in)	No. of Cores	Diam. (in)	No. of Cores
1230	4	5	-	-	-	-	-	-
1277	4	4	4	1	4	4	4	6
1295	4	2	4	2	4	4	4	6
1314	4	6	-	-	-	-	-	-
1392	-	-	4	2	4	5	4	6
1394	4	6	4	2	-	-	-	-
1458	4	6	-	-	-	-	-	-
1465	4	6	4	3	4	4	-	-
1483	4	18	4	3	4	4	4 6	4 2
1500	-	-	-	-	4	5	6	6
1517	4	5	-	-	-	-	-	-
1518	-	-	4	3	-	-	-	-

Table 9-3 summarizes the number of cores, by lift, that were evaluated in this research and previous studies. Note that not all available cores were analyzed and that this report includes data from earlier analyses, new analyses of previously obtained cores, and analyses of new cores. In this sense, this report is a comprehensive review of the SH 21 data covering13 years of pavement data and three TxDOT projects (0-458, 0-1314, and 0-1872).

Table 9-3. Summary of the Extracted and Recovered Lifts, SH 21.

Station	1989			1992			1996			2002		
	Top	Middle	Bottom	Top	Middle	Bottom	Top	Middle	Bottom	Top	Middle	Bottom
1277	1	1	2	0	1	0	*1*	0	*1*	*2*	0	*2*
1295	0	0	0	1	*1*	1	*1*	0	*1*	*2*	0	*2*
1392	0	0	0	0	0	0	*1*	*1*	*1*	*2*	0	*2*
1394	1	1	1	1	1	1	0	0	0	0	0	0
1465	0	*2*	0	0	3[a]	1	*1*	0	*1*	*2*	0	*2*
1483	0	*2*	0	1	3[a]	1	*1*	0	*1*	*2*	0	*2*
1500	0	0	0	0	0	0	*1*	0	*1*	*2*	0	*2*
1518	0	0	0	0	1	0	0	0	0	0	0	0

[a] Measured in this research and by Lunsford (1994).
[*] Italicized figures indicate measurements of this study.

Table 9-4 summarizes low-shear-rate values of η* and carbonyl area for each of the lifts studied at the various stations and each of the five years. Where noted, the values are from Lunsford (1994). The viscosity values are summarized in Figure 9-2 for the top lifts and Figure 9-3 for the bottom lifts. Note that where we would expect an increasingly harder material over time on a lift-by-lift and station-by-station basis, this is not universally true. Through 1996 in each of those instances where there are early-year data available for comparison, there was, in fact, monotonic hardening. However, for most of the 2002 cores, there has been little or no additional hardening, and in some cases, there has even been softening. This result was unexpected but is seen in enough of these data and in the LTPP data reported below that we believe it is a correct observation.

These results were checked carefully. For each lift in each core, at least two extraction and recovery replicates were conducted, more if these two showed a significant discrepancy. Measurements were accepted as close matches if the difference was within 10 percent. The carbonyl area and the viscosity values given in Table 9-4 are the averages of the accepted readings. The results leave little room to attribute the inconsistency to experimental or measurement errors. The most likely cause of this inconsistency is the penetration of the fresh asphalt binder from the seal coat through the voids of the original pavement and even to the bottom lift. The seal coat was overlaid two years before the cores were taken.

Table 9-4. Viscosity and Carbonyl Area of the Recovered Binders.

Station	Lift	1989[a]		1992[a]		1996 Wheel Path		2002 Wheel Path		2002 Center Path	
		η^*_o [b]	CA	η^*_o [b]	CA	η^*_o [b]	CA	η^*_o [b]	CA	η^*_o [b]	CA
1277	Top	11400	0.94	-	-	56230	1.31	78190	1.39	67130	1.49
	Middle	8200	0.99	18200	1.08	-	-	-	-	-	-
	Bottom	8500	0.88	-	-	42685	1.27	56705	1.34	52020	1.44
1295	Top	-	-	30200	1.21	56420	1.31	85165	1.42	45050	1.28
	Middle	-	-	45480	1.28	-	-	-	-	-	-
	Bottom	-	-	14000	1.03	39900	1.19	26600	1.03	35565	1.2
1392	Top	-	-	-	-	42700	1.3	47235	1.38	42785	1.27
	Middle	-	-	-	-	23000	1.12	-	-	-	-
	Bottom	-	-	-	-	19540	1.02	11875	0.9	12172	0.84
1394	Top	-	0.88	20800	1.04	-	-	-	-	-	-
	Middle	-	0.94	15800	1.08	-	-	-	-	-	-
	Bottom	-	1.11	30000	1.25	-	-	-	-	-	-
1465	Top	-	-	-	-	52335	1.22	34690	1.14	40945	1.23
	Middle	-	-	22500	1.3	-	-	-	-	-	-
	Bottom	-	-	45300	1.26	80160	1.41	21090	1.06	27220	1.17
1483	Top	-	-	13000	1.12	26060	1.24	30080	1.28	-	-
	Middle	-	-	15500	1.09	-	-	-	-	-	-
	Bottom	-	-	24300	1.23	33285	1.26	34940	1.31	-	-
1500	Top	-	-	-	-	43600	1.3	40350	1.21	-	-
	Middle	-	-	-	-	-		-	-	-	-
	Bottom	-	-	-	-	24690	1.02	32640	1.1	-	-
1518	Top	-	-	-	-	-	-	-	-	-	-
	Middle	-	-	15000	1.01	-	-	-	-	-	-
	Bottom	-	-	-	-	-	-	-	-	-	-

[a] Lunsford (1994).

[b] η^*_o were measured at 0.1 rad/s and 60 °C.

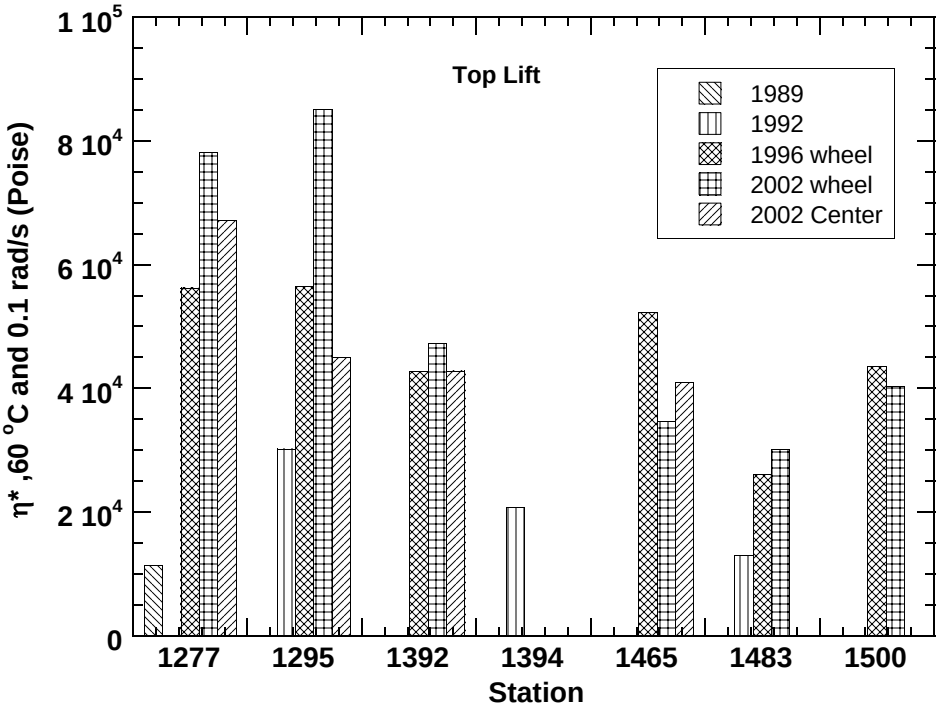

Figure 9-2. Values of η^*_o for the Top Lifts of SH 21.

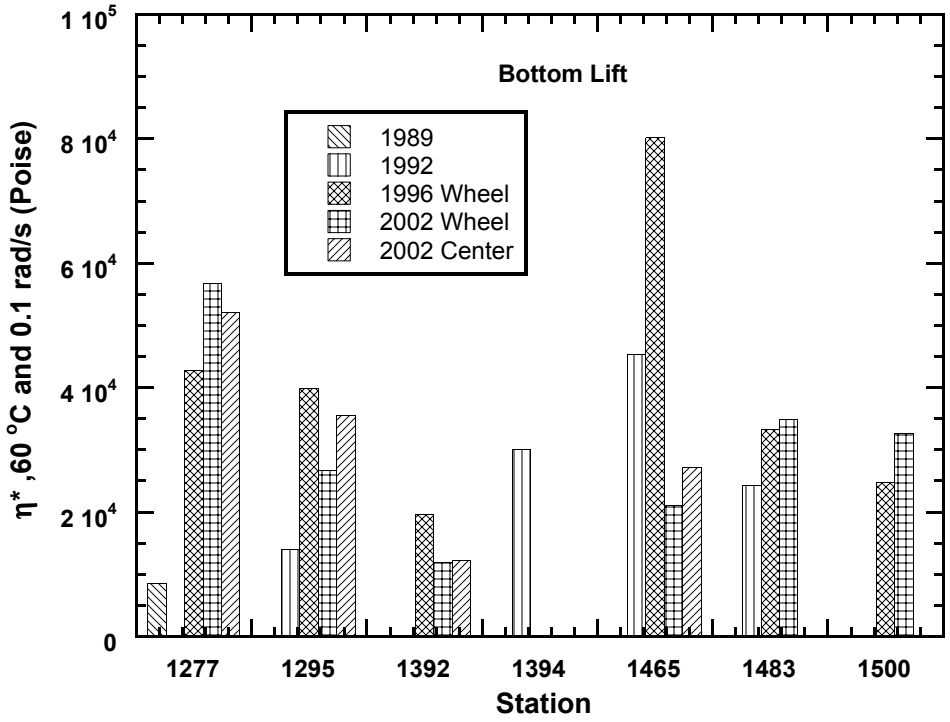

Figure 9-3. Values of η^*_o for the Bottom Lifts of SH 21.

A hardening susceptibility plot for the data of Table 9-4 are shown in Figure 9-4. For each station and lift for which we have sufficient data, η^*_o is plotted versus the FTIR carbonyl area. The hardening susceptibility of a binder is the slope of its line on this plot and indicates how much the binder hardens in response to a given amount of aging (increase in CA). Note that of the six correlations shown, half have a HS of approximately four, and half are about six. The laboratory-aged binder (obtained at the time of construction) shows an HS of from 4.0 to 4.7 and agrees well with one group of the recovered binders. The value of HS is characteristic of a given binder and the value of six for three of the lift-station combinations is significantly outside the bounds of measurement error, leading to the conclusion that a different binder was used in some portions of the paving project. This result is not surprising, given the different lifts and the thirteen-month construction time span.

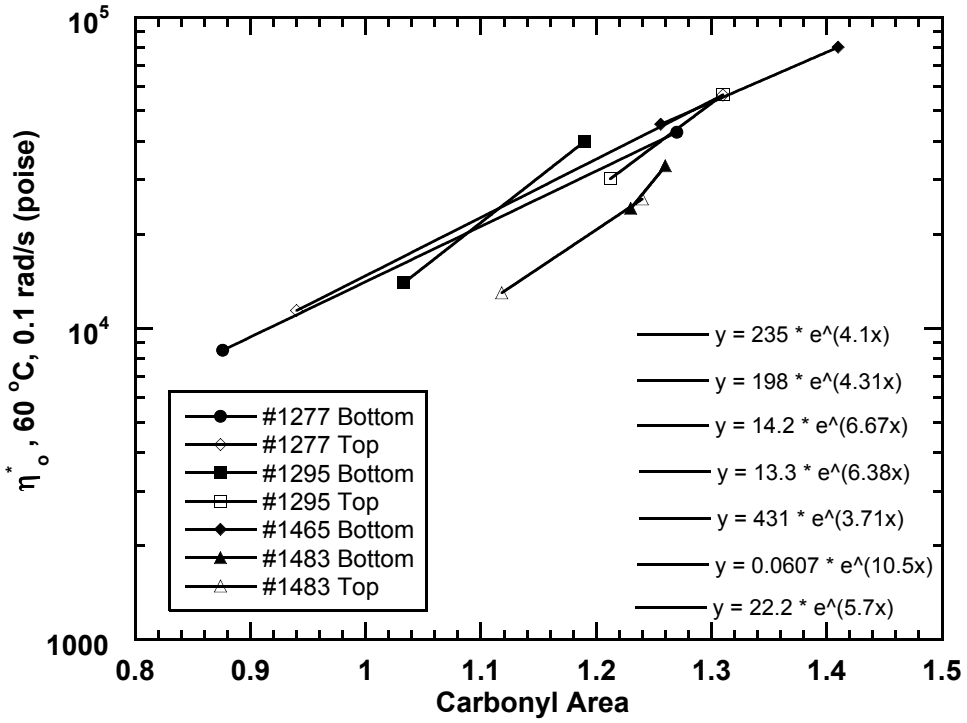

Figure 9-4. Hardening Susceptibilities from 1989, 1992, and 1996 Cores.

Figure 9-5 shows the hardening susceptibility of Exxon AC-20 aged in the laboratory under candidate conditions for an aging test (Chapter 6) and those SH 21 binders recovered from 1989, 1992, and1996 cores that are considered to be the same Exxon AC-20. Note the very good agreement between the lab- and pavement-aged binder HS values in spite of the offset of several sets of data. Cores taken in 2002 are not included in this comparison because the seal coat, placed in 2000, apparently seeped into the lower pavement layers.

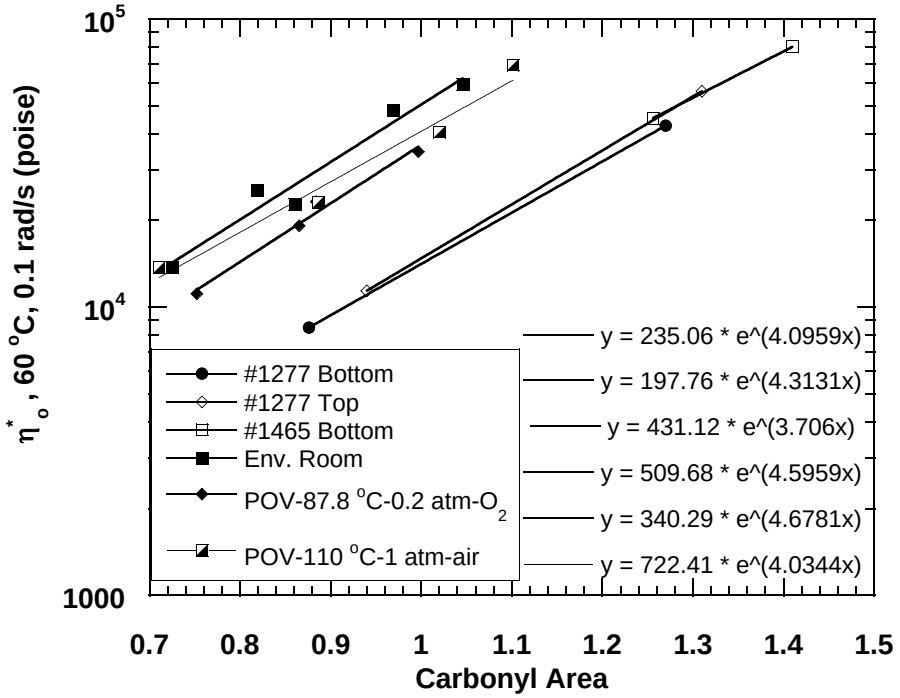

Figure 9-5. Hardening Susceptibilities of Exxon AC-20 from Lab- and Field-Aged Binder.

In addition to the low-shear-rate complex viscosities, the dynamic shear modulus (G') and dynamic viscosity (η') were measured on binders recovered from the 1996 and 2002 cores. These properties, measured at 44.7 °C and 10 rad/s and time-temperature superposition shifted to 15 °C and 0.005 rad/s, were of interest in view of the excellent correlation between ductility at 15 °C and 1 cm/min and the DSR function G'/(η'/G') at 15 °C and 0.005 rad/s (Chapter 4). These properties and the DSR function could be used to track the pavement aging of a binder in a way that should relate to the long-term pavement cracking performance of the binder. Table 9-5 reports these viscoelastic properties. Also shown are the values of the DSR function G'/(η'/G') and an estimated value of ductility, calculated from the ductility-DSR function correlation reported in Chapter 4 by using the equation shown in Figure 4-12.

Table 9-5. DSR Values of SH 21 Recovered Binder.

Station	Section	Year/Path	G' [a] (MPa)	η' [a] (MPa·s)	η'/G' (s)	DSR-Function G'/(η'/G') MPa/s	Calculated Ductility (Cm)
1277	Bottom	1996 Wheel	0.2146	66.0	307.4	0.000698	5.63
		2002 Center	0.2959	85.8	289.9	0.001021	4.76
		2002 Wheel	0.2727	74.6	273.6	0.000997	4.81
	Top	1996 Wheel	0.3237	92.4	285.3	0.001135	4.55
		2000 Center	0.3347	86.5	258.6	0.001294	4.29
		2000 Wheel	0.4011	93.3	232.7	0.001724	3.78
1295	Bottom	1996 Wheel	0.1745	62.2	356.6	0.000489	6.58
		2002 Center	0.1867	67.4	360.9	0.000517	6.42
		2002 Wheel	0.1175	51.2	436.1	0.000269	8.56
	Top	1996 Wheel	0.2623	75.6	288.2	0.00091	5.01
		2002 Center	0.237	74.6	314.9	0.000753	5.45
		2002 Wheel	0.4453	99.2	222.9	0.001998	3.54
1392	Bottom	1996 Wheel	0.0717	39.2	547.2	0.000131	11.75
		2002 Center	0.0346	26.1	754.6	0.000046	18.64
		2002 Wheel	0.0332	25.2	759.5	0.000044	19.05
	Top	1996 Wheel	0.2004	64.8	323.6	0.000619	5.93
		2002 Center	0.1893	61.7	325.9	0.000581	6.10
		2002 Wheel	0.2022	63.3	313.2	0.000646	5.83
1465	Bottom	1996 Wheel	0.3325	90.3	271.5	0.001225	4.40
		2002 Center	0.1172	50.0	426.9	0.000275	8.49
		2002 Wheel	0.0884	44.7	505.8	0.000175	10.35
	Top	1996 Wheel	0.2519	77.2	306.5	0.000822	5.24
		2002 Center	0.1809	63.1	348.7	0.000519	6.41
		2002 Wheel	0.1609	60.3	375.1	0.000429	6.97
1483	Bottom	1996 Wheel	0.1619	70.0	431.9	0.000374	7.41
		2002 Wheel	0.1656	63.5	383.7	0.000432	6.95
	Top	1996 Wheel	0.106	46.7	440.5	0.000241	8.99
		2002 Wheel	0.0926	42.1	455.1	0.000203	9.68
1500	Bottom	1996 Wheel	0.0902	43.1	477.6	0.000189	10.01
		2002 Wheel	0.1464	57.0	389.3	0.000376	7.39
	Top	1996 Wheel	0.136	53.7	394.9	0.000344	7.68
		2002 Wheel	0.181	62.2	343.3	0.000527	6.37

[a] Measured at 44.7 °C and 10 rad/s and then time-temperature shifted to 15 °C and 0.005 rad/s.

In order to add binder data from earlier measurements of the 1989 and 1992 cores (for which the more complete DSR measurements were not available), estimates of the DSR function were made based upon a comparison of function values to the low-shear-rate complex viscosity. Figure 9-6 shows the DSR function plotted versus η* measured at 60 °C and 0.1 rad/s (used as an approximate value of the limiting low-shear-rate complex dynamic viscosity, η^*_o) using both pavement binder and three methods of laboratory aging. The correlation is very good ($r^2 = 0.937$) and was used to estimate the DSR function values for the values of η^*_o that were previously reported on the 1989 and 1992 cores. (As will be discussed further, below, this correlation also was used to estimate the separate values of G' and η' in the DSR function by noting the specific path that this particular asphalt follows on the G' versus η' map.)

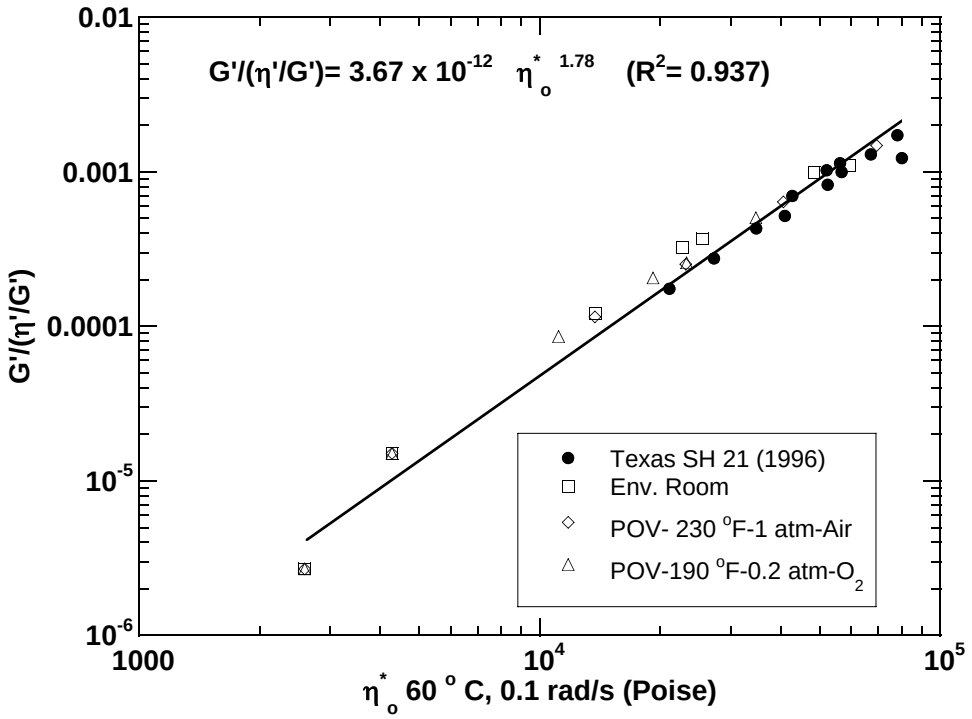

Figure 9-6. G'/(η'/G') Versus η^*_o Correlation.

Values of the DSR function estimates for binder recovered from the 1989 and 1992 cores, together with their measured values of η^*_o and measured data for the 1996 and 2002 cores are reported in Table 9-6. Corresponding estimates of ductility for all of these cores are reported in Table 9-7. The estimates are calculated from the ductility versus DSR function correlation described above and in Chapter 4.

Table 9-6. Values of η^*_o and the DSR Function for the SH 21 Cores.

Station	Lift	1989[a]		1992[a]		1996 Wheel Path		2002 Wheel Path		2002 Center Path	
		η^*_o	DSR Func.	η^*_o	DSR Func.	η^*_o	DSR Func.	η^*_o	DSR Func.	η^*_o	DSR Func.
1277	Top	11400	0.000064	-	-	56230	0.001135	78190	0.001724	67130	0.001294
	Middle	8200	0.000036	18200	0.0001477	-	-	-	-	-	-
	Bottom	8500	0.000038	-	-	42685	0.000698	56705	0.000977	52020	0.001021
1295	Top	-	-	30200	0.0003648	56420	0.00091	85165	0.001998	45050	0.000753
	Middle	-	-	45480	0.0007575	-	-	-	-	-	-
	Bottom	-	-	14000	0.000093	39900	˚0.000489	26600	0.000269˚	35565	0.000517˚
1392	Top	-	-	-	-	42700	0.000619	47235	0.000646	42785	0.000581
	Middle	-	-	-	-	23000	-	-	-	-	-
	Bottom	-	-	-	-	19540	0.000131	11875	0.000044	12172	0.000046
1394	Top	-	-	20800	0.0001875	-	-	-	-	-	-
	Middle	-	-	15800	0.0001148	-	-	-	-	-	-
	Bottom	-	-	30000	0.0003605	-	-	-	-	-	-
1465	Top	-	-	-	-	52335	0.000822	34690	0.000429	40945	0.000519
	Middle	-	-	22500	0.0002157	-	-	-	-	-	-
	Bottom	-	-	45300	0.0007522	80160	0.001225	21090	0.000175	27220	0.000275
1483	Top	-	-	13000	0.000081	26060	0.000241	30080	0.000203	-	-
	Middle	-	-	15500	0.0001109	-	-	-	-	-	-
	Bottom	-	-	24300	0.0002475	33285	0.000374	34940	0.000432	-	-
1500	Top	-	-	-	-	43600	0.000344	40350	0.000527	-	-
	Middle	-	-	-	-	-	-	-	-	-	-
	Bottom	-	-	-	-	24690	0.000189	32640	0.000376	-	-
1518	Top	-	-	-	-	-	-	-	-	-	-
	Middle	-	-	15000	0.0001046	-	-	-	-	-	-
	Bottom	-	-	-	-	-	-	-	-	-	-

[a] The DSR function of the 1989 and 1992 cores were estimated from the G /(η /G) versus η^*_o correlation.

Table 9-7. Estimated Ductility Values for the SH 21 Cores.

Station	Lift	1989		1992		1996		2002 Wheel		2002 Center	
		η^*_o	Est. Duct.	η^*_o	Est. Duct.	η^*_o	Est. Duct.	η^*_o	Est. Duct.	η^*_o	Est. Duct.
1277	Top	11400	16.1	-	-	56230	4.54	78190	3.78	67130	4.29
	Middle	8200	20.8	18200	11.15	-	-	-	-	-	-
	Bottom	8500	20.3	-	-	42685	5.63	56705	4.85	52020	4.76
1295	Top	-	-	30200	7.49	56420	5.01	85165	3.54	45050	5.44
	Middle	-	-	45480	5.43	-	-	-	-	-	-
	Bottom	-	-	14000	13.7	39900	6.58	26600	-	35565	-
1392	Top	-	-	-	-	42700	5.93	47235	5.82	42785	6.1
	Middle	-	-	-	-	23000	-	-	-	-	-
	Bottom	-	-	-	-	19540	11.75	11875	18.99	12172	18.63
1394	Top	-	-	20800	10.04	-	-	-	-	-	-
	Middle	-	-	15800	12.46	-	-	-	-	-	-
	Bottom	-	-	30000	7.53	-	-	-	-	-	-
1465	Top	-	-	-	-	52335	5.24	34690	6.97	40945	6.41
	Middle	-	-	22500	9.44	-	-	-	-	-	-
	Bottom	-	-	45300	5.45	80160	4.39	21090	10.35	27220	8.48
1483	Top	-	-	13000	14.52	26060	8.99	30080	9.69	-	-
	Middle	-	-	15500	12.65	-	-	-	-	-	-
	Bottom	-	-	24300	8.88	33285	7.41	34940	6.95	-	-
1500	Top	-	-	-	-	43600	7.68	40350	6.37	-	-
	Middle	-	-	-	-	-	-	-	-	-	-
	Bottom	-	-	-	-	24690	10.01	32640	7.39	-	-
1518	Top	-	-	-	-	-	-	-	-	-	-
	Middle	-	-	15000	12.98	-	-	-	-	-	-
	Bottom	-	-	-	-	-	-	-	-	-	-

Comparison of Field and Laboratory Hardening Rates

Of particular interest to this project is the rate at which pavement binders harden due to oxidation. Hardening results in an embrittlement of the binder that decreases its ability to sustain deformation without cracking. Three questions are especially relevant: 1) How quickly does hardening occur on the road? 2) How do hardening rates vary with pavement depth? and 3) How do pavement hardening rates compare to laboratory hardening rates? From the data reported above, we reviewed two hardening rate parameters and compared them to their corresponding laboratory hardening rates.

The first of these hardening properties is the ZSV, approximated by η^* measured at 60 °C and 0.1 rad/s. Figure 9-7 shows changes in η^*_o over time. As was noted before from Figure 9-4 and based on common HS, the top and bottom lifts of station 1277 are likely constructed from the same asphalt. The same can be said for the bottom and top lifts of station 1295. However, while the two lifts appear to be the same at each station, these two stations do not appear to have the same asphalt because of their different hardening susceptibilities (Figure 9-4). Thus, some care is warranted in comparing their hardening rates. With that caution, note that the 1277 bottom and top lifts have the same hardening rates from 1989 to 1996 (0.23 ln poise/year). Recall that the top lift is 0 to 2 inches from the surface of the pavement and the bottom lift ranges from 4 to 6 inches below the surface. A hardening rate that deep into the pavement being the same as the top 2 inches is a surprise. However, the 1465 bottom lift, apparently the same binder because of its HS, appears to have a lower hardening rate, 0.14. However, comparing the two lifts at station 1295, we see that the bottom lift rate is actually higher than that of the top lift (0.26 ln poise/year versus 0.16) and these rates vary by the same amounts as the 1277 rates and the 1465 rate. Further, lift 1483 top, which has approximately the same hardening susceptibility as the 1295 bottom and top lifts, has essentially the same hardening rates as the 1295 top lift (0.17 versus 0.16 ln poise/year). Also, the 1277 middle lift has a hardening rate of 0.27 ln poise/year, but its hardening susceptibility was 8.6 (Figure 9-4), and so how its rate should compare to the other lifts is open to question. The second hardening property that was assessed was the DSR function $G'/(\eta'/G')$, and these results are shown in Figure 9-8. The rates follow the same trends and lead to the same conclusions as the ZSV and will not be discussed further.

So, while there is some uncertainty to the data that is complicated by a fairly limited data set, the indications to date are that asphalt hardening is not seriously impeded by a few inches (4 inches in this work) of dense-graded pavement above it. This result seems contrary to intuition, however, based on the dual assumptions of impeded access to oxygen by pavement at deeper levels and lower summertime temperatures below the surface. On the other hand, pavements do breathe as daily temperature fluctuations pump air in and out of the pavement and temperatures below the surface are not cooled as quickly as the surface by nighttime decreases in air temperature. The net result to date is that more data are needed to add statistical weight to this conclusion regarding hardening rate as a function of pavement depth. In the meantime, it is a very intriguing result that bears on the issues of pavement performance, pavement maintenance and rehabilitation, and perpetual pavements.

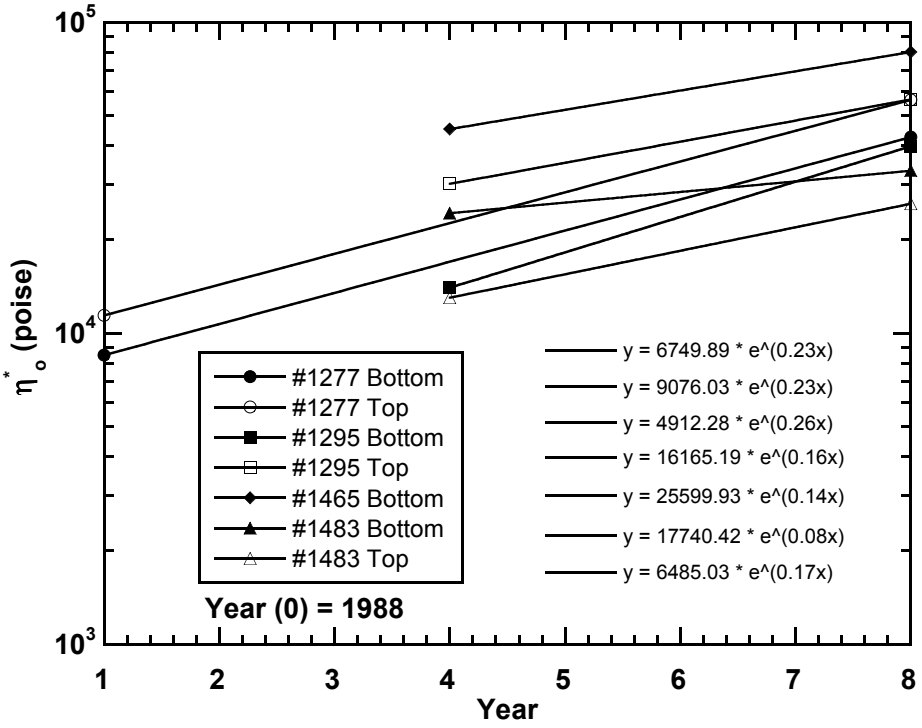

Figure 9-7. Binder η^*_o Hardening Over Time in SH 21.

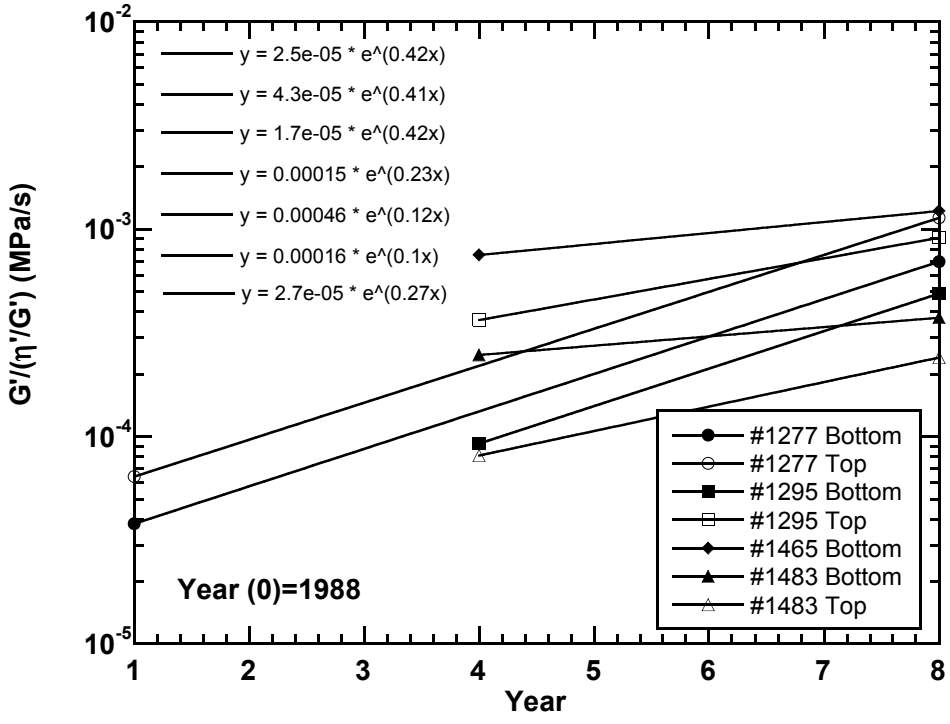

Figure 9-8. Binder DSR Function Hardening Over Time in SH 21.

Figures 9-9 and 9-10, respectively, show η^*_o and DSR function values over time that result from 60 °C environmental room aging and PAV aging at 90 °C in thin (0.86 mm) films. The data were reported in Chapter 6. The two points shown at zero time, are the unaged and post RTFOT aged values, with the latter used to approximate hot-mix plant and construction aging; these points fall well below the constant-rate aging period and define the beginning of the initial jump. Shown on each aging line for the two laboratory aging methods are points that correspond roughly to the binder condition after four and eight years in the pavement (1992 and 1996 cores). These cores were chosen because the pavement binder is beyond the initial jump by this time, and the 2002 cores are almost certainly impacted by the chip seal and overlay that were placed in 2000 and, thus, do not give a reliable indication of pavement aging (discussed below). Station 1277 values were taken to represent road aging rates, although, as has been seen in previous graphs, there is considerable variability, station to station and lift to lift, in actual levels of aging. This variability may be due largely to the state of the binder upon leaving the hot-mix plant. These comparisons suggest that one year in SH 21 is very roughly equivalent to one month in the environmental room and 10 hours in the PAV (90 °C, 20 atm air, 0.86 mm films).

The third question to be addressed was how binder hardening rates from pavements compare to laboratory hardening rates. For this calculation, we used the hardening rates of stations 1277 (both top and bottom lifts) and 1465 bottom as these binders had the same hardening susceptibility as the binder studied in the laboratory. Laboratory values of hardening rates (both ln viscosity and ln DSR function during the constant-rate period) at several aging conditions were reported in Chapter 6. Results from two of these conditions are summarized in Table 9-8 along with comparisons between the laboratory and field aging rates. Based on these calculations, and subject to the data limitations discussed above, we estimate that the environmental room constant-rate aging is about 15 times faster than in the pavement, or, in other words, one month in the environmental room is about 15 months in the pavement, once the initial jump is past. This relative hardening rate is about the same whether viscosity or the DSR function is adopted as the measure of hardening. It should be noted that this estimate is valid only for SH 21 and subject to considerable error. Nevertheless, it is probably the best estimate available anywhere. Note that the PAV aging in thin films, 90 °C and for 20 hours, accelerates aging by a factor of the order of 1000. Thus, about nine hours in the PAV (90 °C, 20 atm air, 0.86 mm films) ages approximately one year in the field, after the initial jump.

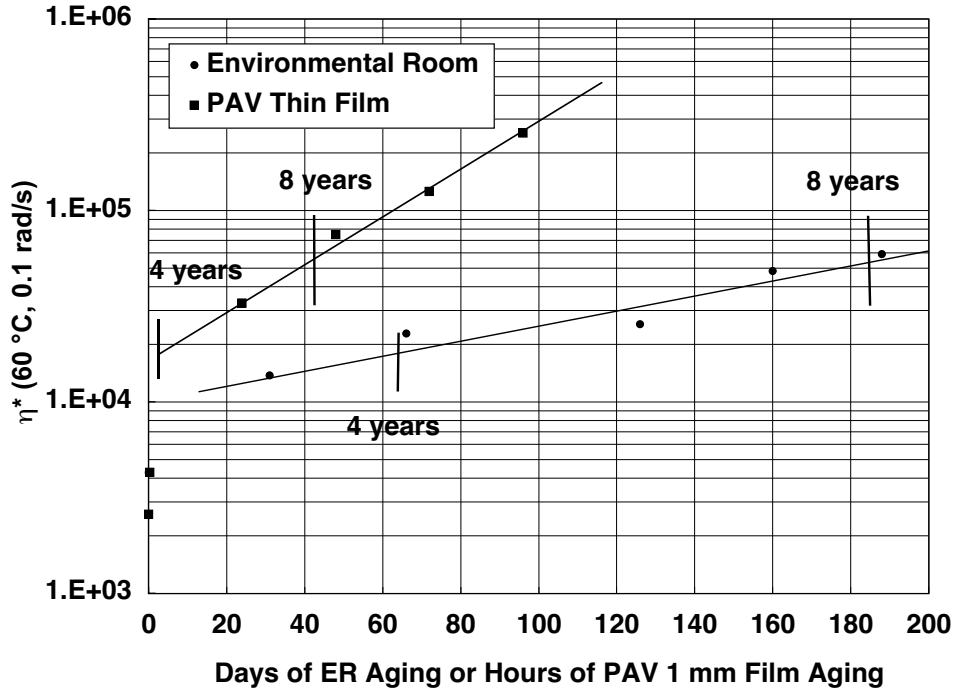

Figure 9-9. η_o* Hardening Rates: ER versus Thin-Film PAV versus SH 21.

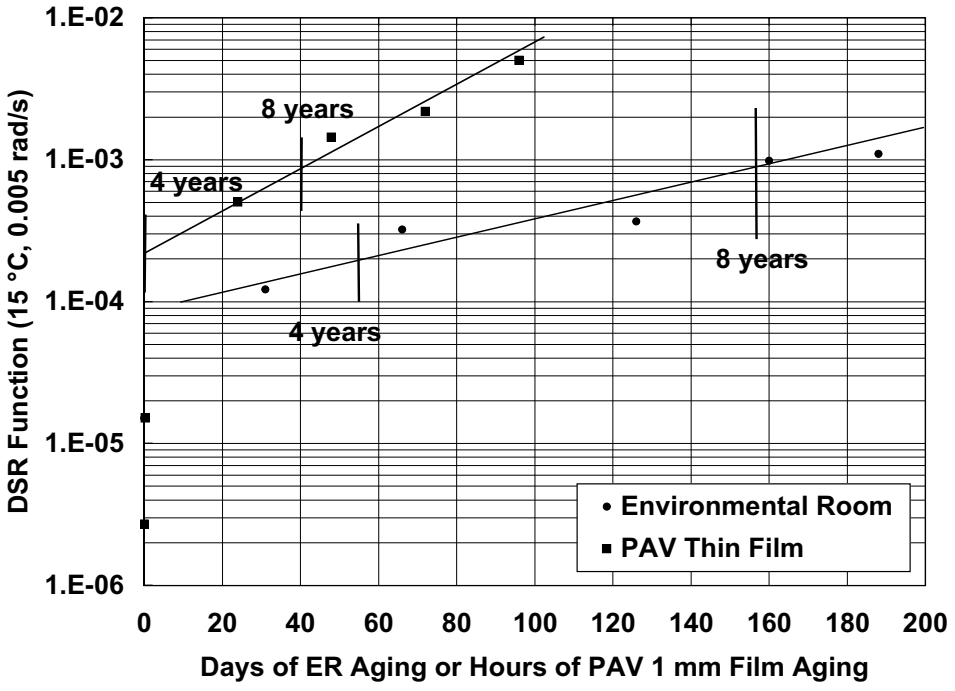

Figure 9-10. DSR Function Hardening Rates: ER versus Thin-Film PAV versus SH 21.

Table 9-8. Field and Laboratory Exxon AC-20 Hardening Rates.

Aging Method	η^*_o Hardening Rate[a] (η^*_{HR}) (ln(Poise)/day)	$\frac{(\eta^*_{HR})}{(\eta^*_{HR})_{Field}}$	DSR Function Hardening Rate (R_{HR}) (ln(MPa/s/day)	$\frac{(R_{HR})}{(R_{HR})_{Field}}$
POV at 90 °C, 20 atm Air	0.673	1225	0.74	812
Environmental Room	0.0088	16	0.014	15
Field (SH 21)[b]	0.000549	1	0.000911	1

[a] Constant-rate Period hardening rate; laboratory values are from Chapter 6.
[b] From stations 1277 (T and B) and 1465 (B), including 1989 cores; thus, these rates may not be out of the initial jump period and may be somewhat high.

Tracking Pavement Aging

In Chapter 4, a relationship between ductility and DSR properties was reported that provides a rationale for tracking binder pavement aging to the point of road performance failure (Figure 4-11). All asphalts that have been studied (twenty to date) follow this same correlation, in spite of having rather distinct DSR properties as indicated by their decidedly different aging paths across a G' versus η'/G' map (Figure 4-10a). Furthermore, literature reports suggest that a value of 15 °C ductility in the range of 3 cm is a danger threshold for pavement failure. Thus, tracking pavement binder properties across this DSR map as it approaches the 3-cm boundary could be expected to relate to age-related pavement performance.

Figure 9-11 compares field-aged binder from two stations of SH 21 to three laboratory-aging conditions. The stations reported are those that are the same binder as that sampled when the pavement was placed, based on hardening susceptibility. Note that, for each station and year, there are two identical symbols, indicating top and bottom lifts of that station. In general, the top lift is more aged than the bottom, and this result serves to identify the top versus the bottom lift. Each of these symbols is an average of at least two replicate recovery extractions. Note that the pavement binders trace a rather well-defined path from lower right to upper left as the binder ages. The dashed lines are lines of constant 15 °C ductility and are calculated from the correlation reported in Chapter 4. The environmental-room aging path lies very close to the pavement binder path. The POV-aged materials are somewhat offset from the pavement binder, due to the different aging conditions.

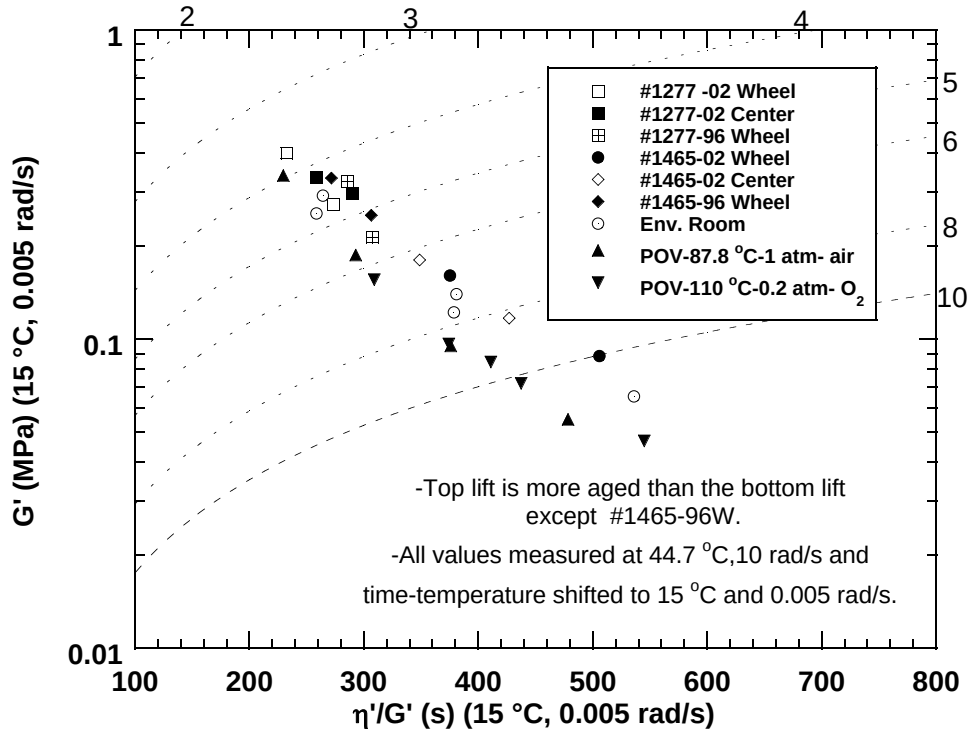

Figure 9-11. The G' versus η'/G' Map of Lab- and Field-Aged Exxon AC-20 (Dashed lines are constant 15 °C ductility, cm).

Figure 9-12 includes all of the stations studied from 1996 and 2002 cores. Again, both top and bottom lifts are included, and each symbol is an average of multiple replicates. In spite of having different HS values, binders from the other stations follow the same aging path, not necessarily an expected result. Note that in most cases the top lift is more heavily aged than the bottom lift, although the difference is surprisingly small in some cases. A good example is station 1277, which shows little difference between top and bottom lifts and also little difference between 1996 and 2002 cores. The most heavily aged SH 21 binder was recovered from station 1295 2002 cores in the wheel path and had a calculated ductility of 3.5 cm. (The Crescent Drive sample was recovered from a city street for comparison and is decades old; hence its very low ductility, less than 3 cm. It should be noted that the condition of this pavement is very poor.) We might expect that SH 21 would be close to age-related failure, based on the literature reports of ductility and pavement performance. However, this is not necessarily true and likely depends upon the overall pavement system stiffness.

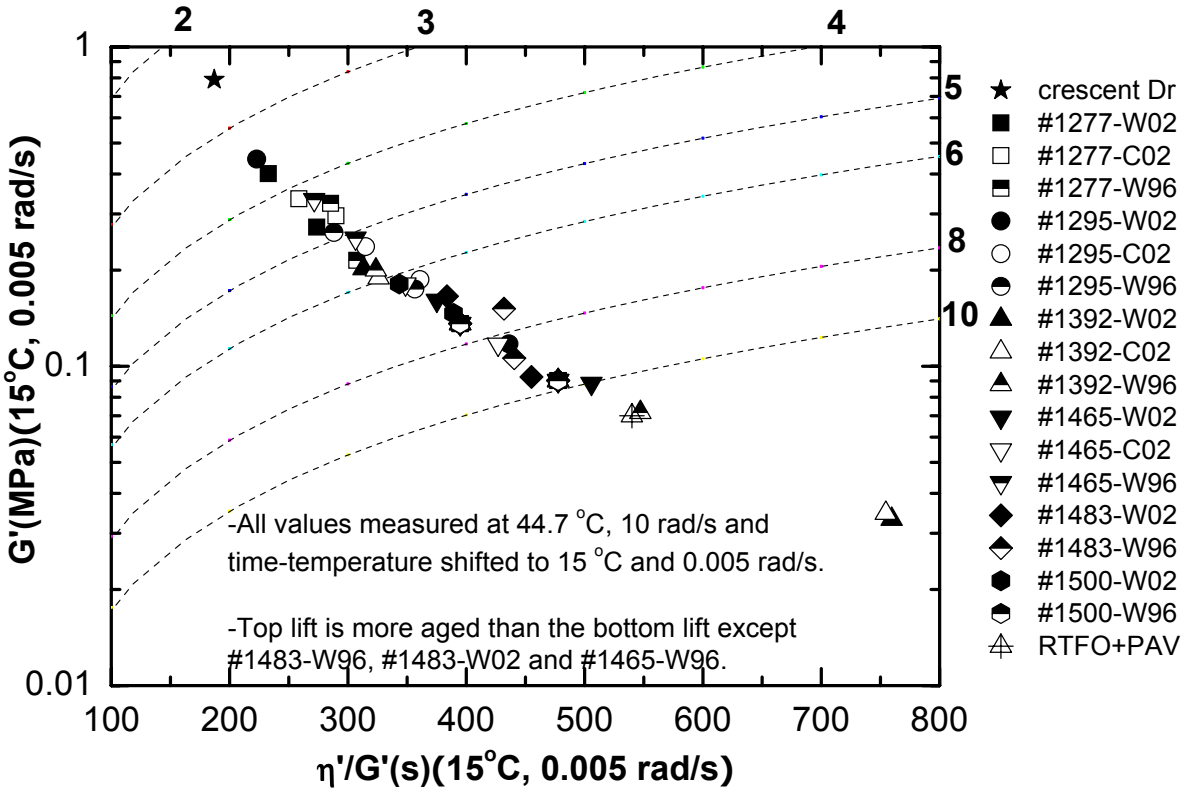

Figure 9-12. The G' versus η'/G' Map for All SH 21 Recovered Binders (Dashed lines are constant 15 °C ductility, cm).

The DSR function values reported in Table 9-6 (both measured values, for 1996 and 2002 cores, and estimated values, for pre-1996 cores) are plotted versus year in Figure 9-13. This shows the dramatic change in hardening rate between 1996 and 2002. One could hypothesize that this rate change is the result of the seal coat and overlay blocking air to the now-deeper lifts. However, this explanation would not account for the actual reduction in hardening that has occurred in several cases. The reduction also occurs in bottom lifts, leading to speculation that the seal coat penetrates inches into the pavement. This is an intriguing possibility that should be studied further. LTPP results that bear on this conclusion are reported in the next section.

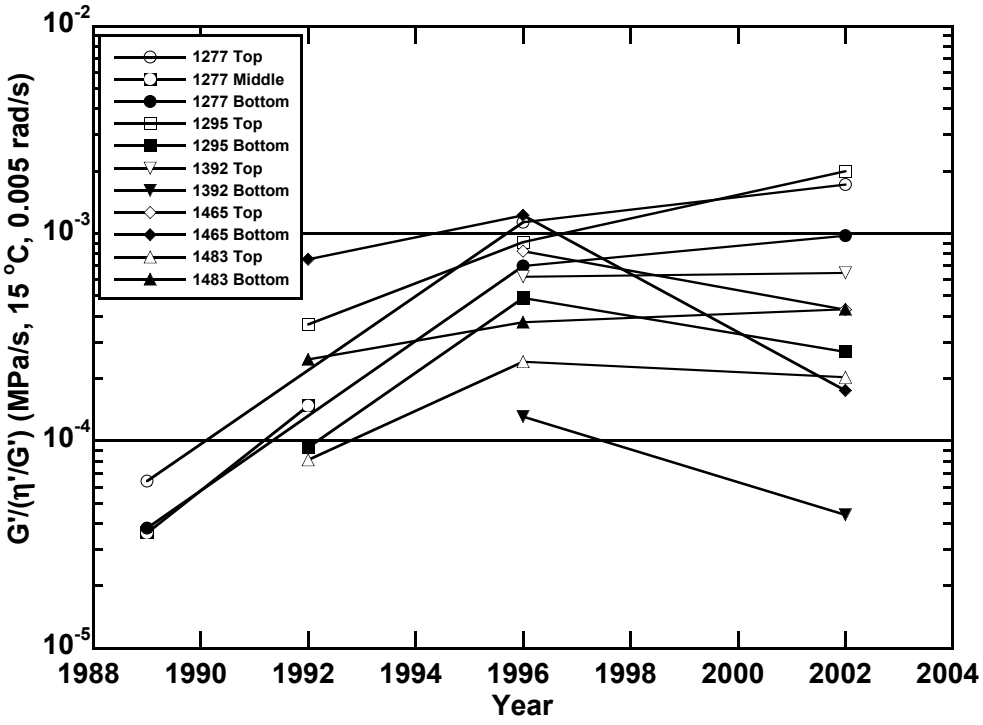

Figure 9-13. DSR Function Values of Recovered Binders, All Years.

The range of calculated ductilities (and also DSR function values) of the recovered binders is rather surprising. At one extreme is station 1392 bottom, a 2002 core with a calculated ductility in excess of 20 cm (low DSR function). At the other extreme is another 2002 core, station 1295 top (high DSR function), as mentioned above. This wide range, in large part, is likely due to the seal coat and overlay(s) placed in July 2000, in addition to the apparent considerable range in starting values, probably as the result of different hot-mix plant aging. Note that the same lift was sampled in each year in spite of the overlay; i.e., the top lift, prior to 2000 was the surface lift, whereas after 2000, the top lift was no longer at the surface.

Figure 9-13 gives a more complete view of binder pavement aging over an extended period of time. This figure includes all top and bottom lift data in Table 9-6 for station 1277, but it should be noted that for the pre-1996 data the points are plotted based on estimates. It was previously explained that values of the DSR function were estimated from ZSV values together with the correlation for the Exxon AC-20 binder shown in Figure 9-6, and these values are shown in Table 9-6. However, these estimates are not sufficient for plotting points on the DSR map because the separate values of G' and η'/G' are not known. However, by using the known path for this binder across the DSR map (Figure 9-12), these individual values can be determined (for the presumed value of the DSR function) by trial and error and then the point located on the map. For comparison, the Exxon AC-20 PAV-aged (100 °C, 20 hour, after RTFOT) sample also is plotted (using ZSV value of 16,000 poise from Chapter 3, Figure 3-6) by the same estimation procedure.

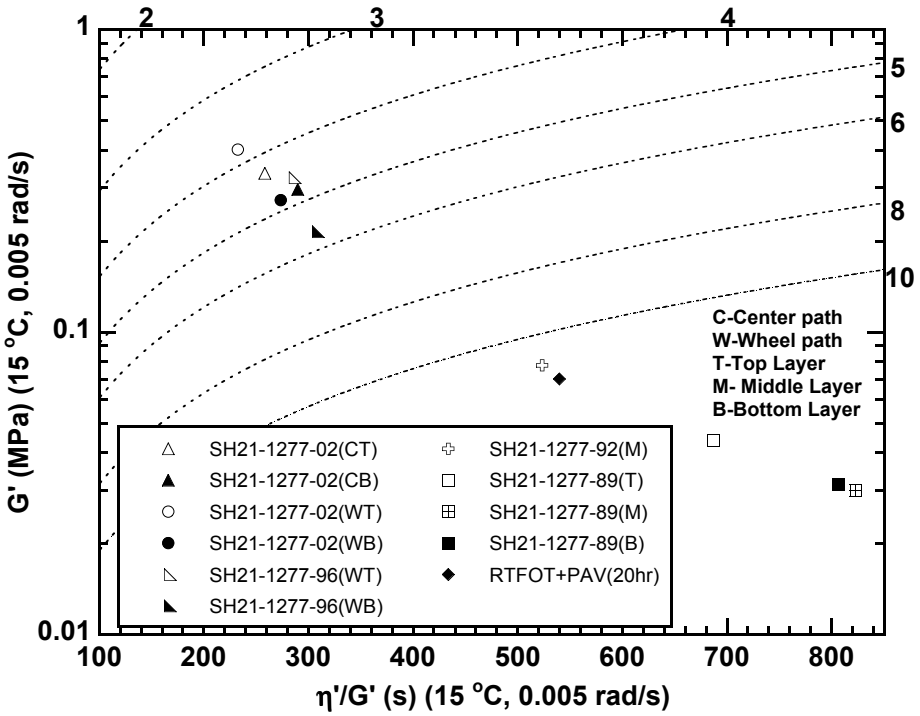

Figure 9-14. Movement of Binder Across the DSR Map, Station 1277.

During service, the binder from these 1277 lifts moves from the lower right to the upper left on the DSR map. The binder recovered from the 1989 cores is at the lower right in Figure 9-14, and the binder from the 2002 cores is at the upper left where calculated ductility values range from 4 to 5 cm. In 1992, the binder was near 10 cm, and by 1996, it was between 5 and 6 cm. For the most part, the recovered binders from these 1277 lifts show a relentless track across the DSR map. For comparison, the RTFOT plus PAV point is aged to about 12 cm, close to the 1992 recovered binder value. It should be noted that the 2002 binders likely are softened by the seal coat placed in 2000, as discussed below, accounting for the relatively small decrease in calculated ductility from 1996 to 2002, compared to the changes observed in prior years.

Station 1465 provides an interesting contrast to 1277, and these data are shown in Figure 9-15. The binder from station 1465 (bottom lift) recovered in 1992 aged in the pavement to a ductility near 5 cm, comparable to the 1996 value for station 1277. This 1465 lift binder evidently started out much more heavily aged at the time of pavement placement than did the 1277 lift binders. This difference also was seen in Figure 9-13 where the 1992 data for 1465 bottom unquestionably has the highest DSR function value. Then, in 1996, the binder ductility has fallen to nearly 4 cm. By 2002, however, a sharp reversal has occurred that we believe is due to the seal coat placed in July 2000. The 2002 binder ductility values range from 8 to 10 cm, significantly greater than the 1996 value, or even the 1992 value. These are surprising results that are well out of line with measurement error.

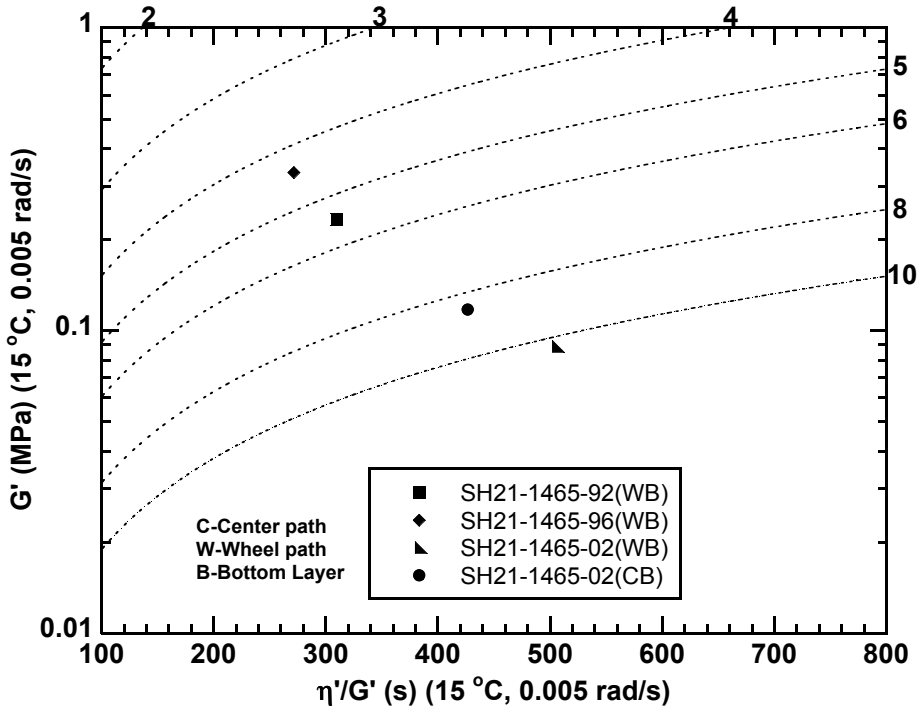

Figure 9-15. Movement of Binder Across the DSR Map, Station 1465.

From these results, we conclude that for this binder and this pavement, the RTFOT plus 20-hour PAV aging corresponded to about four years in the pavement after hot-mix plant and placement aging. Also, 14 years in the pavement aged the binder to a ductility of approximately 4 cm, short of the 3 cm level that might suggest approaching failure. However, it should be remembered that the seal coat appears to have slowed or even reversed aging to a significant degree.

Further comparisons of field aging rates to laboratory aging are useful. Recall that asphalts age in an initial rapid aging period, and this is followed by a constant-rate period that continues indefinitely, at least from a practical viewpoint, in the absence of diffusion limitations. See for example Figure 6-1 in which aging during the constant-rate period can be described by a straight line whose zero-time intercept is termed the initial jump and whose slope is the aging rate after the initial jump is completed (see the discussion in Chapter 6). To put some time scale to the initial jump, short-term aging (RTFOT or hot-mix aging) is not sufficient to move past this rapid-rate region. Consequently, time comparisons of aging tests with each other or with field aging, as is the current interest, is not straightforward.

Texas LTPP Pavements

The LTPP sites studied in this project were identified earlier (Figure 9-1 and Table 9-1). Table 9-9 provides additional pavement details. Note that pavement construction varies significantly from site to site. The thinnest pavement is 1.8 inches and the thickest is 12.9 inches. And, of course, there are multiple lifts and even seal coats and overlays that complicate performance analysis considerably. Also, note that six pavements went out of study before 2002 and were not available for a second coring (48-1049, 48-1050, 48-1060, 48-1109, 48-3679, and 48-3689), and one pavement was placed in 1991, so there was no 1989-1990 core (48-3835).

Experimental Data

For each core, one layer was targeted for study, the original surface layer (OSL in Table 9-9) at the time the pavement was first constructed. In some cases, this was the current surface layer (48-1049, 48-1060, 48-1109, 48-2108, 48-3679, and 48-3689); for others, it was buried below other layers (48-1046; e.g., which was converted to I 40 in 1971, requiring a much thicker pavement). Ideally, it would have been desirable if each LTPP site could have been studied over time. However, as noted above, only seven of the 16 sites provided cores for both 1989-1990 and 2002 cores (Table 9-1). Nine sites provided cores for only one year. For pavements having overlays on top of the olriginal surface layer (OSL), testing these layers would provide additional valuable data on binder condition versus time in the road, but such additional tests were beyond the resources of this project.

Each core was either sawn or cleaved into lifts (while frozen), and the target lift was further broken into pieces. Then, in two replicates (A and B) the broken core was sampled, extracted, and recovered, and the binder analyzed. Binder physical properties, including the estimated binder ductility (based on the correlation presented in Chapter 4), appear in Table 9-10.

Tracking Pavement Aging

The DSR properties for both replicate extractions for each core are plotted on the DSR function map in Figures 9-16 and 9-17. Figure 9-16 shows data for which cores were taken in two years; Figure 9-17 shows data for which a core was taken in only one year. In both figures, the 1989-90 cores are denoted with solid symbols, whereas the 2002 cores are indicated with open symbols. Note that these LTPP data points are much more spread out along a given constant-ductility curve (dashed line) than were the SH-21 data, as would be expected for a variety of binders that likely follow different aging paths across the G' versus η'/G' map. For easy reference, the date that the pavement OSL was placed is noted in parentheses in the legend for the 1989-1990 cores. Additionally, the legend for the 2002 cores contains any relevant information on maintenance to the road. For example, 48-1056 had a strip seal treatment in 1988 (before the 1989 coring) and a seal coat in 2000. Replicate samples generally gave very similar results with the estimated ductility differing by less than 1 cm. The only exceptions to this degree of similarity are for 2002 cores and may have been caused mostly by sampling of the broken core combined with maldistribution of the seal coat material throughout the core.

Table 9-9. Details of the Pavement Layers for the LTPP Sites.

LTPP Site	Road/County	Top Layer	2nd Layer	3rd Layer	4th Layer	5th Layer	6th Layer	7th Layer	Total (in)
48-1046	IH 40 Carson	HMA (0.4)1971	O/L HMA (1.7)1971	I/L Geotextile (0.1)1971	HMA (1.9)1971	HMA (6.4)1971	OSL HMA (1.1)5/55	HMA (1.3)	12.9
48-1049	US 59 Nacogdoches	OSL HMA (1)1984	HMA (3.6)	S/C (0.5)					5.1
48-1050	SH105 Grimes	OSL HMA (1)1984	S/C (0.8)						1.8
48-1056	US 83 Ochiltree	S/C (0.4)7/00	S/S 10/88	OSL HMA (1.8)1969					2.2/1.8
48-1060	US 77 Refugio	OSL HMA (1.7)1986	HMA (5.8)						7.5
48-1068	SH 19 Lamar	O/L HMA (1.5)11/00	S/C 7/28/99	S/F 10/92	OSL HMA (3.1)1985	HMA (7.8)			12.4
48-1109	SH 19 Walker	OSL HMA (0.9)1984	HMA (5.4)						6.3
48-1168	FM 564 Wood	S/C (0.4)2001	S/E 1991	OSL HMA (0.8)1985	S/C (0.4)				1.6
48-2108	Loop 197 Galveston	OSL HMA (3)1985							3
48-2133	Loop 363 Bell	S/C (0.4)8/00	OSL HMA (1.6)1984	S/C (0.6)					2.6/2.2
48-3679	SH 103 Angelina	OSL HMA (1.6)1988							1.6
48-3689	US 190 Polk	OSL HMA (1.1)1987	HMA (1.6)	S/C (0.4)					3.1
48-3769	US 62 El Paso	S/C rubber (0.4)1986	OSL HMA (2)1976						2.4
48-3835	SH 6 Brazos	O/L (1.8)6/00	O/L S1.5/N5.5 6/00	CR/S (0.4)9/92	OSL HMA (1.8)1991				S5.5/N9.5
48-6086	IH 37 Live Oak	O/L HMA (1.5)1985	S/C (0.2)1985	OSL HMA (1.2)1971	HMA (1.2)	HMA (6.1)			10.2
48-9005	FM 1560 Bexar	O/L HMA (1.1)9/98	S/C (0.4)9/98	OSL HMA (1.1)1986	S/C (0.4)				3/1.5

CR/S-Crack Seal; HMA-Hot-Mix Asphalt; I/L-Inner Layer; O/L-Overlay; OSL-Original Surface Layer; S/C-Seal Coat; S/E-Edge Seal; S/S-Strip Seal

Table 9-10. Binder Properties of the LTPP Cores.

LTTP Site		Const Date	Road / County	1989 or 1990					2002				
				η_o(poise) at 60 °C 0.1 rad/s	η'(MPa•s)[a] at 15 °C 0.005 rad/s	G'(MPa)[a] at 15 °C 0.005 rad/s	DSR Func[a] at 15 °C 0.005 rad/s	Calc Duct (cm)	η_o*(poise) at 60 °C 0.1 rad/s	η'(MPa•s)[a] at 15 °C 0.005 rad/s	G'(MPa)[a] at 15 °C 0.005 rad/s	DSR Func[a] at 15 °C 0.005 rad/s	Calc Duct (cm)
48-1046	A	9-1-55	I 40	813,087	79.14	0.70434	0.006268	2.1	55,580	38.38	0.14396	0.000540	6.3
	B		Carson	516,476	73.43	0.5784	0.004556	2.5	40,180	30.17	0.10378	0.000357	7.56
48-1049	A	6-1-84	US 59	36,820	34.72	0.1095	0.000345	7.7	NA	NA	NA	NA	NA
	B		Nacogdoches	41,970	35.68	0.11618	0.000378	7.4	NA	NA	NA	NA	NA
48-1050	A	3-1-84	SH 105	95,710	92.75	0.45016	0.002185	3.4	N/A	NA	NA	NA	NA
	B		Grimes	89,280	85.92	0.41668	0.002021	3.5	NA	NA	NA	NA	NA
48-1056	A	6-1-69	US 83	56,790	23.12	0.09331	0.000377	7.4	18,070	11.57	0.03806	0.000125	12
	B		Ochiltree	65,420	22.95	0.09733	0.000413	7.1	15,960	11.17	0.03135	0.000088	14
48-1060	A	3-1-86	US 77	83,730	57.17	0.2434	0.001036	4.7	NA	NA	NA	NA	NA
	B		Refugio	97,620	73.65	0.32246	0.001412	4.1	NA	NA	NA	NA	NA
48-1068	A	11-1-85	SH 19	NA	NA	NA	NA	NA	39,990	30.68	0.10172	0.000337	7.75
	B		Lamar	NA	NA	NA	NA	NA	38,680	25.42	0.08387	0.000277	8.46
48-1109	A	2-1-84	SH 19	78,760	56.83	0.2295	0.000927	5.0	NA	NA	NA	NA	NA
	B		Walker	91,870	57.96	0.24424	0.001029	4.8	NA	NA	NA	NA	NA
48-1168	A	9-1-85	FM 564	NA	NA	NA	NA	NA	30,760	39.34	0.09441	0.000227	9.23
	B		Wood	NA	NA	NA	NA	NA	41,990	59.36	0.1721	0.000499	6.53
48-2108	A	8-1-85	Loop 197	68,820	77.84	0.29428	0.001113	4.6	173,860	101.68	0.58064	0.003316	2.84
	B		Galveston	64,850	65.51	0.24098	0.000886	5.1	160,283	103.7	0.58198	0.003266	2.85
48-2133	A	5-1-84	Loop 363	52,810	54.54	0.18262	0.000611	6.0	55,810	54.73	0.1921	0.000674	5.72
	B		Bell	60,040	59.1	0.20676	0.000723	5.5	50,630	53.48	0.17566	0.000577	6.12
48-3679	A	6-1-88	SH 103	34,030	40.97	0.12188	0.000363	7.5	NA	NA	NA	NA	NA
	B		Angelina	28,720	36.48	0.10092	0.000279	8.4	NA	NA	NA	NA	NA
48-3689	A	4-1-87	US 190	20,810	25.81	0.06049	0.000142	11.4	NA	NA	NA	NA	NA
	B		Polk	19,990	24.44	0.05519	0.000125	12.0	NA	NA	NA	NA	NA
48-3769	A	6-1-76	US 62	50,410	45.21	0.18428	0.000751	5.5	49,380	47.94	0.18874	0.000743	5.48
	B		El Paso	67,130	50.97	0.22948	0.001033	4.7	76,330	61	0.29018	0.001380	4.17
48-3835	A	10-1-91	SH 6	NA	NA	NA	NA	NA	40,270	77.57	0.21238	0.000581	6.1
	B		Brazos	NA	NA	NA	NA	NA	35,590	66.85	0.16582	0.000411	7.1
48-6086	A	6-1-71	I 37	21,230	38.06	0.08192	0.000176	10.3	56,980	41.44	0.1445	0.000504	6.5
	B		Live Oak	24,800	41.37	0.09758	0.000230	9.2	55,240	39.55	0.13692	0.000474	6.67
48-9005	A	7-1-86	FM 1560	50,060	76.3	0.25248	0.000000	5.2	33,090	46.95	0.13674	0.000398	7.21
	B		Bexar	55,780	84.41	0.29678	0.000000	4.7	27,760	33.5	0.08791	0.000231	9.16

NA- Not Available; A and B are replicate extractions.

[a] η', G' measured at 45 °C, 10 rad/s and converted to 15 °C, 0.005 rad/s by TTSP. DSR Function is G'/(η'/G').

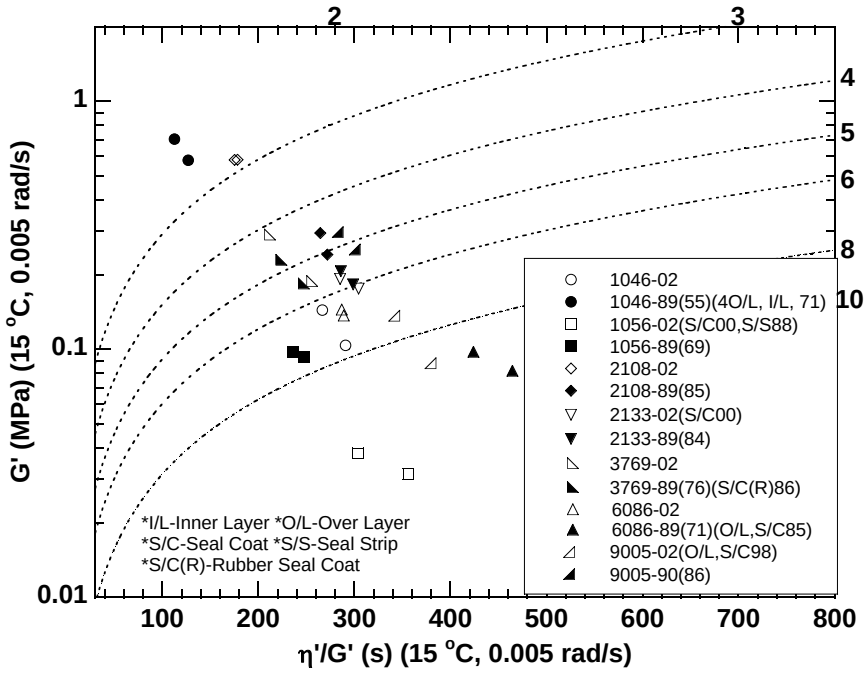

Figure 9-16. DSR Function Map for LTPP Sites That Have Cores in Two Years.

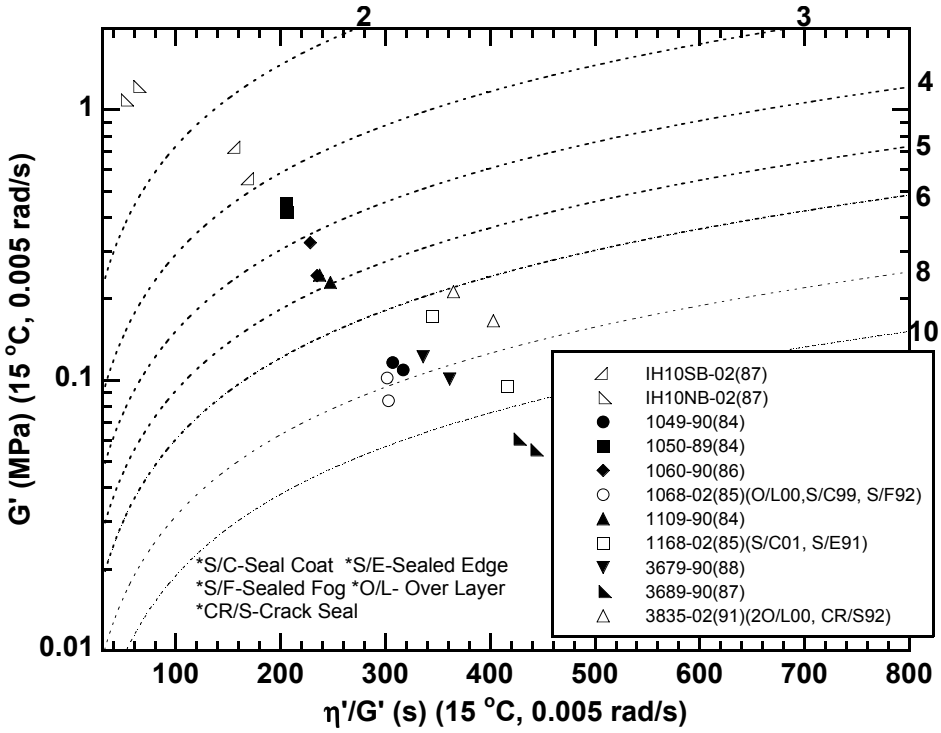

Figure 9-17. DSR Function Map for LTPP Sites That Have Only One Core.

In the normal course of aging, a binder moves across the G' versus η'/G' map toward the top left corner. This was observed to be the case for all laboratory-aged binders that have been studied and was the case for SH 21 until the 2002 cores that we believe were softened by seal-coat penetration.

While this normal trend is followed by two of the LTPP sites shown in Figure 9-16 (48-2108 and 48-6086), for the others it is not, with binders either not stiffening (48-2133 and 48-3769) or actually softening with time (48-1046, 48-1056, and 48-1168). We believe that this non-stiffening behavior also is due to seal coats applied to the pavements, and this hypothesis is discussed, below.

Effect of Seal Coats on Binder Stiffness

The LTPP binders of Figures 9-16 and 9-17 are plotted again in Figure 9-18 in the form of calculated ductility versus years of service of the OSL (time from placement to coring), irrespective of whether this lift has been overlaid or not. Also included in this figure are the data from station 1277 of Texas SH 21. Sites for which there are multiple data points are connected by arrows, and key LTPP sites are identified by their site number. Finally, pavements that have not been treated with a seal coat (or strip seal) of any kind are indicated by solid symbols, while those that have are indicated by open symbols.

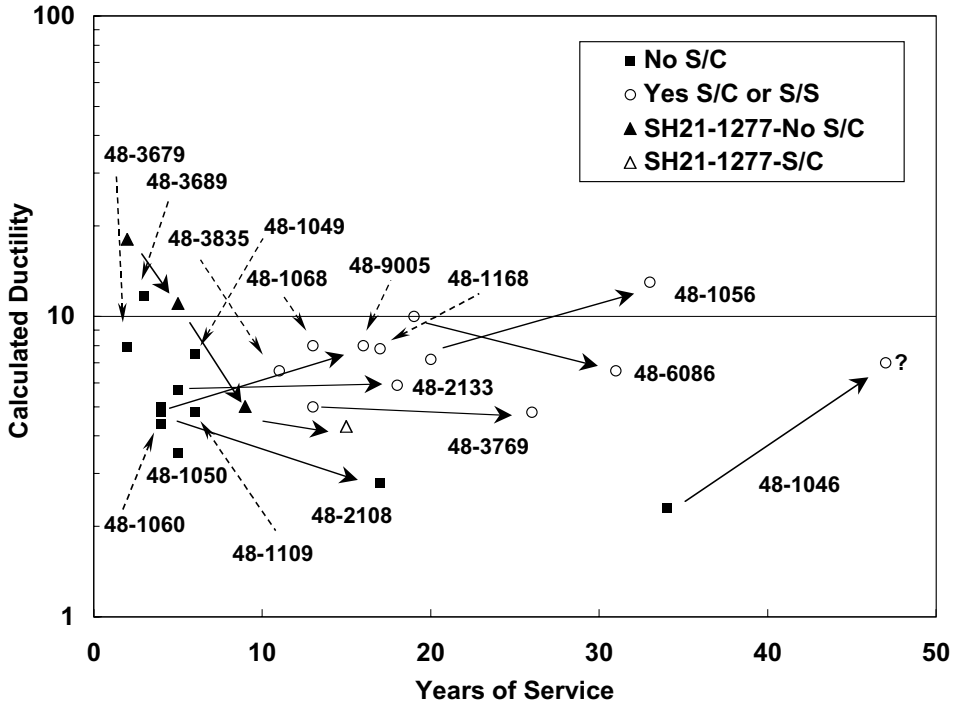

Figure 9-18. Binder Calculated Ductility as Pavements Age and Effect of Seal Coats.

The striking feature of Figure 9-18 is that there is a fairly clear dividing line between binders from pavements that have not been treated with sealant and those that have. Binders to the right of the SH 21 path are high in both service life and ductility and also have been exposed to a sealant. Of particular note are sites 48-1046, 48-1056, and 48-9005, all of which experienced dramatic increases in binder ductility upon additional years of service and had seal coats placed between the first (1989-1990) coring and the second (2002). Site 48-1056 also had a strip seal in 1988, before the first coring and this likely accounts for its fairly high ductility after 20 years of service. This interpretation of site 48-1046 is somewhat questionable, however, as the OSL is some 10 inches below the seal coat, and it seems quite surprising that a pavement layer this far down from the surface would be so greatly affected by a seal coat.

Sites 48-2133 and 48-3769 show no change in ductility with service beyond the first coring, contrary to expectations, but these sites also had seal-coat exposure. Site 48-2133 had a seal coat placed in 2000. It is plausible that the OSL was softened by the seal coat to a higher ductility than the first coring and then continued to age after the seal coat just enough to bring the binder back to the first-coring ductility. Site 48-3769 had no seal coat between the first and second coring, but it too showed no net decrease in binder ductility. In this case, we speculate that the seal coat first softened the binder in the OSL, giving it a fairly high ductility for a 13-year old binder (placed in 1976 and cored in 1989), and then may actually have protected the binder against further hardening. This protection could be two fold as the seal coat contained a rubber modifier. These modifiers have been shown to retard the hardening effects of oxidation, but also, it is possible (and this is pure speculation) that small rubber particles served to seal the OSL from further access to air. If so, this is potentially a very important mechanism for furthering pavement life, and this hypothesis bears further study.

Sites 48-2108 and 48-6086 were mentioned earlier as the two LTPP sites that continued to harden over time. Note that both of these sites had no seal coat of any kind between the first and second corings. It should also be noted, however, that 48-6086 had a seal coat placed in 1985, together with a new overlay. This seal coat apparently resulted in the OSL having a much higher calculated ductility (10 cm) in 1990 than would be expected after 19 years of service. Then, with no further seal coats between corings, continued aging reduced its ductility from that point on.

The recovered binders that have not been exposed to sealants are mostly in fairly young pavements with the exception of 48-2108 and 48-1046 (both previously discussed) and have all gone out the LTPP study for various reasons, mostly because of extensive rehabilitation or reconstruction. Information that has been reported is:

- 48-1049 – reconstructed because of extensive rutting (supposedly on adjacent section of the highway), last visited 3/28/96;
- 48-1050 – reconstructed because of extensive oppoing lane fatigue, last visited 5/11/95;
- 48-1060 – reconstructed with no record of the reason, last visited 1/5/99;
- 48-1109 – reconstructed with no record of the reason, last visited 5/8/01;

- 48-3679 – reconstructed because of extensive block cracking throughout the section, last visited 7/18/97; and
- 48-3689 – reconstructed because of extensive block cracking throughout the section, last visited 5/28/99.

Of these sites, 48-1050 is especially interesting because of its fatigue cracking and low ductility. In 1989 its ductility was down to 3.5 cm after only five years on the road. By 1995 it was taken out of study and reconstructed, evidently because of fatigue cracking. It is impossible to say what its ductility was at that point, but it was certainly below 3 cm and very possibly as low as 2 cm at 15 °C, 1 cm/min elongation rate. This level of ductility would place the pavement well within the range of susceptibility to fatigue cracking that has been reported in the literature. Incidentally, 48-1050, 48-1060, and perhaps 48-1109 all reached a significant level of aging early in their pavement's life, compared to other pavements. While it is unknown how much this aging contributed to their early demise, we suspect that it is a strong element.

Binder Brittleness, Pavement Stiffness, and Fatigue Cracking

Besides binder ductility, a second element that must be present in order for a pavement to fail due to cracking under load is deformation. Even though the binder is very brittle, if the pavement system is stiff enough to prevent deformation under load, the binder still may not reach its failure strain. Pavement falling wheel deflectometer (FWD) data are reported in Figures 9-19 (for the LTPP cores of Figure 9-16) and 9-20 (for the cores of Figure 9-17). These are sensor 1 data reported in LTPP Data Pave 3.0, normalized to a 550 kPa (9 kip) load.

The FWD data span a wide range of behavior. Some pavements are quite stiff and stable in that their deflections are low (arbitrarily taken to be less than 200 microns) and constant over time (sites 48-1046, 48-1049, 48-1060, 48-2108, 48-3689, 48-3835, and 48-6086). By contrast, others have deflections as high as 1200 microns and increase over the life of the pavement.

In spite of the fact that it is difficult to draw definitive conclusions from these pavements, comparisons of performance, ductility, and FWD data are useful. Perhaps sites 48-2108 and 48-1046 are the most interesting. These pavements both have low calculated ductilities, less than 3 cm, but still performed without cracking failure, perhaps due to their high degree of pavement stiffness (low FWD deflections). A low ductility can be sustained provided the pavement system is stiff enough to prevent excessive deformation under load. Site 48-1050, on the other hand, most likely had a similar ductility but apparently failed due to fatigue cracking when the pavement stiffness was not sufficient to prevent deformation beyond its limits (FWD deformations in excess of 800 microns at the time it was taken out of study). Other pavements have continued to perform well even though deflections seem high (48-1056 and 48-1168), but their ductility values are high also, apparently due to the seal coats. Others are more moderate in both deformations and ductilities (48-2133 and 48-3769) and continue in service. From these results, we draw the conclusion that aged, brittle binders coupled with insufficient strength in the pavement system can lead to pavement fatigue-cracking failure.

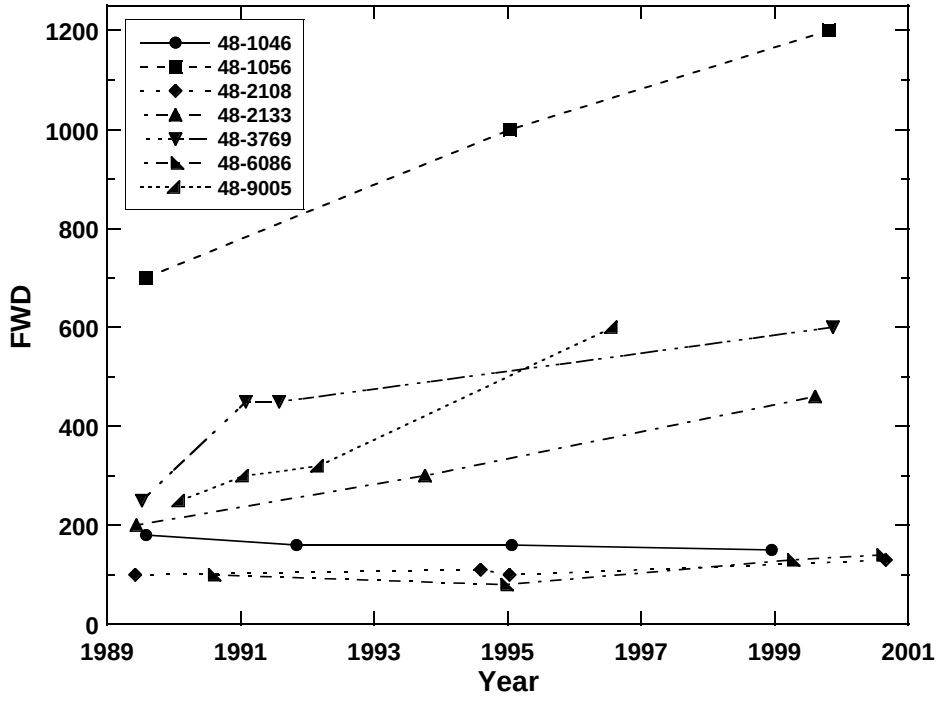

Figure 9-19. FWD Data for LTPP Sites of Figure 9-14.

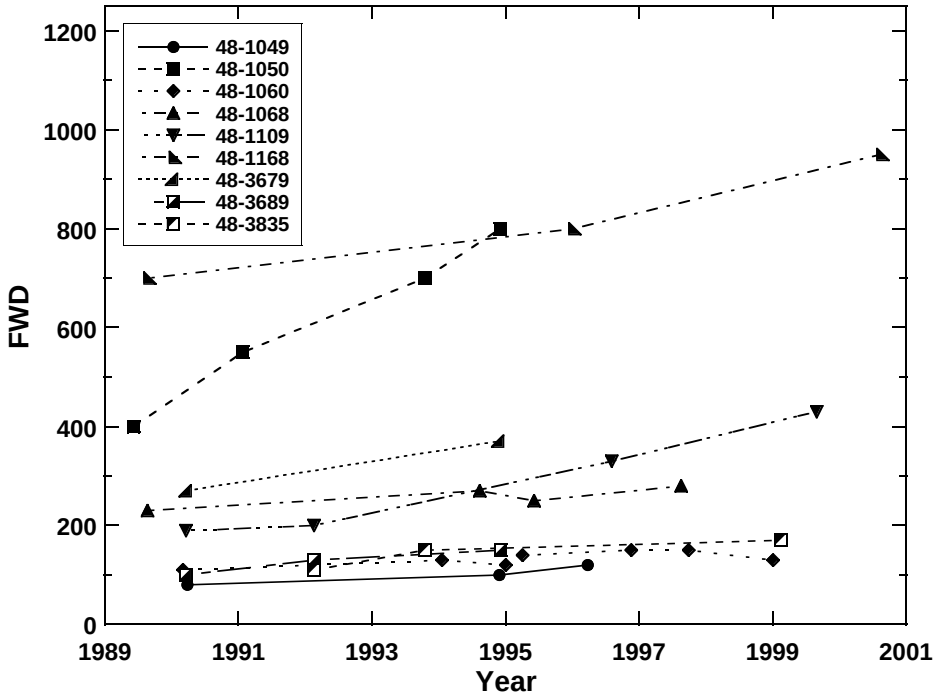

Figure 9-20. FWD Data for LTPP Sites of Figure 9-15.

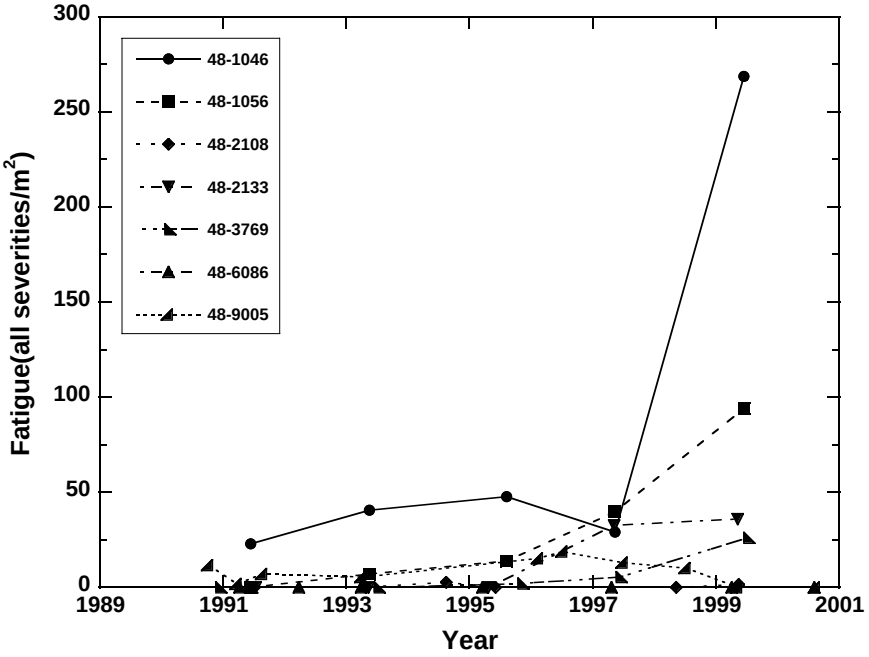

Figure 9-21. Fatigue Cracking for LTPP Sites of Figure 9-14.

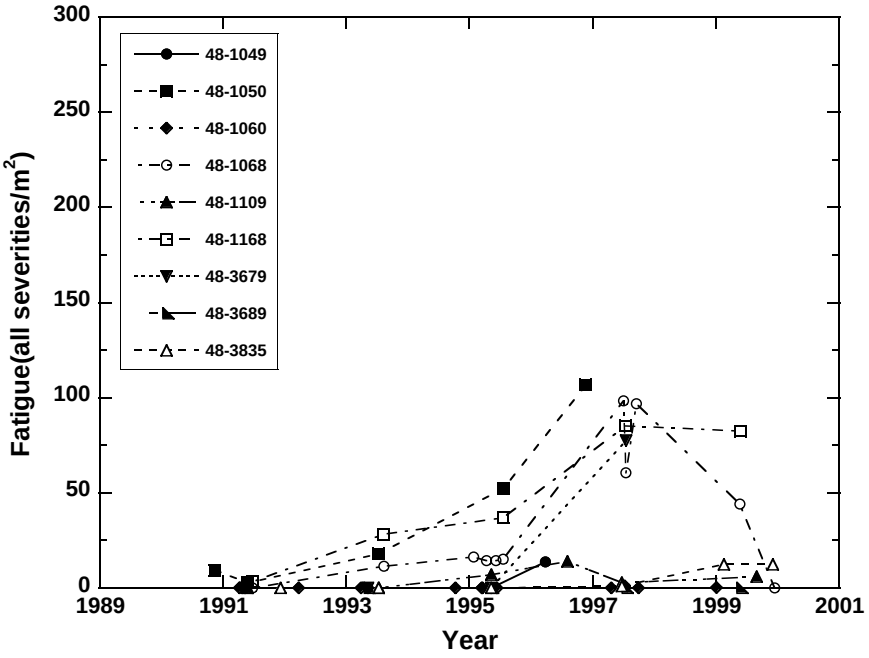

Figure 9-22. Fatigue Cracking for LTPP Sites of Figure 9-15.

Other Pavements

Two other pavement cores were evaluated in the course of this project. These were the northbound and southbound lanes of the IH 10 frontage road over the SP & MP railroad (the Hollywood Overpass) in Beaumont, Jefferson County, Texas. Both pavements were stated to be approximately 15 years old (constructed in approximately 1987), two inches of asphalt cement pavement over a box-beam bridge construction. The northbound lane was stated to be "very oxidized" whereas the southbound lane was considered to be "like new." This characterization was the result of the southbound pavement surface being very black in color, whereas the northbound surface was much more of a faded gray color.

The cores were extracted and the binders recovered, following the same procedures that were used for SH 21 and the LTPP cores. Binder DSR properties were measured, and the results are plotted in Figure 9-17 together with the single-year LTPP data. The binder DSR properties appear in Table 9-11. Both recovered binders were, in fact, quite aged, with the northbound binder (calculated ductility of 1.3 cm) somewhat more hardened than the southbound (ductility of 2.7 cm). In fact, the northbound lane's binder was stiffer than any other pavement binder tested. Based upon the preceding discussion, we might expect that this binder would be too brittle to hold up without cracking. However, the box beam construction of the overpass likely provides an extremely stiff system that prevents excessive deformations. FWD data are not available for this site, however.

Table 9-11. Binder Properties of the IH 10 Frontage Road Binders.

Site		η_0* (Poise) @60 °C, 0.1 rad/s	η' (MPa*s)[a] @15 °C, 0.005 rad/s	G' (MPa)[a] @15 °C, 0.005 rad/s	DSR Func[a] @15 °C, 0.005 rad/s	Calc Duct (cm)
IH 10 N	A	929,880	77.97	1.2190	0.019059	1.31
Northbound	B	1,668,514	56.32	1.0864	0.020956	1.26
IH 10 S	A	196,999	114.31	0.7269	0.004622	2.45
Southbound	B	172,873	94.64	0.5559	0.003265	2.86

[a] η', G' measured at 45 °C, 10 rad/s and converted to 15 °C, 0.005 rad/s by TTSP. DSR Function is G'/(η'/G').

So, the question of why one lane looks "new" and the other "very oxidized" was not the result of drastically different binder. Instead, the different appearances were due to the use of different aggregates. The pavement that looks quite black appears to be constructed using an aggregate that is referred to as traprock, which is a basaltic aggregate from a source in Uvalde.

SUMMARY AND RECOMMENDATIONS

Extensive investigations of selected Texas highway pavements has provided new information on changes in binder properties over time. These studies included SH 21 west of Bryan, Texas, plus 16 LTPP GPS pavements. They were conducted to provide information on pavement performance as it relates to recovered binder properties and also to provide data on comparisons between pavement and laboratory binder oxidation rates and changes in physical properties. From these studies, a number of conclusions and recommendations have been reached.

Findings

- There is some evidence that seal coats may penetrate below the surface of a pavement, even in dense-graded mixes, under the right conditions. Many of the pavements that were tested failed to provide definitive determinations of a critical value of the binder DSR function or of pavement binder aging rates because binder stiffening over time showed anomalous trends. These observed anomalies (reversals in stiffening) could be explained by seal coat penetration, if it occurred to a significant degree.

- If, in fact, seal coats are able to penetrate into the pavement, then they may provide a significant opportunity to rejuvenate pavements in place. For those pavements where the binder stiffening anomalies may be explained by seal coat penetration, the supposed rejuvenation reversed approximately 10 to 15 years of pavement aging. Other pavement data suggest that a specially designed seal coat may be able to halt pavement aging.

- The DSR function $G'/(\eta'/G')$, measured at 44.7 °C and 10 rad/s but converted to 15 °C and 0.005 rad/s, appears to be an excellent function for tracking pavement aging.

- Pavements oxidize at surprisingly uniform rates with depth, even for dense-graded mixes.

- Brittle binders can be tolerated in stiff pavement systems. Thus, an appropriate limiting DSR function value depends on the stiffness of the pavement system.

- For a stiff pavement system (FWD values less than 200 and stable over time), DSR function values of 0.003 (ductility =3 at 15 °C, 10 cm/min) can be tolerated, but this value may be an approximate limit for avoiding age-related failure. For pavements with FWD values of 400 or more, a DSR function of 0.0009 (ductility = 5) appears to be an approximate limit.

- RTFOT plus PAV aging corresponds to approximately hot-mix aging plus three years of pavement aging on SH 21. This corresponds to a DSR function of approximately 1.2×10^{-4} MPa/s and a 15 °C, 1 cm/min ductility of approximately 12 cm.

- To age the SH 21 binder past the initial jump level, it took approximately RTFOT plus 10 hours in the PAV at 20 atm air, 90 °C, 0.86-mm thick films or RTFOT aging plus 20 to 30

days in the environmental room at 60 °C or about three years in the SH 21 pavement (after hot-mix plant aging).

- After the initial jump level of aging has been reached, one month of aging in the 60 °C environmental room was equivalent to 15 months (roughly one year) on SH 21. This calibration will vary with climate and binder composition, compaction, and probably mix design.

- After the initial jump level of aging has been reached, 11 hours of aging in the PAV aging apparatus at 90 °C, 20 atm air, 0.86-mm thick films was equivalent to approximately 12 months (approximately one year) on SH 21.

- On SH 21, aggregate did not alter the oxidation hardening susceptibility or the path on the G' versus η'/G' map followed by an asphalt from laboratory values. This suggests that aggregates do not have a large impact on asphalt oxidation reactions.

Recommendations

- The use of penetrating seal coats to rejuvenate underlying pavement should be evaluated. Rejuvenating seal coats should use materials that are specially designed to produce a more ductile and slower aging binder in the pavement.

- The use of crumb-rubber modified asphalt (CRMA) as a sealcoat to halt the oxidation of underlying pavement should be studied further and implemented as appropriate.

- Falling weight deflectometer measurements together with measurements of binder ductility (through the DSR function) should be implemented as a method for evaluating remaining pavement life and scheduling seal coats to rejuvenate the underlying pavement and to halt or drastically slow further hardening. A combination of a low stiffness pavement and a brittle binder leads to cracking failure.

CHAPTER 10. RECOMMENDED TEST PROCEDURE FOR PREDICTING AGE-RELATED CRACKING OF ASPHALTS

The purpose of this protocol is to provide a test to identify asphalts that might be expected to fail prematurely as a result of rapid loss of ductility on aging and to provide a procedure for evaluating binders in existing pavements. The new binder test includes the following steps: first, the asphalt is subjected to RTFOT or SAFT (stirred air-flow test) aging to simulate the hot-mix operation; then, it is subjected to longer term aging to simulate road aging. Finally, the asphalt is analyzed with the DSR and the function G'/(η'/G') is determined at 44.7 °C (112.5 °F) and 10 rad/s, which was shown in Chapter 5, to correlate well with ductility measured at 15 °C and 1 cm/min. A critical value of the ductility of 3 cm was chosen because the literature indicates that few, if any, pavements can survive at this value, plus this value appears to be consistent with field results from this project. From the correlation presented in Chapter 4 for unmodified materials, this ductility value corresponds to a DSR function of 0.003 MPa/s (at 15 °C, 0.005 rad/s).

As discussed in Chapter 6, we conducted an extensive study of various aging conditions to find a condition that correlates reasonably well with low-temperature atmospheric pressure aging as measured in the 60 °C (140 °F) environmental room. At the same time, the conditioning must be such that the test time is reasonable. Based on these studies, we recommend a procedure.

PROCEDURE FOR UNMODIFIED ASPHALTS

Evaluation of New Binders

Test equipment: standard PAV; 4 cm by 7 cm aluminum trays; DSR

Test Conditions: 90 °C, 20 atm air for 32 hours

Sample Preparation: 2.4 grams of asphalt are weighed into a 4 cm by 7 cm aluminum tray. The tray is heated slightly to obtain a uniformly thick film of asphalt in the tray. This produces an asphalt film approximately 0.857 mm thick.

Operation: Two trays will fit in each of the PAV shelves. Once the vessel is loaded and sealed, operation is identical to the standard PAV procedure at 90 °C except that the aging time is 32 hours.

Measurement of the DSR Function: Sufficient asphalt is removed from the tray, and G' and η' are measured at 44.7 °C and 10 rad/s and converted to the function G'/(η'/G') at 15 °C and 0.005 rad/s by dividing by 2000 (obtained from the frequency ratio, 10 rad/s/0.005 rad/s). Note that G'/(η'/G') = G'ω/tan δ.

Evaluation: If the value of $G'/(\eta'/G')$ is larger than 0.003 MPa/s, the asphalt fails.

Comment: This procedure is tentative, as insufficient replication has been made at each condition, and more asphalts, especially those likely to fail, should be tested. In the meantime, it would be informative to routinely run these tests, as it will be found that asphalts that have the same performance grade may perform quite differently on the test. It may also be found that some unmodified asphalts with high upper PG grade will perform poorly in the test.

Evaluation of Pavement Binder Remaining Life

Extraction and Recovery of Pavement Binder: An extraction and recovery procedure should be followed that effectively extracts the binder from the aggregate, protects against binder hardening or softening in dilute solution with solvent, and leaves essentially no solvent in the hardened pavement binder.

Break apart the pavement cores (after separating the lifts either by sawing or by freezing and then cleaving apart) into small pieces with a hammer before solvent extracting the binder from the aggregate. Approximately 130 g of core material is extracted to obtain about six g of binder (assuming the core is 5 percent binder, by weight). Extract the core material in three successive washes: one wash of 100 mL toluene followed by two washes of a mixture of 15 mL ethanol plus 100 mL toluene. After the binder is extracted from the aggregate, filter the solvent five times using basket coffee filters to remove all aggregate particles from the binder solution.

Recover the binder from the solvent with a rotovap apparatus. A specially designed rotavap "flask" that uses a straight glass tube and mates with a 55-mm diameter ointment tin is preferred. Recover the binder from solution in 100 mL batches and retain the binder from each batch in the ointment tin so that the recovered binder is accumulated in the same tin. These batch recoveries are referred to as the primary solvent removal during which solvent evaporation is sufficient to prevent contact of the asphalt with oxygen.

During primary solvent removal, the bath temperature is kept at 100 ^{o}C (212 ^{o}F) to avoid hardening or softening of the asphalt in dilute solution (Burr et al., 1993). When solvent condensation has slowed to one drop per minute, increase the bath temperature to 173.9 ^{o}C (345 ^{o}F), introduce nitrogen at the rate of 1000 mL/min to prevent asphalt oxidation, and continue to remove solvent for 30 min after reaching this temperature to ensure sufficient final solvent removal. The extraction and recovery procedure takes from three to four hours for each sample of pavement.

Recover binder in at least two replicate batches of core material, best done for each identifiable lift of the core (or a specific lift of interest), to assess variability and to ensure accuracy. The properties of the recovered binder are compared to each other or to other lifts, paths, or years. When inconsistencies occurr in these recovered binder properties, additional replicates should be extracted, up to four replicates total for a given station and lift.

Measurement of the DSR Function: The recovered pavement binder is tested for DSR properties at 44.7 ºC and 10 rad/s and converted to the function $G'/(\eta'/G')$ at 15 ºC and 0.005 rad/s by dividing by 2000 (obtained from the frequency ratio, 10 rad/s/0.005 rad/s). Note that $G'/(\eta'/G') = G'\omega/\tan\delta$.

Evaluation: A value of $G'/(\eta'/G')$ larger than 0.003 MPa/s at 15 ºC, 0.005 rad/s (ductility of about 3 cm at 15 ºC, 1 cm/min) is taken to be a critical value for pavement binder failure, although this number should be climate dependent. A value of 0.0009 MPa/s (ductility of about 5 cm) is believed to be approaching a value that will lead to pavement cracking.

A critical level of this DSR function varies with pavement, according to its pavement stiffness, and evaluation of the pavement binder is best considered in concert with FWD data.

Comment: This evaluation procedure is tentative and should be implemented on a trial basis to build a database of pavement properties and conditions.

PROCEDURE FOR MODIFIED ASPHALTS

We are not recommending a definite pass-fail procedure for modified asphalts. It is clearly shown in Chapter 5 that the DSR-ductility correlation does not hold for modified asphalts because their fundamental rheology is so different from conventional materials. It has also been shown that accelerated aging procedures are even less reliable for these materials (Glover et al., 2000). Even so, these measurements could be useful for modified asphalts.

As seen in Chapter 5, all modified asphalts have ductilities better than those indicated for unmodified asphalts at a given value of the DSR function. The difference is small for small amounts of modifier but quite large for some materials. If the aging procedure indicates a lower aging rate, it is very likely that the modifier is slowing the decrease in ductility and increasing ultimate life.

CHAPTER 11. SUMMARY OF INVESTIGATIONS, FINDINGS, AND RECOMMENDATIONS

This project was designed to answer questions about the adequacy of Superpave specifications and, in particular, to find a specification superior to the Superpave G*sin δ function that does not satisfactorily predict fatigue cracking. Also, there has been an on-going concern that the PAV does not accurately simulate hardening of asphalts in pavements. Finally, with the increasing use of modifiers, there is concern about the applicability of Superpave specifications to these materials and also about the effect of modifiers on water susceptibility.

We addressed all of these questions in this project with emphasis on developing a new long-term performance test that would use new aging conditions and a new measurement, still based on the DSR instrument, that would relate to excessive oxidative hardening and subsequent fatigue. The literature contains data that indicate that ductility measured at lower temperatures ranging from 10 to 15 °C (50 to 59 °F) correlates well with the conditions of old roadways, so a correlation was desired between ductility and DSR measurements. Field verification also was an important part of this project.

SUMMARY OF INVESTIGATIONS

This project was a comprehensive study directed at developing an improved method of screening asphalt binders for long-term pavement performance, and it included studies of aged binders recovered from pavements. This work involved a fresh look at:

- asphalt binder oxidation methods and their effects on binders (including polymer modified binders);
- the effect of binder aging on Superpave performance properties, especially low-temperature BBR S and m; and
- studies of the role of other properties important to durability that are not included in Superpave.

The work culminated in a new binder aging and testing protocol for predicting the long-term performance of asphalt binders in pavements. Specifically, this work included:

- fundamental studies of asphalt oxidation, especially of the effect of oxygen pressure on asphalt hardening rates, important for understanding the suitability of accelerated aging procedures such as the PAV;
- studies of the suitability of the PAV as a conditioning procedure for assessing long-term binder durability;

- studies of the effect of aging on low-temperature asphalt properties;

- investigations to develop an appropriate DSR function that relates to long-term binder durability in pavements and that can be readily measured with existing DSR equipment;

- investigations of the impact of polymer modifiers on binder properties and on binder durability;

- extensive studies of accelerated aging methods to determine an appropriate procedure for conditioning asphalt that has the combined objectives of accurately representing long-term pavement aging while at the same time being able to be performed in a reasonable length of time;

- investigations of the effect of modifiers on water susceptibility; and

- studies of binders recovered from pavement cores to test conclusions about binder properties and performance and to calibrate laboratory aging rates to field aging rates.

SUMMARY OF FINDINGS

A New DSR Function for Predicting Age-Related Failure

An excellent correlation was found for unmodified asphalts between ductility (at 15 °C, 1 cm/min) below 10 cm and the DSR function G'/(η'/G') at 15 °C and 0.005 rad/s. This correlation was coupled with a new aging procedure in a tentative specification that should guard against failure caused by premature asphalt hardening and consequent fatigue cracking. This method appears to be a good predictor of asphalt resistance to failure due to oxidative hardening. The method is not effective for modified asphalts.

The ductility-DSR correlation was originally developed for DSR measurements at 15 °C and 0.005 rad/s. These conditions were shifted to provide for measurement at 44.7 °C and 10 rad/s by using the time-temperature superposition principle to produce a method that is easily accessible to standard laboratory rheological equipment and methods.

For modified asphalts, the DSR-ductility results were complex. Generally for a given value of the DSR function, the ductility was better than indicated by the DSR function correlation for unmodified asphalts. Larger amounts of modifier produced increasing values of ductility for a given function value. This result was very asphalt dependent, however, so no general correlation could be found.

For modified asphalts, force-ductility measurements showed that modifiers change the extensional behavior of binders by providing stability while the binder is in the flow regime and, in some cases, by increasing the failure stress of the binder. These effects can result in much

improved binder ductility for unaged or lightly aged binders.

As modified binders oxidize, the asphalt hardens, and the improvement to ductility imparted by modifiers decreases. After enough aging, the improvement is gone, and modified binders perform no better than their aged unmodified counterpart. Nevertheless, modifiers appear to provide added life to binders. A critical issue remains as to whether the life extension is cost effective, and answers will rely on the actual amount of life extension and the cost of the modification.

Ductility and aging results indicate that polymer modifiers generally improve asphalt hardening rates but the amount of improvement is modifier and asphalt dependent. Styrene butadiene styrene or styrene butadiene rubber at small concentrations (1 percent) do not have much beneficial effect on binder hardening.

Even though a ductility-DSR correlation does not seem to exist for modified binders, a direct tension-ductility correlation does. This may allow using a Superpave instrument (DT) in lieu of the ductility apparatus, which, although not as convenient to use as the DSR, is much more convenient than ductility apparatus.

A New Aging Procedure

The recommended aging procedure uses the PAV apparatus but is modified by taking advantage of the higher average aging rate when the asphalt is aged in thinner films. This change, combined with a somewhat longer aging time, results in more extended binder aging and, thus, a more rigorous test of durability than the standard PAV method. At the same time, the resulting rankings of aged materials are more representative of rankings that are obtained from aging at atmospheric air pressure and 60 °C. In theory, replacing pavement-condition aging with aging at higher temperatures and pressures is incorrect because different asphalts' aging rates accelerate differently by the different conditions. But a wide variety of conditions were tested, and hardening rates were compared to those obtained in the 60 °C (140 °F) environmental room. Asphalts were aged in both the standard PAV and a POV apparatus. Aging conditions were evaluated on the basis of time and relative deviation from the environmental room results, which required months of aging. Any change in time, pressure, temperature, and film thickness can change the relative rankings of asphalts, but conditions were found that agree surprisingly well with the 60 °C environmental room results.

Tests measured low-temperature properties, BBR S and m and direct tension failure strain, for asphalts aged in the standard PAV procedure and in the environmental room, both after RTFOT aging. The properties for PAV-aged asphalts agreed remarkably well with the properties obtained after 38 days in the environmental room, although longer times in the PAV did not correlate as well with any specific longer time in the environmental room.

The PAV can be eliminated and BBR determinations estimated after RTFOT aging (or an alternative hot-mix aging procedure) only, based on values of $G^*/\sin\delta$ at 58 °C. The amount of error in this estimation procedure appears to be acceptable.

From age-hardening results at a variety of conditions of temperature and pressure, a number of comparisons can be made. Especially notable are that 122 days at 60 °C, 1 atm air

corresponds to 32 hours at 90 °C, 20 atm air and 377 hours at 88 °C, 1 atm air, all after RTFOT aging. All of these tests were in nominally 0.86-mm (0.034 in) thick films.

Water susceptibility was determined for several asphalts with and without modifiers, and the results indicated that the modifiers did not greatly affect the water susceptibility.

A New Trial Specification

The DSR function was coupled with the new aging procedure in a tentative specification that should guard against failure caused by premature asphalt hardening and consequent fatigue cracking. This method appears to be a good predictor of asphalt resistance to failure due to oxidative hardening. The method is not effective for modified asphalts, but an alternative direct tension procedure for modified materials shows promise.

New Pavement Aging Results

There is some evidence that seal coats may penetrate below the surface of a pavement, even in dense-graded mixes, under the right conditions. Many of the pavements that were tested failed to provide definitive determinations of a critical value of the binder DSR function or of pavement binder aging rates because binder stiffening over time showed anomalous trends. These observed anomalies (reversals in stiffening) could be explained by seal coat penetration, if it occurred to a significant degree.

If, in fact, seal coats are able to penetrate into the pavement, then they may provide a significant opportunity to rejuvenate pavements in place. For those pavements where the binder stiffening anomalies may be explained by seal coat penetration, the supposed rejuvenation reversed approximately 10 to 15 years of pavement aging. Other pavement data suggest that a specially designed seal coat may be able to halt pavement aging.

The DSR function $G'/(\eta'/G')$, measured at 44.7 °C and 10 rad/s but converted to 15 °C and 0.005 rad/s, appears to be an excellent function for tracking pavement aging.

Pavements can oxidize at surprisingly uniform rates with depth, even for dense-graded mixes.

Brittle binders can be tolerated in stiff pavement systems. Thus, an appropriate limiting DSR function value depends on the stiffness of the pavement system. For a stiff pavement system (FWD values less than 200 and stable over time), DSR function values of 0.003 MPa/s (ductility =3 at 15 °C, 1 cm/min) can be tolerated, but this value may be an approximate limit for avoiding age-related failure. For pavements with FWD values of 400 or more, a DSR function of 0.0009 (ductility = 5) is tentatively taken to be an approximate limit.

The Superpave PAV procedure (RTFOT plus PAV) ages binders at Texas conditions to a level that is approximately equal to hot-mix aging plus four years on the road, based on SH 21 data. This corresponds to a DSR function of approximately 1.2x10-4 MPa/s and a 15 °C, 1 cm/min ductility of approximately 12 cm. This time will depend upon how much the binder is aged before placement, however., compared to RTFOT aging. This is not a very severe level in the context of pavement life.

One month of aging in the 60 °C environmental room was equivalent to approximately one year of aging in SH 21, after the initial jump is past. This calibration will vary with climate, binder composition, and air voids.

On SH 21, aggregate altered neither the oxidation hardening susceptibility nor the path followed on the G' versus η'/G' map, compared to laboratory aging of the binder. This comparison suggests that aggregates do not have a large impact on asphalt oxidation reactions.

RECOMMENDATIONS

For TxDOT Evaluation or Implementation

TxDOT laboratories should begin evaluating the proposed long-term durability specification procedure to gain familiarity with it and with the performance of various asphalts, preliminary to implementation. The test calls for RTFOT or equivalent aging followed by aging in the PAV apparatus at 90 °C and 20 atm air but in thin (0.86 mm) films and for an extended time of 32 hours. This level of aging is approximately equivalent to 122 days at 60 °C and is about three times more aging than the Superpave PAV procedure provides. This procedure is followed by DSR function measurement to determine the asphalt's remaining flexibility after the extended aging.

The use of penetrating seal coats to rejuvenate underlying pavement should be evaluated. Rejuvenating sealcoats should use materials that are specially designed to produce a more ductile and slower aging binder in the pavement.

Falling weight deflectometer measurements together with measurements of binder ductility (through the DSR function) should be implemented as a method for evaluating remaining pavement life and scheduling seal coats to rejuvenate the underlying pavement and to

halt or drastically slow further hardening. A combination of a low stiffness pavement and a brittle binder leads to cracking failure.

TxDOT laboratories should evaluate using the abbreviated procedure for determining low-temperature, Superpave properties immediately after the hot-mix aging test, without PAV conditioning.

Recommended Further Studies

Further study is recommended in the following areas:

- the use of sealcoats, such as crumb-rubber modified materials, designed specifically to halt oxidation of the underlying pavement;

- development of a method for determining binder stiffness in mixtures and pavement cores, as a means of assessing remaining life, especially important for modified materials for which extraction and recovery is unproven;

- polymer modification to understand the cause of the benefit degradation that occurs due to aging and whether this can be improved by adjusting asphalt composition;

- the effect of asphalt composition on polymer benefit;

- the effect of modifier on binder failure stress; and

- the use of direct tension measurements to characterize polymer ductility and durability.

CHAPTER 12. REFERENCES

Anderson, D.A., and T.W. Kennedy. (1993) Development of SHRP Binder Specification. *Proc. Assoc. Asphalt Paving Technol.*, Vol. 62, pp. 481-507.

Anderson, D.A., D.W. Christensen, and H. Bahia. (1991) Physical Properties of Asphalt Cement and the Development of Performance-Related Specifications. *Proc. Assoc. Asphalt Paving Technol.*, Vol. 60, pp. 437-475.

Anderson, D.A., D.W. Christensen, R. Dongre, M.G. Sharma, J. Runt, and P. Jordhal. (1990) Asphalt Behavior at Low Service Temperatures. *FHWA-RD-88-078*, Federal Highway Administration, McLean, VA.

Anderson, D.A., D.W. Christensen, H.U. Bahia, R. Dongre, M.G. Sharma, C.E. Antle, and J. Button. (1994) *Binder Characterization and Evaluation, Volume 3: Physical Characterization*. SHRP A-369, Strategic Highway Research Program/National Research Council. Washington, D.C., p 31.

Anderson, D.A., D.W. Christensen, R. Roque, and R.A. Robyak. (1992) Rheological Properties of Polymer Modified Emulsion Residue. In ASTM STP 1108: *Polymer Modified Asphalt Binders*, K.R. Wardlaw and S. Shuler (Eds.), American Society for Testing and Materials, San Antonio, TX, pp. 20-34.

Anderson, D.I., D.E. Peterson, and M. Wiley. (1976) Characteristics of Asphalts as Related to the Performance of Flexible Pavements. *Research Report No. UDOT-MR-76-6*, State of Utah Department of Transportation.

Asphalt Binders, K.R. Wardlaw and S. Shuler (Eds.), American Society for Testing and Materials, San Antonio, TX, pp. 55-60.

Asphalt Institute. (1994) Performance Graded Asphalt Binder Specification and Testing. *SuperPave series No. 1 (SP-1)*.

ASTM D113-86. (1994) Standard Test Method for the Ductility of Bituminous Materials. Annual Book of ASTM Standards, Vol. 04.03, pp. 23-25.

ASTM D4124. (1994) Standard Test Methods for Separation of Asphalt into Four Fractions. Annual Book of ASTM Standards, Vol. 04.03, pp. 432-437.

Bahia, H.U., and D.A. Anderson. (1993) Glass Transition Behavior and Physical Hardening of Asphalt Binders. *Proc. AAPT*, Vol. 62, p. 93.

Boudart, M. (1991) *Kinetics of Chemical Process*; Butterworth-Heinemann, Stoneham, MA.

Bouldin, M.G., and J.H. Collins. (1992) Influence of Binder Rheology on Rutting Resistance of Polymer Modified and Unmodified Hot Mix Asphalt. In ASTM STP 1108: *Polymer Modified*

Bouldin, M.G., J.H. Collins, and A. Berker. (1991) Rheology and Microstructure of Polymer/Asphalt Blends. *Rubber Chemistry and Technology*, Vol. 64, pp. 577-600.

Bullin, J.A., C.J. Glover, R.R. Davison, M.S. Lin, J.M. Chaffin, M. Liu, and C. Eckhardt. (1997) Development of Superior Asphalt Recycling Agents, DOE Final Progress Report No. DOE/AL/94460.

Burr, B.L., R.R. Davison, C.J. Glover, and J.A. Bullin. (1990) Solvent Removal from Asphalt, *Transp. Res. Rec., 1269,* pp. 1-8.

Burr, B.L., R.R. Davison, H.B. Jemison, C.J. Glover, and J.A. Bullin. (1991) Asphalt Hardening in Extraction Solvents, *Transp. Res. Rec.,* 1323, pp. 70-76.

Burr, B. L., C.J. Glover, R.R. Davison, and J.A. Bullin. (1993) A New Apparatus and Procedure for the Extraction and Recovery of Asphalt Binder from Pavement Mixtures, *Transp. Res. Rec.,* 1391, pp. 20-29.

Burr, B.L., R.R. Davison, C.J. Glover, and J.A. Bullin. (1994) Softening of Asphalts in Dilute Solutions at Primary Distillation Conditions, *Transp. Res. Rec.,* 1436, pp. 47-53.

Chaffin, J.M., M. Liu, R.R. Davison, C.J. Glover, and J.A. Bullin. (1997) Supercritical Fractions as Asphalt Recycling Agents and Preliminary Aging Studies on Recycled Asphalts. *Ind. Eng. Chem. Res.*, Vol. 36 (3), pp. 656-666.

Chipps, J.F. (2001) *The Industrial Manufacture of Tire Rubber-Modified Asphalts with Enhanced Rheological Performance and Improved Longevity*. Ph.D. Dissertation, Texas A&M University, College Station, TX.

Christensen, D.W. and D.A. Anderson. (1992) Interpretation of Dynamic Mechanical Test Data for Paving Grade Asphalt Cements. *J. Am. Assoc. Paving Technol.*, Vol. 61, pp. 67-98.

Cipione, C.A., R.R. Davison, B.L. Burr, C.J. Glover, and J.A. Bullin. (1991) Evaluation of Solvents for the Extraction of Residual Asphalt from Aggregates, *Transp. Res. Rec.*, 1323, pp. 47-52.

Clark, R.C. (1958) Practical Results of Asphalt Hardening on Pavement Life. *Proc. Assoc. Asphalt Paving Technol.*, Vol. 27, pp. 196-208.

Collins, J.H., M.G. Bouldin, R. Gelles, and A. Berker. (1991) Improved Performance of Paving Asphalts by Polymer Modification. *Proc. Assoc. Asphalt Paving Technol.*, Vol. 60, pp. 43-79.

Corbett, L.W. (1979) Dumbbell Mix for Better Asphalt. *Hydrocarbon Processing*, Vol. 58, pp. 173-177.

Davison, R.R., J.A. Bullin, C.J. Glover, B.L. Burr, H.B. Jemison, A.L.G. Kyle, and C.A. Cipione. (1989) Development of Gel Permeation Chromatography, Infrared and Other Tests to Characterize Asphalt Cements and Correlate with Field Performance. *Research Report No. 458*, Texas State Dept. of Highways and Public Transportation.

Davison, R.R., J.A. Bullin, C.J. Glover, J.R. Stegeman, H.B. Jemison, B.L. Burr, A.L. Kyle, and C.A. Cipione. (1991) Design and Manufacture of Superior Asphalt Binders. *FHWA/TX-91/1155-1F*.

Davison, R.R., J.A. Bullin, C.J. Glover, J.M. Chaffin, G.D. Peterson, K.M. Lunsford, M.S. Lin, M. Liu, and M.A. Ferry. (1994) Verification of an Asphalt Aging Test and Development of Superior Recycling Agents and Asphalts, Texas Dept. of Transportation Research Report No. 1314.

Dhalaan, M.A., F. Balghunaim, I.A. Dhubaib, and A.S. Noureldin. (1992) Field Trials with Polymer Modified Asphalts in Saudi Arabia. In ASTM STP 1108: *Polymer Modified Asphalt Binders*, K.R. Wardlaw and S. Shuler (Eds.), American Society for Testing and Materials, San Antonio, TX, pp. 203-223.

Domke, C.H. (1999) *Asphalt Compositional Effects on Physical and Chemical Properties*. Ph.D. Dissertation, Texas A&M University, College Station, TX.

Domke, C.H., R.R. Davison, and C.J. Glover. (1999) Effect of Oxidation Pressure on Asphalt Hardening Susceptibility. *Transp. Res. Rec.*, Vol. 1661, pp. 114-121.

Domke, C.H., R.R. Davison, and C.J. Glover (2000) Effect of Oxygen Pressure on Asphalt Oxidation Kinetics. *Ind. Eng. Chem. Res.*, Vol. 39 (3), pp. 592-598.

Domke, C.H., R.R. Davison, C.J. Glover, and J.A. Bullin. (1997) The Effect of Asphaltenes on SHRP Superpave™ Specifications. Presented at Symposium #635 "Advances in the Chemistry of Asphaltene and Related Substances," at the 5th North American Chemical Congress, Cancun, Mexico, November 11-15.

Domke, C.H., M. Liu, R.R. Davison, J.A. Bullin, and C.J. Glover. (1997) Study of Strategic Highway Research Program Pressure Aging Vessel Procedure Using Long-Term, Low-Temperature Aging Experiments and Asphalt Kinetics. *Trans. Res. Rec.*, Vol. 1586, pp. 10-15.

Doyle, P.C. (1958) Cracking Characteristic of Asphalt Cement. *Proc. Assoc. Asphalt Paving Technol.*, Vol. 27, pp. 581-597.

Ferry, J.D. (1980) *Viscoelastic Properties of Polymers*, 3rd edition, John Wiley & Sons, New York, p. 82.

Fromm, H.J., and W.A. Phang. (1970) Temperature Susceptibility Control in Asphalt Cement Specifications. *Report IR 35*, Ontario Department of Highways.

Gahvari, F. (1997) Effect of Thermoplastic Block Copolymers on Rheology of Asphalt. *J. of Materials in Civil Engineering*, pp. 111-116.

Gallagher, K.P, H.U. Gahia, J.D. Guerra, and J. Keating. (1996) Influence of Air-Blowing on the Performance-Related Properties of Paving Asphalt. *Transp. Res. Rec.*, Vol. 535, p. 29.

Glover, C.J., R.R. Davison, J.A. Bullin, C.K. Estakhri, S.A. Williamson, T.C. Billiter, J.F Chipps, J.S. Chun, P. Juristyarini, S.E. Leicht, and P. Wattanachai. (2000) A Comprehensive Laboratory and Field Study of High Cure Asphalt-Rubber Materials. Texas Dept. of Transp. Research Report No. 1460.

Goodrich, J.L (1988) Asphalt and Polymer Modified Asphalt Properties Related to the Performance of Asphalt Concrete Mixes. *Proc. Assoc. Asphalt Paving Technol.*, Vol. 57, pp. 116-175.

Halstead, W.J. (1963) The Relation of Asphalt Ductility to Pavement Performance. *Proc. Assoc. Asphalt Paving Technol.*, Vol. 32, pp. 247-270.

Halstead, W.J. (1984) Relation of Asphalt Chemistry to Physical Properties and Specifications. *Research Report No. FHWA/VA-84/85*, Virginia Department of Highways and Transportation.

Harper, C.A. (1996) *Handbook of Plastics, Elastomers, and Composites*, 3rd edition, McGraw-Hill, pp. 5, 12.

Harrigan, E.T., R.B. Leahy, and J.S. Youtcheff (Eds). (1994) *The SUPERPAVE Mix Design System Manual of Specifications, Test Methods, and Practices*. Strategic Highway Research Program/National Research Council. Washington, D.C.

Heukelom, W. (1966) Observations on the Rheology and Fracture of Bitumens and Asphalt Mixes. *Proc. Assoc. Asphalt Paving Technol.*, Vol. 36, pp. 358-396.

Hills, J.F., and D. Brien. (1966) The Fracture of Bitumens and Asphalt Mixes by Temperature Induced Stresses. Discussion in *Proc. Assoc. Asphalt Paving Technol.*, Vol. 35, pp. 292-309.

Hoare, T.R., and S. Hesp. (2000) Low-Temperature Fracture Testing of Asphalt Binders: Regular and Modified Systems. *Transp. Res. Rec.*, Vol. 1728, p. 36.

Huang, S.C., M. Tia, and B.E. Ruth. (1996). Laboratory Aging Methods for Simulation of Field Aging of Asphalts. *J. of Materials in Civil Engineering*, Vol. 8 (3), pp. 147-152.

Hubbard, P., and H. Gollomb. (1937) The Hardening of Asphalt with Relation to Development of Cracks in Asphalt Pavements. *Proc. Assoc. Asphalt Paving Technol.*, Vol. 9, pp. 165-194.

Hveem, F.N., E. Zube, and J. Skog. (1963) Proposed New Tests and Specifications for Paving Grade Asphalts. *Proc. Assoc. Asphalt Paving Technol.*, Vol. 32, p. 2.

Ista, E.J., and F.S. Choquet. (1992) The Determination of Bitumen and Recycled Tire Rubber Content in Rubberized Asphalt Road Mixtures. In ASTM STP 1108: *Polymer Modified Asphalt Binders*, K.R. Wardlaw and S. Shuler (Eds.), American Society for Testing and Materials, San Antonio, TX, pp. 224-233.

Jamieson, I.L., and M.M. Hattingh. (1970) The Correlation of Chemical and Physical Properties of Bitumens with Their Road Performance. *Australian Road Research Conf. Proc.*, Vol. 5, pp. 293-324.

Jemison, H.B., B.L. Burr, R.R. Davison, J.A. Bullin, and C.J. Glover. (1992) Application and Use of the ATR, FTIR Method to Asphalt Aging Studies. *Fuel Sci. and Technol. Intl.*, Vol. 10, pp. 795-808.

Jemison, H.B., R.R. Davison, C.J. Glover, and J.A. Bullin. (1991) Evaluation of Standard Oven Tests for Hot-Mix Plant Aging. *Transp. Res. Rec.*, Vol. 1323, pp. 77-84.

Jemison, H.B., R.R. Davison, C.J. Glover, and J.A. Bullin. (1995) Fractionation of Asphalt Materials by Using Supercritical Cyclohexane and Pentane. *Fuel Sci. And Technol. Intl.*, Vol. 13 (5), pp. 605-638.

Jennings, P.W., and J.A. Pribanic. (1985) The Expanded Montana Asphalt Quality Study Using High Pressure Liquid Chromatography. *Research Report FHWA/MT-85/001*, State of Montana Department of Highways.

Jennings, P.W., J.A. Pribanic, W. Campbell, K.R. Dawson, and R.B. Taylor. (1980) High Pressure Liquid Chromatography as a Method of Measuring Asphalt Composition. *Research Report FHWA-MT-7930*, State of Montana Department of Highways.

Kandhal, P.S. (1977) Low-Temperature Ductility in Relation to Pavement Performance. In ASTM STP 628: *Low-Temperature Properties of Bituminous Materials and Compacted Bituminous Paving Mixtures*, C.R. Marek (Ed.), American Society for Testing and Materials, Philadelphia, PA, pp. 95-106.

Kandhal, P.S., and W.C. Koehler. (1984) Significant Studies on Asphalt Durability: Pennsylvania Experience. *Transp. Res. Rec.*, Vol. 999, pp. 41-50.

Kandhal, P.S., and M.E. Wenger. (1973) Evaluation of Properties of AC-20 Asphalt Cements. *Transp. Res. Rec.*, Vol. 468, pp. 56-64.

Kanhal, P.S., and M.E. Wenger. (1975) Asphalt Properties in Relation to Pavement Performance. *Transp. Res. Rec.*, Vol. 544, pp. 1-13.

Kaufman, H.S. (1978) *Introduction to Polymer Science and Technology: an SPE Textbook.* John Wiley & Sons, New York, NY, p. 312.

Knorr, D.B., Jr., Davison, R.R. and Glover, C.J. (2002) The Effect of Various Aging Techniques on Asphalt Low-Temperature Properties, *Transp. Res. Rec.*, 1810, pp. 9-16.

Kumar, A., and R.K. Gupta. (1998) *Fundamentals of Polymers*. McGraw-Hill, New York, NY.

Larson, R.G. (1999) *The Structure and Rheology of Complex Fluids*. Oxford University Press, New York, NY, p. 107.

Lau, C.K., K.M. Lunsford, C.J. Glover, R.R. Davison, and J.A. Bullin. (1992) Reaction Rates and Hardening Susceptibilities as Determined from POV Aging of Asphalts. *Transp. Res. Rec.*, Vol. 1342, pp. 50-57.

Lee, D.Y. (1968) Development of a Laboratory Durability Test for Asphalt. *HRB Report*, Vol. 231, p. 34.

Lee, D.Y. (1973) Asphalt Durability Test Correlations in Iowa. *Hwy. Res. Rec.*, Vol. 468, pp. 43-60.

Lee, D.Y., and R.J. Huang. (1973) Weathering of Asphalts as Characterized by Infrared Multiple Internal Reflection Spectra. *Anal. Chem.*, Vol. 46, p. 2242.

Leicht, S.E., P. Juristyarini, R.R. Davison, and C.J. Glover. (2001) An Investigation of Oxidative Curing on the Properties of High Cure Asphalt Rubber, *Petroleum Sci. and Technol.*, 19(3&4), pp. 317-334.

Lesueur, D., J.F. Gerard, P. Claudy, J.M. Letoffe, J.P. Planche, and D. Martin. (1996) A Structure-Related Model to Describe Asphalt Linear Viscoelasticity. *J. Rheology,* Vol. 40 (5), pp. 813-836.

Lewandowski, L.H. (1994) Polymer Modification of Paving Asphalt Binders. *Rubber Chemistry and Technology,* Vol. 67, pp. 447-480.

Lin, M.S., C.J. Glover, R.R. Davison, and J.A. Bullin. (1995a) The Effects of Asphaltenes on Asphalt Recycling and Aging. *Transp. Res. Rec.*, Vol. 1507, pp. 86-95.

Lin, M.S., J.M. Chaffin, R.R. Davison, C.J. Glover, and J.A. Bullin. (1998) A New Suspension Viscosity Model and Its Application to Asphaltene Association Thermodynamics and Structures.

Lin, M.S., J.M. Chaffin, M. Liu, C.J. Glover, R.R. Davison, and J.A. Bullin. (1996) The Effect of Asphalt Composition on the Formation of Asphaltenes and Their Contribution to Asphalt Viscosity. *Fuel Sci. and Technol. Intl*, Vol. 14 (1&2), pp. 139-162.

Lin, M.S., K.M. Lunsford, C.J. Glover, R.R. Davison, and J.A. Bullin. (1995b) The Effects of Asphaltenes on the Chemical and Physical Characteristics of Asphalts. In *Asphaltenes: Fundamentals and Applications*, E.Y. Sheu and O.C. Mullins (Eds.), Plenum Press, New York, NY, pp. 155-176.

Linde, S., and U. Johansson. (1992) Thermo-Oxidative Degradation of Polymer Modified Bitumen. In ASTM STP 1108: *Polymer Modified Asphalt Binders*, K.R. Wardlaw and S. Shuler (Eds.), American Society for Testing and Materials, San Antonio, TX, pp. 244-253.

Liu, M. (1996) *The Effects of Asphalt Fractional Composition on Properties*. Ph.D. Dissertation, Texas A&M University, College Station, TX.

Liu, M., J.M. Chaffin, R.R. Davison, C.J. Glover, and J.A. Bullin. (1997a) Reactivity of Asphalt Supercritical Fractions. *Ind. Eng. Chem. Res.*, Vol. 36 (6), pp. 2177-2183.

Liu, M., J.M. Chaffin, R.R. Davison, C.J. Glover, and J.A. Bullin. (1998a) Changes in Corbett Fraction Composition During Oxidation of Asphalt Fractions. *Transp. Res. Rec*., Vol. 1638, pp. 40-46.

Liu, M., M.A. Ferry, R.R. Davison, C.J. Glover, and J.A. Bullin. (1998b) Oxygen Uptake as Correlated to Carbonyl Growth in Aged Asphalts and Asphalt Corbett Fractions. *Ind. Eng. Chem. Res.*, Vol. 37, pp. 4669-4674.

Liu, M., M.S. Lin, J.M. Chaffin, R.R. Davison, C.J. Glover, and J.A. Bullin. (1997b) Compositional Optimization for a Superior Asphalt Binder. *Petroleum Sci. and Technol.*, Vol. 15 (1&2), pp. 471-493.

Liu, M., M.S. Lin, J.M. Chaffin, R.R. Davison, C.J. Glover, and J.A. Bullin. (1998c) Oxidation Kinetics of Asphalt Corbett Fractions and Compositional Dependence of Asphalt Oxidation. *Petroleum Science and Technology,* Vol. 16 (7&8), pp. 827-850.

Liu, M., K.M. Lunsford, R.R. Davison, C.J. Glover, and J.A. Bullin. (1996) The Kinetics of Carbonyl Formation in Asphalt. *AIChE J.*, Vol. 42 (4), pp. 1069-1076.

Lu, X., and U. Isacsson. (1999) Chemical and Rheological Characteristics of Styrene-Butadiene-Styrene Polymer-Modified Bitumens. *Transp. Res. Rec.*, Vol. 1661, pp. 83-92.

Lunsford, K.M. (1994) *The Effect of Temperature and Pressure on Laboratory Oxidized Asphalt Films with Comparison to Field Aging*. Ph.D. Dissertation, Texas A&M University, College Station, TX.

Madrid, R.C. (1997) *Compositional Evaluation of Asphalt Binder Recycling Agents*. M.S. Thesis, Texas A&M University, College Station, TX.

Martin, K.L., R.R. Davison, C.J. Glover, and J.A. Bullin. (1990) Asphalt Aging in Texas Roads and Test Sections. *Transp. Res. Rec.*, Vol. 1269, pp. 9-19.

McCrum, N.G., C.P. Buckley, and C.B. Bucknall. (1997) *Principles of Polymer Engineering*, 2nd Edition, Oxford Science Publications, p. 140.

McLeod, N.W. (1972) A 4-Year Survey of Low Temperature Transverse Pavement Cracking on Three Ontario Test Roads. *Proc. Assoc. Asphalt Paving Technol.*, Vol. 41, pp. 424-493.

Mullins, O.C., and E.Y. Sheu (Eds.). (1998) In *Structures and Dynamics of Asphaltenes*, Plenum Press, New York, NY, pp. 267-302.

Muncy, H.W., G.N. King, and J.B. Prudhomme. (1987) Improved Rheological Properties of Polymer-Modified Asphalts. In ASTM STP 941: *Asphalt Rheology: Relationship to Mixture*. O.E. Briscoe (Ed.), American Society for Testing and Materials, Nashville, TN, pp. 146-165.

Newman, J.K. (1998) Dynamic Shear Rheological Properties of Polymer-Modified Asphalt Binders. *Journal of Elastomers and Plastics*, Vol. 30, pp. 245-263.

Petersen, J.C. (1984) Chemical Composition of Asphalt as Related to Asphalt Durability-State-of-the-Art. *Transp. Res. Rec.*, Vol. 999, pp. 13-30.

Petersen, J.C. (1998) A Dual, Sequential Mechanism for the Oxidation for Petroleum Asphalts. *Pet. Sci. & Tech.*, Vol. 16, p. 1023.

Petersen, J.C., J.F. Branthaver, R.E. Robertson, P.M. Harnsberger, J.J. Duvall, and E.K. Ensley. (1993) Effects of Physicochemical Factors on Asphalt Oxidation Kinetics. *Transp. Res. Rec.*, Vol. 1391, p. 1.

Peterson, G.D., R.R. Davison, C.J. Glover, and J.A. Bullin. (1994) Effect of Composition on Asphalt Recycling Agent Performance. *Transp. Res. Rec.*, Vol. 1436, pp. 38-46.

Pfeiffer, J.P., and R.N.J. Saal. (1940) *J. Phys. Chem.*, Vol. 44, p. 139.

Quddus, M.A., S.N. Sarwar, and F. Khan. (1995) The Chemical Composition of Catalytic Air Blown Asphalt. *Fuel*, Vol. 74, p. 684.

Readshaw, E.E. (1972) Asphalt Specifications in British Columbia for Low Temperature Performance. *Proc. Assoc. Asphalt Paving Technol.*, Vol. 43, pp. 562-581.

Reese, R.E. (1997) Properties of Aged Asphalt binder Related to Asphalt Concrete Fatigue Life. *Proc. Assoc. Asphalt Paving Technol*., Vol. 66, pp. 604-632.

Reese, R.E., and J.L. Goodrich. (1993) California Desert Test Road – a Step Closer to Performance Based Specifications. *Proc. Assoc. Asphalt Paving Technol.*, Vol. 62, pp. 247-313.

Ruan, Y., Davison, R.R., and Glover, C.J. (2003) An Investigation of Asphalt Durability: Relationships between Ductility and Rheological Properties for Unmodified Asphalts, *Petroleum Science and Technology*, 21(1&2), pp. 231-254.

Shuler, T.S., J.H. Collins, and J.P. Kirkpatrick. (1987) Polymer-Modified Asphalt Properties Related to Asphalt Concrete Performance. In ASTM STP 941: *Asphalt Rheology: Relationship to Mixture*, O.E. Briscoe (Ed.), American Society for Testing and Materials, Nashville, TN., pp. 179-193.

Skog, J. (1967) 'Setting' and Durability Studies on Paving Grade Asphalts. *Proc. Assoc. Asphalt Paving Technol.*, Vol. 36, pp. 387-420.

Srivastava, A., P.C. Hopman, and A.A. Molenaar. (1992) SBS Polymer Modified Asphalt Binder and Its Implications on Overlay Design. In ASTM STP 1108: *Polymer Modified Asphalt Binders*, K.R. Wardlaw and S. Shuler (Eds.), American Society for Testing and Materials, San Antonio, TX, pp. 309-329.

Stegeman, J.R., R.R. Davison, C.J. Glover, and J.A. Bullin. (1991) Supercritical Fractionation and Reblending to Produce Improved Asphalts. *Proceedings of the International Symposium: Chemistry of Bitumens*, Rome, Italy, Vol. 1, pp. 336-381.

Stoffels, S.M., R. Roque, and T. Farwana. (1994) Evaluation and Field Validation of Proposed SHRP Binder Specification for Thermal Cracking. *Transp. Res. Rec.*, Vol. 1436, pp. 1-10.

Strategic Highway Research Program. (1993) *SHRP Materials Reference Library: Asphalt Cements: A Concise Data Compilation*, National Research Council, Washington D.C.

Tayebali, A.A., J.L. Goodrich, J.B. Sousa, and C.L. Monismith. (1992) Influence of the Rheological Properties of Modified Asphalt Binders on the Load Deformation Characteristics of the Binder-Aggregate Mixtures. In ASTM STP 1108: *Polymer Modified Asphalt Binders*, K.R.

Wardlaw and S. Shuler (Eds.), American Society for Testing and Materials, San Antonio, TX, pp. 77-96.

Texas Department of Transportation. (1995) Prediction of Moisture Induced Damage to Bituminous Paving Materials Using Molded Specimens. *Manual of Testing Procedures*. Section 10. Tex-531-C.

Vallerga, B.A., and W.J. Halstead. (1971) The Effect of Field Aging on Fundamental Properties of Paving Asphalts. *Highway Research Record*, Vol. 361, pp. 71-92.

Vassiliev, N.Y. (2001) *Studies of Asphalt Air Blowing and Development of a New Air Blowing Technique for Simulation of Asphalt Short-Term Aging*. M.S. Thesis, Texas A&M University, College Station, TX.

Welborn, J.Y. (1984) Physical Properties as Related to Asphalt Durability: State of the Art. *Transp. Res. Rec.*, Vol. 999, pp. 31-36.

Welborn, J.Y., E.R. Oglio, and J.A. Zenewitz. (1966) A Study of Viscosity-Graded Asphalt Cements. *Proc. Assoc. Asphalt Paving Technol.*, Vol. 35, pp. 19-60.

Williams, M.L., R.F. Landel, and J.F. Ferry. (1955) The Temperature Dependence of Relaxation Mechanisms in Amorphous Polymers and Other Glass Forming Liquids. *J. Am. Chem. Soc.*, Vol. 77, pp. 3701-3707.

APPENDIX A:

ADDITIONAL DSR FUNCTION AGING PROCEDURES DATA

Table A-6-1. Viscosity Hardening Rate and Initial Jump for All PAV and POV Aged Asphalts.

	Test #1 100 ºC 20 atm Air		Test #2 90 ºC 20 atm Air		Test #3 100 ºC 5 atm O_2		Test #4 110 ºC 1 atm O_2		Test #5 110 ºC 1 atm Air	
	HR[a]	IJ[b]	HR[a]	IJ[b]	HR[a]	IJ[b]	HR[a]	IJ[b]	HR[a]	IJ[b]
AAA-1	2.24	0.25	1.32	1.67	1.97	2.20	2.12	0.99	0.60	1.46
AAB-1	1.95	0.53	0.98	2.10	1.82	2.23	1.80	1.82	0.74	1.39
AAD-1	2.00	0.71	1.23	2.44	2.04	2.43	1.74	2.08	0.88	1.55
AAF-1	1.40	1.06	0.88	2.69	1.32	2.96	1.70	1.74	0.58	1.79
ABM-1	0.45	1.13	0.40	1.61	0.48	1.68	0.51	1.25	0.32	0.83
AAM-1	1.24	1.84	0.83	2.65	1.02	3.13	1.27	2.24	0.65	1.84
AAS-1	1.18	1.30	0.79	2.00	1.20	2.35	1.22	2.12	0.62	1.32
Lau4	1.25	0.74	0.67	1.90	1.29	1.81	1.16	1.68	0.54	1.12
TS2K	1.47	1.67	0.89	2.29	1.38	2.66	1.37	2.28	0.85	1.37

[a] HR unit = ln(poise)/day; [b] IJ unit = ln(poise)

Table A-6-1. Viscosity Hardening Rate and Initial Jump for All PAV and POV Aged Asphalts (Contd.).

	Test #6 100 ºC 1 atm O_2		Test #7 93 ºC 1 atm O_2		Test #8 88 ºC 0.2 atm O_2		Test #9 82 ºC 1 atm O_2	
	HR[a]	IJ[b]	HR[a]	IJ[b]	HR[a]	IJ[b]	HR[a]	IJ[b]
AAA-1	0.93	1.77	0.53	1.89	0.11	1.31	0.21	1.26
AAB-1	0.74	2.12	0.64	1.74	0.11	1.66	0.20	1.69
AAD-1	1.03	2.06	0.64	2.18	0.14	1.65	0.21	2.03
AAF-1	0.79	1.96	0.38	2.49	0.13	1.55	0.17	2.22
ABM-1	0.30	1.14	0.18	1.43	0.04	0.90	0.07	1.32
AAM-1	0.89	1.97	0.52	2.33	0.13	1.81	0.17	2.20
AAS-1	0.76	1.71	0.51	1.69	0.08	1.56	0.17	1.62
Lau4	0.73	1.23	0.43	1.43	0.09	1.23	0.13	1.59
TS2K	0.92	1.76	0.55	1.79	0.14	1.65	0.16	2.07

[a] HR unit = ln(poise)/day; [b] IJ unit = ln(poise)

Table A-6-2. DSR Function Hardening Rate and Initial Jump for PAV and POV Aged Asphalts.

	Test #1 100 ºC 20 atm Air		Test #2 90 ºC 20 atm Air		Test #3 100 ºC 5 atm O_2		Test #4 110 ºC 1 atm O_2		Test #5 110 ºC 1 atm Air	
	HR[a]	IJ[b]	HR[a]	IJ[b]	HR[a]	IJ[b]	HR[a]	IJ[b]	HR[a]	IJ[b]
AAA-1	1.80	3.20	1.25	3.87	2.39	3.78	1.90	3.36	0.67	3.31
AAB-1	1.64	3.31	1.07	4.06	1.43	4.92	1.49	4.28	0.87	3.00
AAD-1	1.48	3.41	1.31	3.69	1.88	4.04	1.59	3.47	0.87	2.73
AAF-1	1.32	4.78	0.80	6.33	0.89	7.03	1.33	5.68	0.73	4.75
ABM-1	0.86	3.83	0.75	4.86	0.89	4.97	1.00	4.05	0.80	2.82
AAM-1	1.15	3.74	0.80	4.49	1.20	4.10	0.94	4.54	0.65	3.61
AAS-1	1.15	2.90	0.76	3.70	1.03	4.18	1.06	3.88	0.73	2.62
Lau4	1.44	2.97	0.74	4.57	1.25	4.62	1.14	4.43	0.86	2.87
TS2K	1.13	2.38	0.68	2.89	1.00	3.25	1.00	2.87	0.67	2.05

[a] HR unit = ln(MPa/s)/day; [b] IJ unit = ln(MPa/s)

Table A-6-2. DSR Function Hardening Rate and Initial Jump for PAV and POV Aged Asphalts (Contd.).

	Test #6 100 ºC 1 atm O_2		Test #7 93 ºC 1 atm O_2		Test #8 88 ºC 1 atm Air		Test #9 82 ºC 1 atm O_2	
	HR[a]	IJ[b]	HR[a]	IJ[b]	HR[a]	IJ[b]	HR[a]	IJ[b]
AAA-1	0.99	3.72	0.60	3.73	0.15	2.92	0.24	3.16
AAB-1	0.79	4.08	0.76	3.53	0.13	3.37	0.20	3.75
AAD-1	1.09	3.21	0.59	3.58	0.13	2.99	0.21	3.31
AAF-1	0.86	5.19	0.47	5.76	0.20	4.33	0.18	5.53
ABM-1	0.65	3.71	0.37	4.33	0.10	3.28	0.16	4.23
AAM-1	0.91	3.64	0.52	4.07	0.14	3.49	0.16	4.11
AAS-1	0.80	3.22	0.57	3.17	0.08	3.07	0.18	3.09
Lau4	0.91	3.43	0.50	3.74	0.12	3.27	0.18	3.89
TS2K	0.81	2.21	0.50	2.19	0.12	2.18	0.14	2.51

[a] HR unit = ln(MPa/s)/day; [b] IJ unit = ln(MPa/s)

Table A-6-3. Viscosity and DSR Function Data after Aging in ER.

	Aging Time in Environmental Room (60 ºC, 1 atm Air)						
	2 mos	4 mos	6 mos	9 mos	12 mos	15 mos	22 mos
η* at 60ºC, 0.1 rad/s (poise)							
TX03-E	27,690	46,520	64,280				
TX03-A		8543	14,100	23,390	33, 640		
TX03-B	8039	13,680	19,980	26,290	47,100		
TX03-F	24,010	44,260	85,760	247,800			
TX03-G	3977	5,617	6726	10,290			
TX03-N	18,840	29,710	43,700	92,890			
TX03-T	19,660	35,630	60,400	144,500			
TX03-U	12,790	24,970	32,130	109,700			
TX03-V	16,570	31,010	44,380	101,200			
TX03-W	32,590	65,380	82,650	155,400			
Function at 44.7ºC, 10 rad/s (MPa/s)							
TX03-E	4.08×10^{-4}	7.76×10^{-4}	1.47×10^{-3}	2.40×10^{-3}	4.35×10^{-3}		
TX03-A	6.02×10^{-5}	1.82×10^{-4}	3.20×10^{-4}	6.89×10^{-4}	1.31×10^{-3}	2.62×10^{-3}	7.55×10^{-3}
TX03-B	7.44×10^{-5}	2.01×10^{-4}	4.03×10^{-4}	8.63×10^{-4}	1.66×10^{-3}	2.84×10^{-3}	
TX03-F	1.95×10^{-4}	5.92×10^{-4}	1.66×10^{-3}	4.50×10^{-3}			
TX03-G			3.74×10^{-5}	5.86×10^{-5}	3.04×10^{-4}		
TX03-N	1.44×10^{-4}	2.48×10^{-4}	4.67×10^{-4}	1.45×10^{-3}			
TX03-T	1.20×10^{-4}	3.11×10^{-4}	6.73×10^{-4}	1.88×10^{-3}			
TX03-U	1.37×10^{-4}	3.62×10^{-4}	6.88×10^{-4}	1.93×10^{-3}			
TX03-V	1.34×10^{-4}	2.70×10^{-4}	4.77×10^{-4}	1.14×10^{-3}	1.83×10^{-3}		
TX03-W				2.20×10^{-3}	3.72×10^{-3}		

Table A-6-4. Viscosity and DSR Function Data After POV Aging.

	POV 100 ºC, 1 atm O_2			POV 100 ºC, 20 atm Air	
	24 hours	52 hours	72.25 hours	24 hours	30 hours
η* at 60ºC, 0.1 rad/s (poise)					
TX03-E	21,850	80,450	132,400	61,750	55,920
TX03-A	54,710	12,490	30,630	9550	10,700
TX03-B	958,300	23,640	37,880	14,110	16,270
TX03-F	255,400	188,300	317,900	91,750	141,200
TX03-G	66,200	7724	14,470	6237	8123
TX03-N	192,000	79,310	269,800	40,040	65,220
TX03-T	231,300	96,700	319,400	61,390	98,980
TX03-U	146,500	108,600	260,100	46,850	74,220
TX03-V	161,700	200,600	621,900	74,870	115,300
TX03-W	260,400	359,200	932,200	179,300	272,500
Function at 44.7ºC, 10 rad/s (MPa/s)					
TX03-E	3.24×10^{-4}	1.71×10^{-3}	2.64×10^{-3}	1.45×10^{-3}	1.25×10^{-3}
TX03-A	2.20×10^{-5}	1.96×10^{-4}	6.11×10^{-4}	1.24×10^{-4}	1.55×10^{-4}
TX03-B	4.91×10^{-5}	3.90×10^{-4}	8.49×10^{-4}	1.69×10^{-4}	2.28×10^{-4}
TX03-F	3.80×10^{-4}	3.19×10^{-3}	4.91×10^{-3}	1.58×10^{-3}	2.45×10^{-3}
TX03-G	1.48×10^{-5}	5.83×10^{-5}	1.94×10^{-4}	3.56×10^{-5}	7.22×10^{-5}
TX03-N	2.46×10^{-4}	1.19×10^{-3}	3.07×10^{-3}	6.93×10^{-4}	1.04×10^{-3}
TX03-T	3.51×10^{-4}	1.05×10^{-3}	3.30×10^{-3}	8.14×10^{-4}	1.46×10^{-3}
TX03-U	2.49×10^{-4}	1.26×10^{-3}	2.86×10^{-3}	5.85×10^{-4}	1.06×10^{-3}
TX03-V	3.58×10^{-4}	1.70×10^{-3}	4.26×10^{-3}	7.38×10^{-4}	1.22×10^{-3}
TX03-W	7.32×10^{-4}	2.65×10^{-3}	6.03×10^{-3}	1.59×10^{-3}	2.52×10^{-3}

Table A-6-5. Viscosity and DSR Function Data After POV Aging.

	POV 100 ºC, 5 atm Air			
	24 hours	29 hours	52.75 hours	76.75 hours
η* at 60ºC, 0.1 rad/s (poise)				
SHRPAAD-1		29,010	32,690	87,200
SHRP AAF-1		28,400	33,820	90,610
TS2K		59,760	92,600	240,100
TX03-E		20,400	39,040	86,220
TX03-F		26,950	45,090	127,100
TX03-U		16,010	32,090	93,840
TX03-W		64,020	144,700	387,100
TS2K		52,820	54,370	66,560
TX03-EM		25,980	34,000	78,830
TX20-FM	23,510	13,470	17,710	24,000
TX03-UM		21,130	27,650	36,168
TX03-WM		139,500	174,400	217,964
Function at 44.7ºC, 10 rad/s (MPa/s)				
SHRPAAD-1		$1.84x10^{-4}$	$2.40x10^{-4}$	$5.87x10^{-4}$
SHRP AAF-1		$6.40x10^{-4}$	$7.35x10^{-4}$	$2.76x10^{-3}$
TS2K		$5.75x10^{-4}$	$8.00x10^{-4}$	$1.84x10^{-3}$
TX03-E		$2.78x10^{-4}$	$8.44x10^{-4}$	$1.88x10^{-3}$
TX03-F		$2.67x10^{-4}$	$5.94x10^{-4}$	$2.14x10^{-3}$
TX03-U		$1.46x10^{-4}$	$3.64x10^{-4}$	$1.20x10^{-3}$
TX03-W		$6.14x10^{-4}$	$1.45x10^{-3}$	$3.41x10^{-3}$
TS2K		$3.20x10^{-4}$	$4.36x10^{-4}$	$6.47x10^{-4}$
TX03-EM		$4.06x10^{-4}$	$9.62x10^{-4}$	$1.77x10^{-3}$
TX20-FM		$7.63x10^{-5}$	$1.48x10^{-4}$	$3.15x10^{-4}$
TX03-UM	$2.25x10^{-4}$	$2.44x10^{-4}$	$3.82x10^{-4}$	$5.96x10^{-4}$
TX03-WM		$3.24x10^{-4}$	$4.62x10^{-3}$	$6.57x10^{-3}$

APPENDIX B:

ADDITIONAL DSR FUNCTION HARDENING KINETICS GRAPHS

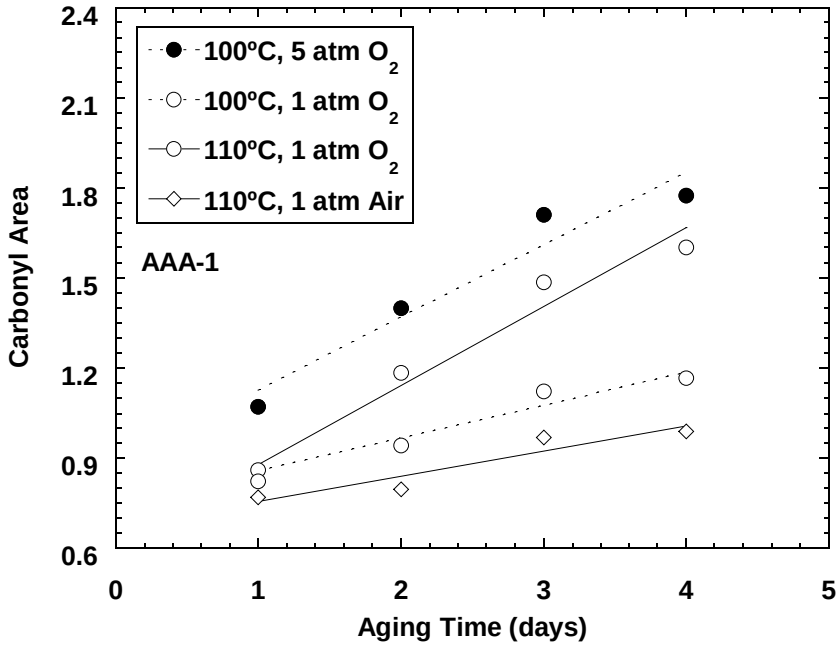

Figure B-7-1. Carbonyl Area versus Aging Time for SHRP AAA-1.

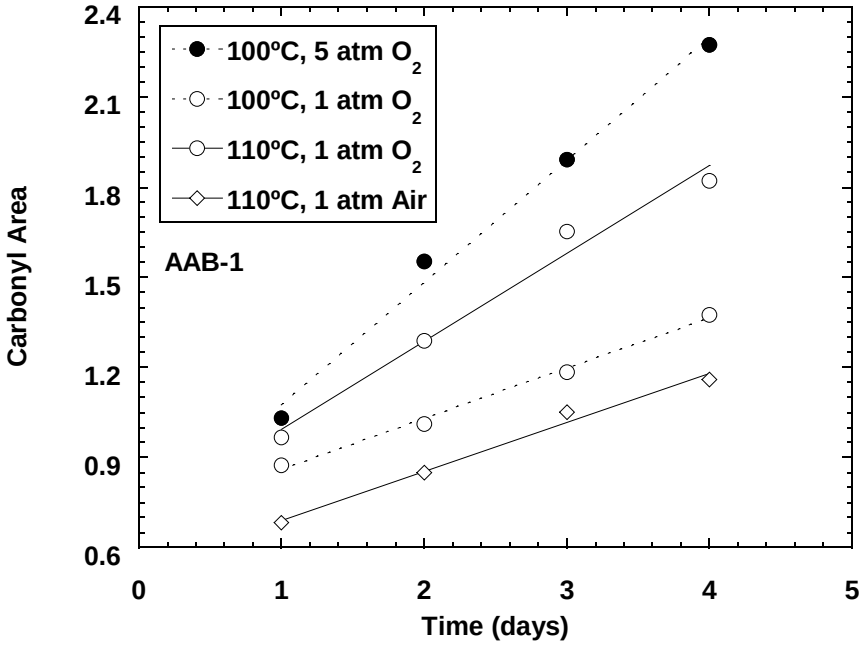

Figure B-7-2. Carbonyl Area versus Aging Time for SHRP AAB-1.

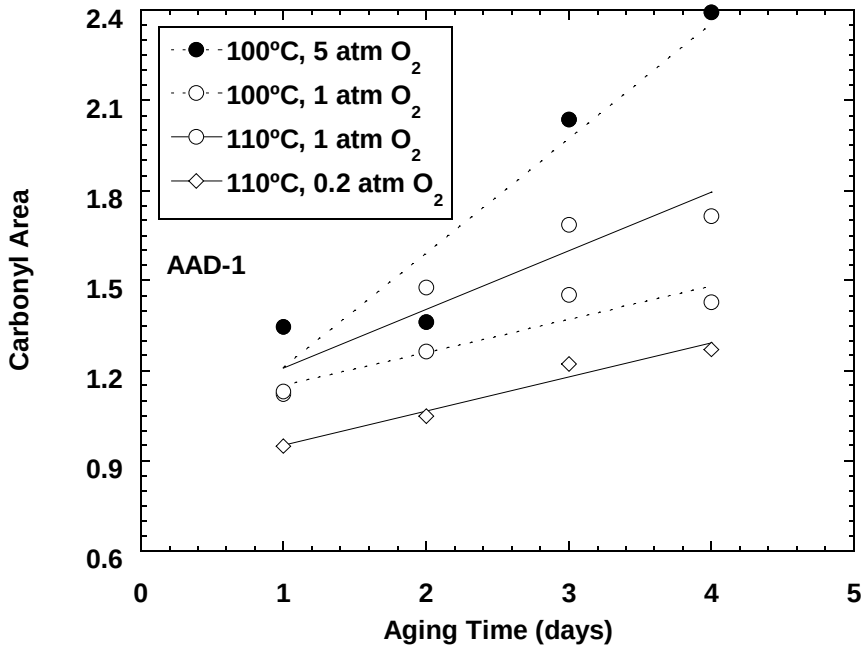

Figure B-7-3. Carbonyl Area versus Aging Time for SHRP AAD-1.

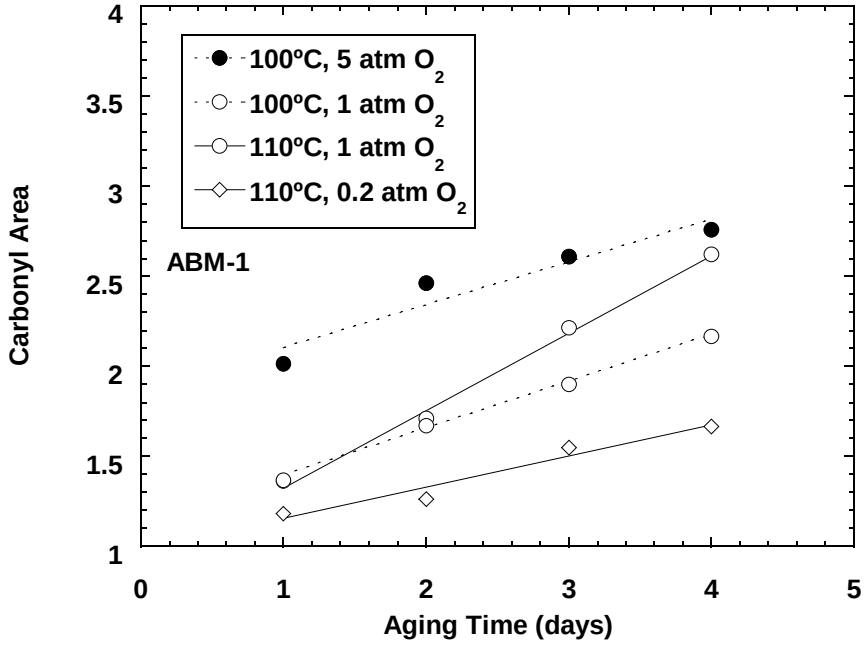

Figure B-7-4. Carbonyl Area versus Aging Time for SHRP ABM-1.

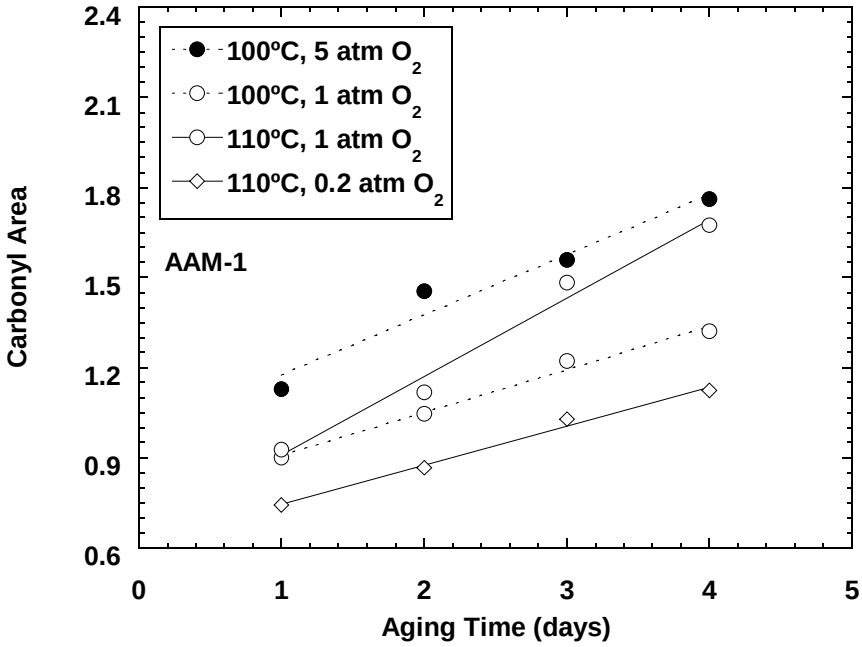

Figure B-7-5. Carbonyl Area versus Aging Time for SHRP AAM-1.

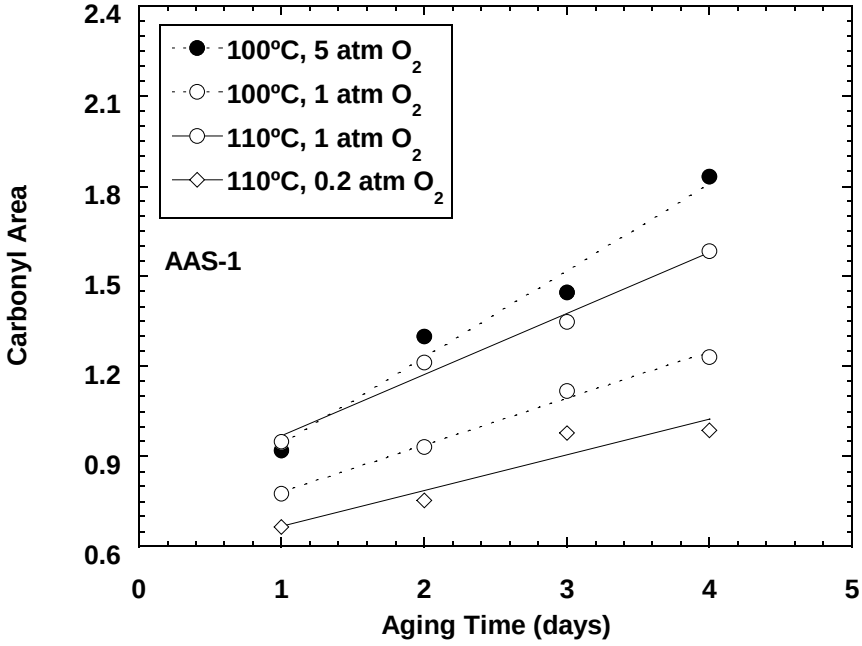

Figure B-7-6. Carbonyl Area versus Aging Time for SHRP AAS-1.

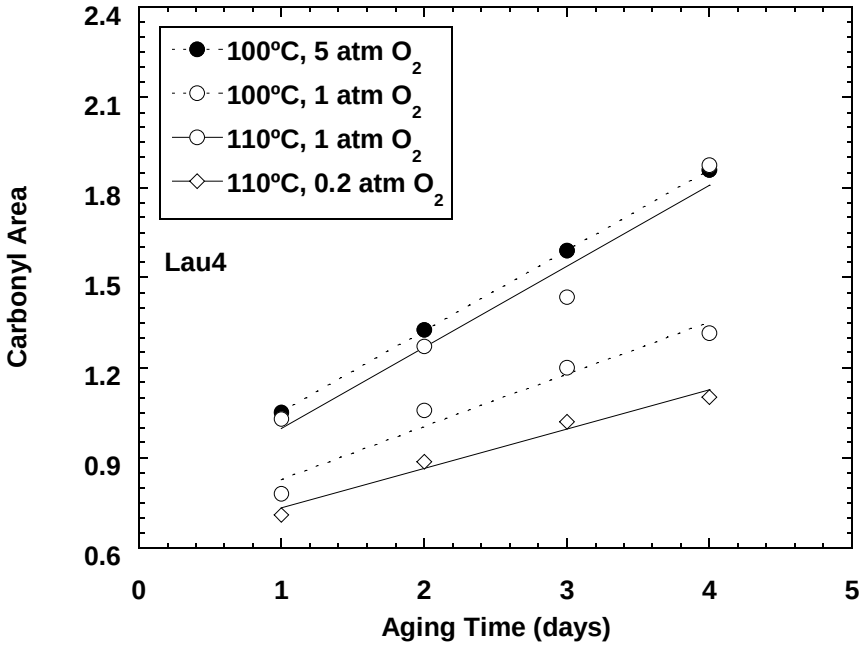

Figure B-7-7. Carbonyl Area versus Aging Time for Lau4.

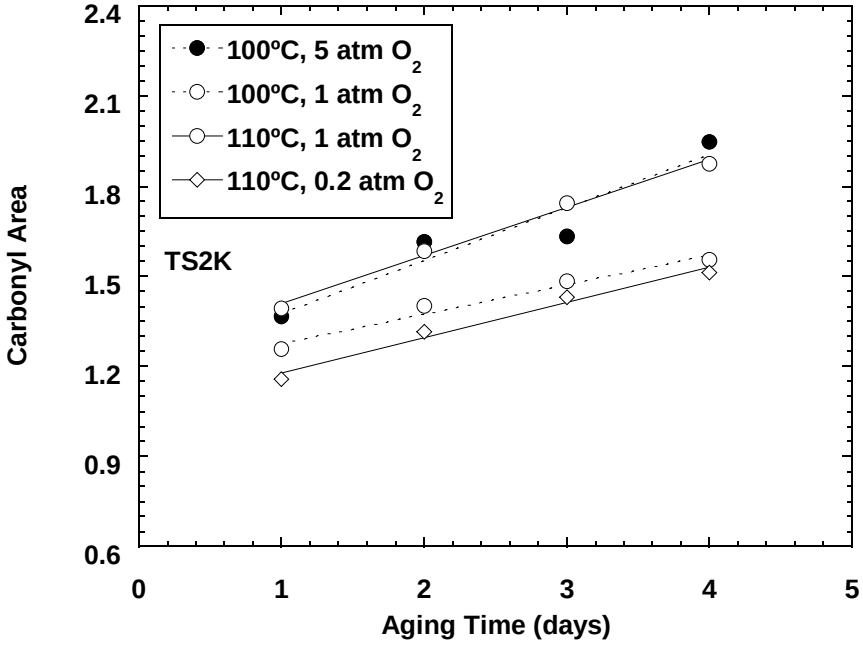

Figure B-7-8. Carbonyl Area versus Aging Time for TS2K.

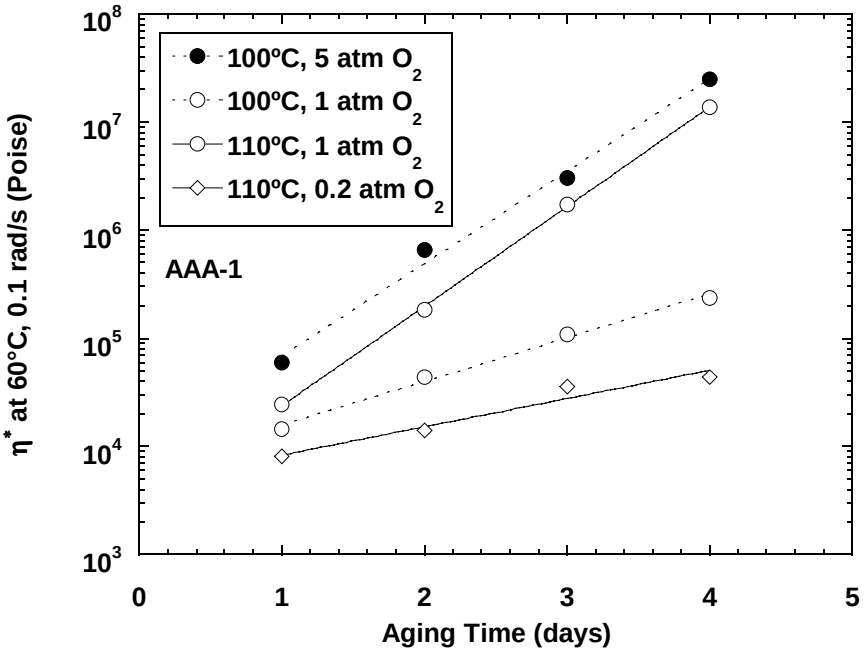

Figure B-7-9. Viscosity Hardening Rate for SHRP AAA-1.

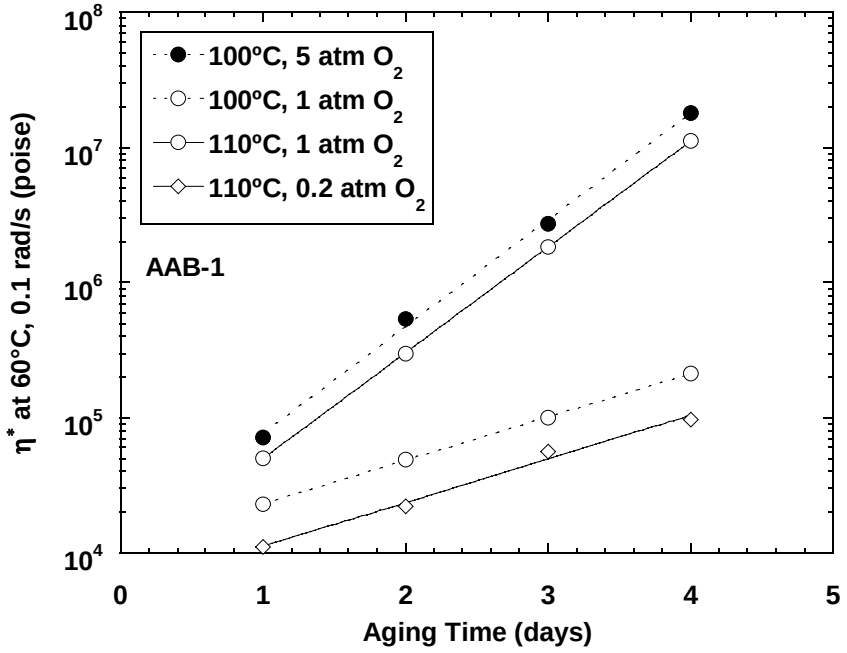

Figure B-7-10. Viscosity Hardening Rate of SHRP AAB-1.

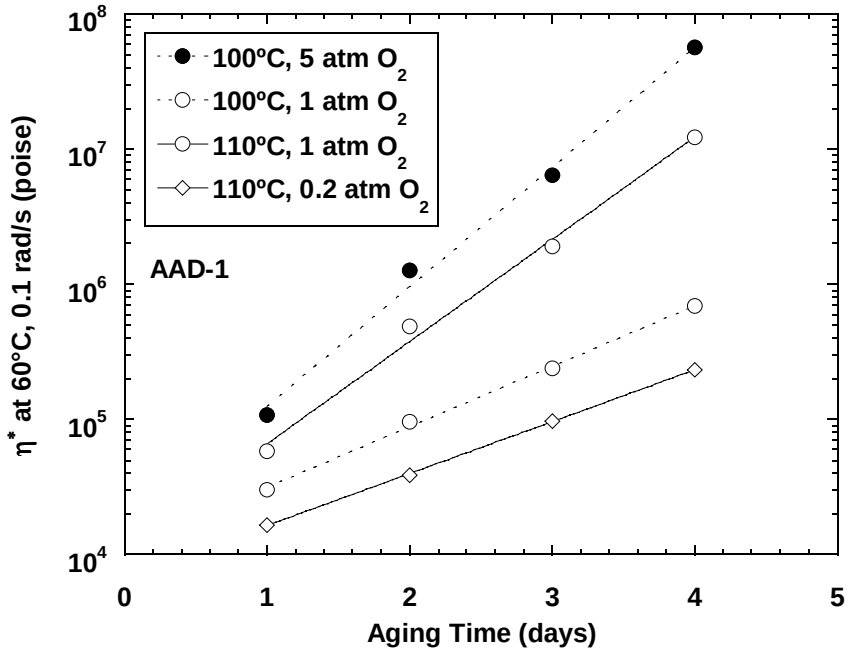

Figure B-7-11. Viscosity Hardening Rate of SHRP AAD-1.

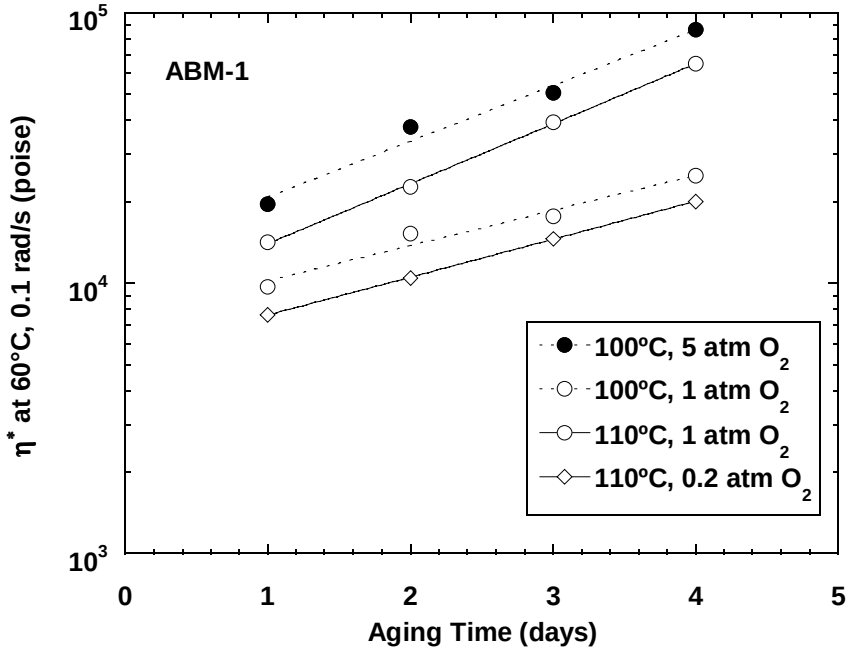

Figure B-7-12. Viscosity Hardening Rate of SHRP ABM-1.

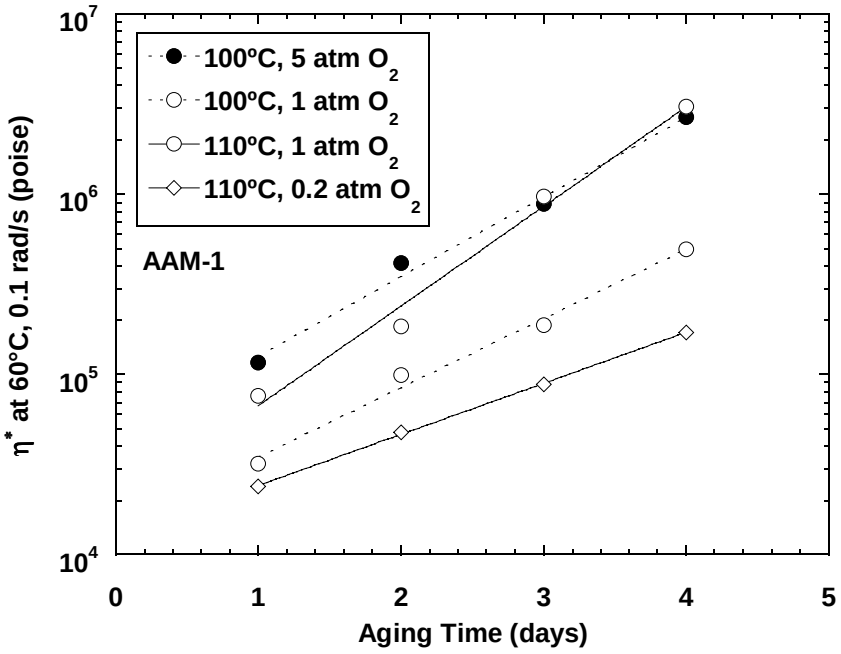

Figure B-7-13. Viscosity Hardening Rate of SHRP AAM-1.

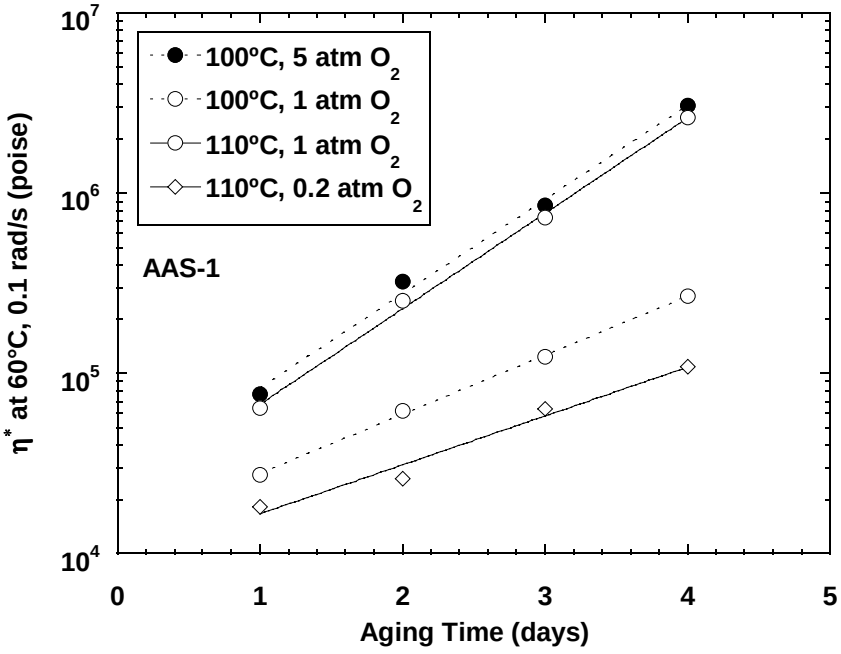

Figure B-7-14. Viscosity Hardening Rate of SHRP AAS-1.

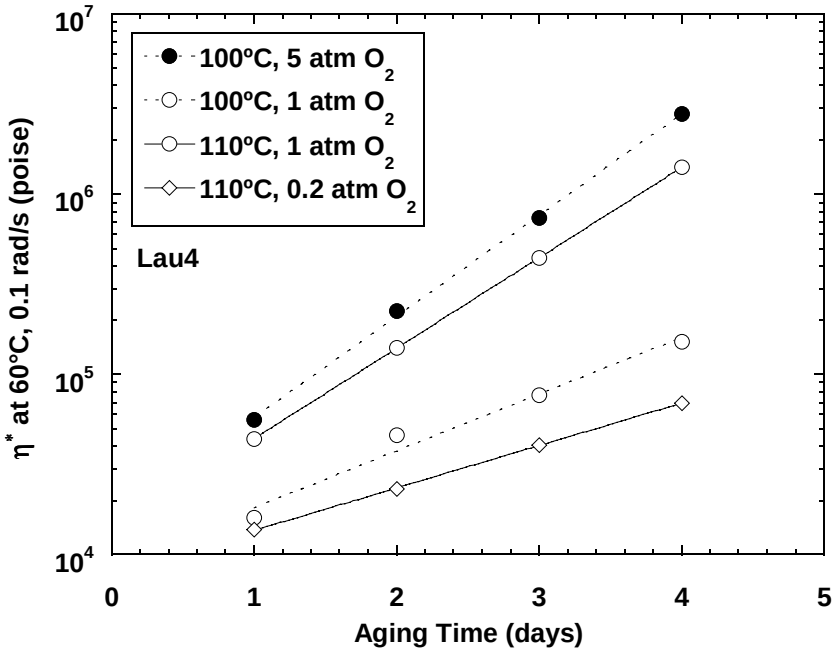

Figure B-7-15. Viscosity Hardening Rate of Lau4.

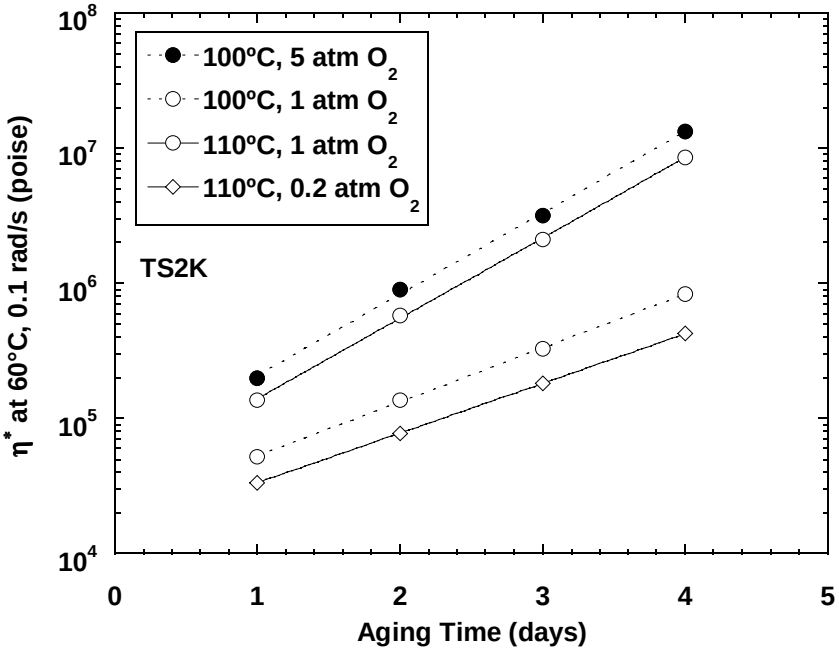

Figure B-7-16. Viscosity Hardening Rate of TS2K.

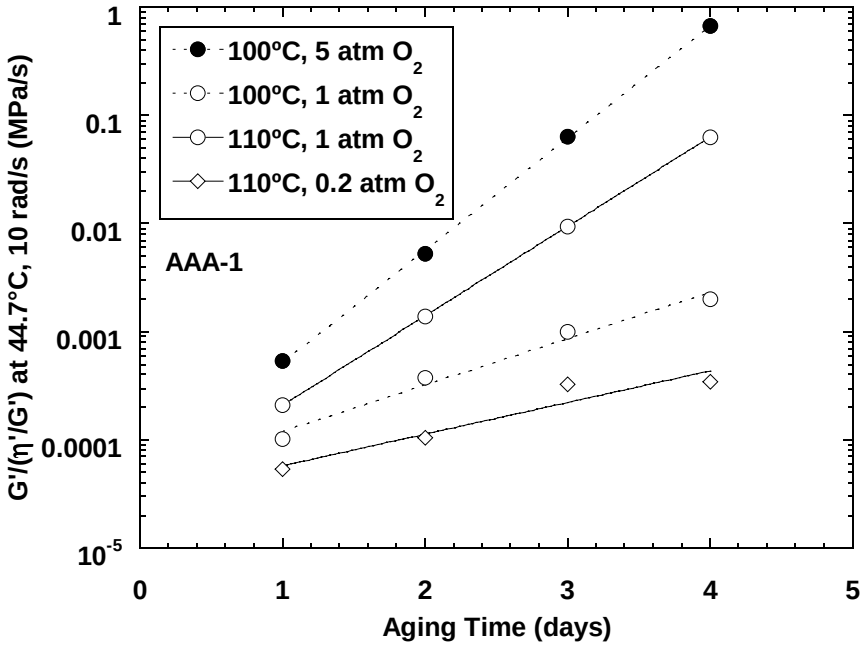

Figure B-7-17. DSR Function Hardening Rate of SHRP AAA-1.

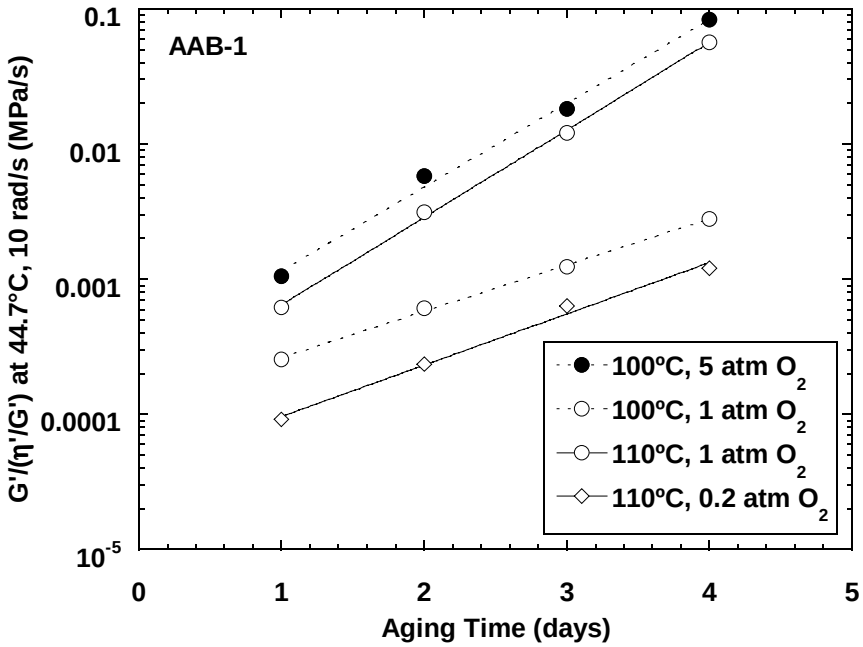

Figure B-7-18. DSR Function Hardening Rate of SHRP AAB-1.

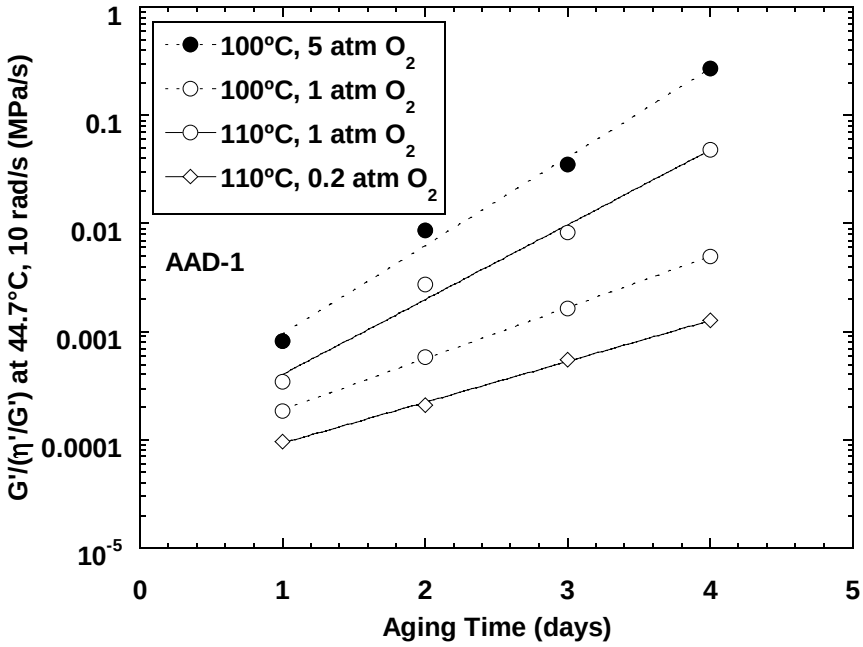

Figure B-7-19. DSR Function Hardening Rate of SHRP AAD-1.

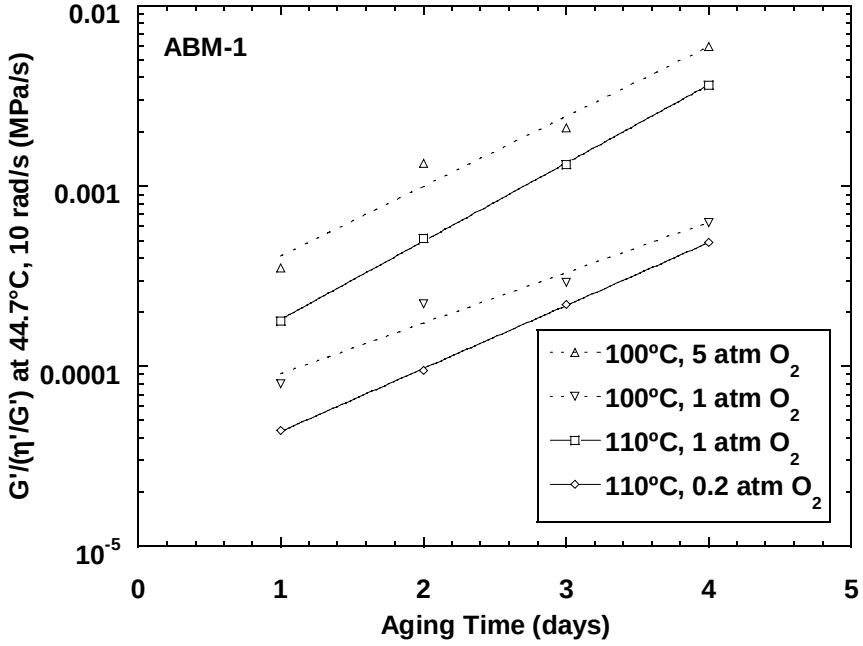

Figure B-7-20. DSR Function Hardening Rate of SHRP ABM-1.

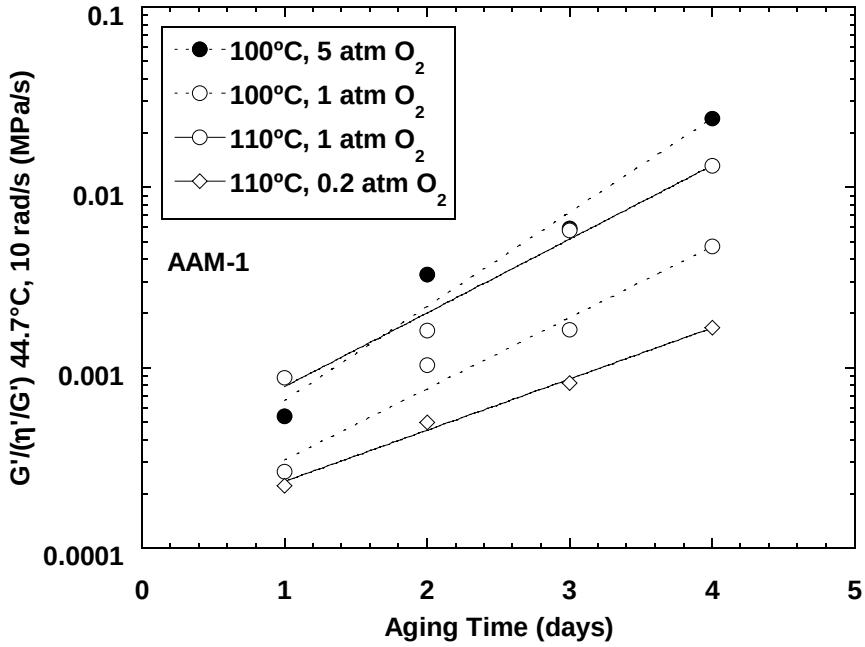

Figure B-7-21. DSR Function Hardening Rate of SHRP AAM-1.

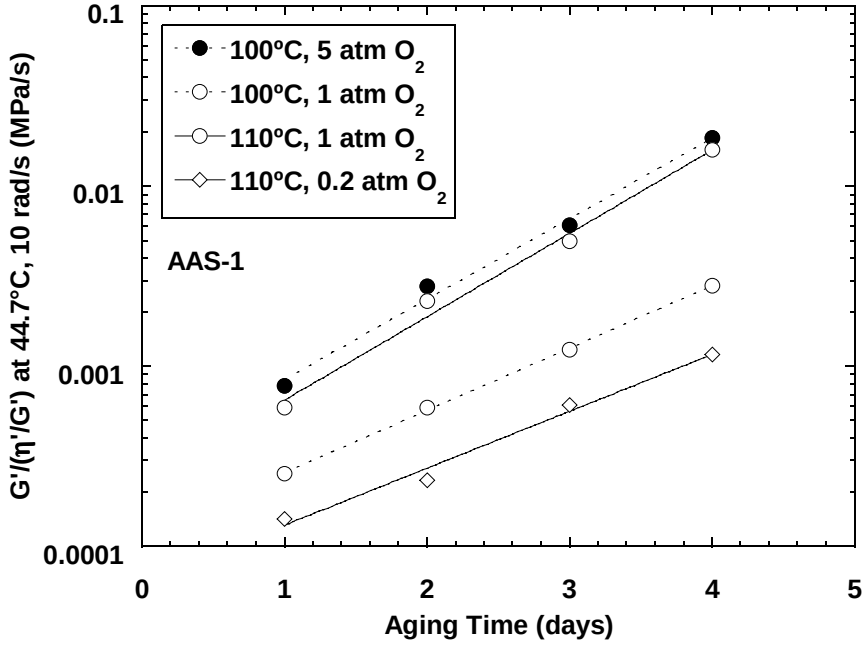

Figure B-7-22. DSR Function Hardening Rate of SHRP AAS-1.

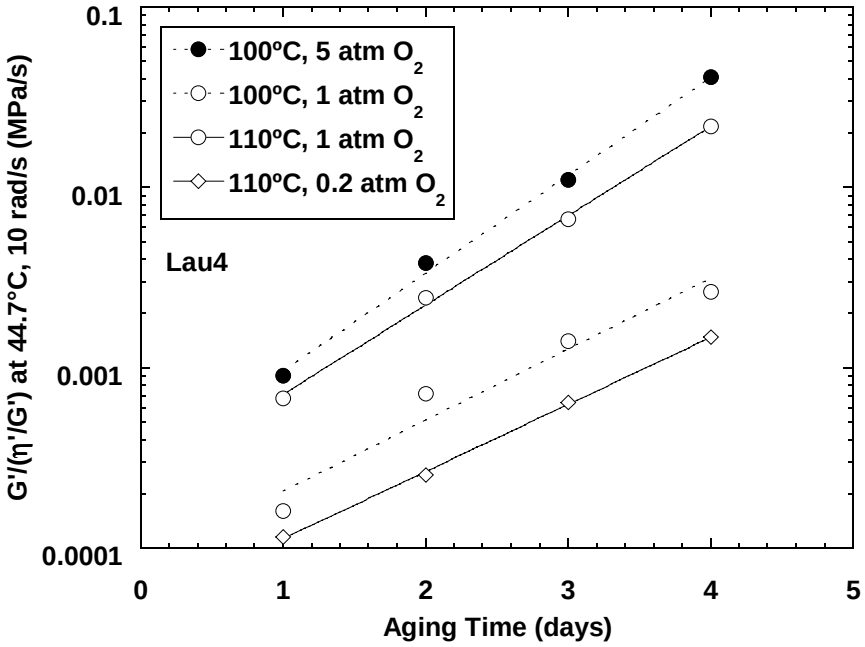

Figure B-7-23. DSR Function Hardening Rate of Lau4.

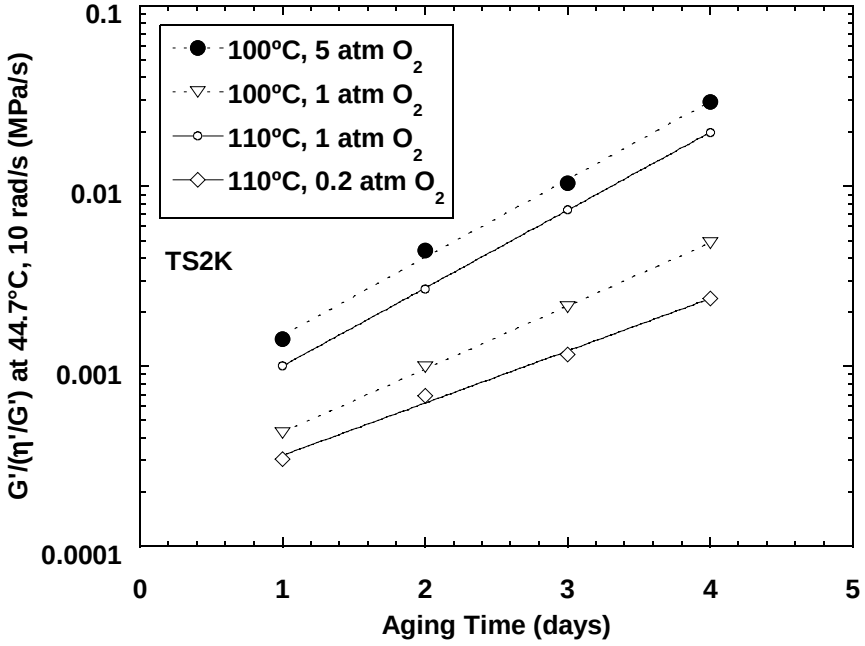

Figure B-7-24. DSR Function Hardening Rate of TS2K.

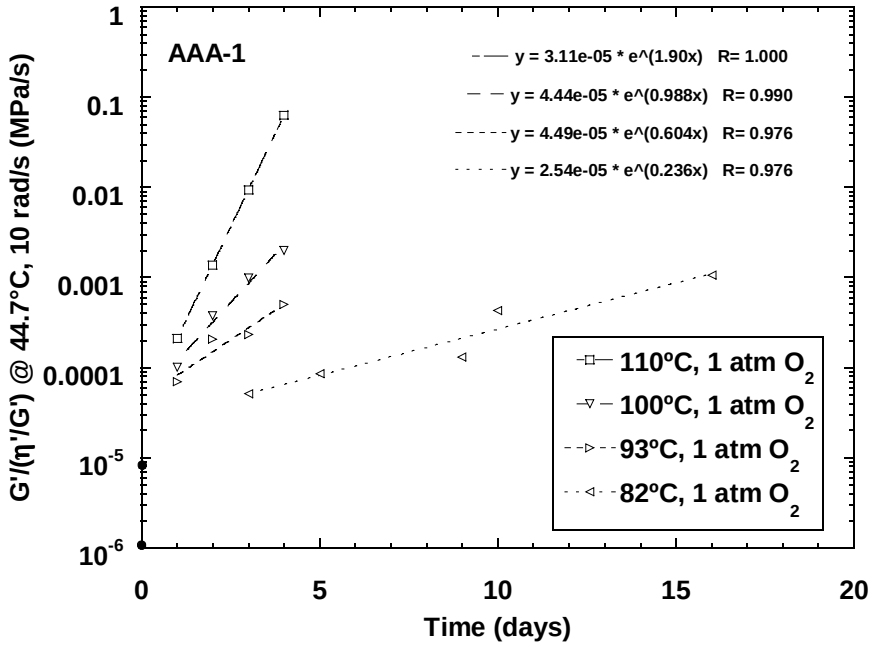

Figure B-7-25. DSR Function Hardening Rate of SHRP AAA-1, Varying Temperature.

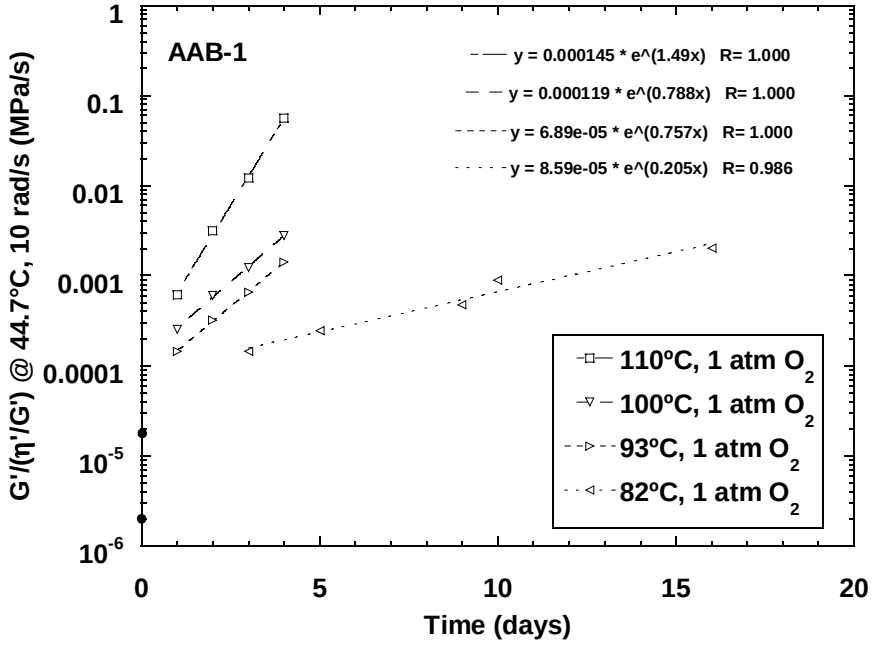

Figure B-7-26. DSR Function Hardening Rate of SHRP AAB-1, Varying Temperature.

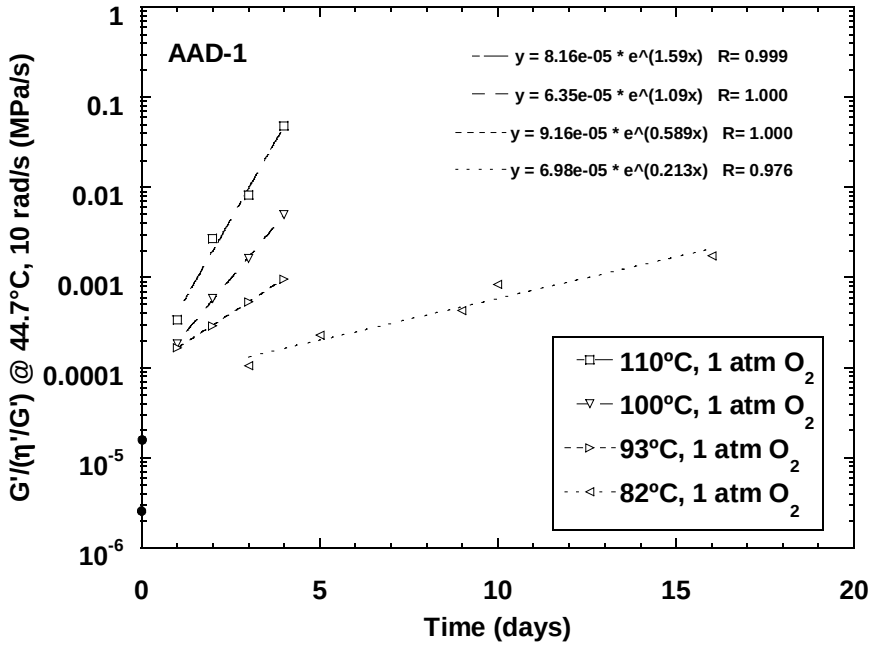

Figure B-7-27. DSR Function Hardening Rate of SHRP AAD-1, Varying Temperature.

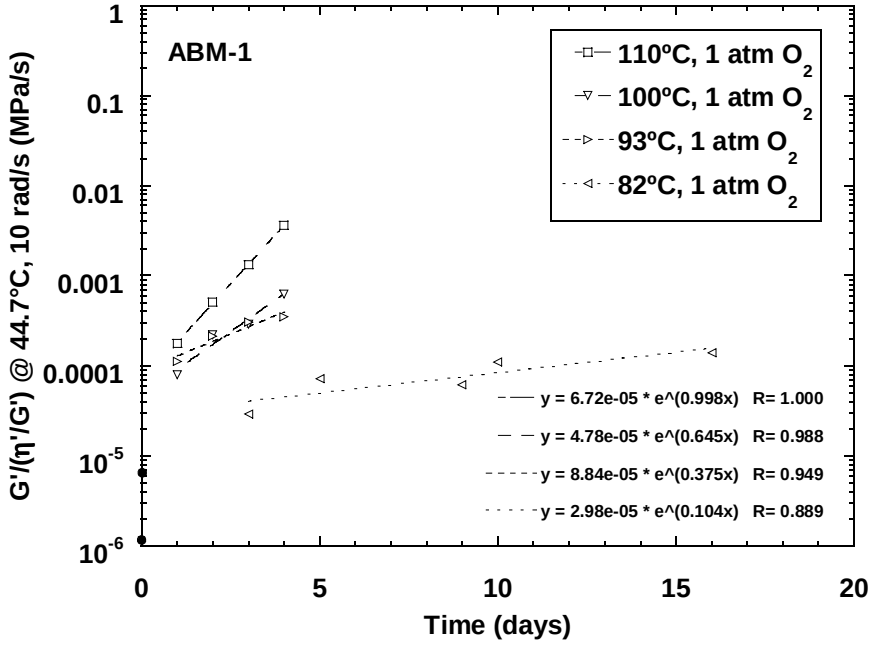

Figure B-7-28. DSR Function Hardening Rate of SHRP ABM-1, Varying Temperature.

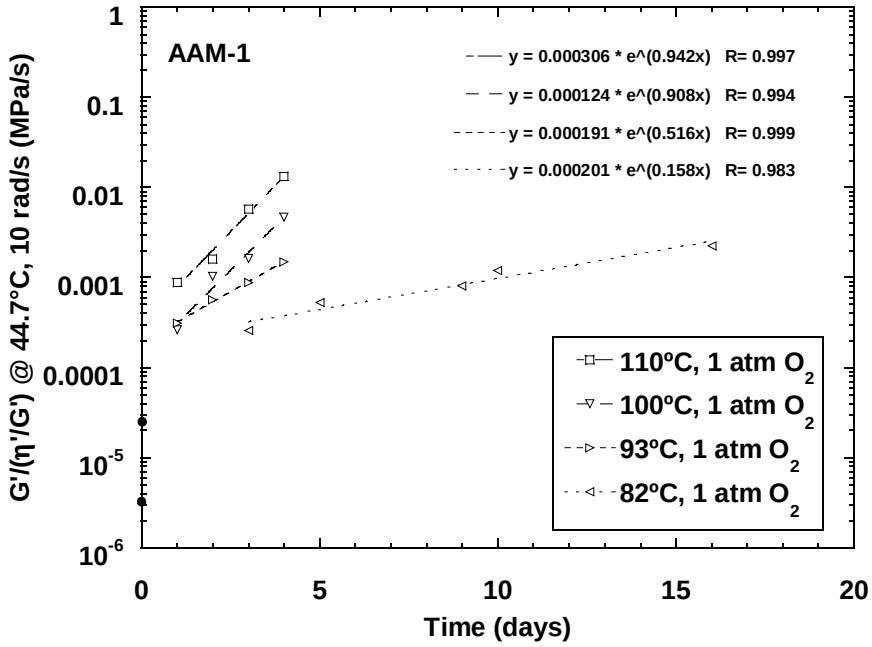

Figure B-7-29. DSR Function Hardening Rate of SHRP AAM-1, Varying Temperature.

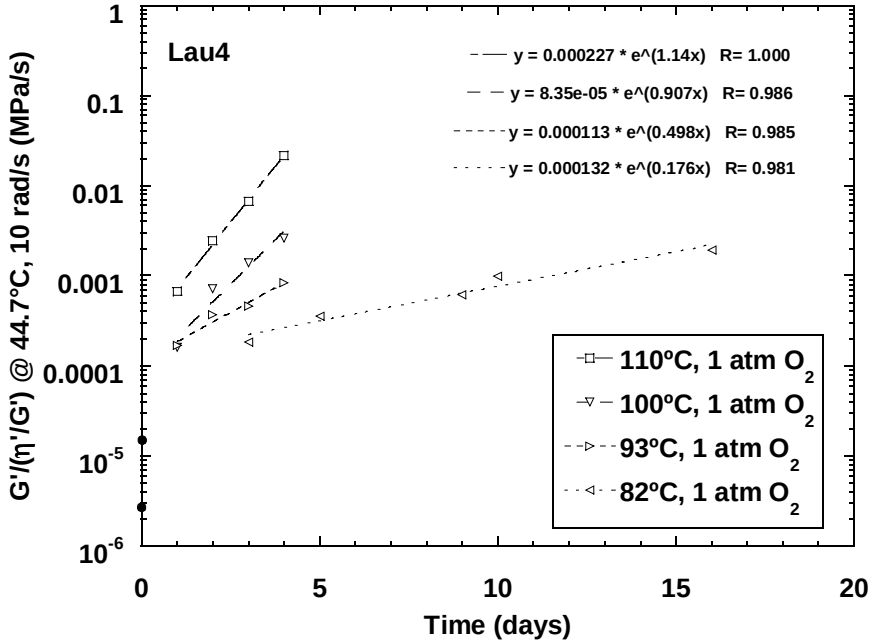

Figure B-7-30. DSR Function Hardening Rate of Lau4, Varying Temperature.

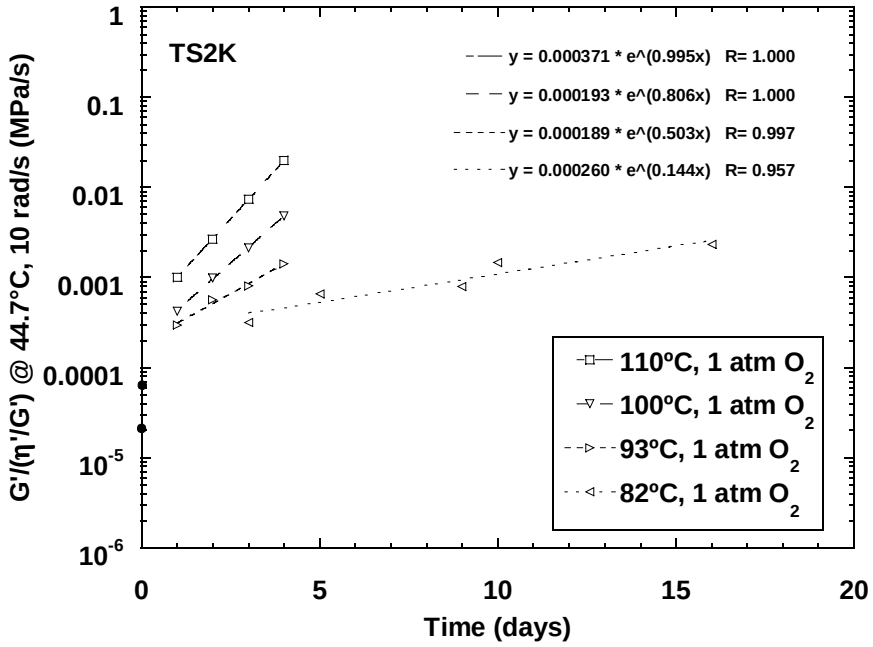

Figure B-7-31. DSR Function Hardening Rate of TS2K, Varying Temperature.

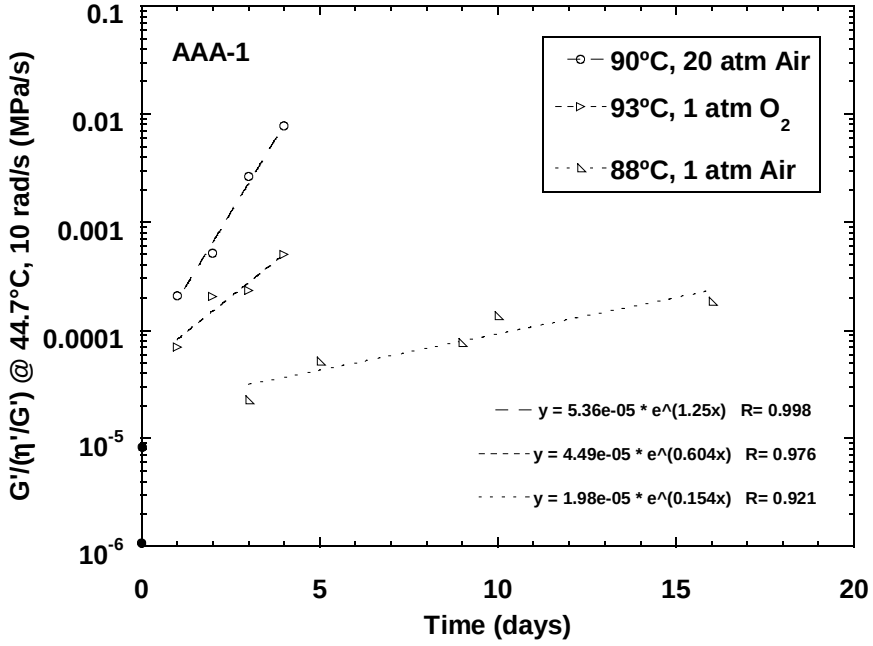

Figure B-7-32. DSR Function Hardening Rate of SHRP AAA-1, Varying Pressure.

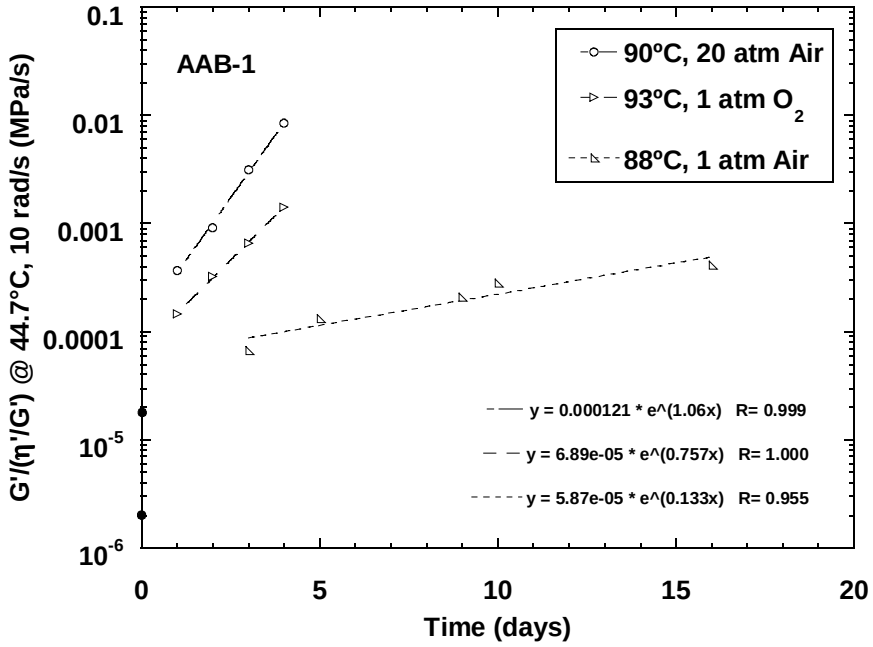

Figure B-7-33. DSR Function Hardening Rate of SHRP AAB-1, Varying Pressure.

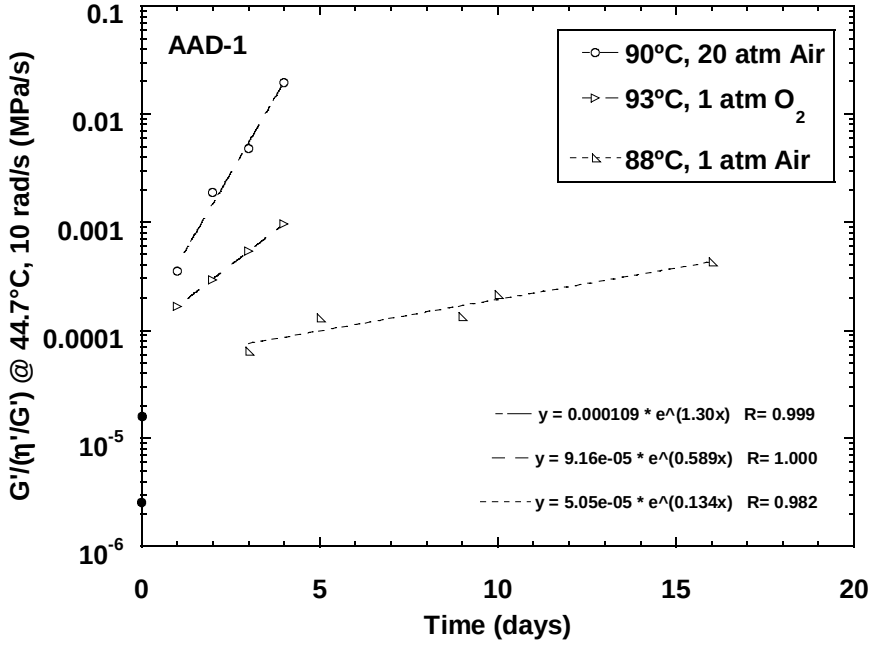

Figure B-7-34. DSR Function Hardening Rate of SHRP AAD-1, Varying Pressure.

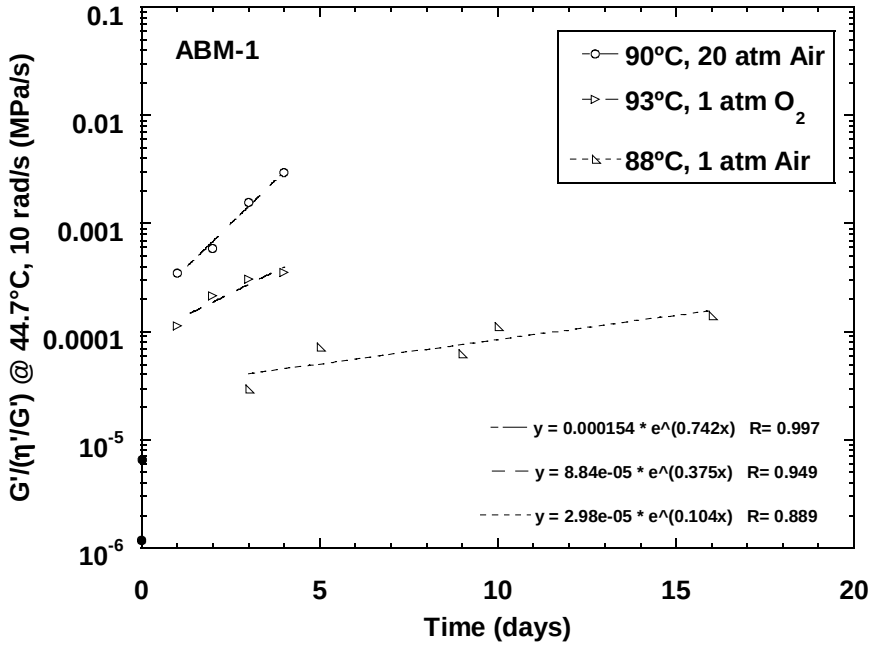

Figure B-7-35. DSR Function Hardening Rate of SHRP ABM-1, Varying Pressure.

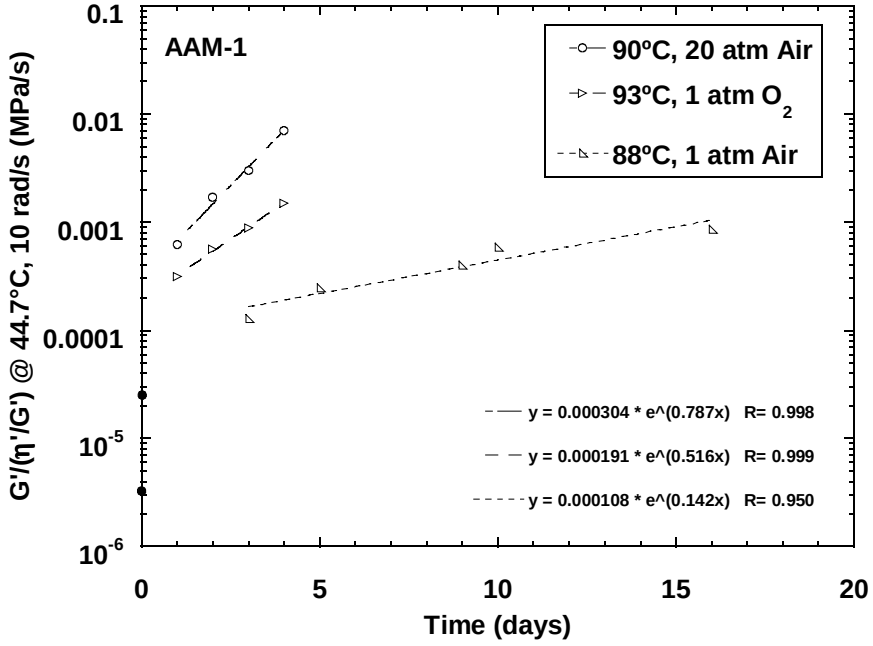

Figure B-7-36. DSR Function Hardening Rate of SHRP AAM-1, Varying Pressure.

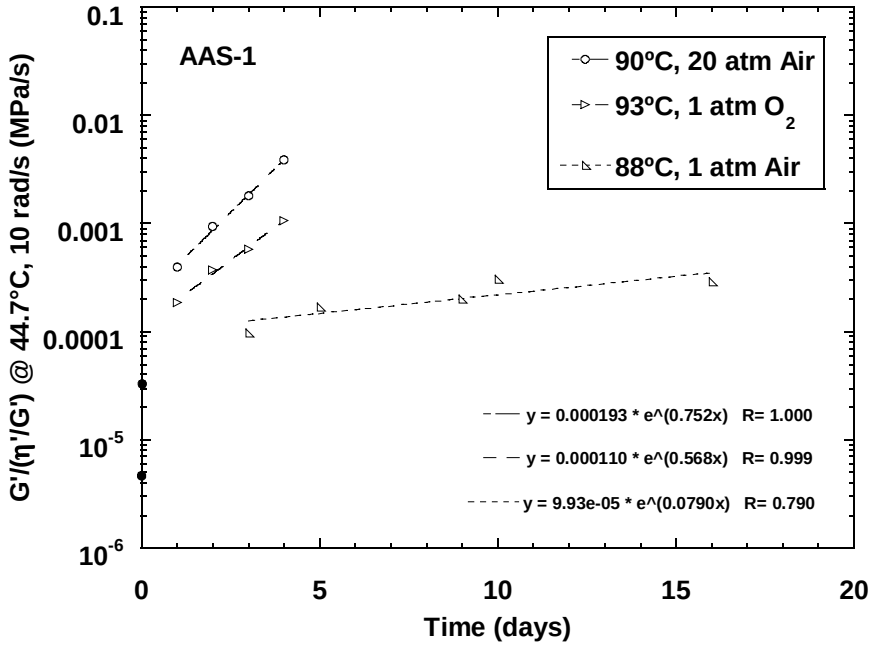

Figure B-7-37. DSR Function Hardening Rate of SHRP AAS-1, Varying Pressure.

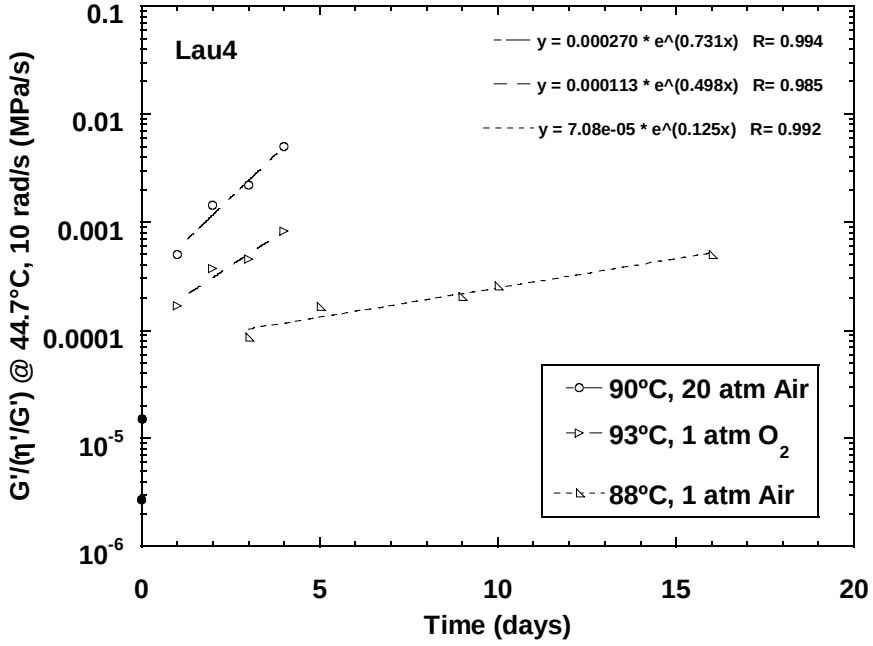

Figure B-7-38. DSR Function Hardening Rate of Lau4, Varying Pressure.

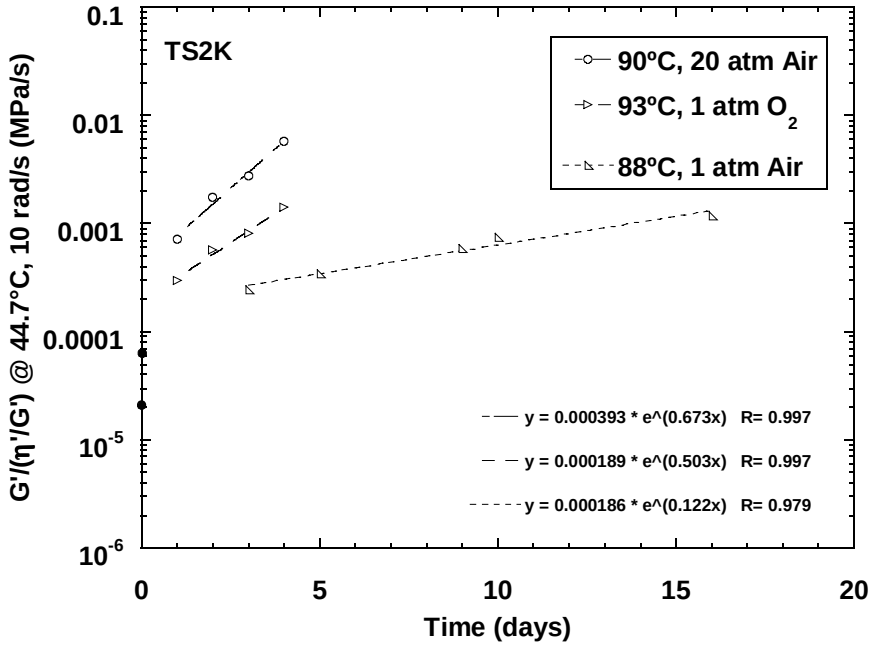

Figure B-7-39. DSR Function Hardening Rate of TS2K, Varying Pressure.

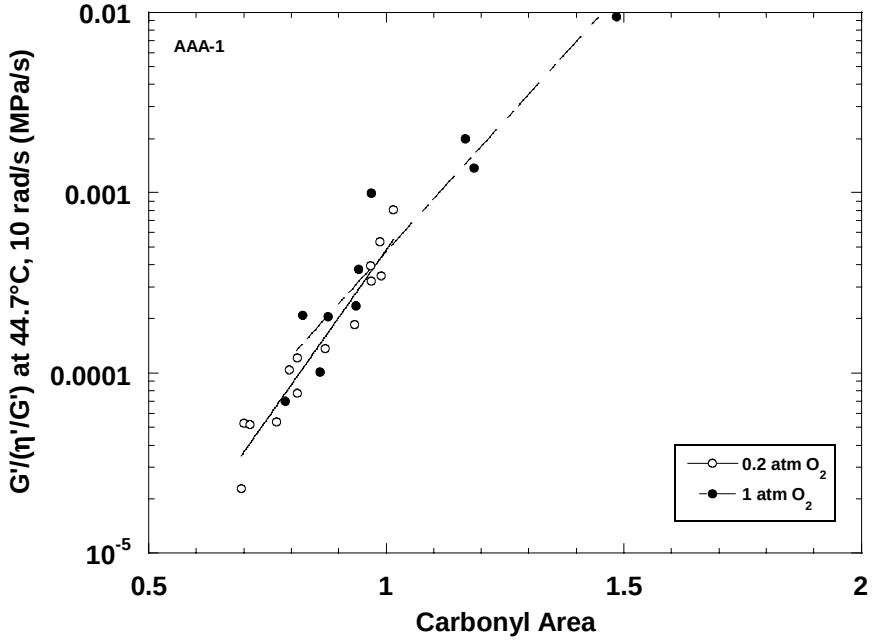

Figure B-7-40. DSR Function Hardening Susceptibility of AAA-1.

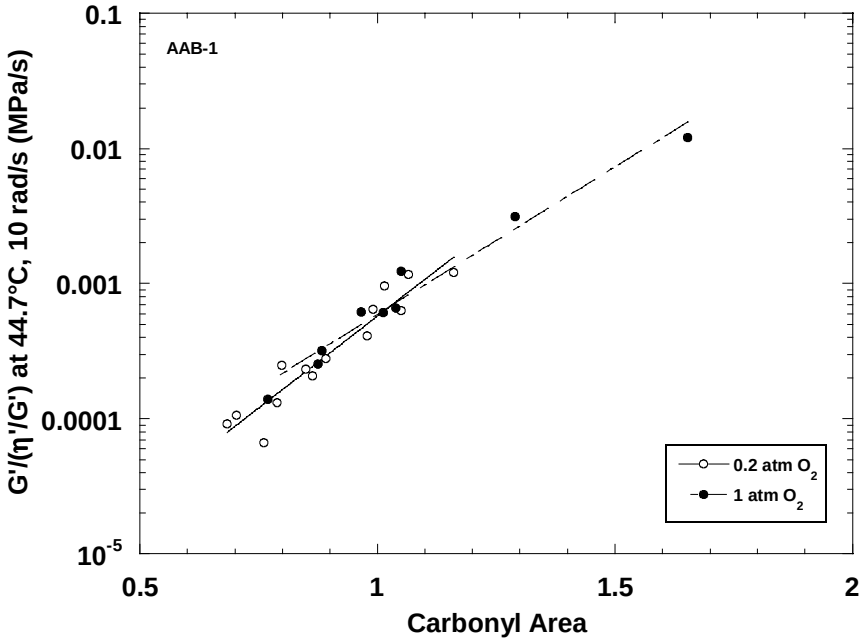

Figure B-7-41. DSR Function Hardening Susceptibility of AAB-1.

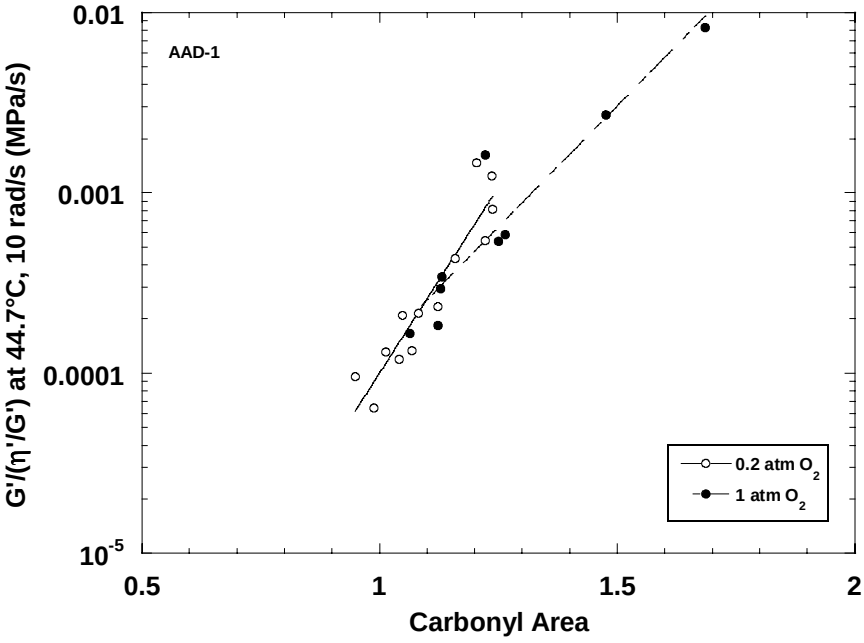

Figure B-7-42. DSR Function Hardening Susceptibility of AAD-1.

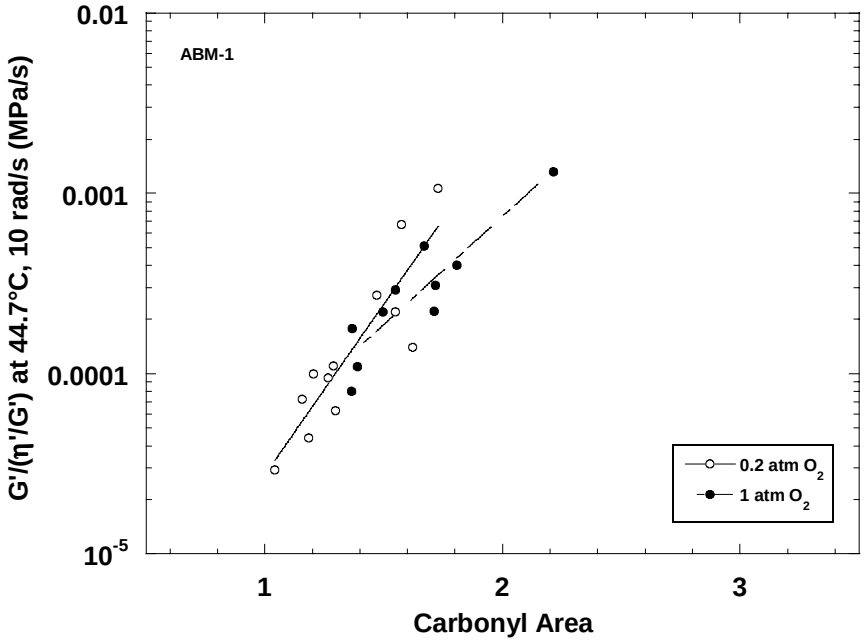

Figure B-7-43. DSR Function Hardening Susceptibility of ABM-1.

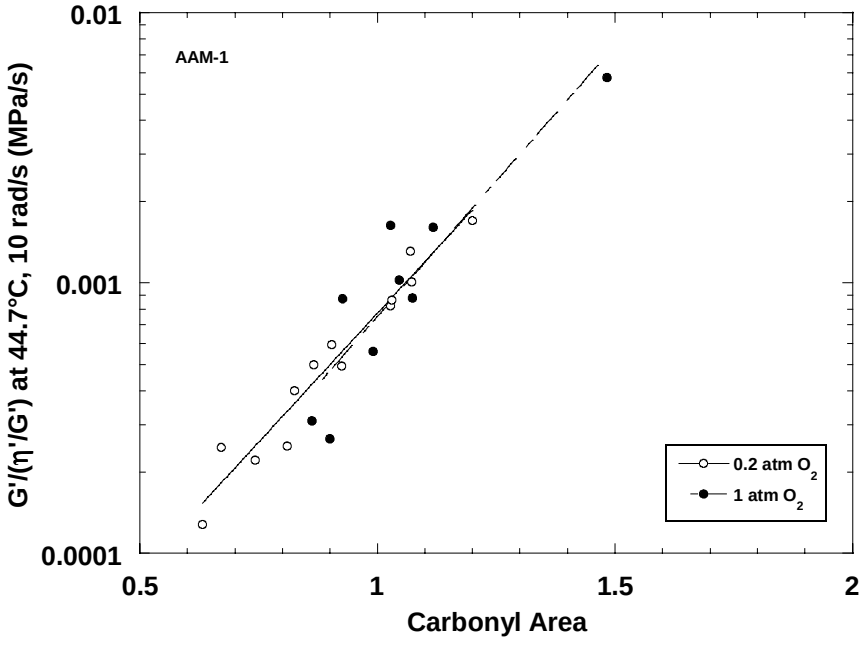

Figure B-7-44. DSR Function Hardening Susceptibility of AAM-1.

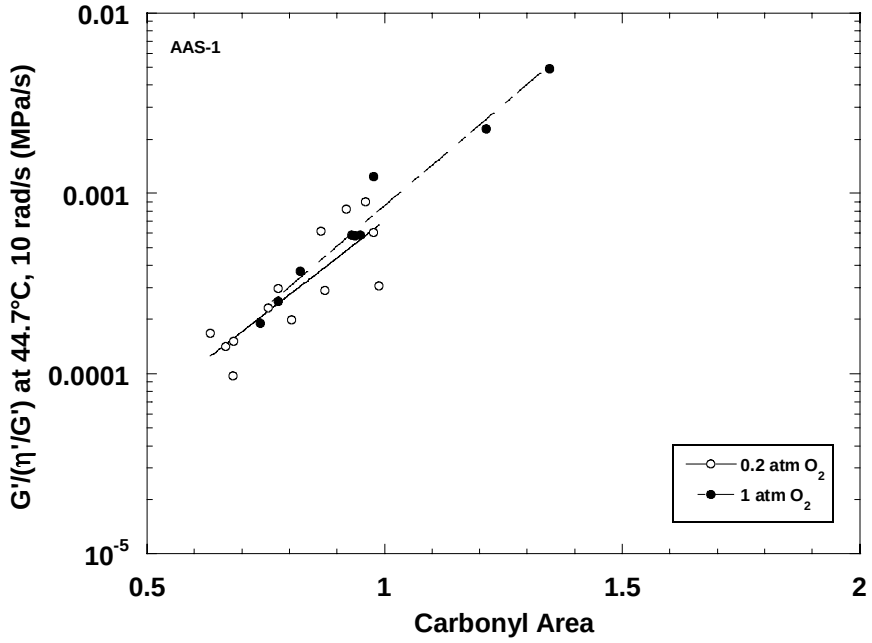

Figure B-7-45. DSR Function Hardening Susceptibility of AAS-1.

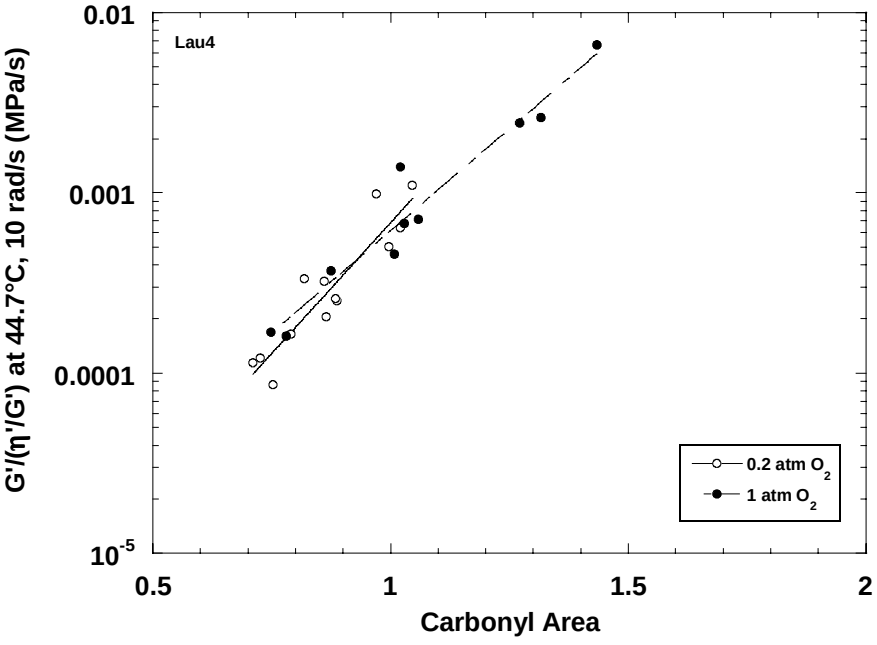

Figure B-7-46. DSR Function Hardening Susceptibility of Lau4.